The effect of geometry on acoustic emission.

EL-DARDIRY, S.M.A.

1980

THE EFFECT OF GEOMETRY ON ACOUSTIC EMISSION

by

SAMIR M.A. EL-DARDIRY

B.Sc., M.Sc., M.Phil.

Thesis submitted in partial fulfilment of the requirements for the degree of Doctor of Philosophy of the Council for National Academic Awards.

School of Physics
Robert Gordon's Institute of Technology
ABERDEEN
SCOTLAND

February 1980

CONTENTS

PART FOUR: RESULTS, DISCUSSION AND CONCLUSIONS

PART FIVE: APPENDICES AND REFERENCES

ACKNOWLEDGEMENTS

The author wishes to express his sincere thanks to Dr. R. Hill and Professor N. Langton, at School of Physics, RGIT, for their guidance, constant advice, continued encouragement and fruitful discussion throughout this project.

It is also a pleasure to acknowledge the advice and the many enlightening discussions and general supervision given to the author by Dr. G. Curtis of the Nondestructive Testing Centre, AERE Harwell and for some test facilities made available at the Centre.

The author also wishes to record his appreciation of the award of a studentship grant by the Scottish Education Department, and to the School of Physics at RGIT in providing the facilities which have made this work possible.

Also, the cooperation and technical workshop assistance provided by Mr. A. Mutch and Mr. W. Reeves are acknowledged.

His sincere thanks are also due to the staff of the Computer Unit at RGIT for the unlimited use of the computer facilities.

Finally, the author would like to record his appreciation to Mrs. M. Miara for the very necessary task of typing the manuscript.

DECLARATION

This thesis has been composed by myself and represents the results of a study on Acoustic Emission. The study was carried out in the School of Physics at Robert Gordon's Institute of Technology, Aberdeen, in the period of January 1976 to January 1979. The work of which this is a record is original and all sources of information have been acknowledged by means of reference. No part of the work described has been submitted to any other Institute or University for the purpose of obtaining degrees or other academic qualifications.

S.M.A. EL-DARDIRY

PUBLICATIONS

With R. Hill:

1. The Effect of Geometry on Acoustic Emission, Proc. of The Inst. of Acoustics, 1976.

2. The Influence of Transducer Couplant Thickness on Acoustic Emission Parameters, Proc. of The Inst. of Acoustics, 1977.

3. Variables in the Use and Design of Acoustic Emission Transducers, Proc. of the Int. Conf. on Acoustic Emission, Anaheim, California, Sept. 10-13, 1979.

4. A Theory for Optimisation in the Use of Acoustic Emission Transducers, A paper accepted for publication in the J. Acoust. Soc. Am.

THE EFFECT OF GEOMETRY ON ACOUSTIC EMISSION

ABSTRACT

Acoustic emissions are impulsive elastic waves which are part of the total energy release from many metallurgical phenomena. The emissions signature carry information about the source mechanisms and the present interest of investigators is to identify the acoustic emission sources in terms of material fatigue and fracture parameters in order to determine their severity on the structure components. In practice, the acoustic emission signature from the receiving transducer output is strongly affected by the structure geometry, structure/transducer couplant layer, transducer components and instrumentation characteristics.

The aim of this study was to develop an acoustic emission data processing system and to investigate the effect of piezoelectric transducer structure, couplant and the geometry of test specimen on the transducer output. Theoretical interpretation of acoustic emission parameters are carried out on an arbitrary emission burst and relationships between different parameters, in both time and frequency domains, are investigated in order to achieve a better understanding of the physical meaning of such measures. Data processing systems to record the waveforms of emissions and computer programs to extract several statistical parameters and transform the waveforms to frequency spectra are developed and tested.

To simplify the propagation problem, the theoretical study only predicted the pressure transmission coefficient for the case of a plane longitudinal wave incident on the couplant and transducer components in normal direction. Several transmission cases are considered theoretically, and an emerged test system was devised to determine experimentally the applicability of the theoretically predicted transmission curves. The study shows how the observed acoustic emission parameters are influenced by the transmission geometry and variation in couplant thickness. It is suggested that a PVC adhesive tape, under certain conditions, is a good selection as transducer couplant.

An attempt was made, using the developed data processing system and couplant, to touch on the important highlights of the effect of the specimen geometry on the received acoustic emission waveforms. It is found that the series of the theoretical relationships between different acoustic emission parameters correspond rather well with the experimental results. In the case of simulated acoustic emission source in plates, the results indicated that the received bursts are of normal distribution with zero mean as well as the bursts derivative function. The linear relationship between the natural logarithm of the burst number of counts and the corresponding threshold squared value for an individual burst can be used to characterise the burst energy, duration time and the central frequency.

PART ONE

INTRODUCTION

CHAPTER ONE

INTRODUCTION

1.1 FOREWORD

The use of acoustic emission monitoring technique in numerous engineering nondestructive testing applications and scientific research has experienced very rapid growth in the past two decades. This growth was given marked impetus by the increasing use of high stressed structures such as nuclear plants, aircraft, space vehicles and oil pipe lines and with the development of means of detecting and analysing the emission by electronic and computerized equipment.

The term 'acoustic emission (A.E.)' or 'stress wave emission (SWE)' is applied to the elastic stress waves generated during a wide variety of dynamic processes such as dislocation motion and crack propagation in material deformation and failure.

The history of acoustic emission technology starts with work of Joseph Kaiser*, 1950, whose doctoral investigation included monitoring of a variety of materials for the emission of sound energy while the material was being subjected to external loads. Kaiser established the immediately irreversible

---

*J. Kaiser: Untersuchunger "Uber das Auftreten Gerauschen bien Zugversuch (An Investigation into the Occurrence of Noises in Tensile Tests), Ph.D. Thesis, Techn. Hochsh. Munchen, 1950.

characteristic of the acoustic emission during repeated loading. This phenomenon came to be named the Kaiser effect. Because of the many problems encountered not much work was done until the mid 1960's, when research and development efforts started to apply the technique for monitoring of flaws and crack growth. Recently, significant advances in the location of flaws in engineering structures have been established by computerized multiple transducer triangulation systems and considerable success had already been achieved relating acoustic emission to fracture mechanics parameters. In comparison, the basic scientific understanding of many aspects of acoustic emission is still inadequate. Little attention has been paid to the large effects of the specimen geometry and the transducer components on the signal that is detected. The characterization of acoustic emission signals requires a sophisticated system of large data processing, developing more understanding of the signal waveforms and wave propagation within the structural geometry being monitored and in the detecting transducer components.

The acoustic emission from the original source will be modified by the path characteristics between the source and the transducer interfaces and by the boundary conditions of these interfaces. It is expected that the acoustic emission event at the source will be of short duration, impulsive in nature, and lasting in the very short time range (nanoseconds). The frequency spectrum of this event will be uniformly distributed over a very broadband frequency.

Inside the propagation structure this source spectrum is likely to be modified by a series of factors which will cause the source event to be distorted before it reaches the transducer. These processes of modification are intrinsic attenuation, frequency dispersion, mode conversion, specimen resonance and transducer/shoe/coupling layers resonance. Before the original wave reaches the structure surface its amplitude decreases inversely with distance from the source if spherical propagation nature can be assumed. At the specimen or structural surface it will be converted to shear and surface waves along with the reflected longitudinal waves. If the propagation structure is relatively thin, Lamb waves will be generated instead. Surface and Lamb waves maintain their amplitude at greater distances from the source as their amplitude decreases as the square root of the distance from the source. In addition, the propagated modes will suffer more distortion from reflections and interactions with microstructures along the transmission path. At the transducer face a variety of wave propagational modes will exist which carry a number of superimposed frequencies, and therefore the frequency content of the stress waves will be modified and no longer uniformly distributed, as it was at the source.

The detecting transducer is the major critical element in analysing the acoustic emission signal and getting information about the source event. Although transducers of several types were tried, they are now almost always piezoelectric, and are usually undamped or lightly damped so that sensitivity is maintained. It is important to realise that a transducer of this kind cannot measure the acoustic emission event itself but only its effect. The transmission of the propagated waves into the transducer active element is a rather complicated problem. The geometrical and physical construction and acoustic matching of the transducer components as well as the transducer couplant with the structure are all important factors in the final transducer output electrical signal. It is important for a realistic quantification of the acoustic emission source to study the interaction of the transducer components including the couplant. Most of the measured acoustic emission parameters and consequent analysis can be misleading and significantly affected by the characteristics of the transmission system.

In summary, a better understanding of the geometry problems is necessary in order to establish the basic limitations and possibilities of a valuable technological tool.

The work reported in this thesis represents an exploration of these problems. The rest of this chapter reviews some important aspects dealing with the present understanding of acoustic emission. This is by no means a complete review as the volume of the published work is too large and comprehensive reviews can be found elsehwere (1-4). In addition to this introductory chapter, the thesis is divided into five other chapters. In Chapter Two, a statistical interpretation of acoustic emission parameters is investigated because of their extreme importance in the computation and data processing system. The emission waveform is explored in detail and the concepts of threshold counting, zero-crossing counts and peaks distribution are discussed. Signal analysis computer programs are developed to determine digitally some statistical parameters and frequency spectra of the acoustic emission burst in the absence of commercial equipment.

The transmission theory which considers the PZT-active-element as combined with other material is considered in Chapter Three. Because the acoustic emission piezoelectric transducer with its plastic or metallic shoe, backing medium, couplant and propagation structure has the effect of a complicated transmission geometry, it will be assumed that the transmitted waves are longitudinal. The details of experimental design and associated data preprocessing, acquisition and display systems, are emphasized in Chapter Four. Chapter Five presents the theoretical and experimental results which are obtained from the transmission theory and models. It is found that the acoustic emission transducer output is governed by the geometry of the transducer components and its acoustic couplant to the structure. Considerable effort has gone into determining the transmission characteristics of commercial transducers and a standard couplant material was proposed.

In Chapter Six, a comparison is made between the acoustic emission waveforms simulated in a variety of specimen geometries using a variety of materials. The significance of the propagation geometry to acoustic emission measurements is also emphasized.

In short, it is found that the transmission characteristics of the propagation structure, transducer components and couplant play a vital role in the frequency characteristics and the measured parameters of the transducer output.

1.2 NATURE OF THE ORIGINAL AND OBSERVED ACOUSTIC EMISSION SIGNALS

The original acoustic emission source events are generally thought of as step or delta functions (5) due to the nature of the generating source, so that the emissions contain a broadband spectrum of frequencies. Microdynamical deformation processes such as twinning (6), martensitic phase transformation (7-10) and dislocation motion (11-17) are examples of acoustic emission sources.

The principal process in the generation of acoustic emission by dislocation motion can be explained by the local lags of dislocation motion. During such postpone there is an accumulation of dislocations accompanied by a blocking and at localized sections high stresses having increased energy appear. During the deformation process there is a spontaneous release of the blocking which leads to a deformation step generating an acoustic emission. From the point of view of fracture mechanics and in practice, a crack never grows uniformly and its growth rate pulsates both in magnitude and direction (18). During the advance of the crack, acoustic emission is likely to be emitted from the crack tip by this non-uniform crack steplike motion

(b) Continuous Emission;Continuous emission is continuous nonperiodic signals detected from rapidly occurring acoustic emission events. The signal energy level is 1-10 electron volts (21) and characterized by a wide frequency spectrum the upper limit of which is evaluated at 30 MHz (28). Generally, the continuous emission appears as random noise of low amplitude in which individual events cannot be distinguished (12). It is recognisable as an apparent increase in the electronic noise level. In tensile tests where uniform strains are distributed fairly evenly throughout the volume of test specimen, continuous emission is likely to be observed.

However, intermediate cases may be observed in practice as continuous emission is a limiting case of high rate, low amplitude bursts. Therefore, the division of the emission into the two classes is a matter of convenience in discussing such experimental results (20) and not really a satisfactory classification.

1.3 ACOUSTIC EMISSION TRANSDUCTION

The criteria for detection of acoustic emission signatures is that sufficient elastic energy at the source must be converted into elastic stress waves for the output of the transducer to rise above the background noise level. Transducers attached to the surface of the structure detect the stress wave information as it reaches the transducer/structure interface. Acoustic emission transducers can be generally classified into two separate categories:

and with the rapid increase in the load of the material. In the occurrence of martensite phase transformations in metals and alloys, redistributions of atoms occur and as a result of this high rate of transformation and the constraints due to this surrounding matrix, acoustic emissions are generated.

Because of attenuation, reflections, mode conversions in the transmission path and transducer structure and resonance, the signal at the transducer output is in random waveform and approximates a complex decaying exponential (19, 20). Two basic types of acoustic emission signals are generally observed in experiment by many investigators (21, 22):-

(a) Burst Emission: Individual emission events which appear as well defined discrete short pulses of complicated form and can be distinguished from each other (12). Burst emissions are characterised by a duration of 10^{-4}-10^{-8} seconds (23,24). The amplitude can range from below the noise level, i.e. less than a few microvolts at the transducer output to greater than 6 volts or more, in some materials, as reported by Radon and Pollock (25). The burst energy level has been determined to be 10^{10}-10^{14} electron volts (21). Burst type emissions are observed where large localised strains occur (26) or when discrete events such as microcracking (27) or phase transformation takes place.

(a) Resonant Piezoelectric: usually used to detect waves with frequencies centred on particular narrowband frequencies ranging from 20 KHz to 5 MHz in 100-200 KHz bandwidths. No detailed information about the shape or time duration of the acoustic emission as it originated is gained with these transducers.

(b) Non-resonant Transducers: e.g. capacitive transducers (29), polymeric foil (30) and the absolute displacement measuring laser interferometer (31). They can be used to detect acoustic emission with frequencies ranging from DC to 30 MHz (29-34). These transducers offer many important advantages over the resonant piezoelectric devices in research laboratories, e.g. no acoustical impedance matching couplant is required, the waveform of the acoustic emission is not modified by the transducer structure and geometry, they can be absolutely calibrated and have inherent broadband and flat frequency response. These have the disadvantages of being difficult to operate, necessitating specimen surface preparation, and being too delicate for field work. The main disadvantage however is the low sensitivity in general. Sensitivity is an important factor when the stress wave source is weak, as it often is in emission from ductile metals, and when the stress wave is further dissipated in the material under test. Speake (31) states that resonant piezoelectric transducers are an order of magnitude more sensitive than broadband piezoelectric transducers and two orders of magnitude more sensitive than either capacitive transducers or the absolute displacement measuring laser interferometer.

Most applications of acoustic emission have used piezoelectric transducers principally because of their high sensitivity, low sensitivity to mechanical noise and good signal-to-noise ratio. They can also easily be designed to respond to particular wave types; e.g. longitudinal or shear waves. On the other hand, details of the piezoelectric transducer vibrating modes are hard to come by. A number of authors (35-39) have shown experimentally that the modes of a vibrating transducer are very complicated and do not resemble the one-dimensional vibrations basis which has been given by Mason (40) and used by others (41). Shaw and Sujir (39) have measured the displacement distributions on the surface of transducers vibrating in air or liquid and as a result very complex modes were obtained. The main problem however is the extreme difficulty in calibration. Part of the reason for this is measuring stress wave amplitudes at the transducer/structure interface, though recent advances in laser interferometry (31) have to some extent solved this problem. Despite these difficulties, however, several other calibration techniques have been developed and are in current use (31, 42-48). Considerable progress was made by Breckenridge et al (49) who developed a method for obtaining the waveforms of simulated acoustic emission sources which were unmodified by the resonances of the specimen or the transducer. Their technique was based on the comparison of two signals at the transducer, one from the event in question and one from an artificial event of known waveform. For a standard source event they used a step function of stress which was realized experimentally by fracturing a glass capillary at the centre of one flat surface of a large cylindrical aluminium alloy transfer block. In order to have a broadband transducer they used a DC-biased electrostatic transducer with an air gap dielectric. They found that measurements of the waveform both on the same surface as the source and on the opposite surface yielded results that agreed remarkably well with theoretical predictions. An important conclusion from the work was that there is no important difference between the vertical displacement at the epicentral point produced by a source event on the surface and that produced by a similar event in the interior.

More recently, Hsu, Simmons, and Hardy (50) have numerically computed the displacement as a function of time at an arbitrary point on an infinite plate due to an arbitrary point source force function. Nearly perfect experimental agreement with their theory was obtained by using a reproducible step-function stress release pulse as a simulated acoustic emission signal and a wideband capacitive transducer as a receiver.

1.4 ACOUSTIC EMISSION PARAMETERS AND APPLICATIONS

The information which can be gained about the acoustic emission source is very much dependent on the characteristics of the detecting and recording equipment, and consequently of the parameters measured. Such structure evaluation and technical information is based on the presence of correlations between the acoustic emission parameters and the parameters characterizing material defects and their dynamics of growth. In this section, only general parameters and relationships in use are presented. Our view will be discussed further in Chapter Two.

1.4.1 RINGDOWN COUNTING

This is defined as the total number of times that the acoustic emission transducer output crosses a preset threshold. The sensitivity of the system is a function of the threshold level and the detecting system gain, and consequently the maximum sensitivity is restricted by the background and electronic noise. The main advantages of ringdown counting however are that it is easy to measure and that it provides a single number to be related to other engineering test parameters.

A number of authors (51-53) assumed that the acoustic emission burst is an exponentially decaying sinusoid of period T and decaying constant β i.e.:

$$V(t) = V_p \, e^{-\beta t} \sin(2\pi t/T) \tag{1.1}$$

where $V(t)$ is the transducer output voltage at time t, and V_p is the voltage at time $t = 0$. Then, the total number of threshold crossings in the burst ΣN, can be related to the burst peak voltage V_p and the threshold level V_ℓ, and to the burst total energy E_T, assuming that V_p is proportional to the square root of the burst energy with proportionality constant ψ:

$$\Sigma N = \frac{1}{T\beta} \ln (V_p/V_\ell) \tag{1.2}$$

$$\Sigma N = \frac{1}{T\beta} \ln (\psi\sqrt{E_T}/V_\ell) \tag{1.3}$$

Equations (1.2) and (1.3) have been used to relate the burst energy and the total number of ringdown counts in studying fibre fractures and resulting strain energy release in Al_3Ni composites (51). They have also been applied with some success by Tetelman and Chow (52) to predict acoustic emission counts during microcracking in tensile tests. However, both relationships depend on the period T of the sinusoid and the exponential decay constant β, being constant during a test. This is unlikely to be the case, as internal reflections in the specimen and the specimen resonance will change during a test as cracking occurs. The signal attenuation has also been noted to be increased after the specimen has yielded (54). The burst waveform is also important and is not a simple sinusoidal decay as assumed above, which is to be expected due to multiple reflections in the specimen and transducer structure (19, 55). Dumousseau (56) also points out that if the peak-amplitude distribution law changes, so does the relation between energy and ringdown counts.

The relationship between the total number of ringdown counts and crack tip stress intensity factor K has been investigated (57-63). The following general relationships have been obtained:

$$\Sigma N = A\ K^m \tag{1.4}$$

where A and m are constants. A wide range of values of m has been reported for a variety of materials and geometries. Generally it can be considered that the best fitting with experimental data is provided by an exponent m varying from 1-22(61,64). The reason for such a wide variation is the effect of variation of the volume of the stressed part in the crack tip and also the effect of deformation rate, specimen thickness and notch depth.

Palmer and Heald (57) developed another relation as:

$$\Sigma N = D\ S \tag{1.5}$$

where S is the plastic zone size and D is a material constant depending on heat treatment, cold work, etc.

Work has also been carried out on the relation between ΣN and the crack opening displacement (COD), δ, and the form:

$$\Sigma N = B\ \delta^{b} \tag{1.6}$$

has been observed, where B and b are constants (65).

Equation (1.4) was obtained considering the hypothesis that the emission rate (number of counts per unit time) is proportional to the growth rate of the amount of material plastically deformed in the region of the crack tip. In the simplest case of uniform single-axis tensile stress σ_o of an infinite plate having a central crack of length ℓ, the crack tip stress intensity factor is equal to (18):

$$K = \sigma_o \; (\pi\ell/2)^{\frac{1}{2}}$$

and therefore equation (1.4) becomes:

$$\Sigma N = A\sigma_o^m \; (\pi\ell/2)^{\frac{1}{2}m} \tag{1.7}$$

which relates the total number of counts to the crack length. This can be the base for monitoring of the magnitude of defects and approximates the time of rupture corresponding to the critical value $K = K_c$ and consequently the critical value of ΣN.

Sinclair et al (66) found that in fatigue of A533B steel and other steels the numbers of acoustic emission bursts were proportional to the fatigue crack area.

1.4.2 MAXIMUM AMPLITUDE AND AMPLITUDE DISTRIBUTION

Opinions have also been expressed of relationships between acoustic emission amplitude and the magnitude of defects (21, 67).

The acoustic emission maximum amplitude can be related to the strain energy release during crack propagation. The elastic energy release due to a microcrack propagating across a single grain has been considered as (27, 52):

$$E = \frac{\sigma^2}{2Y} d^3 \qquad (1.8)$$

where d is the material grain diameter, with Young's modulus Y, over which the applied stress σ is relaxed as the crack propagates. The maximum amplitude V_p, can then be estimated by assuming that it is proportional to the emission energy (51):

$$V_p = C \sqrt{\Delta E} = \frac{C}{\sqrt{2Y}} \sigma \; d^{3/2} \qquad (1.9)$$

where C is a constant. It was found that the maximum amplitude was proportional to the load drop per unit specimen thickness for a range of crack increments, from single grain microcracks to 1 cm. macrocrack in steel (68).

Green (21) discusses the correlation between the acoustic emission amplitude characteristics and an increment of length of a fatigue crack and also its rate of growth.

The amplitude distribution technique has been used by many workers to distinguish between different deformation mechanisms in materials (69, 70). Analysis carried out by Ono (63) suggests that continuous emission amplitudes, regardless of the signal bandwidth, follow a Rayleigh distribution. Other authors (71, 72) also suggest that the amplitude distributions follow cumulative power laws of the form:

$$n_\ell = V_\ell^{-s} \tag{1.10}$$

where n_ℓ is the number of emissions with amplitude greater than trigger level V_ℓ , and s is a constant.

Radon and Pollock (25) have related strain energy released and cracking mechanism to emission distribution in aluminium alloys. Many investigations have also been carried out on ductile crack growth in various materials (19, 62, 68, 73) and it appears that different deformation mechanisms in material can be distinguished by applying the amplitude distribution technique on the acoustic emission produced.

1.4.3 EMISSION ENERGY

The energy of acoustic emissions have been related to the strain energy released by different source mechanisms (11, 25, 71, 74, 75). Two methods are used: RMS voltmeters (pulse integrating method) and pulse peak amplitude squaring method. The amplitude squaring method is dependent on the burst duration and the characteristics of the burst waveform. Beattie and Jaramillo (76) claimed that the emission energy is not so sensitive to the emission waveform as ringdown counting and, therefore, is not so sensitive to transducer and specimen resonances. This seems, however, questionable and depends on the recording systems used.

A number of researchers (51, 77-79) have correlated the energy as measured by peak amplitude squaring method and the total energy in the burst waveform. Harris and Bell (77) have investigated the relation between energy and ringdown counts and concluded that there was no significant advantage in either for the detection of cracking. Dumousseau (56) has found that the RMS energy recording is likely to give less spread in results than other recording methods especially ringdown counting. Mirabile (11) has related the energy released in plastic deformation and brittle fracture with the acoustic emission energy detected from a steel heat treated to give different fracture modes. He stated that the energy parameter was a better measure to distinguish ductile from brittle cracking fracture than ringdown counting. Radon and Pollock (25) noted that the fraction of strain energy going to acoustic emissions increases as the fracture energy increases. This is an important fact as most models for energy contained in acoustic emissions assume that a constant fraction of the total strain energy released goes into stress waves (52).

1.4.4 FREQUENCY ANALYSIS

Frequency analysis is another type of signal processing that has recently received considerable attention as the fine structure of the emission spectrum can yield much information about the source mechanisms. The time domain and frequency domain can be interchanged by means of Fourier or inverse Fourier transformation.

Stephens and Pollock (80) demonstrate the feasibility of spectral analysis semiquantitively. The analysis has been used by various other authors (6, 75, 81). Woodward and Harris (81) analysed individual emission signals in a single parameter. The median frequency was computed for each spectrum. They defined the median frequency as the frequency which divides the spectrum into two segments of equal area, and hence equal energy.

Despite the distortion due to transmission and resonances, it seems possible to use the frequency analysis in distinguishing between different source mechanisms (5, 64, 80-87). Graham and Alers (84) have shown that the frequency spectra of emission from A533B steel become relatively lower in frequency as crack growth begins. Ono and Ucisik (82) correlate changes in the amplitude of specimen resonance frequencies with changes in microscopic fracture processes in high strength aluminium alloys. Fleischmann et al (85) distinguish between two mechanisms of deformation in tensile tests on mild steel by frequency spectra.

In summary, although the ringdown counting is a useful and widely used parameter the results must be interpretated with care and the problems of wave propagation and detection must be taken into account. The relationships given by equations (1.2) and (1.3) are derived on the basis of the very simplified exponentially decaying sinusoid of emission waveform, equation (1.1). At the present time, the actual relationships are still to be found only empirically by experiments, equations (1.4)-(1.7) and (1.10). It is clear that considerable work has to be carried out in the direction of basic theoretical understanding of acoustic emission parameters. This is necessary to make such measurements successfully and to interpret them correctly.

1.4.5 SOME APPLICATION AREAS

At present acoustic emission is employed for the testing of materials and structural integrity. In material testing, acoustic emission can be applied to a wide variety of materials (4). Tests have been made on pure and composite materials in both flawed and originally unflawed conditions. Acoustic emission tests on flawed materials not only confirm the existence of a dynamic crack or deformation but can also be employed to locate it (88,89) and even estimate the velocity at which it is developing. Flaws can be detected and located by loading the material specimen or engineering structure. The presence of cracks alters the loads at which plastic deformation begins (18) and consequently alters the acoustic emission patterns as the specimen is loaded (61). Growing cracks can be studied during stress corrosion cracking (90), high cycle fatigue test (91,92) and heat treatment (93). Acoustic emission tests on unflawed materials are valuable where knowledge of the characteristics and fracture strength of the materials is needed with reference to their use in structures such as pressure vessels (94).

An early study of the practical use of fracture analysis in both flawed and unflawed specimens, aluminium and beryllium, was made by Dunegan, Harris and Tatro (60). The suggestion was made in the article that acoustic emission data obtained in such experiments might be used in nondestructive testing of engineering structures.

There have been several studies of composite materials (51), carbon fibre reinforced plastics, cfrp, (95), fibre glass reinforced epoxies (96), and graphite epoxies (97). Dean and Kerridge (98) suggest an immersion technique to solve the problem of copious emissions from cfrp, which do not necessarily indicate deformation affecting the mechanical properties of the composite. Their technique has proved to monitor acoustic emission activity with less uncertainty and seems more convenient for production scale testing.

Structural integrity tests have been carried out on a wide variety of structures. Pressure vessels, for nuclear and petroleum industries especially tend to be the most common (99-102). Acoustic emission is also employed in in-service tests of structural integrity. Gopal (103) underlines the value of continuous monitoring of hydrostatic tests and during the normal operation of nuclear power plant. In-service acoustic emission monitoring has also been successfully applied to steam-methane reformer furnaces (104) despite problems of high noise level and skin temperature.

Acoustic emission techniques have also been employed in conjunction with in-processing tests to detect and provide quantitative data on flaws. The monitoring of weld defects during welding processes was developed by many investigators (105, 106). The occurrence of a fissure during the cooling of welds is indicated by the emission of signals, reception of which makes it possible to detect the fault. This has been used successfully in monitoring nuclear power component welds (107-109). Many of the applications of acoustic emission monitoring in nuclear reactors are in the in-service surveillance of welds. Such an application requires multi-channel computerized source-location capability (110). The background noise during welding can make the application formidable. At the other extreme is the testing of old welds in pipes that have experienced corrosion and a variety of structural loading (111).

Acoustic emission techniques have also had their problems however at the industrial level. The present technology cannot provide direct data on flaw characteristics, such as size, depth, and type. Industrial usage is, at present, confined mainly to source location and proof testing especially in large structures because of the difficulty in assigning source event types to acoustic emission in a systematic way. Doubts as to the reliability of information provided by the emitted signals have existed (112). Many of these are due to a lack of knowledge of the significance of parameters in common use, such as total number of counts, to characterize the emission. Furthermore, most of the information in an acoustic emission is discarded by the use of this parameter. Considerable work needs to be done on the effect of propagation geometry on acoustic emission waveforms and other measured parameters. New quantities are required and needed to be correlated with the metallurgical, mechanical and geometrical characteristics of structure (55). The implication is that the problems of propagation and transduction transfer functions (113, 114) in industrial applications appear surmountable.

In the light of the above points it was decided to develop a data processing system which could extract more information from the emission burst than just the number of ringdown counts.

1.5 MODES OF PROPAGATION AND ATTENUATION

Acoustic emission sources might occur in the bulk or on the surface of the structure under investigation. The stress waves are radiated in all directions through the bulk and along the surface of the structure where they are absorbed or reflected. In solid media through which these waves are propagated, there can be two main types of waves, namely, the longitudinal and the shear waves. The picture of the transmission of acoustic emission becomes complicated at the transducer face because at the boundaries of the propagation medium and the layers of the transducer components, for instance: couplant layer and transducer protective shoe, an incident longitudinal wave will produce four waves in the general case, namely, longitudinal reflected and shear reflected waves and two analogous refracted waves. The same holds for an incident shear wave which produces a longitudinal reflected and a shear reflected wave and a similar pair of refracted waves. Each of these modes has its own characteristic velocity and rate of attenuation, both of which are frequency dependent, in general. Thus, the stress wave signal arriving at the transducer active element is expected to be complex in its waveform and frequency content. This is the chief peculiarity of the propagation of acoustic emission.

Work by Kroll (115) and Egle and Tatro (86) showed that specimen resonances as well as transducer resonances were evident in the detected signal and different vibration modes of the test specimen were excited by the source. Egle and Tatro concluded that the specimen and transducer respond to frequencies near to their own resonant frequencies and therefore they act as filters in the system. Stephens and Pollock (80) undertook a theoretical analysis of the longitudinal modes of a test specimen and confirmed that the emission spectra are influenced by structural resonances. Fowler and Papadakis (116) presented a study of simulated acoustic emission waves in thin plates, concentrating on the first arrivals in the detecting signal. Theoretical and experimental work has also been performed by Fitch (117) on the effect of multiple reflections on the detected acoustic emission signal. Preliminary investigation by Hill and El-Dardiry (55) suggested that the frequency analysis is able to detect changes in specimen geometry.

On the other hand, Graham and Alers (83, 84) misinterpreted the effect of specimen geometry on frequency spectra by locating the acoustic emission transducer on the specimen very close to the source of the burst (white noise generator). They concluded that mode conversion during multiple reflection, specimen size and geometry have no effect on the spectra of emission received and the frequency content of an acoustic emission burst is related to the mechanisms which produced it.

1.5.1 LONGITUDINAL AND SHEAR WAVES

The complex acoustic emission source events are known to be expressed as a sum of harmonic oscillations by means of Fast Fourier Transform. When the wavelength of a harmonic component is significantly small compared with a heterogeneity, such as thickness or grain size the propagation of the stress waves can be derived for appropriate boundary conditions by solving the general wave equation (118):

$$\mu\nabla^2 \hat{u} + (\lambda+\mu)\, \nabla(\nabla.\hat{u}) = \rho \frac{\partial^2 \hat{u}}{\partial t^2} \tag{1.11}$$

where $\hat{u}$ is the particle displacement vector, t is the time variable, ρ is the density, λ and μ are the two Lame constants and ∇^2 is the Laplacian operator ($\nabla^2 = \partial^2/\partial x^2 + \partial^2/\partial y^2 + \partial^2/\partial z^2$). All the solutions of equation (1.11) can be formed from a combination of a vector potential function $\hat{\psi}$ and scalar potential function ϕ such that:

$$\hat{u} = \nabla\phi + (\nabla \times \hat{\psi}) \tag{1.12}$$

if ϕ and $\hat{\psi}$ are solutions to the equations:

$$C_L^2 \nabla^2 \phi = \partial^2 \phi / \partial t^2$$

$$C_S^2 \nabla^2 \hat{\psi} = \partial^2 \hat{\psi} / \partial t^2, \text{ and}$$

$$\nabla . \hat{\psi} = 0$$

where C_L and C_S are the velocity of longitudinal and shear waves. Both longitudinal and shear waves can exist simultaneously in a solid as a result of mode conversion. However, the exact solution of the wave equation cannot be obtained when reflections from the free surfaces are involved. Snell's law describes the direction that beams of various reflected and refracted modes take. Several conditions are possible (119).

In metals, the stress waves travel with a modest amount of attenuation in frequency range of 0-1 MHz. The attenuation coefficient α depends on the absorption and scattering processes occurring in the structure. The absorption process converts the wave energy into heat, while scattering redistributes the energy to other wave modes where they are finally absorbed by absorption mechanisms. The attenuation coefficient, α, can be expressed as (120):

$$\alpha = \alpha_a + \alpha_s$$

where α_a is the absorption attenuation coefficient, and α_s is the scattering attenuation coefficient. Generally, the attenuation coefficient as a function of frequency can be fitted approximately by the following formula:

$$\alpha = a\,f + b\,f^4 \qquad (1.13)$$

in which the coefficients 'a' and 'b' are determined by the physical properties of the solid. Both longitudinal and shear waves have an attenuation dependent upon frequency of this form with coefficient 'b' approximately six times larger for shear waves than for longitudinal waves. As a result, one might expect to find, in a case where the transducer is located far away from the source, that the mode of propagation is predominantly longitudinal.

Birchon (121) mentioned that an attenuation of 2 - 3 dB/m. over 2-3 metres was observed by a sensor resonant at around 400 KHz in a reasonably clean homogeneous microstructure steel plate. He also found that attenuation can rise above 20 dB across welds.

Another dynamic factor which can affect the wave attenuation in material under stress is the change in specimen geometry under load. It has been noted by Gillis and Hamstad (54) that signal attenuation increases during yield in tensile tests. This was related to the dissipation of stress wave energy in pinned dislocation segments as indicated by Granato and Lücke (122).

This factor could have important consequencies when emissions have to travel through yielded regions, leading to distortion of both the amplitude and frequency spectra.

1.5.2 DISPERSIVE MEDIUM AND LAMB MODES

In a case of such medium where the thickness of the material ℓ is small compared to the wavelength of the acoustic waves, the different frequency components propagate with difference velocities so that after the waves have travelled some distance the different frequency components are separated in space and arrive at the transducer at different times. This is the case of a dispersive medium in which the principal propagation modes are the symmetric and antisymmetric Lamb modes.

Egle and Brown (123) have summarized the possible resonance frequencies of Lamb waves as follows:

$$\left.\begin{aligned} f_{1s,m} &= (2m-1)\, C_S/\sqrt{2}\;\ell \\ f_{2s,m} &= (2m-1)\, C_L/\;2\;\ell \\ f_{3s,m} &= m\, C_S/\ell \\ f_{4s,m} &= m\, C_S\, C_L\;/\sqrt{C_L^2 - C_S^2}\;\ell \end{aligned}\right\} \qquad (1.14)$$

$$\left.\begin{aligned} f_{1a,m} &= 2m\, C_S / \sqrt{2}\, \ell \\ f_{2a,m} &= m\, C_L/\ell \\ f_{3a,m} &= (2m-1)\, C_S/2\ell \\ f_{4a,m} &= x_m\, C_L\, C_S / \sqrt{C_L^2 - C_S^2}\, \ell \end{aligned}\right\} \quad \begin{array}{c}(1.14)\\ (\text{contd.})\end{array}$$

In these equations f, is the wave frequency, 's' stands for symmetric mode type and 'a' for antisymmetric mode, m is positive integer and the value of x_m are the roots of:

$$\tan x_m = x_m \left\{ \left[2 - \left(\tfrac{1}{\xi}\right)^2\right]^2 / \left[1 - \left(\tfrac{1}{\xi}\right)^2\right] \right\}$$

where $\xi = C_S/C_L$

An important characteristic of equations (1.14) is that the mode frequencies depend only on the plate thickness and longitudinal and shear wave velocities and not on the width of the plate.

The total number of symmetrical modes N_s and antisymmetrical modes N_a that are possible in a plate of given thickness ℓ at a frequency f are given by Viktorov (124) as:

$$N_s = 1 + \left[\ell/\lambda_S\right] + \left[(\ell/\lambda_L) + \tfrac{1}{2}\right] \qquad (1.15)$$

$$N_a = 1 + \left[\ell/\lambda_L\right] + \left[(\ell/\lambda_S) + \tfrac{1}{2}\right] \qquad (1.16)$$

where the square brackets in this case indicate the nearest integer part of the number that they enclose.

Egle and Brown conducted a series of simulated acoustic emission-propagation experiments on plates of various thicknesses and concluded that the structure geometry introduces peaks in the received spectra corresponding to the resonance frequencies which may be estimated from Lamb's wave theory as given by equations (1.14).

The attenuation mechanism of Lamb waves is a more complicated one because of the possible occurrence of dispersion in the phase and group velocities. Viktorov gives the following expressions:

$$\sigma_{\delta sm} = A_{sm}\,\sigma_{\alpha} + B_{sm}\,\sigma_{\beta} \tag{1.17}$$

$$\sigma_{\delta am} + A_{am}\,\sigma_{\alpha} + B_{am}\,\sigma_{\beta} \tag{1.18}$$

where $\sigma_{\delta sm}$ and $\sigma_{\delta am}$ are the Lamb wave attenuation factors per wavelength, σ_{α} and σ_{β} are the attenuation factors for a given frequency per longitudinal and shear wavelength respectively, and the coefficients $A_{sm,am}$ and $B_{sm,am}$ are dependent on the type and order of Lamb's wave, specimen thickness, and Poisson ratio. These coefficients also depend very strongly on ℓ/λ and consequently on the mode frequency.

1.5.3 SURFACE WAVES

Surface waves can also be generated when the thickness of the material is large in comparison with the wavelength and by mode conversion on the surface of the specimen. The amplitude decay of surface waves due to scattering and absorption is typical of longitudinal and shear waves since the surface wave is a combination of these waves. Press and Healy (125) consider σ_α, σ_β, and σ_γ as the attenuation factors for a given frequency per longitudinal, shear and surface wavelength respectively then state the following relationship:

$$\sigma_\gamma = T\,\sigma_\alpha + (1-T)\,\sigma_\beta \qquad (1.19)$$

where $T = 16\bar{\xi}^2(1-\bar{\eta}^2)/\,\bar{\eta}^2(3\bar{\eta}^4 - 16\,\bar{\eta}^2 - 16\bar{\xi}^2 + 24)$, and $\bar{\eta}$ and $\bar{\xi}$ are complex values given by $\bar{k}_S/\bar{k}_R$ and $\bar{k}_L/\bar{k}_S$ respectively, and $\bar{k}$ is the corresponding complex wave number for each mode. It can be seen, from equation (1.19), that the surface wave attenuation factor per wavelength σ_γ is a linear combination of the longitudinal and shear wave attenuation factors. For all the materials the contribution of σ_β in equation (1.19) is much greater than σ_α, i.e. the surface waves attenuation factor is governed mainly by the shear wave attenuation factor σ_β. For steel and aluminium T takes the values of 0.11 and 0.07 respectively (124).

The effects of specimen surface conditions on the acoustic emission number of counts have been investigated by Tsoi and Egle (126).

Aluminium specimens with different surface finishes were subjected to tensile fatigue loading. Observations of the emission signals show that detectable emission occurs earlier in the specimens with rougher surface finish and that transverse surface scratches result in detectable emission earlier than longitudinal scratches.

In summary, if the acoustic emission parameters recorded using a transducer on the specimen surface is to be related to the source inside the test body, consideration has to be made of what happens to these parameters in travelling from the source to the transducer face. As it is mentioned above emission information is travelling through a material by a number of different types of wave modes each with its own characteristic velocity and attenuation rate both of which are frequency dependent. In the light of the discussion in this Section, this consideration is clearly hard to investigate as only a fraction of the entire information will be detected via the transducer.

PART TWO

THEORETICAL INVESTIGATIONS

CHAPTER TWO

STATISTICAL INTERPRETATION AND DIGITAL COMPUTATION OF ACOUSTIC EMISSION PARAMETERS

Several digital signal processing methods for representing acoustic emission bursts are presented in this chapter. Brief mention is also made of the practical considerations in the choice of analysis parameters. The name of the computer programme is given at the end of each section and the computer algorithms are listed in the Appendices.

2.1 INTRODUCTION

In most of the acoustic emission measuring systems whether they are used in site tests or for laboratory research, the systems provide an electrical signal "burst" which is related to the original acoustic emission event. The burst waveform depends on the transducers used in monitoring the structure and the rest of the measuring system transfer functions. Although the original acoustic emission pulse or event will be coloured by all these transfer functions, the resulting burst signal should contain information about the original metallurgical mechanism (5). The task of the signal analysis technique adopted, is ideally, to identify different types of flaws in engineering structures and materials and to assess their severity.

Unfortunately, acoustic emission bursts cannot be described by an exact mathematical formula and therefore, they are non-deterministic and realistic theoretical correlation with engineering parameters is quite difficult to establish (13,17,68,127). Consequently, the the observed acoustic emission electrical signal 'burst' captured from the electronic system will be described simply as a function of time by a universal set of data $\{x(t)\}$ throughout this study. In general, acoustic emission bursts are non-stationary random signals (128)as their statistical properties can vary from one subset of a relatively short-time period to another. Therefore, they can only be characterized by statistical parameters and theories similar to those of stationary random signals if a test of stationarity is performed on the detected bursts before proceeding to further statistical analyses.

The method of analysis and representation of the acoustic emission burst is central to almost every area of acoustic emission technology and research. Unfortunately, the methods of analysis and measurement of acoustic emission bursts varies. This seems to be more a matter of accident and convenience rather than valid scientific 'design'.

The main purpose of this chapter is to present some methods for digital processing and to represent the detected burst in the form of statistical parameters. The concepts of burst amplitude, threshold counting, zero-crossing count and the use of the burst envelope technique will be discussed. There are two reasons for using digital signal processing rather than signal processing via analog electronic equipment. First, by using a digital computer, a wide variety of digital signal processing techniques can be applied to acoustic emission burst signals. Secondly, the more sophisticated processing techniques, are in many cases, difficult to achieve with commercial analog equipment which is often expensive and may only allow one parameter to be measured.

The following references are of particular significance to this study; Papoulis (129,130), Otnes and Enochson (131),Mayer (132), Newland (133),Bendat and Piersol (134), and Rice (135).

2.2 STATIONARITY OF ACOUSTIC EMISSION BURSTS

A stationary signal can be defined as a signal whose statistical properties do not change with time (130). Although only some of the measuring parameters and analyses applied to stationary signals may be applied to non-stationary or transient data, no attempts to test the stationarity of acoustic emission bursts are to be found in the acoustic emission literature. This is necessary before a suitable analysis technique or measurement parameter can be chosen.

A useful test of stationarity and non-stationarity trends in either the mean or the variance of the burst data set can be done by subdividing the entire acoustic emission record of data into M time slices. From each one, a short-time averaged mean square value can be obtained. The parameter to be considered is termed a 'reverse arrangement' (133) and can be estimated as follows.

Suppose the short-time averaged mean square values are denoted by:-

$$X_1, X_2, \ldots\ldots, X_m$$

Define a reverse arrangement as occurring every time as:

$$X_j \geqslant X_i; \quad j>i \text{ and } i = 1, 2, \ldots\ldots, M-1$$

For a given value of the index i, if the number of reverse arrangements is denoted by R_i, then the total number of reverse arrangements, R_t, can be calculated as:

$$R_t = \sum_{i=1}^{M-1} R_i$$

R_t should be divided by a reference value in order to obtain the signal percentage stationarity. The reference value can be calculated from the number of the short-time slices M. Consider the fact that X_1 is equally likely to be larger or less than the succeeding (M-1) members of a random sequence. Therefore, the average number of reverse arrangements, $E\{R_1\}$ when considering X_1 compared to the remaining members is:

$$E\{R_1\} = \frac{M-1}{2}$$

Similarly, X_2 compared with the (M-2) remaining members as:

$$E\{R_2\} = \frac{M-2}{2}$$

and continuing for the rest of the slices leads to:

$$E\{R_3\} = \frac{M-3}{2}$$

$$\cdots\cdot \qquad \cdots\cdot$$

$$E\{R_{M-2}\} = \frac{2}{2}$$

and $$E\{R_{M-1}\} = \frac{1}{2}$$

Finally, the average value of the reference R_T is obtained by adding up all these individual averages, i.e.:

$$E\{R_T\} = \sum_{i=1}^{M-1} E\{R_i\} = \frac{1}{2} \sum_{i=1}^{M-1} i$$

$$= \frac{M(M-1)}{4}$$

Then, the expectation value of the total number of reverse arrangement is equal to one-half of the sum of the first (M-1) integers. Consequently, the reference value R_T may be calculated from the total number of short-time slices M as:

$$R_T = 2\ E\{R_T\} = \frac{M(M-1)}{2}$$

R_T represents the maximum number of reverse arrangements.

Nevertheless, it must be emphasised here that the test has many limitations as far as certain types of data records are concerned and is not a general test. As an example, if the mean square value jumps and returns to its original level after a period of time and if the test were being applied over this entire subset of data, the test would probably be inadequate. This is because, although too many reverse arrangements would occur over the first portion of the data, too few would most likely occur in the latter part to obtain an overall value which was not unusual. For this possibility, the burst waveform must always be visually inspected after the digitization process to make sure that there is no such sudden jump away from the zero voltage centre.

In this study, the stationarity tests were applied to each data record and when the signal has less than 100% stationarity, the calculated percentage stationarity will be mentioned.

Computer Program:-

NAME: STATM.FOR APPENDIX: 2.A.

2.3 TIME DOMAIN BURST ANALYSIS

The objective of digital representation of the acoustic emission burst signal is to prepare a numerical data set as accurately as possible so that other statistical parameters can be calculated from the digital representation. Some rather simple, but useful, characterizations can be derived by simple computation on the waveform itself, i.e.: upon a digital representation of the analogue waveform. Correct data format in the record file can also be tested by displaying the digitized waveform on a computer display unit and pre-stationarity test can also be done.

Computer Program:

NAME: TIMPLT.FOR APPENDIX: 2.B

2.3.1 MAXIMUM PEAK-TO-PEAK AMPLITUDE

The maximum peak-to-peak amplitude of the acoustic emission burst can be of some use in distinguishing between different acoustic emission sources generated from similar specimen design and loading conditions. It has been suggested by Nakamura (62) as a useful parameter for recognising specific deformation processes in the presence of background noise. Even though it should be used in conjunction with other parameters to give more confident picture of the acoustic emission burst.

The analytical procedures to measure the maximum peak-to-peak amplitude can be summarized as follows:

(i) Search for the maximum positive amplitude $|x(t)|_{max}$:

i.e. $|x(t)|_{max} = \max \{x_i(t): i = 1, 2, \ldots\ldots N\}$

and search for the maximum negative amplitude; $|x(t)|_{min}$

i.e. $|x(t)|_{min} = \min \{x_i(t): i = 1, 2, \ldots\ldots N\}$

(ii) Calculate the maximum peak-to-peak amplitude as:

$$\text{Max. P-P Amplitude} = |x(t)|_{max} - |x(t)|_{min}$$

This parameter is simple to measure but cannot be used as an individual parameter to describe such bursts.

Computer Program:

NAME: COUNT.FOR APPENDIX: 2.C.

2.3.2. BURST SHAPE AND THRESHOLD CROSSING

The number of counts and count rate using a fixed threshold level seems to be the preferred parameter for many workers in acoustic emission technology. Quantitative comparisons of different work is difficult because the shape distribution of the bursts has usually been ignored. In order to accomplish better understanding of these parameters and evaluate some relationships between them and corresponding parameters in the frequency domain, a fundamental analysis is presented in this section. The work is based upon a generalization of Rice's (135) theory of random noise analysis. Rice's approach is based on the analysis of the autocorrelation function of the noise signal x(t). Our approach will be concerned with the change in the burst shape as function of time. The analysis is based on the assumption that the signal x(t) is a stationary random process and the threshold crossing statistics is obtained from the joint distribution density function $p(x, \dot{x})$. A burst waveform that crosses the level x_ℓ per unit time is sketched in Fig. 2.1. Suppose it is possible to define the burst signal time-derivative $\dot{x}(t)$ and let the joint probability density function of x and $\dot{x}$ to be $p(x, \dot{x})$. The probability that the instantaneous value of x(t) at time t, lies within the amplitude range x_ℓ and $x_\ell + dx_\ell$ and at that time the rate of change of x(t) lies between $\dot{x}_\ell$ and $\dot{x}_\ell + d\dot{x}_\ell$; i.e. the strip between x_ℓ and $x_\ell + dx_\ell$ is being crossed with a rate of change between $\dot{x}_\ell$ and $\dot{x}_\ell + d\dot{x}_\ell$ is given by*:

$$P\{x_\ell \leqslant x(t) \leqslant x_\ell + dx_\ell \text{ and } \dot{x}_\ell \leqslant \dot{x}(t) \leqslant \dot{x}_\ell + d\dot{x}_\ell\} =$$

$$\int_{x_\ell}^{x_\ell + dx_\ell} \int_{\dot{x}_\ell}^{\dot{x}_\ell + d\dot{x}_\ell} p(x,\dot{x})\, dx\, d\dot{x}$$

This expression also represents the time interval which, during unit time, is spent by signal x(t) within the strip dx_ℓ while moving with

*See Ref.(134) page 27 and Ref.(133)page 12.

speed $\dot{x}_\ell$. The duration of a single crossing of the strip is given by:

$$\frac{dx_\ell}{|\dot{x}_\ell|}$$

where the absolute sign has to be taken since it is immaterial whether the rate of change $\dot{x}_\ell$ is positive or negative. Dividing the total time being spent within the strip by the duration of one crossing, gives the mean number of crossings per unit time; with rate of change $\dot{x}(t)$ as crossing frequency of the threshold level x_ℓ:-

$$n(x_\ell , \dot{x}_\ell) = |\dot{x}_\ell| \; p \; (x, \dot{x}) \; d\dot{x} \qquad (2.1)$$

The total number of crossings with an arbitrary rate of change $\dot{x}_\ell$ per unit time is therefore:

$$n(x_\ell) = \int_{-\infty}^{+\infty} |\dot{x}_\ell| \; p(x, \dot{x}) \; d\dot{x} \qquad (2.2)$$

Since the numbers of upward positive crossings (n+) and downward negative crossing (n^-) of line x_ℓ will be equal, then the crossing frequency for x(t) to exceed a given value x_ℓ will be $\frac{n(x_\ell)}{2}$.
In particular, the number of passages through the zero level is called the number of zero-crossings (n_o) and can be expressed as:-

$$n_o = \int_{-\infty}^{+\infty} |\dot{x}_\ell| \; p \; (o,\dot{x}) \; d\dot{x} \qquad (2.3)$$

If $x(t)$ and $\dot{x}(t)$ are independent and $\dot{x}(t)$ has a normal distribution with zero mean, i.e. $N(0,\sigma_{\dot{x}}^2)$, then:

$$p(x,\dot{x}) = p(x)\,p(\dot{x})$$

$$= p(x)\,\frac{1}{\sigma_{\dot{x}}\sqrt{2\pi}}\,e^{-\frac{\dot{x}_\ell^2}{2\sigma_{\dot{x}}^2}} \tag{2.4}$$

where $\sigma_{\dot{x}}$ is the standard deviation of the random variable $\dot{x}$ of the stationary random process $\dot{x}(t)$.

Substituting into equation (2.2) yields:

$$n(x_\ell) = \int_{-\infty}^{+\infty} |\dot{x}_\ell|\,p(x)\,\frac{1}{\sigma_{\dot{x}}\sqrt{2\pi}}\,e^{-\frac{\dot{x}_\ell^2}{2\sigma_{\dot{x}}^2}}\,d\dot{x} \tag{2.5}$$

By using the standard integration: (See Ref. (133) page 9)

$$\int_0^\infty \dot{x}\,e^{-\frac{\dot{x}^2}{2\sigma_{\dot{x}}^2}}\,d\dot{x} = \sigma_{\dot{x}}^2$$

equation (2.5) becomes:

$$n(x_\ell) = \left(\frac{2}{\pi}\right)^{\frac{1}{2}} \sigma_{\dot{x}}\,p(x) \tag{2.6}$$

and if $x(t)$ is also normal; i.e. $N(0,\sigma_x^2)$, then:

$$n(x_\ell) = \frac{1}{\pi}\,\frac{\sigma_{\dot{x}}}{\sigma_x}\,e^{-\frac{x_\ell^2}{2\sigma_x^2}} \tag{2.7}$$

and therefore

$$n_o = \frac{1}{\pi} \frac{\sigma_{\dot{x}}}{\sigma_x} \tag{2.8}$$

Equation (2.8) is similar to the one derived by Rice and mentioned by Ono (63).

In implementing zero crossing measurements digitally, there are a number of important considerations. Although the basic algorithm requires only a comparison of signs of each two successsive samples, special care must be taken in the sampling processing. Noise and D.C. offset have disastrous effects on zero crossing measurements. However, these factors will be treated in Chapter Four which deals with acoustic emission electrical signal preprocessing.

Detailed discussion is presented in Section (2.6). The computer algorithm COUNT which computes the number of zero-crossings will be mentioned in the next section.

2.3.3 DISTRIBUTION OF PEAKS AND THE PROBABILITY DENSITY FUNCTION OF THE BURST ENVELOPE

Another method of analysing acoustic emission is to study the distribution of peaks in a single burst. In Fig. 2.1, a peak maximum occurs if:

$$\dot{x}(t) = 0 \text{ and } \ddot{x}(t) < 0$$

Since $\dot{x}(t)$ has to change from positive to negative within the interval dt, the probability for a maximum within the intervals dt and dx_ℓ is:

$$P\{\text{Max. in } dx_\ell dt\} = P\{x_\ell < x(t) < x_\ell + dx_\ell;\ \dot{x}_\ell > \dot{x}(t) = 0 > \dot{x}_\ell - d\dot{x}_\ell;\ -\infty < \ddot{x}(t) < 0\}$$

Denoting the joint probability density of x, $\dot{x}$, and $\ddot{x}$ by $p(x, \dot{x}, \ddot{x}; t)$, then:

$$P\{\text{Max. in } dx_\ell\ dt\} = \int_{-\infty}^{0} p(x, 0, \ddot{x}; t)\ dx_\ell\ (-\ddot{x}dt)\ d\ddot{x}$$

The above equation is obtained by substituting ($d\dot{x} = \ddot{x}dt$) into the first equation given in section (2.3.2) and making the other necessary alterations.
therefore:

$$P\{\text{Max. in } dx_\ell\ dt\} = -dx_\ell\ \ dt \int_{-\infty}^{0} \ddot{x}\ p\ (x, 0, \ddot{x}; t)\ d\ddot{x} \qquad (2.9)$$

From the above equation, the probability of a maximum within unit time above a certain threshold level L is: (where x_ℓ = L in Eq. (2.9)).

$$P\{\text{Max.} > L \text{ per unit time}\} = -\int_{L}^{\infty} dx \int_{-\infty}^{0} \ddot{x}\ p\ (x, 0, \ddot{x}; t)\ d\ddot{x} \ (2.10)$$

This probability is also equal to the expected number N{L} of of maxima occur above x=L per unit time. Integration over a given period of time renders the expected number of maxima, within the period. In the stationary case; $p(x,\dot{x},\ddot{x};t)$ does not depend on t.

Now, if the acoustic emission burst x(t) is a stationary random process with a narrow frequency band, its waveform has the appearance of a sine wave with slow random amplitude and frequency modulation as in Fig. 2.2. One may assume that there is only one single maximum or minimum between two zero-crossings. Therefore, of n_o zero-crossings only n_L have, in the average, an amplitude larger than the threshold level L.

Therefore, approximately:

$$P\{\text{Max.}>L \text{ per unit time}\} = \frac{n_L}{n_o}$$

Consider the fact that:

$$P_M(L) = \int_L^{\infty} p(L)\, dL = \frac{n_L}{n_o}$$

Then, one can write the following equation for the probability density of maximum greater than a threshold level L:-

$$p(L) = -\frac{dP_M(L)}{dL} = -\frac{1}{n_o}\frac{dn_L}{dL} \qquad (2.11)$$

Again x(t) is stationary, normal with zero mean and independent of its derivative $\dot{x}(t)$ which is also normal $N(0, \sigma_{\dot{x}}^2)$ with zero mean. Then they are uncorrelated and (130):

$$E\{x(t)\ \dot{x}(t)\} = E\ \{x(t)\}\ E\ \{\dot{x}(t)\} = 0$$

Therefore, they are also orthogonal. Simply, the previous condition may be written in the following form:

$$E\{x\ \dot{x}\} = 0$$

Similarly: $$E\{\dot{x}\ \ddot{x}\} = 0$$

This assumption is not necessarily valid for $E\{x\ddot{x}\}$ and in general:-

$$\begin{aligned} E\{x\ \ddot{x}\} &= \lim_{T\to\infty} \frac{1}{2T} \int_{-T}^{T} x\ \ddot{x}\ dt \\ &= \lim_{T\to\infty} \frac{1}{2T} \left(\left[x\dot{x}\right]_{-T}^{T} - \int_{-T}^{T} \dot{x}^2\ dt \right) \\ &= -E\ \{\dot{x}^2\} = -\sigma_{\dot{x}}^2 \end{aligned}$$

and for 3-dimensional normal distributions x, y and z with almost zero mean values one can write (Ref. (134) page 65):

$$p(x,y,z) =$$

$$\frac{1}{(8\pi^3|\delta|)^{\frac{1}{2}}} e^{-\frac{1}{2|\delta|}(C_{11}x^2+C_{22}y^2+C_{33}z^2+2C_{12}xy+2C_{23}yz+2C_{31}zx)}$$

where: δ is the covariance matrix of C_{ij} defined by:-

$$\delta = \begin{bmatrix} \sigma_x^2 & \sigma_{xy} & \sigma_{xz} \\ \sigma_{xy} & \sigma_y^2 & \sigma_{yz} \\ \sigma_{xz} & \sigma_{yz} & \sigma_z^2 \end{bmatrix}$$

$|\delta|$ is the determinant of δ and

C_{ij} is the absolute cofactor value in determinant $|\delta|$ i.e.

$$C_{11} = \sigma_y^2\ \sigma_z^2 - \sigma_{yz}^2 \qquad C_{22} = \sigma_z^2\ \sigma_x^2 - \sigma_{xz}^2$$

$$C_{33} = \sigma_x^2\ \sigma_y^2 - \sigma_{xy}^2 \qquad C_{12} = \sigma_{xz}\ \sigma_{yz} - \sigma_z^2\ \sigma_{xy}$$

$$C_{23} = \sigma_{xy}\ \sigma_{xz} - \sigma_x^2\ \sigma_{yz} \qquad C_{31} = \sigma_{xy}\ \sigma_{yz} - \sigma_y^2\ \sigma_{xz}$$

and $\sigma_x^2 = E\{x^2\}$; $\sigma_y^2 = E\{y^2\}$; $\sigma_z^2 = E\{z^2\}$

$\sigma_{xy} = E\{xy\}$; $\sigma_{xz} = E\{xz\}$ and $\sigma_{yz} = E\{yz\}$

Substituting into the previous equation using:-

$$x = x(t), \quad y = \dot{x}(t) = 0, \quad z = \ddot{x}(t), \quad \sigma_{xy} = \sigma_{yz} = 0$$

and $\sigma_{xz} = -\sigma_{\dot{x}}^2$

the joint probability density function $p(x, 0, \ddot{x})$ becomes:-

$$p(x,0,\ddot{x}) = \frac{1}{(8\pi^3 \beta)^{\frac{1}{2}}} e^{-\left[\frac{1}{2\beta}\left(\sigma_{\dot{x}}^2 \sigma_{\ddot{x}}^2 x^2 + 2\sigma_{\dot{x}}^4 x\ddot{x} + \sigma_x^2 \sigma_{\dot{x}}^2 \ddot{x}^2\right)\right]} \tag{2.12}$$

where:

$$\beta = \sigma_{\dot{x}}^2 \left(\sigma_x^2 \sigma_{\ddot{x}}^2 - \sigma_{\dot{x}}^2\right)$$

Substituting (2.12) into (2.10) and differentiating Eq. (2.10), in accordance with Eq. (2.11) with respect to the threshold level L, after lengthy manipulation, one obtains, for the probability density of the envelope:

$$P_M(L) = \frac{1}{\sigma_x}\left(\frac{1-\alpha^2}{2\pi}\right)^{\frac{1}{2}} e^{-\frac{L^2}{2\sigma_x^2(1-\alpha^2)}} + \frac{L}{2\sigma_x^2}\,\alpha\left[1 + \operatorname{erf}\left(\frac{L\alpha}{\sigma_x(2-2\alpha^2)^{\frac{1}{2}}}\right)\right] e^{-\frac{L^2}{2\sigma_x^2}} \tag{2.13}$$

where

$$\alpha = \frac{n_o^+}{N};$$

$$n_o^+ = \frac{1}{2\pi} \frac{\sigma_{\dot{x}}}{\sigma_x};$$

$$\text{erf}(x) = \frac{2}{(\pi)^{\frac{1}{2}}} \int_o^x e^{-t^2} dt;$$

and

$$N = -\int_{-\infty}^{+\infty} dx \int_{-\infty}^{o} \ddot{x}\, p(x,0,\ddot{x})\, d\ddot{x} \qquad (2.14)$$

i.e. N is the total number of maxima per unit time, independent of their magnitude.

It can be shown that α must lie in the interval (0-1), i.e.:

$$0<\alpha<1$$

The upper limit, $\alpha = 1$, corresponds to the case of a narrow frequency band signal and in this case:

$$N = \frac{n_L}{2}$$

Furthermore, in the case of a narrow frequency band equation (2.13) reduces to a Rayleigh distribution:

$$P_M(L) = \frac{L}{\sigma_x^2} e^{-\frac{L^2}{2\sigma_x^2}} \qquad (2.15)$$

A measure of the accuracy of the Rayleigh distribution for an assumed narrow frequency band can be obtained by determining how the number of maxima and zero-crossings compare.

Equation (2.13) is the general solution for the burst envelope and applies of any signal x(t) having an arbitrary probability distribution. If x(t) is a normal distribution function one may drive equation (2.15) simply by substituting equation (2.7) into (2.11) and substituting for n_o from equation (2.8).

If, on the other hand, α is very small then we have the case where the mean number of maxima is much greater than that of zero-crossings. Such a situation is sketched in Fig. 2.3. In this case the ratio α approaches zero for the ideal broad-band signal and equation (2.13) goes over into a normal distribution i.e.:

$$P_M(L) = \frac{1}{(2\pi)^{\frac{1}{2}}\sigma_x} e^{-\frac{L^2}{2\sigma_x^2}} \tag{2.16}$$

One can easily realize that if x(t) at the very beginning is not normal the evaluation of equation (2.10) not only presents great difficulties but also there is no possibility of determining $p(x, \dot{x}, \ddot{x}; t)$.

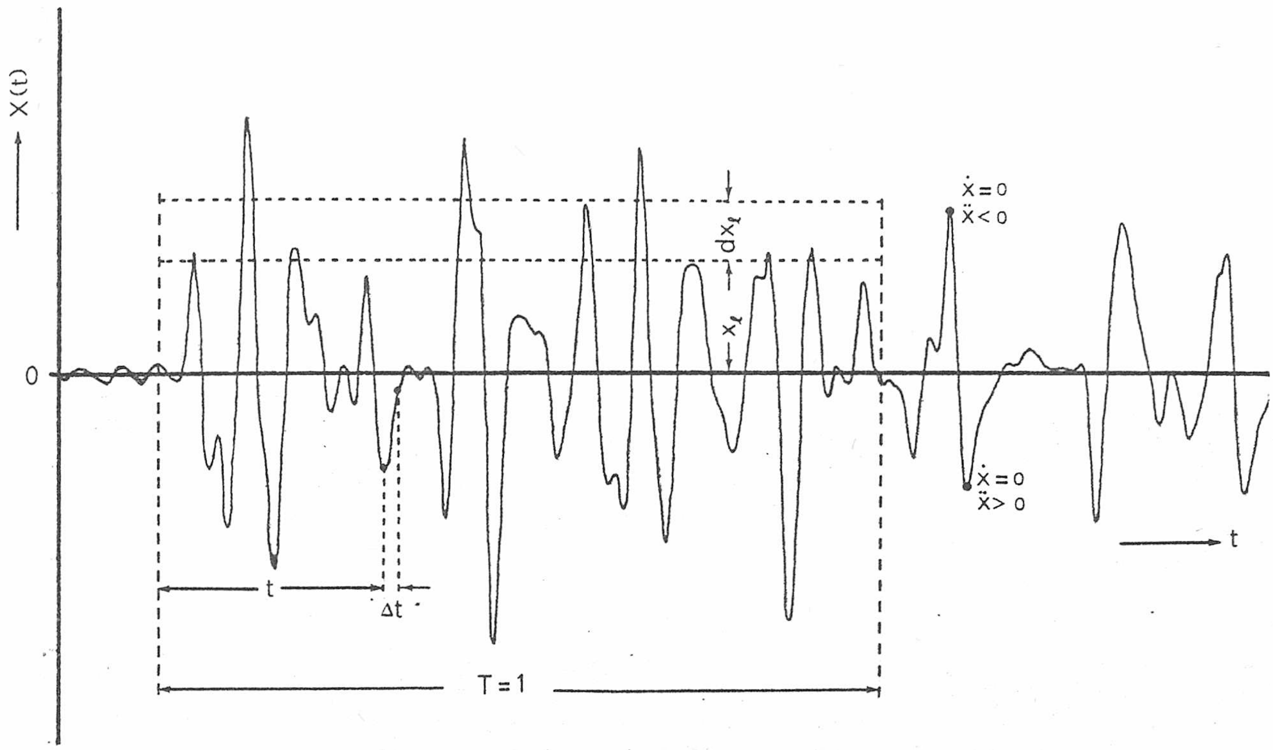

FIGURE 2.1 : The Concept of Threshold Crossings per Unit Time.

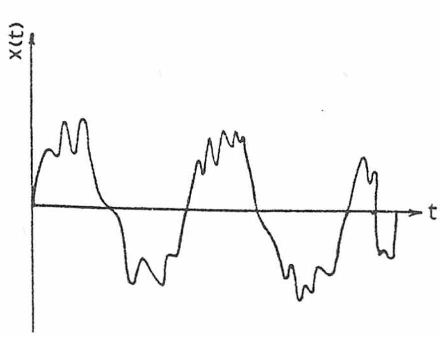

FIGURE 2.3 : The Number of Maxima is Larger than the Number of Zero-Crossing ($\propto \rightarrow o$)

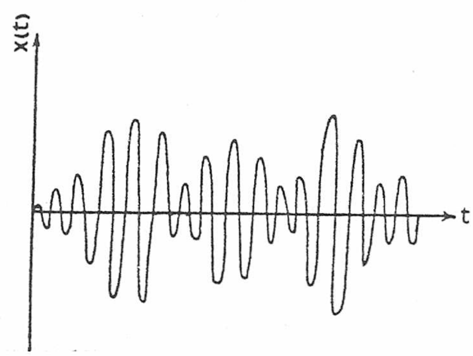

FIGURE 2.2 : Stationary Signal x(t) with a Narrow Frequency Band.

Computer Algorithm:-

The parameters which appear to be of particular interest as a result of the previous discussion can be divided into three groups:-

(i) Evaluation of the largest and smallest value in a burst signal of record period T which defines the signal maximum peak-to-peak amplitude. This value is printed out by running the program COUNT and the corresponding algorithm is mentioned in Section 2.31.

(ii) Distribution of the peak values, the threshold counting and the number of zero-crossings. These are also calculated by using the programme COUNT. Numerical results and/or graph plotting can be obtained as required by running this program.

(iii) The envelope of the burst maxima and minima, their distribution and time locations are calculated by running the programme PEAK.FOR (Appendix 2.D). The procedure for locating those values is as follows:

For the maxima, the subset $\{x_i(t)\}_{max}$ is calculated such that

$$x_i(t) - x_{i-1}(t) > 0$$

and $$x_i(t) - x_{i+1}(t) > 0$$

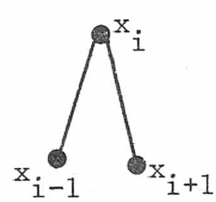

For the minima, the subset $\{x_i(t)\}_{min.}$ is evaluated such that,

$$x_i(t) - x_{i-1}(t) < 0$$

and $$x_i(t) - x_{i+1}(t) < 0$$

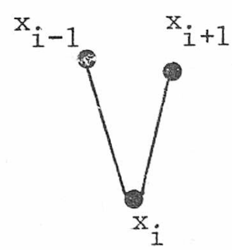

2.3.4 ENERGY MEASUREMENTS

The instantaneous signal energy at time t may be represented by:

$$\Delta E_i(t) \equiv \Delta t\ x_i^2(t) \tag{2.17}$$

where Δt is the time interval between two successive time records. The total energy in an acoustic emission burst can be calculated from the time domain as:

$$E_T \equiv \Delta t \sum_{n=1}^{N} x_i^2(t) = T\,\overline{x^2(t)} = T\,\sigma_x^2 \tag{2.18}$$

where: T is the burst period.

Another energy representations have been used by other authors (79,136) is the mean-square value of the burst (m.s.), i.e.: $\overline{x^2(t)}$ or σ_x^2 and the root-mean-square (r.m.s.), i.e.: $(\overline{x^2(t)})^{\frac{1}{2}}$ or σ_x. Clearly the relationship between different representations is:-

$$E_T \equiv T.(r.m.s.)^2 = T.(m.s.)$$

However, the burst energy can only be calculated from equation (2.18) and both the r.m.s. and m.s. may only be used as a measure of amplitude.

The signal period T must be considered in such burst energy analysis and must be long compared with the period of the lowest frequency component in the burst. Furthermore, bursts having the same r.m.s. or m.s. value can indeed have very different waveforms and the total energy will not provide a unique definition of a burst. Also, it is to be expected that the function E(t) in equation (2.17) would display time varying energy amplitude properties of the acoustic emission burst x(t).

For graphic representation, the instantaneous energy will fluctuate very rapidly depending on the exact details of the burst waveform (137). Also, these values are very sensitive to large signal level because the square of the signal level is used. Two relatively simple ways of alleviating this problem are used in this study. One way is to use equation (2.17) and accumulate the instantaneous energy up to a particular time in the signal i.e.:

$$\overset{\Lambda}{E}_i(t) = \left(\sum_{n=1}^{i-1} x_n^{\,2}(t)\ \Delta t \right) + x_i^{\,2}(t)\ \Delta t \qquad i>1$$

i.e.

$$\overset{\Lambda}{E}_i(t) = \sum_{n=1}^{i} E_n\ (t) \qquad i = 1, 2, \ldots N$$

(2.19)

where $\overset{\Lambda}{E}_i(t)$ represents the accumulated energy at time t_i and Λ is the symbolism used for "increment". Plotting $\overset{\Lambda}{E}_i(t)$ against time gives the 'energy increment' graph.

Another approach is to evaluate an 'energy decrement' graph which has been calculated using the formula:-

$$\check{E}_i(t) = E_T - \sum_{n=1}^{i} E_n(t) \qquad i = 1, 2, \ldots N \tag{2.20}$$

where $\check{E}_i$ is the instantaneous energy value at time t in the energy decrement graph and v is the symbolism used for "decrement".

The significance of both $\hat{E}_i(t)$ and $\check{E}_i(t)$ is that they provide a good representation of the burst waveform in terms of its decay value, noise level and shape. The slope in both $\check{E}_i(t)$ and $\hat{E}_i(t)$ for the noise level is much smaller than for the active portion of the burst if not zero.

Computer programs:-

1. $\hat{E}_i(t)$:	NAME:	ENERGY INC.FOR	APPENDIX: 2.E
2. $\check{E}_i(t)$:	NAME:	ENERGY DEC.FOR	APPENDIX: 2.F

2.4 FREQUENCY DOMAIN ANALYSIS

Frequency analysis has traditionally been one of the most important acoustic emission analysis techniques. If the acoustic emission burst x(t) in its short-time interval can be considered stationary, then its Fourier transform should give a good spectral representation of the burst during that time interval. In this study a few programs needed to be written to make use of the Singleton's

Fast Fourier Transform algorithm (138).

The Fourier transform evaluates the different frequency sinusoids and their respective amplitudes. These combine to form a waveform. Mathematically, this relationship is given by:-

$$X(f) = \int_{-\infty}^{+\infty} x(t)\, e^{-j2\pi f t}\, dt \qquad -\infty<f<\infty \qquad (2.21)$$

where the time domain burst x(t) decomposed into a series of sinusoids. X(f) is the Fourier transform of x(t), $j = \sqrt{-1}$.

The inverse transform is defined as:

$$x(t) = \int_{-\infty}^{+\infty} X(f)\, e^{j\,2\pi f t}\, df \qquad -\infty<t<\infty \qquad (2.22)$$

In equations (2.21) and (2.22) both t and f are continuous variables. For sample analysis, the numerical integration of equation (2.21) can be written as:

$$X(f) = \sum_{i=0}^{N-1} x_i(t)\, e^{-j\,2\pi f_k t_i}\, (t_{i+1} - t_i) \qquad (2.23)$$

where k = 0, 1, 2, ..., N-1.

In general, the Fourier transform is a complex quantity and:

$$X(f) = X_r(f) + j\, X_i(f) = |X(f)|\, e^{j\theta(f)} \qquad (2.24)$$

where:

$X_r(f)$ is the real part of the Fourier transform;

$X_i(f)$ is the imaginary part of the Fourier transform;

$|X(f)|$ is the magnitude of Fourier spectrum of $x(t)$ and is calculated as:-

$$|X(f)| = \left[X_r^2(f) + X_i^2(f)\right]^{\frac{1}{2}} \qquad (2.25)$$

$\theta(f)$ is the phase angle of the Fourier transform and can be calculated by:-

$$\theta(f) = \tan^{-1} \frac{X_i(f)}{X_r(f)}$$

The power spectrum density (PSD) is calculated from equation (2.25) as:-

$$PSD = |X(f)|^2 \qquad (2.26)$$

It can be shown that if there are N data points in the burst $x(t)$, then the computational time is proportional to N^2 which requires excessive machine time for large N. In 1965, Cooley and Tukey (139) published their mathematical algorithm which has become known as the Fast Fourier Transform (FFT). The FFT reduces the computing time of equation (2.21) to a time proportional to $(N \log_2 N)$. For example if N = 1024 data points as used in this study, the FFT becomes very economical in terms of computation time. It is over one hundred times faster than the straightforward one.

Nevertheless, as the speed of the computation was of little concern, Singleton's algorithm is combined with the scaling and and plotting subroutines. A few programs have been written to carry out different computational procedures. All these programs were tested with various theoretical pulse functions and digitized using continuous sine waves of differing frequency. The test frequencies were chosen to cover the frequency-band of interest and it was found that the digitized frequency values are in excellent agreement with the standard theoretical transform.

However, more details on this subject and the problems associated with using the FFT can be found in the references mentioned in Section (2.1).

Computer Programs:-

1.	NAME: SPECT.FOR	APPENDIX: 2.G
2.	NAME: SPECTM.FOR	APPENDIX: 2.H

2.5 THEORETICAL RELATIONSHIPS BETWEEN DIFFERENT PARAMETERS

This section discusses and provides a number of relationships between different parameters which have been considered in the preceding sections.

(i) In the case of a relatively narrow-band acoustic emission burst the probability density function of the peaks (which is given by equation (2.15)), follows a Rayleigh distribution. Considering equation (2.18) and an acoustic emission burst x(t) with zero expectation and normal distribution $N(0,\sigma_x^2)$ (the signal normality can be tested by using the programme MSES listed in Appendix 2.I) one can write the following relationship between the burst total energy and its peaks distribution function:

$$P_M(L) = \frac{L}{\overline{E}_T} e^{-\frac{L^2}{2\overline{E}_T}} \qquad (2.27)$$

where $\overline{E}_T = E_T/T = \sigma_x^2$

The expected number of peaks (number of counts) exceeding the threshold level L can be calculated by:

$$\Sigma N = f_o \int_L^{\infty} P_M(L)\, dL \qquad (2.28)$$

where f_o is the central frequency of the acoustic emission burst.

Combining equations (2.27) and (2.28) yields:-

$$\Sigma N = \frac{f_o}{\bar{E}_T} \int_{-L}^{\infty} L\, e^{-\frac{L^2}{2\bar{E}_T}}\, dL$$

i.e.
$$\Sigma N = f_o\, e^{-\frac{L^2}{2\bar{E}_T}} \tag{2.29}$$

Therefore, the number of counts ΣN is an exponential function of the quantity $(-L^2/2\bar{E}_T)$. It will be shown later in chapter (6) that the energy contained in the transducer signal depends on the volume of the monitored specimen. If so, equation (2.29) can be used to relate the number of counts per burst, the threshold level and the specimen volume.

The central frequency f_o is a function of the number of zero-crossing and is almost equal to $\frac{n_o}{2}$ for an ideal narrow-frequency band. Then, if ln (ΣN) is plotted versus L_i^2 for individual acoustic emission bursts, equation (2.29) clearly suggests a straight line fit. The straight line has a slope which is proportional to the ratio $\frac{T}{E_T}$ and also to the specimen volume. The intercept with (ln ΣN) axis should define the number of zero-crossings, the burst central frequency and duration. Consequently, the intercept value might be used to estimate one of these parameters if others can be measured or defined.

(ii) For fixed threshold counting, i.e.: when L is constant in equation (2.29) and for bursts with a constant period T, the relationship between ΣN or the count rate $\dot{N}$ and the burst energy is also in an exponential form. This means the straight line fitting suggested by Harries and Bell (77) does not in fact exist, at least, theoretically. The reason for the observed linear fitting might be due to the lack of graphic scaling or the experimental set up which confined the results in the approximately linear **region** of the exponential curve. This fact can be also realized by studying the two experimental graphs given by Beattie (140). Tests were conducted on a PRD-epoxy filament-wound bottle and Beattie reported that the individual bursts had a frequency content centred around 200 kHz and were about 75 μ sec long. The variation of both the total energy and total counts with the applied pressure were plotted as two separate curves. Fig. 2.4 shows experimental data, remeasured from this reference, plotted together with numerically calculated points. The experimental representation shows an exponential relationship between the total energy and the total counts similar to the theoretical curve.

(iii) Considering equation (2.22), the time domain waveform can be reconstructed from the burst Fourier coefficients as follows:

$$x(t) = \sum_{n=0}^{N-1} \left\{ X_r(f_n) \cos 2\pi f_n t + X_i (f_n) \sin 2\pi f_n t \right\} \tag{2.30}$$

the first and second derivatives take the forms:-

$$\dot{x}(t) = 2\pi \sum_{n=0}^{N-1} f_n \left\{ -X_r(f_n) \sin 2\pi f_n t + X_i (f_n) \cos 2\pi f_n t \right\} \tag{2.31}$$

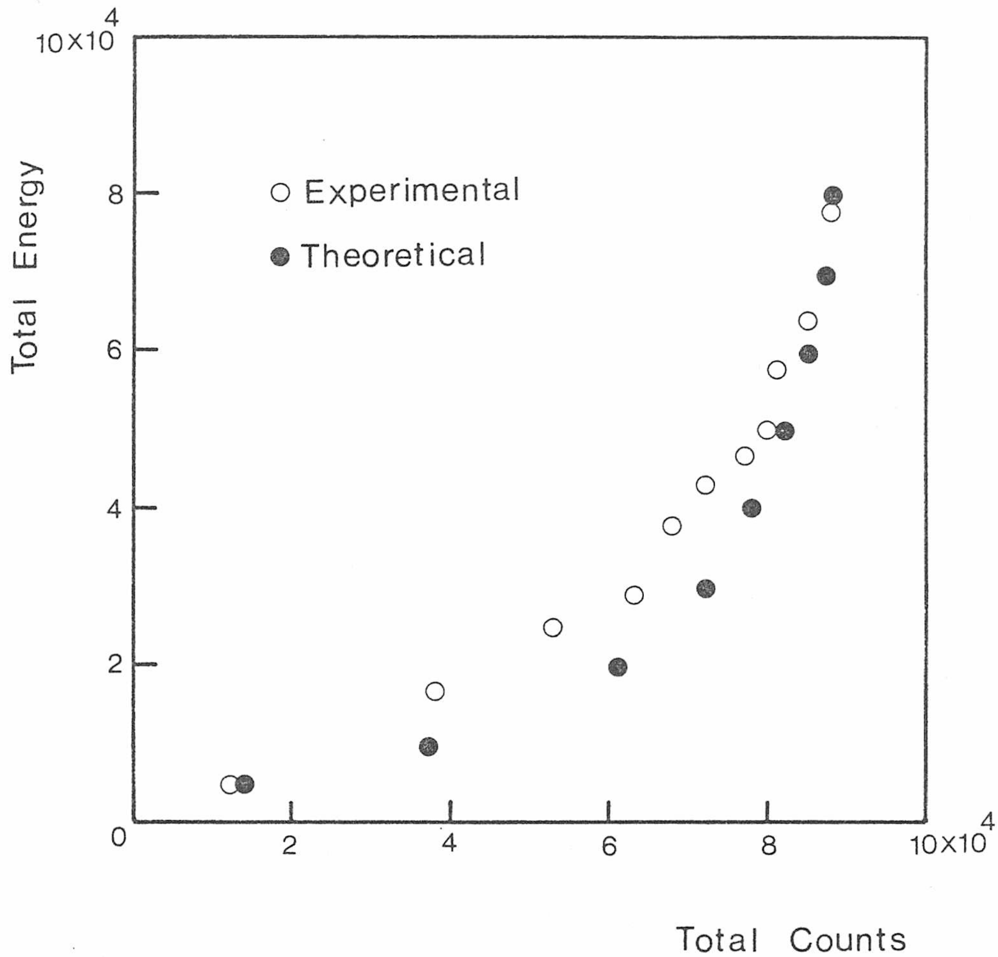

FIGURE 2.4 : An Example of the Exponential Relationship between the Total Counts and the Total Energy in Individual Acoustic Emission Bursts. Experimental Data are from Burst Test of PRD-Epoxy Bottle (Estimated from Fig.4, Ref. 140). The Theoretical Points are the Numerical Plotting of Eq.(2.29), Based on the Experimental Constants : $V_\ell = \sqrt{2}$ Volts and $f_0 = 200$ KHz.

and $$\ddot{x}(t) = 4\pi^2 \sum_{n=0}^{n-1} f_n^{\ 2} \left\{ -X_r(f_n) \cos 2\pi f_n t - X_i(f_n) \sin 2\pi f_n t \right\}$$

(2.32)

It is the characteristic of the Fourier transform that the calculated area under $x^2(t)$ in the time domain is proportional to the area calculated from the corresponding frequency spectrum graph. Therefore, it follows from equations (2.18), (2.25), and (2.30–2.32) that:-

$$\int x^2(t)\, dt \equiv \int X(f)\, df \equiv \sigma_x^{\ 2} \qquad (2.33)$$

; $$\int \dot{x}^2(t)\, dt \equiv 4\pi^2 \int f^2\, X(f)\, df \equiv \sigma_{\dot{x}}^{\ 2} \qquad (2.34)$$

and $$\int \ddot{x}^2(t)\, dt \equiv 16\,\pi^4 \int f^4\, X(f)\, df \equiv \sigma_{\ddot{x}}^{\ 2} \qquad (2.35)$$

Equations (2.33)–(2.35) are useful for comparing acoustic emission parameters in both the time domain and frequency domain.

(a) The integrated area under the frequency spectrum curve represents the total power in the burst which is equivalent to that calculated from the time domain.

(b) The second moment of the burst frequency spectrum ($\int f^2\, X(f)\, df$) is equivalent to the integration under the square value of the first derivative of the time domain representation.

(c) The fourth moment in the frequency domain ($\int f^4 X(f)\, df$) corresponds to integration under the square values of the second derivative of the burst function.

(d) The values of σ_x^2, $\sigma_{\dot{x}}^2$ and $\sigma_{\ddot{x}}^2$ used in the foregoing sections could now be numerically evaluated. This is another advantage in using digital computation analysis in acoustic emission measurements.

(iv) Using the preceding relationships a general correlation between the number of zero-crossings and the burst frequency spectrum can now be stated.

The number of zero-crossing is given in equation (2.8) by:-

$$n_o = \frac{1}{\pi} \frac{\sigma_{\dot{x}}}{\sigma_x}$$

then

$$n_o = 2 \left\{ \frac{\int f^2 X(f)\, df}{\int X(f)\, df} \right\}^{\frac{1}{2}}$$

and $n_o^+ = \dfrac{n_o}{2}$

Therefore, the number of zero-crossing can be used as a simple method to describe the burst in the frequency domain.

(v) In Section (2.3.3) the analysis of the burst peak distribution leads to a Rayleigh distribution given by equation (2.15) for a narrow-band acoustic emission burst which is assumed to have a normal distribution in the time domain representation. To estimate the number of maxima and minima in arbitrary acoustic emission burst given in Fig. 2.1 one can assume that the number of maxima is equal to half the number of the total zero-crossings of the function $\dot{x}(t)$. This function is the derivative of the original burst function $x(t)$. Half the zero-crossings of $\dot{x}(t)$ can be calculated from a formula corresponding to that given by equation (2.8). By analogy:-

$$n_{max} = \frac{1}{2\pi} \frac{\sigma_{\ddot{x}}}{\sigma_{\dot{x}}} \qquad (2.37)$$

Substituting for $\sigma_{\ddot{x}}$ and $\sigma_{\dot{x}}$ from equations (2.34) and (2.35), equation (2.37) becomes:

$$n_{max} = \left\{ \frac{\int f^4 X(f)\, df}{\int f X(f)\, df} \right\}^{\frac{1}{2}} \qquad (2.38)$$

The total number of maxima and minima for fairly symmetrical burst may be considered as:

$$N_{Total} = 2\, n_{max} \qquad (2.39)$$

2.6 CONCLUSIONS

One of the main advantages of using digital analysis in acoustic emission studies is the flexibility provided. A large number of different analysis parameters can be performed on each burst record by a digital computer which otherwise would need a separate analog electronic instrument.

In this chapter a wide variety of digital analysis techniques have been suggested for application to acoustic emission bursts. These techniques have varied in complexity and will provide information about the original burst waveform. Attention has been focussed, almost exclusively, on the theoretical analyses of burst signals. Parameters such as ring-down counting, burst amplitude and the burst energy can be applied in a wide range of situations. Most of the techniques mentioned will be applied to a variety of acoustic emission experiments and the results will be discussed later.

In the past, only a few models have been proposed (26,51,67) which mathematically simulate acoustic emission bursts. These models had different limitations and provided an approximate relationship between some of the acoustic emission parameters and engineering parameters (77,141).

As mentioned before, acoustic emission bursts are non-deterministic functions and cannot be represented by a mathematical model. Therefore the analysis carried out in the preceding sections has been developed for an arbitrary burst described by x(t). The assumed normality and stationarity characteristics do not restrict the analysis described in this chapter. These assumptions of burst signal normality and stationarity are also included in other mathematical models even though the authors have not mentioned it clearly in their work. Onoe (142) represents some graphs of actual acoustic emission waveforms detected while monitoring welded structures and all show the assumed normality and stationarity.

The number of counts and count rate, used as general parameters for representing the acoustic emission burst in the time domain are insufficient if they are employed alone. The use of these parameters will only be successful provided that the threshold level can be kept in a fixed position and the distribution of peaks can be provided.

Studying equations (2.27) and (2.29) reveals that to measure either the burst number of counts or total energy the following parameters should be mentioned:-

(a) The transducer resonance frequency, applied frequency-band and the observed central frequency.

(b) The specimen geometry and dimension.

(c) The burst duration time.

Differentiation between different bursts or sources may be done by analysing their peaks amplitude distributions because in this case, all amplitudes of each burst are counted.

The number of zero-crossings may be introduced as one of the acoustic emission parameters. This is very simple to measure. For digital analysis, a zero-crossing can be said to occur between two sampling instants t and t+1 if:-

$$\text{sign } x(t) \neq \text{sign } x(t+1)$$

Nevertheless, the number of zero-crossings is trivial to implement and can only be used as a gross estimate of the frequency spectrum. Its use may be motivated when using a very narrow frequency-band.

CHAPTER THREE

THE TRANSMISSION THEORY AND ACOUSTIC EMISSION TRANSDUCERS

This chapter deals with the general theory, and the analytical calculations for various multilayer systems. In order to study the influence of the components of acoustic emission transducers on the detected response, particularly the effect of the couplant layer and transducer protective shoe, the sound pressure transmission coefficient of a plane ultrasonic longitudinal elastic wave has been investigated for a number of multilayer systems; namely, three-, four-, five-, and six-layer systems.

In all transmission models, a longitudinal wave is assumed to travel normal to the interfaces from the propagation medium through intermediate layers and the PZT-element to the air or another backing material. In a three-layer model, the intermediate layer can represent either the couplant layer or the transducer protective shoe. The four-layer model represents the case of a narrow-band transducer in which both couplant and transducer shoes are considered. The transmission solution for a five-layer model describes broad-band transducers in practical use. Finally, the six-layer model is investigated in order to verify experimentally the previous cases.

3.1 INTRODUCTION

Acoustic emission transducers generally have the configuration shown in Fig. 3.1. The piezoelectric element is the main part of the device and is usually a longitudinally poled lead zirconate titanate ceramic "PZT-5A". The low face of the PZT-element is always attached to the acoustic emission propagation medium, usually via some protective shoe. The upper one is left free and in contact with air in the case of a narrow-band device, or backed by an absorptive damping backing material in the case of a broad-band device. In the case of a transducer operated at its fundamental resonance the PZT element's two faces are separated by a distance equal to one-half wavelength. The various layers on the bottom face make the whole transducer act as a multilayer transmission system. The most important layers, affecting the transducer response should be the transducer protective layer, i.e. the transducer shoe and the couplant layer.

The acoustic emission transducer is a complicated transmission system with reflections occurring at all faces of its components; i.e. the couplant layer, the protective shoe, the PZT-element and the backing material or air.

The transmission problem for plane longitudinal elastic waves incident normally on a multilayer system consisting of an infinite set of alternate parallel layers of two different media was first treated by Lindsay et al (143) in 1934. The analysis was

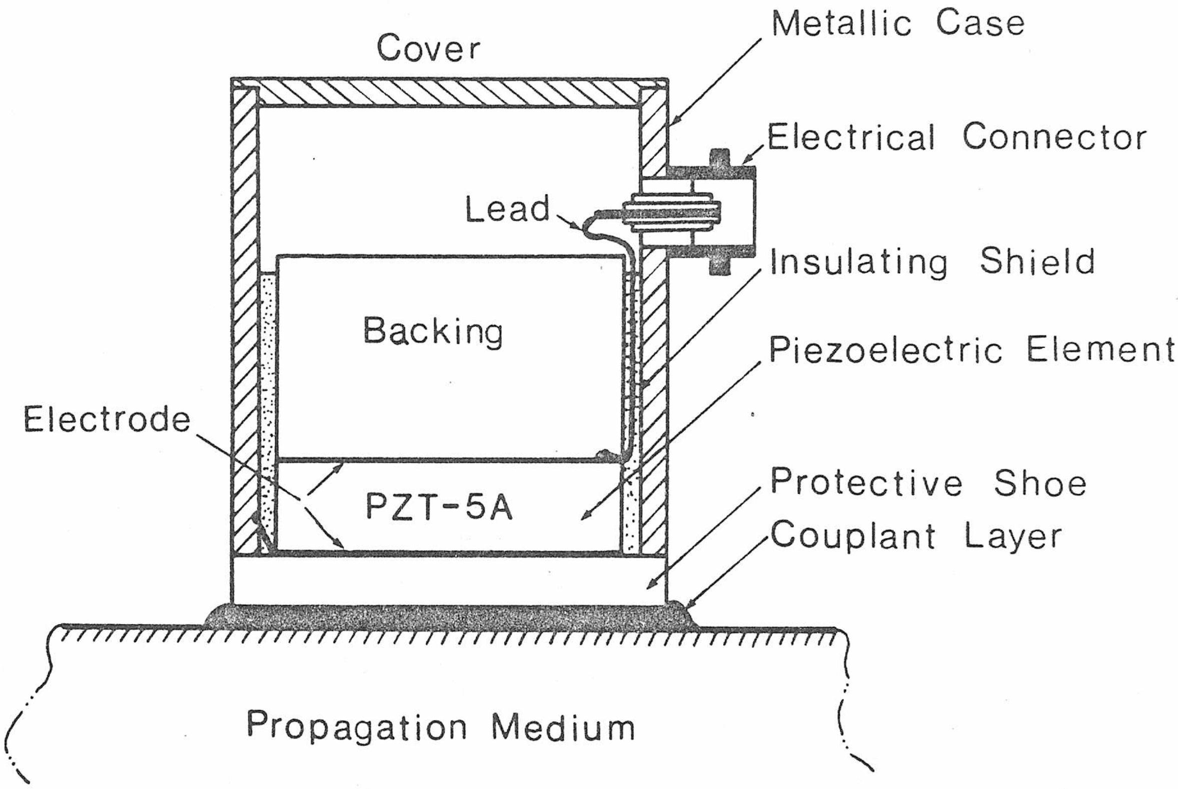

FIGURE 3.1 : General Configuration of Acoustic Emission Transducer Loaded to a Propagation Medium.

extended to the case of oblique transmission for the particular cases of an infinite series of alternating layers of two different fluid media, and, when one of the layers is solid (144). In these early studies, the analytical investigations indicated that multi-layer systems are acting as a low-pass elastic wave filter in which transmission and reflection bands are dependent on the angle of incidence.

The derivation published by Thomson (145)in 1950, considers the problem of the transmission of plane elastic wave at oblique incidence through a system consisting of any number of parallel plates of different materials and thicknesses. In this system, the equations for one layer were related to those of the adjoining layers by the continuity of particle velocity normal and shearing stresses at the interfaces. Unfortunately, the equations obtained by Thomson made the severely restrictive assumption that the shear modulus is constant throughout all layers and use of continuity of shear strain at the interfaces rather than the appropriate shear stress. This was apparently first corrected by Haskell (146)in 1953, so that the formulated equations were applicable to more general cases.

For more than twenty years the problem was left without experimental verification or any theoretical improvement. In 1975, the case of a single solid layer surrounded by liquid media was studied experimentally by Barnard et al (147). They used the equations published by Brekhovskikh, (148)which are identical to

Thomson's, to compare theory with the observed results. Because Thomson's equations are valid for a single layer plate in a liquid medium the calculated results are valid since only this case was considered. In the same year, Cook and Lovejoy (149)published some experimental results for transmission through two laminated plates in an aqueous medium with no theoretical verification. The measurements were made to determine the relative transmission loss, reflectivity at normal incidence versus frequency, and transmission loss (discrete frequency) versus angle of incidence.

More recently, Folds and Loggins (150) made another correction to the previously suggested solutions, but again they have only considered transmission systems which are surrounded by a liquid. They treated the transmission problem more generally, and presented considerable experimental data in order to verify the theoretical work. The variation in sound pressure transmission coefficient is investigated in the frequency range 100-700 KHz for one, two, and three solid layers immersed in water. The transmission coefficient versus incidence angle at constant frequency was also presented. However, the experimental results suffer from many 'overshoots' and the curves are shifted with respect to corresponding theoretical graphs with no satisfactory reason given for this discrepancy.

All the published experimental work considers the transmission as a problem in underwater acoustics. Hydrophones are always employed as receivers and the transmission systems were surrounded by a liquid or in most cases water. The maximum number of layers which are included in these theoretical studies is limited to three solid plates and two identical liquid media surrounding the transmission system (i.e. they apply only to special cases of transmission systems).

The purpose of the present study is to investigate the effect of the transducer geometry on the received acoustic emission signal. The transducer components have a limited diameter (say 20 mm as maximum). Consequently, normally incident longitudinal waves travelling parallel to the device centre have been used in order to decrease experimental errors. Theoretically, infinite lateral extension has been assumed. When the PZT-5A element has to be considered as one of the transmission layers, symmetrical excitation has been suggested to reduce the influence of the piezo-electric element inhomogeneity on the output signal.

A simple multilayer transmission theory has been investigated which required fewer material constants in the theoretical calculations. Most of these properties could be measured accurately.

3.2 THE PROBLEM OF THE MULTILAYER SYSTEM

The usual method for obtaining a solution for multilayer transmission systems is to represent the system by a set of simultaneous equations involving all the variables in the network (151).

Such a method is quite common, but it is complicated for more than a three-layer system. There are as many equations as variables in the system, in spite of the fact that only the relationship between the input and the output variables is required to calculate the transmission or the reflection coefficient.

In the following sections, the solution of the pressure and velocity simultaneous equations is first considered for the transmission via three-layer system as given by Kinsler and Frey. Then a considerably simpler procedure is introduced which solve the problem without any need to solve the simultaneous equations. This method is used thereafter to deal with the more complicated systems.

3.3 GENERAL ASSUMPTIONS

In all transmission systems, a plane elastic longitudinal undamped wave is assumed to strike the multilayer system as shown in Fig. 3.2. To simplify the problem, only the normal incident case will be considered. The following assumptions are made:

(a) the X-axis is oriented in a direction normal to the plane-boundaries and the layers are numbered from left to right in the direction of propagation of the incident wave,

(b) the elastic wave originates in the first layer and proceeds through the second and subsequent layers to emerge into the last layer, n,

(c) the first boundary is located between medium one and two at which $x_1 = 0$ and $x_2 = 0$ (see Fig. 3.2),

(d) the layers are assumed to be of infinite extent in the Y and Z direction,

(e) a reflected wave will be produced in the first medium when the incident wave is striking the first boundary, and a transmitted wave in medium two and so on in the subsequent media 3, 4, ... to n,

(f) the reflected wave in medium n will be ignored ($P_{rn} = 0$) as there is no further reflected boundary in this layer,

(g) even though the bounded media would produce multiple reflections and transmissions at the boundaries surrounding it, (152,153)it is sufficient to suppose that there is only one wave in each direction. Provided that the boundary conditions are satisfied, these will include all of the individual components,

(h) The boundary conditions require continuity of normal wave pressures and particle velocities at the interfaces between layers,

(i) The absorption of sound in the layers can be neglected,

(j) The fact that, during the transmission process, the PZT-element does actually extract some energy from the acoustic wave and convert it to an electrical one is neglected. This approximation is correct only if the transducer is open circuit (154). It has been pointed out by de Klerk (155) that the great mismatch in electrical impedance between the transducer and the amplifier would indicate that very little signal is lost in such manner. Nevertheless, the amount of energy extracted from the acoustic wave may be determined by the transducer electromechanical conversion efficiency.

3.4 FUNDAMENTAL EQUATIONS

Consider a multilayer system consisting of n parallel plane-homogeneous elastic layers with different thicknesses ℓ_h where h = 2, 3, ... n-1 and characteristic impedances Z_ℓ where ℓ = 1, 2, ... n (Fig. 3.2). The general representation of the pressures and particle velocities for each medium can be written as the following:

For medium 1:

$$p_{i1} = A_1 e^{j(\omega t - k_1 x_1)} \tag{3.1}$$

$$v_{i1} = \frac{p_{i1}}{Z_1} \tag{3.2}$$

$$p_{r1} = B_1 e^{j(\omega t + k_1 x_1)} \tag{3.3}$$

$$v_{r1} = -\frac{p_{r1}}{Z_1} \tag{3.4}$$

For medium 2:

$$p_{t2} = A_2 e^{j(\omega t - k_2 x_2)} \tag{3.5}$$

$$v_{t2} = \frac{p_{t2}}{Z_2} \tag{3.6}$$

$$p_{r2} = B_2 e^{j(\omega t + k_2 x_2)} \tag{3.7}$$

$$v_{r2} = - \frac{p_{r2}}{Z_2} \qquad (3.8)$$

For medium q: where 1<q<n

$$p_{tq} = A_q \, e^{j(\omega t - k_q x_q)} \qquad (3.9)$$

$$v_{tq} = \frac{p_{tq}}{Z_q} \qquad (3.10)$$

$$p_{rq} = B_q \, e^{j(\omega t + k_q x_q)} \qquad (3.11)$$

$$v_{rq} = - \frac{p_{rq}}{Z_q} \qquad (3.12)$$

And for the last medium n which is assumed to be semi-infinite:

$$p_{tn} = A_n \, e^{j(\omega t - k_n x_n)} \qquad (3.13)$$

$$v_{tn} = \frac{p_{tn}}{Z_n} \qquad (3.14)$$

Therefore for a system of n layers there are 2(2n-1) boundary conditions to be satisfied. These lead to the same number of homogeneous simultaneous equations. In general, the n-layer system can be represented by a group of equations which may be summarised as:

$$p_{t\ell} = A_\ell \, e^{j(\omega t - k_\ell x_\ell)} \qquad (3.15)$$

$$v_{t\ell} = \frac{p_{t\ell}}{Z_\ell} \qquad (3.16)$$

$$p_{rm} = B_m e^{j(\omega t + k_m x_m)} \quad (3.17)$$

and $$v_{rm} = - \frac{p_{rm}}{Z_m} \quad (3.18)$$

where in equations (3.15) and (3.16): $\ell = 1, 2, 3, \ldots; n$

and in equations (3.17) and (3.18): $m = 1, 2, 3, \ldots; (n-1)$

and where:

p_{il} and v_{il}: the pressure and particle velocity amplitudes of the incident wave in the first medium

p_{rm} and v_{rm}: the pressure and particle velocity amplitudes of the reflected wave in medium m

A's and B's: complex constants representing the maximum pressure amplitudes of the transmitted and reflected waves

j: imaginary unit ($\sqrt{-1}$)

ω: the wave angular velocity $= 2\pi f = \frac{2\pi C_L}{\lambda}$, radian s^{-1}

k: the wave constant $= \frac{\omega}{C_L} = \frac{2\pi f}{C_L} = \frac{2\pi}{\lambda}$, m^{-1}

x: distance, m

t: time, s

C_L: longitudinal wave velocity, m s^{-1}

f: the wave frequency, Hz

λ: wavelength, m

Z: the medium characteristic impedance $= \rho C_L$, Kg m^{-2} s^{-1} (MKS rayl)

ρ: the volume density, Kg m^{-3}.

The complex constant allows for phase differences between the system broundaries. In equations (3.1)-(3.18) the plus signs correspond to the forward wave in X-direction, and the minus signs correspond to the reverse direction.

In each medium the total pressure and velocity equations can be calculated from the following equations:

for the first and subsequent media up to medium (n - 1):

$$P_m = p_{tm} + p_{rm}$$

$$= A_m e^{j(\omega t - k_m x_m)} + B_m e^{j(\omega t + k_m x_m)} \tag{3.19}$$

$$V_m = v_{tm} + v_{rm}$$

$$= \frac{p_{tm}}{Z_m} - \frac{p_{rm}}{Z_m}$$

$$= \frac{1}{Z_m} A_m e^{j(\omega t - k_m x_m)} - B_m e^{j(\omega t + k_m x_m)} \tag{3.20}$$

and for the last medium n:

$$P_n = p_{tn} = A_n e^{j(\omega t - k_n x_n)} \tag{3.21}$$

$$V_n = v_{tn} = \frac{p_{tn}}{Z_n} = \frac{1}{Z_n}\left[A_n e^{j(\omega t - k_n x_n)}\right] \tag{3.22}$$

At the boundary between two media m and m + 1, $x_m = \ell_m$ and $x_{m+1} = 0$, (Fig. 3.1), the particle velocity and the sound pressure must change continuously from one medium to the next therefore:

$$P_m = P_{m+1} \tag{3.23}$$

and

$$V_m = V_{m+1} \tag{3.24}$$

If the condition of continuity at the boundaries is applied on all the interfaces between the system layers using equations (3.23) and (3.24), a set of simultaneous equations can be developed to set the appropriate quantities equal. By eliminating all the complex constants (i.e. A's and B's) from these equations except A_1 and A_n, the magnitude of the amplitude ratio A_n/A_1 can be obtained, which represents the sound pressure transmission coefficient (α_{pn}):

$$\alpha_{pn} = \left|\frac{A_n}{A_1}\right| \tag{3.25}$$

The sound power transmission coefficient can be calculated from the equation:

$$\alpha_{tn} = \left|\frac{A_n}{A_1}\right|^2 \frac{Z_1}{Z_n} \tag{3.26}$$

and the phase angle of the complex ratio A_1/A_n is a measure of the amount by which the phase of the incident wave at $x_1 = 0$ or $x_2 = 0$, i.e. on the first boundary, leads that of the transmitted wave at the last boundary $(n-1)\rightarrow(n)$ and the medium n.

3.5 CASE ONE: THREE-LAYER SYSTEM

Consider three different layers separated by two plane boundaries. These boundaries are normal to the X-axis and each one passes through an origin from which the position in the right side layer is to be measured. If a plane longitudinal wave is incident on the first boundary from the first medium, normal to the boundary, then part of the energy passes on into the second medium in the form of a plane wave and part is reflected at the boundary and goes back into the first medium. The same process will be repeated on the second boundary between the second and the third medium.

The solution for the three-layer system (151)is included to enable a comparison to be made with more complex systems presented in Sections (3.8, 3.9 and 3.10).

In Fig. 3.2, if the system consists of three layers i.e. n = 3, one can write ten equations governing all the variables in this system. The first eight equations would be similar to equations (3.1) - (3.8) in Section 3.4, and the last two can be written as:

$$p_{t3} = A_3 \, e^{\,j(\omega t - k_3 x_3)} \tag{3.27}$$

and

$$v_{t3} = \frac{p_{t3}}{Z_3} \tag{3.28}$$

Satisfying the continuity conditions of the pressures and particle velocities at each boundary gives:

At boundary (1)→(2): $x_1 = 0$ and $x_2 = 0$

a. continuity of pressure:

$$\{p_{i1} + p_{r1}\}_{x_1=o} = \{p_{t2} + p_{r2}\}_{x_2=o}$$

and from equations (3.1), (3.3), (3.5) and (3.7):

$$A_1 + B_1 = A_2 + B_2 \tag{3.29}$$

b. continuity of particle velocity:

$$\{v_{i1} + v_{r1}\}_{x_1=o} = \{v_{t2} + v_{rs}\}_{x_2=o}$$

and from equations (3.1) - (3.8):

$$\frac{A_1 - B_1}{Z_1} = \frac{A_2 - B_2}{Z_2} \tag{3.30}$$

At boundary (2)→(3): $x_2 = \ell_2$ and $x_3 = 0$

a. continuity of pressure:

$$\{p_{t2} + p_{r2}\}_{x_2=\ell_2} = \{p_{t3}\}_{x_3=o}$$

and from equations (3.5), (3.7) and (3.27):

$$A_2 e^{-jk_2\ell_2} + B_2 e^{jk_2\ell_2} = A_3 \tag{3.31}$$

b. continuity of particle velocity:

$$\left\{ v_{t2} + v_{r2} \right\}_{x_2 = \ell_2} = \left\{ v_{t3} \right\}_{x_3 = o}$$

and from equations (3.6), (3.8) and (3.28):

$$\frac{A_2 e^{-jk_2\ell_2} - B_2 e^{jk_2\ell_2}}{Z_2} = \frac{A_3}{Z_3} \tag{3.32}$$

By eliminating B_1, B_2 and A_2 from equations (3.29), (3.30)-(3.32), the amplitude ratio A_3/A_1 can be evaluated as follows:

from equations (3.29) and (3.30):

$$A_1 = \frac{A_2 + B_2}{2} + \frac{Z_1}{Z_2} \frac{A_2 - B_2}{2} \tag{3.33}$$

then, A_2 and B_2 can be represented as function of A_3 by combining equations (3.31) and (3.32):

$$A_2 = \frac{1}{2} A_3 \left(1 + \frac{Z_2}{Z_3}\right) e^{jk_2\ell_2}$$

$$B_2 = \frac{1}{2} A_3 \left(1 - \frac{Z_2}{Z_3}\right) e^{-jk_2\ell_2}$$

substituting in equation (3.33):

$$A_1 = \frac{1}{4 Z_2 Z_3} \left[(Z_1 + Z_2)(Z_2 + Z_3) e^{jk_2\ell_2} + (Z_2 - Z_1)(Z_3 - Z_2) e^{-jk_2\ell_2} \right] A_3 \qquad (3.34)$$

In trigonometric form equation (3.34) may be written as:

$$A_1 = \frac{A_3}{2} \left[(1 + \frac{Z_1}{Z_3}) \cos k_2\ell_2 + j (\frac{Z_1}{Z_2} + \frac{Z_2}{Z_3}) \sin k_2\ell_2 \right] \qquad (3.35)$$

The magnitude of the complex ratio A_3/A_1 represents the sound pressure transmission coefficient between three layers; α_{p3}:

i.e. $\alpha_{p3} = |\frac{A_3}{A_1}|$

$$= \frac{2 Z_3}{\left((Z_1 + Z_3)^2 \cos^2 k_2\ell_2 + (Z_2 + \frac{Z_1 Z_3}{Z_2})^2 \sin^2 k_2\ell_2\right)^{\frac{1}{2}}} \qquad (3.36)$$

and the sound power transmission coefficient α_{t3} can be expressed by:

$$\alpha_{t3} = |\frac{A_3}{A_1}|^2 \frac{Z_1}{Z_3}$$

$$= \frac{4 Z_1 Z_3}{(Z_1 + Z_3)^2 \cos^2 k_2\ell_2 + (Z_2 + \frac{Z_1 Z_3}{Z_2})^2 \sin^2 k_2\ell_2} \qquad (3.37)$$

Canella (156)used equation (3.36) to study the effects of different couplant layers in ultrasonic contact testing. The advantage of using ultrasonic transducers with a relatively high resonant frequency (>2 MHz) suppressed and thus prevented the low frequency radial modes of the transducers influencing the results. Experiments were carried out near the transducer thickness modes, so that results were not affected by the interference of reflected waves from the transducers crystal 'element' rear face (157). Furthermore, the transducers were highly damped and the reflected wave amplitude, for transducers operated at frequency very close to that of the thickness mode, was too small to effect the results. Three-layer Theory does not take into account the sympathetic resin which is used as a transducer shoe. Canella's work is the only experimental study which has been published describing the effect of the couplant layers on the received ultrasonic pulse amplitude.

In a previous paper Hill and El-Dardiry (55) considered the effects of the transducer intermediate layers on acoustic emission parameters. Equation (3.37) was used to calculate the variation of the sound power transmission coefficient with frequency for a variety of coupling thicknesses. Although only a simple transmission model (propagation medium- couplant- PZT element) has been considered and the effect of the transducer protective shoe was ignored, the theoretical calculations showed a marked variations of the transmission coefficient over 1 MHz frequency -band. The condition of acoustic emission transducers is different from that of ultrasonic non-destructive testing transducers. The acoustic emission transducers may detect bursts with various frequency components. Therefore, the detection frequency band is required to be as wide as possible depending on the transducer sensitivity and the electronic equipment. Then, the acoustic emission transducers are not always operated at their thickness mode and the interference of the reflected wave on the PZT-element rear face must be considered.

From the application point of view, the three-layer solution may be used in an approximate calculations when designing acoustic emission transducers. Either equation (3.36) or (3.37) could be used in preliminary investigations to increase the narrow-band transducer efficiency by ensuring a good acoustic matching between the material to be monitored and the PZT-element. In the case, of a narrow-band transducer, the shoe material and thickness could be selected to suit the transducer central operating frequency (Chapter Five).

3.6 MATRICES APPROACH TO MULTILAYER TRANSMISSION SYSTEMS

In Section 3.5, the solution of 10 equations was required to calculate the transmission coefficient of a three-layer system. Here, a characteristic matrix is defined for each bounded layer and the entire multilayer system is considered as the product of the total matrices. In this way, the transmission coefficient for the whole system is calculated by straight-forward multiplication, without any need to solve the system simultaneous equations and without reference to the intermediate internal variables A_2, A_3... A_{n-1}, B_1, B_2 .... and B_n (see Section 3.4). This analytical technique is well known in electrical circuit theory and electrical power transmission systems.

Consider the first three layers in Fig. 3.2, the total pressure and particle velocity at any point in medium 2 can be determined by putting m = 2 in equations (3.19) and (3.20):

$$P_2 = A_2 \, e^{j(\omega t - k_2 x_2)} + B_2 \, e^{j(\omega t + k_2 x_2)} \tag{3.38}$$

$$V_2 = \frac{A_2}{Z_2} \, e^{j(\omega t - k_2 x_2)} - \frac{B_2}{Z_2} \, e^{j(\omega t + k_2 x_2)} \tag{3.39}$$

These equations can be represented in matrix form as:

$$\begin{vmatrix} P_2 \\ V_2 \end{vmatrix} = \begin{vmatrix} e^{-jk_2x_2} & e^{jk_2x_2} \\ \frac{1}{Z_2} e^{jk_2x_2} & -\frac{1}{Z_2} e^{jk_2x_2} \end{vmatrix} \begin{vmatrix} A_2 \\ B_2 \end{vmatrix} e^{j\omega t} \tag{3.40}$$

Equation (3.40) is a set of two linear algebraic equations which can be used in solving the transmission problem.

At the boundary (1)→(2), $x_2 = 0$:

$$\begin{vmatrix} P \\ V \end{vmatrix}_{(1)\to(2)} = \begin{vmatrix} 1 & 1 \\ \frac{1}{Z_2} & -\frac{1}{Z_2} \end{vmatrix} \begin{vmatrix} A_2 \\ B_2 \end{vmatrix} e^{j\omega t} \tag{3.41}$$

and at the boundary (2)→(3), $x_2 = \ell_2$:

$$\begin{vmatrix} P \\ \\ V \end{vmatrix}_{(2)\to(3)} = \begin{vmatrix} e^{-jk_2\ell_2} & e^{jk_2\ell_2} \\ \\ \frac{e^{-jk_2\ell_2}}{Z_2} & -\frac{e^{jk_2\ell_2}}{Z_2} \end{vmatrix} \begin{vmatrix} A_2 \\ \\ B_2 \end{vmatrix} e^{j\omega t} \tag{3.42}$$

From the continuity conditions of pressure and particle velocity at the boundaries (1)→(2) and (2)→(3):

$$\begin{vmatrix} P \\ \\ V \end{vmatrix}_{(1)\to(2)} = \begin{vmatrix} P_1 \\ \\ V_1 \end{vmatrix} \quad \text{and} \quad \begin{vmatrix} P \\ \\ V \end{vmatrix}_{(2)\to(3)} = \begin{vmatrix} P_3 \\ \\ V_3 \end{vmatrix} \tag{3.43}$$

By eliminating A_2 and B_2 equations (3.41) – (3.43) yield:

$$\begin{vmatrix} P_1 \\ \\ V_1 \end{vmatrix} = \begin{vmatrix} 1 & 1 \\ \\ \frac{1}{Z_2} & -\frac{1}{Z_2} \end{vmatrix} \begin{vmatrix} e^{jk_2\ell_2} & e^{jk_2\ell_2} \\ \\ \frac{e^{-jk_2\ell_2}}{Z_2} & -\frac{e^{jk_2\ell_2}}{Z_2} \end{vmatrix} \begin{vmatrix} P_3 \\ \\ V_3 \end{vmatrix} \tag{3.44}$$

Assuming:

$$Q = \begin{vmatrix} e^{-jk_2\ell_2} & e^{jk_2\ell_2} \\ \\ \frac{e^{-jk_2\ell_2}}{Z_2} & -\frac{e^{jk_2\ell_2}}{Z_2} \end{vmatrix} \tag{3.45}$$

The inverse matrix Q^{-1} is defined by:

$$Q^{-1} = \frac{\text{adj }\{Q\}}{|Q|}$$

where $|Q|$ is the determinant of matrix Q:

$$|Q| = -\frac{2}{Z_2} \tag{3.46}$$

and adj {Q} is the adjoint matrix of matrix Q and can be obtained by setting out a matrix of cofactors of matrix Q as:

$$\text{cof.}\{Q\} = \begin{vmatrix} -\dfrac{e^{jk_2\ell_2}}{Z_2} & -\dfrac{e^{-jk_2\ell_2}}{Z_2} \\ \\ -e^{jk_2\ell_2} & e^{-jk_2\ell_2} \end{vmatrix}$$

Now, if this cofactor matrix is transposed, matrix obtained is the adjoint matrix; so:

$$\text{adj }\{Q\} = \begin{vmatrix} -\dfrac{e^{jk_2\ell_2}}{Z_2} & -e^{jk_2\ell_2} \\ \\ -\dfrac{e^{-jk_2\ell_2}}{Z_2} & e^{-jk_2\ell_2} \end{vmatrix} \tag{3.47}$$

and substitution of Q^{-1} in equation (3.44) yields:

$$\begin{vmatrix} P_1 \\ \\ V_1 \end{vmatrix} = \begin{vmatrix} 1 & 1 \\ \\ \dfrac{1}{Z_2} & -\dfrac{1}{Z_2} \end{vmatrix} \begin{vmatrix} \dfrac{e^{jk_2\ell_2}}{2} & \dfrac{Z_2\, e^{jk_2\ell_2}}{2} \\ \dfrac{e^{-jk_2\ell_2}}{2} & -\dfrac{Z_2\, e^{-jk_2\ell_2}}{2} \end{vmatrix} \begin{vmatrix} P_3 \\ \\ V_3 \end{vmatrix}$$

$$= \begin{vmatrix} \dfrac{e^{jk_2\ell_2} + e^{-jk_2\ell_2}}{2} & \dfrac{Z_2\,(e^{jk_2\ell_2} - e^{-jk_2\ell_2})}{2} \\ \dfrac{1}{Z_2}\left(\dfrac{e^{jk_2\ell_2} - e^{-jk_2\ell_2}}{2}\right) & \dfrac{e^{jk_2\ell_2} + e^{-jk_2\ell_2}}{2} \end{vmatrix} \begin{vmatrix} P_3 \\ V_3 \end{vmatrix}$$

Expressing the exponential functions of $jk_2\ell_2$ in trigonometric form:

$$\begin{vmatrix} P_1 \\ V_1 \end{vmatrix} = \begin{vmatrix} \cos k_2\ell_2 & j\ Z_2\ \sin k_2\ell_2 \\ \dfrac{j\ \sin k_2\ell_2}{Z_2} & \cos k_2\ell_2 \end{vmatrix} \begin{vmatrix} P_3 \\ V_3 \end{vmatrix} \tag{3.48}$$

and in matrix notation:

$$T_1 = C_2\ T_3 \tag{3.49}$$

where:

$$T_1 = \begin{vmatrix} P_1 \\ V_1 \end{vmatrix} \quad ; \quad T_3 = \begin{vmatrix} P_3 \\ V_3 \end{vmatrix}$$

$$C_2 = \begin{vmatrix} \cos k_2\ell_2 & j\ Z_2 \sin k_2\ell_2 \\ \dfrac{j\ \sin k_2\ell_2}{Z_2} & \cos k_2\ell_2 \end{vmatrix}$$

i.e. T is a vector whose components (P, V) are the total pressure and the total velocity inside a terminal medium, and C is the characteristic matrix given above.

The matrix C_2 contains variable elements k_2, ℓ_2 and Z_2 which only represent the physical and geometrical properties of this particular layer. Therefore, equation (3.49) represents a transmission system in which two unbounded layers T_1 and T_3 are terminated by a complete bounded layer which is characterized by matrix C_2.

The general representation for a system of a number of layers n having n-2 of bounded layers can be written as:

$$\left.\begin{array}{lll}
T_1 \ (\text{terminal}) & = C_2 \, T_{(2)\to(3)} & \text{'a'} \\
T_{(2)\to(3)} & = C_3 \, T_{(3)\to(4)} & \text{'b'} \\
T_{(3)\to(4)} & = C_4 \, T_{(4)\to(5)} & \text{'c'} \\
\cdots\cdots & = \cdot\cdot \ \cdots\cdots\cdots & \\
T_{(i-1)\to(i)} & = C_i \, T_{(i)\to(j)} & \text{'i'} \\
\cdots\cdots & = \cdot\cdot \ \cdots\cdots\cdots & \\
T_{(n-1)\to(n)} & = C_{n-1} \, T_n \ (\text{terminal}) & \text{'n'}
\end{array}\right\} \quad (3.50)$$

where vector $T_{(i)\to(j)}$ represents the total pressure and particle velocity at the boundary (i)→(j) which separates medium i and j, Fig. 3.3.

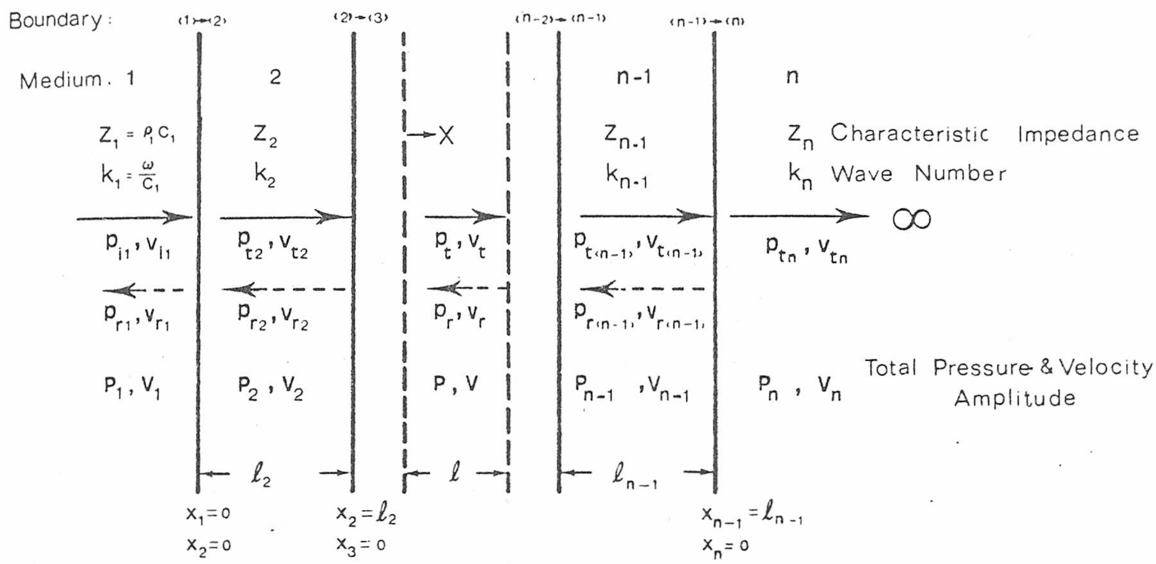

FIGURE 3.2 : The Transmission of the Normally Incidence Longitudinal Plane Wave Through a Multilayer System.

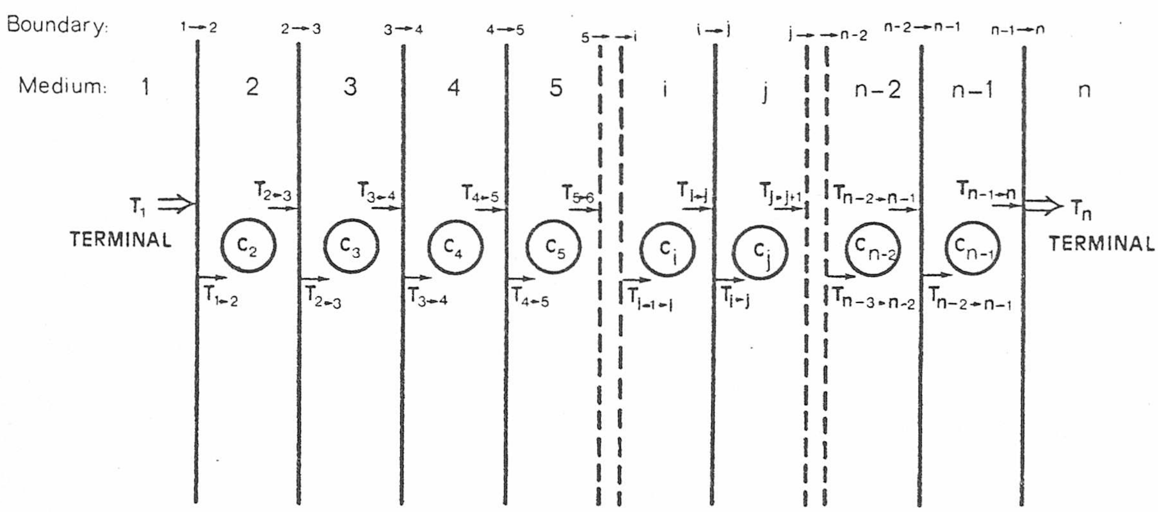

FIGURE 3.3 : Matrix Representation of Transmission System of n Layers " Equation (3.50) ".

By a series of substitutions in equation (3.50), the intermediate $T_{(i)\rightarrow(j)}$'s can be eliminated yielding:

$$T_1 = C_2 \; C_3 \; C_4 \; C_5 \; \ldots\ldots C_{n-1} \; T_n \tag{3.51}$$

or, in condensed form:

$$T_1 = \left\{ \prod_{i=2}^{n-1} C_i \right\} \cdot T_n \tag{3.52}$$

Equation (3.52) is in matrix format and the order of matrices C's must be as that in equation (3.51). The evaluation of the sound power or pressure transmission can then be done simply by using equation (3.52) and is only a matter of 2x2 matrix multiplication followed by some simple algebra. It can be seen that there are the same number of 2x2 matrices as there are complete bounded layers in the transmission system. Each layer in the system can be identified with a single corresponding matrix. The matrix C_i, for example, depends only on the properties of the i^{th} bounded layer. The entire problem can be solved once the number of layers and their properties are specified. It is also important to note that the addition of a layer having a unit matrix will not affect the properties of the system. This condition is applicable to resonant transducers which designed for operation at their thickness mode and will reduce the multilayer transmission system by one layer.

3.7 ALTERNATIVE DERIVATION FOR THREE-LAYER SYSTEM (CASE ONE)

This case has been considered in Section 3.5 by solving a set of ten simultaneous equations which represent the system. The case is reconsidered in this section in order to lay down the basics of the matrix method which will be applied to complicated systems. It should be noted that the final medium is assumed to be semi-infinite in extent so that the reflected wave at that end can be ignored.

The pressure and velocity equations for medium 1 at $x_1 = 0$ (boundary (1)→(2)) are obtained from equations (3.19) and (3.20) as:

$$P_1 = (A_1 + B_1)\, e^{j\omega t} \qquad (3.53)$$

$$V_1 = \frac{1}{Z_1}(A_1 - B_1)\, e^{j\omega t} \qquad (3.54)$$

Equations (3.21) and (3.22) for medium 3, at boundary (2)→(3), i.e. $n = 3$ and $x_3 = 0$, give :

$$P_3 = A_3\, e^{j\omega t} \qquad (3.55)$$

$$V_3 = \frac{A_3}{Z_3}\, e^{j\omega t} \qquad (3.56)$$

Substitute in equation (3.52) for n = 3 and in matrix form:

$$\begin{vmatrix} A_1 + B_1 \\ \\ \dfrac{A_1 - B_1}{Z_1} \end{vmatrix} e^{j\omega t} = \begin{vmatrix} \cos k_2\ell_2 & j\, Z_2 \sin k_2\ell_2 \\ \\ \dfrac{j \sin k_2\ell_2}{Z_2} & \cos k_2\ell_2 \end{vmatrix} \begin{vmatrix} A_3 \\ \\ \dfrac{A_3}{Z_3} \end{vmatrix} . \; e^{j\omega t}$$

which can be considered again as two equations:

$$A_1 + B_1 = A_3(\cos k_2\ell_2 + j \frac{Z_2}{Z_3} \sin k_2\ell_2) \tag{3.57}$$

$$A_1 - B_1 = A_3\, Z_1 \left(\frac{j \sin k_2\ell_2}{Z_2} + \frac{1}{Z_3} \cos k_2\ell_2\right) \tag{3.58}$$

by adding equations (3.57) and (3.58):

$$2\, A_1 = A_3 \left[(1 + \frac{Z_1}{Z_3} \cos k_2\ell_2 + j\, (\frac{Z_1}{Z_2} + \frac{Z_2}{Z_3}) \sin k_2\ell_2\right] \tag{3.59}$$

Equation (3.59) is similar to equation (3.35) in Section 3.5.

3.8 CASE TWO: FOUR-LAYER SYSTEM

This case is considered to assist in designing the acoustic emission narrow-band transducers. In the four-layer model, the PZT-element will be assumed to be a semi-infinite medium, see Fig. 3.4, so that the reflected wave from the rear surface of this layer could be ignored. This assumption will be discussed in Chapter 5.

For four-layer transmission system equation (3.52) yields:

$$T_1 = C_2\ C_3\ T_4 \tag{3.60}$$

where T_1 is a column matrix containing the total sound pressure and particle velocity in the propagation medium (unbounded layer 1),

C_2 is a 2 x 2 square matrix which contains the physical and acoustical properties (Z_2, ℓ_2, k_2) of the couplant layer (bounded layer 2),

C_3 is a 2 x 2 square matrix which contains the physical and acoustical properties (Z_3, ℓ_3, k_3) of the transducer shoe (bounded layer 3), and

T_4 is a column matrix which contains the total sound pressure and particle velocity in the PZT-element (unbounded layer 4).

Written in matrix form equation (3.60) becomes:

$$\begin{vmatrix} A_1 + B_1 \\ \\ \dfrac{A_1 - B_1}{Z_1} \end{vmatrix} = \begin{vmatrix} \cos k_2\ell_2 & j\ Z_2 \sin k_2\ell_2 \\ \\ \dfrac{j \sin k_2\ell_2}{Z_2} & \cos k_2\ell_2 \end{vmatrix} \begin{vmatrix} \cos k_3\ell_3 & j\ Z_3 \sin k_3\ell_3 \\ \\ \dfrac{j \sin k_3\ell_3}{Z_3} & \cos k_3\ell_3 \end{vmatrix}$$

$$\begin{vmatrix} A_4 \\ \\ \dfrac{A_4}{Z_4} \end{vmatrix} \tag{3.61}$$

Putting:

$$a_1 = d_1 = \cos k_2 \ell_2$$

$$b_1 = j\, Z_2 \sin k_2 \ell_2$$

$$c_1 = \frac{j \sin k_2 \ell_2}{Z_2}$$

and;

$$a_2 = d_2 = \cos k_3 \ell_3$$

$$b_2 = j\, Z_3 \cos k_3 \ell_3$$

$$c_2 = \frac{j \sin k_3 \ell_3}{Z_3}$$

into equation (3.61) gives:

$$\begin{vmatrix} A_1 + B_1 \\ \dfrac{A_1 - B_1}{Z_1} \end{vmatrix} = \begin{vmatrix} a_1 & b_1 \\ c_1 & d_1 \end{vmatrix} \begin{vmatrix} a_2 & b_2 \\ c_2 & d_2 \end{vmatrix} \begin{vmatrix} A_4 \\ \dfrac{A_4}{Z_4} \end{vmatrix}$$

$$\begin{vmatrix} A_1 + B_1 \\ \dfrac{A_1 - B_1}{Z_1} \end{vmatrix} = \begin{vmatrix} a_1 a_2 + b_1 c_2 \\ c_1 a_2 + d_1 c_2 \end{vmatrix} \begin{vmatrix} a_1 b_2 + b_1 d_2 \\ c_1 b_2 + d_1 d_2 \end{vmatrix} \begin{vmatrix} A_4 \\ \dfrac{A_4}{Z_4} \end{vmatrix} \qquad (3.62)$$

Again the matrices equation (3.62) represents two equations and the complex constant B_1 can be eliminated:

$$2\,A_1 = A_4\,(a_3 + \frac{1}{Z_4}\,b_3 + Z_1\,c_3 + \frac{Z_1}{Z_4}\,d_3) \qquad (3.63)$$

in which:

$$a_3 = a_1 a_2 + b_1 c_2$$

$$= \cos k_2\ell_2 \cos k_3\ell_3 - \frac{Z_2}{Z_3} \sin k_2\ell_2 \sin k_3\ell_3$$

$$b_3 = a_1 b_2 + b_1 d_2$$

$$= j\,\{ Z_3 \cos k_2\ell_2 \sin k_3\ell_3 + Z_2 \sin k_2\ell_2 \cos k_3\ell_3 \}$$

$$c_3 = c_1 a_2 - d_1 c_2 \qquad (3.64)$$

$$= j\{\frac{1}{Z_3} \sin k_2\ell_2 \cos k_3\ell_3 + \frac{1}{Z_3} \cos k_2\ell_2 \sin k_3\ell_3 \}$$

and

$$d_3 = c_1 b_2 + d_1 d_2$$

$$= -\frac{Z_3}{Z_2} \sin k_2\ell_2 \sin k_3\ell_3 + \cos k_2\ell_2 \cos k_3\ell_3$$

On substituting from equation (3.64) into equation (3.63) it follows that:

$$A_1 = \frac{A_4}{2} \left\{ (R_1 \cos k_2\ell_2 \cos k_3\ell_3 - R_2 \sin k_2\ell_2 \sin k_3\ell_3) + j\,(R_3 \sin k_2\ell_2 \cos k_3\ell_3 + R_4 \cos k_2\ell_2) \right\} \qquad (3.65)$$

where: $$R_1 = 1 + \frac{Z_1}{Z_4}$$

$$R_2 = \frac{Z_2}{Z_3} + \frac{Z_1 Z_3}{Z_2 Z_4}$$

$$R_3 = \frac{Z_1}{Z_2} + \frac{Z_2}{Z_4}$$

$$R_4 = \frac{Z_1}{Z_3} + \frac{Z_3}{Z_4}$$

The sound pressure transmission coefficient can be determined from equation (3.65) as:

$$\alpha_{p4} = \left| \frac{A_4}{A_1} \right| \tag{3.66}$$

and the sound power transmission coefficient can be calculated by:

$$\alpha_{t4} = \left| \frac{A_4}{A_1} \right|^2 \frac{Z_1}{Z_4} \tag{3.67}$$

3.9 CASE THREE: FIVE-LAYER SYSTEM

When broad-band transducers are to be employed, the five-layer system should be considered in order to obtain the change in the transmission value over the frequency range of interest. This is also the case when a narrow-band transducer is operated over a wide frequency range (see Section 5.5). In this case the PZT layer must be considered as a bounded medium and account must also be given to the effect of the reflected wave from its rear surface. Another layer is added (see Fig. 3.5) which for most acoustic emission transducers is air (e.g. Dunegan/Endevco transducers).

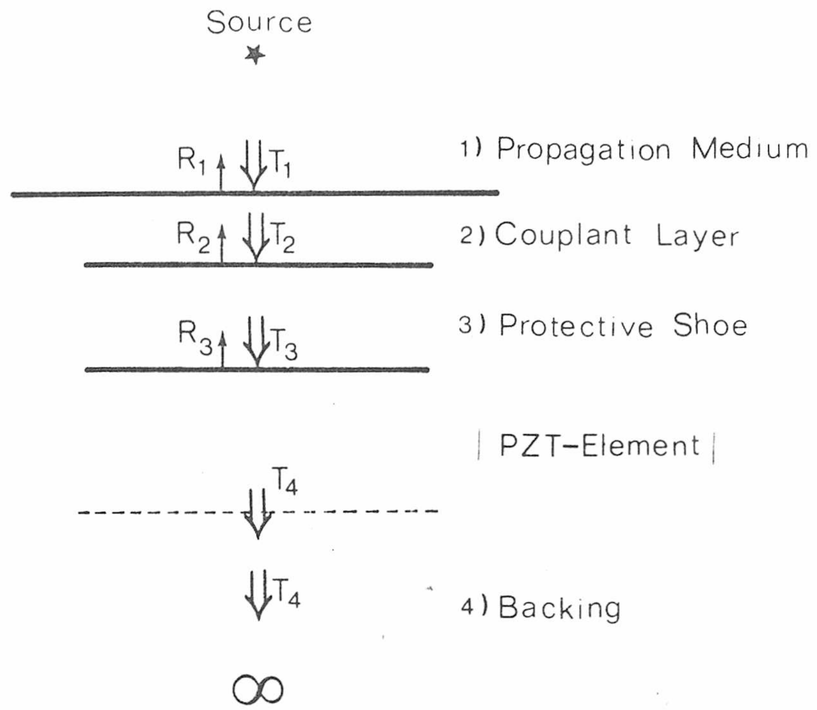

FIGURE 3.4 : Four-Layer Transmission Model for a Narrow-Band Transducer.
T: Transmitted Wave
R: Reflected Wave

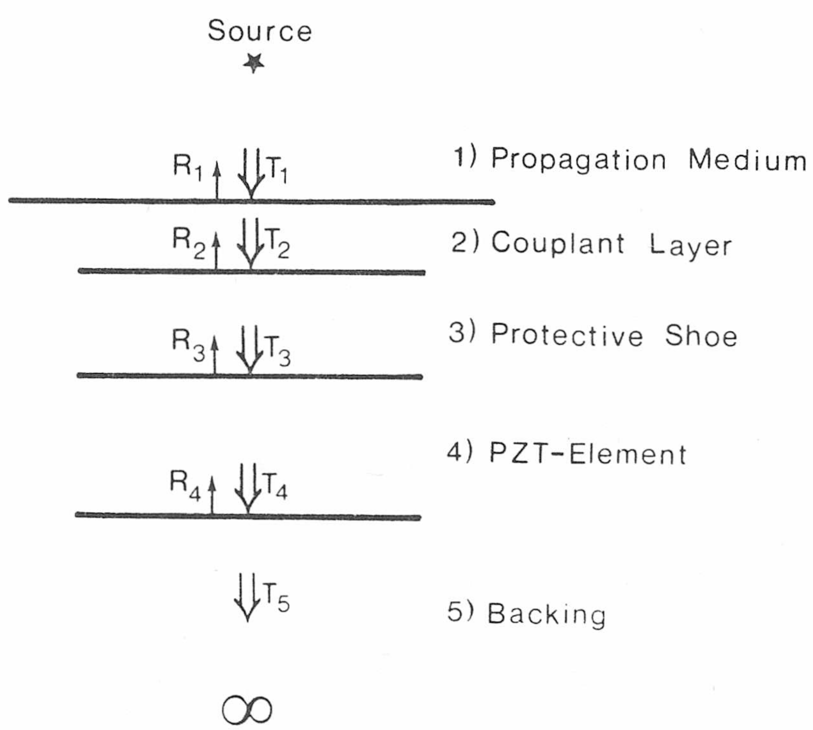

FIGURE 3.5 : Five- Layer Transmisson Model for a Broad-Band Transducer.
T: Transmitted Wave
R: Reflected Wave

For a five-layer system, equation (3.52) gives:

$$T_1 = C_2\ C_3\ C_4\ T_5 \tag{3.68}$$

and from equations (3.62) and (3.64); $C_2 x C_3$ is given by:

$$C_2 x C_3 = \begin{vmatrix} a_3 & b_3 \\ c_3 & d_3 \end{vmatrix}$$

Then, in matrices form equation (3.68) becomes:

$$\begin{vmatrix} A_1 + B_1 \\ \dfrac{A_1 - B_1}{Z_1} \end{vmatrix} = \begin{vmatrix} a_3 & b_3 \\ c_3 & d_3 \end{vmatrix} \begin{vmatrix} \cos k_4\ell_4 & j\ Z_4 \sin k_4\ell_4 \\ \dfrac{j \sin k_4\ell_4}{Z_4} & \cos k_4\ell_4 \end{vmatrix} \begin{vmatrix} A_5 \\ \dfrac{A_5}{Z_5} \end{vmatrix}$$

eliminating B_1 from the resulting two equations gives:

$$\begin{aligned} A_1 = \frac{A_5}{2} \Big\{ \quad & (F_1 \cos k_2\ell_2 \cos k_3\ell_3 \cos k_4\ell_4 \\ & -F_2 \sin k_2\ell_2 \sin k_3\ell_3 \cos k_4\ell_4 \\ & -F_3 \cos k_2\ell_2 \sin k_3\ell_3 \sin k_4\ell_4 \\ & -F_4 \sin k_2\ell_2 \cos k_3\ell_3 \sin k_4\ell_4 \ ) \\ & + j(\ F_5 \cos k_2\ell_2 \sin k_3\ell_3 \cos k_4\ell_4 \end{aligned}$$

$$+F_6 \cos k_2\ell_2 \cos k_3\ell_3 \sin k_4\ell_4$$

$$+F_7 \sin k_2\ell_2 \cos k_3\ell_3 \cos k_4\ell_4$$

$$\left.-F_8 \sin k_2\ell_2 \sin k_3\ell_3 \sin k_4\ell_4 \quad)\right\} \qquad (3.69)$$

where:

$$F_1 = 1 + \frac{Z_1}{Z_5} \qquad F_2 = \frac{Z_2}{Z_3} + \frac{Z_1 Z_3}{Z_2 Z_5}$$

$$F_3 = \frac{Z_3}{Z_4} + \frac{Z_1 Z_4}{Z_3 Z_5} \qquad F_4 = \frac{Z_2}{Z_4} + \frac{Z_1 Z_4}{Z_2 Z_5}$$

$$F_5 = \frac{Z_1}{Z_3} + \frac{Z_3}{Z_5} \qquad F_6 = \frac{Z_1}{Z_4} + \frac{Z_4}{Z_5}$$

$$F_7 = \frac{Z_1}{Z_2} + \frac{Z_2}{Z_5} \qquad F_8 = \frac{Z_1 Z_3}{Z_2 Z_4} + \frac{Z_2 Z_4}{Z_3 Z_5}$$

The sound pressure transmission coefficient can be calculated from equation (3.69) by:

$$\alpha_{p5} = \left|\frac{A_5}{A_1}\right| \qquad (3.70)$$

and the sound power transmission coefficient as:

$$\alpha_{t5} = \left|\frac{A_5}{A_1}\right|^2 \frac{Z_1}{Z_5} \qquad (3.71)$$

3.10 CASE FOUR: SIX-LAYER SYSTEM

The previous transmission systems are sufficient to represent the behaviour of acoustic emission transducers in practice. However, in designing the experimental device to verify the theoretical investigation, the results were affected by specimen resonances. The source of the resonance peaks was attributed to the multireflection of the propagated waves at the specimen free surfaces. To overcome this problem the whole experimental system has to be immersed in a water tank which introduced the need to solve the transmission problem for a six-layer system.

In this case equation (3.52) gives:

$$T_1 = C_2\ C_3\ C_4\ C_5\ \ T_6 \tag{3.72}$$

Substituting the corresponding values for matrices C_2, C_3, C_4 and C_5 and using the matrices product from the previous case the final relationship for six-layer case becomes:

$$\begin{aligned} 2\,A_1 = A_6 \Big\{ & (S_1 \cos k_2\ell_2 \cos k_3\ell_3 \cos k_4\ell_4 \cos k_5\ell_5 \\ & +S_2 \sin k_2\ell_2 \sin k_3\ell_3 \sin k_4\ell_4 \sin k_5\ell_5 \\ & -S_3 \sin k_2\ell_2 \sin k_3\ell_3 \cos k_4\ell_4 \cos k_5\ell_5 \\ & -S_4 \cos k_2\ell_2 \sin k_3\ell_3 \sin k_4\ell_4 \cos k_5\ell_5 \\ & -S_5 \sin k_2\ell_2 \cos k_3\ell_3 \sin k_4\ell_4 \cos k_5\ell_5 \\ & -S_6 \cos k_2\ell_2 \cos k_3\ell_3 \sin k_4\ell_4 \sin k_5\ell_5 \end{aligned}$$

$$-S_7 \sin k_2\ell_2 \cos k_3\ell_3 \cos k_4\ell_4 \sin k_5\ell_5$$

$$-S_8 \sin k_2\ell_2 \cos k_3\ell_3 \sin k_4\ell_4 \cos k_5\ell_5 \;)$$

$$+ j(S_9 \cos k_2\ell_2 \cos k_3\ell_3 \cos k_4\ell_4 \sin k_5\ell_5$$

$$+S_{10} \cos k_2\ell_2 \cos k_3\ell_3 \sin k_4\ell_4 \cos k_5\ell_5$$

$$+S_{11} \cos k_2\ell_2 \sin k_3\ell_3 \cos k_4\ell_4 \cos k_5\ell_5$$

$$+S_{12} \sin k_2\ell_2 \cos k_3\ell_3 \cos k_4\ell_4 \cos k_5\ell_5$$

$$-S_{13} \sin k_2\ell_2 \sin k_3\ell_3 \cos k_4\ell_4 \sin k_5\ell_5$$

$$-S_{14} \cos k_2\ell_2 \sin k_3\ell_3 \sin k_4\ell_4 \sin k_5\ell_5$$

$$-S_{15} \sin k_2\ell_2 \cos k_3\ell_3 \sin k_4\ell_4 \sin k_5\ell_5$$

$$-S_{16} \sin k_2\ell_2 \sin k_3\ell_3 \sin k_4\ell_4 \cos k_5\ell_5) \Big\} \tag{3.73}$$

where:

$$S_1 = 1 + \frac{Z_1}{Z_6} \qquad S_2 = \frac{Z_2\,Z_4}{Z_3\,Z_5} + \frac{Z_1\,Z_3\,Z_5}{Z_2\,Z_4\,Z_6}$$

$$S_3 = \frac{Z_2}{Z_3} + \frac{Z_1\,Z_3}{Z_2\,Z_6} \qquad S_4 = \frac{Z_3}{Z_4} + \frac{Z_1\,Z_4}{Z_3\,Z_6}$$

$$S_5 = \frac{Z_2}{Z_4} + \frac{Z_1\,Z_4}{Z_2\,Z_6} \qquad S_6 = \frac{Z_4}{Z_5} + \frac{Z_1\,Z_5}{Z_4\,Z_6}$$

$$S_7 = \frac{Z_2}{Z_5} + \frac{Z_1 Z_5}{Z_2 Z_6} \qquad S_8 = \frac{Z_3}{Z_5} + \frac{Z_1 Z_5}{Z_3 Z_6}$$

$$S_9 = \frac{Z_1}{Z_5} + \frac{Z_5}{Z_6} \qquad S_{10} = \frac{Z_1}{Z_4} + \frac{Z_4}{Z_6}$$

$$S_{11} = \frac{Z_1}{Z_3} + \frac{Z_3}{Z_6} \qquad S_{12} = \frac{Z_1}{Z_2} + \frac{Z_2}{Z_6}$$

$$S_{13} = \frac{Z_1 Z_3}{Z_2 Z_5} + \frac{Z_2 Z_5}{Z_3 Z_6} \qquad S_{14} = \frac{Z_1 Z_4}{Z_3 Z_5} + \frac{Z_3 Z_5}{Z_4 Z_6}$$

$$S_{15} = \frac{Z_1 Z_4}{Z_2 Z_5} + \frac{Z_2 Z_5}{Z_4 Z_6} \qquad S_{16} = \frac{Z_1 Z_3}{Z_2 Z_4} + \frac{Z_2 Z_4}{Z_3 Z_6}$$

The sound pressure transmission coefficient can be determined as:

$$\alpha_{p6} = \frac{A_6}{A_1} \tag{3.74}$$

and the sound power transmission coefficient is given by:

$$\alpha_{t6} = \left| \frac{A_6}{A_1} \right|^2 \frac{Z_1}{Z_6} \tag{3.75}$$

3.11 CONCLUSIONS

There are 2(2n–1) boundary conditions to be satisfied for a transmission system of n layers. The conditions are continuity of two pressure components and two velocity components in each layer except that of layer n. This is the last layer in such system and since it is assumed to be semi-infinite in extent, it has only one pressure and one particle velocity component. These give 2(2n–1) homogeneous simultaneous equations to determine the ratio between the incident and transmitted sound pressure amplitude.

One of the most useful concepts in the analysis of the multilayer wave transmission system is the idea of the characteristic matrix of the bounded layer C_i, equation (3.52). Each bounded layer in the normal incident longitudinal wave transmission system may therefore be represented by 2x2 square matrix operator for which the elements along the principal diagonal are real and equal ($\cos k_i \ell_i$), the off-diagonal elements are imaginary ($j\, Z_i \sin k_i \ell_i$, $j \sin k_i \ell_i / Z_i$), and the determinant is unity.

The entire multilayer system may then be represented by the matrix product of the individual matrices. In general, the form of the product matrix differs from that of the individual matrices in that the elements along the principal diagonal are unequal.

However, it was shown that matrices method representation leads to a simple and straightforward technique for the analytical investigation. The results are represented in final format which is suitable for computation.

Relationships connecting the transmitted longitudinal wave amplitude into acoustic emission transducer components have been investigated for particular number of multilayer models in order to study the effect of the monitoring geometry on the received acoustic emission bursts.

PART THREE

DATA HANDLING AND EQUIPMENT

CHAPTER FOUR

DATA ACQUISITION AND PROCESSING

The recording of acoustic emission transducer response is strongly dependent on the instrumentation system selected and the method of processing the collected data. During the course of this study, an acoustic emission data acquisition and processing system was developed to gather and process acoustic emission transient waveforms.

The aim of this chapter is to explain the instrumentation, devices, techniques, data collection and processing used.

4.1 EQUIPMENT, MATERIALS AND DEVICES

Figure 4.1 shows a general diagram which summarises the equipment, materials and devices and their function as used in the experimental studies. Some features of these experimental tools are described in this section while the general characteristics of the routine electronic equipment are given in Appendix 4.A. Detailed experimental set-up will be mentioned in the next section.

(1) The Transducers:

A piezoelectric transducer was used as an acoustic emission source. This was a commercial Meccasonic broad-band 5 MHz transducer, highly damped to reduce ringing to a minimum and produce a stress impulse with a broad power spectrum.

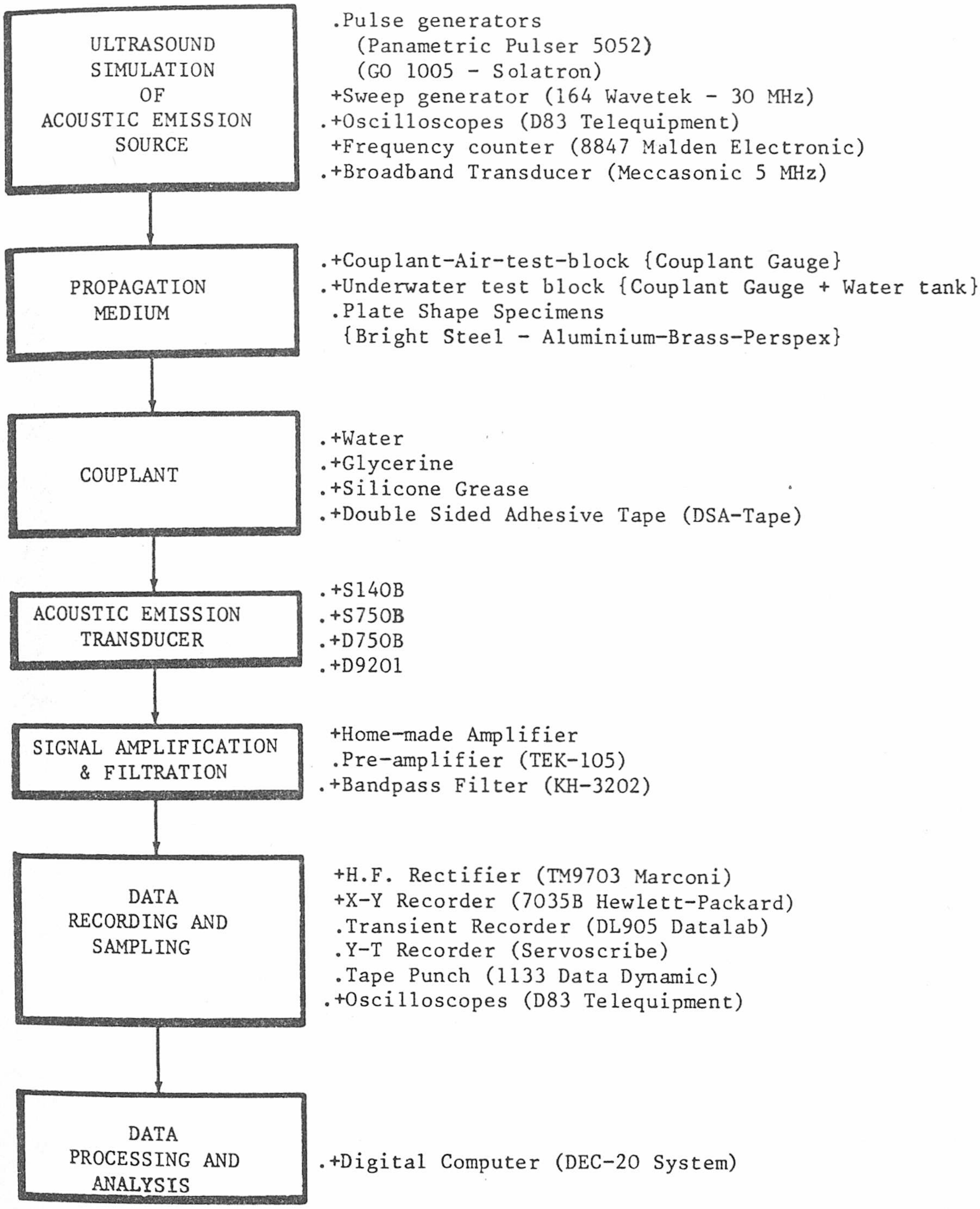

FIGURE 4.1 : A Summary Diagram of Equipment, Materials and Devices Used in The Experiments Set-up.
+ Continuous Wave Experiments.
. Repeated Pulse Experiments.

Figure 4.2 shows a typical CRO photograph of the transducer response using a 40 V pulse and a reflector of 4.75 mm diameter (measurement carried out at Harwell). The transducer is 5 mm in diameter to approximate a point source. The piezoelectric simulated source was used because the duration and waveform of the stress wave can be easily controlled and the source is stable and continuously repeatable. For continuous wave measurements, the same source transducer was used as a sender.

Acoustic emission transducers used were manufactured by Dunegan/Endevco. These transducers are constructed using a piezoelectric PZT-5A ceramic disc which has been polarised and cemented to an epoxy protective shoe. The manufacturers calibration curves as reproduced from the original sheets, supplied with the transducers are shown in Fig. 4.3 (a,b,c and d). These figures show their frequency response using the spark-bar impulse calibration technique (42). Some physical parameters are given in Table 4.1.

(2) Couplants:

Initially, three couplant media were used in this study: water, silicone grease and glycerine diluted in water to different densities. When the need for couplant standardization became important, a different couplant material was used. The material was double-sided adhesive (DSA) tape. Double-sided adhesive tape consists of polyvinyl chloride (PVC) sheet which has a similar specific acoustic impedance to that of the acoustic emission

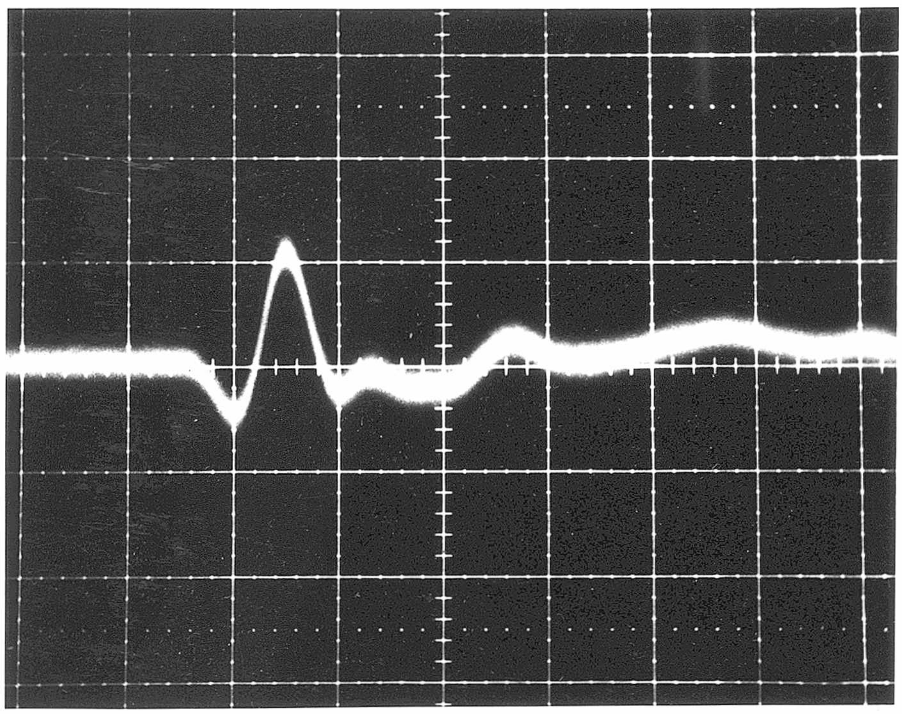

FIGURE 4.2 : A Photograph for Pulse Excitation of
the 5MHz Sender Transducer.
(Horizontal Scale: 0.2 μs/Div.)

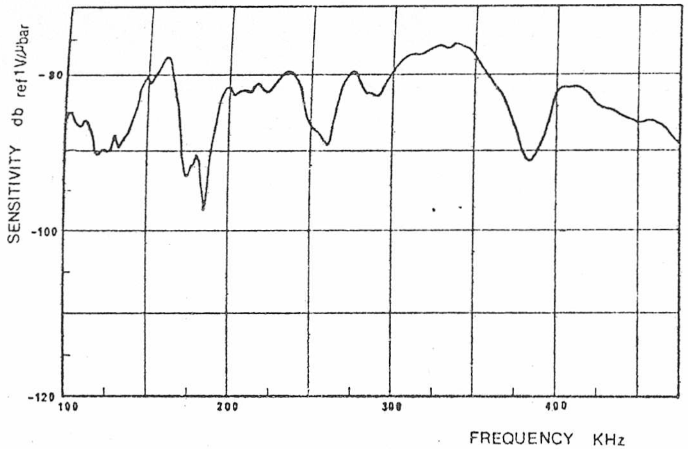

(a) For S140B

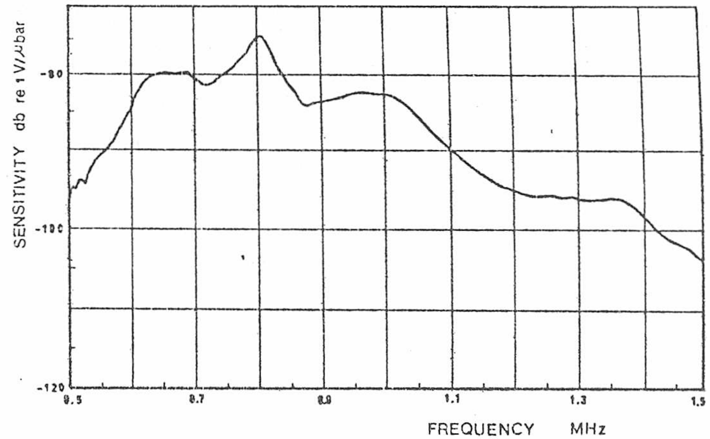

(b) For S750B

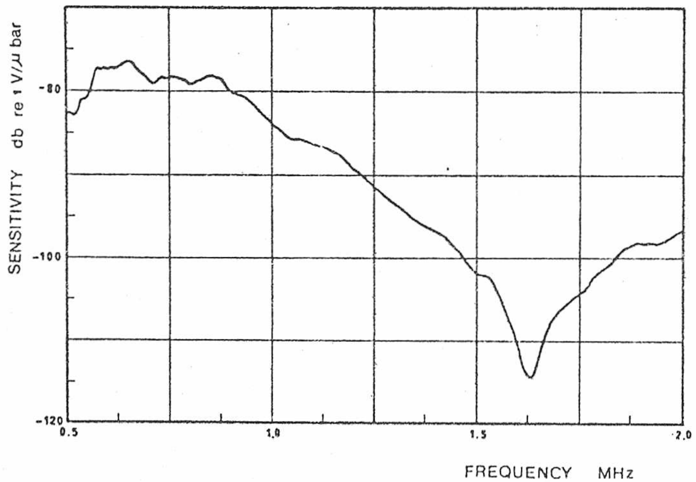

(c) For D750B

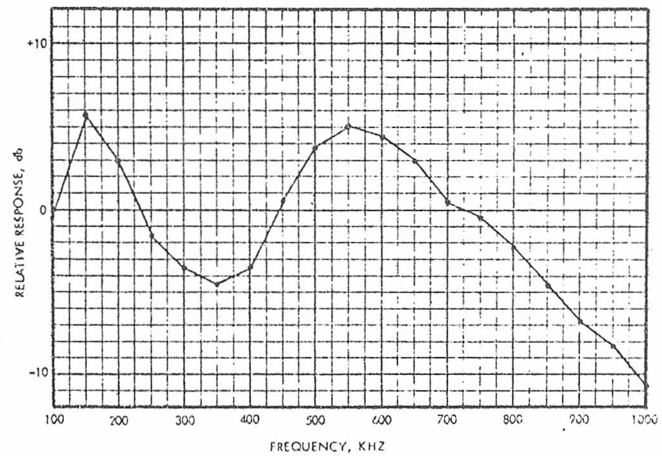

(d) For D9201

FIGURE 4.3 : Calibration Charts of Acoustic Emission Transducers Using the Spark-Bar Impulse Technique.

Table 4.I Some Physical Parameters of the Commercial Acoustic Emission Transducers

Physical Parameter	Transducers: S140B	Transducers: S750B D750B	Transducers: D9201
Frequency-band	Narrow		Broad
Mode Sensitivity	Longitudinal		Shear
Peak Sensitivity*	-75 dB ref. 2 volt per microbar		-85 dB ref 1V/μbar (Average)
Directionality**	-2 dB Typical (Max-Min)		(NA)
Case Material	Aluminium		St.St.
<u>Protective Shoe:</u>			
Material:	Black Epoxy		Alumina 99% (AL_2O_3)
diameter (mm)	19.84		-
thickness (mm)***	3.125		0.5
Sp. Acoustic Impedance kg. m^{-2} s^{-1}	2.5×10^6 $		42.5×10^6 $$
longitudinal wave velocity m s^{-1}	2550 $		10700 $$
<u>PZT-5A element:</u>			
diameter (mm) *$	12.7		(NA)
thickness (mm)*$	6.35	2.9	(NA)
Sp. Acoustic Impedance (kg m^{-2} s^{-1})$$	33.7×10^6(R)		33.7×10^6
longitudinal wave velocity (m s^{-1})$$	4350		4350
Design	single ended	single ended (D750B: Differential)	differential ended

* obtained by ultrasonic calibration (manufacture data sheet)
** obtained by spark-bar impulse calibration (manufacture data)
***measured and confirmed by the manufacturer (158).
$ measured (at Harwell).
$$ measured
*$ The transducers are X-rayed by us and confirmed by Hamstad (159).
(R) This value was also used by Pace (158).
(NA) not available.

transducer protective shoe. It provides almost constant couplant thickness over the whole transducer surface. It would be expected to support both longitudinal and shear waves. In use it does not need any rubber-band or special clip to hold the transducer onto the specimen body being monitored. It has high resistance to water, acids, alkalis and temperature and can be used to attach the transducer to both ferrous and non-ferrous materials for a long time without change in either structure or the transducer surface. The acoustical and physical properties of the couplant media are summarized in the following table:

TABLE 4.II: THE VALUES OF LONGITUDINAL WAVE VELOCITY AND ACOUSTIC IMPEDANCE FOR DIFFERENT COUPLANT MEDIA

Couplant Medium	Longitudinal Wave Velocity ($m.s^{-1}$)	Acoustic Impedance x 10^{-6} $Kg.m^{-2}$ s^{-1}
Water	1500	1.5
Glycerine (1260 $Kg.m^{-3}$ 'density')	1920	2.48
Silicone Grease*	1050	1.077
DSA Tape	2350	2.48

*measured (as published data could not be traced).

-other data are compiled from published works and textbooks.

Before using DSA tape, surfaces must be cleaned. A solvent with the following composition was used for all specimens and transducer surface cleaning.

Ether	30% (in volume)
Chloroform	30%
Petroleum Ether	25% (B.P. 40-60^{o}C)
Toluene	15%

(3) Propagation Specimens:

In order to study the effect of the propagation body geometries on acoustic emission signals a simple geometry was needed. A number of plate shapes was used. Table 4.111 gives the code, dimension and material of each specimen used (Chapter Six) in studying and relating the acoustic emission parameters. The surface finish of each specimen was used as received (rolled bars).

TABLE 4.III: SPECIMENS GEOMETRY AND MATERIAL

Code No.	Material	DIMENSION, mm L x W x T	Surface Finish* CLA, Microns	
			Long.	Trans.
GS1	Bright Steel	995 x 50 x 12.5	1.8	1.1
GS2	" "	690 x 50 x 6	0.3	0.9
GS3	" "	330 x 50 x 12.5	2.5	1.6
GS4	" "	330 x 50 x 6	1.2	0.6
GS5	" "	330 x 30 x 30	1.7	0.8
GS6	" "	330 x 25 x 12.5	1.4	1.9
GA	Aluminium	330 x 25 x 12.5	0.75	1.3
GB	Brass	995 x 50 x 12.5	0.28	1.0
GP	Perspex	995 x 50 x 12.5	0.02	0.09

*CLA is the Central Line Average.

Long. ≃ measured in the rolling direction (L).

Trans. ≃ measured in the transverse direction (W).

(4) The Couplant Gauges:

The basic mechanical fixture for positioning the acoustic emission transducer so that the couplant thickness could be varied is shown in Fig. 4.4. This device was used for experiments in air. An ultrasonic source was provided by exciting the 5 MHz Meccasonic transducer (B). The source transducer was coupled to the top centre of the aluminium test block (X) of diameter 100 mm and height 20 mm which acted as a propagation body. The top and bottom surfaces of the block were machined to a high degree of parallelism and were polished. When results were taken, the source transducer was kept in the same position under a load of 300 gm (A) to achieve a constant and stable acoustic contact. A commercial acoustic emission transducer (C) was adjusted in the top of a guiding block (D) so that its face was parallel to the bottom of the test block and exactly opposite the source transducer. In all couplant experiments the excitation was applied to one face of the aluminium block (X) while the acoustic emission transducer was placed on the opposite face to sense the direct longitudinal wave generated by the source. The guiding block was mounted on the head of the micrometer (G) by which the couplant thickness was controlled and measured. Measurements were made in one direction of the micrometer to avoid backlash problems, starting with the maximum couplant thickness and ending with the minimum. The micrometer had two turns per mm travel, with 200 subdivision per turn. Figure 4.5a shows a detailed plan view of the guiding aluminium block (D).

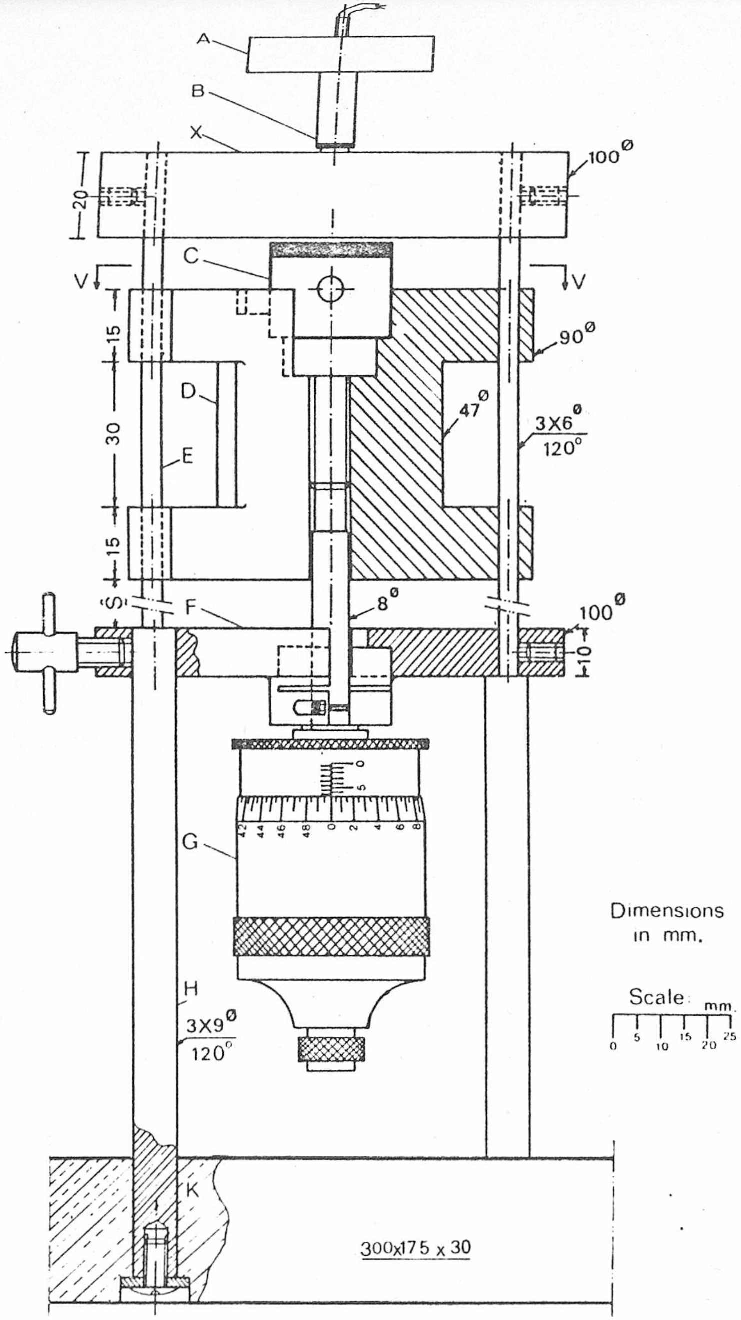

FIGURE 4.4 : Elevation Drawing of the Couplant Gauge, Designed to Locate the Acoustic Emission Transducer with Controlled Couplant Thicknesses.

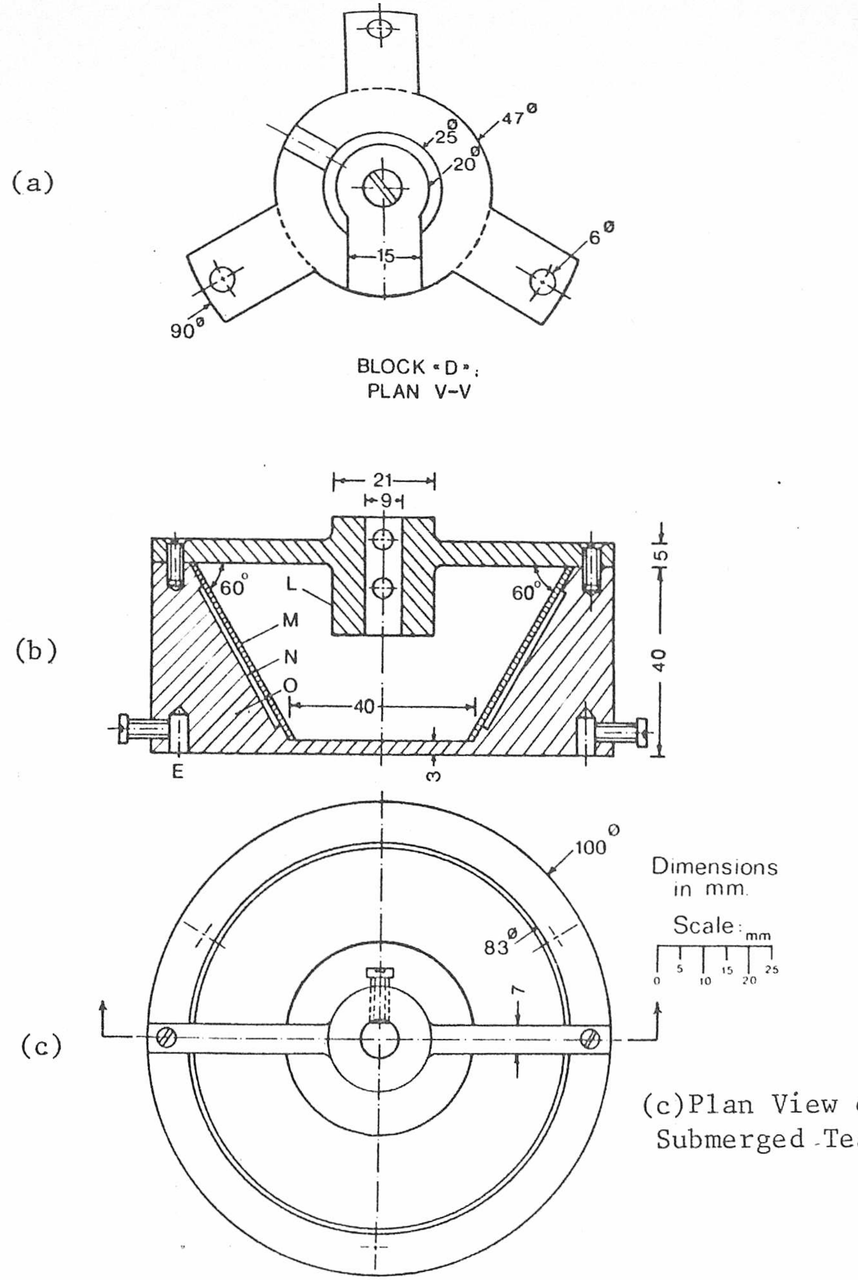

(c)Plan View of The Submerged Test Block

FIGURE 4.5 : (a) Plan V-V of the Couplant Gauge Guided Block (D).
(b) Elevation Cross-Section in the Submerged Test Block.

For the experiments underwater, another test block was designed to replace (X). This was used to overcome the problems arising from acoustic resonances in block (X). The dimensions of the second test block are shown in Fig. 4.5b and c. The source transducer was held in the mechanical holder (L). The cup-shape was given to the test block in order to suppress the formation of standing waves between the block boundaries. All the possible scaped waves from the transmitted acoustic beam will go multi-reflections inside the semi-cone shape of (O) and towards its narrow corner away from the diaphragm (P). Finally, these unwanted waves will be either transmitted into the water tank through the outer surface of the text block or trapped in the narrow corner of (O).

The inside wall of the test block was machined in a way to perform; when it was covered with a thin sheet of perspex (M); an air gap (N). This construction made the inside wall of (O) to act as a perfect reflector to prevent any wave inside (O) from passing through and interfering with the transmitted one.

Since the transmission theory is developed for a plane wave incident into the test block and subsequent transducer layers, care was taken to keep the propagation diaphragm (P) in the farfield of the transmitting transducer. The expression D^2/λ was used to determine the minimum distance to the farfield, where D is the diameter of the transmitter transducer active element (5 mm) and λ is the wavelength of the pressure wave in water.

The lowest longitudinal thickness resonance in 3 mm thickness aluminium plate occurs at approximately 1.07 MHz. Therefore no specimen resonance exists in the experimental frequency range (500-1000 KHz).

(5) The Water Tank:

The underwater experiments were made in a laboratory fresh-water test tank of 1x1x1 meter. The couplant gauge was immersed vertically (upside-down) in the centre of the tank. To avoid reflections from the bottom of the tank, a thick layer of sand covered by rubber was used as an aid in absorbing reflections at the tank bottom. Couplant thickness could be adjusted from above the water level and no problems were experienced from the tank walls or liquid/air surface reflections within the tank.

(6) The Main Electronic Equipment:

A variation of electronic equipment was used in this study (see Fig. 4.1). The important features of the signal amplification and the transient recorder will be discussed in this section, while those for the remainder of the system are listed in Appendix 4.A.

Signal Amplifiers:

Two signal amplifiers were used in this study. A pre-amplifier (model TEK-105) and a home-made amplifier. The Tek pre-amplifier gave a fixed gain of 40 dB and was used in most of the specimen geometry experiments. The pre-amplifier frequency response curve is shown in Fig. 4.6a. The input voltage was 10 microvolts (RMS). It can be seen that the upper-fall off frequency limit begins beyond 1 MHz. This is quite satisfactory since the upper-frequency limit was 1 MHz in all the experimental work.

In the early stage of this study, a home-made amplifier was used. The frequency response curve is shown in Fig. 4.6b for a constant sinusoidal input voltage. The graph shows unsatisfactory behaviour of the response curve over the frequency bandwidth of interest. This amplifier was used in experiments where the variation in gain with frequency was unimportant.

The Transient Recorder:

A DL905 Datalab transient recorder has been used to capture and digitize the transient acoustic emission waveforms (bursts). These can be continuously displayed on an oscilloscope or plotted on a Y-T chart recorder. A digital record may also be obtained by interfacing the unit to a paper tape punch machine.

When the acoustic emission waveform is recorded, it is stored as a number of equally spaced points representing the amplitude of the waveform at discrete moments in time. Each sample of the signal is converted into a digital number and stored in memory. The instrument has 1024 words of memory, given amplitude resolution of one part in 256 (8 bits), and maximum sampling rate of 5 MHz.

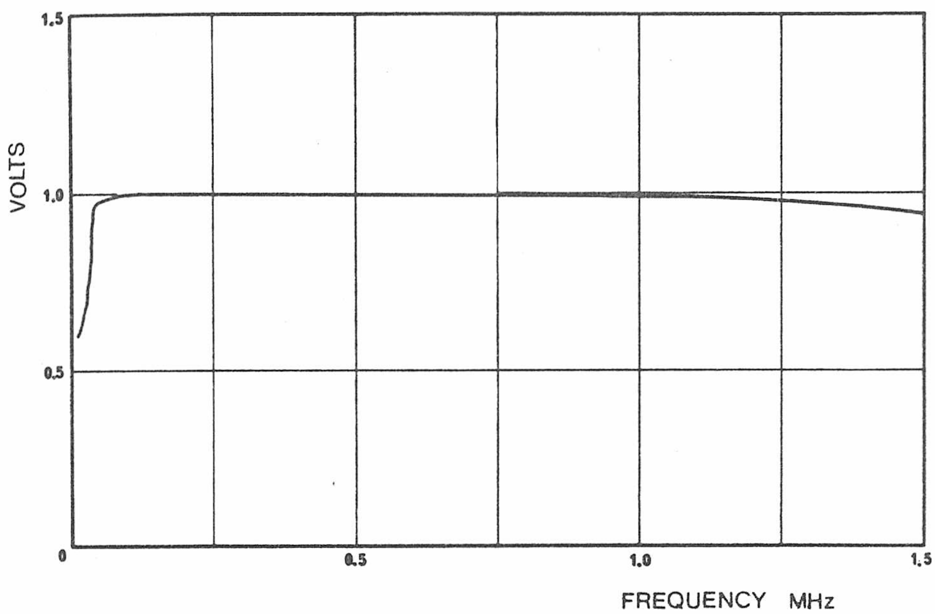

FIGURE 4.6 (a) : The Frequency Response of the TEK-105 Pre-Amplifier.

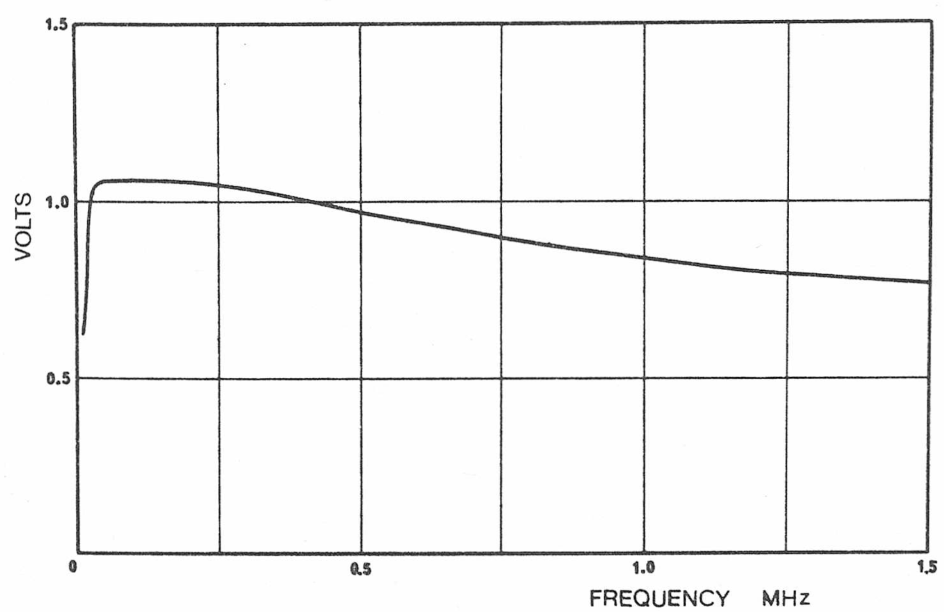

FIGURE 4.6 (b) : The Frequency Response of the Home-Made Amplifier.

The first 1000 points of the record stored in the memory of the instrument are reconstructed via a digital to analogue converter as a repeating sequence of 1000 analogue values, so that the reconstructed waveform may be viewed continuously by connecting a CRO to the X and Y terminals of the unit.

It is necessary to consider the sample interval and its relationship to the frequency content of the signal to be recorded. As the number of samples in a single record is fixed to 1024, a change in record length (sweep time) is accompanied by a change in sample interval. The sample interval is calculated as 1/1000 part of the sweep time and defines the maximum frequency that may be recorded for any sweep time (when carrying out computation, this scaling process is carried out through a computer subroutine named SCALE which is called at the very beginning of each data processing main program "see Appendix 4.B"). Due to the discrete sampling nature of the unit it was necessary to ensure that aliasing does not occur. It was, therefore, necessary to use the pass-band filter which limits the high frequency content of the signal.

The unit volts full scale setting determines full sensitivity of the unit input amplifier. As the input signal is digitized to 8 bit accuracy (one part in 256) the smallest quantity that will be digitized is:

$$\frac{1}{256} \text{ X Full Scale Setting (V)}$$

It follows that best resolution is obtained by setting this control to value, V, so that the peak to peak value of the input signal is as near the full scale voltage as possible without overloading the input range. Signals that have exceeded the dynamic range of the analogue to digital converter will be seen and digitized as clipped waveforms on the record (when carrying out computation the volt scale is read from the subroutine SCALE and the voltage scaling operation is done on the samples record throughout the read subroutines READA and READAB "see Appendix 4.C").

4.2 EXPERIMENTAL TECHNIQUES

In this section the experimental configuration will be described with the experiments being grouped according to general type. A system diagram is given that should serve as a guide to system configuration and equipment selection.

4.2.1 CONTINUOUS WAVE DIRECT FREQUENCY RESPONSE

The technique is intended to measure, by means of continuous sine wave, the direct frequency response of the propagation medium, couplant and transducer multilayer system. Figure 4.7 shows schematic block diagram of the electronic system used in this technique. The simulated acoustic emission source transducer was driven by sweeping a continuous sine wave of constant amplitude over the desired frequency band in 100 seconds. The heart of the test system is the Wavetek sweep frequency generator which provides a constant amplitude output signal. The starting and stopping frequency were selected as desired using a monitoring oscilloscope and the frequency counter (see Wavetek instruction manual 3/77). The sweep-out connector from the Wavetek generator provides the voltage, proportional to the sweep frequency, which was connected to the X-axis of the X-Y recorder to obtain a plot of amplitude versus frequency.

The acoustic emission transducer response (from '3') was amplified, filtered and fed to the Y-axis of the X-Y recorder. The experimental set-up was employed in two different couplant gauge conditions.

(1) Air Couplant Experiments: in which the transmission block (X), Fig. 4.4, was used in air with transmission system shown in the left of fig. 4.7.

(2) Submerged Couplant Experiments: in which the transmission block (O), in Fig. 4.5b and c, was used, The whole couplant gauge was submerged vertically in the centre of the water tank (except the micrometer). The transmission direction inside the water tank was upward to the acoustic emission transducer '3'.

The submerged couplant experiments were devised to determine the transmission characteristics of acoustic emission transducers. As these experiments were almost free of interference from reflected waves and specimen resonances, a comparison with the theoretically

predicted transmission coefficient at corresponding frequencies could be made.
The stability of the whole system was such that a complete plot over the desired frequency-band could be repeated within ± 0.5 dB.

4.2.2 INDIVIDUAL REPEATED PULSE EXPERIMENTS

The primary goal in these type of experiments was to record the acoustic emission burst signals amplified from the receiver transducer output. Figure 4.8 is schematic block diagram of the typical experimental set-up used in this case.

The experiments basically involve the recording of the acoustic emission "burst" on paper tape at the laboratory followed by computer processing and analysis of this data. In general, the system may be applied to any signal which is measurable as a voltage and is a function of time.

In fig. 4.8 the simulated acoustic emission transducer was driven by a short electrical pulse from one of the pulse generators. The output response of the acoustic emission transducer was amplified through the 40 dB constant gain pre-amplifier (the pre-amplifier is the external part of a TEK-105 Stress Wave Emission Processor). The amplified signals were then filtered through the band-pass filter which was set to provide a 20 KHz - 1 MHz bandpass for each signal.

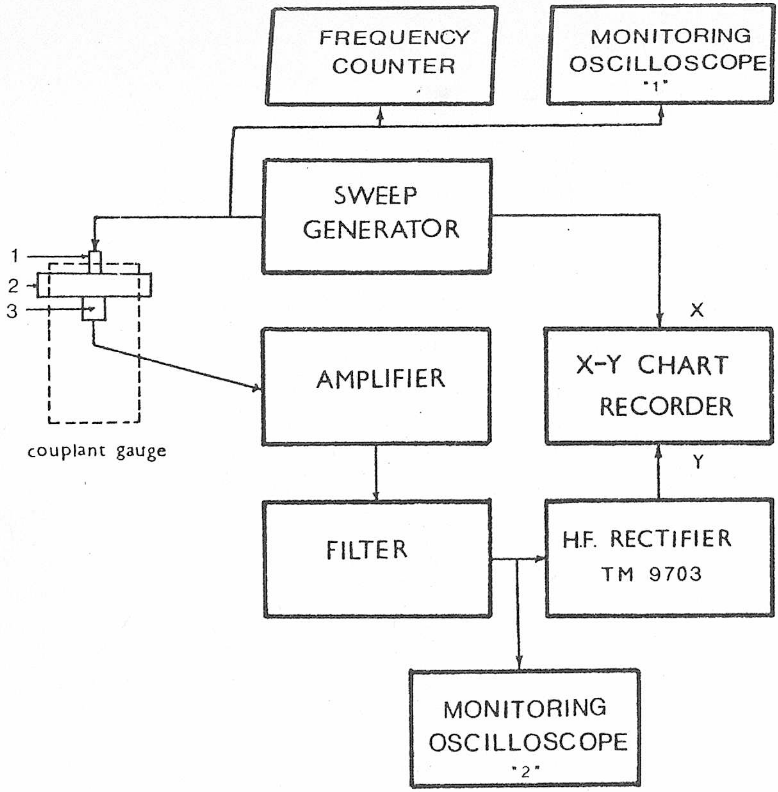

FIGURE 4.7 : Schematic Block Diagram of the Electronic System for the Determination of the Direct Frequency Response of the Acoustic Emission Transducers Using Swept Sine Wave.

1. Transmitter Transducer
2. Transmitting Test Block
3. Acoustic Emission Transducer

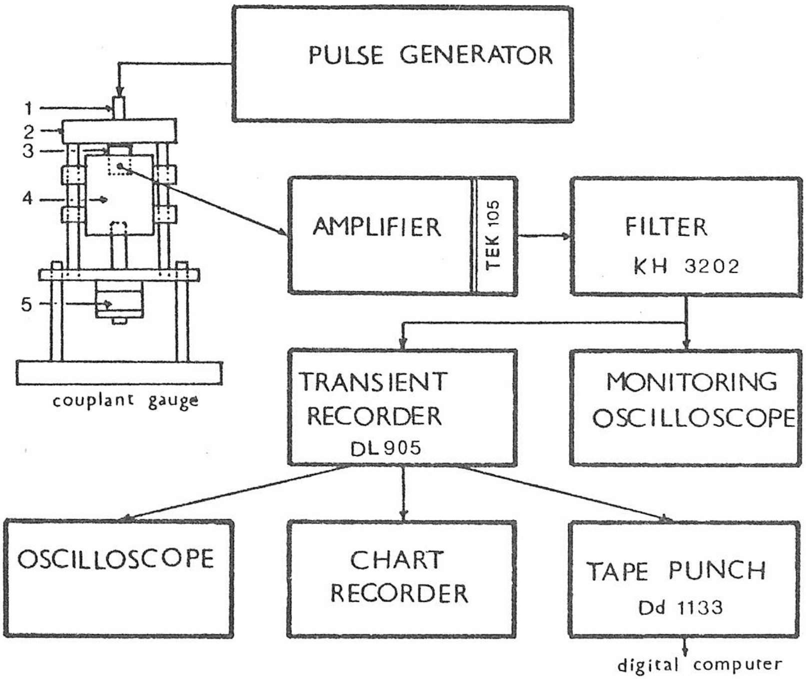

FIGURE 4.8 : Block Diagram of Instrumentation for Recording Individual "Acoustic Emission Bursts".

The filtered signals were digitized with the transient recorder (DL 905). One digitizing rate of 0.5 μs/point was used. By Nyquist's theorem, this provided accurate spectral analysis up to a frequency of 1 MHz. As the storage capacity of the transient recorder was 1024 points, the first 0.5 ms (corresponding to 1000 points) of each signal was digitized and recorded on paper tape. Then the data was transferred on paper tape to the Institute DEC-20 computer for processing and graph plotting.

One of the two oscilloscopes was used to monitor the whole detected acoustic emission signal as it came out of the filter, and the second one to display and observe the digitized signal.

4.3 BURST DATA HANDLING AND PROCESSING

This section describes the acoustic emission data handling and processing system which has been developed. The complete system is a combination of electronic signal acquisition and computer data processing. Data off paper tape is fed to the Institute central computer for processing and plotting. Each of the main programs (which have been mentioned in Chapter Two) can be run from terminal and have the ability to call data files from the computer magnetic disc, open, read and close the file being used. Figure 4.9 shows the complete data computation and display system.

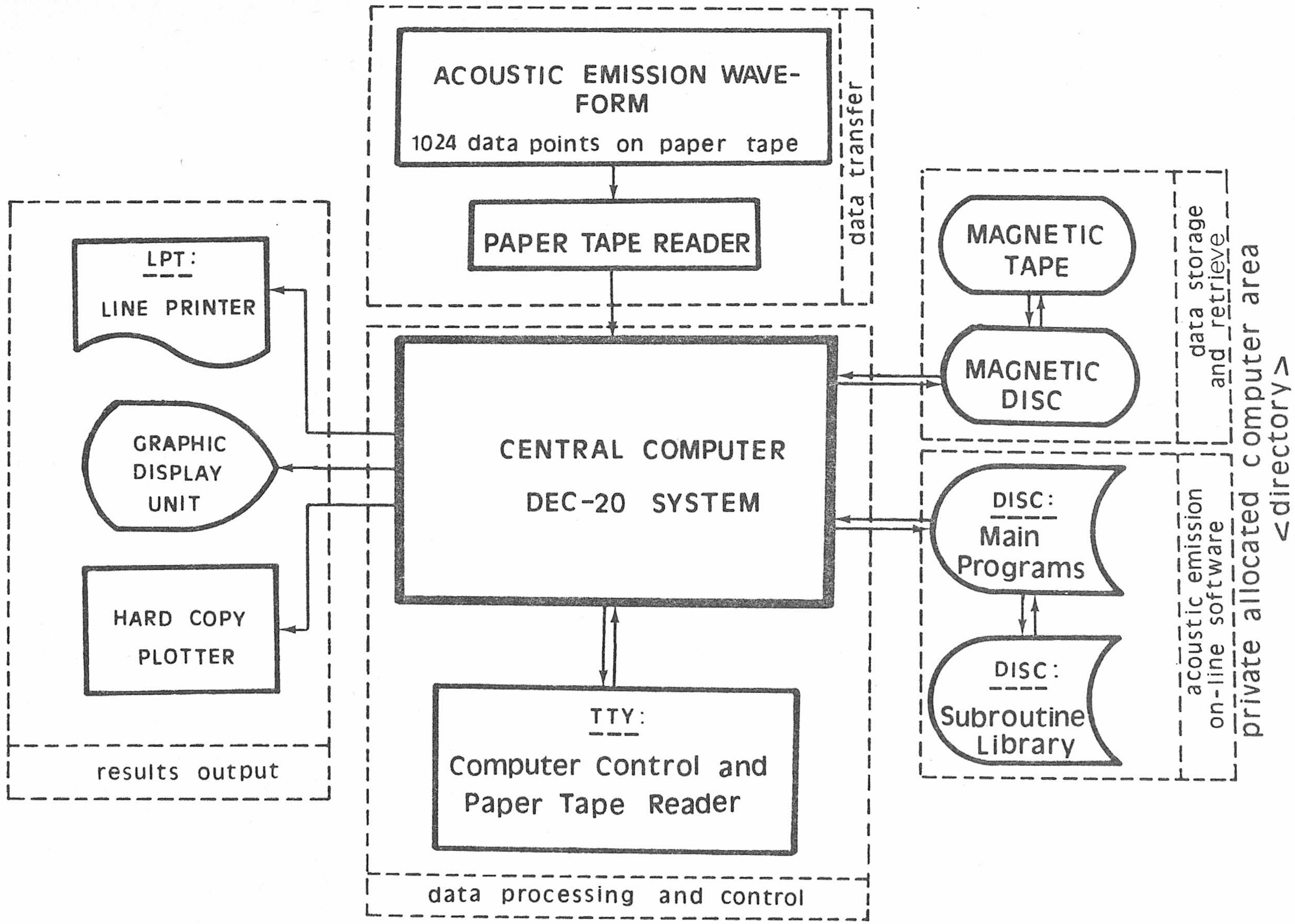

FIGURE 4.9 : Acoustic Emission Data Transfer, Computation and Display System.

Data Transfer and Storage:

After the acoustic emission test has been completed, the test data records are read from the paper tape either through the laboratory teletype terminal or through the central computer paper tape fast reader and transmitted to special located area where it is stored on magnetic disc. However, both methods were inefficient, being time consuming and subject to reading errors. The teletype direct data transfer was achieved by using a short program (in ALGOL) on the DEC-20 system to read the data from paper tape and store it in a PAPER.TAP data file (which should be renamed into XXXX.DAT).

Testing of Data File Contents:

When the data file has been transmitted on disc file, all the contents of the file are listed first on fast display terminal (VDU). This is a very important step in the system since the data can be given an examination for obvious digitization and format errors. The total number of data points must also be checked. The data file can be assessed for editing using the computer command option for error editing. The editing feature of the DEC-20 system permits rapid correction of data errors prior to processing. It is also essential that the format of the data file to be uniform to match the program to which it is to be read from the stored file. The format of the data file must be as follows:

```
64 (16 ( I3, 1X))
```

one space (1)

number of digits in each figure (3)

number of figures in each line

number of lines in each file

To end the editing session, the editing command EU must be used after the last asterisk (*) to remove the line numbers from data file.

Verification also can take place by inspecting the data file plot. This was always done, before performing any frequency analysis, by plotting the signal in its time domain using the TIMPLT program (see Section 2.3).

After verification and format changes and once the data file was established as correct it would be given the extension name (.DAT). The data file is now available for processing by any of the programs mentioned in Chapter Two.

General Computational Sequence:

The general computational sequence which is carried out on the burst data file is shown in Fig.4.10. The computational programs and subroutines have been written in FORTRAN and applied to a maximum of 1024 points. All data files were subjected to general preprocessing operations through subroutines as follows:

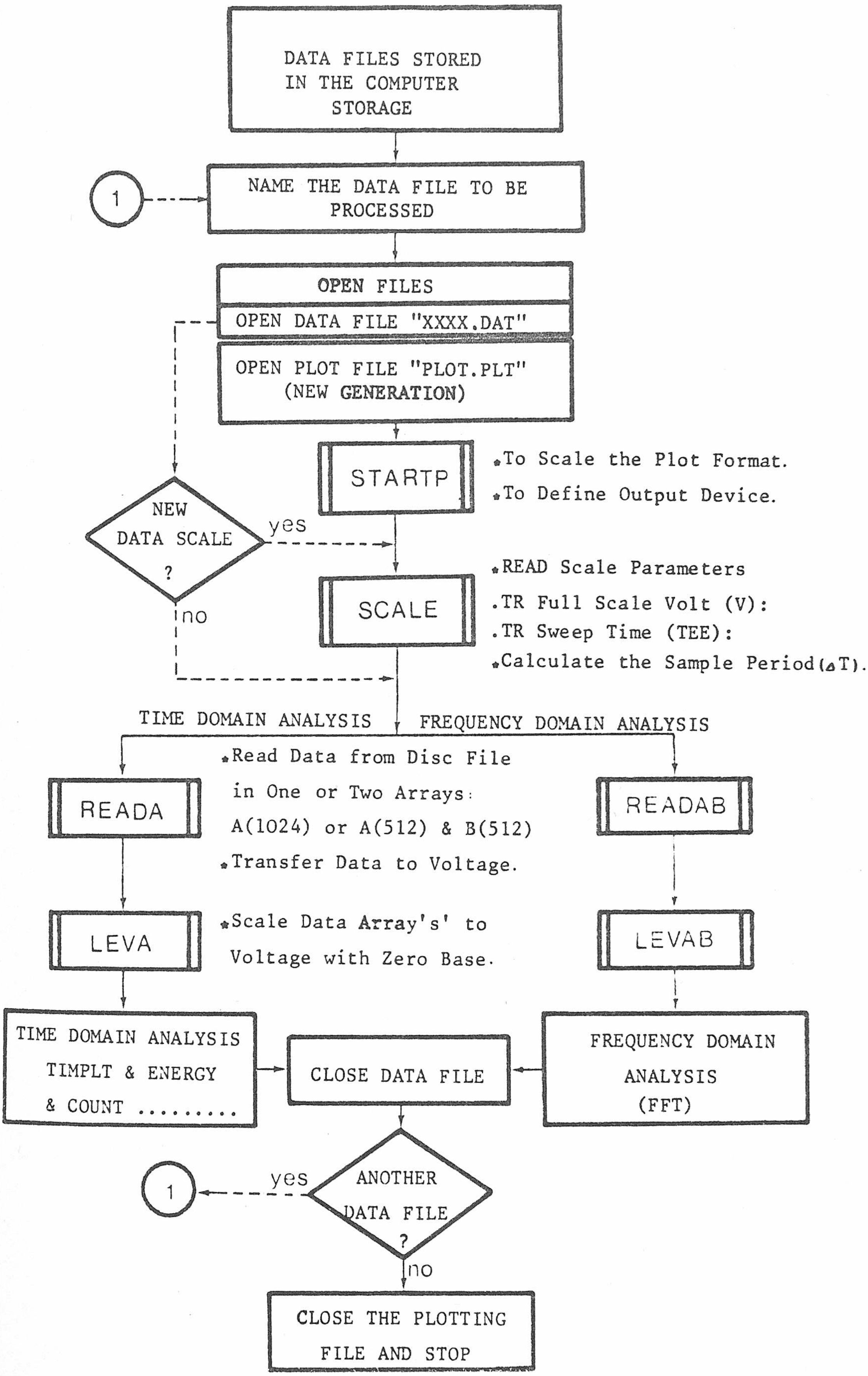

FIGURE 4.10 : General Computational Analysis of the Bursts Data.

î Converting the Data Record to Voltage Values:

The data points in each record were digitized into 1024 words of three digits positive numbers through the transient recorder. The value of each word (data point) is varied from (000) to (255) representing the variation in the signal amplitude according to the full scale setting of the transient recorder. These values are related to an arbitrary base value. To convert these values to others which are equal to the input voltage, the digitized numbers after being read into the computer central processing unit were multiplied by the proportional ratio:

$$\frac{V}{RESOLN}$$

i.e. $\dfrac{V}{2^B - 1}$ or $\dfrac{V}{255}$

where:

V is the voltage full scale setting of the transient recorder,

RESOLN is 'the dynamic range of the transient recorder - 1',

and B is the number of bits in each word (8).

This operation has been done through the subroutine READA or READAB (Appendix 4.C).

ii Separation of the DC Component from the Digitized Record:

Because the data points from the transient recorder are measured from an arbitrary DC level which varies from one record to another, the second step in the data processing procedure was to determine the mean value and then separate out the DC component before subsequent processing. This step has been done either through LEVA or LEVAB subroutines (Appendix 4.D) depending on the nature of the subsequent analysis. First, the total record mean value was calculated as:

$$\bar{x} = \frac{1}{N} \sum_{n=1}^{N} x_n'(t)$$

where N is the number of data samples (1024) and $x'(t)$ are the data values which have been converted as mentioned in (i). Second, the data values $x_n'(t)$ were transformed to have a zero mean value. The new time history record is defined as:

$$x_n(t) = x_n'(t) - \bar{x} \qquad n=1,2,\ldots\ldots N$$

The mean value of the new record $x_n(t)$ is now equal to zero.

The sample standard deviation in its time domain can now be calculated as:

$$\sigma_{xt} = \left[\frac{\sum_{n=1}^{N} x_n^2(t)}{N} \right]^{\frac{1}{2}}$$

In Chapter Two, this transformed data record was used in all the analysis.

4.4 SAMPLING AND DIGITAL PLOTTING

The digital representation of acoustic emission burst records is directly related to the burst signal waveform. Digitization techniques are all based on the sampling theory which says that any band-limited signal can be exactly reconstructed from samples taken periodically in time if the sampling rate is twice the highest frequency of the signal (160). In applying the sampling theorem to a digital acoustic emission waveform there are two main concerns; if the signal bandwidth is W in Hertz, then the sampling period must be;

$$\Delta T < \frac{1}{2W}$$

if the samples are represented as B-bit binary words, then the bit rate is

$$2\,B\,W \text{ bits/second}$$

In our system:

$W = 1$ MHz, $B = 8$ bits

therefore: The bit rate $= 16 \times 10^{6}$ bits/second

$\Delta T = 0.5 \times 10^{-3} / 10^{3}$ (number of samples in each record)

$= 0.5\ \mu s$

Therefore, the sampling period was kept in order of 1/2W(the Nyquist rate). Using the bandpass electronic filter, the highest frequency to be evaluated is restricted by (161):

$$F_{max} = \frac{1}{2\Delta T}$$

where T is the sampling period, i.e. the time interval between two successive points.

The computer programs were written to evaluate most of the acoustic emission parameters mentioned in Chapter Two. The programs were tested with standard functions which generate test data arrays instead of the experimental data files. Both the resulting numerical values and plotted graphs were found to be satisfactory. The programs are fully interactive and made use of the full data file capability of the DEC-20 system. In addition to acoustic emission applications, the programs can handle any time based data.

Throughout the computer programs, the plot format is controlled to produce A4 size graphs if the plotting factor is made zero (or return value. If 0.8 is given instead it results in a half A4 paper size plot. In both cases zero (or return) must be given to the "TEKPLT" factor request in subroutine STARTP (Appendix 4.E).

To increase the plotting resolution, the number of points to be plotted can be selected. Once any plotting program is run, the plotting instructions are stored in a plot file named PLOT.PLT, which can be used to view the plot file graphs on the graphics terminal using the computer system command:

@ RUN RGT:TEKPLT

and if the screen plot is found to be satisfactory a hard copy may be produced by using the system command:

@ PLOT

In the same way as the data file, the plotting file PLOT.PLT is temporary and should be renamed to be a coded permanent file before using the command @ PLOT.

PART FOUR

RESULTS, DISCUSSION AND CONCLUSIONS

CHAPTER FIVE

THEORETICAL AND EXPERIMENTAL DETERMINATION OF THE TRANSMISSION CHARACTERISTICS OF TRANSDUCTION MULTILAYER SYSTEMS

5.1 INTRODUCTION

In Chapter Three, theory was developed considering the transmission of ultrasonic waves normally travelling through a system of multilayers. Here, theoretical calculations and experiments are reported which attempt to verify and assess the suitability of this theory in explaining the behaviour of acoustic emission transducers. Experiments are also described which attempt to verify the effect of changes in multilayer parameters on quantities commonly measured to quantify acoustic emission signals.

Some of the existing commercial transducers will be considered in detail to emphasise the effect of the couplant layer on the transducer response. In the experimental sections, the couplant medium as well as thickness are regarded as variable parameters. To avoid the problems arising from the transmission block resonances, the six-layer transmission system will be also investigated for water and silicone grease as couplant layers.

It was assumed in Chapter Three that the transducer components are of infinite extent in the lateral dimensions. Therefore, it is important to maintain these dimensions at least of order of magnitude of the corresponding wavelength. This restriction was limited the validity of the analysis presented to frequency above 400 KHz.

5.2 PRESENTATION OF DATA

The four transmission models discussed in Chapter Three were programmed to yield the sound pressure transmission coefficient as a function of frequency. The pressure transmission coefficient, α_{pn}, is plotted on a decibel scale as the PTC level, i.e.:

$$\text{PTC (in dB)} = 20 \log_{10} \alpha_{pn}$$

$$= 20 \log_{10} |An/A_1| \qquad (5.1)$$

where α_{pn} is the calculated value of the PTC for n layers. The physical and acoustical properties of materials used in the theoretical analysis are listed in Appendix 5.A.

As the investigation progresses to consider the four-five-and six-layer models only the couplant layer was considered as a variable parameter in each model.

It should be stressed that the transmission theory is only applied to calculation of the net transmission coefficient and not the absolute value of the output voltage or current from acoustic emission transducers. Techniques involving the output voltage or current would need to include the piezoelectric transduction process in the analysis.

5.3 USE OF THREE-LAYER TRANSMISSION THEORY

One of the most used multilayer theories is that for three layers. This model provides both direct insight into sound transmission and the transmission coefficient is easily evaluated. Many different combinations of media may be explored in a short time. One can also divide any complex system into three-layer sub-systems by neglecting the effect of one or two layers. This approximation, however, is reasonable enough for single frequency transducers such as those employed for ultrasonic non-destructive testing (154,162). In acoustic emission it is impossible to estimate the source central frequency and a wide frequency band must be used in most monitoring situations.

In these circumstances, the three-layer model has restricted application to acoustic emission transduction. The model can only be used at the preliminary investigation stage of a very narrow-band transducers. However, it is useful in selecting a suitable material for the transducer shoe.

Equation (3.36) was programmed (CPNG3.FOR Appendix 5.B) to plot the PTC level as a function of frequency for variation of layers combinations. Each figure represents one three-layer combination.

The first is assumed to be in an infinite extent in the direction opposite to the wave propagation and the second (having four arbitrary thicknesses of 1, 2, 3 and 5 mm) represents the transducer shoe. The third medium consists of the PZT-element and is assumed to be of an infinite extent into the direction of the wave propagation, so that no account is taken of waves interference between the transmitted wave and the reflected from the rear surface. This assumption is applicable to a perfectly damped transducers and with the piezoelectric elements operating at the thickness mode. In all graphs the plotting resolution is 2 KHz.

5.3.1 COUPLANT-SHOE-PZT APPROXIMATE MODEL

This arrangement represents a simple transducer structure and considers different transducer couplant media, various transducer protective shoes combined with a PZT-5A piezoelectric element. The effect of the material being monitored and the couplant thickness are ignored at this stage.

Figures 5.1 (a-d) show the calculated variations of PTC level with frequency for silicone grease couplant. In Fig. 5.1 (a), the PTC level is calculated for four thicknesses of aluminium shoe. The minimum PTC level (valley) is 5.75 dB and the maximum value is 10.82 dB. For the thin aluminium shoe (1 mm), the PTC increases slowly with frequency and generally its PTC level values are the lower than those for other shoe thicknesses over the whole frequency

FIGURE 5.1 : Curves of Theoretical Pressure Transmission Coefficient Level Plotted Against Frequency for a Three-layer System:

Silicone Grease-Shoe-PZT

(a) Silicone Grease-Aluminium-PZT
(b) Silicone Grease-Stainless Steel-PZT
(c) Silicone Grease-Epoxy-PZT
(d) Silicone Grease-Perspex-PZT

Keys:

Symbol	Shoe Thickness (mm)
o	1.0
Δ	2.0
+	3.0
x	5.0

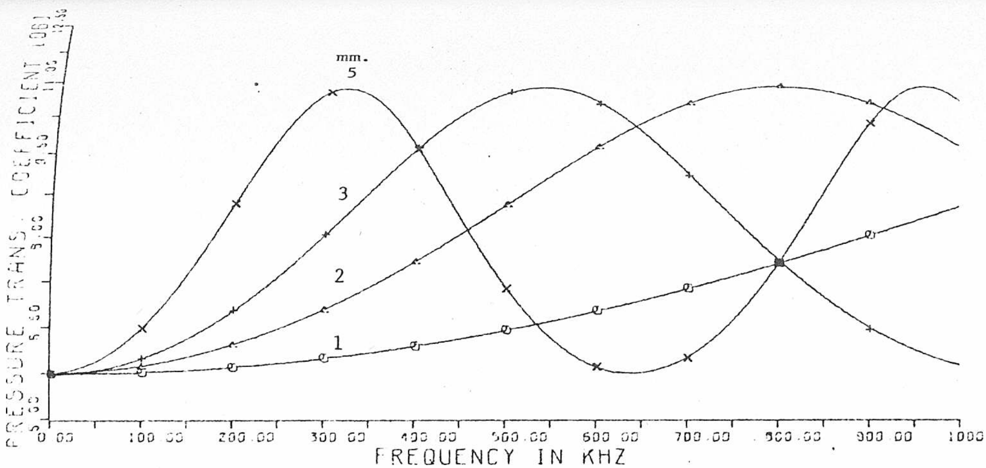

FIG. 5.1 (a) : Silcone Grease - Aluminium - PZT

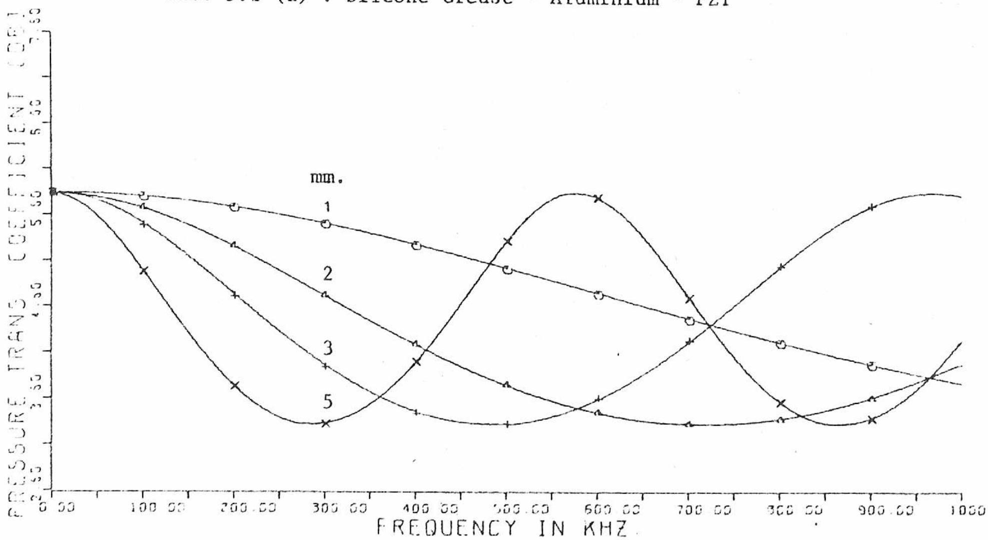

FIG. 5.1 (b) : Silicone Grease - Stainless Steel - PZT

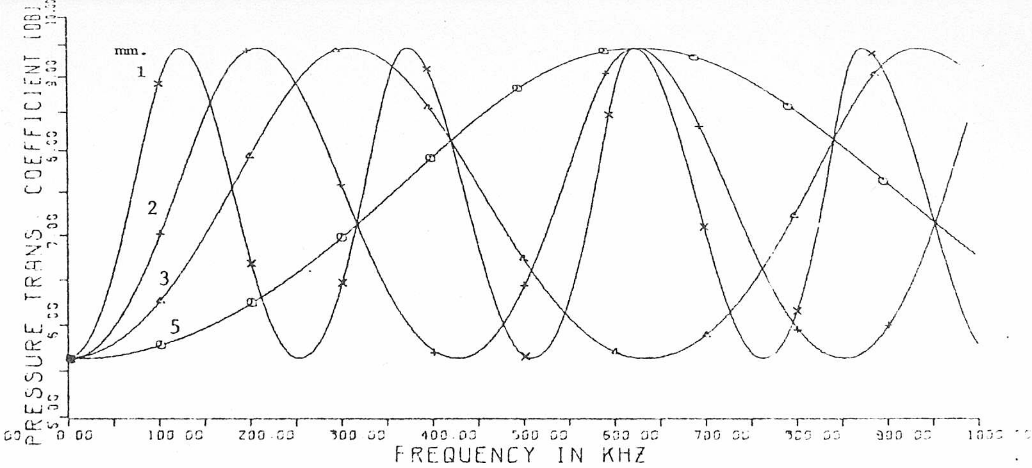

FIG. 5.1 (c) : Silicone Grease - Epoxy - PZT

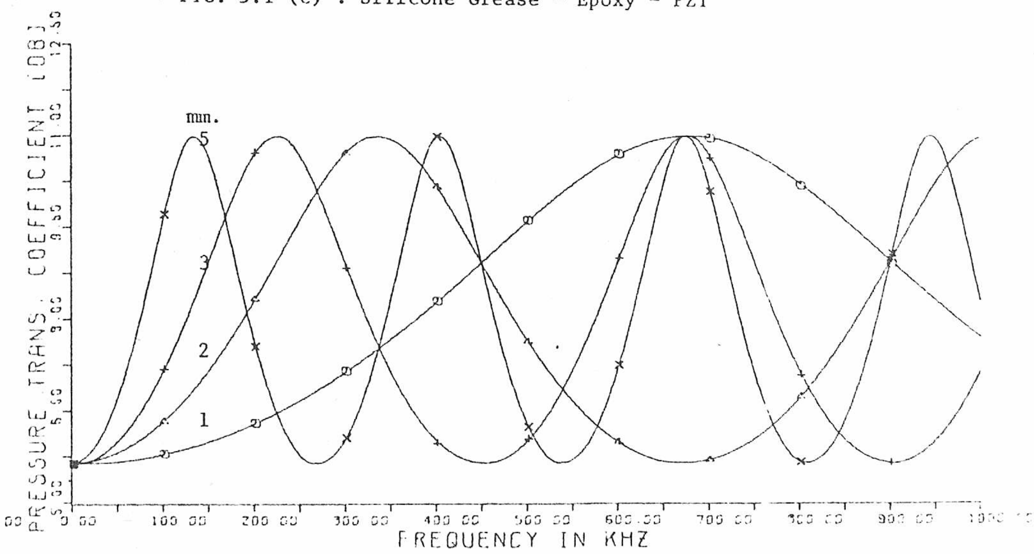

FIG. 5.1 (d) : Silicone Grease - Perspex - PZT

band. It is also the only curve which shows no resonances within the frequency range of interest, as the first transmission peak occurs beyond the highest frequency considered (1.6 MHz). As the thickness increases the frequency of the PTC peak moves down in frequency and its bandwidth decreases. Obviously to improve the resonance transducer efficiency, using an aluminium shoe, the thickness of this layer should be carefully chosen. For example, 2 mm aluminium shoe should be employed with resonance transducer of 800 KHz central frequency. Similarly, a 500 KHz resonance transducer should have 3 mm aluminium shoe. Generally, one can say aluminium shoes exhibit PTC peaks corresponding to the integer odd number of quarter-wavelengths ($n\lambda_2/4$). Then, the PTC resonance frequencies can simply be calculated as:

$$f_r = n\ C_2/4\ \ell_2 \tag{5.2}$$

where:

- n is an odd integer number (1, 3, 5, ...),
- C_2 is the longitudinal wave velocity in the second medium, and
- ℓ_2 is the thickness of the second layer.

Referring to Tables 4.I, 4.II and 5.A (Appendix 5.A) for Z values. Equation (5.2) can be applied, in general, when:

$$Z_1 < Z_2 < Z_3 \tag{5.3}$$

Fig. 5.1(b) shows the case for a stainless-steel shoe. The PTC peak frequencies appear at values corresponding to the stainless-steel half wavelengths, i.e.:

$$f_r = m\, C_2/2\ell_2 \tag{5.4}$$

where m = 1, 2, 3, ...

It is clear that the system impedance arrangement takes the form:

$$Z_1 < Z_2 > Z_3 \tag{5.5}$$

In this transmission system, the PTC curves have maxima of 5.75 dB and minima of 3.2 dB. In this case, the PTC level decreases as frequency increases in the low frequency range (0-300 KHz).

Figure 5.1(c) shows the case for an epoxy resin shoe. In this case, the acoustic impedances obey the inequality given by equation (5.3), i.e.: $Z_1 < Z_2 < Z_3$. The PTC peak frequencies correspond to f_r in equation (5.2), i.e.: they exist for quarter-wavelength resonance of the epoxy resin layer. The curves show that using epoxy resin, as a transducer shoe, the PTC level increases and the transducer becomes more efficient in comparison with those having a stainless-steel shoe. In this case one can see narrow-band transmission peaks. For the thicker shoe more peaks occur in the same bandwidth and the difference between the PTC maxima (peaks) and minima (valleys) is larger than those for metallic shoe.

The sound PTC curves for perspex shoes shown in Fig. 5.1 (d) are similar to those of epoxy resin as the acoustic impedances of both materials are similar.

Figures 5.2 (a-d), show the calculated PTC transmission curves using glycerine (ρ = 1260 $Kg.m^{-3}$) as couplant and aluminium, stainless-steel, perspex and plastic as different transducers shoes having different thicknesses. Although the general characteristics of these graphs are much the same as those which calculated for silicone grease (Figure 5.1) it can be seen that the maximum PTC values are lower (in particular with perspex shoes, down from 13.3 dB for silicone grease couplant to 7.2 dB using glycerine couplant). In the case of metallic shoes, the difference appears to be very small (a fraction of a decibel). This is simply because the change in Z_1/Z_2(see equation (3.36)) is too small to effect the results. The PTC curves for the case of epoxy resin are not given as the acoustic impedance of glycerine and epoxy are the same so that no reflection will occur at the glycerine/epoxy boundary. A flat PTC curve (5.4 dB) would occur in this case.

These curves suggested that the transducer shoe materials may be classified into the following groups:-

FIGURE 5.2 : Curves of Theoretical Pressure Transmission Coefficient Level Plotted Against Frequency for a Three-layer System:

Glycerine-Shoe-PZT

(a) Glycerine-Aluminium-PZT
(b) Glycerine-Stainless Steel-PZT
(c) Glycerine-Perspex-PZT
(d) Glycerine-Plastic-PZT

Keys:

Symbol	Shoe Thickness (mm.)
o	1.0
Δ	2.0
+	3.0
x	5.0

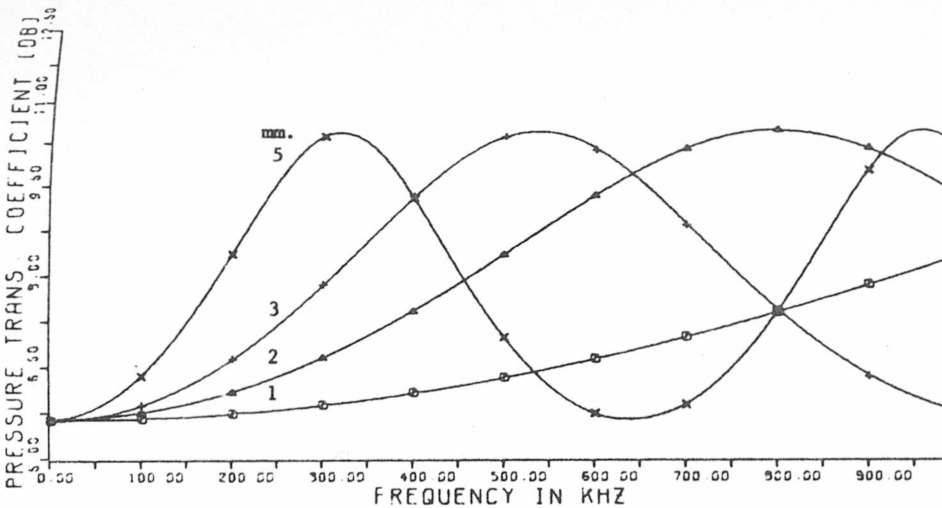

FIG. 5.2 (a) : Glycerine - Aluminium - PZT

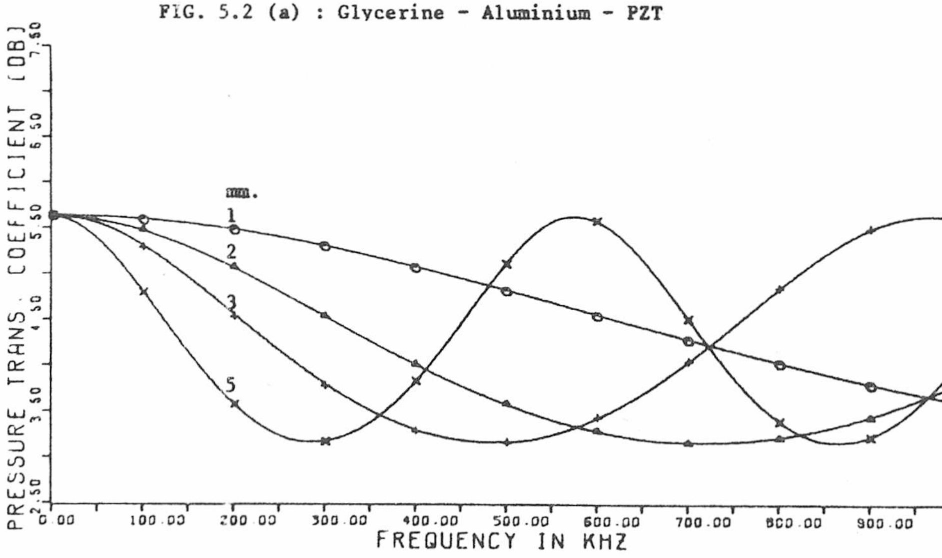

FIG. 5.2 (b) : Glycerine - Stainless Steel - PZT

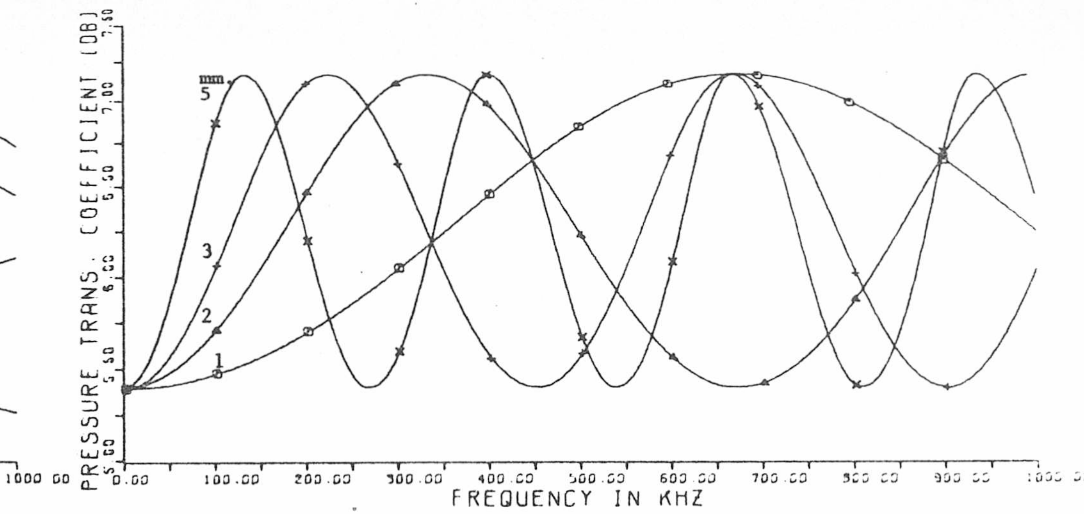

FIG. 5.2 (c) : Glycerine - Perspex - PZT

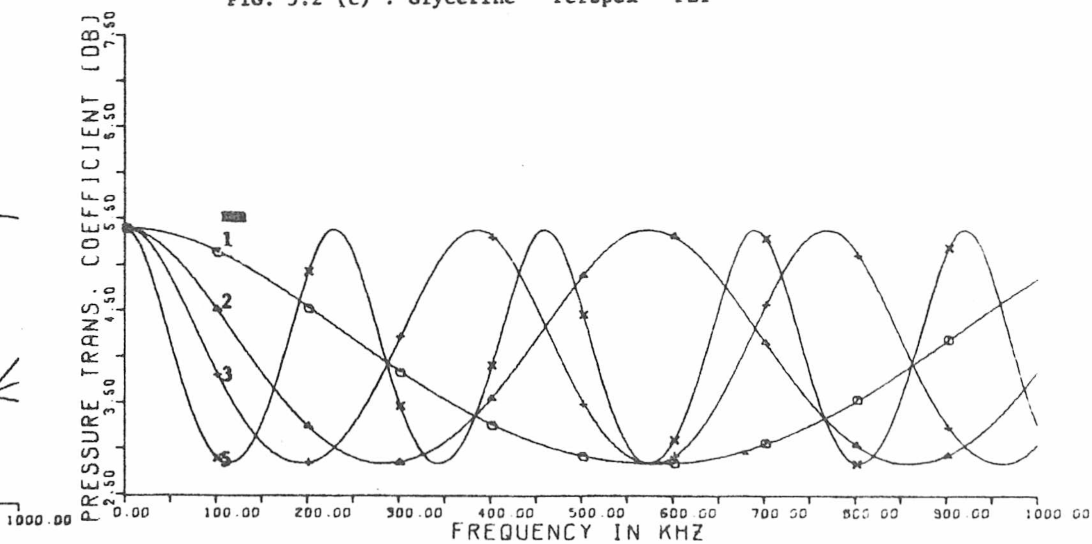

FIG. 5.2 (d) : Glycerine - Plastic - PZT

i - Polymer Shoes: (such as perspex, epoxy resin, and polystyrene). The acoustical characteristics of these materials and the couplant layer are alike and both are smaller than those for the PZT-element. In this case, the PTC curves are characterised by PTC peaks with a narrow bandwidth and larger differences between maxima and minima. At low frequency range (0-120 KHz), the sound PTC increases with frequency. The resonant frequency can be simply calculated by equation (5.2) for quarter-wave resonance. The characteristic impedance values generally follow the order $Z_1 < Z_2 < Z_3$. An example of a different arrangement in this group is glycerine-plastic-PZT system shown in Fig. 5.2(d), where the characteristic impedance arrangement takes the form:

$$Z_1 > Z_2 < Z_3 \tag{5.6}$$

This impedance arrangement is similar in effect to the arrangement $Z_1 < Z_2 > Z_3$ (although medium 2 boundary conditions differ) as only the net transmission coefficient is concerned. In this case, the plastic shoe would yield the same shape transmission curves as that for the 'metallic group' (e.g. stainless steel shoe). The similarity can be seen by comparing Figures 5.2(b) and 5.2(d). Further comparison will be made in the next Section.

ii - Light Metal Shoes: This group includes metallic shoes whose acoustic impedance is smaller than that for PZT-element. The impedance arrangement of the transmission system will remain similar to those for the polymer group (i.e.: $Z_1 < Z_2 < Z_3$). An aluminium shoe is an example of this group. The main characteristic of this group is the effect of the large wave velocity on the transmission peaks. It can be seen from Figure 5.1(a) that the PTC peaks have a wider frequency bandwidth than for the case of polymer shoes. Also, the maxima and minima are in the same order as those for polymer group.

iii - Metallic Shoes: This group represents a well known transmission system which is similar to the case of an immersed solid-plate in water or a liquid discussed by many authors (147,149). The system impedance arrangement is $Z_1 < Z_2 > Z_3$, and the peaks frequencies appear at the shoe half-wavelength as given in equation (5.4). The PTC values decrease with frequency at low frequency band (0 $\sim$ 120 KHz) and the peak PTC value is lower than the corresponding value for polymers and light metal shoes. On the other hand, the difference between maxima and minima is much smaller and the peak bandwidth is much larger than those for the previous groups.

Table 5.I summarizes the main features of different shoe groups. The optimum shoe thickness are calculated for different materials to achieve maximum PTC at 140 KHz and 750 KHz. These are the nominal resonant frequencies of the transducers used in this study. The calculated values for metallic shoes at 140 KHz are shown to be impractical. The table also indicates the second harmonic thicknesses for some polymer shoes when the fundamental is less than 1 mm thick. The calculated features for water and oil as couplant are also presented for comparison.

5.3.2. COUPLANT AND TRANSDUCER SHOE OPTIMIZATION

An approximate method to optimize a transducer shoe thickness can be carried out by using the three-layer transmission model. The model is also useful for preliminary investigation on the effect of the couplant media and the transducer shoe material on the frequency spectra and the expected transducer sensitivity. In this section, three couplant media have been considered with nine different shoe materials. The transducer central frequency is assumed to be 750 KHz, and the shoe thickness was optimized to achieve a maximum PTC at this frequency. Equation (3.36) was programmed (DTHREE.FOR and CPDC3.FOR; Appendix 5.C) to allow for different central frequencies as well as different couplant and shoe characteristics to be input.

TABLE 5.I Calculated PTC Values and Optimum Shoe Thickness

for Different Couplants and Transducer Shoe Materials

Transducer Sheo	Grease			Oil*			Water			Glycerine			Optimum thick, mm.	
	MAX. PTC	MIN. PTC	DIFF.	MAX. PTC	MIN. PTC	DIFF.	MAX. PTC	MIN. PTC	DIFF.	MAX. PTC	MIN. PTC	DIFF.	140 KHz	750 KHz
<u>Metallic Shoes:-</u>														
Steel	5.75	3.00	2.76	5.69	2.96	2.73	5.64	2.94	2.71	5.4	2.81	2.59	(21.44)	4.01
Stainless Steel	5.75	3.23	2.52	5.69	3.20	2.50	5.64	3.17	2.48	5.4	3.03	2.37	(20.69)	3.87
Copper	5.75	3.43	2.32	5.69	3.40	2.30	5.64	3.37	2.27	5.4	3.23	2.17	(17.90)	3.35
Brass	5.75	4.21	1.53	5.69	4.18	1.52	5.64	4.14	1.50	5.4	4.00	1.43	(16.8)	3.14
<u>Light Metal Shoes:-</u>														
Aluminium	10.82	5.75	5.07	10.63	5.69	4.93	10.46	5.64	4.82	9.66	5.4	4.26	(11.47)	2.15
<u>Polymer Shoes:-</u>														
Perspex	13.32	5.75	7.57	12.02	5.69	6.33	11.00	5.64	5.36	7.17	5.4	1.77	4.83	0.91 2.71
Epoxy	11.96	5.75	6.21	10.54	5.69	4.85	9.45	5.64	3.80				4.56	0.86 2.56
										5.4	5.4	0.0	any	any
Polystyrene	11.91	5.75	5.16	10.49	5.69	4.8	9.39	5.64	3.76				4.21	0.79 2.31
										5.4	2.84	2.56	8.22	1.54 3.08

PTC values are in dB

*Data are presented for oil with $Z_2 = 1.3 \times 10^6$ Kg s^{-1} m^{-2} and $C_2 = 1400$ m s^{-1}.

Figure 5.3 allows comparison of the transmission curves for silicone grease couplant and various shoe materials. The first optimum thickness (fundamental resonance) was used in calculation unless it was found to be less than 1 mm thick. In this case, the second harmonic thickness is considered. This is always the case for polymer transducer shoes. All transmission systems presented have approximately similar PTC values at very low frequency (i.e. when $\lambda_2 >> \ell_2$) or $k_2 \ell_2 << 1$ as well as when $k_2 \ell_2 \simeq n\pi$; i.e.: when $\sin k_2 \ell_2 \simeq o$ and $\cos k_2 \ell_2 \simeq 1$. By substituting in equation (3.36) with these values:

$$\alpha_{3p} = \frac{2Z_2}{Z_1+Z_3} \tag{5.7}$$

This expression coincides with the pressure transmission coefficient calculated for the case of transmission across a boundary between two media. Therefore, for very thin layers or at very low frequency, the PTC is independant on the intermediate layer properties and thickness. The calculated PTC value for silicone grease/PZT boundary using equation (5.7) is found to be 5.75 dB. This represents the system PTC at very low frequency and the minimum values for polymer and light metals (Al) transducer shoes (i.e.: for $Z_2 < Z_3$).

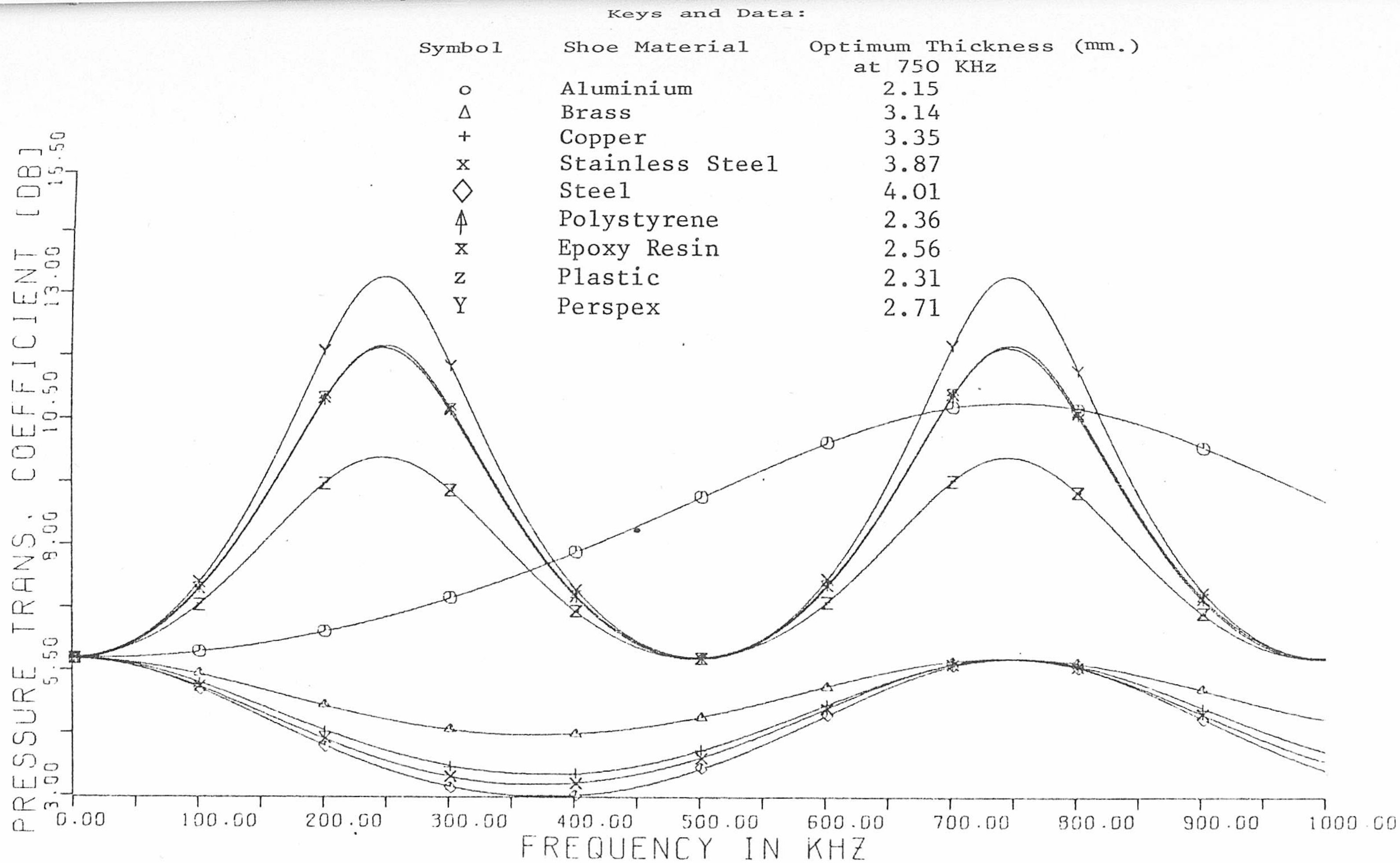

FIGURE 5.3 : Calculated Pressure Transmission Coefficient in dB versus Frequency. The Optimum Shoe Thickness is Calculated for 750 KHz.

System:

Silicone Grease-Shoe-PZT

Figure 5.4 shows the calculated PTC curves for water couplant. In comparison with silicone grease, the overall decrease in PTC values can be seen. This can be attributed to the increase of the Z_1/Z_3 ratio in equation (3.36). The maximum PTC of the aluminium shoe system becomes higher with respect to the epoxy and polystyrene shoe curves with no great change in the PTC curves for metallic transducer shoes (see Table 5.I for numerical values).

The case of using glycerine couplant (ρ = 1260 $Kg.m^{-3}$) is shown in Fig. 5.5. Generally, in comparison with the previous cases, all the curves show smaller PTC values over the whole frequency range. Aluminium appears to be the most efficient shoe in this case followed by the perspex shoe. Epoxy and polystyrene give almost constant PTC values close to 5.4 dB. This is because of the good acoustic matching between these materials and the glycerine couplant.

An interesting observation on the behaviour of the curve for the plastic shoe can now be made. Although plastic shoes have small characteristic impedance and longitudinal wave velocity ($Z = 1.8 \times 10^6$ $Kg.s^{-1}.m^{-2}$, C_L = 2300 m s^{-1}), the PTC values coincide exactly with the steel shoe curve in this case. Therefore, the method of calculating the PTC value for peaks and valleys would be similar to those for the metallic group.

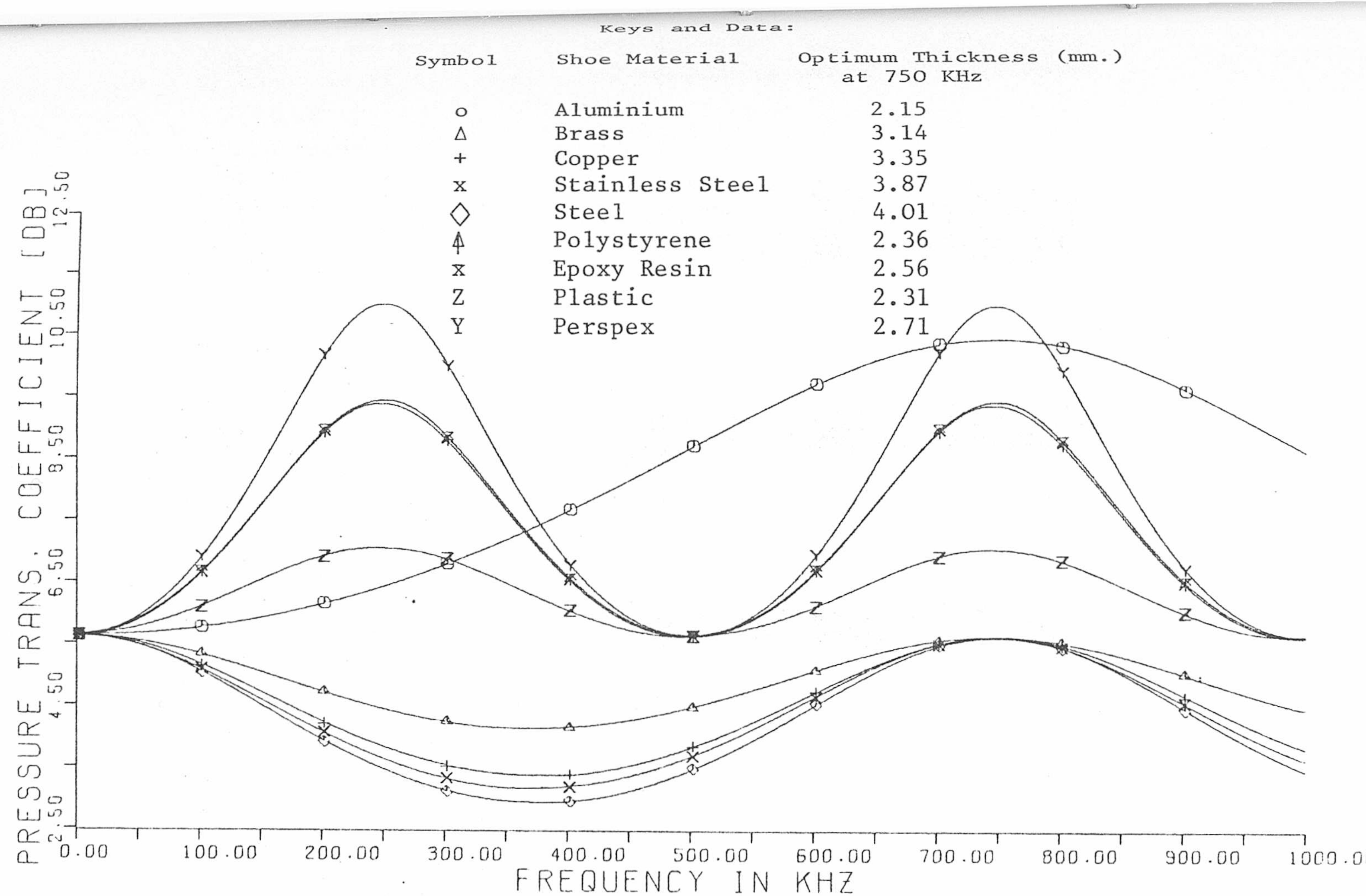

FIGURE 5.4 : Calculated Pressure Transmission Coefficient in dB versus Frequency. The Optimum Shoe Thickness is Calculated for 750 KHz.

System:

Water-Shoe-PZT

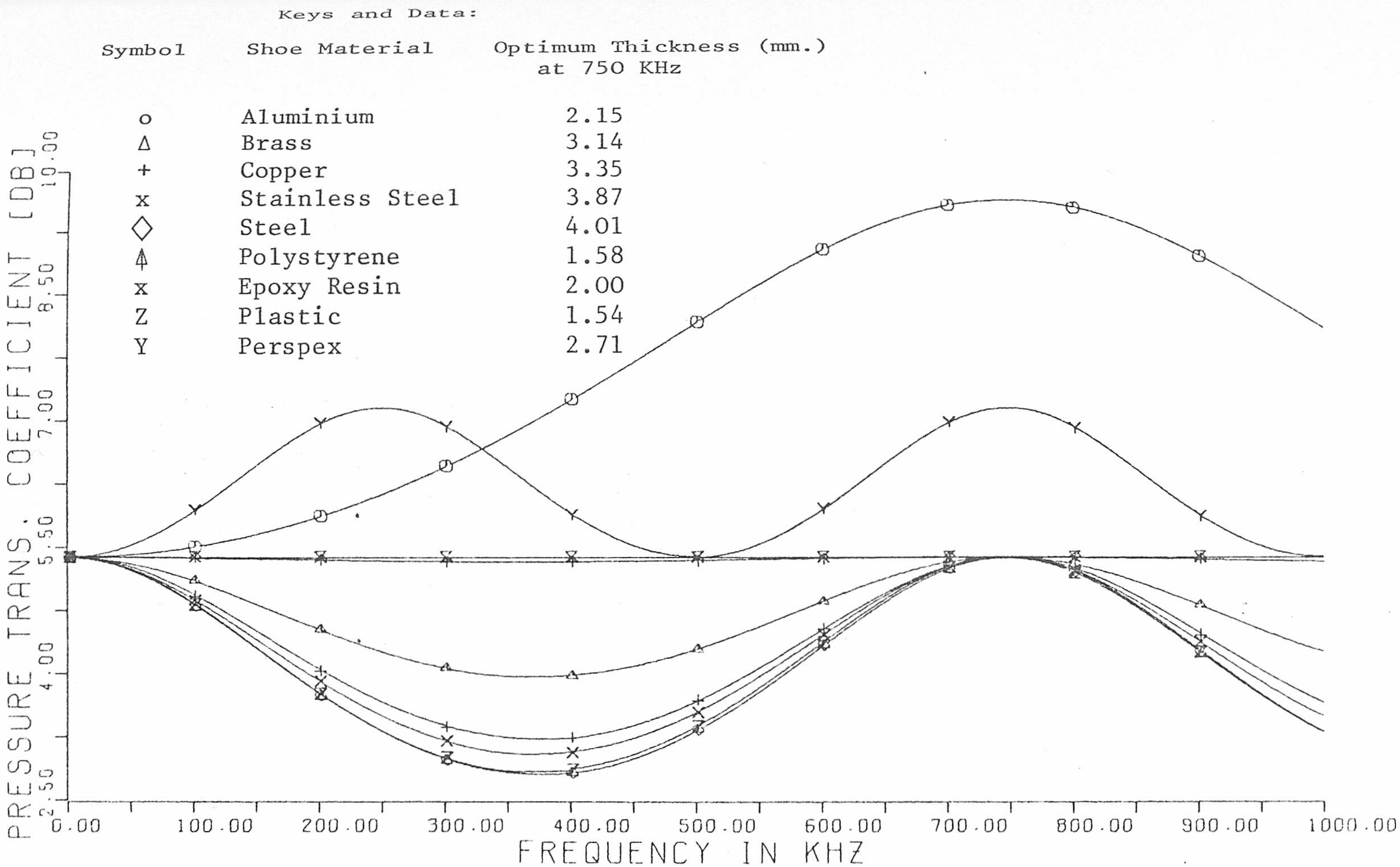

FIGURE 5.5 : Calculated pressure Transmission Coefficient in dB versus Frequency. The Optimum Shoe Thickness is Calculated for 750 KHz.

System:

Glycerine (1260 $Kg.m^{-3}$)-Shoe-PZT

It is worthwhile to mention also that for transducers having an epoxy protective shoe, it is likely to minimize the effect of couplant thickness on the received transducer response if glycerine is used as couplant. Indeed, as can be seen in Fig. 5.5, this advantage is at the price of the net transmission efficiency.

In summary, the optimum shoe thickness for polymer transducer shoes is found to be around 2.5 mm and most suitable for narrow-band resonant transducers. An aluminium shoe gives a similar transmission curves to a polymer shoe (as $Z_2<Z_3$). For these groups the maximum PTC may be directly calculated from equation (3.36) by substituting $\sin k_2\ell_2 = 1$ and $\cos k_2\ell_2 = o$, i.e.: from

$$\alpha_{3p} = \frac{2Z_2Z_3}{Z_2^2+Z_1Z_3} \tag{5.8}$$

which is dependent on the shoe acoustical properties. On the other hand, the minimum PTC value for these groups (equation (5.7)) is dependent only on the couplant layer and not on the shoe properties. For metallic transducer shoes the situation is the other way around, i.e.: the maximum transmission should be calculated from equation (5.7) and the minimum from equation (5.8).

5.3.3 PROPAGATION MEDIUM AND TRANSDUCER SHOE

In the earlier sections, the propagation of normal incident longitudinal wave from a couplant medium through the transducer protective shoe and PZT-element was discussed. In all cases the propagation medium has to be ignored. In this section, the three-layer transmission model is used to investigate approximately the effect of the propagation medium on the transmission characteristics when the couplant layer has to be neglected. The validity of this approximation is dependent on two essential assumptions; first, the couplant thickness is too small to be considered and second, the PZT-element is operated within a very narrow frequency-band around its thickness mode frequency.

Two common metals, steel and aluminium, are considered as examples of propagation media because of the significant difference between their acoustic impedances.

Figure 5.6(a) shows the pressure transmission coefficient curves of a hypothetical stainless steel shoe transducer which is loaded to steel medium. The fluctuations between maximum and minimum transmission are seen to be very small (0.03 dB) as the transducer shoe and propagation medium are well matched and the PTC level is centred around -1.55 dB. The optimum shoe thickness at 750 KHz is 1.94 mm. The case of aluminium shoe is shown in Fig. 5.6(b) with maximum PTC of -1.56 dB and with a -4.16 dB minimum.

FIGURE 5.6 : Calculated Pressure Transmission Coefficient in dB versus Frequency for a Steel Propagation Medium.

(a) Steel-Stainless Steel-PZT
(b) Steel-Aluminium-PZT
(c) Steel-Perspex-PZT
(d) Steel-Epoxy-PZT

Keys:

Symbol	Shoe Thickness (mm.)
o	1.0
Δ	2.0
+	3.0
x	5.0

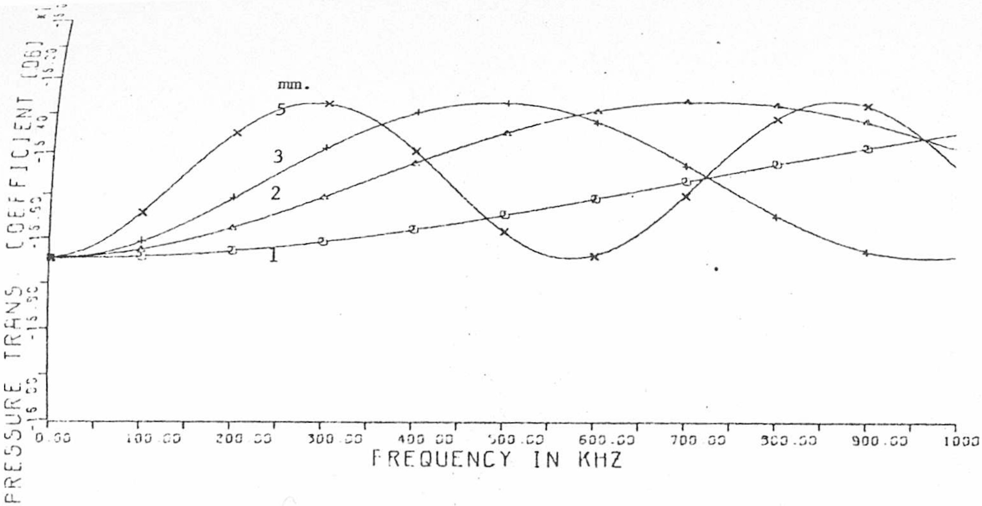

FIG. 5.6 (a) : Steel - Stainless Steel - PZT

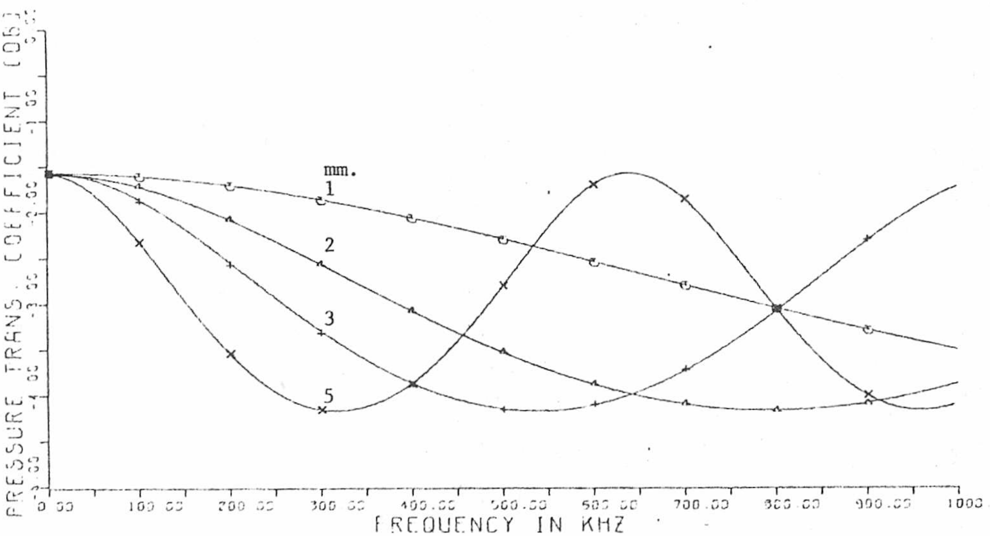

FIG. 5.6 (b) : Steel - Aluminium - PZT

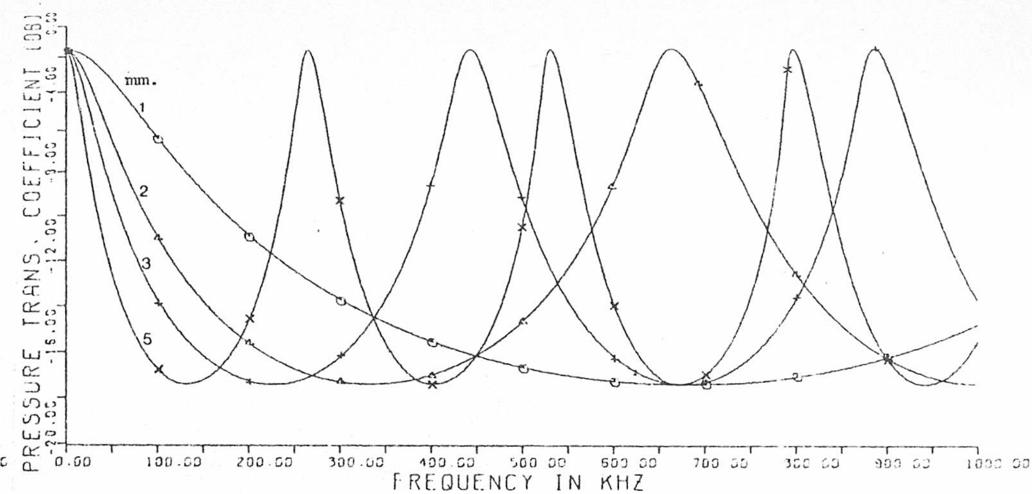

FIG. 5.6 (c) : Steel - Perspex - PZT

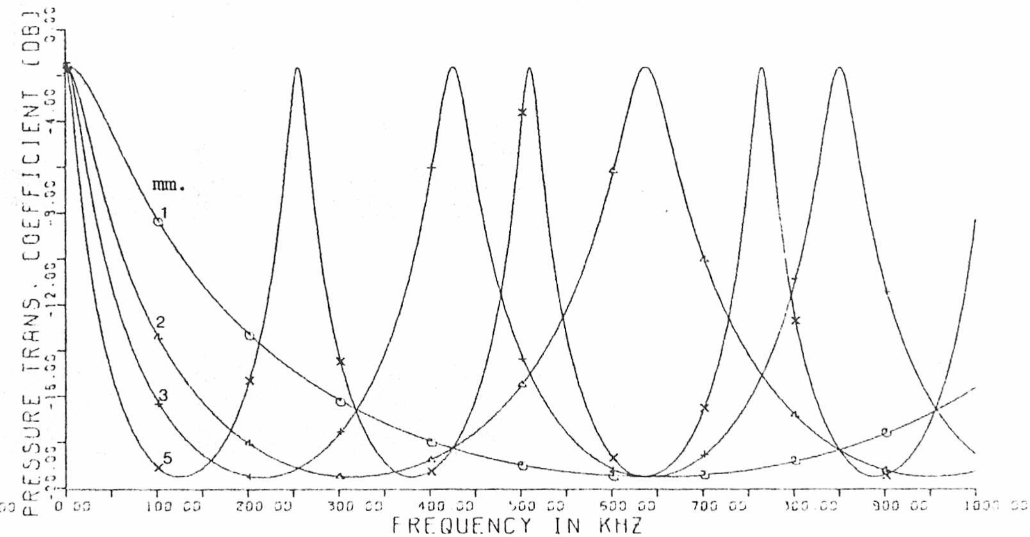

FIG. 5.6 (d) : Steel - Epoxy - PZT

Using different polymer shoes leads to approximately similar transmission curves, as these materials have smaller acoustic impedances compared to the propagation medium and PZT-element. The characteristics of the transmission/frequency curves for perspex and epoxy resin are illustrated in Figures 5.6 (c) and (d) respectively.

Figure 5.7 represents the calculated curves for different shoe materials using an optimum shoe thicknesses in order to achieve maximum PTC at 750 KHz central frequency. All curves are seen to have the same maximum values while the minima are dependent on the acoustic impedance of the shoe material. It is evident from the calculated results that the lower the acoustic impedance of the shoe material the sharper the transmission peaks in the PTC curves. Also the resonance peaks can be seen to be displaced towards the low frequency.

Similar transmission graphs are shown in Figures 5.8 and 5.9 for aluminium as a propagation body. In all cases, it is important to note that the maximum transmission coefficient is increased by about 2.4 dB compared to similar case for steel. Also the overall transmission values are higher over the frequency range. Table 5.II summarizes the main features of Figures 5.6-5.9.

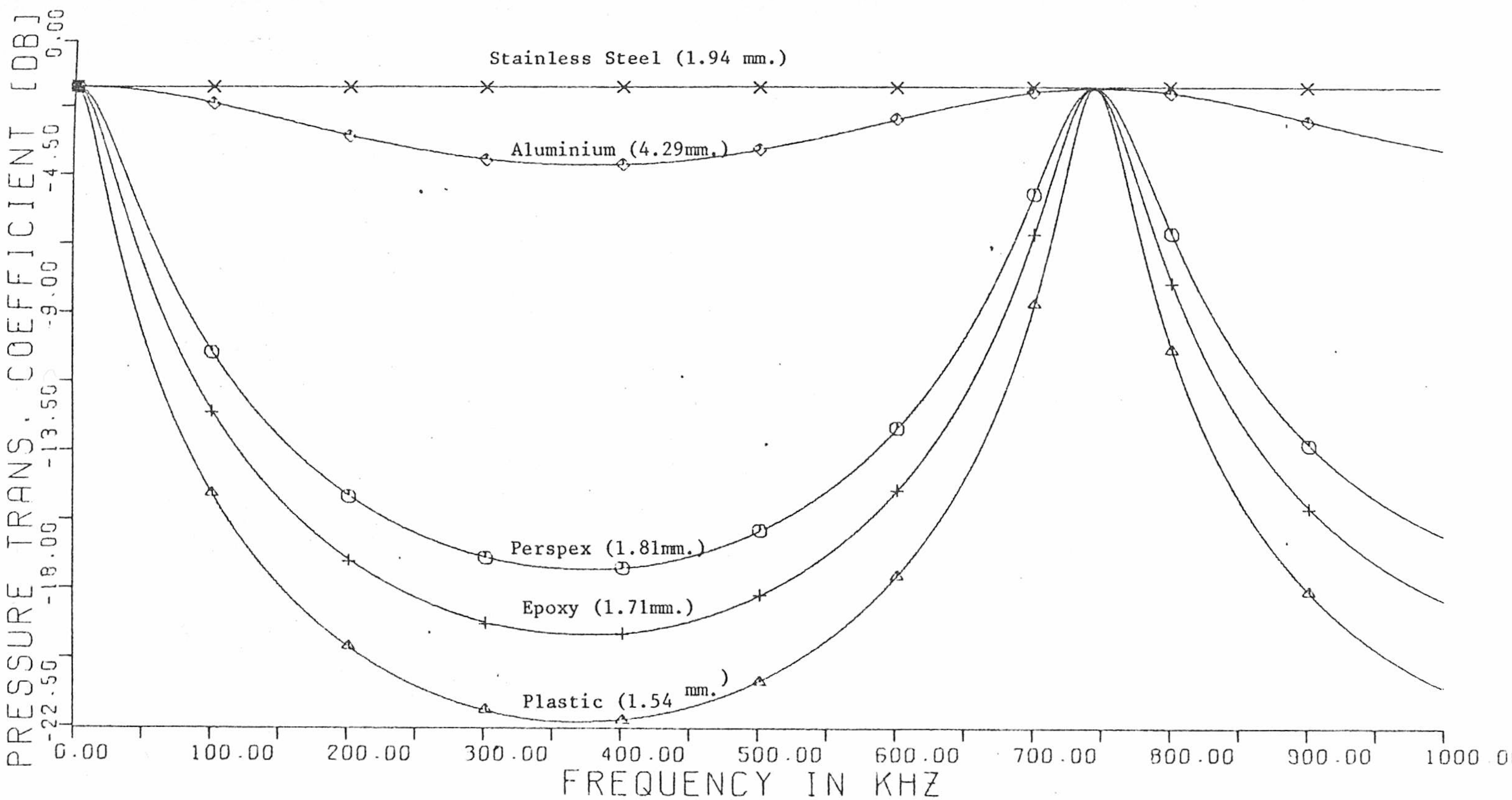

FIGURE 5.7 : Calculated Pressure Transmission Coefficient in dB versus Frequency for Steel-Shoe-PZT. The Shoe Thickness is Optimized to Resonate at 750 KHz.

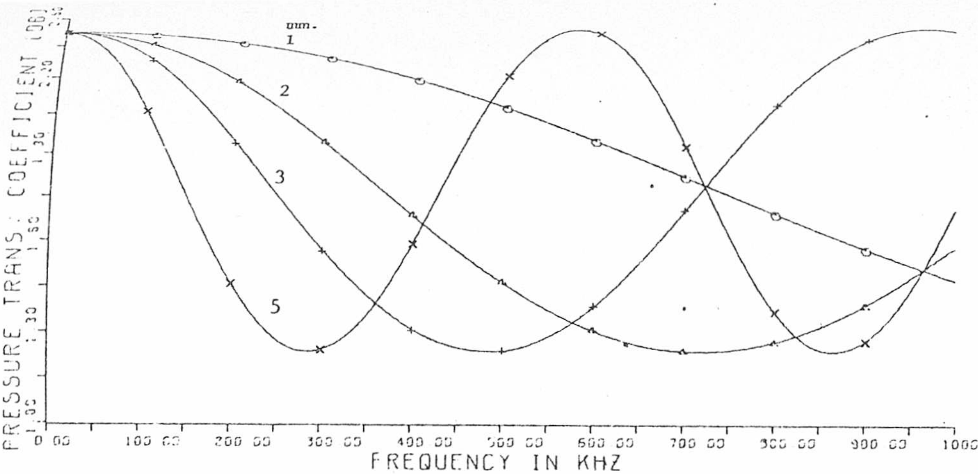

FIG. 5.8 (a): Aluminium - Stainless Steel - PZT

FIGURE 5.8 : Calculated Pressure Transmission Coefficient in dB versus Frequency for an Aluminium Propagation Medium.

(a) Aluminium-Stainless Steel-PZT
(b) Aluminium-Perspex-PZT
(c) Aluminium-Epoxy-PZT

Keys:

Symbol	Shoe Thickness (mm.)
o	1.0
Δ	2.0
+	3.0
x	5.0

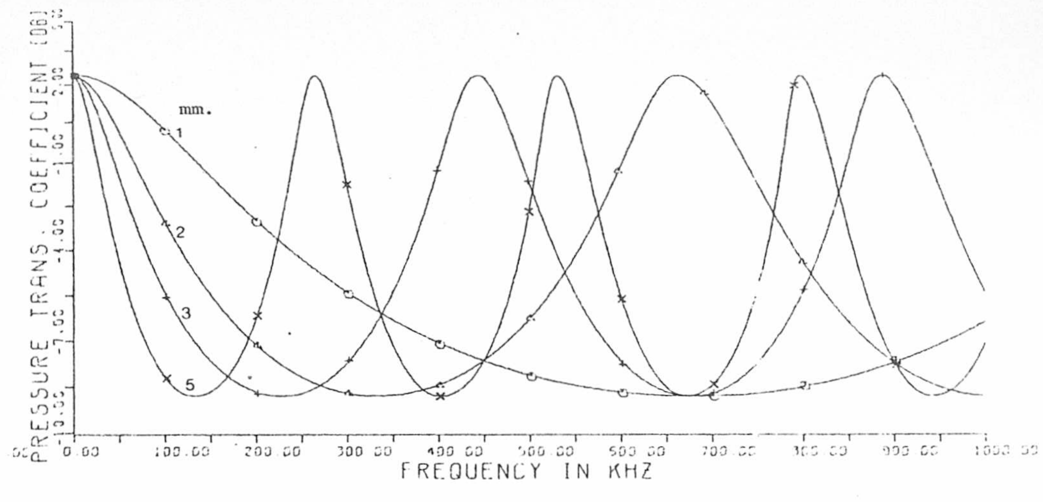

FIG. 5.8 (b) : Aluminium -Perspex - PZT

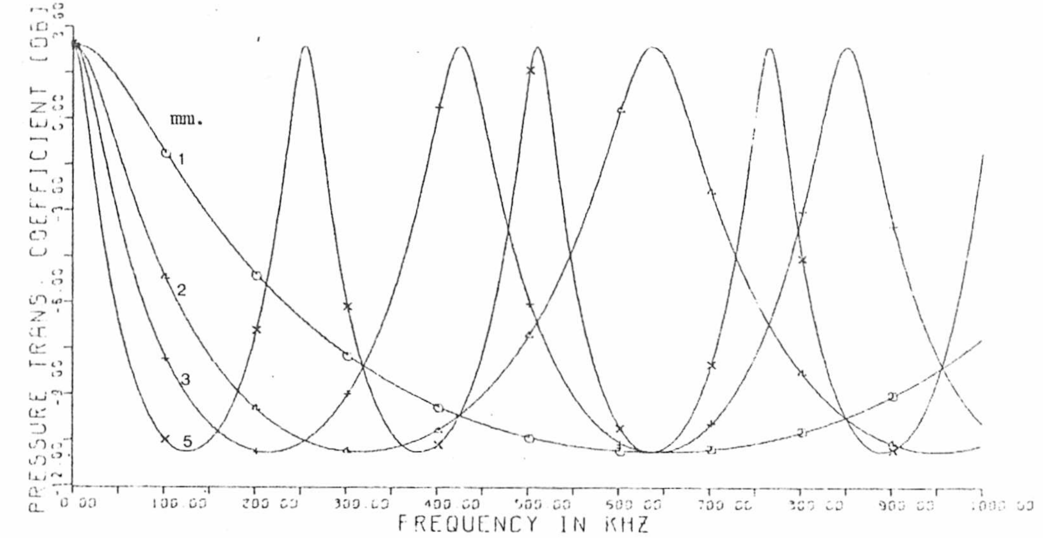

FIG. 5.8 (c) : Aluminium - Epoxy - PZT

Table 5.II The Variation of PTC Maxima and Minima for a Particular Propagation Medium (Summary of Figs.5.7-5.10) {for transmission configuration: Propagation body - Transducer shoe - PZT}

Propagation Medium	Transducer show	Max. PTC dB	Min. PTC dB	diff. dB	opt. shoe thick.mm (750 kHz)
Steel	Stainless Steel	-1.53	-1.56	0.03	1.94
	Aluminium	-1.56	-4.16	2.60	4.29
	Perspex	-1.56	-17.37	15.71	1.81
	Epoxy	-1.56	-19.50	17.94	1.71
	Plastic	-1.59	122.33	20.74	1.54
Aluminium	Stainless Steel	2.42	1.24	1.18	3.87
	Perspex	2.42	-8.79	11.21	1.81
	Epoxy	2.42	-10.87	13.29	1.71
	Plastic	2.41	-13.68	16.09	1.54

5.3.4 DISCUSSION AND CONCLUSIONS

The simple three-layer model allows a prediction of the transmission curves for a variety of transducer protective shoe materials and thicknesses. An analysis of the illustrated results allow us to form the following:

1. It is difficult to produce a reasonable broadband transducer by employing a polymer protective shoe. Although the polymer shoes increase the resonant transducer efficiency, they introduce a resonance peaks around the piezoelectric element thickness mode.

2. An aluminium metallic shoe could provide a relatively broadband transducer with better transmission efficiency. With correct calculation one can obtain the most efficient aluminium shoe thickness over the frequency-band of interest.

3. Using the three-layer model, it is found that the frequency characteristics of the acoustic emission transducer depends essentially on the ratios Z_1/Z_2 and Z_2/Z_3. Two impedance arrangements are possible:

i. Symmetric Impedance Arrangement in which;

$$Z_1 > Z_2 < Z_3 \text{ or } Z_1 < Z_2 > Z_3$$

In this arrangement, the peak characteristics become sharper when the quantity Z_2 (shoe) is chosen to be smaller. The gain in the PTC at resonance is accompanied by a decrease in the transmission bandwidth. It is possible, for this impedance arrangement, (when $\ell_2 = \lambda_2/2$ and $\ell_3 = \lambda_3/2$) to obtain a rise in the pressure transmission coefficient. On the other hand, the PTC value decreases as Z_2 becomes larger than both those for couplant and PZT-element and the transmission bandwidth increases.

ii. A Gradient Impedance Arrangement in which;

$$Z_1 < Z_2 < Z_3 \text{ or } Z_1 > Z_2 > Z_3$$

When the shoe material is chosen so that $Z_1 > Z_2 > Z_3$ the gain in the PTC at resonance reaches that for the symmetric arrangement and is accompanied by an increase in the transmission bandwidth. At low frequencies the PTC increases with frequency and it is possible, in this case, to obtain a rise in transmission for $\ell_2 = \lambda_2/4$.

4. Increasing the couplant acoustic impedance decreases the PTC of the transmission system. This is an important fact and should be taken into consideration when solid couplant is to be used for continuous structure monitoring. Although solid couplant will provide an effective means of mounting the transducer, it will reduce the monitoring system sensitivity.

5. For a particular narrow-band transducer operated at its piezoelectric element thickness mode, the PTC can be improved by optimizing the thickness of the protective shoe. The optimum thickness should be calculated by using an appropriate formula, i.e.: either the quarter-wavelength or half-wavelength depending on the system impedance arrangement.

6. Heavy metallic shoes should be avoided in designing acoustic emission transducers. Poor transmission curves always result in this case. However, an aluminium shoe could replace them if a broadband transducer is sought.

7. The maximum sound pressure transmission coefficient depends on both the acoustical properties of the material being monitored and the piezoelectric element and not on the shoe properties. This is an important phenomenon which indicates that at the shoe resonance thickness, the wave propagates through it without change in magnitude.

8. From the above comments, it can be seen that the aluminium block will be most suitable for our experimental investigation. It enhances the transmission of acoustic emission signals and consequently improves the signal-to-noise ratio.

5.4 THE FOUR-LAYER MODEL AND RESONANT TRANSDUCERS

Transducers operating in their thickness longitudinal resonant modes will be considered in this section. In the following analysis it will be assumed that the thickness of the transducer piezoelectric element is equivalent to $C_{PZT}/2f_o$, where C_{PZT} is the longitudinal wave velocity in the PZT-element and f_o is the operating frequency. In this case, the various media are arranged as follows;

Propagation medium→Couplant→Transducer shoe→Air backing, and the effect of the piezoelectric layer is omitted. This assumption can be realized by substituting $\sin k_2\ell_2 = o$ and $\cos k_2\ell_2 = 1$ in equation (3.36) for a simple three-layer system:

Transducer shoe 'medium (1)'→PZT(2)→Backing(3)

The resulting relationship is similar to that given by equation (5.7). Therefore, for a half-wavelength PZT-element the transmission system is independent of the characteristics of the element.

Figure 3.4 shows the transmission geometry employed in the computations. Equations (3.65) and (3.66) were used to compute the PTC curves for a resonant thickness mode "narrow-band" transducer (CPNG4.FOR; Appendix 5.D). In the results, the propagation medium was chosen as aluminium and the transducer shoe epoxy resin 3.125 mm thick. Silicone grease, water, glycerine (1260 $Kg.m^{-3}$ density) and adhesive tape were used as couplant with different thickness to predict their effect on the transmission curves.

Figure 5.10 shows the PTC curve for silicone grease couplant of 0.02, 0.1, 0.3, 0.5 and 1.0 mm thickness. It should be stressed again that all graphs presented in this section are only valid at a single frequency or very narrow-band corresponding to the piezoelectric element half-wavelength. Consider first the transmission curve for 0.02 mm thickness in which the effect of the couplant layer can be ignored. Three transmission peaks are seen at frequencies of 195, 590, and 985 KHz. It is clear that these peak frequencies correspond to the odd-multiple quarter-wavelength resonances of the transducer shoe which may be determined by:

$$f_p = \frac{(2n-1)}{4} \lambda_{shoe} \quad \text{where } n = o, 1, 2, \ldots .$$

as the system impedance arrangement is that of gradient type ($Z_1 > Z_2 > Z_3$). Table 5.III summarizes the transmission characteristics of Fig. 5.10.

Similar explanations can be given for the case of water and glycerine couplants. Figures 5.11 and 5.12 show the transmission curves for water and glycerine couplants. The characteristic features are summarized in Tables 5.IV and 5.V.

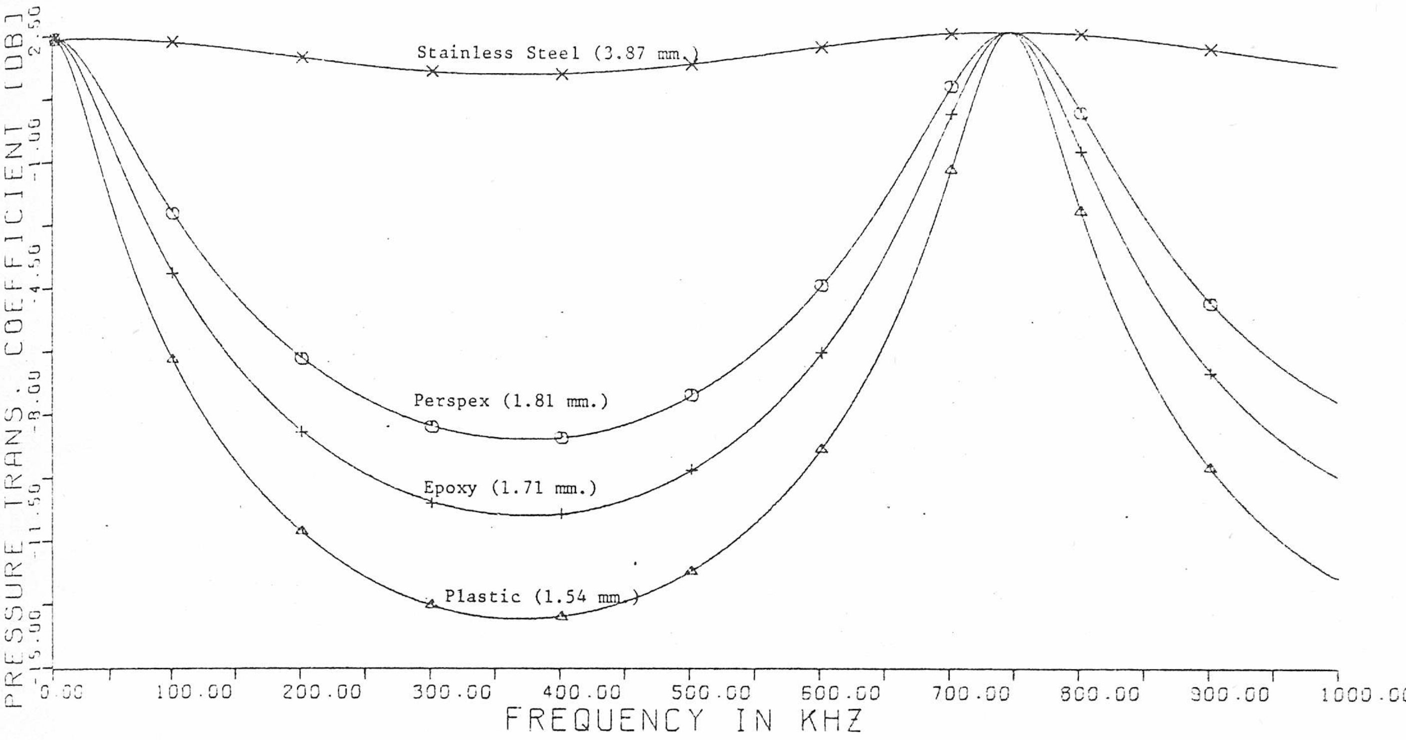

FIGURE 5.9 : Calculated Pressure Transmission Coefficient in dB versus Frequency for Aluminium-Shoe-PZT. The Shoe Thickness is Optimized to Resonate at 750 KHz.

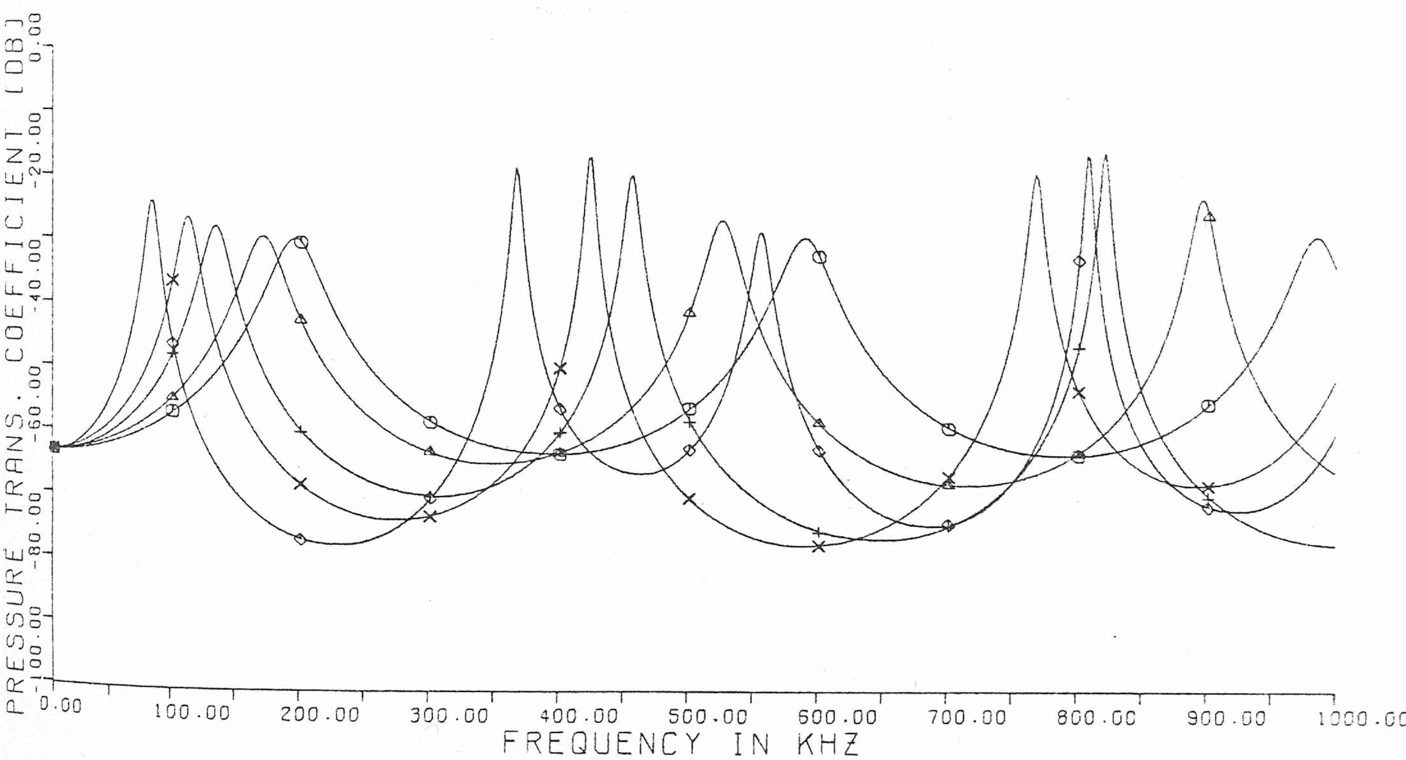

FIGURE 5.10 : Calculated PTC Curves for Resonant Transducers Using Silicone Grease Couplant of Thickness:

O = 0.02 mm., Δ = 0.1 mm., + = 0.3 mm., X = 0.5 mm., and ◇ = 1.0 mm.

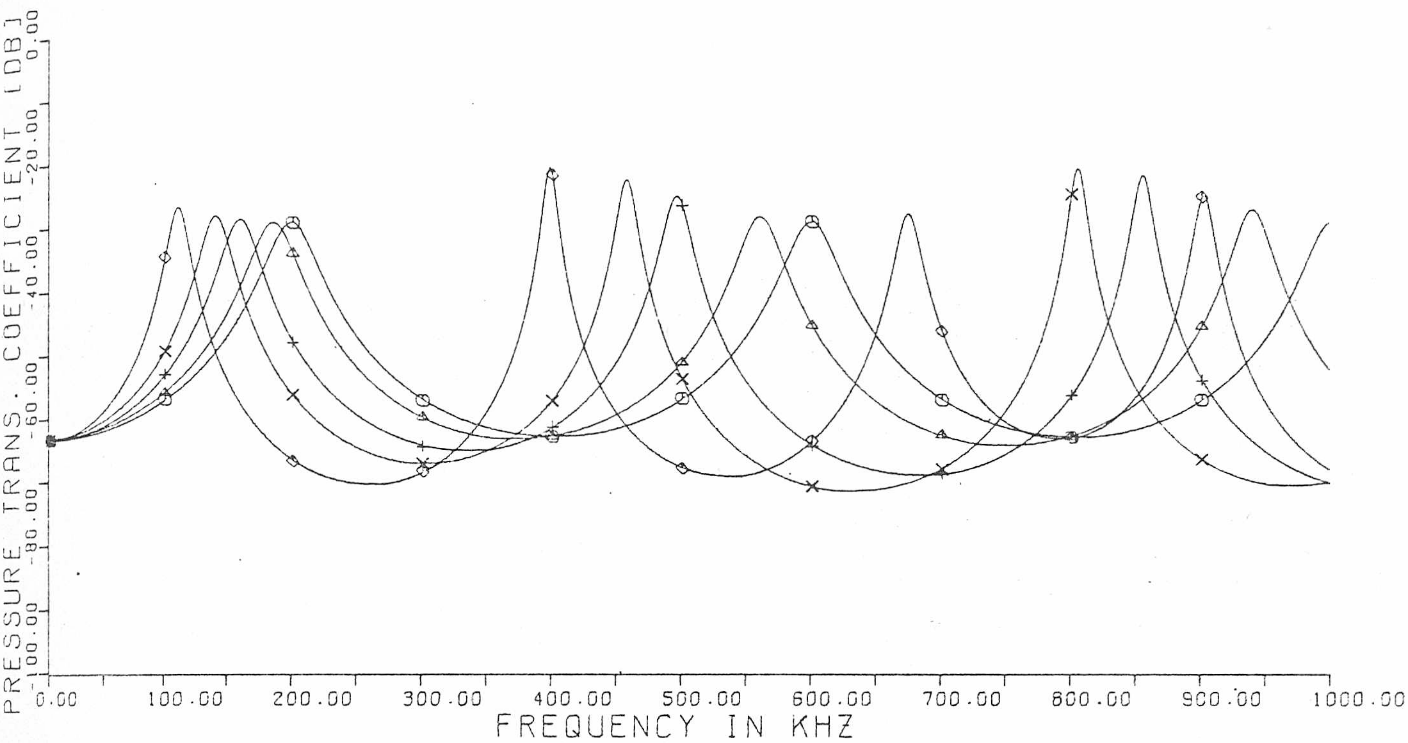

FIGURE 5.11:Calculated PTC Curves for Resonant Transducers Using Water Couplant of Thickness:

0 = 0.02 mm., Δ = 0.1 mm, + = 0.3 mm., X = 0.5 mm., and ◇ = 1.0 mm.

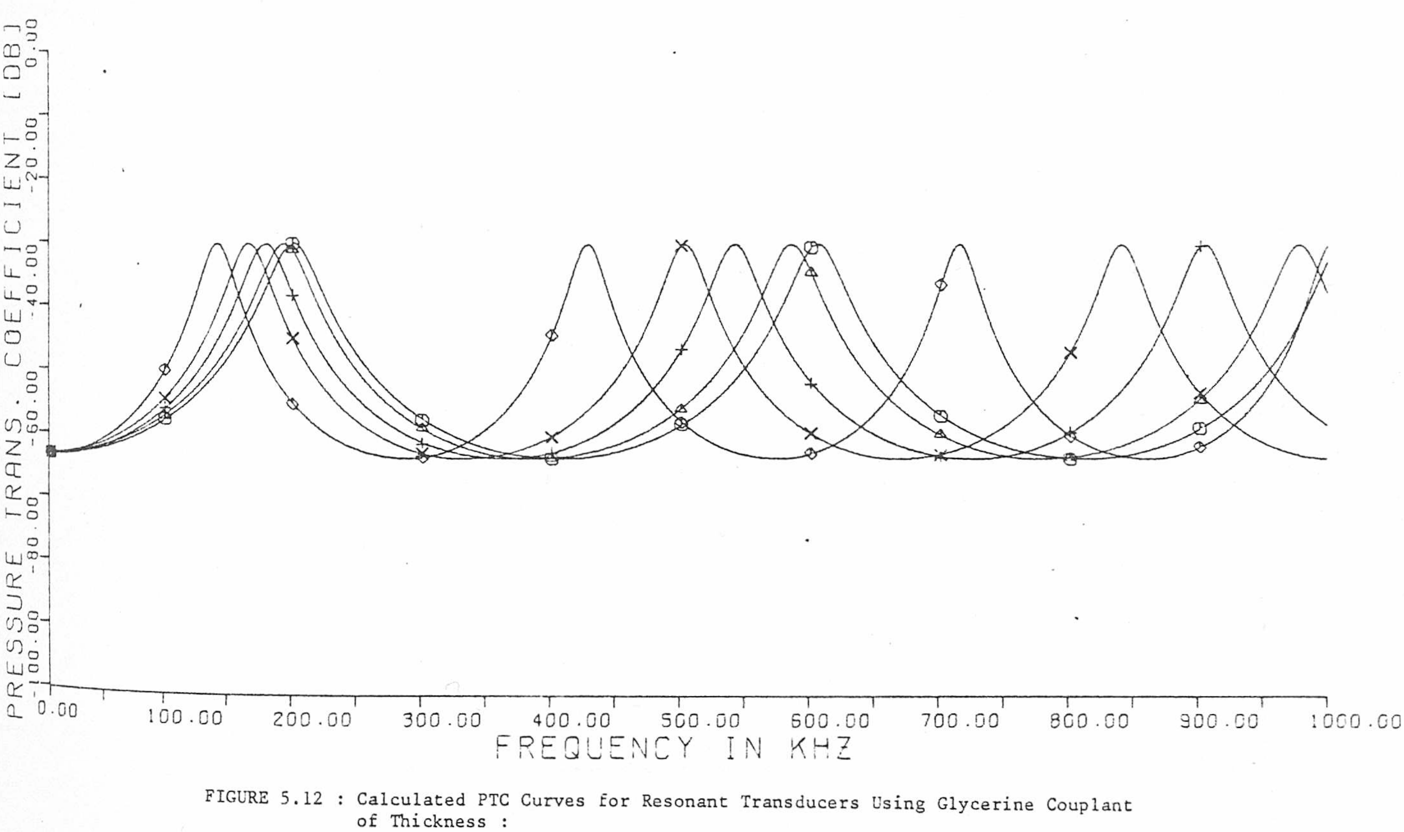

FIGURE 5.12 : Calculated PTC Curves for Resonant Transducers Using Glycerine Couplant of Thickness :

0 = 0.02 mm., Δ = 0.1 mm., + = 0.3 mm., X = 0.5 mm., and ◇ = 1.0 mm.

TABLE 5.III The Main Characteristics of the Transmission Spectra in Fig. 5.10 for Grease Couplant

Group	Couplant thickness (mm)	Frequency* KHz	PTC(dB)*	Group Remarks
1st Peaks	0.02	195	-29.8	PTC Range = 6.2 dB
	0.1	175	-29.5	Frequency Range = 110 KHz
	0.3	135	-27.8	
	0.5	115	-26.4	
	1.0	85	-23.6	
1st Valleys	0.02	.395	-63.3	PTC Range = 14.1 dB
	0.1	355	-64.7	Frequency Range = 165 KHz
	0.3	305	-69.8	
	0.5	280	-73.5	
	1.0	230	-77.4	
2nd Peaks	0.02	590	-29.5	PTC Range = 13.2 dB
	0.1	525	-27.0	Frequency Range = 220 KHz
	0.3	455	-21.3	
	0.5	425	-16.3	
	1.0	(1)370	-20.2	
		(2)555	-29.2	
2nd Valleys	0.02	785	-63.5	PTC Range = 14.0 dB
	0.1	720	-68.1	Frequency Range = 310 KHz
	0.3	645	-76.5	
	0.5	595	-77.5	
	1.0	(1)475	-65.9	
		(2)685	-74.5	
3rd Peaks	0.02	985	-29.2	PTC Range = 12.1 dB
	0.1	895	-23.7	Frequency Range = 430 KHz
	0.3	820	-17.1	
	0.5	770	-20.2	
	1.0	810	-17.2	

*Accuracy: ±2.5 KHz and ±0.05 dB

TABLE 5.IV The Main Characteristics of the Transmission Spectra in Fig. 5.11 for Water Couplant

Group	Couplant thickness (mm)	Frequency* (KHz)	PTC (dB)*	Group Remarks
1st Peaks	0.02	200	-29.7	PTC Ranges 2.0 dB
	0.1	190	-29.7	Frequency Range = 90 KHz
	0.3	160	-29.2	
	0.5	140	-28.8	
	1.0	110	-27.7	
1st Valleys	0.02	400	-63.2	PTC Range = 7.4 dB
	0.1	375	-63.6	Frequency Range = 140 KHz
	0.3	335	-65.4	
	0.5	305	-67.4	
	1.0	260	-70.6	
2nd Peaks	0.02	600	-29.7	PTC Range = 8.5 dB
	0.1	560	-29.1	Frequency Range = 200 KHz
	0.3	500	-26.1	
	0.5	460	-23.1	
	1.0	400	-21.2	
2nd Valleys	0.02	800	-63.2	PTC Range = 85 dB
	0.1	755	-64.6	Frequency Range = 365 KHz
	0.3	680	-69.2	
	0.5	635	-71.7	
	1.0	(1)535	-69.4	
		(2)790	-63.6	
3rd Peaks	0.02	-	-	PTC Range = 6.6 dB
	0.1	940	-27.7	
	0.3	855	-22.7	Frequency Range = 265 KHz
	0.5	805	-21.9	
	1.0	(1)675	-28.5	
		(2)905	-25.9	

*Accuracy: ±2.5 KHz and ±0.05 dB

TABLE 5.V The Main Characteristics of the Transmission

Spectra in Fig. 5.12 for Glycerine Couplant

Group	Couplant thickness (mm)	Frequency* (KHz)	PTC (dB)*	Group Remarks
1st Peaks	0.02	200	-29.8	PTC Range = 0.2 dB
	0.1	195	-29.8	Frequency Range = 55 KHz
	0.3	180	-29.7	
	0.5	170	-29.8	
	1.0	145	-29.9	
1st Valleys	0.02	405		
	0.1	390		Frequency Range - 120 KHz
	0.3	360	163.2	
	0.5	330		
	1.0	285		
2nd Peaks	0.02	605	-29.8	PTC Range = 0.2 dB
	0.1	585	-29.8	Frequency Range = 175 KHz
	0.3	545	-29.9	
	0.5	505	-29.7	
	1.0	430	-29.7	
2nd Valleys	0.02	810		
	0.1	785		Frequency Range = 235 KHz
	0.3	725	-63.2	
	0.5	675		
	1.0	(1)575		
		(2)860		
3rd Peak	0.02	-	-	PTC Range = 0.1 dB
	0.1	980	-29.8	Frequency Range = 265 KHz
	0.3	905	-29.7	
	0.5	840	-29.8	
	1.0	715	-29.7	

*Accuracy: ±2.5 KHz and ±0.05 dB

The following observations are made from the numerical results:

1. Increasing the couplant thickness increases the maximum PTC (peaks) values, e.g. in the case of grease couplant the first group peaks increased from -29.8 dB (PTC) to -23.6 dB and for water from -29.7 dB to -27.7 dB with no significant increase in the case of glycerine couplant (0.1 dB).

2. The transmission peak bandwidths are decreased as the couplant thickness increases. The thicker the couplant the sharper the peaks on the PTC curves. This characteristic is more pronounced in the cases of grease and water couplant than that of glycerine. The reason is that the glycerine has similar acoustical characteristics to the transducer shoe and therefore there is no great reflection or change in the transmitted wave phase at the couplant/shoe boundary.

3. Increasing the couplant thickness decreases the PTC values in the valleys (minimum transmission). These values are also decreased as the frequency is increased for a particular couplant thickness. However, this is not a general trend as for high frequency groups the valley PTC values may increase again (see the second valleys for 1.0 mm of grease, Table 5.III and the same for water couplant of 1.0 mm thickness).

4. Increasing the ratio Z couplant/Z_{shoe} to reach unity has the effect of decreasing the general PTC values over the frequency range. This effect can be seen, in particular, for the high frequency group of peaks for the thicker couplants; e.g. for a couplant thickness of 0.3 mm the second group peak amplitudes decrease from -21.3 dB for grease to -26.1 dB for water and to -29.9 dB for glycerine. This is always accompanied by an increase in PTC minima (valleys). For example, for the same 0.3 mm curves PTC minima increase from -76.5 dB for grease to -69.2 dB for water and to -63.2 dB for glycerine at the second group of valleys.

5. Achieving a good acoustic matching between the transducer couplant and shoe produces less variation in the peak amplitudes and bring the peaks or valleys closer. It can be seen that as $(Z_2/Z_3)\rightarrow 1$, the PTC ranges are reduced substantially from 14.1→6.2 dB for grease couplant, to 8.5→2.0 dB for water, and to 0.2→0.0 for glycerine couplant.

In conclusion, as one is trying to stop the couplant producing minimum perturbation of the transmission curves, it would be realistic to suggest glycerine as a couplant for use with the epoxy resin shoe. Although, glycerine was found to produce satisfactory results, there are problems when using it. In experimental work, it was always difficult to wet both the transducer shoe and the specimen surface. It was also difficult to use glycerine with surfaces not horizontal because it tends to run out from between the surfaces. Glycerine/water mix might also be unstable couplant as changes in density might occur during continuous monitoring due to evaporation.

A series of studies were carried out on some suitable couplant substances. It was found that 0.1 mm thick double sided adhesive tape made from the polymer PVC (Polyvinyl Chloride $CH_2:CHCl$) will produce exactly the same PTC curves as a corresponding layer of glycerine (with + 5 KHz frequency shift of the second and third frequency peaks). In addition, the PVC material has a good resistance to water, acids, alkalis, and alcohols. Another advantage of using the PVC adhesive tape is its large temperature resistance range. The couplant would withstand temperature down to -30° C and up to 45°C for long term monitoring or up to 65° C for a short time monitoring.

5.5 THE FIVE-LAYER MODEL AND ACTUAL TRANSMISSION PERFORMANCE OF ACOUSTIC EMISSION TRANSDUCERS

In practice, acoustic emission transducers in which a PZT piezoelectric element is attached to a plastic shoe are always employed over a range of frequencies. The actual acoustic event can not be considered to emit at a single ultrasonic frequency. Consequently, the transducers can not be chosen to match the event frequency. It is likely that the choice of an acoustic emission transducer is always an arbitrary process and there is no certainty that its resonant transmission characteristics will suit the particular source event. Therefore, in the investigations to follow Dunegan/Endevco commercial transducers will be tested against the theory in the frequency range of 0-1 MHz. This bandwidth covers the frequency bandwidth considered in most earlier acoustic emission work.

5.5.1 THEORETICAL RESULTS

For the transmission model indicated in Fig. 3.5 and described by equations (3.69) and (3.70), ℓ_3 (the shoe thickness) and ℓ_4 (the thickness of the transducer PZT-element) are fixed. The pressure transmission coefficient α_{p5} has an infinite number of maxima at different frequencies. In the frequency range of interest (0-1 MHz), the most prominent maxima are produced when the transducer under investigation (S750 D/E) is loaded to an aluminium specimen (i.e.: $Z_1/Z_4 < 1$) and these maxima are expected to come at or near the PZT thickness resonance with $\lambda_4 = 2\ \ell_4$ and the shoe resonance $\lambda_3 = 2\ \ell_3$; i.e.: at 750 and 408 KHz. The half-wavelength resonance is expected because both the transducer shoe and PZT-element are surrounded by a symmetric impedance arrangement (Section 5.3).

The presence of the couplant layers and the dependence of the transmission coefficient curves on the couplant thickness is illustrated in Figures 5.13-5.15 for silicone grease, water, and glycerine couplant media. These figures are derived from equations (3.69) and (3.70) (using program CPNG5.FOR; Appendix 5.E) and are for the commercial transducer S750 D/E. This transducer consists of a 3.125 mm thickness epoxy resin transducer shoe, and a 2.9 mm thickness air backed PZT-5A piezoelectric element. In these figures, the transducer is loaded into an aluminium propagation medium. In general, the PTC curves vary with frequency and with the couplant thickness and medium. Several values of couplant thickness (0.02, 0.1, 0.2,0.3,0.5 and 1.0 mm) have been considered.

The effect of couplant thickness on the PTC peak amplitude, sharpness and frequency should be especially noted. As the grease couplant thickness, ℓ_2, increases from 0.02 mm, the peaks in the first four resonance groups, are displaced to the lower frequency zone and the peak amplitudes are increased with exception of the third group. It can be also seen for all couplants that the third group of peak amplitudes always decrease as the couplant thickness is increased and the peaks move away from the PZT-element thickness resonance (750 KHz).

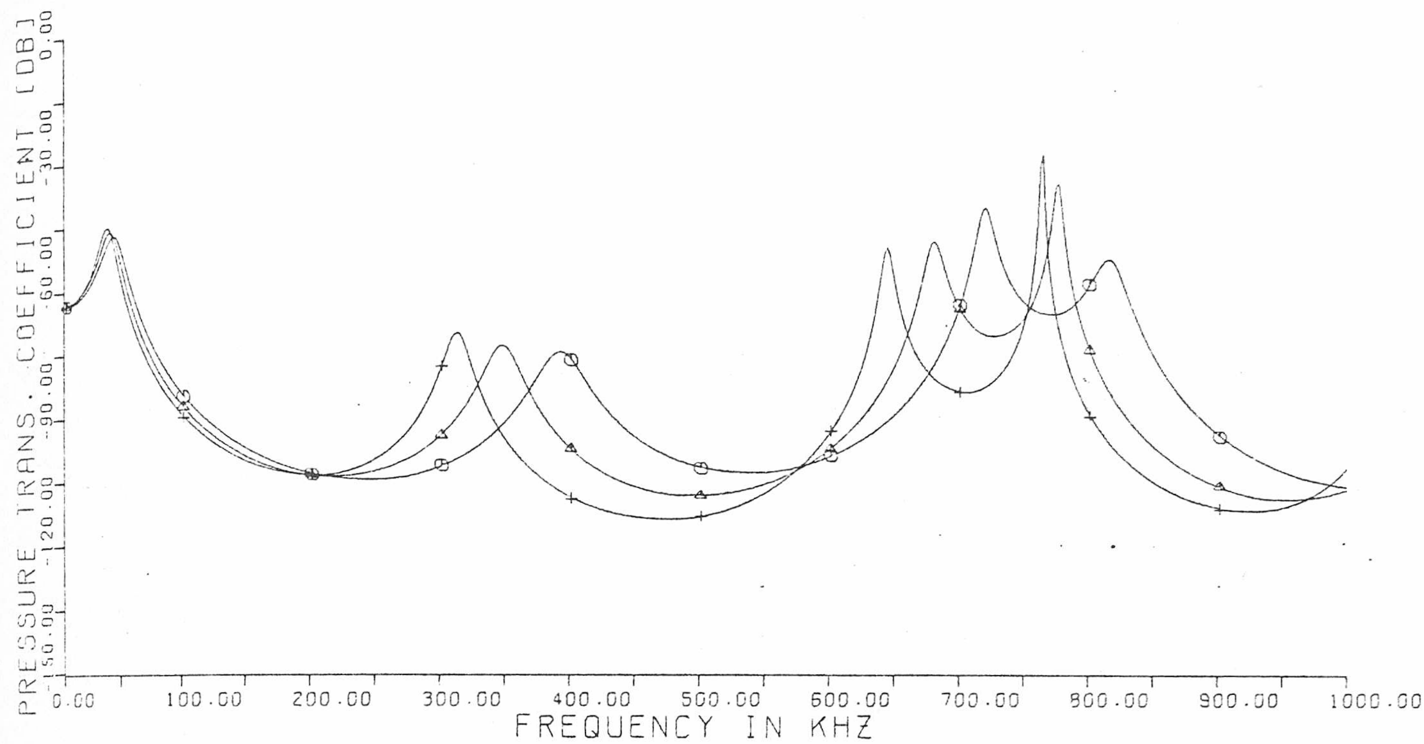

FIGURE 5.13 : The Dependance of the Transmission Coefficient Spectra on the Silicone Grease Couplant Thickness.

(a) For Grease Layer Thickness : O = 0.02, Δ = 0.1, + = 0.2 mm.

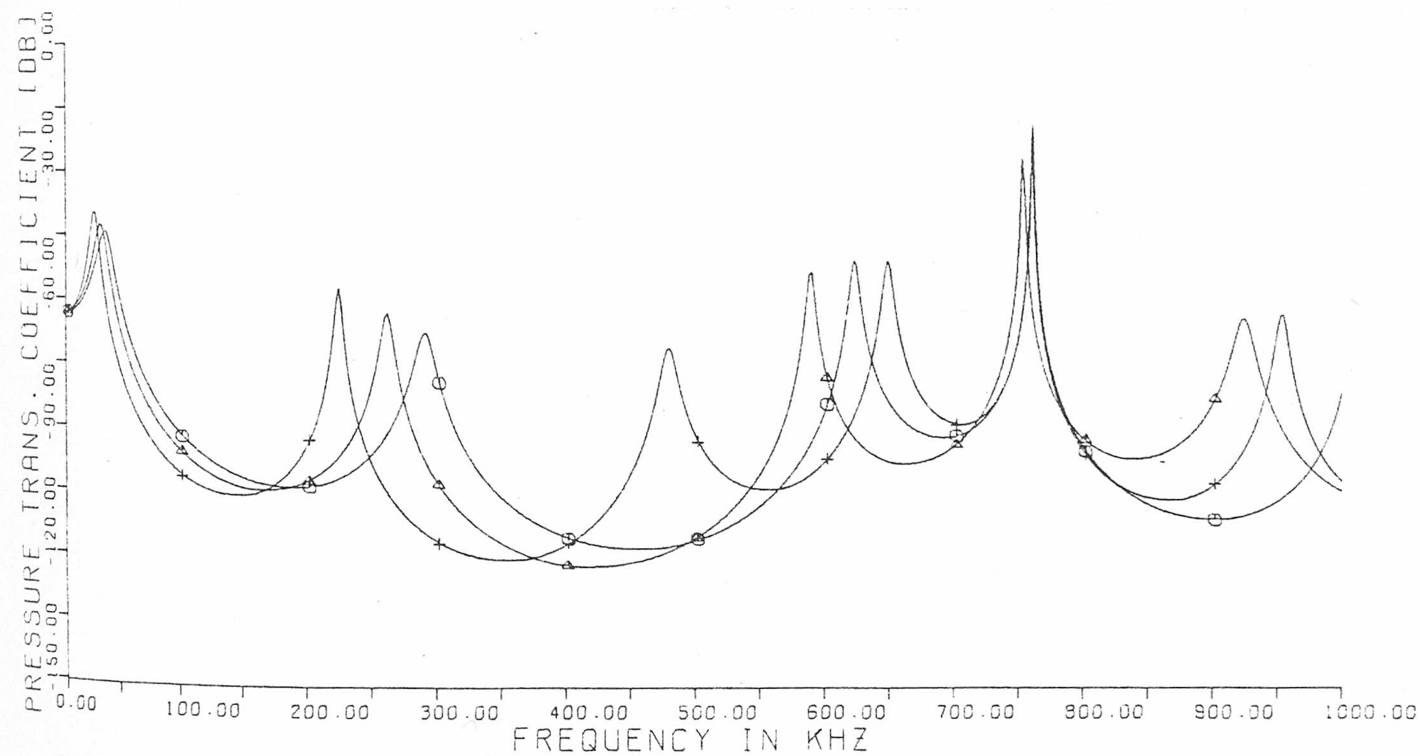

FIG. 5.13 : Continued.

(b) For Grease Layer Thickness : O = 0.3, Δ = 0.5, + = 1.0 mm.

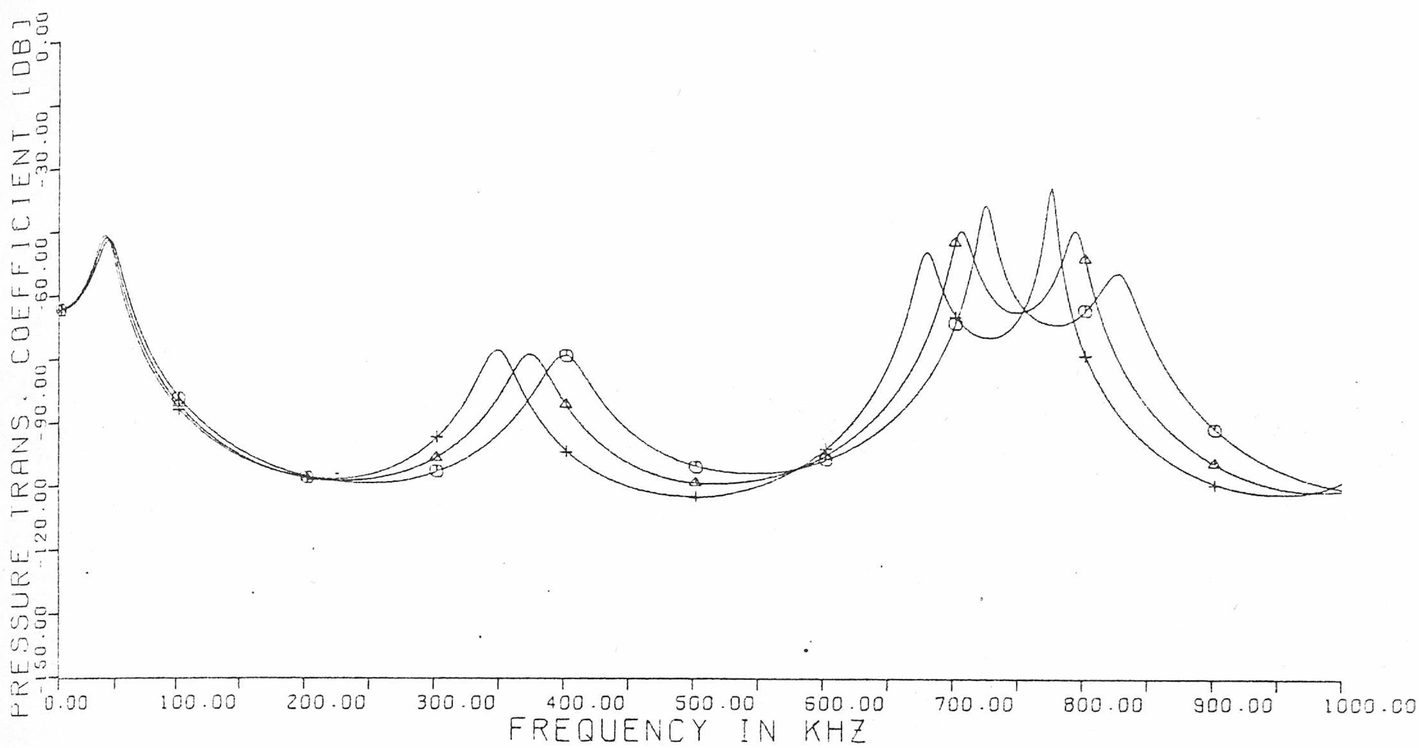

FIGURE 5.14 : The Dependance of the Transmission Coefficient Spectra on the Water Couplant Thickness.

(a) For Water Layer Thickness : O = 0.02, Δ = 0.1, + = 0.2 mm.

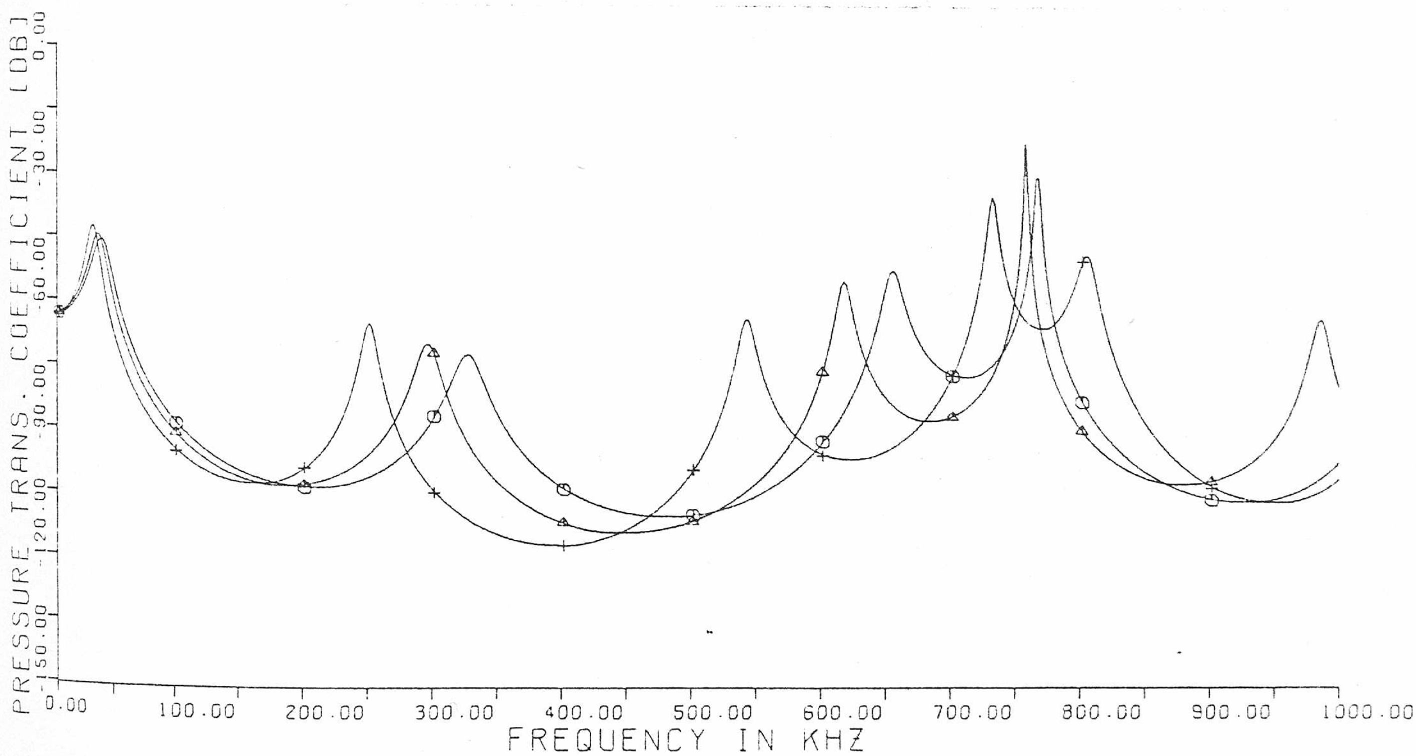

FIG. 5.14 : Continued.

(b) For Water Layer Thickness : O = 0.3, Δ = 0.5, + = 1.0 mm.

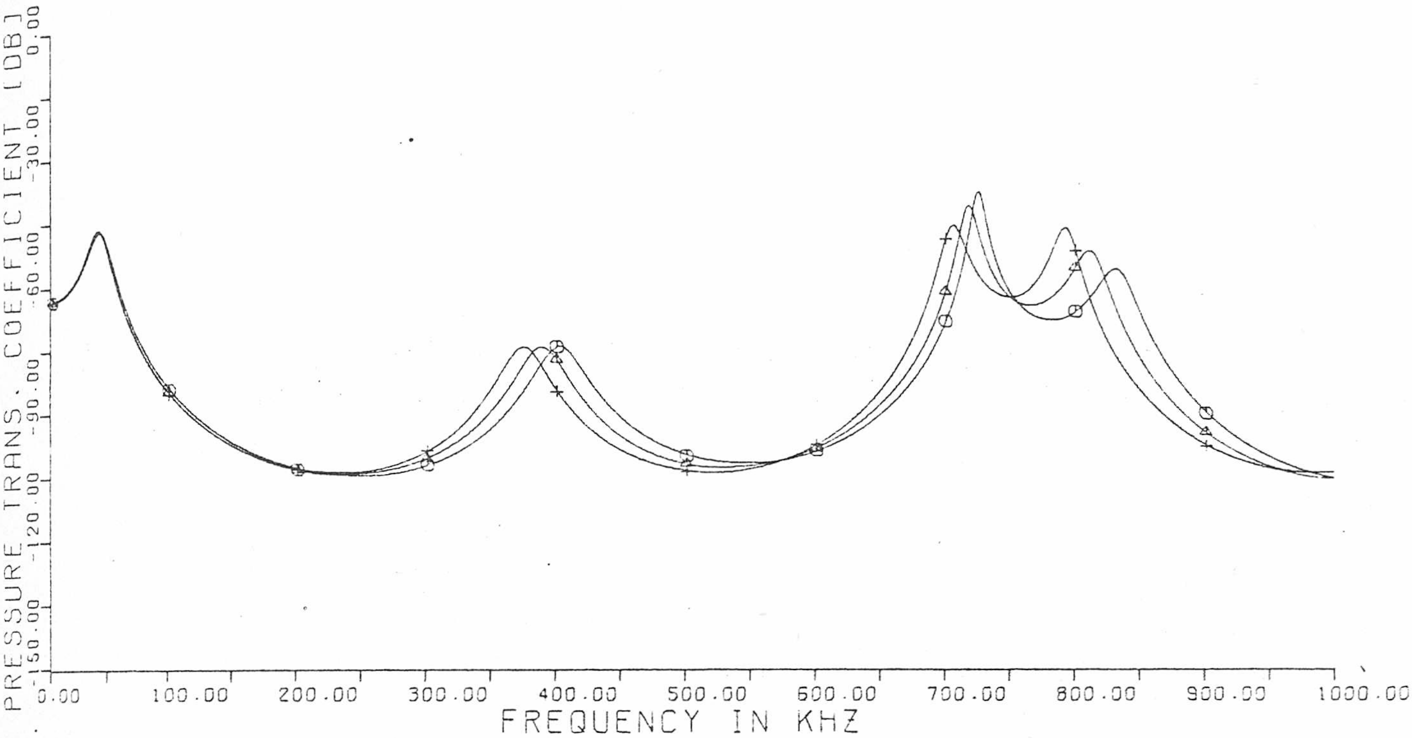

FIGURE 5.15 : The Dependance of the Transmission Coefficient Spectra on the Glycerine Couplant Thickness.

(a) For Glycerine Layer Thickness : O = 0.02, Δ = 0.1, + = 0.2 mm.

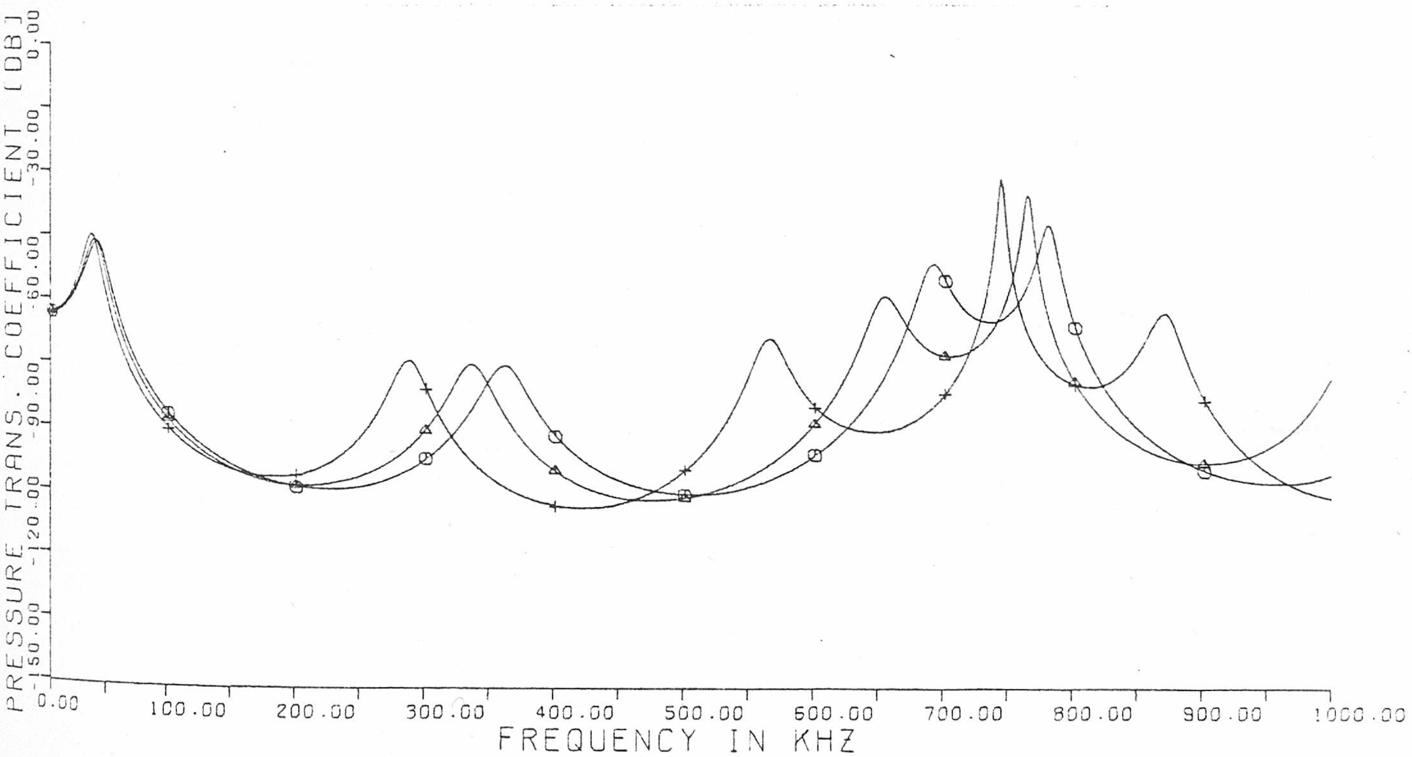

FIG. 5.15 : Continued.

(b) For Glycerine Layer Thickness : O = 0.3, Δ = 0.5, + = 1.0 mm.

As the acoustical properties of the couplant layer becomes closer to that of the transducer shoe, the changes in peaks amplitude and frequencies shift become less pronounced. This can be seen by comparing the main features of the figures which are given in Tables 5VI-5.VIII. Figures 5.15 (a) and (b) show the glycerine couplant widens the peak width and the change in couplant thickness has less effect on shifting the peak frequency and the PTC values. It is interesting to consider the value of the PTC when the thickness of the PZT-element or shoe is half the wavelength as well as its dependance on the ratio Z_i/Z_n (where i = 1, 2, 3, 4 and n = 2, 3, 4, 5 when n ≠ i) which gives 7 different combinations. As $\lambda_4 = 2\,\ell_4$ and $k_4\,\ell_4 = n\pi$, therefore sine $k_4\ell_4 = 0$ and cos $k_4\ell_4 = -1$ and equation (3.69) becomes:

$$A_1 = \frac{A_5}{2}\{(-F_1 \cos k_2\ell_2 \cos k_3\ell_3 + F_2 \sin k_2\ell_2 \sin k_3\ell_3)$$

$$-j(F_5 \cos k_2\ell_2 \text{ sine } k_3\ell_3 + F_7 \sin k_2\ell_2 \cos k_3\ell_3)\} \quad (5.9)$$

This means that the transmission peaks at the PZT-element thickness resonance will be affected by the geometry and the acoustical characteristics of both the couplant layer and transducer shoe where the monitoring material and transducer backing are unchanged. The influence of these components can be seen in the fourth group of peaks (around 750 KHz). The PTC values at 750 KHz (exactly) are independent of the acoustical properties of the PZT-element (i.e.: C_L and Z). Equation (5.9) is similar to equation (3.65)

TABLE 5.VI Numerical Summary of the Main Features of Figure: 5.13 (a) and (b)

For Silicone Grease Couplant (Five-layer Transmission Model)

Group Type	Group Number	Silicone Grease Couplant Thickness, mm*												Range	
		0.02		0.1		0.2		0.3		0.5		1.0		Freq. (KHz)	PTC (dB)
		Freq.	PTC	Freq.	PTC	Freq.	PTC	Freq.	PTC	Freq.	PTC	Freq.	PTC		
Peaks	1	45	-47.0	45	-46.5	40	-45.1	35	-44.1	35	-43.9	25	-41.0	20	6.5
	2	395	-74.7	350	-73.2	315	-70.3	290	167.3	260	-63.9	225	-57.9	170	10.2
	3	720	-41.0	680	-49.4	645	-50.3	625	-53.6	590	-53.0	(1)480 (2)650	-70.8 -51.9	240	29.8
	4	815	-52.9	775	-38.4	765	-23.4	760	-18.6	755	-42.0	760	-19.5	165	34.3
	5	(occurs outside the frequency range of interest,>1MHz)								925	-64.0	955	-64.1		
Valleys	1	245	-104.7	220	-103.9	200	-103.6	185	-103.7	170	-140.3	145	-104.6	100	1.1
	2	535	-103.0	500	-108.4	470	-114.0	450	-117.8	365	-118.5	350	-120.5	185	17.5
	3	770	-66.0	730	-71.0	705	-84.1	690	-91.8	665	-79.9	(1)555 (2)705	-104.1 -88.6	215	38.1
	4	(beyond 1 MHz)		955	-109.2	920	-111.8	900	-110.9	840	-96.8	-865	-106.5		

*Frequency in (KHz) ±2.5

PTC in (dB) ±0.05

TABLE 5.VII Numerical Summary of the Main Features of Figure 5.14 (a) and (b)

For Water Couplant (Five-layer Transmission Model)

Group Type	Group Number	Water Couplant Thickness, mm*												Range	
		0.02		0.1		0.2		0.3		0.5		1.0		Freq. (KHz)	PTC (dB)
		Freq.	PTC	Freq.	PTC	Freq.	PTC	Freq.	PTC	Freq.	PTC	Freq.	PTC		
Peaks	1	45	-47.0	45	-46.9	40	-46.1	40	-45.3	35	-45.2	30	-44.0	15	3.0
	2	400	-74.7	375	-74.4	350	-73.6	330	-72.6	295	-70.2	250	-65.8	150	8.9
	3	725	-39.1	705	-45.7	680	-50.3	655	-52.7	620	-55.9	545	-64.7	280	25.6
	4	825	-55.3	795	-45.4	775	-35.4	765	-35.8	760	-36.0	730	-38.9	95	19.9
	5	(occurs outside the frequency range of interest)								985	-64.3	805	-49.3		
Valleys	1	245	-104.9	230	-104.3	220	-103.7	205	-103.4	190	-103.0	165	-102.5	120	2.4
	2	540	-102.4	520	-104.9	495	-107.9	480	-110.5	450	-114.2	395	-117.1	145	14.7
	3	770	-67.1	750	-64.6	725	-70.5	710	-78.0	685	-88.1	620	-97.0	150	32.4
	4			985	-106.5	950	-107.2	925	-107.1	880	-102.9	770	-66.7	215	40.5
	5	(occurs outside the frequency range of interest, i.e. > 1 MHz)										950	-107.2		

*Frequency in (KHz) ±2.5.

PTC in (dB) ±0.05.

TABLE 5.VIII Numerical Summary of the Main Features of Figure 5.15 (a) and (b)

For Glycerine Couplant (Five-layer Transmission Model)

Group Type	Group Number	Glycerine Couplant Thickness, mm*												Range	
		0.02		0.1		0.2		0.3		0.5		1.0		Freq. (KHz)	PTC (dB)
		Freq.	PTC	Freq.	PTC	Freq.	PTC	Freq.	PTC	Freq.	PTC	Freq.	PTC		
Peaks	1	45	-47.1	45	-46.9	45	-46.9	40	-46.8	40	-45.8	35	-45.6	10	0.5
	2	405	-74.7	390	-74.7	375	-74.8	360	-74.8	335	-74.7	290	-73.7	115	1.1
	3	725	-39.7	720	-41.6	710	-46.8	690	-51.3	655	-58.5	565	-68.5	160	28.8
	4	830	-56.7	815	-52.5	795	-46.9	780	-41.8	765	-34.2	745	-31.0	85	25.7
	5	(occurs outside the frequency range of interest i.e. > 1 MHz)										870	-62.3		
Valleys	1	245	-105.0	235	-104.6	230	-104.2	225	-103.8	210	-102.9	185	-100.9	60	4.1
	2	545	-102.1	535	-103.1	520	-104.1	505	-105.0	480	-106.4	420	-108.1	125	6.0
	3	785	-68.5	770	-65.1	750	-63.2	735	-64.6	705	-72.7	645	-90.3	140	27.1
	4	(beyond 1 MHz)				985	-104.3	955	-102.4	905	-97.6	810	-79.7		

*Frequency in (KHz) ±2.5

PTC in (dB) ±0.05

if Z_5 is replaced by Z_4 (for the backing material) and both will give similar PTC at 750 KHz. This means that the four-layer model can be used when the shoe layer can be omitted, i.e. when $\ell_3 = 0$ or $= n\lambda_3/2$ (where n = 1, 2, 3, ...).

For all couplant media, the shoe resonance appears at about 400 KHz when a thin couplant thickness was used in the calculation. Increasing the couplant thickness shifts the peaks towards the frequency of $\lambda_{shoe} = 4\ \ell_{shoe}$ which is the lower limit of all shifts (204 KHz). The explanation is that when the couplant thickness is small enough not to effect the impedance arrangement between Z_1, Z_3 and Z_4 which is obviously of symmetric form i.e.:

$$Z_1 \text{ (aluminium) } > Z_3 \text{(Epoxy shoe)} < Z_4 \text{ (PZT)}$$

the second group of peaks occur at frequency corresponding to $\lambda_{shoe}/2$. As the couplant thickness increases, its effect on the peaks frequency can no longer be ignored and for 1.0 mm thickness curves, the peak appears at frequencies very close to $\lambda_{shoe}/4$. This transformation of shoe peaks frequency is due to the change in the system impedance arrangement to that of gradient form i.e.

$$Z_2 < Z_3 < Z_4 \quad \text{(see Section 5.3.4)}$$

One can also attribute the increase in the peak amplitude to this arrangement transformation. In Section 5.3, a system with a gradient impedance arrangement shows slightly higher PTC values in comparison with the symmetrical one. It turns out that the variation in the transducer couplant thickness initially affects the fundamental frequency of the transducer shoe. The fundamental shoe resonance will oscillate between the transducer shoe half- and quarter- wavelength values. Therefore, the consequent harmonic resonances will oscillate as a result of the oscillation of the fundamental peak and in some cases will interfere with other transducer components resonance. This interference will cause the "peaks splitting" effect at the transducer main resonance frequency.

The only explanation for the first group of peaks (around 50 kHz) is that as the PTC_{curve} is a function of all the system components, these peaks may be the result of an equivalent layer representing all of medium 2, 3 and 4.

In order to summarize the previous discussion, Figure 5.16 illustrates curves which characterize the resonance shift as a function of the quantity $\ell_2 f_r$ (where f_r is the frequency at which the PZT-element thickness corresponds to half-wavelength and ℓ_2 is the couplant thickness) and for aluminium as a propagation medium. The magnitude of the relative shift in the resonance frequency is plotted along the vertical axis in $\Delta f ^o/_o$ which is defined as follows:-

$$\Delta f = \frac{f_p - f_r}{f_r} \times 100$$

where f_p is the peak resonance frequency calculated for a five-layer system.

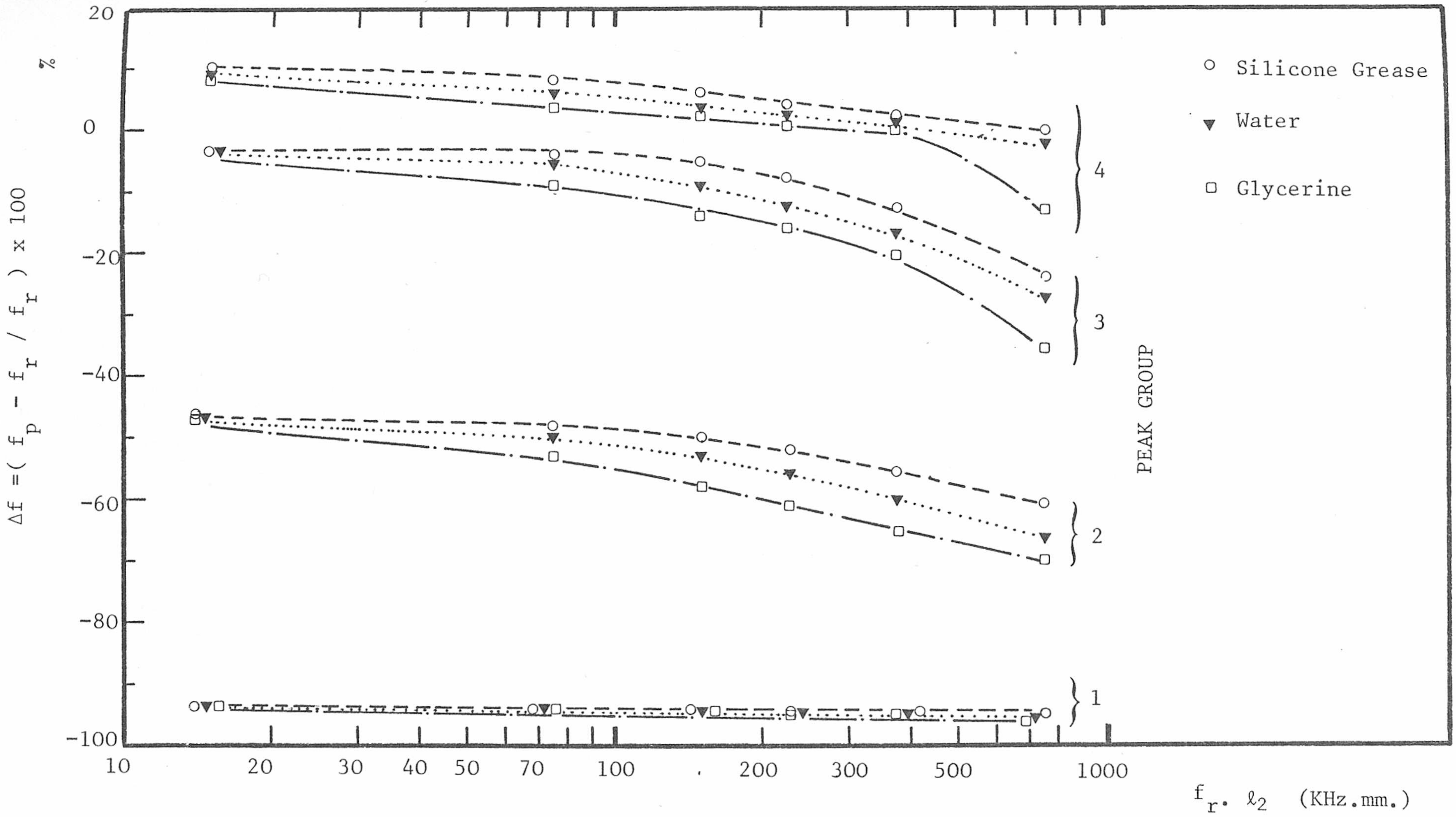

FIGURE 5.16 : Theoretical Characteristics of the Peak Resonance Shift.

5.5.2 EXPERIMENTAL OBSERVATIONS OF THE EFFECT OF COUPLANT CHARACTERISTICS ON ACOUSTIC EMISSION PARAMETERS

The main object of the experiments described in this section is to indicate in a qualitative way how different acoustic emission parameters are influenced by the couplant layer characteristics, and to assess the potential value of the transmission theory.

Initially, the individual repeated pulse technique (Section 4.2.2) was tried to investigate the direct effect of the couplant layer characteristics on the individually detected acoustic emission bursts. However, electronic limitations made it difficult for a good experimental/theoretical comparison to be made so the continuous wave technique was considered. Although the five-layer model represents the practical situation of acoustic emission monitoring, technical problems prevent a quantitative analysis being done.

1. Results for the Individual Repeated Pulse Experiments:

The experimental arrangement was as shown in Fig. 4.8 and the aluminium block (X), Fig. 4.4, was used. The simulated acoustic emission source transducer (A) was driven by a pulse generator with electrical pulses of 1 μs duration, 0.06 s repetition time and 20 volts constant amplitude. The recording system passband was 20-1000 KHz. Silicone grease, water and glycerine of 1140 and 1260 $Kg. m^{-3}$ density were used as couplant media with different thicknesses. A commercial D750 B resonant acoustic emission transducer was used as a receiver and the first 0.5 m s of the detected burst was recorded on a digital transient recorder.

a. Effect on the Time Domain Parameters:

Figure 5.17 (a-d) shows the effect of the change in couplant thickness on the number of counts versus voltage trigger level for individual acoustic emission burst. At any reasonable trigger level, apart from the zero level crossing; say +0.8 volts; the variation in the burst number of counts can be noted for each couplant medium. The difference is maximum in the case of silicone grease couplant (about 36 counts) and smaller for water and glycerine couplants.

Variations in the maximum number of counts (i.e. the number of zero crossings) can also be seen in this figure. For thorough comparison, Fig. 5.18 summarizes these variations for the entire group of couplants. Shifts in the dominant frequencies of the burst spectra are expected. For all couplant media, increasing the couplant thickness should decrease the maximum number of counts as a result of shifting the transmission peaks towards the lower frequency (see Figs. 5.13-5.15). A rough but useful comparison can also be made between Fig. 5.18 and the theoretically calculated shifts shown in Fig. 5.16. Similarity between the smaller gradient value in the case of glycerine could be observed and compared with other cases in both theoretical and experimental representations.

FIGURE 5.17 :

Variation in Emission Number of Counts versus Trigger Level (in VOLTS). Using the Air Block and D750 Transducer.

(a) For Silicone Grease Couplant.

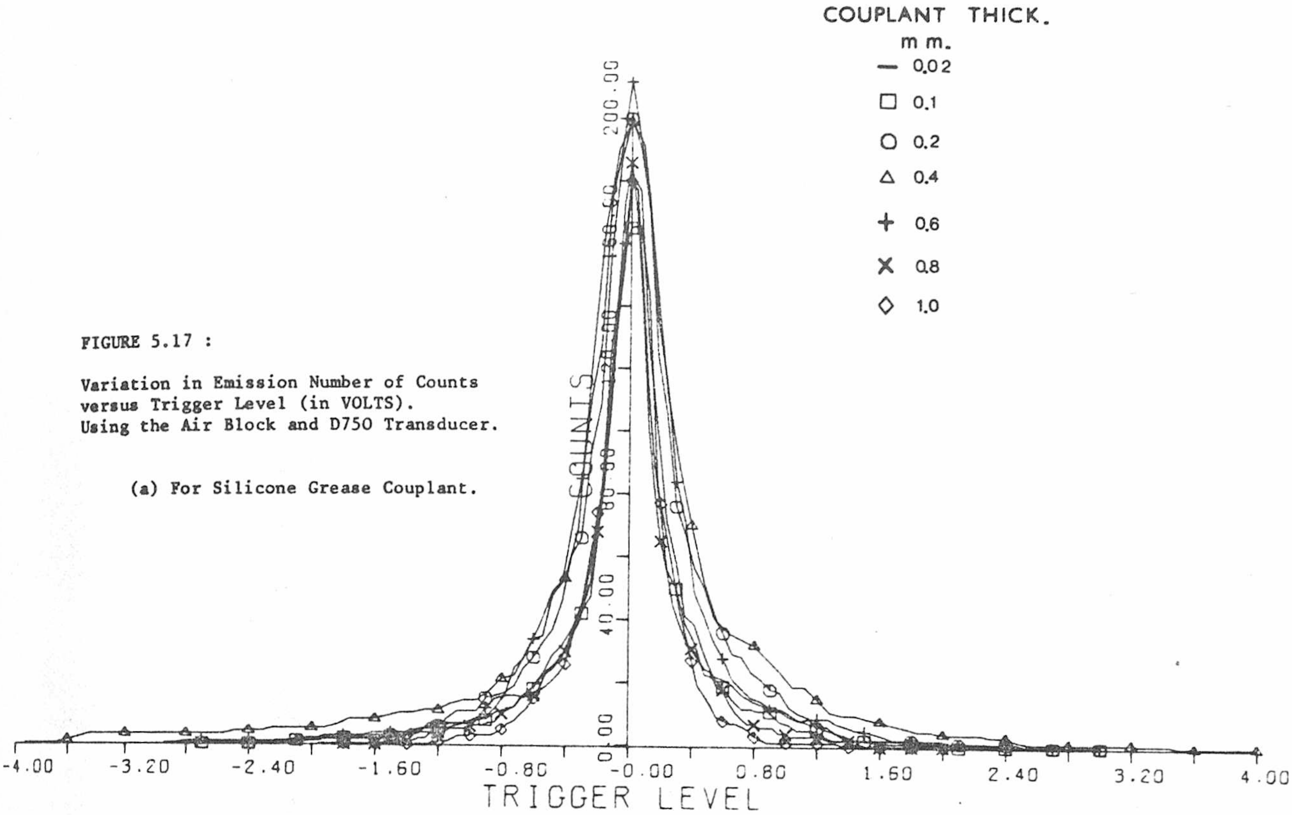

FIGURE 5.17 : Continued.

(b) For Water Couplant

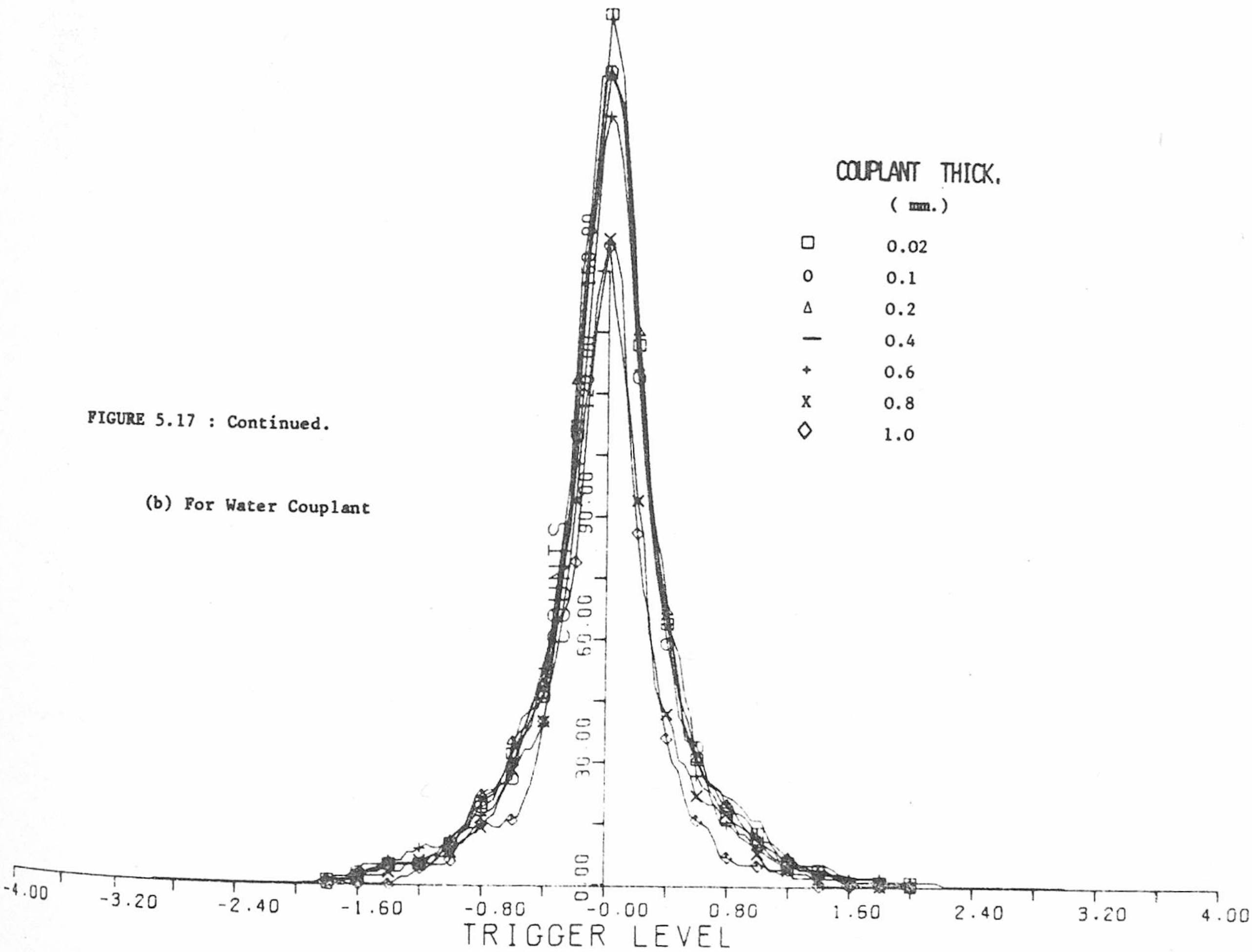

FIGURE 5.17 : Continued.

(c) For Glycerine Couplant
(1140 Kg.m^{-3})

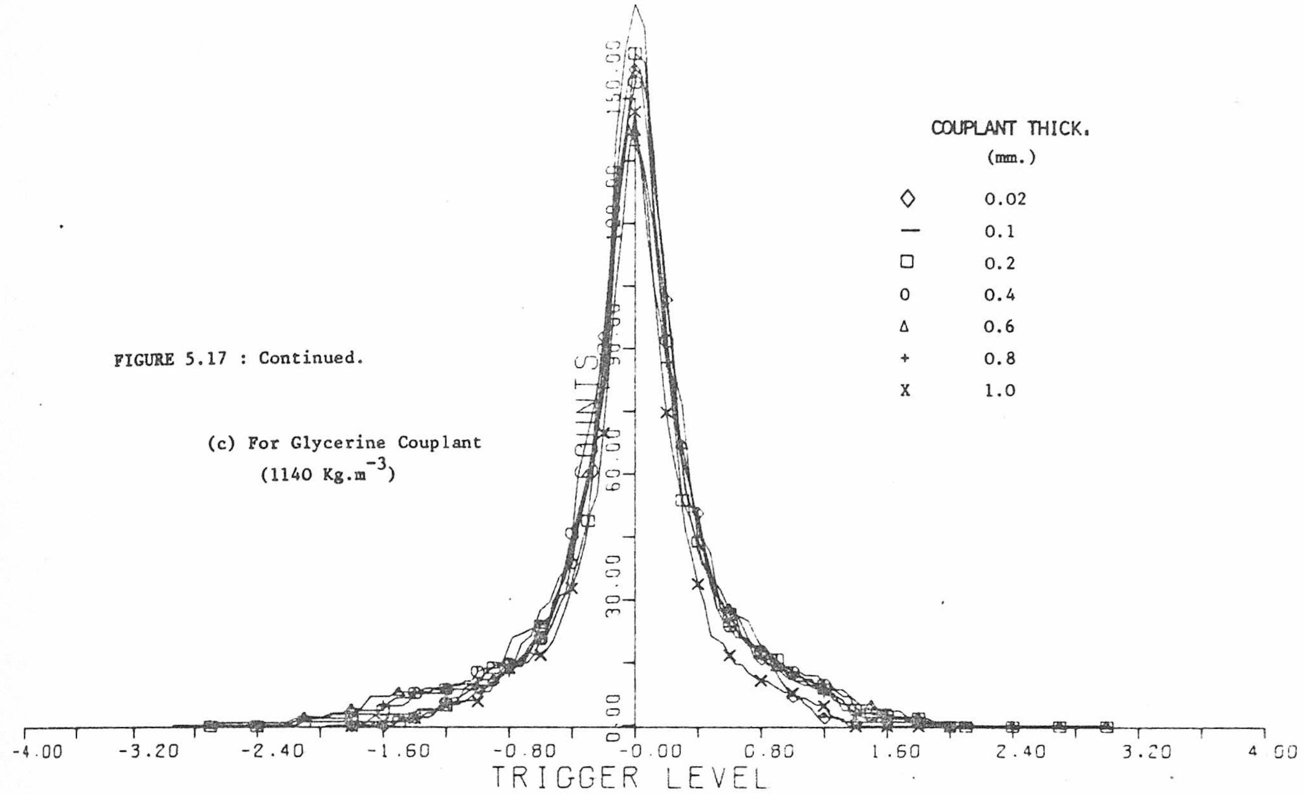

FIGURE 5.17 : Continued.

(d) For Glycerine Couplant
(1260 Kg.m^{-3})

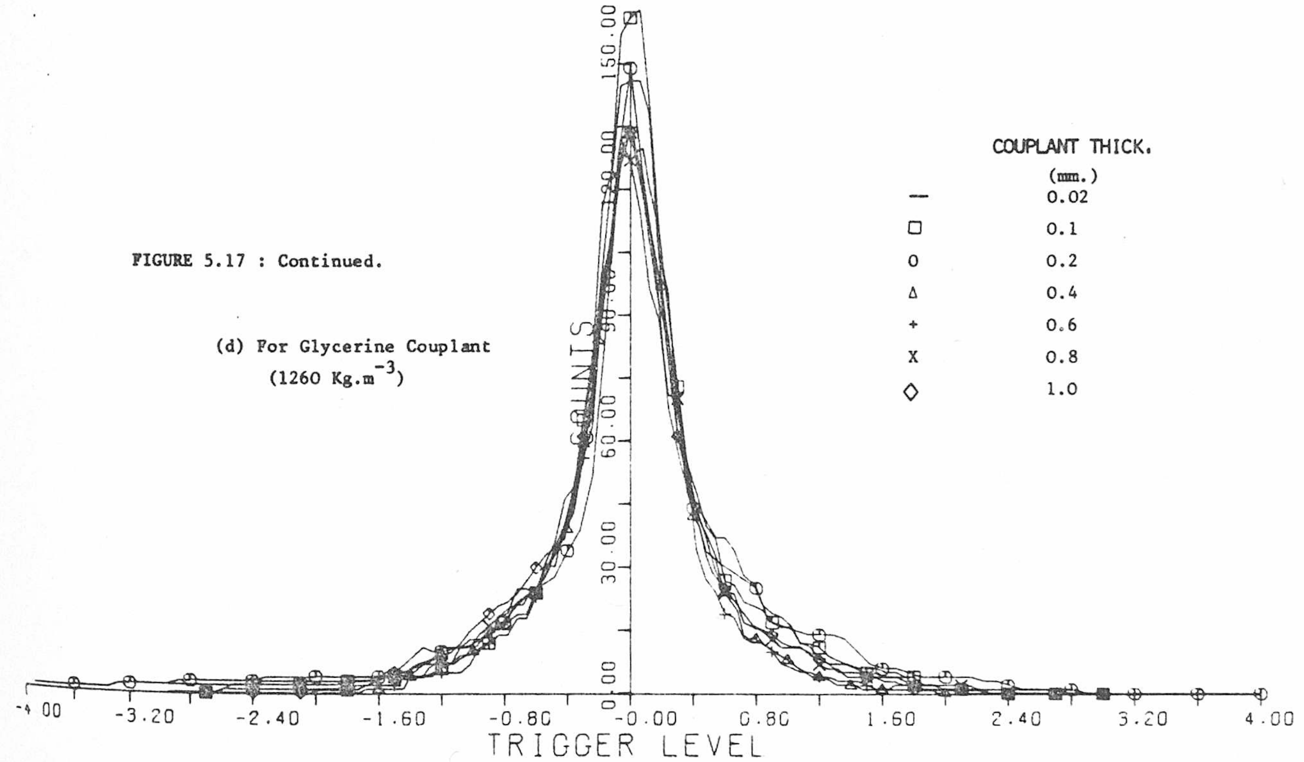

Figure 5.19 shows the variation of the bursts maximum peak-to-peak amplitude. For silicone grease couplant the peak-to-peak amplitudes are extremely varied with thickness. The graph demonstrates that the difference was as large as 4.55 volts and the maximum amplitude was 7.14 volts corresponding to 0.4 mm grease couplant thickness. This amplitude value decreased to 2.59 volts for 1 mm thickness.

In general, the experimental results indicate a great variation in acoustic emission number of counts and amplitude with a grease couplant, i.e. small variation in thickness led to quite a large change in these parameters. These, again, can be generally compared with a change in the corresponding PTC spectra for grease, water and glycerine, Figures 5.13-5.15.

The variations in time domain burst energy decrement are shown in Fig. 5.20 (a-d). The bursts total energy are represented in Fig. 5.21. With reference to Section 2.3.4, each curve summarizes the burst configuration, and the differences between different curves in each group show the influence of changing the couplant thickness. In all cases, using a thin couplant thickness (0.02 mm) does not necessarily achieve efficient transmission over the entire burst frequency-band. However, using glycerine (1260 $Kg.m^{-3}$), generally, improves the burst energy detection and as seen in Fig. 5.21, the average transmitted energy indicated by an arrow is the highest.

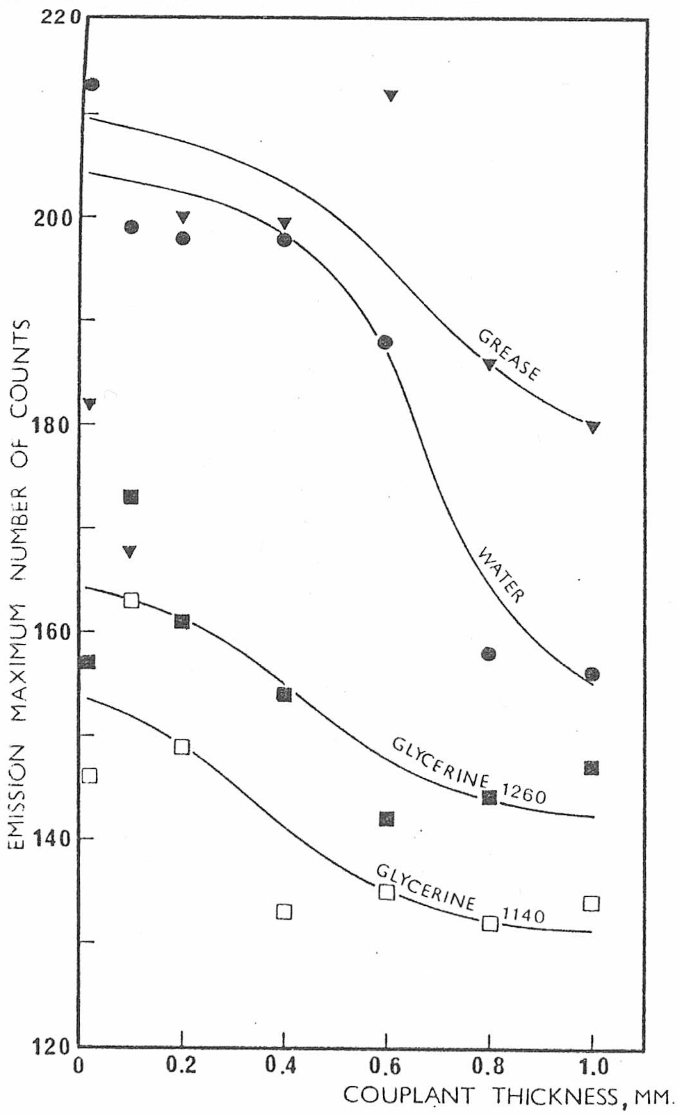

FIGURE 5.18 : Variation in Emission Maximum Number of Counts per One Burst (Number of Zero Crossing).

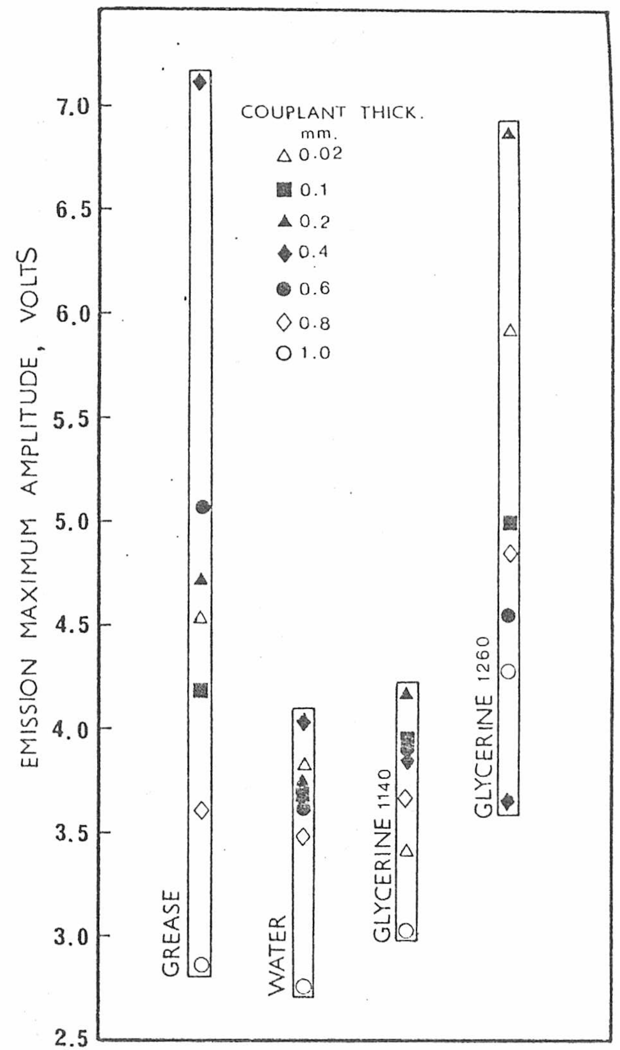

FIGURE 5.19 : Variation in Emission Maximum Amplitude.

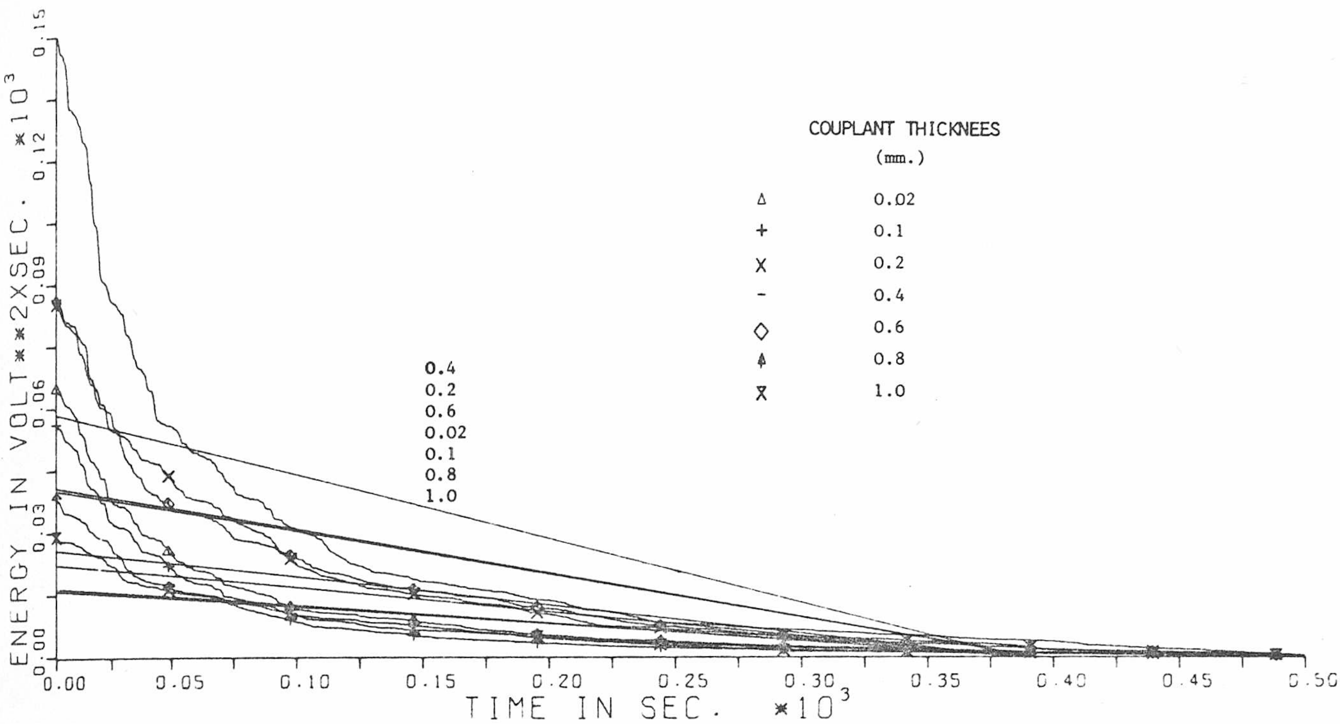

FIGURE 5.20 : Variation in Time Domain Burst Energy Decrement Using D750 Acoustic Emission Transducer and the Block (X) in Air.

(a) For Silicone Grease Couplant.

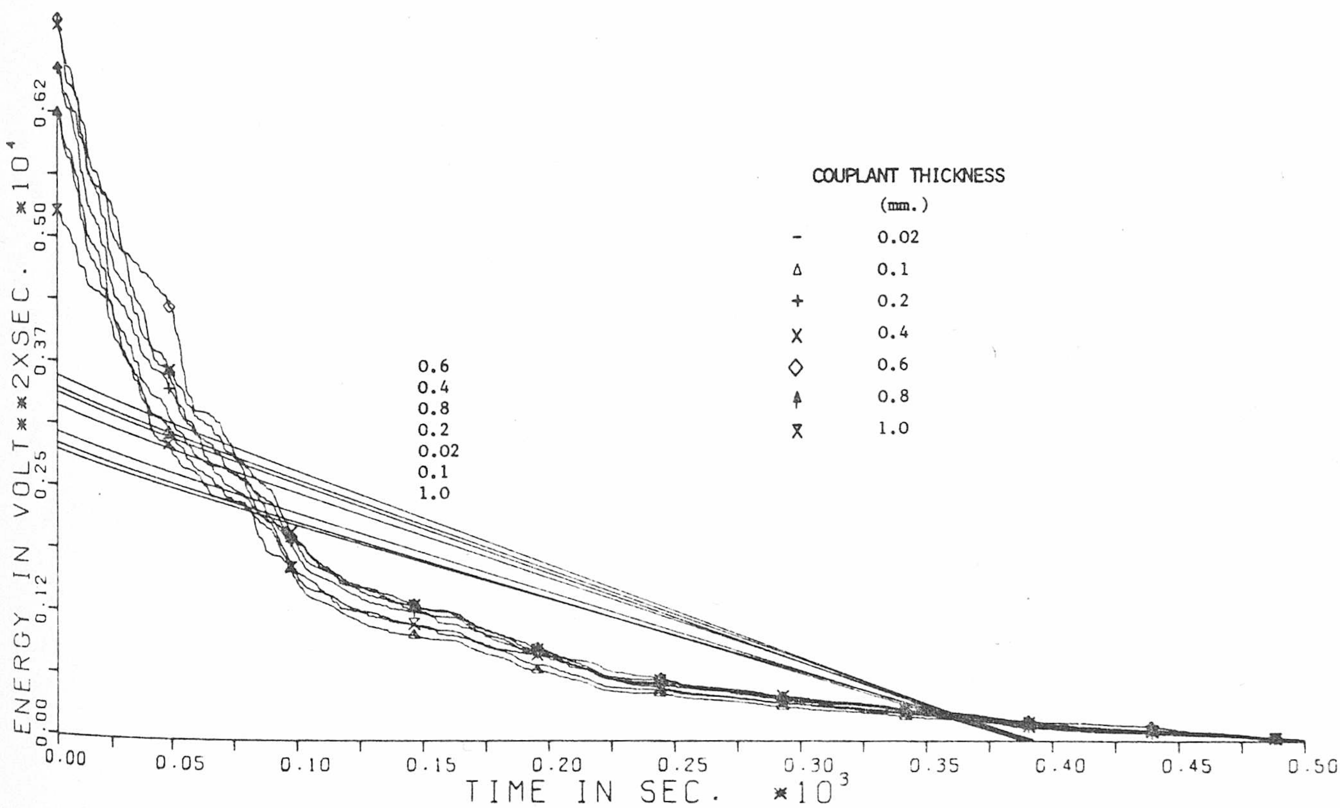

FIGURE 5.20 : Continued.

(b) For Water Couplant

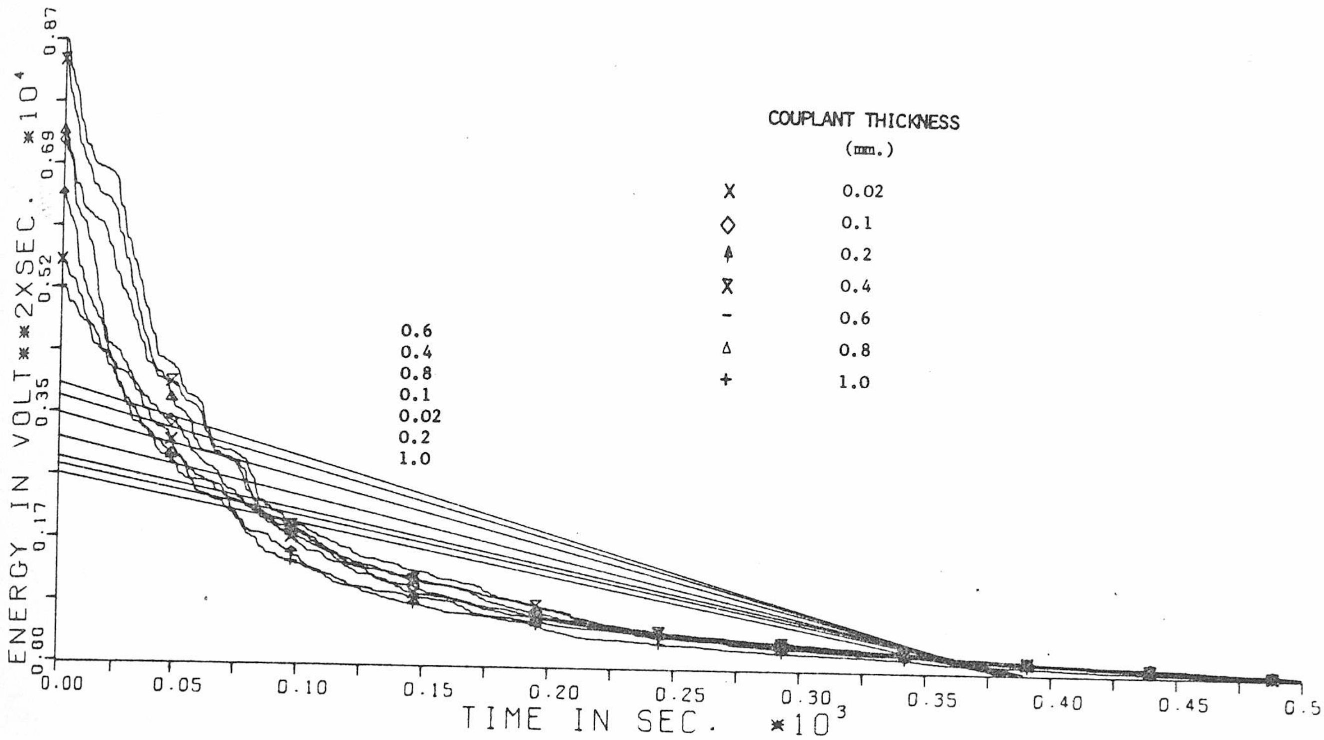

FIGURE 5.20 : Continued.

(c) For Glycerine Couplant (1140 $Kg.m^{-3}$).

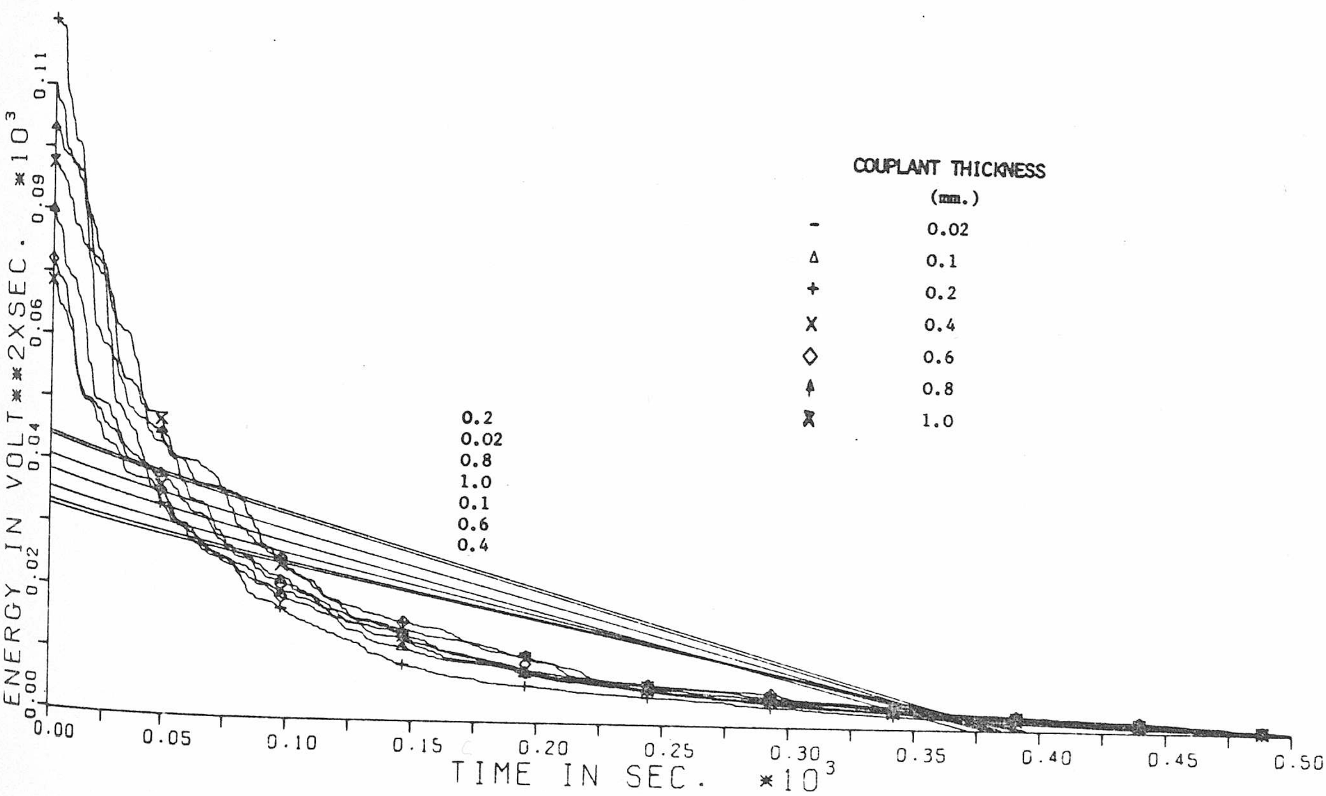

FIGURE 5.20 : Continued.

(d) For Glycerine Couplant (1260 $Kg.m^{-3}$).

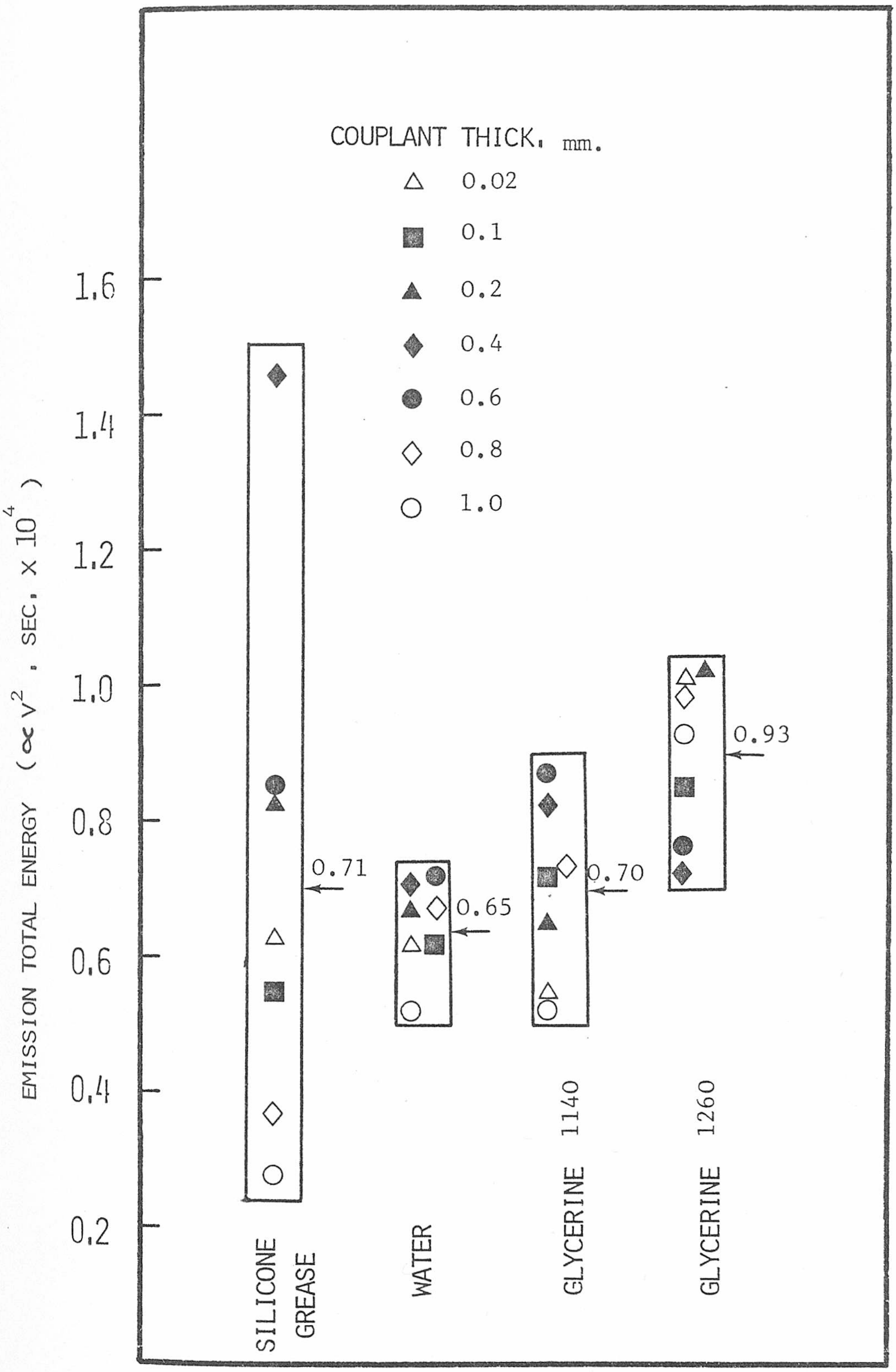

FIGURE 5.21 : Variation in Individual Emission Total Energy and the Average of Transmitted Energy for Each Group of Different Couplant Media.

This can be attributed to the better acoustic matching which has been achieved between the glycerine couplant and the transducer shoe. Water couplant shows less total energy variation with thickness while the deviation was greater when silicone grease couplant was used. In the energy decrement graphs the straight lines defines an enclosed area equivalent to that enclosed by the corresponding energy curve and X-axis.

b. Effects on the Frequency Spectrum:

As it was seen, both the couplant medium and thickness has substantial effect on the acoustic emission burst shape and different time domain parameters. These fluctuations in shape are expected to reflect similar variation in the burst frequency spectrum. Figure 5.22 (a-d) show the frequency spectra for the same data records considered in the previous section. In the case of grease couplant, Fig. 5.22(a), the variation is quite pronounced and more than those for other couplants. However, it proved difficult to relate the variation in these spectra to their corresponding theoretical graphs. Attempts have been made to smooth the frequency spectra but the effect of the "hairy" spectra made this task quite impossible. One technique used was to calculate the relative transmission coefficient from the Fourier magnitude. First, the computed Fourier magnitudes was evaluated as 500 points for each spectrum with 2 KHz frequency resolution; then the average of each 10 points was taken which represents the linear average of the Fourier magnitude over 20 KHz.

Secondly, the ratio between different spectra and that for 0.02 mm couplant thickness was obtained and called the relative transmission (RT). This method allows experimental results to be roughly compared. The results from applying this technique are shown in Figure 5.23 (a-h). In these graphs both relative transmission peaks and antipeaks represent a variation in Fourier magnitude and/or a frequency shift. No satisfactory correlation could be made with the theoretically calculated graphs due to the large errors involved in the smoothing operation and the high noise to signal ratio at frequencies above 500 KHz. In addition, the influence of the propagation block geometry which introduces strong resonances in the frequency response made the comparison hard if not impossible.

The appearance of the strong block resonances could be explained as follows. The stress waves emitted by the 5 MHz broadband transducer diverge slightly in the aluminium block, so that some internal reflection takes place on the cylindrical surface of the block. The reflected waves are partially longitudinal and partially shear. Upon further reflections the shear component is partially reconverted into longitudinal waves which reach the acoustic emission transducer. Owing to differences in velocity and path for the two waves, interference takes place which accounts for the peculiarities in the frequency spectrum curves. The resonances arising from this interference will introduce peaks at different frequencies. Because of the digitization process, each peak will be accompanied with a few side peaks around it with

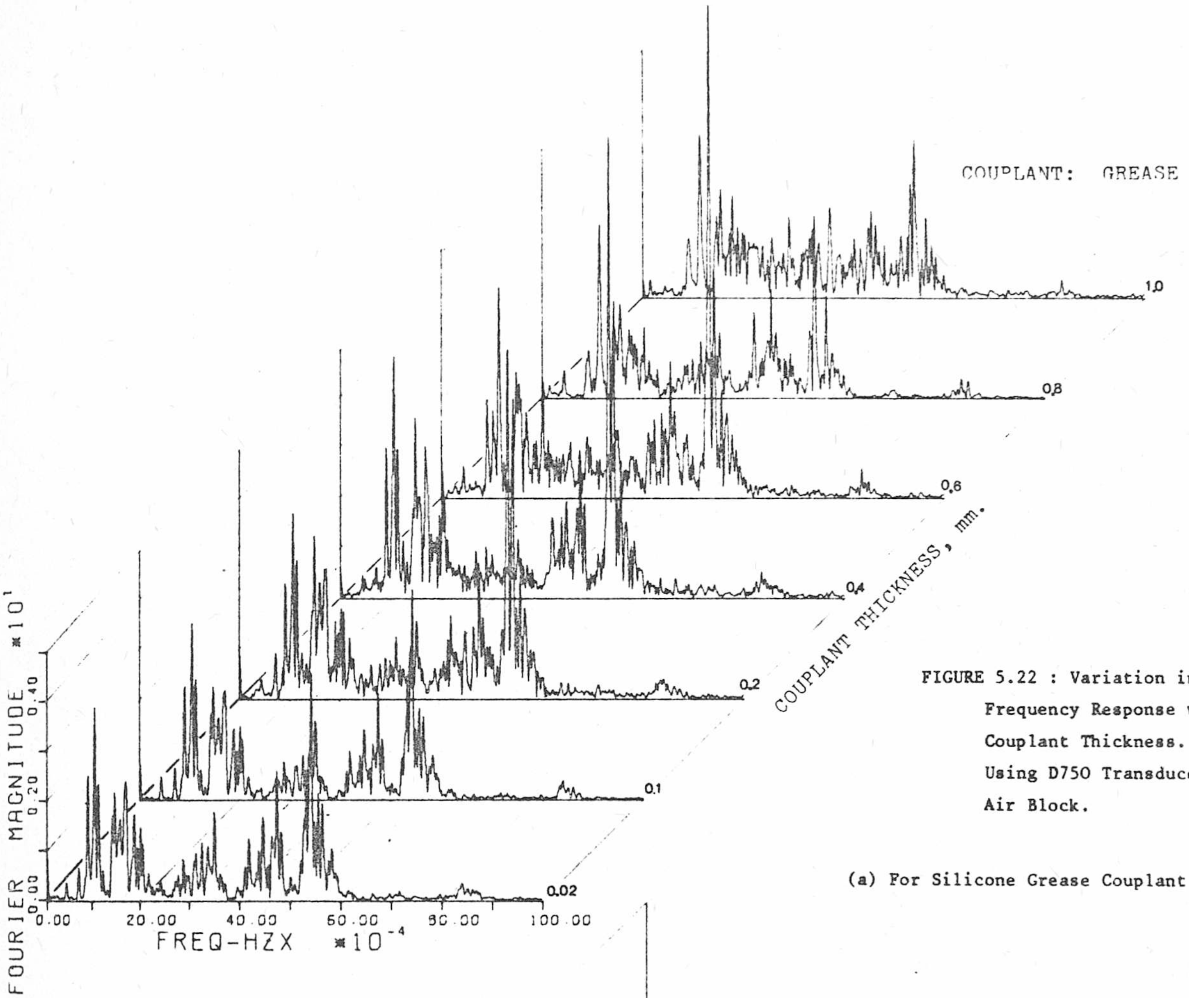

FIGURE 5.22 : Variation in Burst Frequency Response with Couplant Thickness. Using D750 Transducer and Air Block.

(a) For Silicone Grease Couplant.

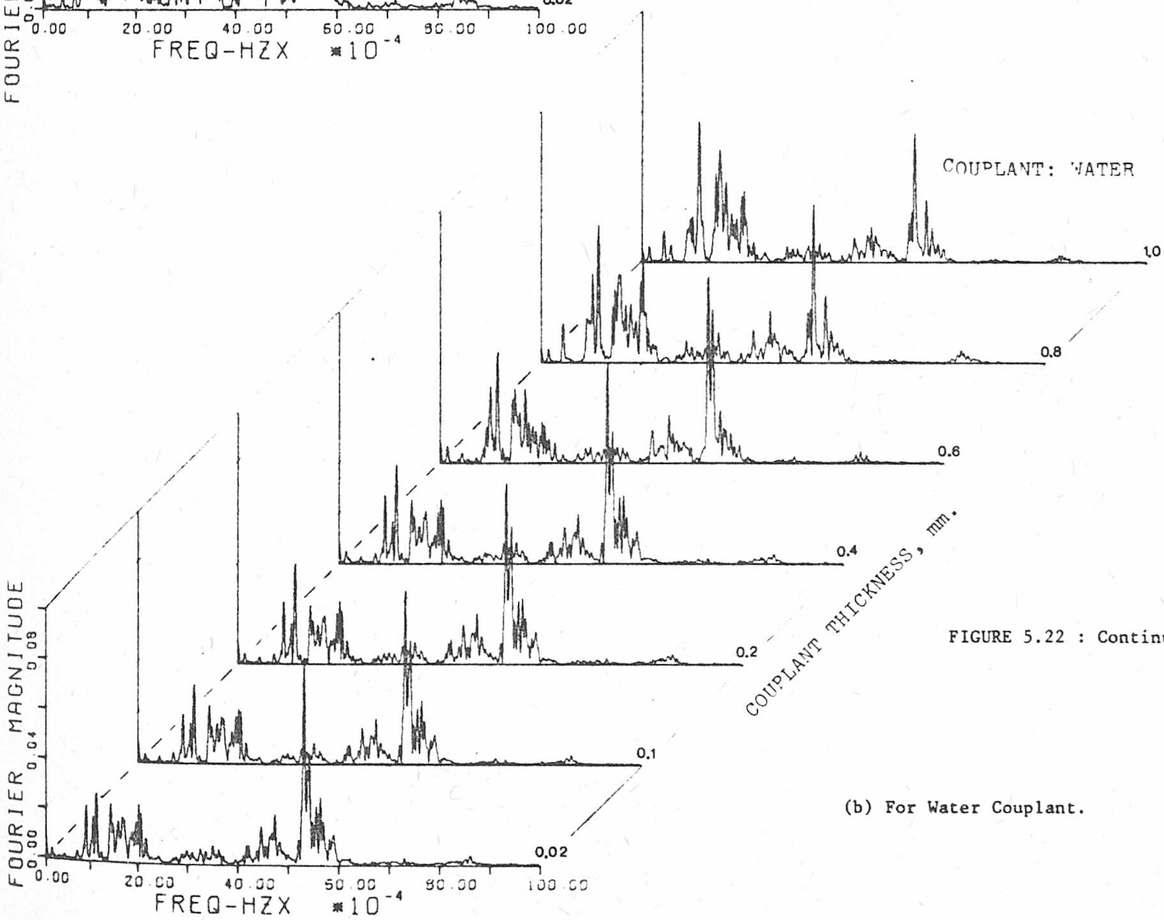

FIGURE 5.22 : Continued.

(b) For Water Couplant.

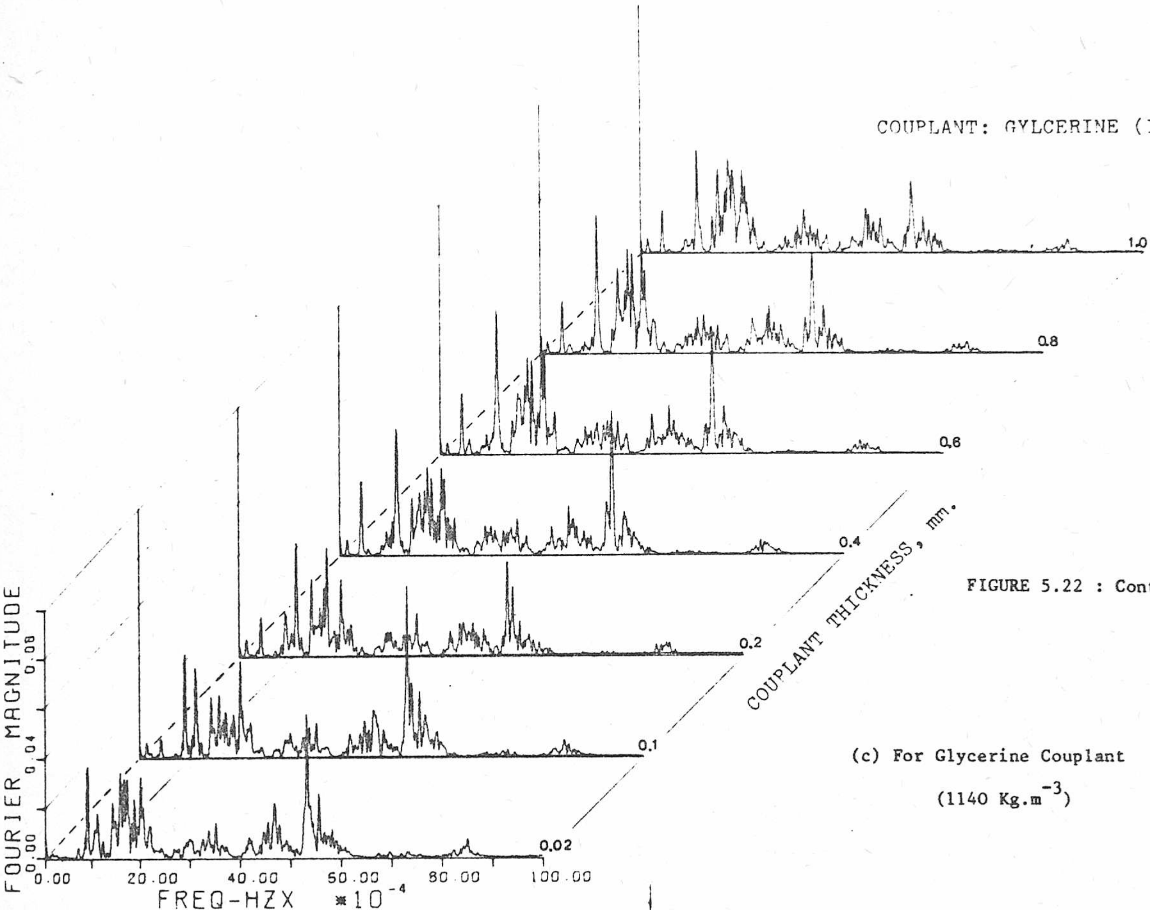

FIGURE 5.22 : Continued.

(c) For Glycerine Couplant

(1140 $Kg.m^{-3}$)

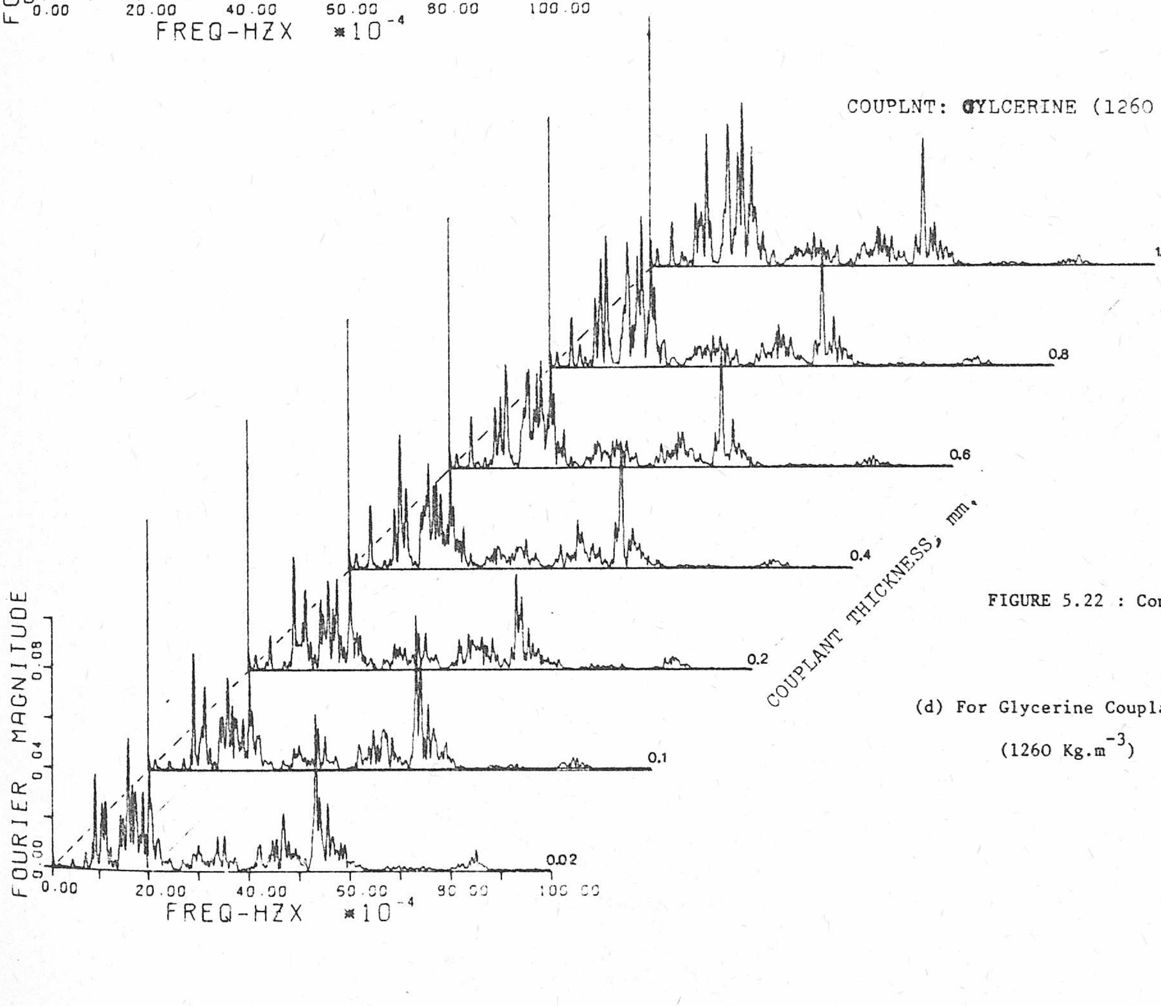

FIGURE 5.22 : Continued.

(d) For Glycerine Couplant

(1260 $Kg.m^{-3}$)

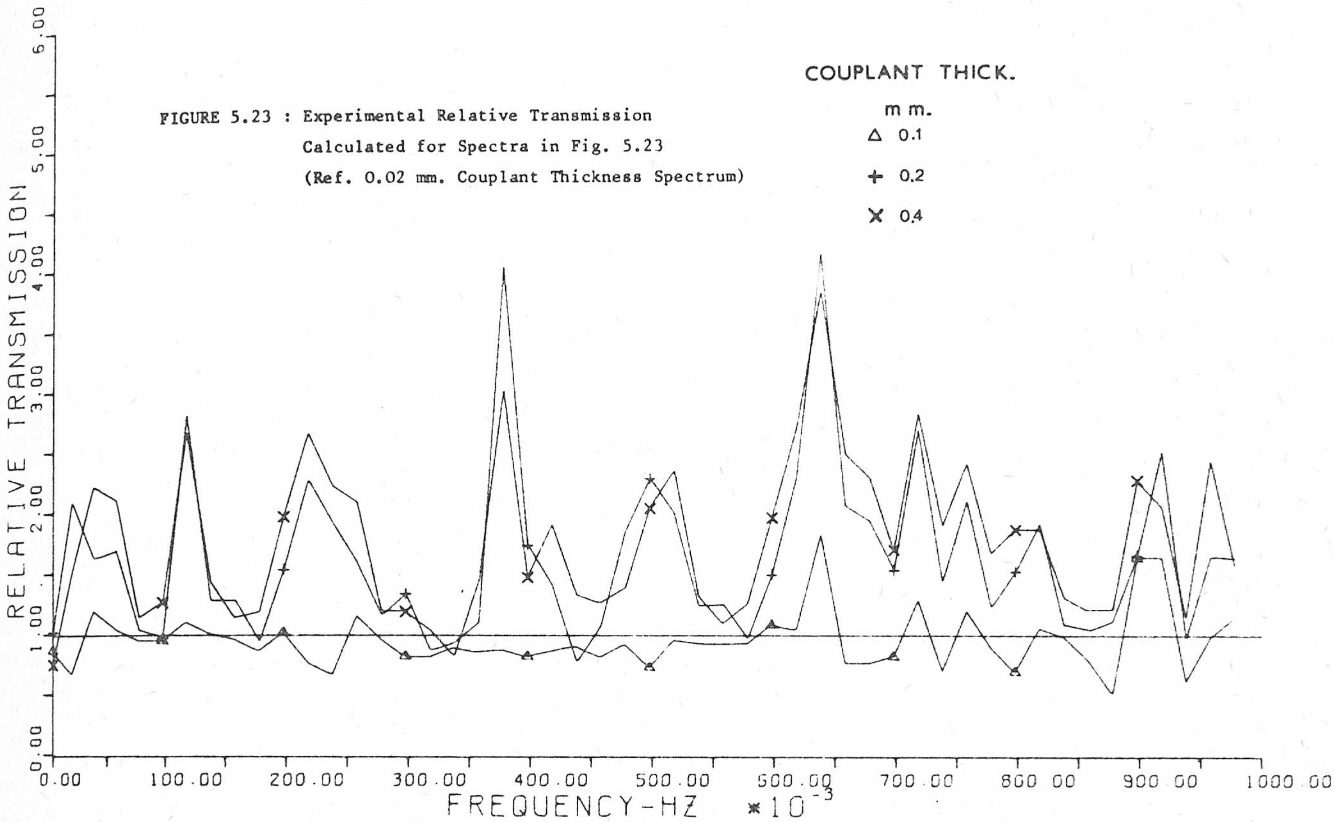

FIGURE 5.23 : Experimental Relative Transmission
Calculated for Spectra in Fig. 5.23
(Ref. 0.02 mm. Couplant Thickness Spectrum)

(a) For 0.1, 0.2, and 0.4 mm. Silicone Grease Couplant

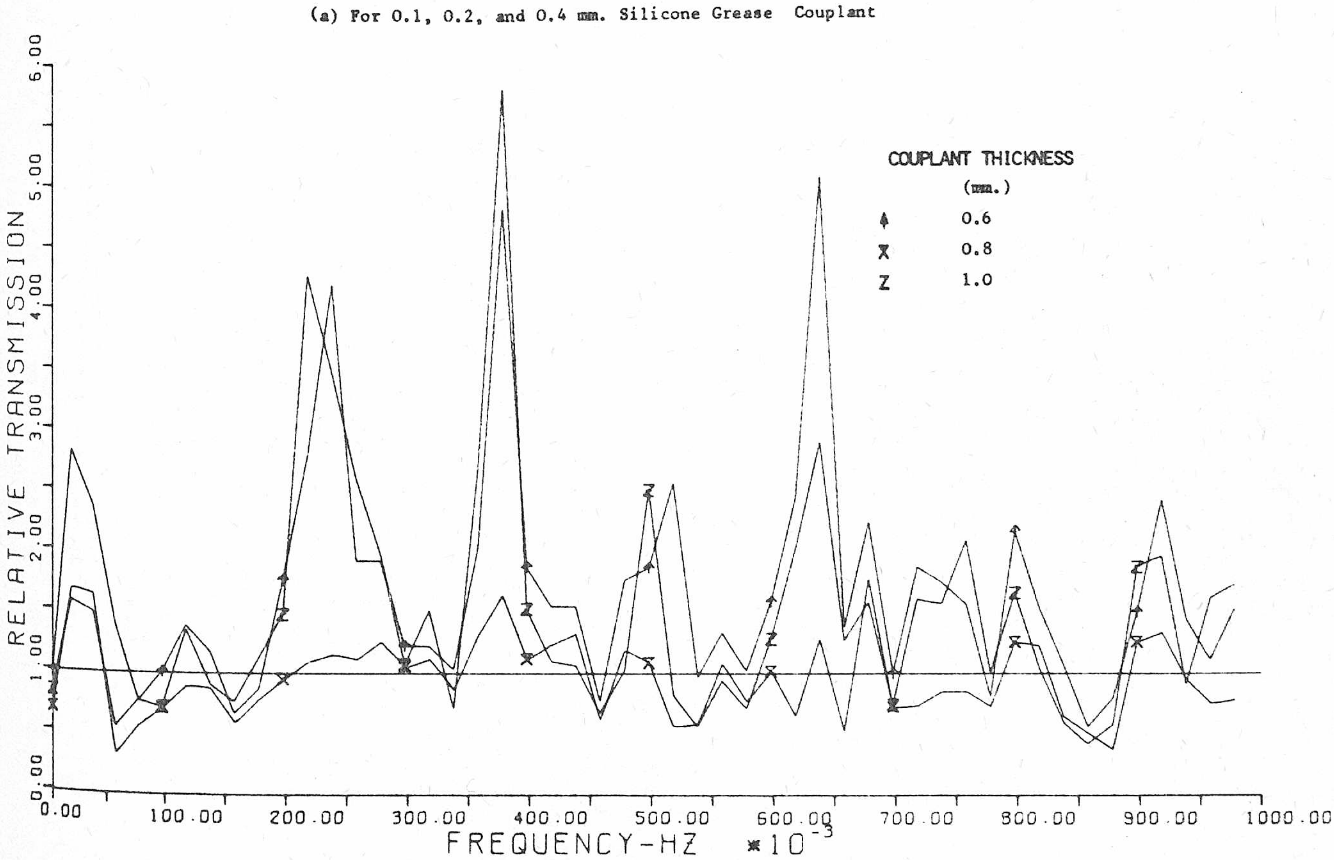

FIGURE 5.23 : Continued.

(b) For 0.6, 0.8, and 1.0 mm. Silicone Grease Couplant.

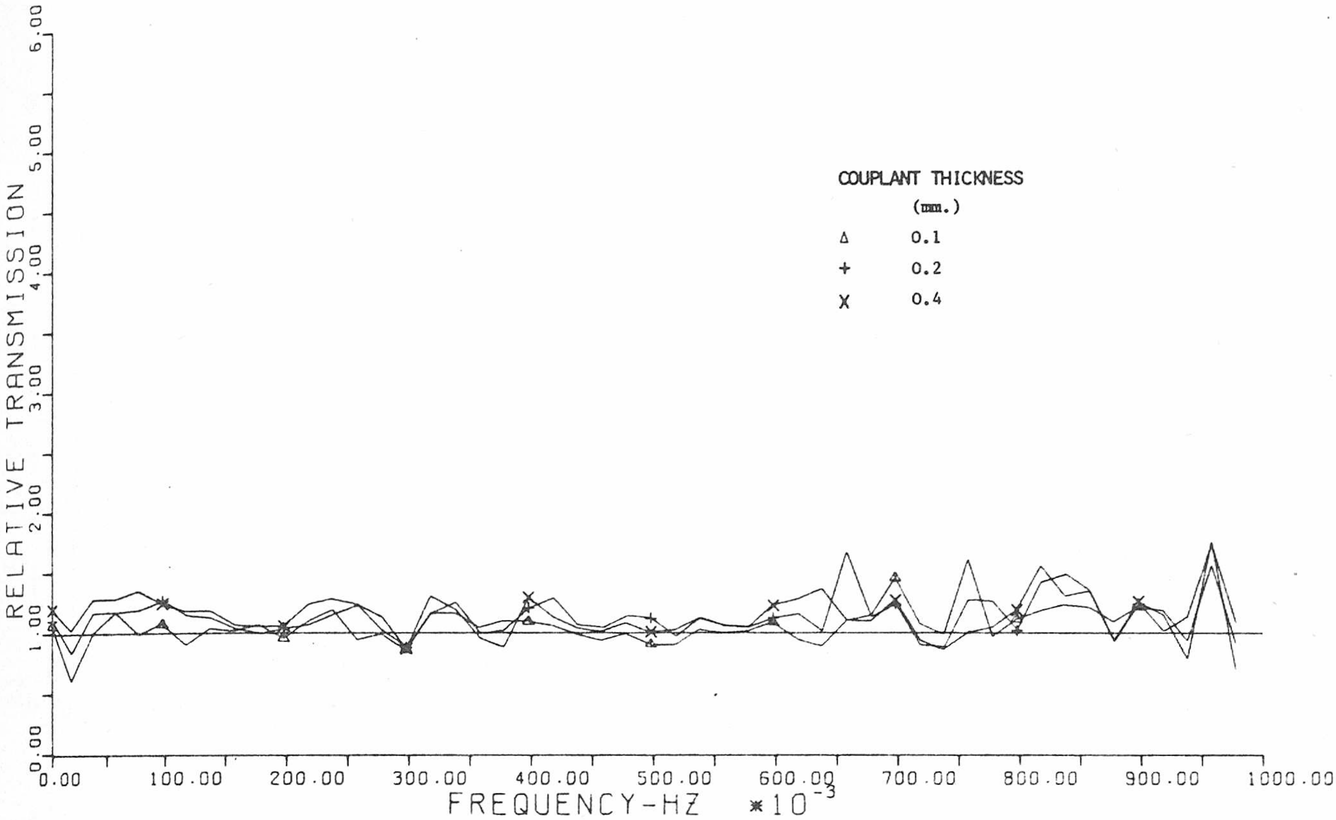

FIGURE 5.23 : Continued.
(c) For 0.1, 0.2, and 0.4 mm. Water Couplant.

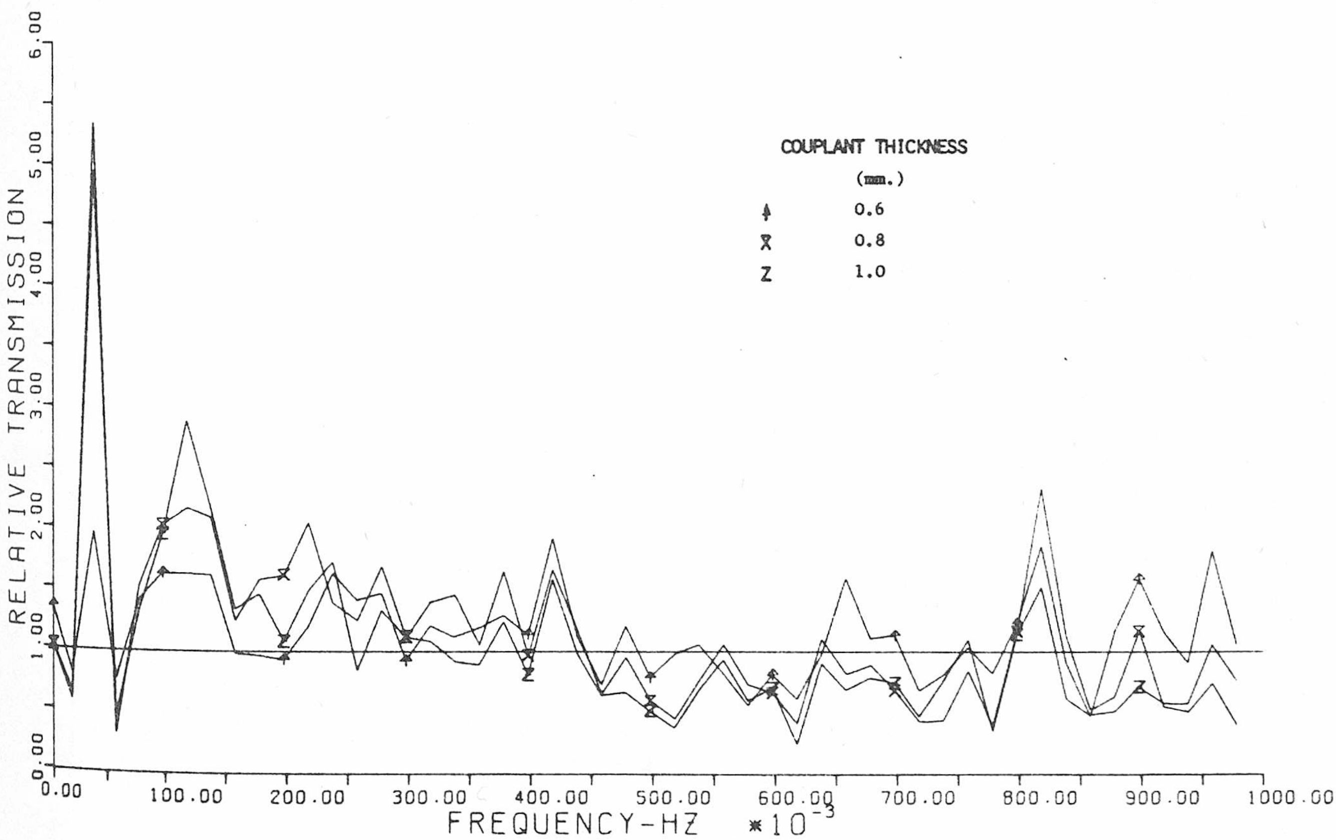

FIGURE 5.23 : Continued.
(d) For 0.6, 0.8, and 1.0 mm. Water Couplant.

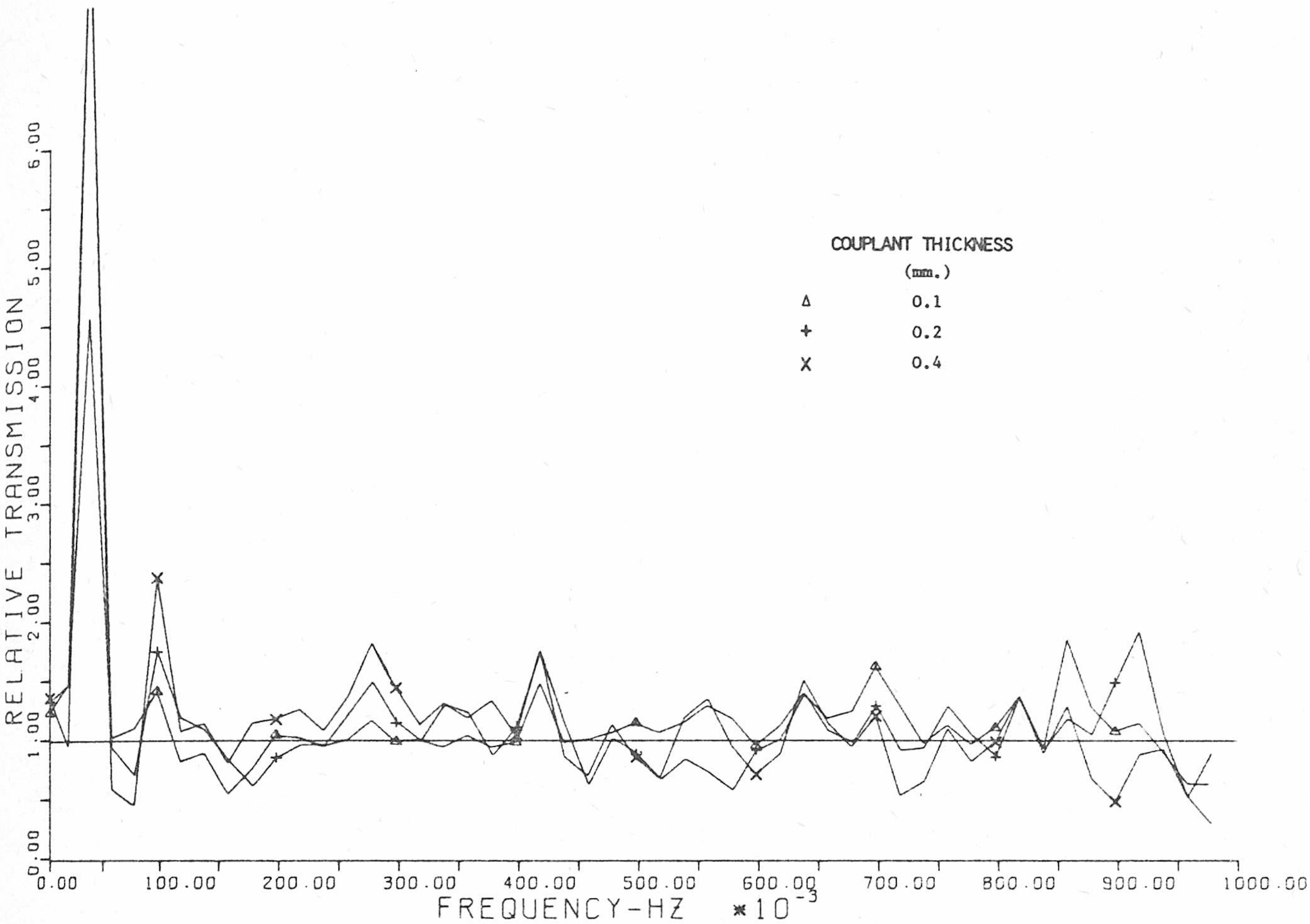

FIGURE 5.23 : Continued.

(e) For 0.1, 0.2, and 0.4 mm. Glycerine Couplant (1140 $Kg.m^{-3}$)

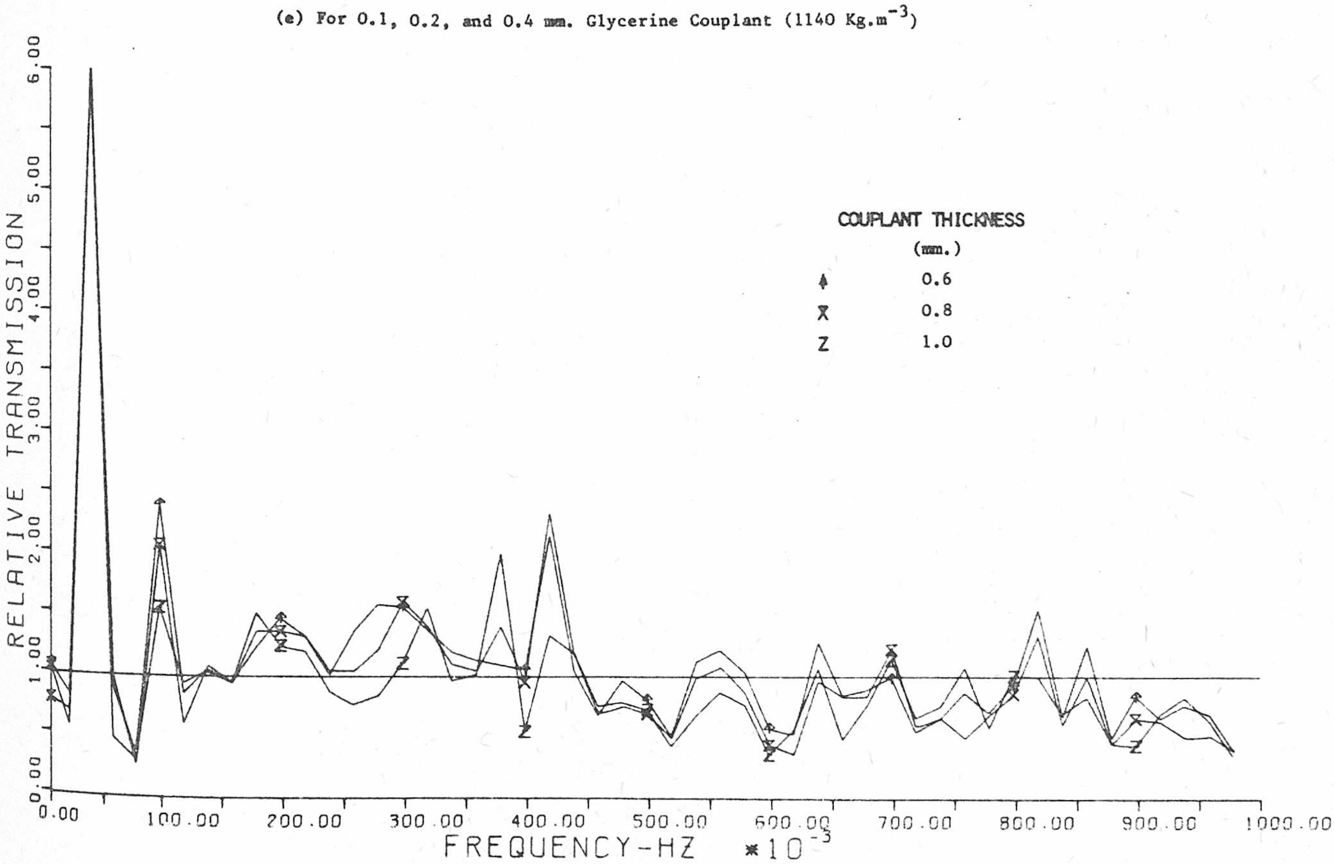

FIGURE 5.23 : Continued.

(f) For 0.6, 0.8, and 1.0 mm. Glycerine Couplant (1140 $Kg.m^{-3}$)

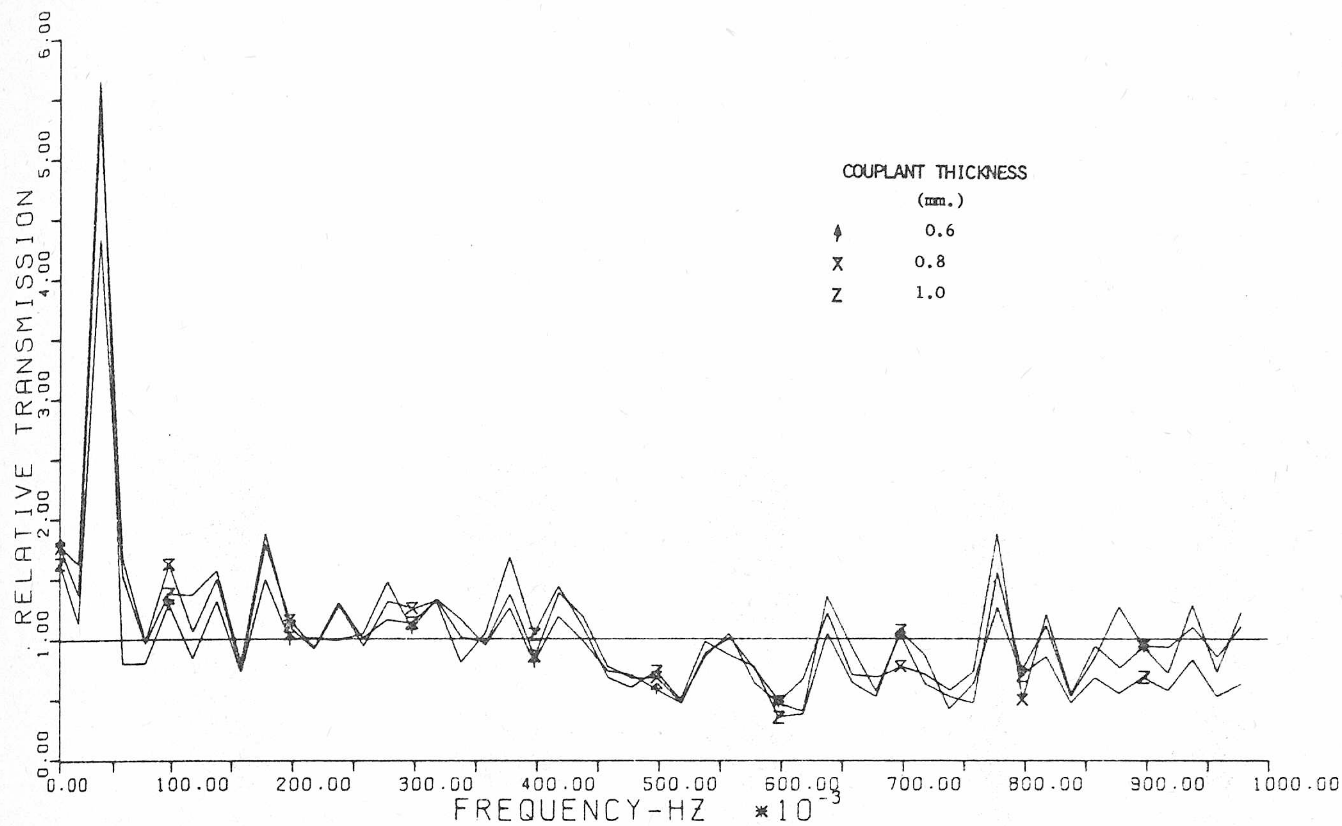

FIGURE 5.23 : Continued.

(h) For 0.6, 0.8, and 1.0 mm. Glycerine Couplant (1260 Kg.m^{-3})

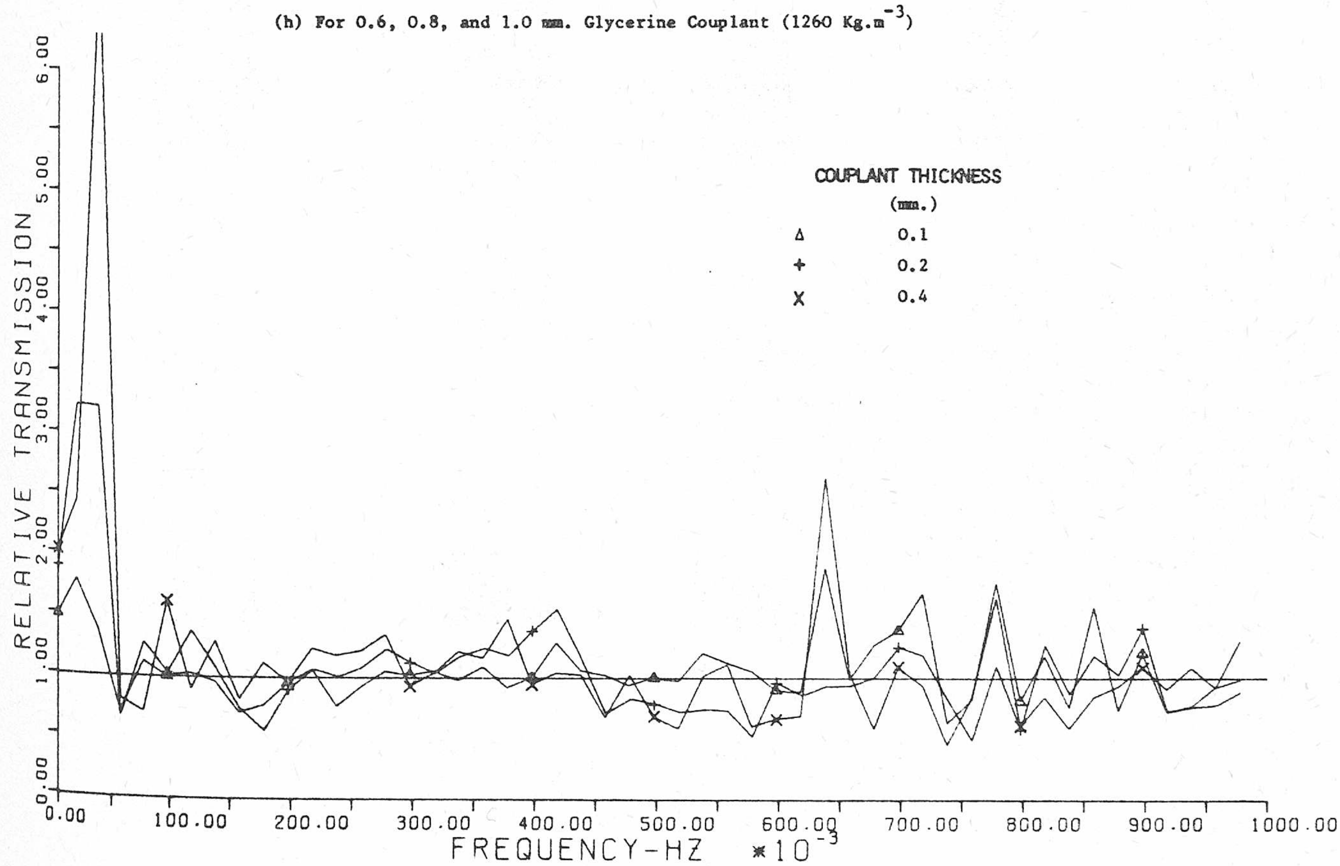

FIGURE 5.23 : Continued.

(g) For 0.1, 0.2, and 0.4 mm. Glycerine Couplant (1260 Kg.m^{-3}).

smaller amplitudes. Interference between the numerous group of peaks makes the interpretations of test results difficult.

II Results for Continuous Wave Experiments:

Since the complex wave form of any impulse can, by means of the Fourier integral, be synthesized by the superposition of a number of simple sinusoidal waves of different amplitude and frequency; continuous wave techniques can be used to examine the frequency response and possibly verify the transmission theory.

Experiments were carried out using the experimental arrangement shown in Fig. 4.7 and the aluminium couplant block (X) in air (Fig. 4.4). The simulated acoustic emission transducer was driven by sweeping a continuous sine wave of 2.4 volts constant amplitude over the frequency band. The propagated signal was received by D750 acoustic emission transducer. A series of experiments were conducted for various frequency ranges.

In all results, the acoustic emission transducer response yielded extremely fast oscillations (see Fig. 5.24) when reasonable sweep time (100 seconds) was used. A fast sweep time (10 seconds) was chosen to average the frequency response. Figures 5.25 (a) and (b) show the variation of the transducer direct frequency response (averaged) when grease was used as couplant medium. The spectral amplitude at the appropriate frequency range are seen to vary considerably with the change in couplant thickness. The peak shifts can also be seen in these graphs at certain frequencies.

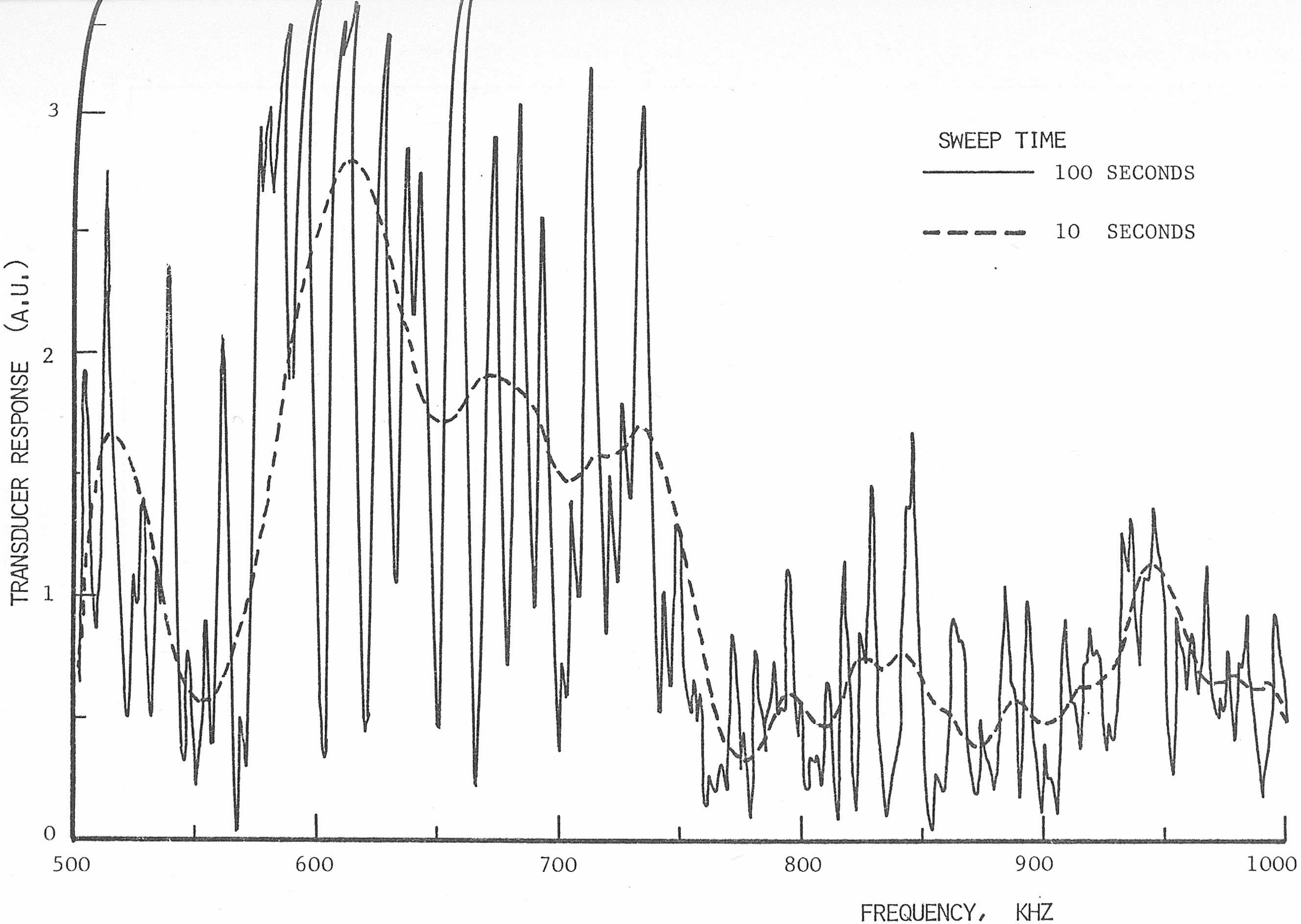

FIGURE 5.24 : Effect of the Propagation Block Vibration Modes on the Transducer Frequency Response. Using D750 Transducer and 0.02 mm. Thickness Silicone grease Couplant.

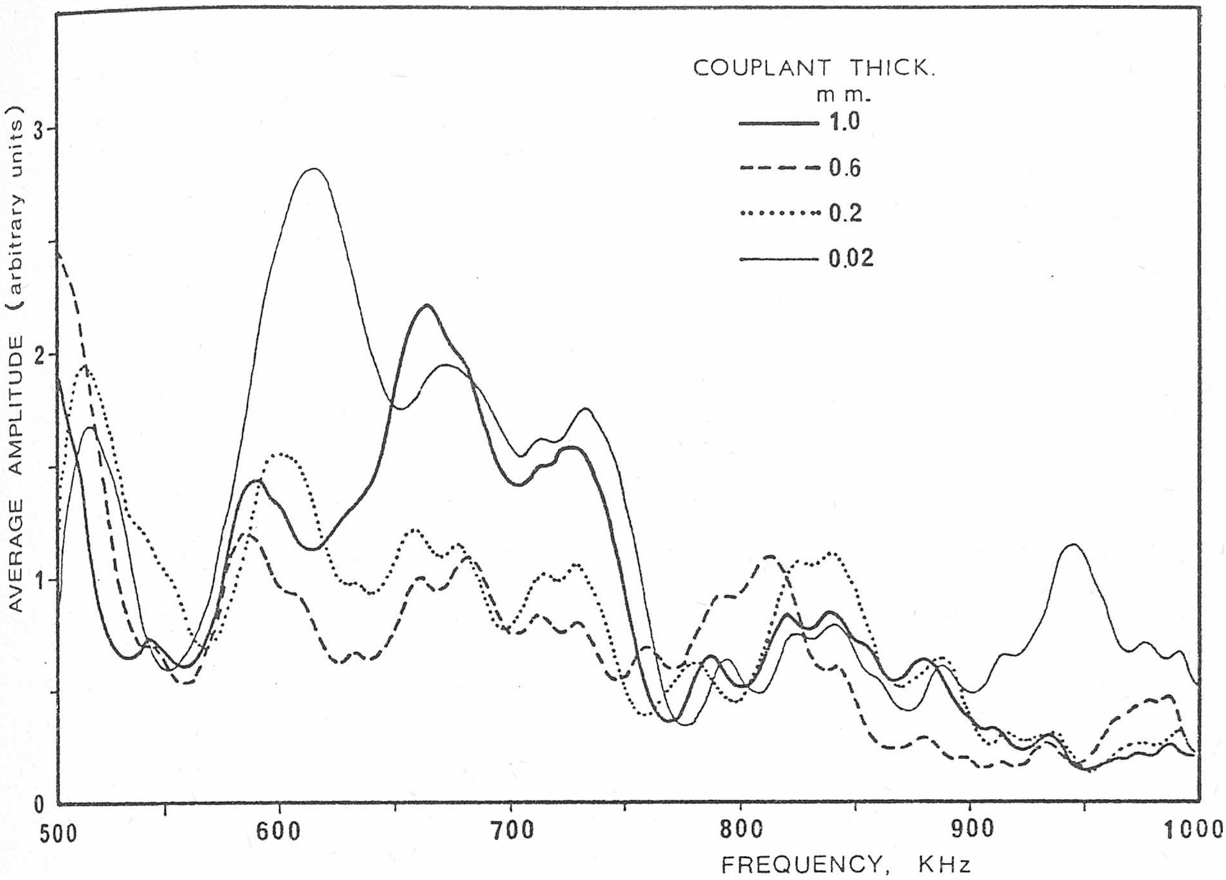

FIGURE 5.25 : Variation in Direct Transducer Frequency Response Using Silicone Grease as a Couplant a Fast Sweeping Time (10 Sec.).

(a) For 0.02, 0.2, 0.6, and 1.0 mm. Silicone Grease Couplant.

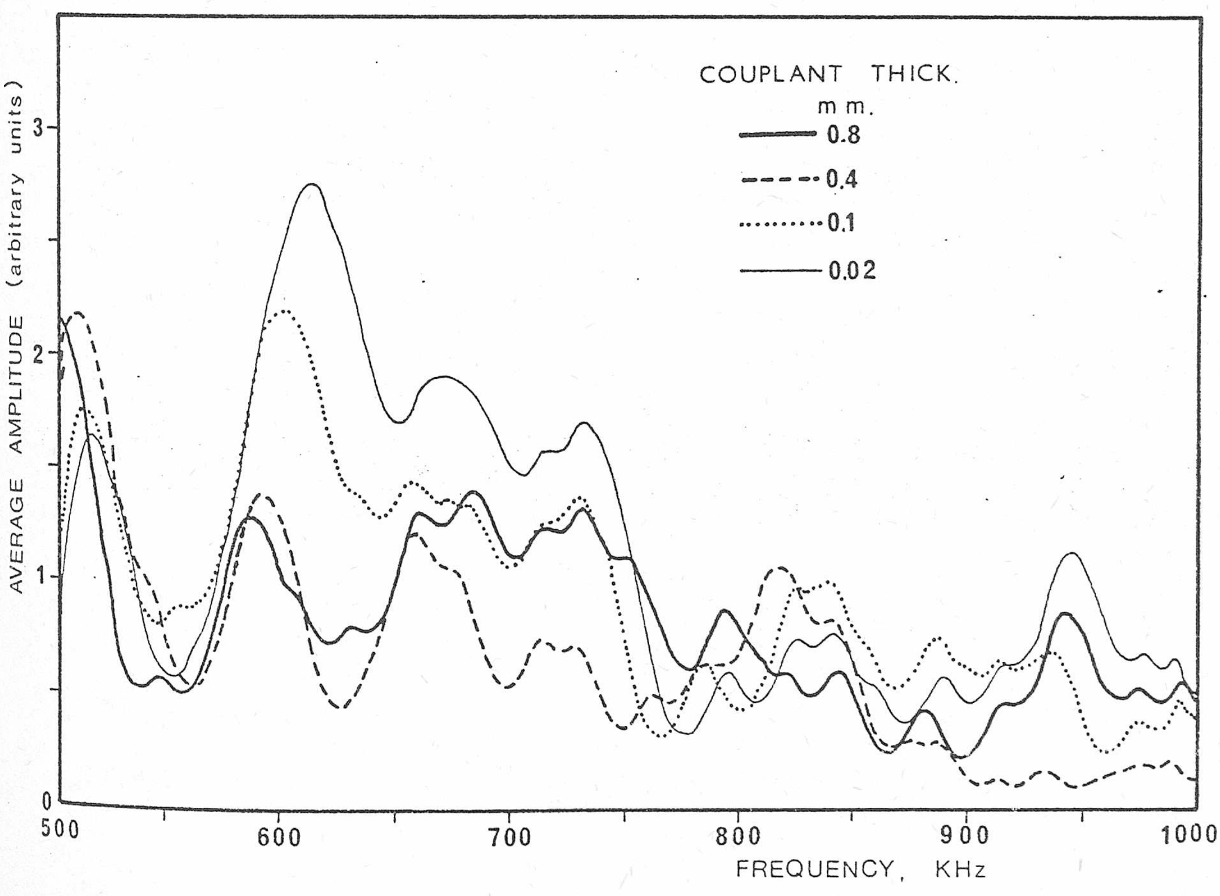

FIGURE 5.25 : Continued.

(b) For 0.02, 0.1, 0.4, and 0.8 mm. Silicone Grease Couplant.

However, an accurate comparison between experimental and theoretical results remain difficult because of the large peak gradient produced with the slow sweep in the original curves. It was also a problem to assess the averaged response as most of the peak values are distorted.

Difficulty in obtaining agreement between experiment and theory was attributed to these block resonances produced by the multiple reflection at the block free surfaces. The surfaces of the block is left free, so that plane waves travelling along the block plane surfaces can be assumed to be perfectly reflected. If, as in the case with the aluminium block in question, the attenuation is sufficiently small, a system of standing waves is set up whenever $\ell_{a\ell} = \frac{n\lambda(a\ell)}{2}$ and approximately $d_{a\ell} = n\lambda(a\ell)/2$, where n, the number of halfwaves is an integer, $\ell_{a\ell}$ is the block thickness and $d_{a\ell}$ is the block diameter. Then the change in frequency required to introduce one more halfwave is

$$\Delta f_1 \frac{C_L(a\ell)}{2\ell_{a\ell}} \quad \text{and} \quad \Delta f_2 = \frac{C_L(a\ell)}{2d_{a\ell}}$$

where $C_L(a\ell)$ is the longitudinal wave velocity in the aluminium block. However, the thickness of the block is not long enough to contain a large number of halfwaves resonance (n x 160 KHz) but it is believed to be a radial reflection from the side surface of the block (simply n x 32 KHz). In effect, small change of frequency results in sudden large change in the transmission amplitude.

Therefore, the signal from the PZT-element depends strongly on the dimensions of the test block and on the frequency.

The S140 transducer was attached to a rectangular aluminium block of 3.5 x 2.5 x 6.5 cm. The PZT-element of this transducer had a natural frequency of 342 KHz. The source transducer was placed on the block opposite to the S140 transducer (on the 6.5 x 3.5 cm surface). The input frequency was swept from 20 to 200 KHz in 100 seconds. A sine wave of 2.4 volts constant amplitude was used. The amplified output was rectified and applied to an X-Y recorder given the curve shown in Fig. 5.26. The peaks correspond to maxima in the response of the whole system.

Instead of rising uniformly to a maximum at about 150 KHz and then falling, the envelope of the record has maxima as if there were beats between too many different sets of waves. This effect appears to be similar to that observed by J. Speake (163) using a laser beam interferometer to excite the surface of a test block.

From the point of view of the wave theory the volume of the aluminium block is seen as a complex vibratory system. Such a system, when excited by a stress wave, carries out its own gradually decaying normal modes of vibration. To clarify this, it is necessary to study the nature of these vibration modes.

The frequencies of the normal modes of vibration which can be obtained from the equation (151):

$$f_r = \frac{C}{2}\left\{\left(\frac{n_i}{x}\right)^2 + \left(\frac{n_j}{y}\right)^2 + \left(\frac{n_k}{2}\right)^2\right\}^{\frac{1}{2}} \qquad (5.10)$$

where C is the propagation velocity in the block material;

x, y and z are the specimen dimension, and

n_i, n_j and n_k = 0, 1, 2, ...

By substituting with the specimen dimension in equation (5.10) gives the specimen normal modes which have been indicated in Fig. 5.26.

5.5.3 CONCLUSIONS

Both the theoretical and experimental results lead to the following conclusion.The change in the couplant layer thickness, even by a small amount, has substantial effect on the transducer response. Most of the acoustic emission parameters are seen to be affected by this small variation.

In general, the theoretically calculated transmission coefficients demonstrate that with an increase in couplant thickness first, there is a shift in the PTC maxima; i.e. a shift in the system resonant frequencies and second, the transmission band diminishes. Thirdly, the PTC and resonance increases or decreases depending on the acoustical characteristics and thickness of the couplant layer.

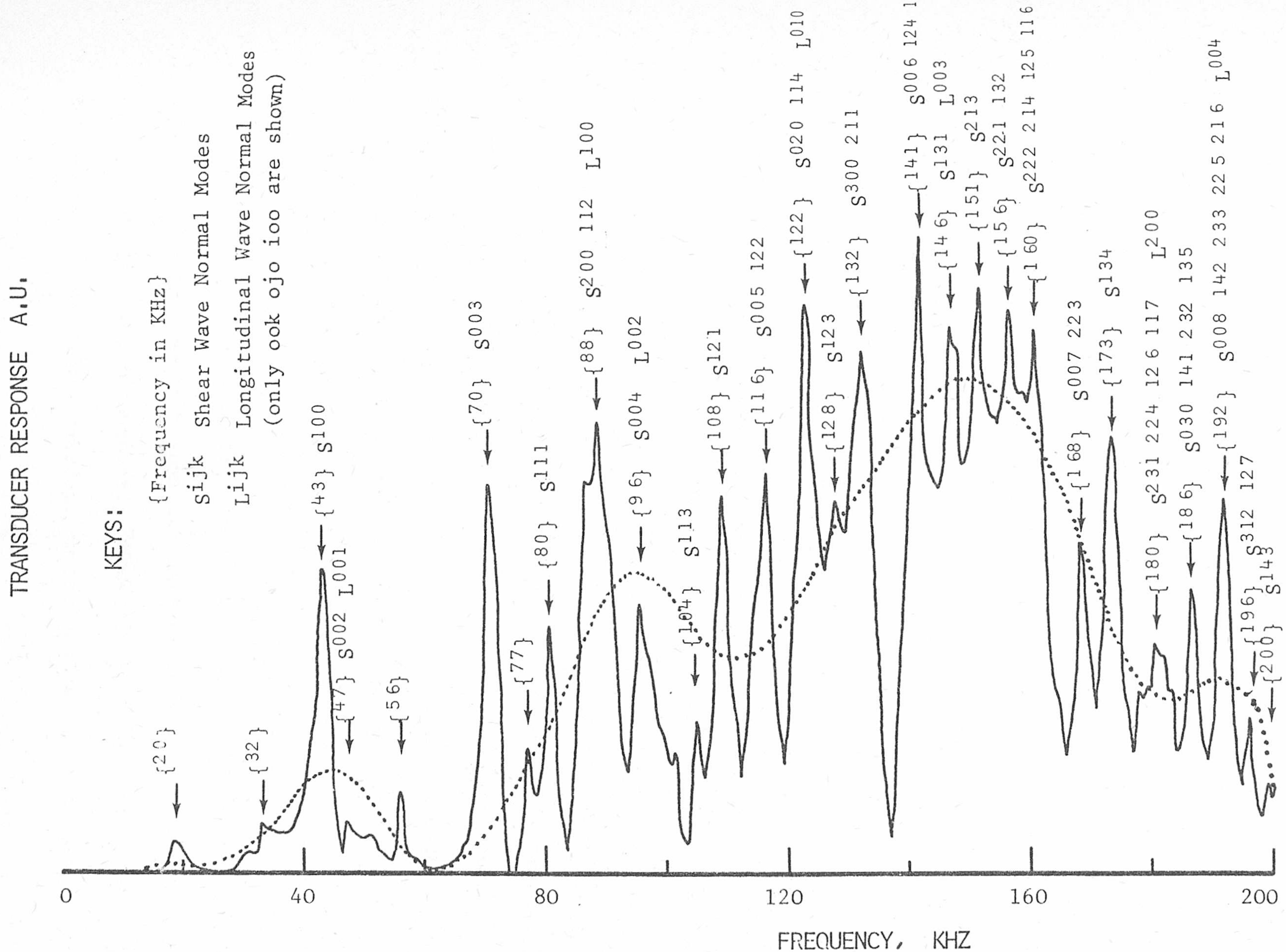

FIGURE 5.26 : The Effect of the Rectangular Aluminium Block (3.5x2.5x6.5 cm.) Vibration Mode on the Acoustic Emission Transducer (S140) Direct Response.

It was necessary to reduce or remove the specimen resonances from the transmission system frequency response in order to compare theoretical and experimental results.

The continuous wave technique was valuable in verifying the theoretical predictions as the input stress wave amplitude can be varied to overcome the problem of low signal sensitivity at frequencies away from the acoustic emission transducer resonance.

This approach will be discussed in the next section using the six-layer model.

5.6 TRANSMISSION THROUGH A SIX-LAYER SYSTEM

So far, it has been postulated that the transmission characteristics of acoustic emission transducers could be predicted by the use of multilayer transmission theory. Experiments carried out using five-layer theory did not verify that the theory was applicable. The difficulties were attributed to the non-uniform specimen geometry resonances. To overcome this problem, several approaches, in addition to the repeated pulse and continuous wave techniques, have been considered. Gated sine wave and warbled continuous sine waves were tried. However, block resonances still proved a problem so that experimental accuracy was still not high enough. Experiments could possibly be done in a semi-infinite fluid which would remove the problem of peaky resonances. However, this approach does not duplicate the practical transduction process as the transducer was not loaded into a solid body.

A compromise transmission system was used by modifying the propagation couplant block as shown in Fig. 4.5 (b and c). The propagation block was designed to be used underwater. The sound beam from the source transducer travels through water first before striking the aluminium diaphragm. The six-layer transmission model has to be investigated for this particular transmission system.

5.6.1 CALCULATION OF TRANSMISSION THROUGH SIX-LAYER

Figure 5.27 (a-e) shows the pressure transmission curves that were theoretically predicted for the experimental configuration using equation (3.74). The pressure transmission coefficients (PTC) are calculated for radiation from water (first medium) into a final medium (air) via four intermediate layers. The second layer consists of the aluminium diaphragm (3mm thick), and the third layer is the silicone grease couplant layer of various thicknesses. The fourth layer is the transducer protective shoe and consists of a 3.125 mm thick epoxy resin shoe. The fifth layer is the transducer PZT-element of the S140 transducer (6.35 mm thick). This transducer was chosen for the final experimental verification because it had the thickest active PZT-element of the available acoustic emission transducers. Therefore, if it were possible to verify the predicted transmission curves by employing this transducer, then, it would mean that better agreement could be expected for other transducers with thinner PZT-elements; i.e. large diameter/thickness ratios.

The transmission curves shown were calculated by using equation (3.74) in conjunction with (3.73) and the computer program CPNG6.FOR (Appendix 5.F). It is worthwhile to note the following characteristics in the transmission curves:

(i) Three principal groups of peaks are common in all couplant thickness graphs. These groups take place at three fixed frequencies 172,514 and 856 KHz. It is evident that these frequencies are harmonic of the fundamental frequency 172 KHz. They could only be related to the PZT-element geometry.

The first group of peaks at 172 KHz corresponds to one-quarter wavelength of the PZT-element. As the couplant thickness increases the peak amplitude decreases until the grease layer thickness extends to 1.4 mm when the peak amplitude starts to increase again. This change in peak amplitude is accompanied by similar changes in the peak bandwidth. The phase differences between the incident wave and the wave transmitted into the air backing medium are almost $|\pi/2|$, as can be seen in the first column of the summary Table 5.IX.

The second principal group of peaks is shown to be at 514 KHz which corresponds to $\ell_5 = 3\lambda_5/4$. Again, as the couplant thickness increases the peak amplitude decreases up to thickness of 0.5 mm. Then, a sudden jump in the amplitude can be noted for 0.9 mm grease couplant thickness (see Fig. 5.27(c)). At this particular couplant thickness the phase difference also has a unique value of about $\pi/3$. Another sudden increase can be also seen for 1.4 mm grease thickness.

The third principal group of peaks in the frequency band of interest occurs at frequency 856 KHz and corresponds to $\ell_5 = 5\lambda_5/4$.

(ii) As the frequency increases from one principal group of peaks to the next, the nonuniformity of the curves becomes more pronounced with the appearance of intermediate relatively less sharp peaks with lower amplitudes. These secondary peaks oscillate in both frequency and amplitude between the two principal groups depending on the selected couplant thickness ℓ_3.

In Fig. 5.27(d), it is possible to follow the change in the transmission efficiency when the secondary peaks have almost disappeared for particular range of couplant thickness (1.0-1.6 mm). At this couplant thickness range, the transmission efficiency decreases, the effect of the change in couplant thickness is small and the curves become more uniform, characterized by only three principal groups of peaks.

Similar curves for water as couplant medium are included in Appendix 5.G. The water couplant curves are qualitatively similar to those for silicone grease.

5.6.2 THE SIX-LAYER EXPERIMENTS

In order to verify the theoretical transmission model experimentally, one must be able to use similar parameters for both the theoretically calculated and experimentally measured transmission characteristics. The experimental configuration is shown in Fig. 5.28 comprising the propagation media and measurement components. The measurement system can be respresented as a series of transfer functions which are all function of frequency.

If a constant voltage and frequency dependent current I (ω) is used to drive the source transducer (1) with transfer function S (ω), the source transducer may be considered as a volume velocity $(m^3\ s^{-1})$ source and the stress wave output from the propagation medium (2) will be a pressure parameter $(N\ m^{-2})$ as explained by Hill and Adams (47). The net output voltage of the acoustic emission transducer $E(\omega)$ will be equal to the original source spectrum modified by a series of connected transfer functions. The transfer function of the six-layer transmission system $X(\omega)$ is equivalent to the pressure transmission coefficient $\alpha_{p6}(\omega)$; i.e. $|A_6/A_1|$ in equation (3.73) modified by the PZT-element transduction transfer function $\tau(\omega)$ which is dependant on the transduction

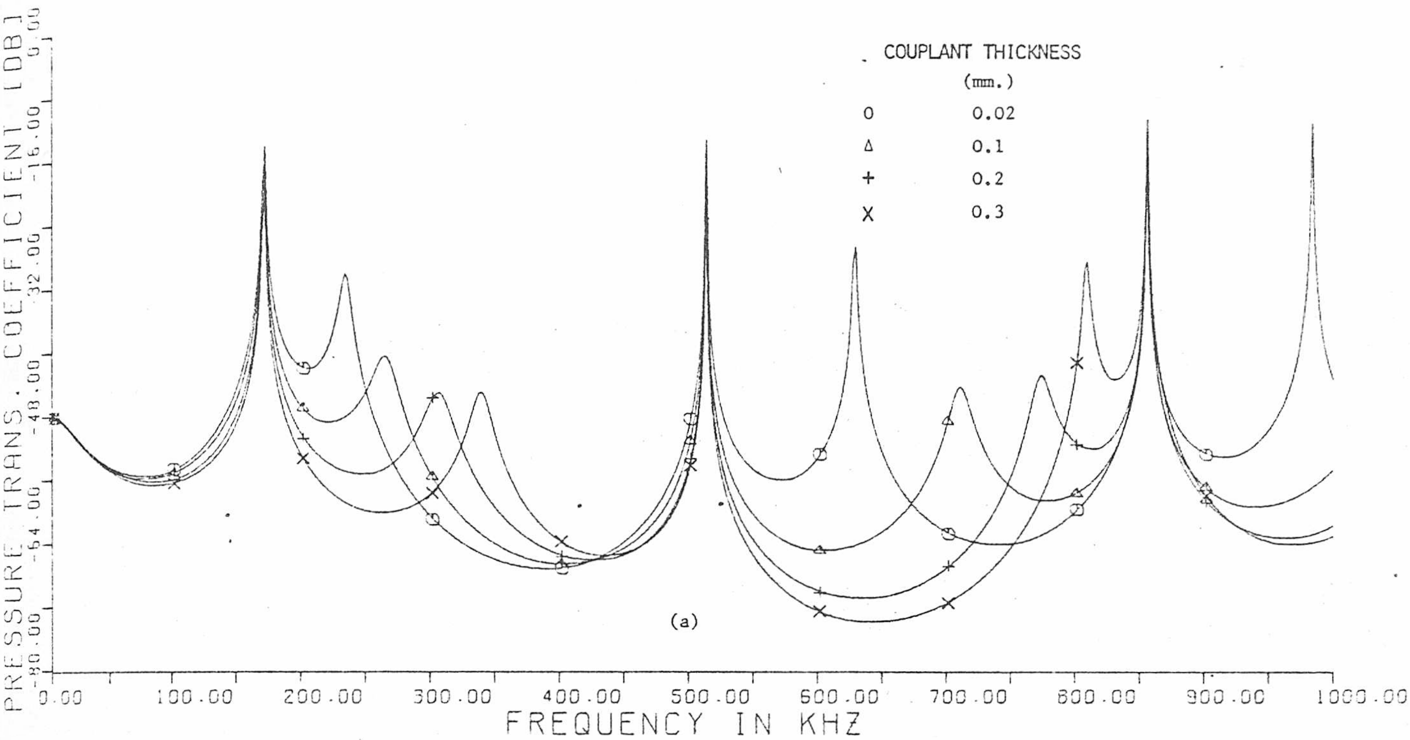

FIGURE 5.27 : Calculated Pressure Transmission Coefficient for the Experimental Six-layer Transmission System Using Silicone Grease Couplant and S140 D/E Transducer.

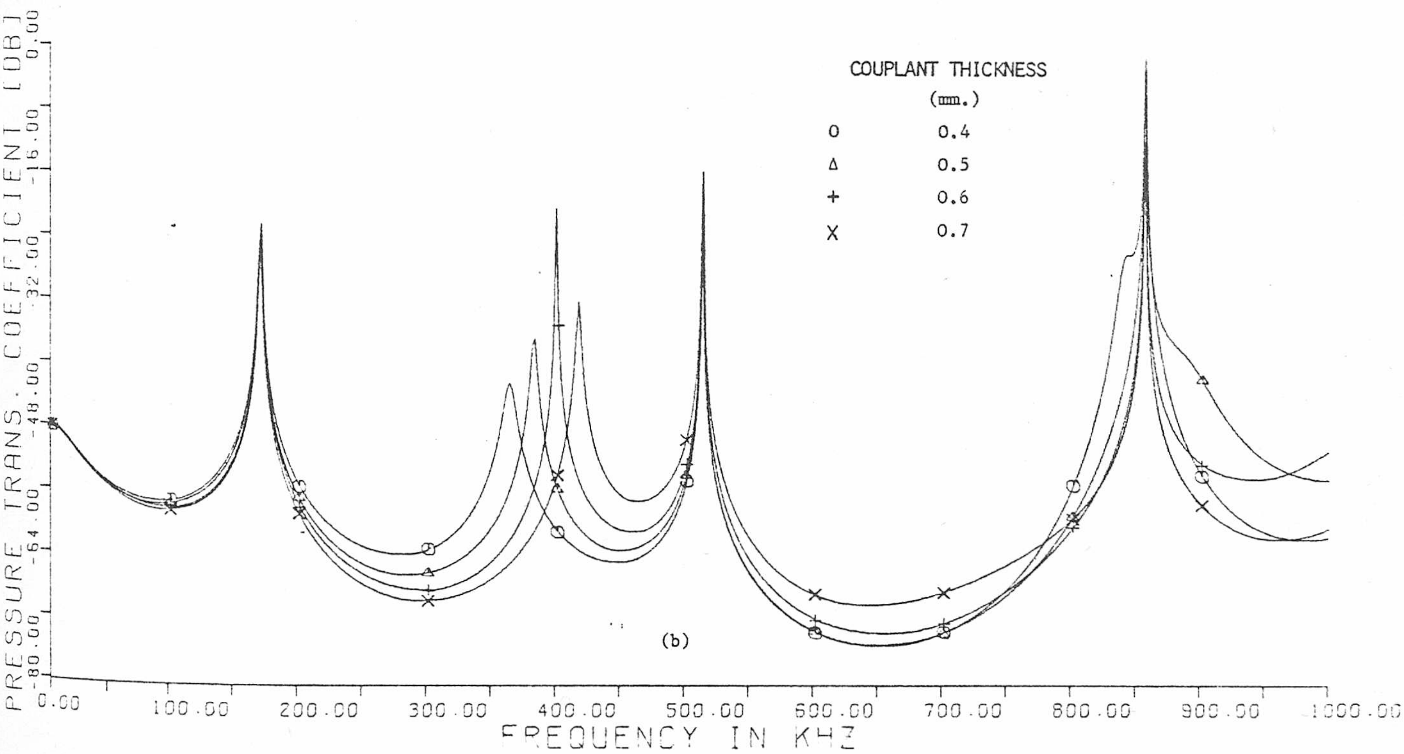

FIGURE 5.27 : Continued.

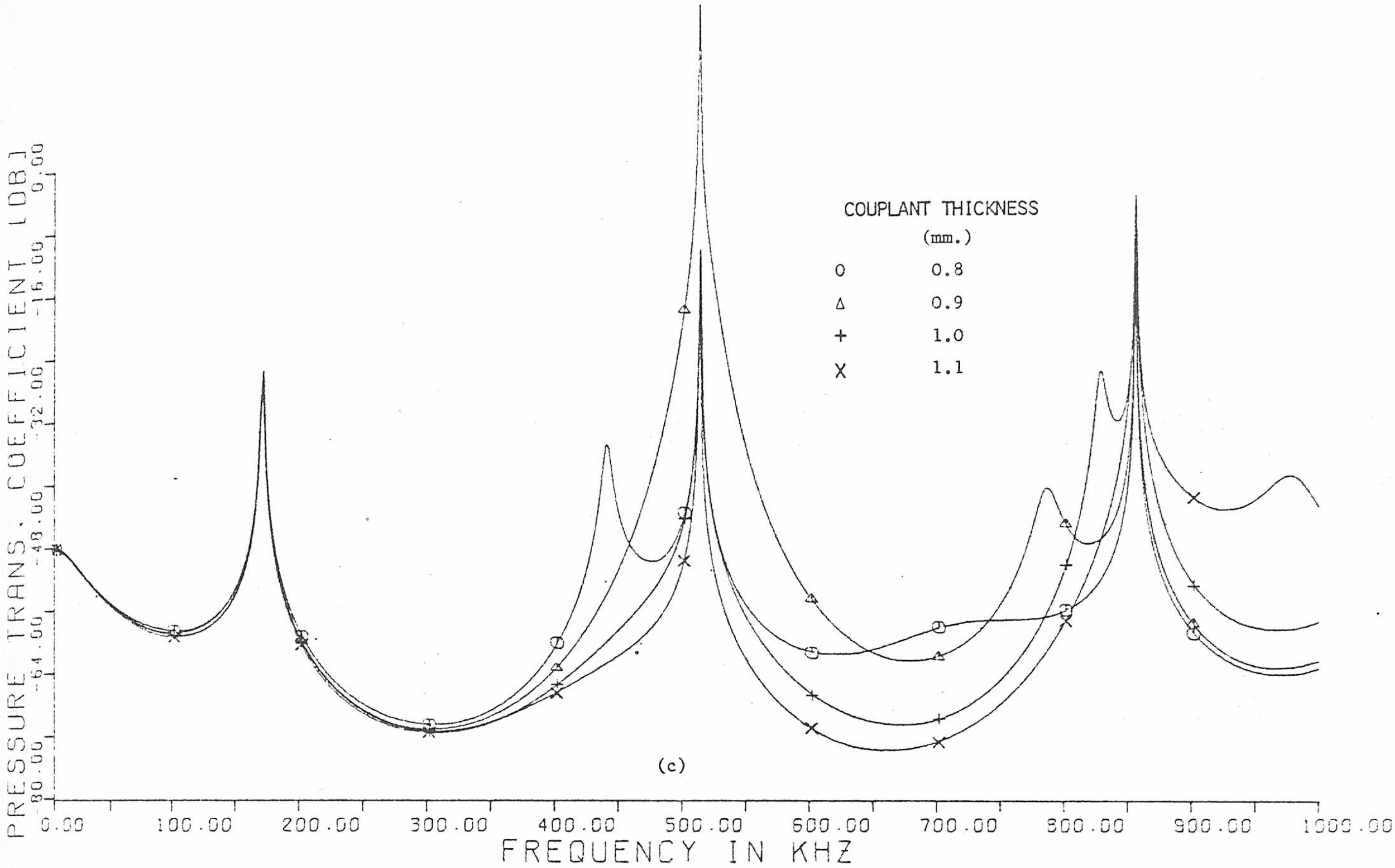

FIGURE 5.27 : Continued.

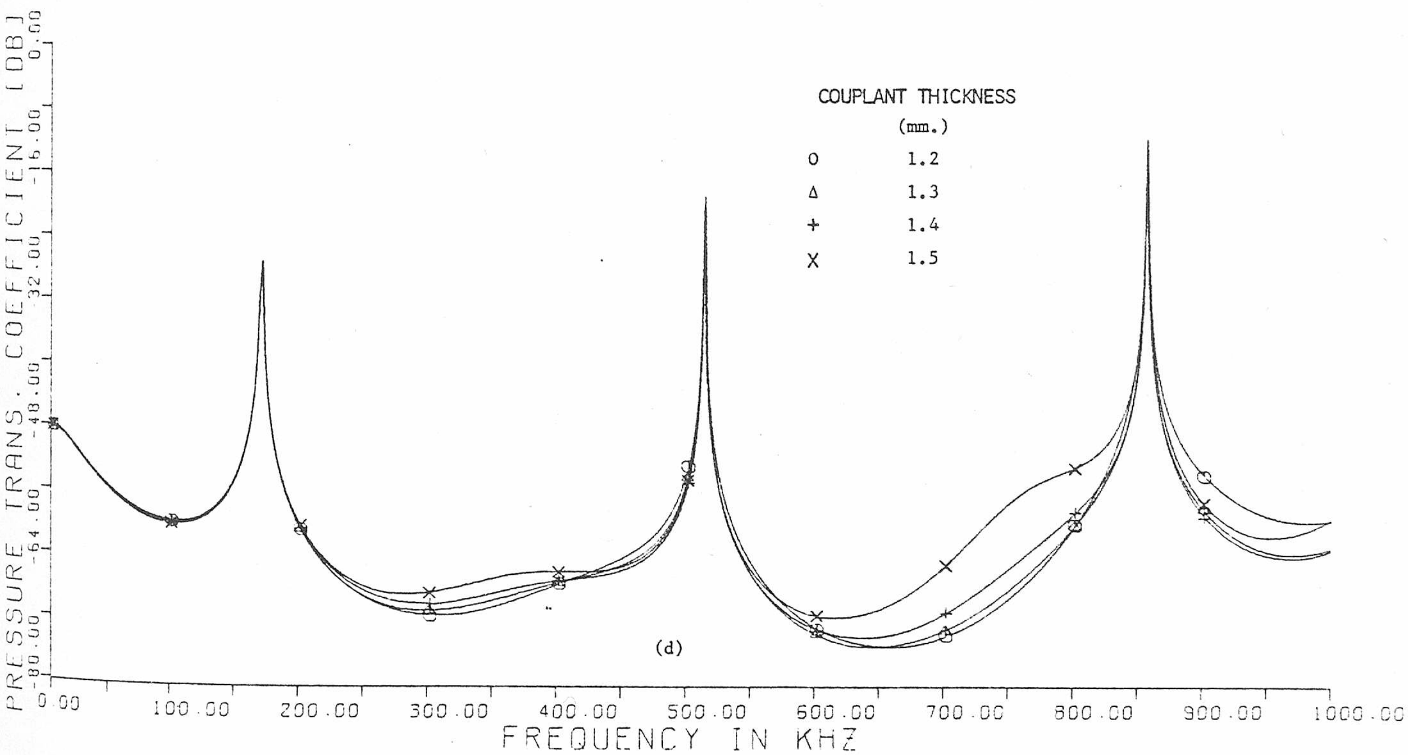

FIGURE 5.27 : Continued.

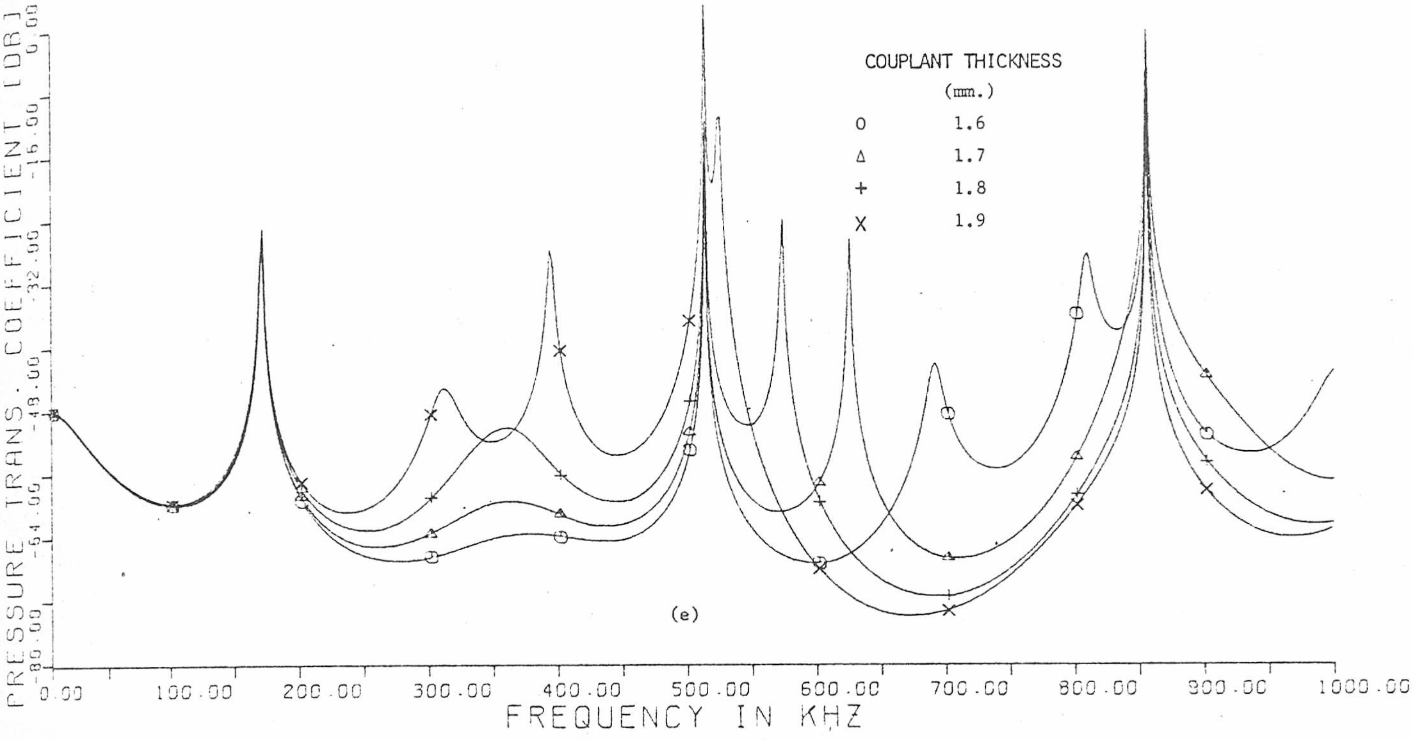

FIGURE 5.27 : Continued.

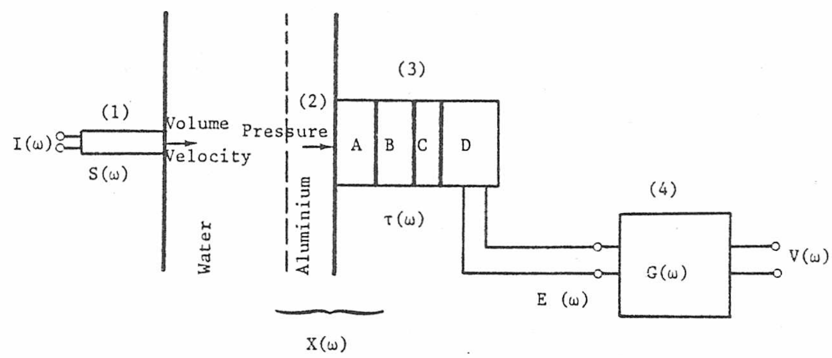

The Transmission System

FIGURE 5.28 : Experimental Configuraton and the System Transfer Functions.

(1) Source Transducer

(2) Propagation Medium

(3) Acoustic Emission Transducer :
A- Couplant Layer
B- Protective Shoe
C- PZT-Element
D- Backing

(4) Electric System

Table 5.IX Summary of the Main Features of Figures 5.28 (a-e) for Silicone Grease Couplant

Couplant Thick. (mm)	172 KHz					514 KHz					856 KHz				
	PTC	P.D.	Freq.	PTC	P.D.	PTC	P.D.	Freq.	PTC	P.D.	PTC	P.D.	Freq.	PTC	P.D.
0.02	-14.26	86.9	234	-30.17	-8.9	-13.34	89.9	630	-27.41	-45.7	-12.89	-83.6	982	-18.10	-30.4
0.1	-16.76	89.9	264	-40.54	0.5	-16.71	-89.9	712	-44.29	-2.1	-14.21	-86.8			
0.2	-19.C7	-87.8	306	-45.19	0.8	-19.09	-89.8	774	-42.85	-4.3	-13.79	89.7			
0.3	-20.83	-86.4	340	-45.04	7.1	-20.27	-89.7	810	-28.47	-27.2	-10.59	84.3			
0.4	-22.21	-85.5	364	-42.05	3.6	-20.57	-89.6				-1.24	61.1			
0.5	-23.32	-84.8	384	-36.59	25.1	-20.03	-89.5				-4.76	-68.3			
0.6	-24.24	-84.3	400	-20.17	-63.6	-18.55	-89.4				-11.72	-81.7			
0.7	-24.97	-83.7	418	-31.90	-4.3	-15.70	-89.3				-14.08	-86.2			
0.8	-25.61	-83.3	440	-34.70	11.8	-10.00	-88.9	788	-40.26	-17.4	-13.97	-89.7			
0.9	-26.06	-82.9				+21.52	58.4	828	-25.38	-19.7	-11.31	85.5			
1,0	-26.41	-82.6				-10.36	89.6				-3.50	69.2			
1.1	-26.67	-82.3				-15.87	-89.9				-2.79	-62.5	980	-36.95	85.7
1.2	-26.84	-82.0				-18.64	-89.8				-11.08	-80.7			
1.3	-26.90	-81.7				-20.08	-89.7				-13.90	-85.7			
1.4	-26.88	-81.4				-0.58	-89.6				-14.13	-89.2			
1.5	-26.76	-81.2				-20.25	-89.6				-11.92	86.4			
1.6	-26.56	-80.8	376	-63.10	85.8	-19.02	-89.4				-5.33	74.2			
1.7	-26.25	-80.5	364	-59.17	81.9	-16.57	-89.3	626	-26.02	-51.7	-0.38	-52.8			
1.8	-25.83	-80.2	360	-50.46	64.9	-11.85	-89.0	574	-23.84	-50.4	-10.33	-79.5			

PTC = The Sound Power Transmission Coefficient ± in dB ±0.005

P.D. = Phase Angle Difference in Degree ± 0.05

Freq. = Frequency ± 1 KHz.

characteristics provided by the PZT ceramic element. Finally the signal voltage output from the transducer is amplified and filtered; i.e. modified by the electronic system transfer function $G(\omega)$ to yield an output voltage $V(\omega)$ which is function of frequency, therefore:

$$V(\omega) = I(\omega).S(\omega).X(\omega).\ \tau(\omega).G(\omega) \tag{5.11}$$

The transfer function of the six-layer transmission system $X(\omega)$ may be represented by its components transfer functions as follows:

$$X(\omega) = P(\omega).C(\omega).W(\omega).Z(\omega) \tag{5.12}$$

where:

$P(\omega)$: is the transfer function of the propagation body (aluminium),

$C(\omega)$: is the transfer function of the couplant layer,

$W(\omega)$: is the transfer function of the transducer protective shoe (epoxy resin), and

$Z(\omega)$: is the transfer function of the PZT-element.

When taking measurements, all the components of the transmission system were kept constant except for the couplant layer which was varied, therefore:

$$X(\omega) = Y(\omega).C(\omega) \quad (5.13)$$

where $Y(\omega)$ is another transfer function representing the six-layer transmission system and independant on the couplant layer characteristics. By substituting in equation (5.11) and for an arbitrary couplant thickness:

$$V(\omega) = I(\omega).S(\omega).Y(\omega).C(\omega).\ \tau(\omega).G(\omega) \quad (5.14)$$

and for measurements at reference couplant thickness:

$$\{V(\omega)\}_{ref.} = I(\omega).S(\omega).Y(\omega).\{C(\omega)\}_{ref.}\ \tau(\omega).G(\omega) \quad (5.15)$$

Taking the ratio between equations (5.14) and (5.15):

$$\frac{V(\omega)}{\{V(\omega)\}_{ref.}} = \frac{C(\omega)}{\{C(\omega)\}_{ref.}} \quad (5.16)$$

As may be seen in equation (3.73), the complex transmission system at a certain frequency and when all the system physical dimensions are kept constant except those for the couplant layer, the transmission coefficient α_{p6} may be considered as a function of the couplant thickness only. Thus the couplant transfer function is directly proportional to the system transmission coefficient, i.e.:

$$C(\omega) \propto \alpha_{p6}(\omega) \quad (5.17)$$

Consequently:

$$\{C(\omega)\}_{ref.} \; \alpha \{\alpha_{p6}(\omega)\}_{ref.} \tag{5.18}$$

By substituting from the last two equations into equation (5.16), it follows:

$$\frac{V(\omega)}{\{V(\omega)\}_{ref.}} = \frac{\alpha_{p6}(\omega)}{\{\alpha_{p6}(\omega)\}_{ref.}} \tag{5.19}$$

Therefore, at a given frequency and couplant thickness the ratio of the transducer output voltage to that at reference couplant thickness $\ell_{ref.}$, should be equal to the corresponding theoretical pressure transmission coefficient ratio at the same frequency.

5.6.3 EXPERIMENTAL VERIFICATION OF THE SIX-LAYER MODEL

The experimental results are extracted from the transducer voltage-frequency response graphs. The transducer direct frequency response was obtained at separate frequency bands depending on the transmission system efficiency and the electronic system sensitivity. Three separate sets of experimental system responses are produced to cover the frequency range of 500-1050 KHz using silicone grease as couplant with various thicknesses. Each set of graphs was obtained by driving the source transducer with a swept sine wave with constant voltage amplitude.

Figures 5.29-5.31 show the transducer S140 direct frequency response for a large variation of couplant layer thickness.

The voltages measured from the frequency response graphs were stored in data files. Each data file contains the transducer amplified output voltage versus couplant thickness at a certain frequency. This data was used to calculate the relative transmitted pressure at individual frequencies.

A comparison between theoretical and experimental results can be seen in Fig. 5.32 (a-p) for silicone grease couplant (using program CP6.FOR; Appendix 5.H). In each graph, the solid line represents the theoretical relative pressure transmission in dB calculated as:

$$20 \log_{10} \frac{\alpha_{p6}(\omega)}{\{\alpha_{p6}(\omega)\}_{ref.}} \qquad (5.20)$$

In equation (5.20) the theoretical reference level, $\{\alpha_{p6}(\omega)\}_{ref.}$, is taken as the maximum transmission coefficient in the couplant thickness range of 0-2.0 mm with 0.004 mm increment. In this case, the maximum relative transmission level is considered as zero level (i.e. zero decibel). The non-connected point were experimentally obtained (as indicated above) and in this case the reference level is the maximum signal voltage of the transducer response at the plotting frequency. The experimental couplant thickness range was 0.1-2.0 mm with 0.1 mm increment and the relative pressure was calculated as:

$$20 \log_{10} \frac{V(\omega)}{\{V(\omega)\}_{max.}} \qquad (5.21)$$

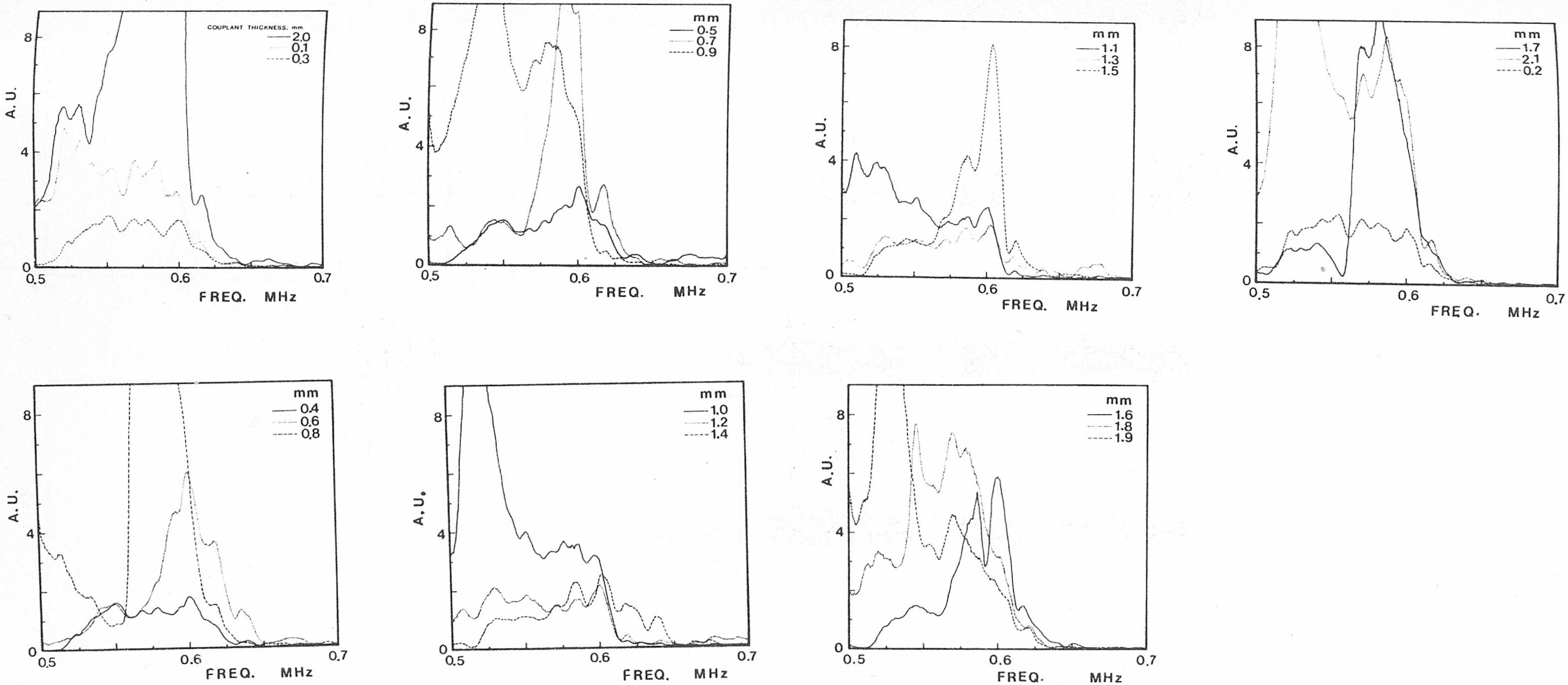

FIGURE 5.29 : Direct Frequency Response of S140 D/E Transducer Using Silicone Grease Couplant.

.Frequency Range : 500-700 KHz
.Source Transducer Input Voltage : 8 Volts
.Output Voltage : 16 mV/A.U.

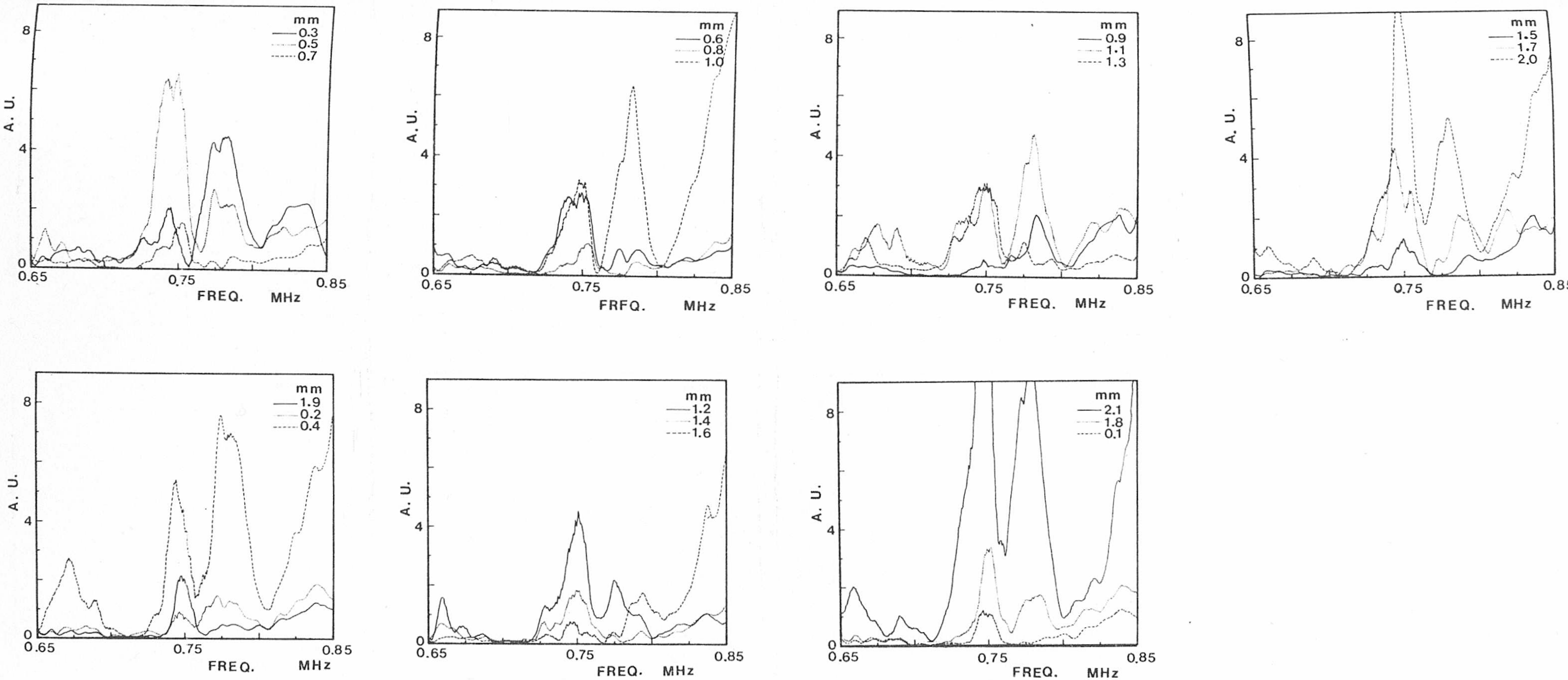

FIGURE 5.30 : Direct Frequency Response of S140 D/E Transducer Using Silicone Grease Couplant.

.Frequency Range: 650-850 KHz
.Source Transducer Input Voltage : 16 Volts
.Output Voltage : 10 mV/A.U.

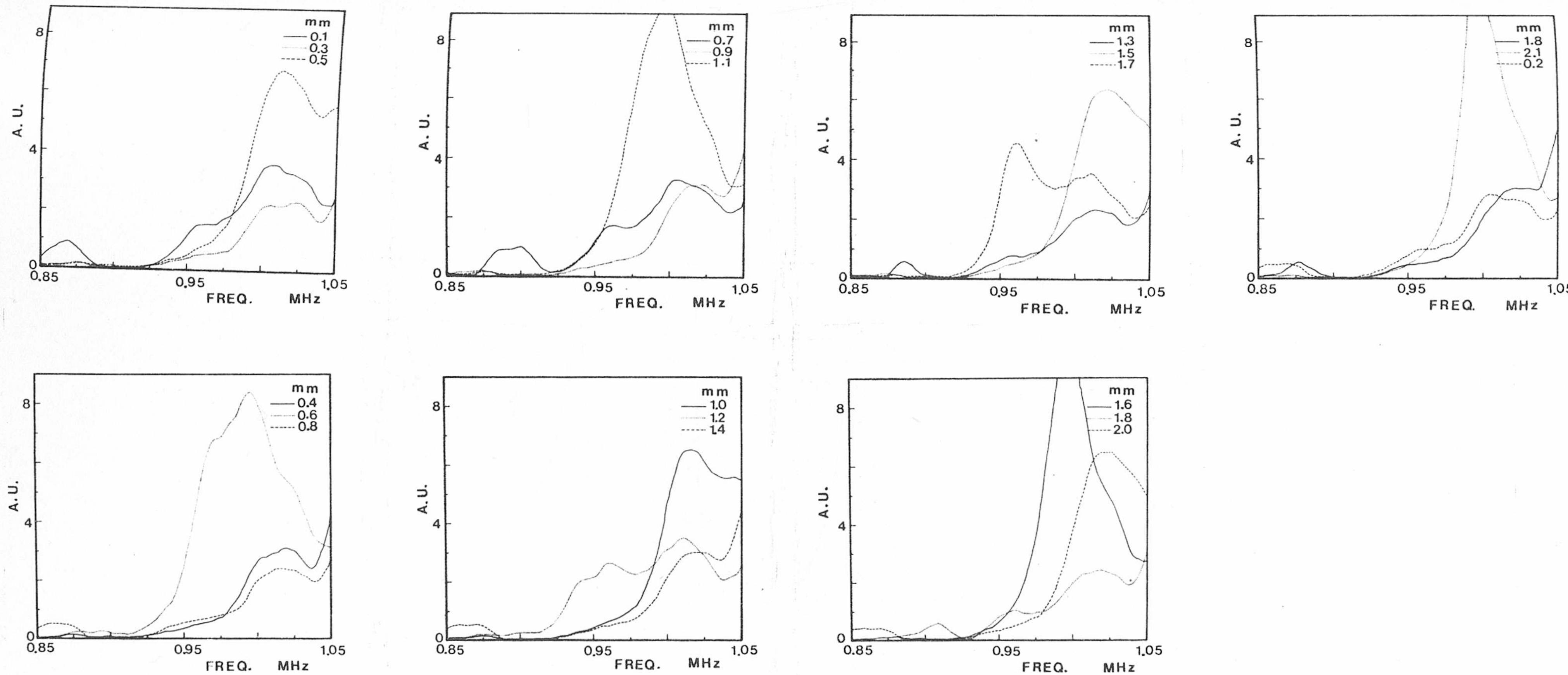

FIGURE 5.31 : Direct Frequency Response of S140 D/E Transducer Using Silicone Grease Couplant.

.Frequency Range : 850-1050 KHz
.Source Transducer Input Voltage : 6 Volts
.Output Voltage : 150 mV/A.U.

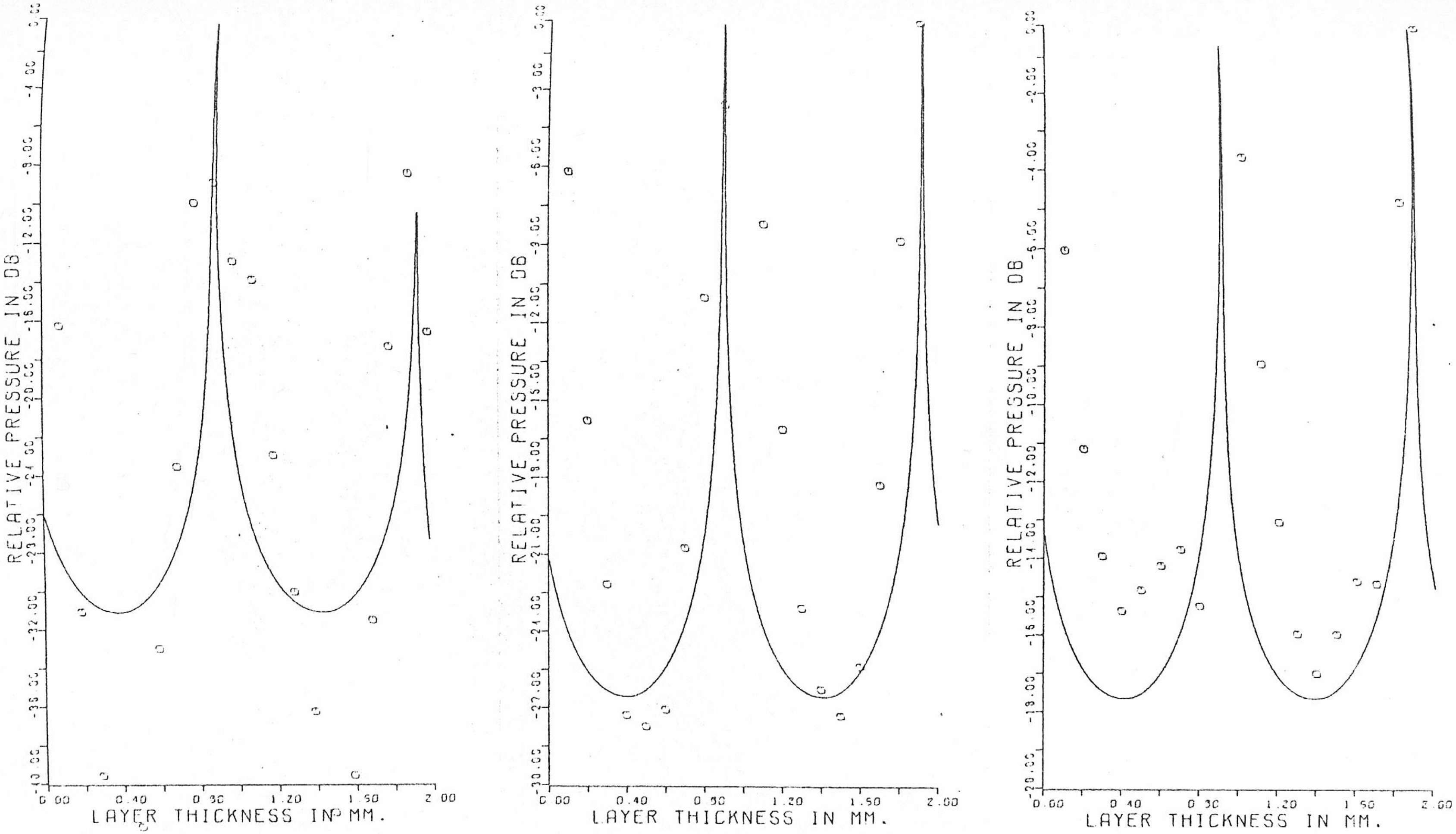

(a) 500 KHz

(b) 520 KHz

(c) 540 KHz

FIGURE 5.32 : Comparison Between Experimental and Theoretical Pressure Relative Transmission as a Function of Silicone Grease Couplant Thickness Using S140 Transducer.

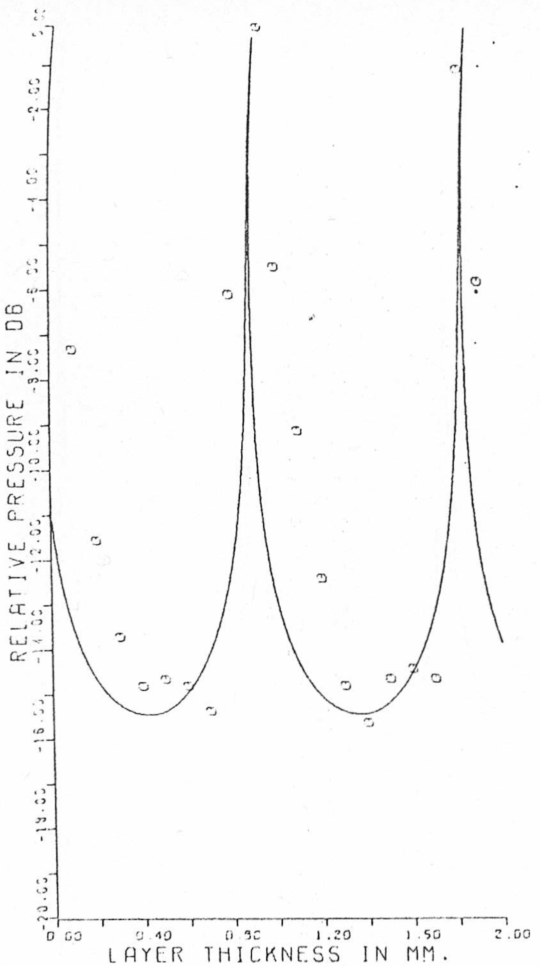

(d) 560 KHz

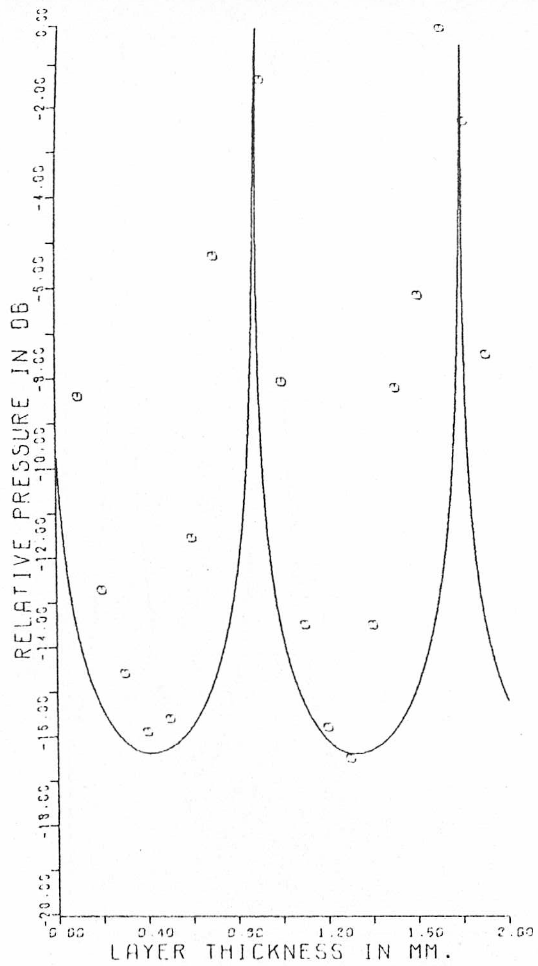

(e) 580 KHz

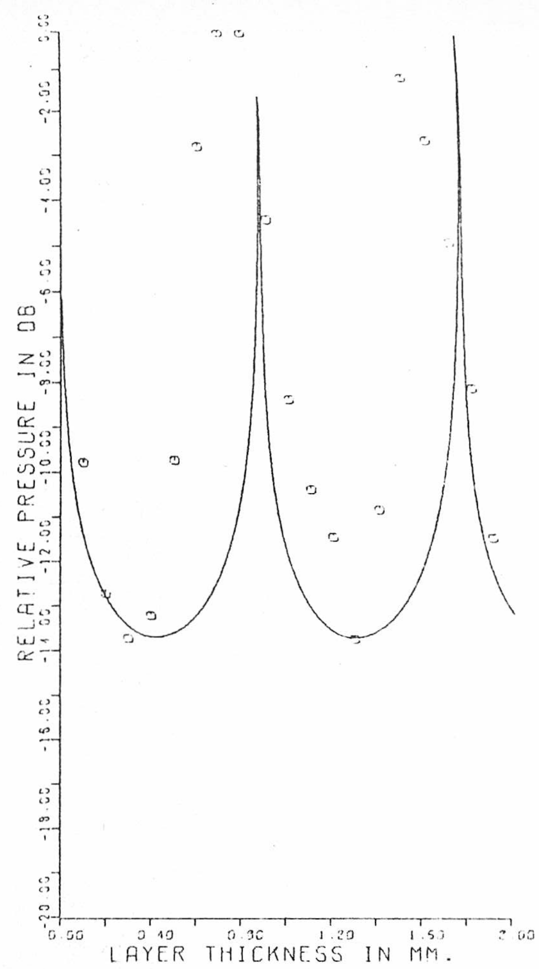

(f) 600 KHz

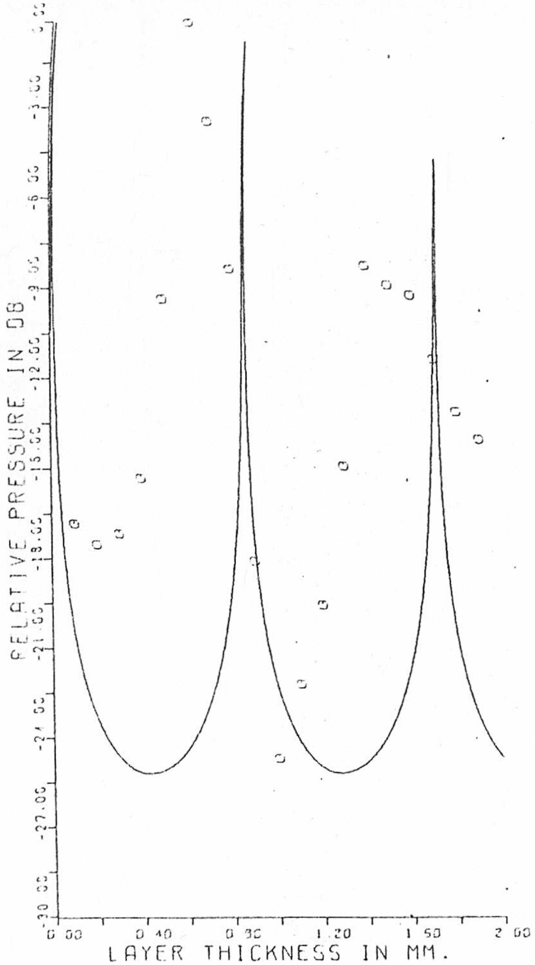

(g) 620 KHz

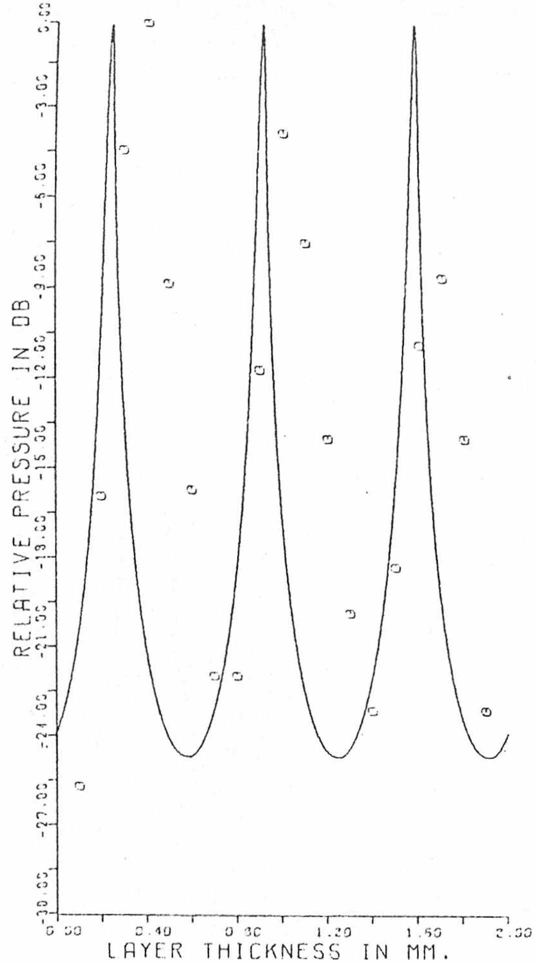

(h) 790 KHz

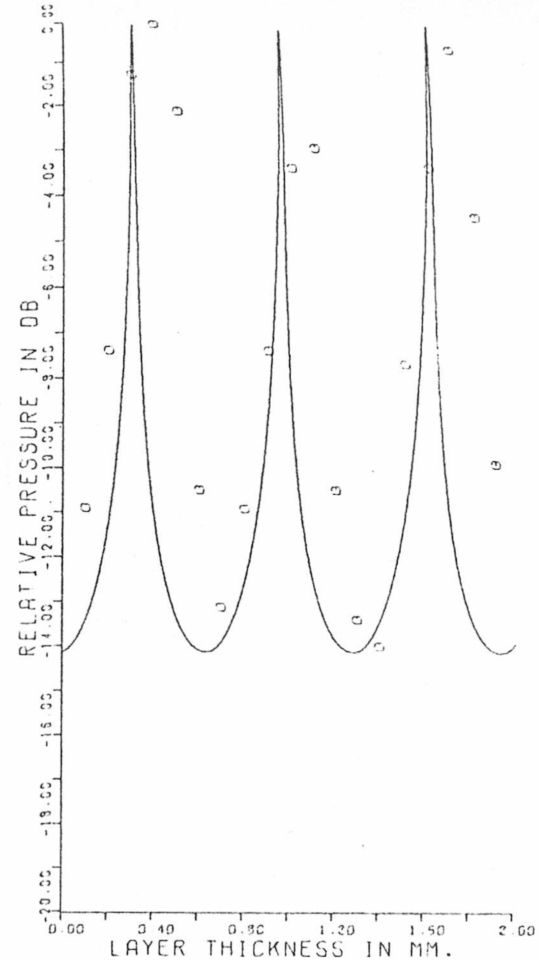

(i) 810 KHz

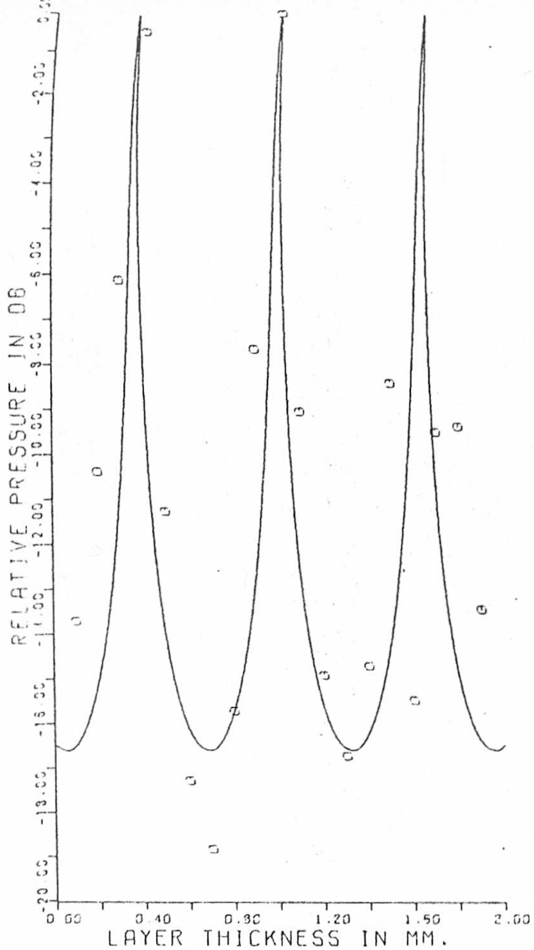

(j) 830 KHz

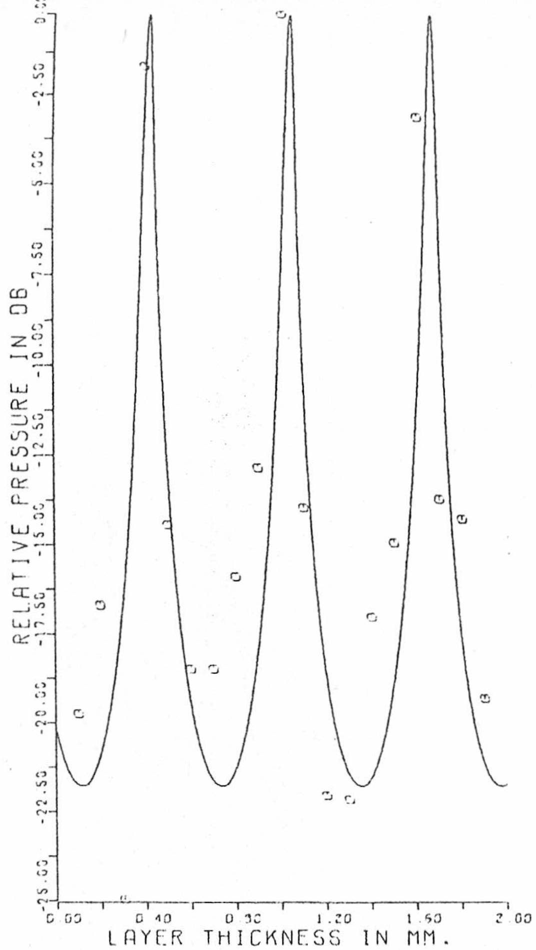

(k) 850 KHz

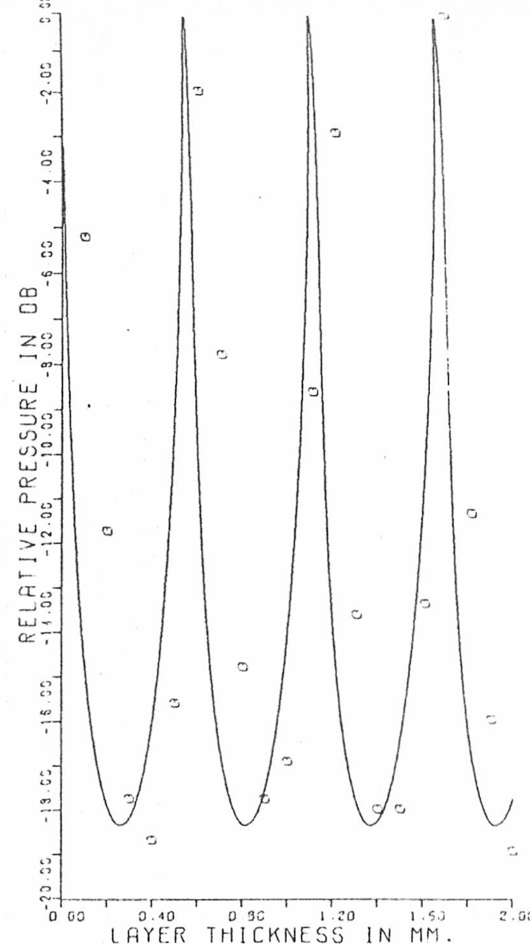

(ℓ) 950 KHz

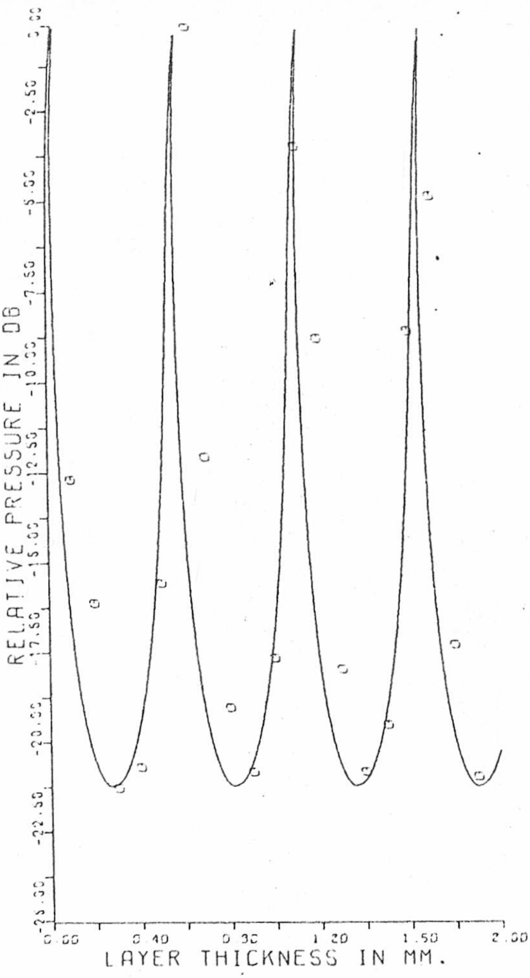
RELATIVE PRESSURE IN DB
0.00
-2.50
-5.00
-7.50
-10.00
-12.50
-15.00
-17.50
-20.00
-22.50
-25.00
0.00
0.40
0.80
1.20
1.60
2.00
LAYER THICKNESS IN MM.

(m) 970 KHz

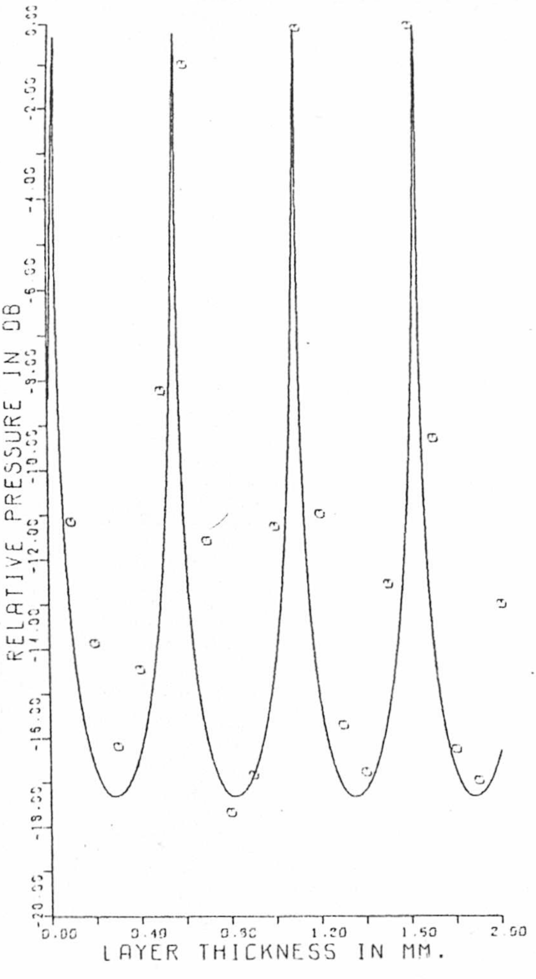

(n) 990 KHz

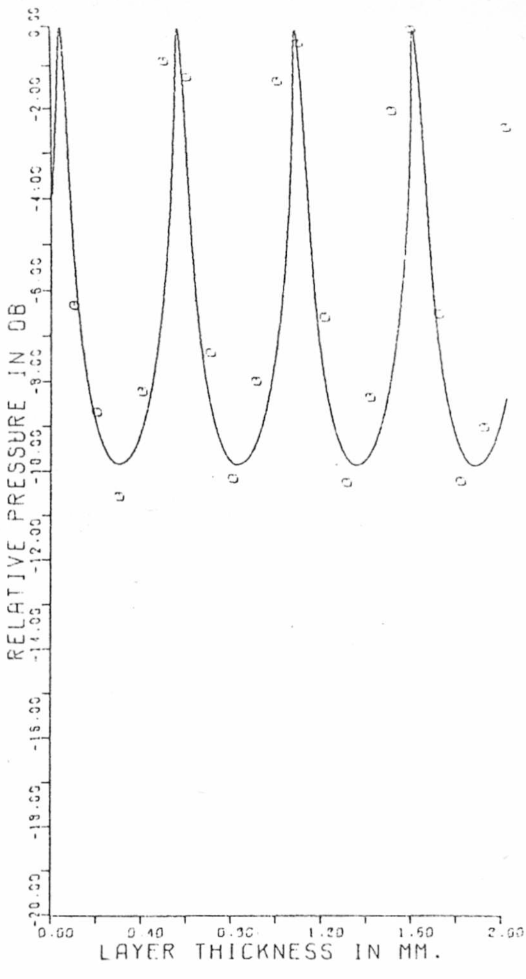

(o) 1010 KHz

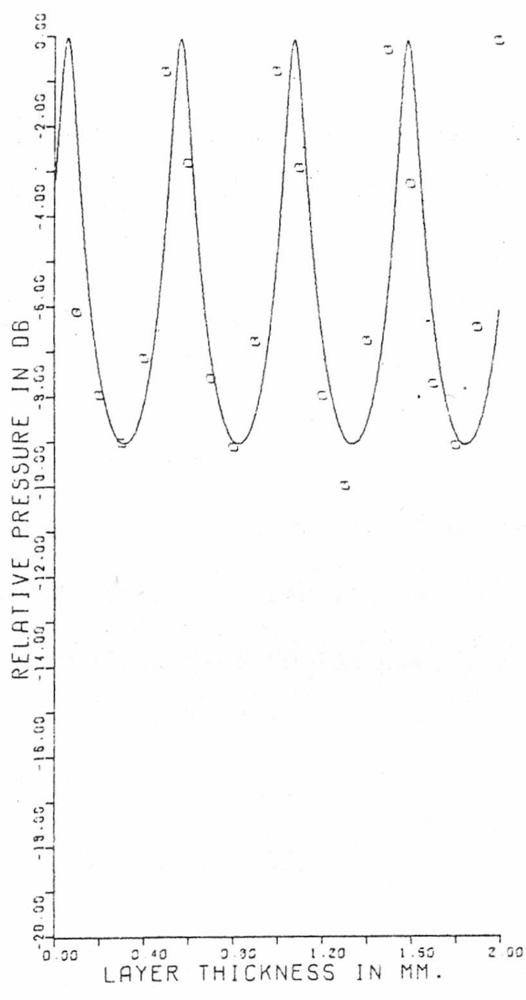

(p) 1030 KHz

The measurements were taken in 20 KHz frequency steps whenever it was possible to obtain reasonable accuracy from the system response curves (Figs. 5.29-5.31).

It can be seen that the results show good agreement between the theoretical and experimental relative transmission values. In particular, at higher frequencies agreement is excellent as the wavelength becomes small in comparison with the diameter of the transducer components.

Experiments were also conducted for water couplant using the same acoustic emission transducer and results can be seen in Appendix 5.I. A second transducer S750 was also used with water couplant (114).

5.6.5 CONCLUSIONS

Results obtained by using the six-layer model and continuous wave technique indicate an excellent agreement with theory over the frequency range from 0.5-1MHz. Therefore, it can be assumed that multilayer transmission theory is generally applicable to multilayer acoustic emission transducers. At the same time, it validates the discussions presented in the earlier sections of this chapter.

5.7 COUPLANT STANDARDIZATION

Results from the previous sections indicate the need to establish a standard couplant and a standard mounting technique. Hartman (164) states in his article 'Towards Standardization of Acoustic Emission Technology'.

"One additional contribution to this area* could be the development of standard forms of describing the pertinent physical and chemical properties of acoustic couplant materials"

The comparison of acoustic emission parameters in the following experiment indicates that consideration should be given to the type of couplant used.

Two acoustic emission transducers were attached to the specimen GS5 (Table 4.III). The first transducer S750 was mounted using silicone grease couplant and held in place with a rubber band. The second transducer D750 was attached to the specimen surface by using the PVC adhesive tape as a couplant with no supporting clips or rubber band. Figure 5.33 shows the position of the two acoustic emission transducers with respect to the simulated source transducer. The source transducer (5 MHz) was driven by a square pulse of length 1.2 μs and amplitude 30 V.

---

*mounting acoustic emission transducer.

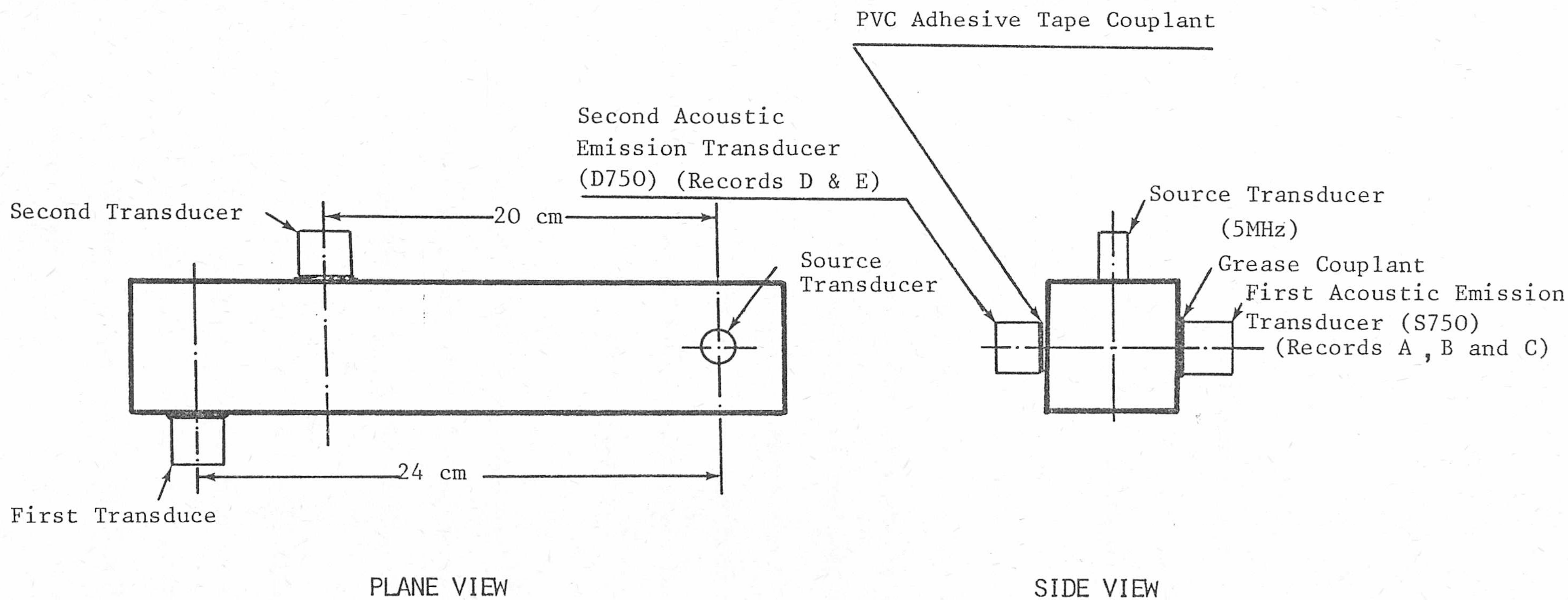

FIGURE 5.33 : Experimental Geometry for Couplant Stability

Three records A, B and C were obtained from the first transducer (with grease couplant) as follows:

A - first attachment

B - second arbitrary attachment (with care to keep the grease couplant and the rubber band under the same conditions as in A)

C - attachment B after 3 hours mounting.

The other two records (D and E) were taken from the second acoustic emission transducer (D750) using the PVC adhesive tape as a couplant. Record D was taken at the time between records A and B. Then the PVC tape was replaced and the second record (E) from this transducer (D750) was taken at the end of the experiment and after the record (C) was taken from the first transducer (S750) (i.e. record E was taken after the second transducer being re-attached for more than 3 hours).

The change in the received acoustic emission waveforms from the first transducer, using grease couplant, together with other calculated parameter are given in Fig. 5.34 (a-d).

It is evident that it is quite difficult to reproduce the same coupling conditions although great care was taken (cases A and B). When using a viscous couplant such as silicone grease, the couplant thickness relaxation with time is also an important factor (see cases B and C).

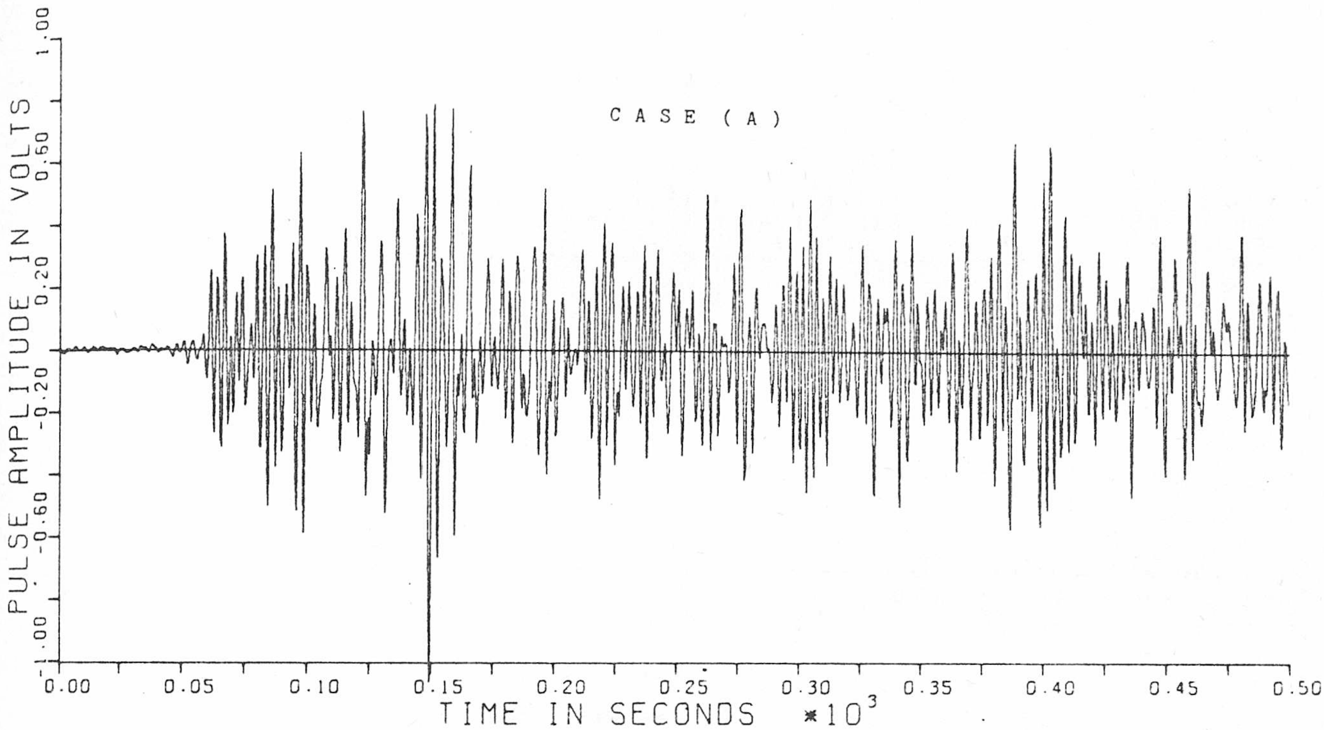

FIGURE 5.34 : Using Silicone Grease Couplant and Traditional Rubber Band as Clip.

(a) Acoustic Emission Waveform

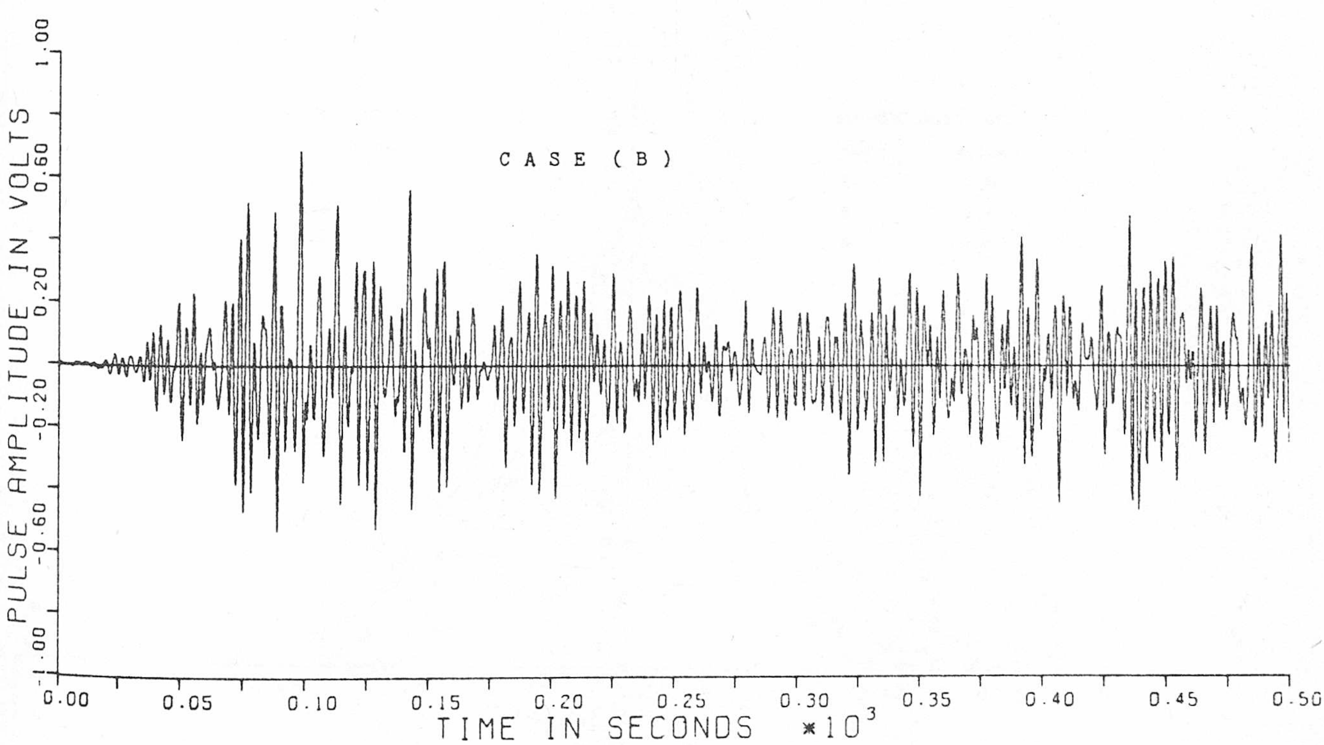

FIGURE 5.34 : Continued.

(a) Acoustic Emission Waveform.

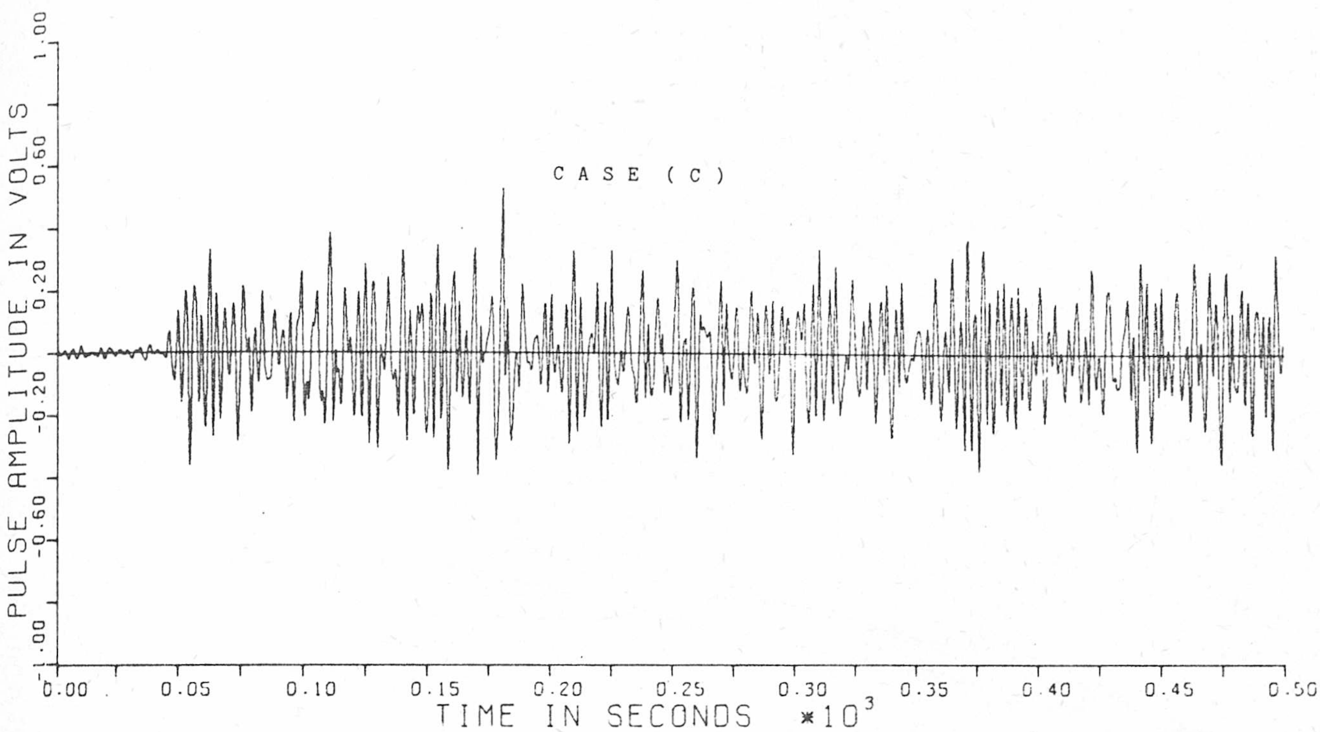

FIGURE 5.34: Continued.

(a) Acoustic Emission Waveform.

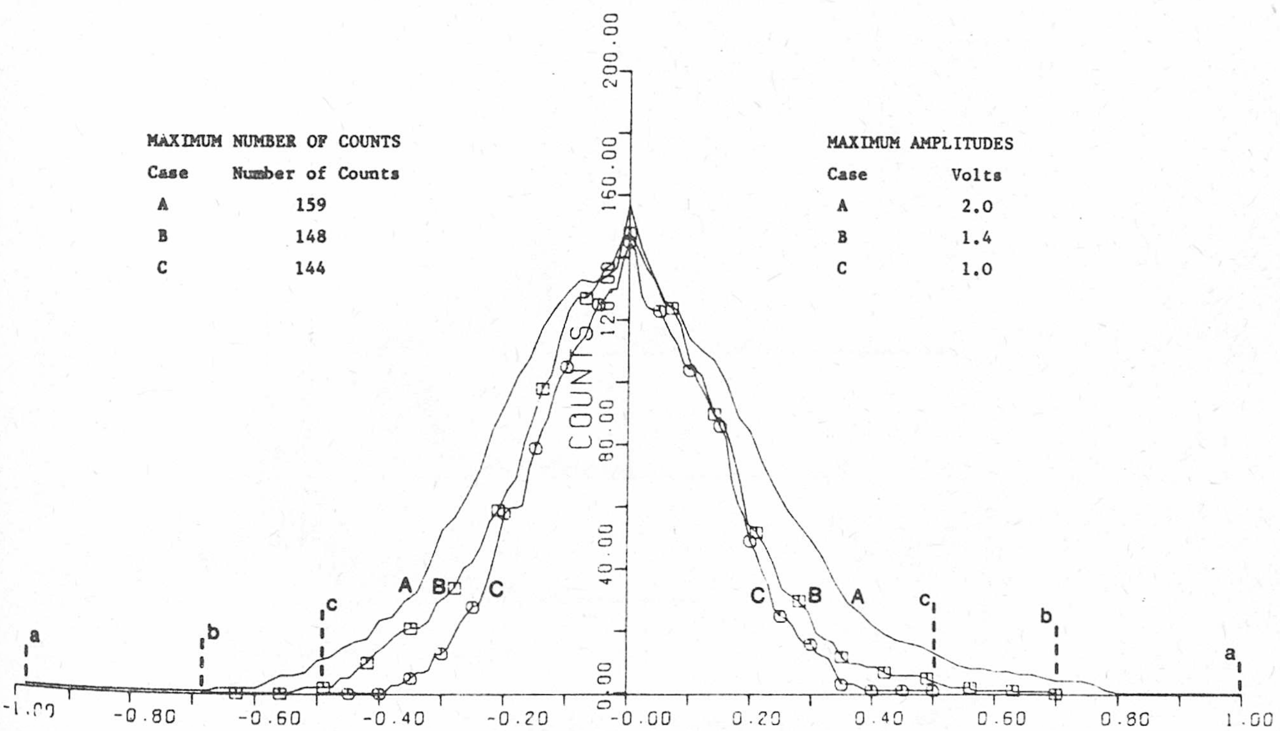

FIGURE 5.34: Continued

(b) Change in Acoustic Emission Amplitude (in Volts) and Number of Counts.

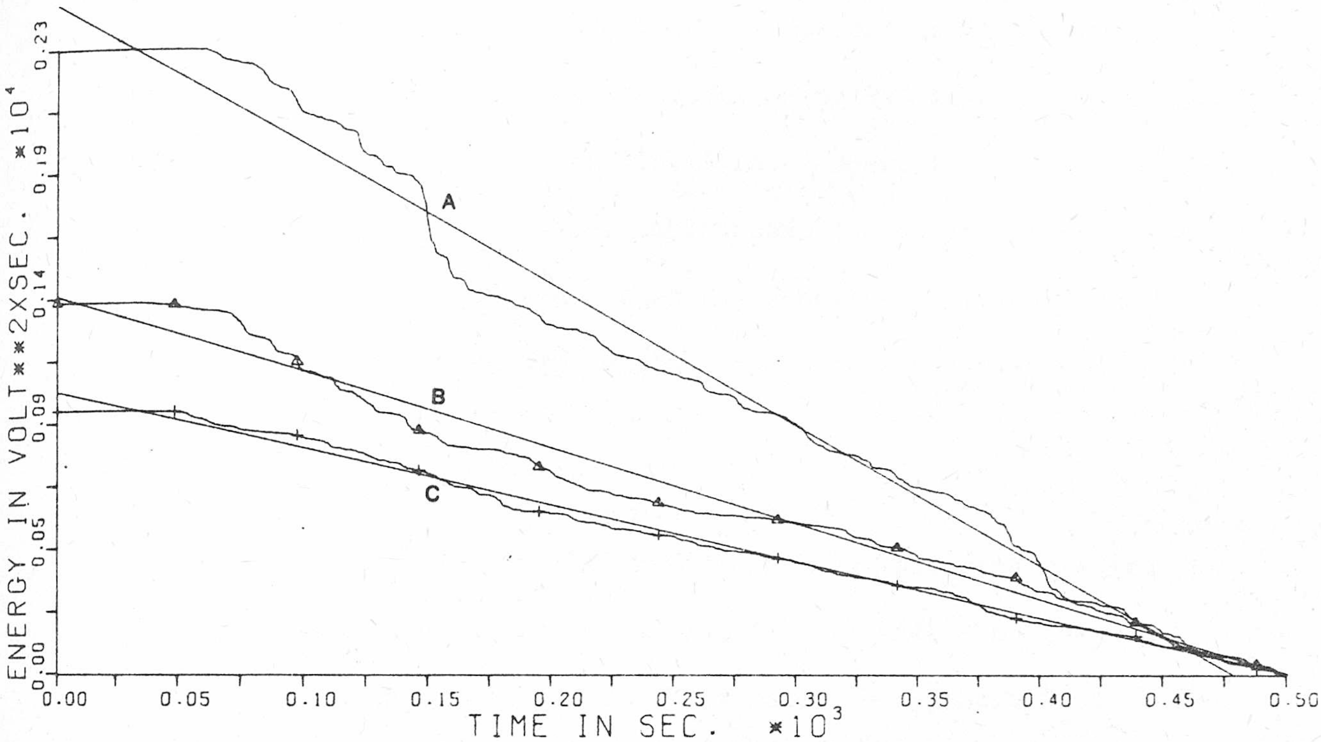

FIGURE 5.34 : Continued.

(c) Change in Acoustic Emission Total Energy and Energy Decrement.

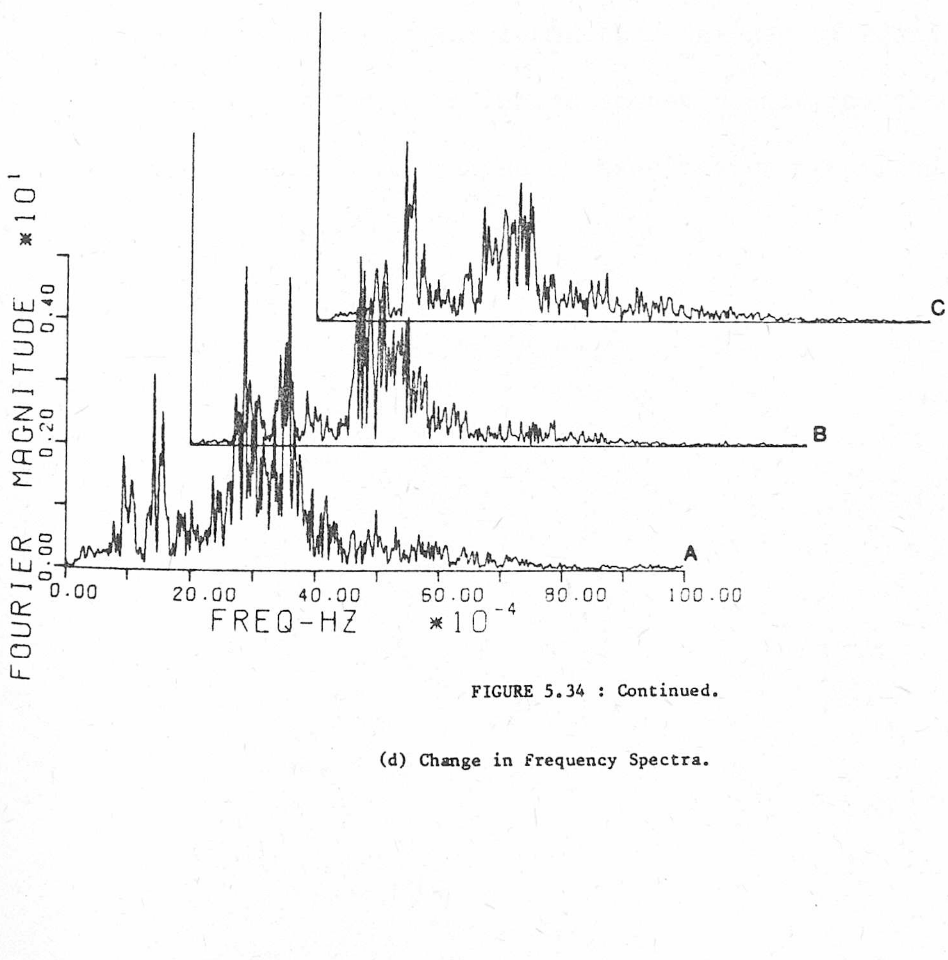

FIGURE 5.34 : Continued.

(d) Change in Frequency Spectra.

A comparison between the frequency components of the two records taken from the second receiver using PVC adhesive tape (records D and E) is shown in Fig. 5.35. Apart from a very small decrease in the spectral amplitudes, the spectra appear very similar. This suggests that the adhesive tape would be a good choice as a standard couplant for acoustic emission measurements.

A comparison between different couplants (silicone grease, water, glycerine and adhesive tape) and their effect on the acoustic emission parameters is illustrated in Appendix 5.J. The air couplant gauge was employed in this experiment and the simulated acoustic emission source transducer was driven by the Panametric pulser (Appendix 4.A). It was found that the use of adhesive tape does not destroy information in the acoustic emission transducer output signal or alter the transducer sensitivity predicted by the theoretical curves.

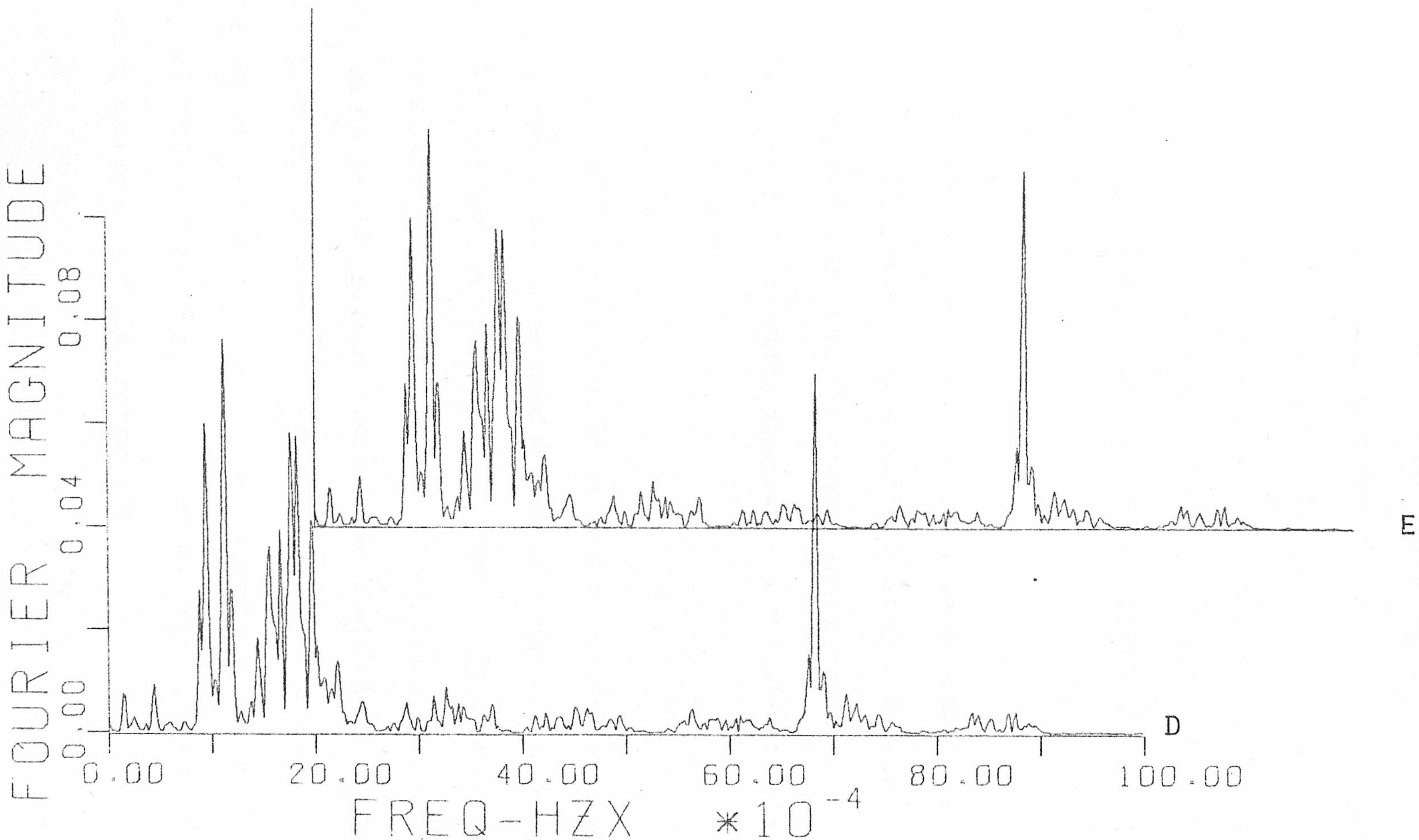

FIGURE 5.35 : A Comparison Between the Frequency Components of Two Different Records Using PVC Adhesive Tape and the Same Source Signal.

5.8 INTEGRATED CONCLUSIONS AND SUGGESTIONS FOR FUTURE STUDIES

The study presented in this chapter has attempted to investigate the influence of the transducer geometry and couplant medium on the received acoustic emission signals. The approach used was the pressure transmission coefficients for the transmission of normally incident longitudinal waves through a series of solid layers. The following general conclusions can be made from both the theoretical and experimental results.

1. The six-layer experiment has shown to be applicable to the transmission of longitudinal acoustic waves into an acoustic emission transducer, and it can be assumed that multilayer transmission theory is generally applicable to multilayer acoustic emission transductions.

2. The five-layer solution is applied to a particular acoustic emission transducer and using this theory the effect of varying the couplant thickness is considered. A complex interaction occurs between transmitted and reflected waves in each layer, but a definite series of peaks in the pressure transmission coefficient values can be identified for the particular set of materials considered. As the couplant thickness is increased these peaks move to lower frequencies resulting in large changes in the sensitivity of the measurement system at certain frequencies.

3. All acoustic emission parameters are critically dependent upon the couplant medium and the variation in its thickness. Unless the thickness of the couplant layer is kept constant over the whole monitoring time and for all specimens, changes observed in acoustic emission parameters are not only due to source differences. For continuous structure monitoring, a solid couplant such as Araldite should be used. For measurements over a limited time it is possible to use the suggested PVC adhesive tape couplant which will provide a good control of the transducer couplant thickness.

4. It is evident that in fulfilling the conditions $Z_{coup} \simeq Z_{shoe}$, one gets less variation in the pressure transmission coefficient curves for a small change in couplant thickness (see Fig. 5.15 for glycerine couplant). Therefore, by careful selection of the transducer shoe design the effect of changes in couplant layer thickness might be reduced.

5. The use of three-and-four-layer transmission results is only possible for single or very narrow-band transducers. They can only be used for preliminary investigation to select a suitable material for the transducer components.

6. Acoustic emission transducers should be designed with an appropriate resonant frequency and the band-width should be stated by the manufacturers in order to obtain the best sensitivity and resolution compatible with the experimental conditions.

7. The transducer performance can be optimized and transducer components selected to give highest possible response. This means better transducer efficiency and a higher signal-to-noise ratio. The multilayer transmission theory has important applications in this aspect. The three-and-four-layer models can be applied to increase the average transmission coefficient with the narrow frequency range in a very narrowband transducer. In a broadband transducer the problem becomes more complicated as one must look at the transmission coefficient over a wide frequency range and the layers matching conditions becomes more critical the number of layers involved. A suggestion for such geometry and design optimization is given in Appendix 5.K.

8. Extension of this investigation will be necessary to consider the piezoelectric terms. Using the five-layer transmission model and taking into account the piezoelectric terms will lead directly to the transducer component transfer function. The evaluation is expected to be taken in the following steps. First, monitoring the structure by more than one transducer to allow the principal beam angle of the emission waves to be evaluated. Second, expanding the transmission theory to include the oblique incident wave and the piezoelectric terms. Then the calculated transducer response should lead to the transducer transfer function.

CHAPTER SIX

THE EFFECTS OF SPECIMEN GEOMETRY

6.1 AIMS

The aims of the experimental work described in this chapter are:

i. to investigate the effects of specimen dimensions and material properties on different acoustic emission parameters, and consequently the sensitivity of such parameters in detecting variation in acoustic emission sources and specimen geometry;

ii. to evaluate experimentally some of the parameter relationships which have been derived theoretically in Chapter Two.

The experiments presented deal only with the problems of acoustic emission propagation and detection in plate specimens.

6.2 EXPERIMENTS

The experiments were performed on commercially available materials. The specimens geometry and material are given in Table 4.III. Each specimen was laid on two sharp wedges, one centimetre, inside, from its opposing ends.

A sharp electrical pulse of 30 nanoseconds width and 125 volts amplitude (about 5 ns rise time) Fig. 6.1, was generated by the Panametric 5052 pulser and introduced into the 5 MHz Mecasonic transducer to simulate a broadband acoustic emission source (Sec. 4.1). This source transducer was coupled to the centre line of the major specimen surface by silicone grease. A constant weight of 300 gm applied to the transducer ensured intimate contact.

The pulse from the source transducer travels in the specimen as acoustic emission waves, which is picked up by the, nominally called, broadband acoustic emission transducer (D9201 Dunegan/Endevco). The receiving transducer was located on the centre line of the same specimen major face using the PVC adhesive tape as couplant medium, Fig. 6.2 The distance between the two transducers was 25 cm and was kept the same for all specimens. The transducer output was amplified by a gain of 40 dB and filtered in a 100-1000 KHz band pass. The filtered signal was then sent to the data processing system as shown in Fig. 4.8. The digitized signals were processed by using the computer programs presented in Chapters Two and Four.

Attention should now be directed to the actual pulse waveform which is assumed to simulate the emission source. Although the 5 MHz transducer was excited by step function electrical pulses, Fig. 6.1, the actual shape of the mechanical pulse entering the specimen surface is unknown. The structure of the source transducer and the grease couplant in addition to the specimen

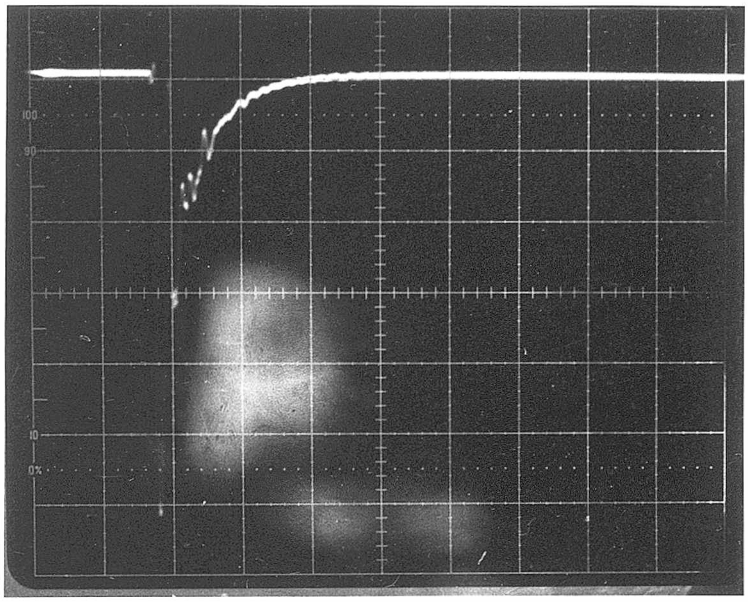

FIGURE 6.1 : The Input Electrical Pulse used to Excite the 5 MHz Source Transducer. (H: 0.1 μs/div. & V: 20 Volts/div.)

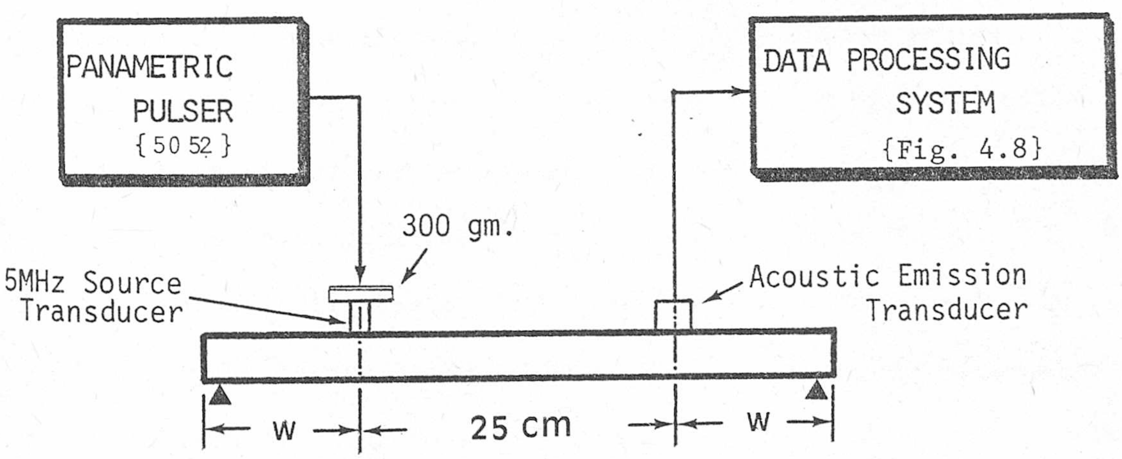

FIGURE 6.2 : Geometry of the Transducers Location on a Plate Specimen.

acoustical parameters will indeed modify the step function shape. However, sources introduced to the steel specimens would be identical.

6.3 RESULTS AND DISCUSSION

The statistical model analysis investigated in Chapter Two in addition to the experimental procedure outlined in the previous section was led to some interesting results which are now presented and discussed.

6.3.1 BURST WAVEFORM ANALYSIS

The first 0.5 m s of the amplified acoustic emission waveforms are shown in Figs. 6.3 (a)through 6.3(i) for different specimen geometries. It is seen that the waveform changes, as might be expected, as the specimen dimensions and material change. A consideration of the normality of each data set $\{\chi_i(t)\}$ would have been of interest to the validity of the theoretical interpretation presented in Chapter Two. Each of the emission bursts, Fig. 6.3, was statistically tested for normality using the program MSES (Appendix 2.I). The bursts statistical properties were obtained and summarized in Table 6.I. The results indicate that, in general, the means of the detected bursts from plate specimens were negligibly small (almost less than 1 mV). Figures 6.4(a)and 6.4(b) contain plots of the two data sets obtained from the specimens GS6 and GA as examples. Similar distributions were obtained for all specimens.

Therefore, the normal distribution assumption, $N(o,\sigma^2_{x(t)})$, seems physically reasonable (Chapter Two).

TABLE 6.I STATISTICAL FEATURES OF THE BURSTS WAVEFORM DISTRIBUTION

Specimen Code	Distribution Characteristics			Stationarity (%)
	Mean $\bar{x}(t)$ Volts(10^{-3})	Variance Volts$^2(10^{-2})$	Standard Deviation Volts(10^{-1})	
Steel:				
GS1	0.458	0.492	0.702	24.2
GS2	0.427	0.449	0.670	10.8
GS3	0.362	0.423	0.650	19.0
GS4	0.999	3.383	1.839	50.0
GS5	0.728	2.557	1.559	14.6
GS6	1.628	5.108	2.260	36.4
Aluminium:				
GA	0.862	2.549	1.597	43.1
Brass:				
GB	0.331	0.365	0.604	36.4
Perspex:				
GP	0.025	0.001	0.027	50.0

On the other hand, it may be observed from Table 6.I that with the exception of the specimen GS4 and GP (50% stationarity) all the waveforms consistently fail the test for stationarity (STATM) of the observed time interval (less than 50% stationarity). This may have some effects on interpretating some parameters and these will be discussed later in Section 6.4.2. However, this is not a serious problem as it can be seen in Fig. 6.3 that there is no sudden jump or periodic fluctuation in the bursts mean level (the zeroth voltage level). Also the validity of the stationarity

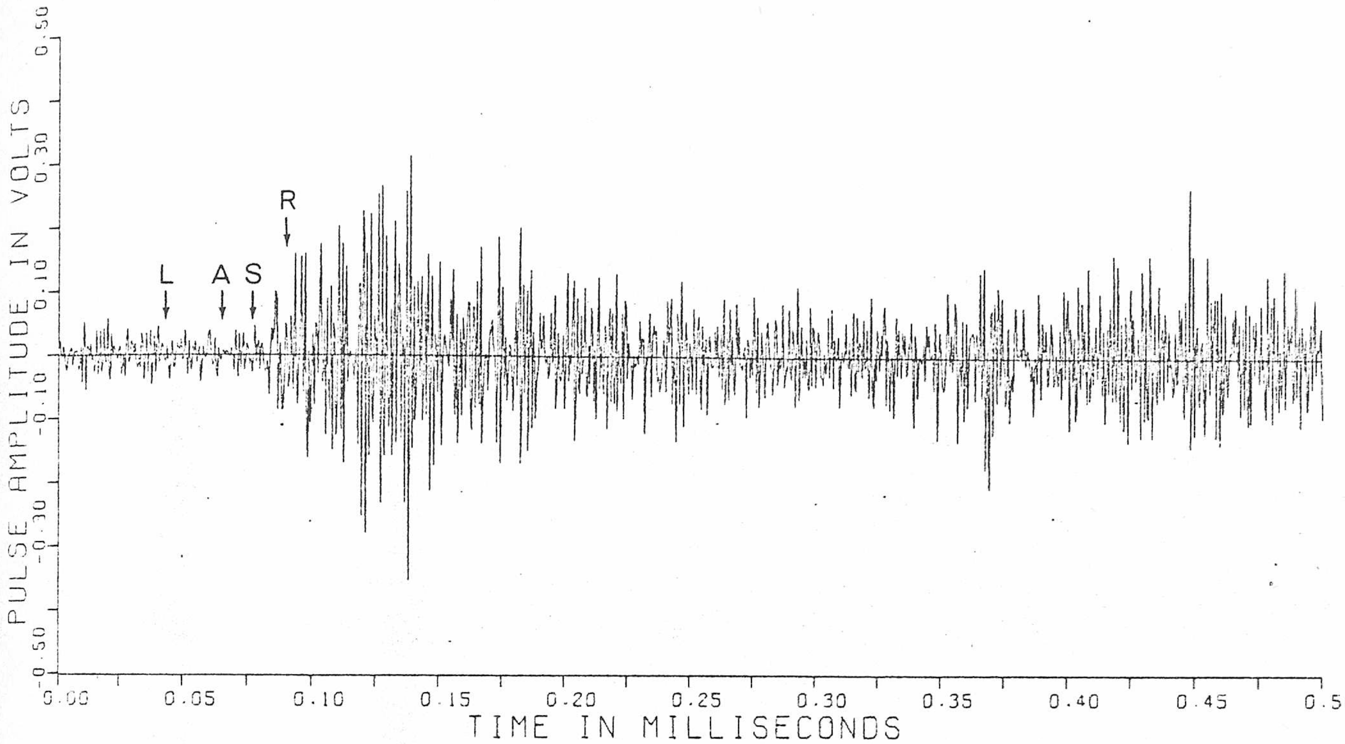

(a) GS1 : Steel Plate 995x50x12.5 mm.

FIGURE 6.3 : Time Domain Acoustic Emission Transducer (D9201 D/E) Response to an Ultrasonic Pulse Source Propagated in Plate Specimens. Transducers are 250 mm. Apart. Arrows Indicate the Arrival Times of the First:

L : Longitudinal Wave
A : Antisymmetric Wave
S : Shear and Symmetric Waves
R : Surface Wave

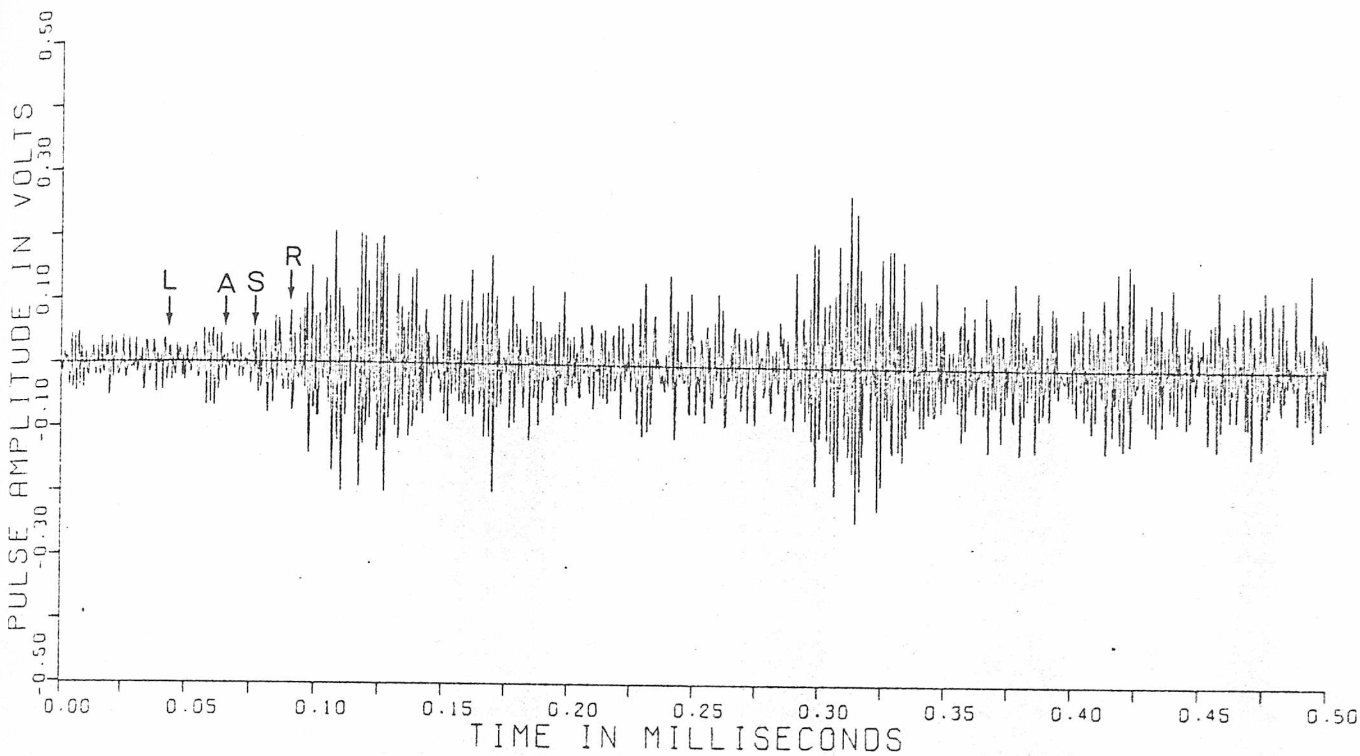

(b) GS2 : Steel Plate 690x50x6 mm.

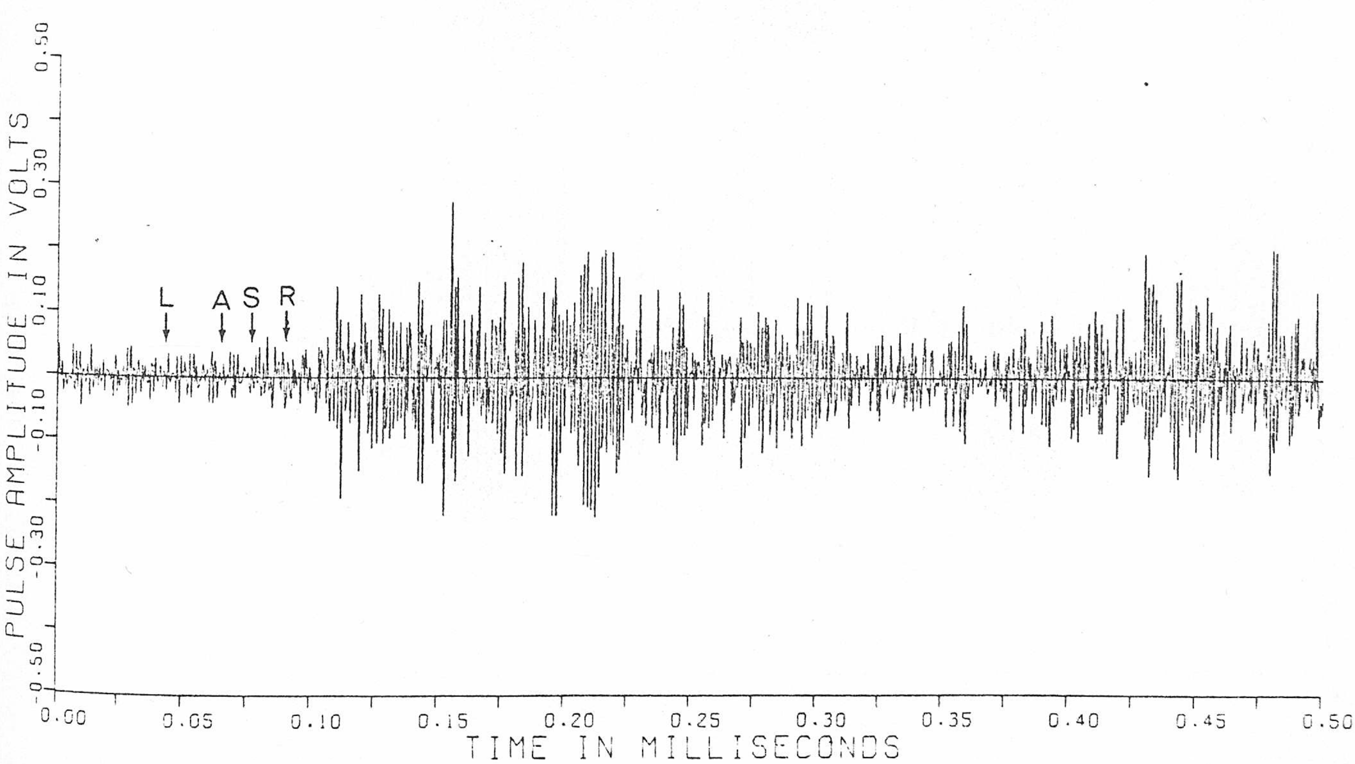

(c) GS3 : Steel Plate 330x50x12.5 mm.

FIGURE 6.3 : Cont.

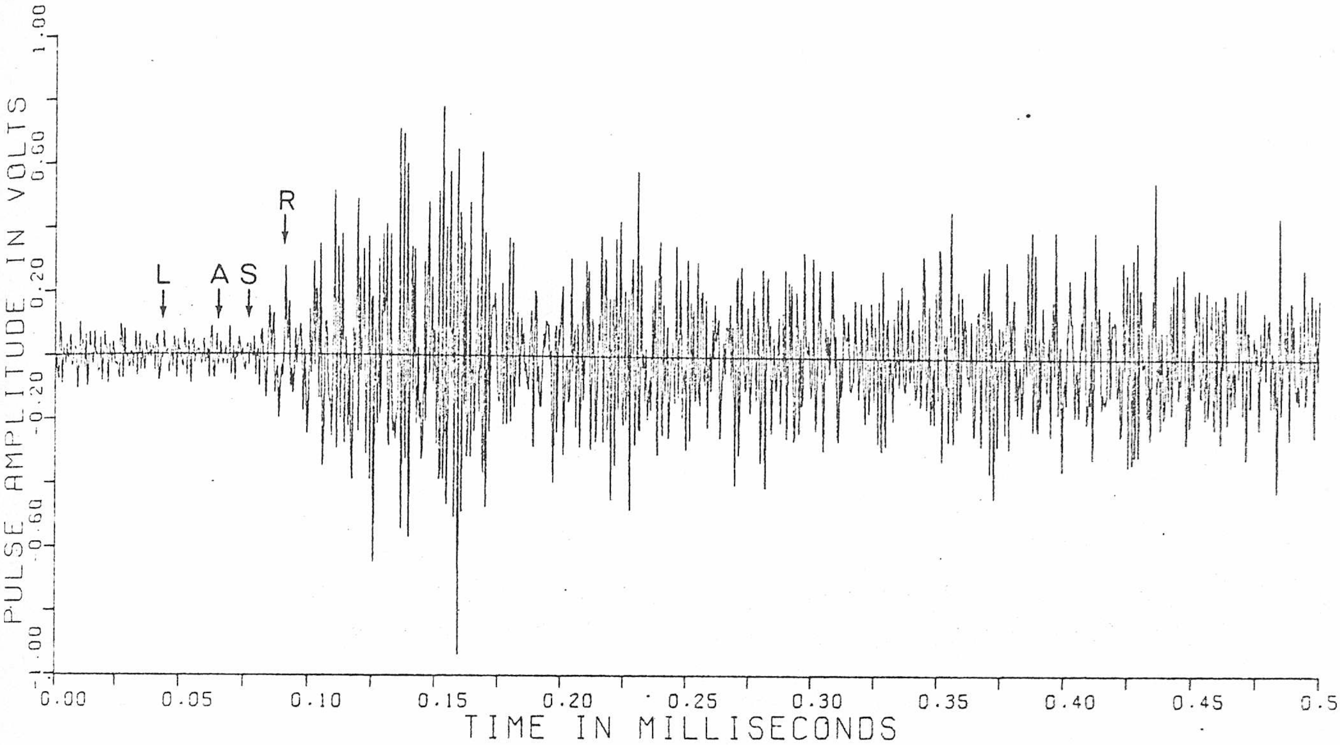

(d) GS4 : Steel Plate 330x50x6 mm.

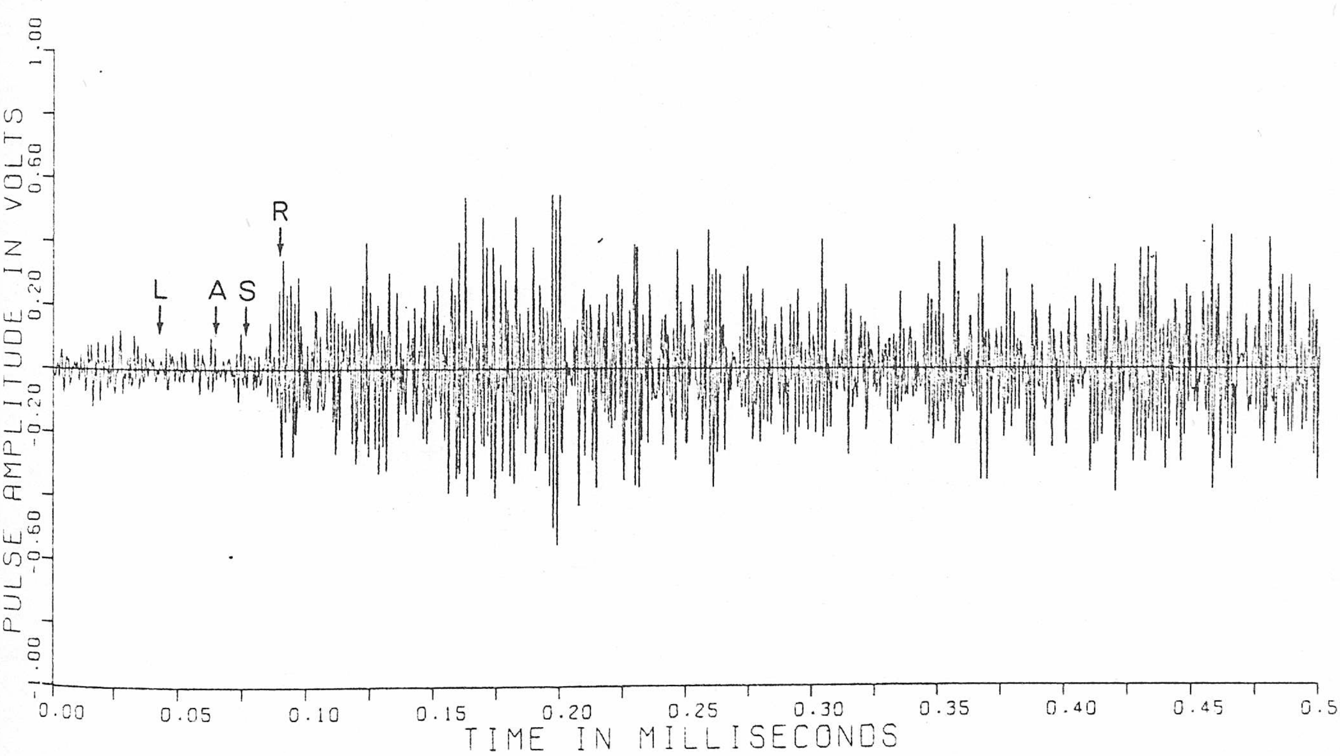

(e) GS5 : Steel Plate 330x30x30 mm.

FIGURE 6.3 : Cont.

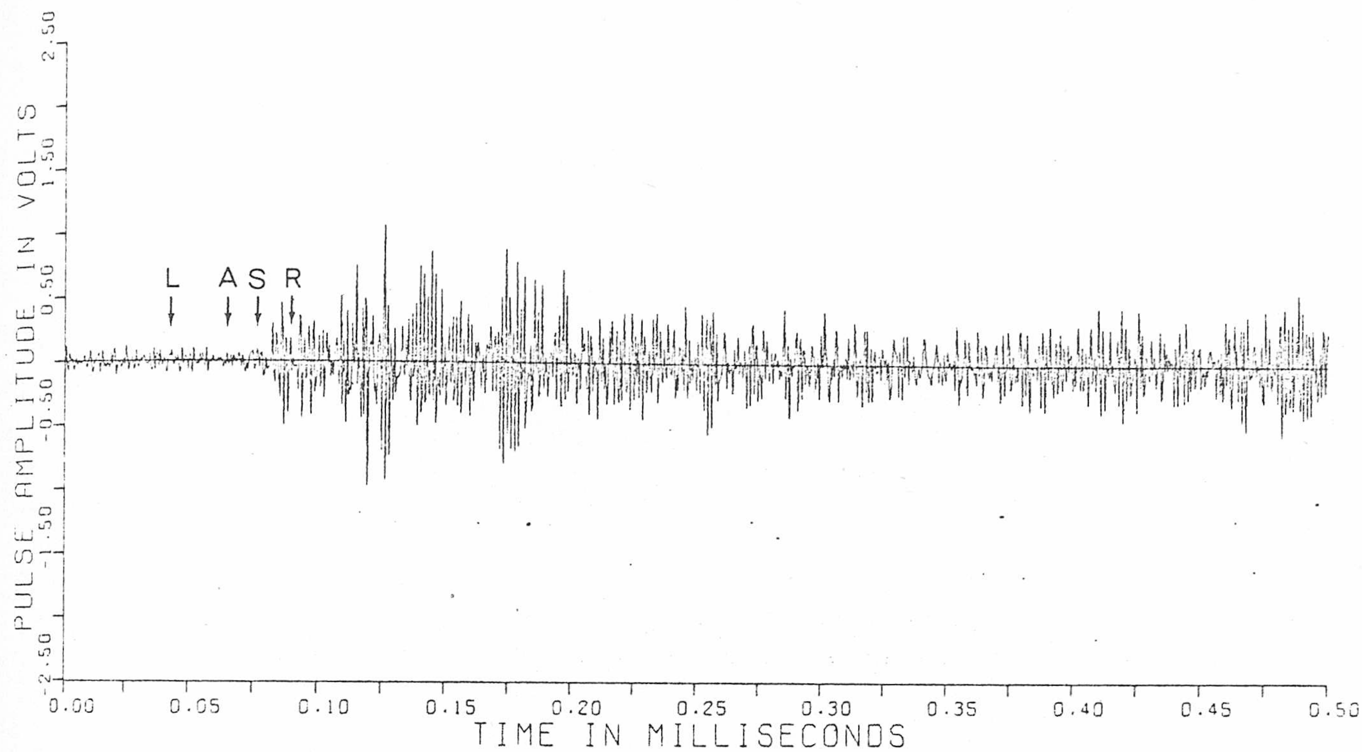

(f) GS6 : Steel Plate 330x25x12.5 mm.

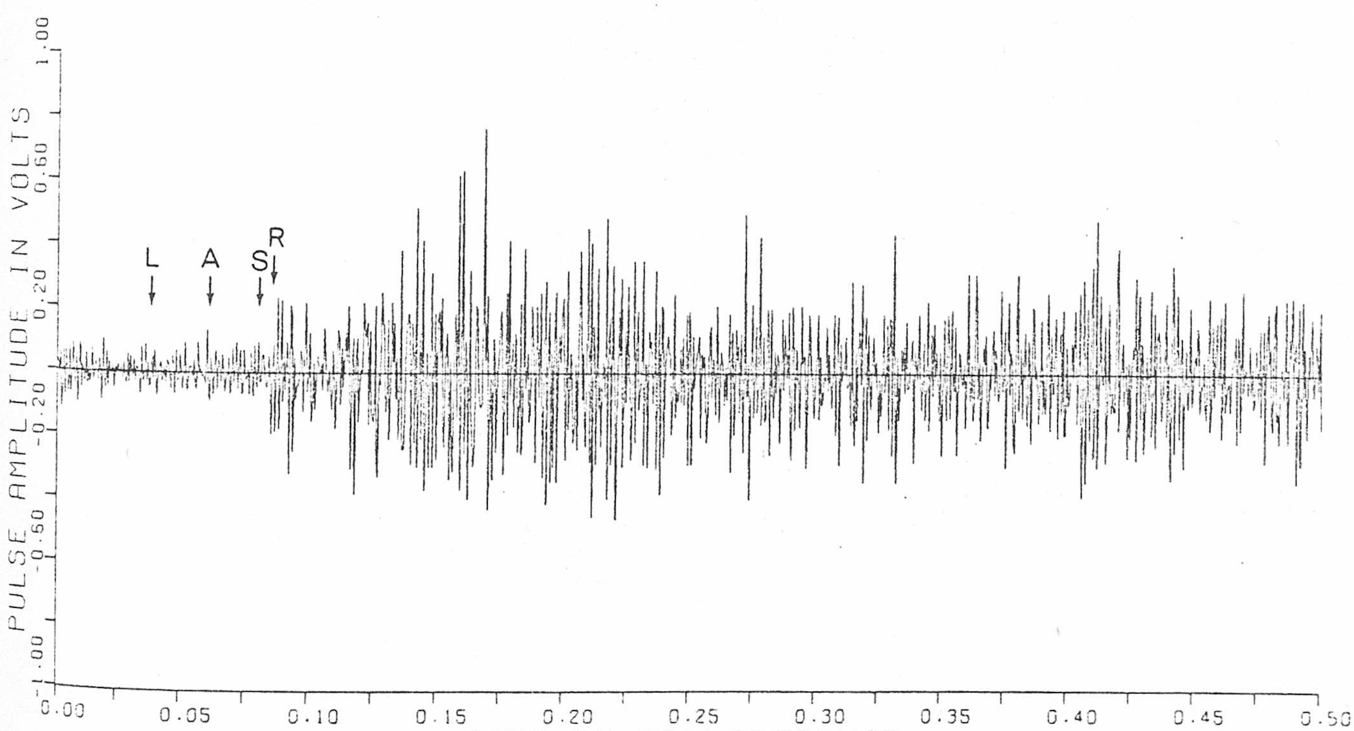

(g) GA : Aluminium Plate 330x25x12.5 mm.

FIGURE 6.3 : Cont.

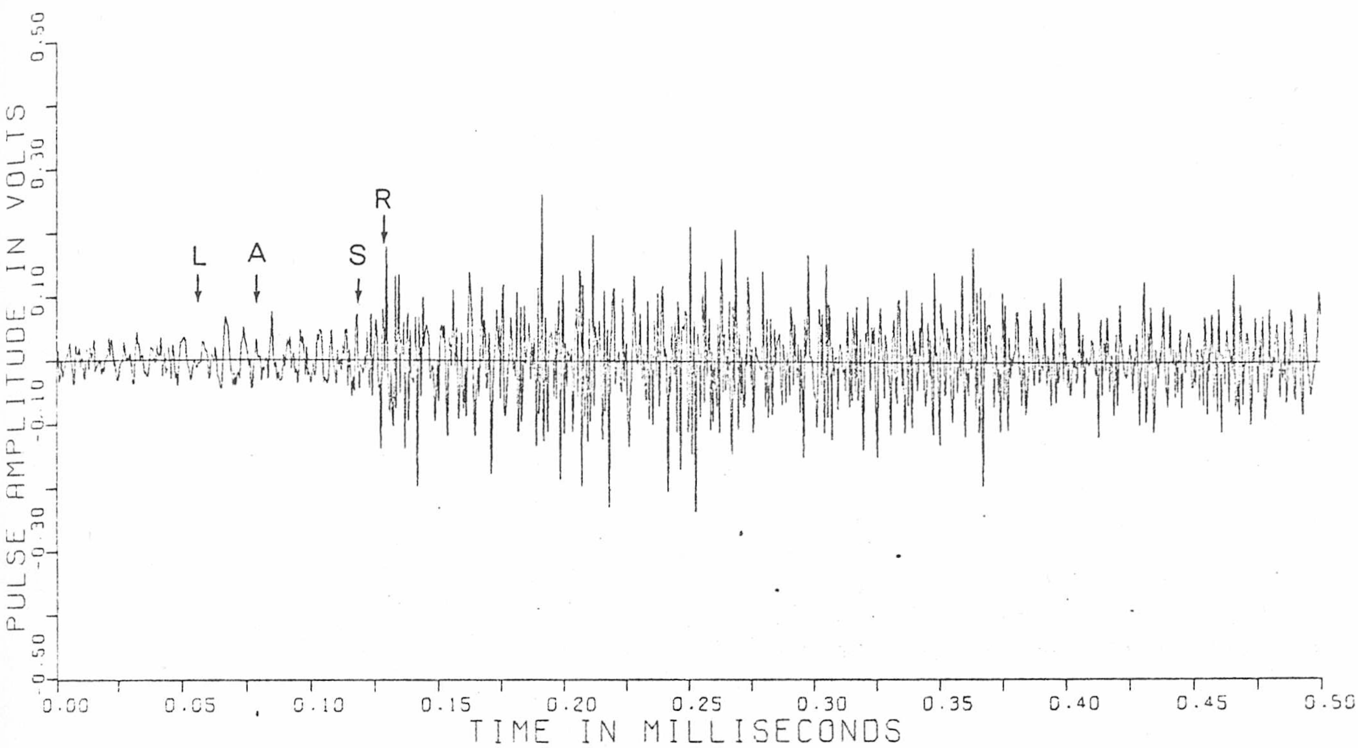

(h) GB : Brass Plate 995x50x12.5 mm.

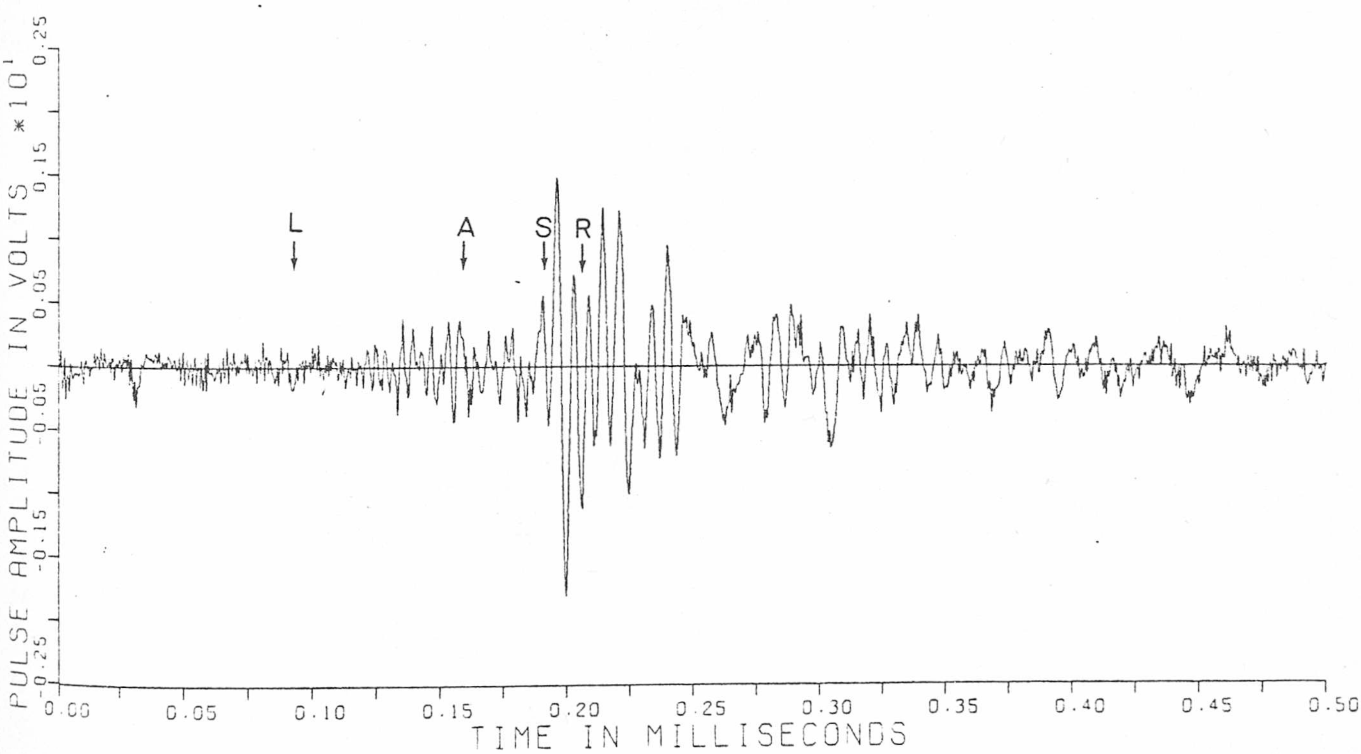

(i) GP : Perspex Plate 995x50x12.5 mm.

FIGURE 6.3 : Cont.

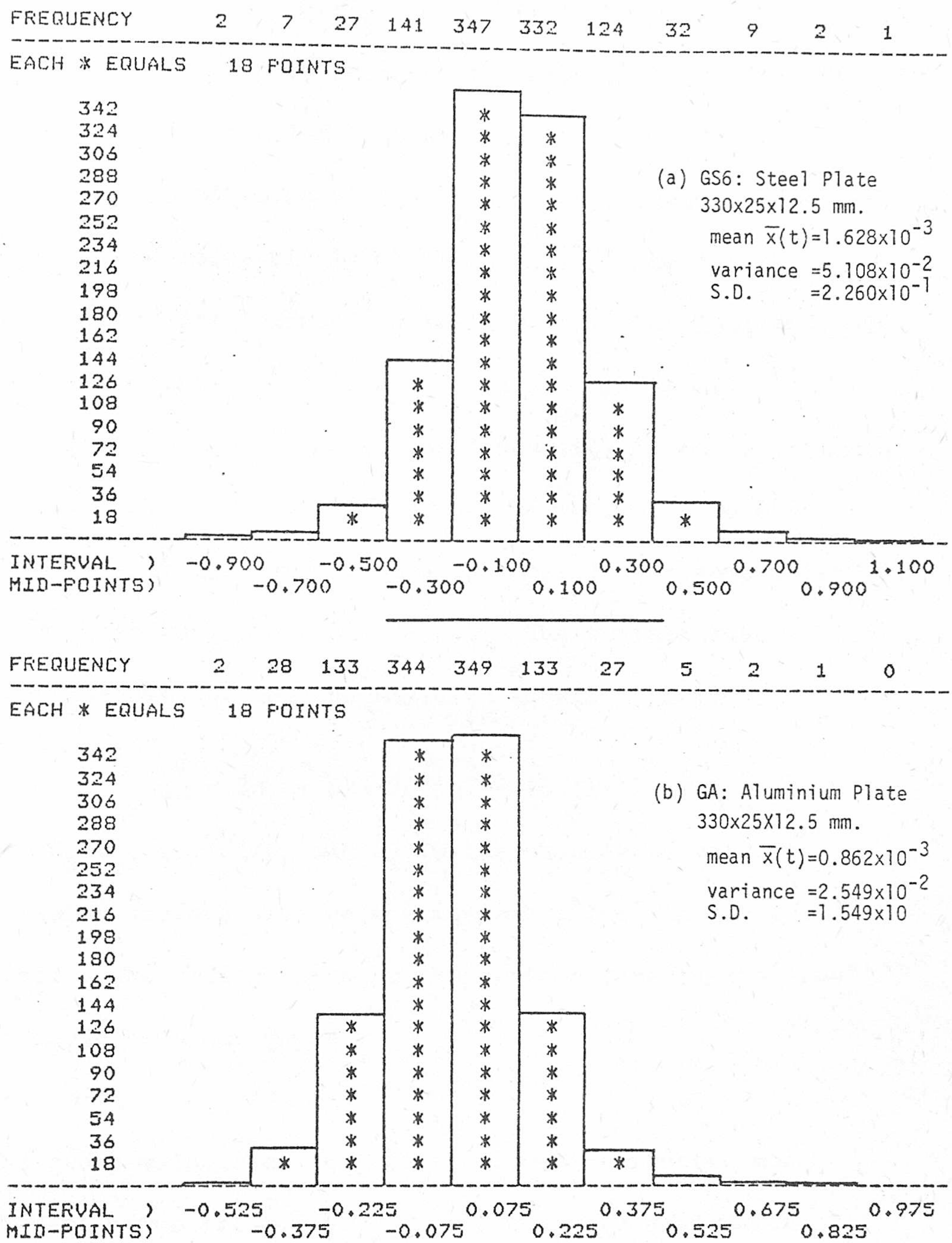

FIGURE 6.4 :Testing for Normality: Example of Two Discrete Frequency Distributions for the Digitized Data of Specimens GS6 and GA.

test is uncertain for the reasons previously mentioned in Section 2.2.

Reference is now made again to the emission bursts in Fig. 6.3 (a-i). The arrows labelled L, S and R on each waveform plot indicated the arrival times of the first longitudanal, shear and surface wave mode respectively. The arrival times for these propagation modes are computed theoretically. For longitudinal mode, the relevant velocity is C_L, which for mild steel is approximately 6000 m s^{-1} (Table 5.A 'Appendix'). For a distance x = 25 cm, the arrival time x/C_L would theoretically be about 42 μs. Similarly for shear mode propagates in the same material, the arrival time would be about 77 μs. The surface wave velocity, C_R, is obtained by solving the Rayleigh equation (124):

$$\eta^6 - 8\eta^4 + 8(3-2\xi^2)\eta^2 - 16\ (1-\xi^2) = 0$$

where $\eta = C_R/C_S$, $\xi = C_S/C_L$ and C_S is the shear wave velocity. The calculated surface wave velocities are listed in Table 5.A (Appendix). The arrival time for the surface wave in the steel specimen would be about 90 μs.

The group velocities for the two lowest symmetric mode $C_{1S,1}$ and antisymmetric mode $C_{1a,1}$ in plate were also calculated by the approximated relations given by Tolstay and Usdin (165) as:

$$C_{1S,1} = C_S \text{ and } C_{1a,1} = 1.2\ C_S$$

The corresponding arrival time for the lowest antisymmetric mode is labelled 'A' on each burst.

Clearly most of the waveforms show no significant change in the amplitude at the corresponding arrival time of either the longitudinal or shear modes. In all bursts, the primary portion of the waveforms is disturbed by the system noise. Because of the low amplitudes of these modes, their arrival times are very poorly marked and sometimes indiscernible in the system noise. Only slight change in the amplitude may be noted at the arrival time of the lowest antisymmetric mode (marked A) on the specimens GS5, GA and GP. Of course, these waveforms were overtested in large scale plots and the relative change in the burst amplitudes were also calculated around the expected arrival times. The changes in the amplitude rates were so small (either negative or positive slope) that the results of the test were regarded as meaningless. Hence these results are not presented.

On the other hand, the large amplitudes are very well pronounced by the arrival of the surface waves (marked R). This can be observed on all burst with the exception of specimen GS3. The record beyond the surface wave arrival is complicated by the arrival of subsequent waves of different modes which have experienced longer paths and multireflection along the specimen boundaries. The final shape is characterized by the specimen dimension and its acoustical properties which can be noted by comparing all bursts with respect to each other. All these complicated waveforms do not obey the exponentially decaying sinusoid model as it is assumed in literatures (51-53).

Recently, Pao et al (166) have theoretically calculated the time history response of the displacements at the surface of a plate due to a perpendicular force on the surface. The analysis is based on the generalized ray theory. Their results show that the response at the same surface is characterized by an amplitude change at the arrival time of the surface wave (Fig. 8(c) Ref. (166)). Such change was absent at the opposite side of the plate. The authors also concluded that beyond the arrival time of the surface wave, the burst shape is built up essentially by the accumulation of rays from second and subsequent groups of different wave modes. Our experimental observation is seen to support the theoretical results given in this reference.

6.3.2 PEAKS DISTRIBUTION AND DENSITY

The envelopes of maximum and minimum peaks together with the peaks densities are compared in Figures 6.5 (a-i) for different specimens (program: PEAK). The plots are presented in the same sequence as for the waveforms given in Figs. 6.3 (a-i). Each peaks' envelope has a rather irregular form of decay, occasioned by the inevitable fluctuation of peak amplitudes caused by disturbances of the sequency of arrival of different wave modes which have experienced various mode conversions at the surfaces of the specimen.

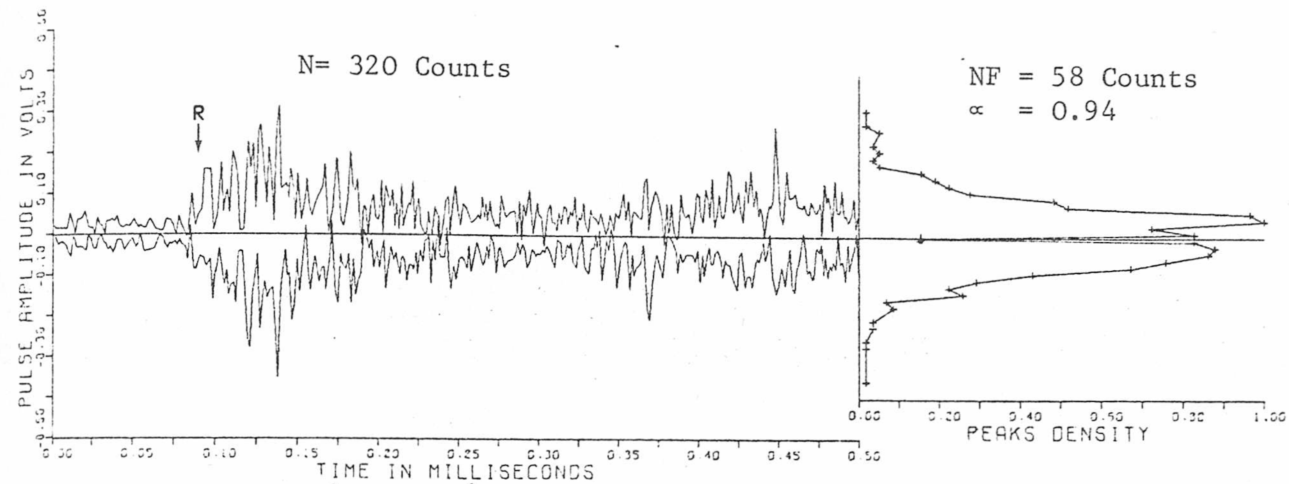

(a) GS1 : Steel Plate 995x50x12.5 mm.

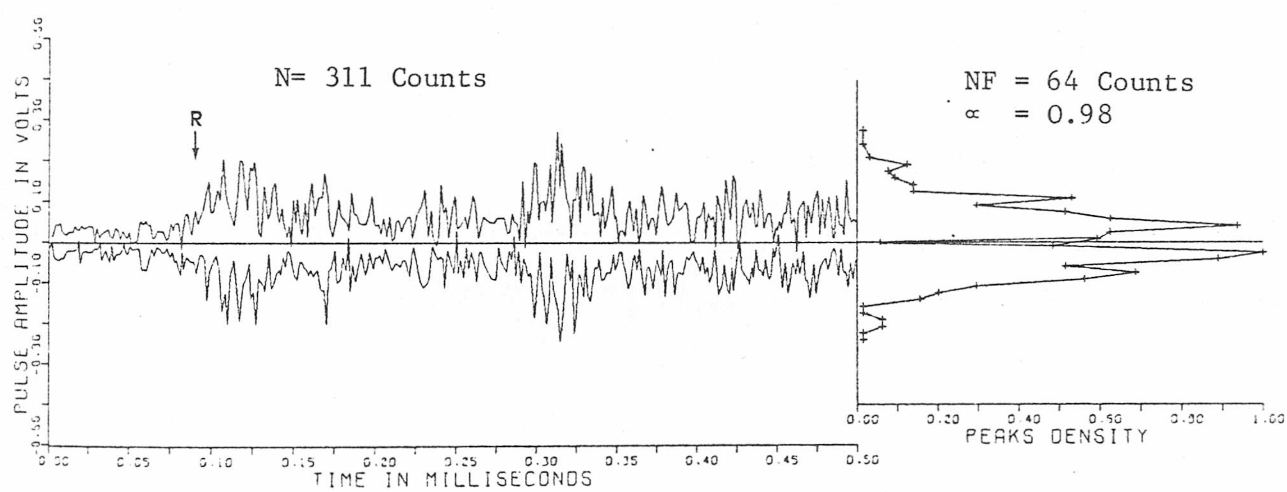

(b) GS2 : Steel Plate 690x50x6 mm.

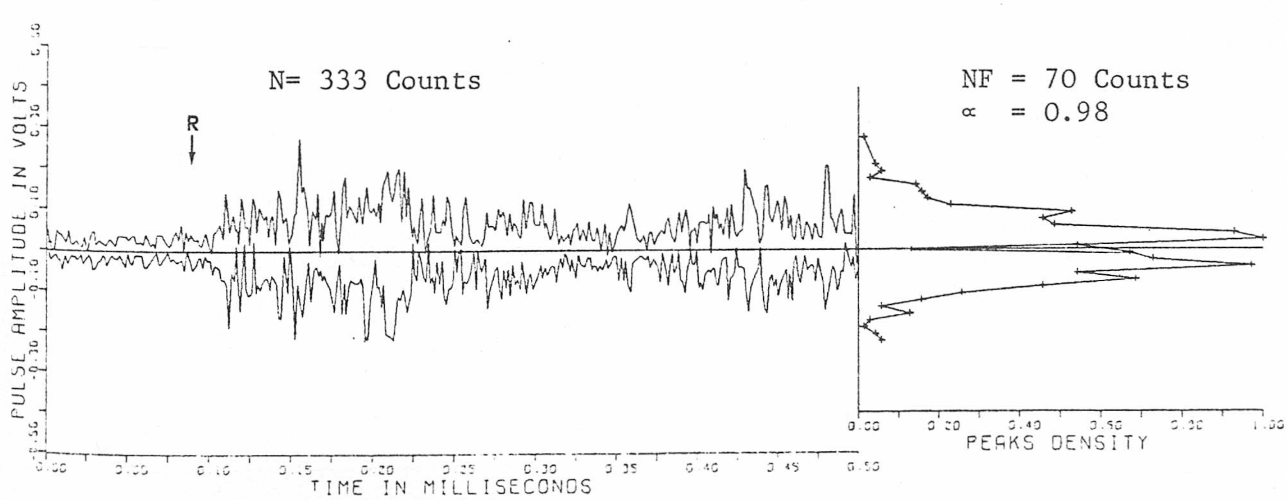

(c) GS3 : Steel Plate 330x50x12.5 mm.

FIGURE 6.5 : Time Domain Envelope of Peaks and The Probability Density (Peaks Density) of the Burst Envelope.

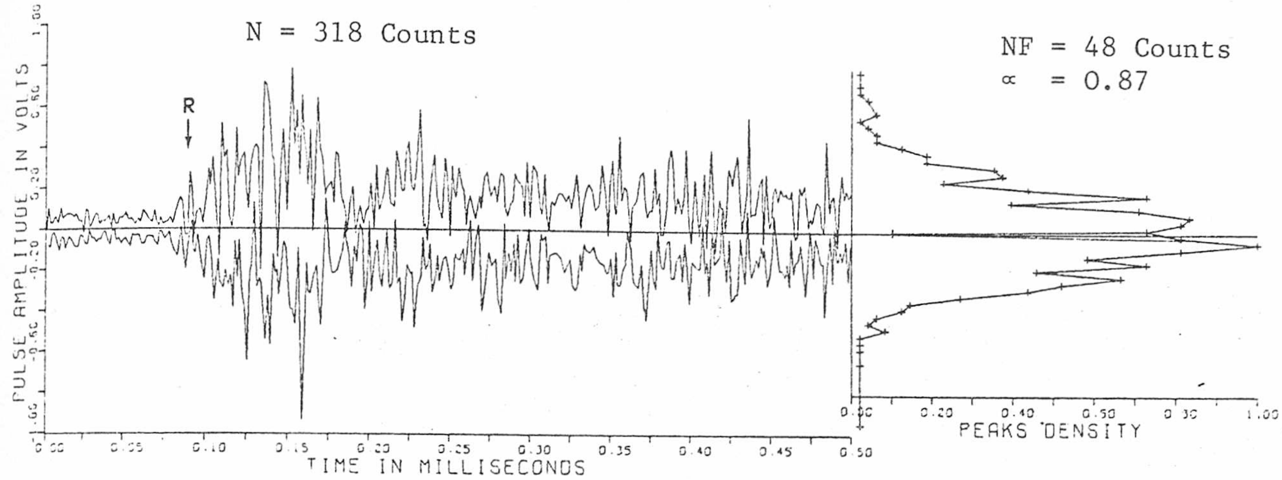

(d) GS4 : Steel Plate 330x50x6 mm.

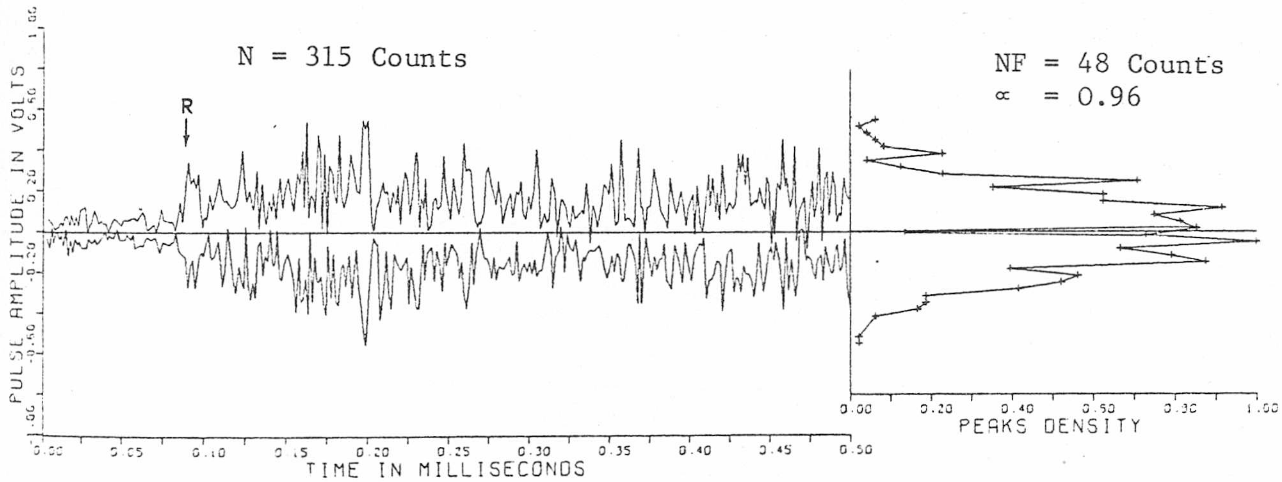

(e) GS5 : Steel Plate 330x30x30 mm.

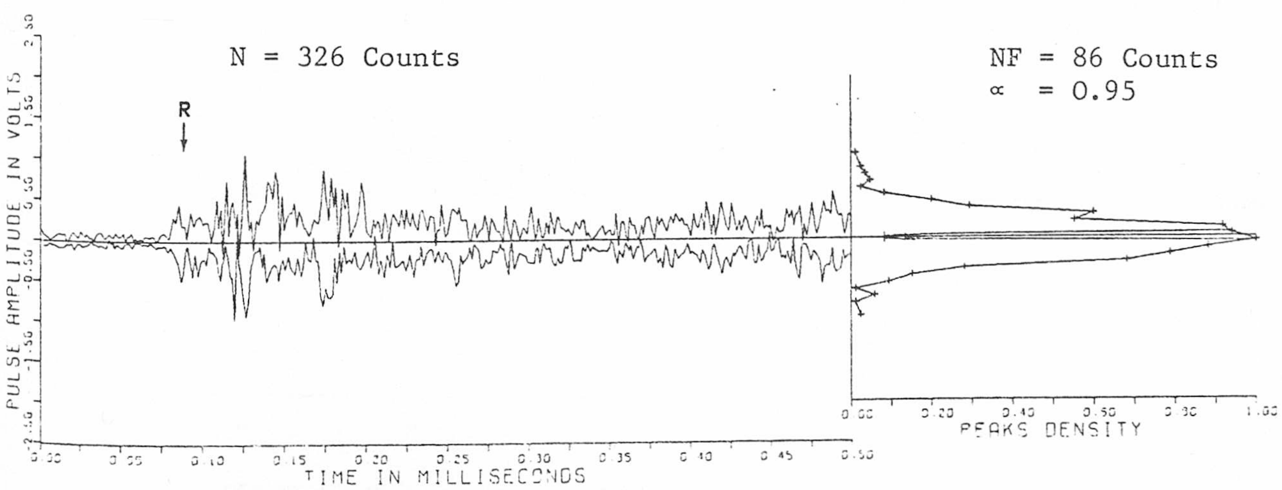

(f) GS6 : Steel Plate 330x25x12.5 mm.

FIGURE 6.5 : Cont.

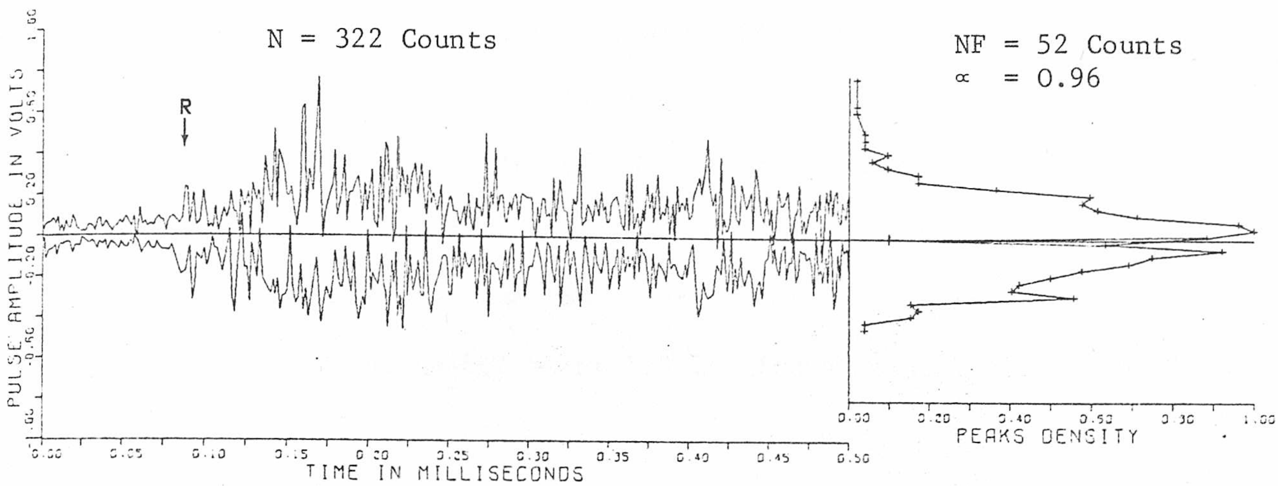

(g). GA : Aluminium Plate 330x25x12.5 mm.

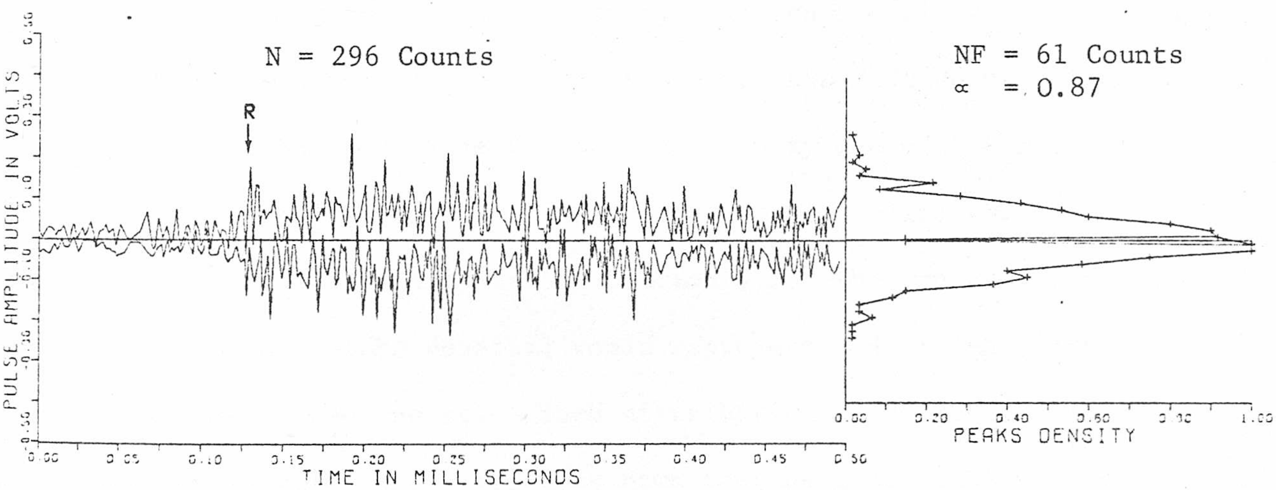

(h) GB : Brass Plate 995x50x12.5 mm.

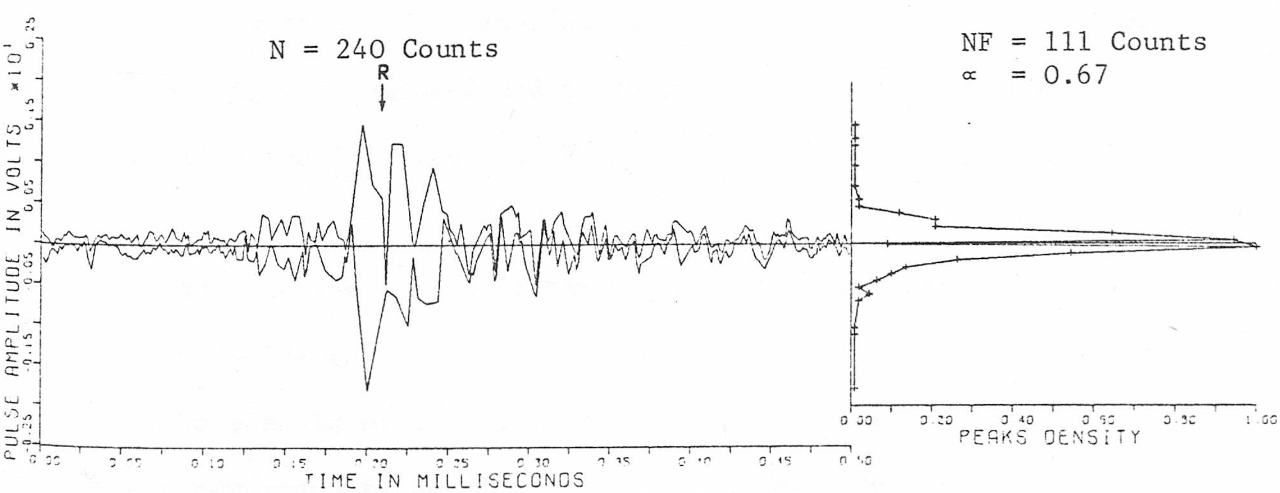

(i) GP : Perspex Plate 995x50x12.5 mm.

FIGURE 6.5 : Cont.

The arrival time of the directly propagated surface wave can be easily distinguished as the first pronounced ridge on the envelope (with the exception of GS6 and GP). The arrow marked 'R' shows the theoretical arrival time in each specimen. The number of maxima, N, is given at the top of each plot for comparison. It was found that the number of maxima is always equal to the number of minima.

Referring to the peaks density plots, on the right, the ordinate scale of each plot is the same as the pulse amplitude scale. The maximum peaks density is normalized to unity and only the values at different amplitudes on a single plot can be compared with each other. It was anticipated in Section 2.3.3 that the burst peaks distribution (peaks density) would represent a Rayleigh distribution for a narrow-band burst. Such distribution is characterized by a density function whose top goes down towards zero (133). The measure of the accuracy of the Rayleigh distribution, α (the ratio of the number of zero-crossings n_o^+ and number of maxima N, i.e. $\alpha = n_o^+/N$) was computed and given on each plot in addition to the normalization factor used, NF.

In this connection it can be noted that α takes a value greater than 0.94 for the specimens GS1, GS2, GS3, GS5, GS6 and GA. It will be seen later that this will have a great effect on the frequency response depending on how the ratio approaches unity. Based on the discussion given in Section 2.3.3, these specimens are expected to show almost one concentrated resonance frequency while the rest of the specimen GS4, GB and GP are expected to exhibit more than one collection of resonance frequencies.

At this end, one can conclude that although a broadband transducer was used to detect the emission, the peaks density resembles a Rayleigh distribution. It is also expected from the peaks distribution that the bursts will show an approximate narrow-band frequency response, in general.

No attempt has been made to obtain further statistical parameters from this presentation. Hopefully, future studies will also establish some relationships between the peaks density distribution and specimen geometry.

6.3.3 ENERGY ANALYSIS IN THE TIME DOMAIN

It is interesting to see how the shapes of the calculated burst energy increment depend upon the specimen geometry. To study this, the energy increment technique, given in Section 2.3.4 was applied and the plots are presented in four groups depending on the specimen geometry and material.

The results are shown in Figures 6.6 (a-d) and the corresponding numerical results are tabulated in Table 6.II. The average increment rate corresponds to the least squares straight line fit to each curve. For scaling reasons, all plots have been made from only the first

1000 data points, as usual, while the numerical data have been calculated from the total of 1024 points per burst.

To demonstrate the effect of specimen material, shown in Fig. 6.6(a) are the energy increment plots for specimens GS1, GB and GP of the same dimension (995 x 50 x 12.5 mm). The energy

TABLE 6.II: TOTAL ENERGY AND THE AVERAGE INCREMENT RATE FOR VARIOUS SPECIMENS

Code	Specimen Geometry		Total Energy $Volts^2Sec.$ (10^{-5})	Average Increment Rate	
	Dimension mm	Volume, m^3 (10^{-3})		Rate, $Volts^2$ (10^{-5})	Correlation
GS1	995x50x12.5	0.622	0.252	0.525	0.97
GS2	690x50x6	0.207	0.230	0.507	0.99
GS3	330x50x12.5	0.206	0.216	0.476	0.98
GS4	330x50x6	0.099	1.732	3.955	0.98
GS5	330x30x30	0.297	1.309	2.859	0.99
GS6	330x25x12.5	0.103	2.608	5.639	0.97
GA	330x25x12.5	0.103	1.305	2.959	0.99
GB	995x50x12.5	0.622	0.187	0.446	0.99
GP	995x50x12.5	0.622	0.370×10^{-3}	0.001	0.93

data set $\{\hat{E}_i(t) = \sum_{n=1}^{i} E_n(t)\}$ for specimen GP is multiplied by a factor of 400 for plotting purposes* (otherwise, the energy curve will coincide with the time axis and no details can be shown). The total energy received from the steel specimen, GS1, is the largest, the next was from brass and the smallest was from the perspex. The order is held for the average increment rate $(d\hat{E}_T/dt)$. Since, the specimens volume, cross-sectional area and the experimental conditions

* This is shown in the reduced plot.

are identical, the variation in the burst energy can only be attributed to the acoustical properties of the specimens material. The steel specimen has an acoustic impedance of about 47×10^6 Kg s^{-1} m^{-2} and a longitudinal wave velocity of 6000 m s^{-1} which are fairly close to those of the shoe material of the receiving transducer (alumina, $A\ell_2O_3$: Z = 42.6×10^6 Kg s^{-1} m^{-2}; C_L = 10700 m s^{-1} 'Table 4.I'). Then comes the brass (Z = 40.6×10^6, C_L = 4500) and finally the perspex with a poor transmission coefficient (Z = 3.2×10^6, C_L = 2700).

The same reason can be given in comparing the curve of aluminium specimen, GA, with steel, GS6, Fig. 6.6(b). Both specimens have identical dimensions of 330 x 25 x 12.5 mm. The transmitted energy to the acoustic emission transducer via the aluminium specimen is shown to be reduced to about 50% of the total energy transmitted via the steel specimen of similar dimensions. The average increment rate is also shown to drop to 50%.

Figure 6.6(c) shows the change in the energy increments received from three steel specimens of different dimensions. Specimens GS2 and GS4 with identical cross-sectional area (50 x 6 mm) are varied only in length. The curves reveal that the increase in specimen length decreases the detected emission energy. The curve for specimen GS1 is displayed in this figure in order to compare the results in the other graphs.

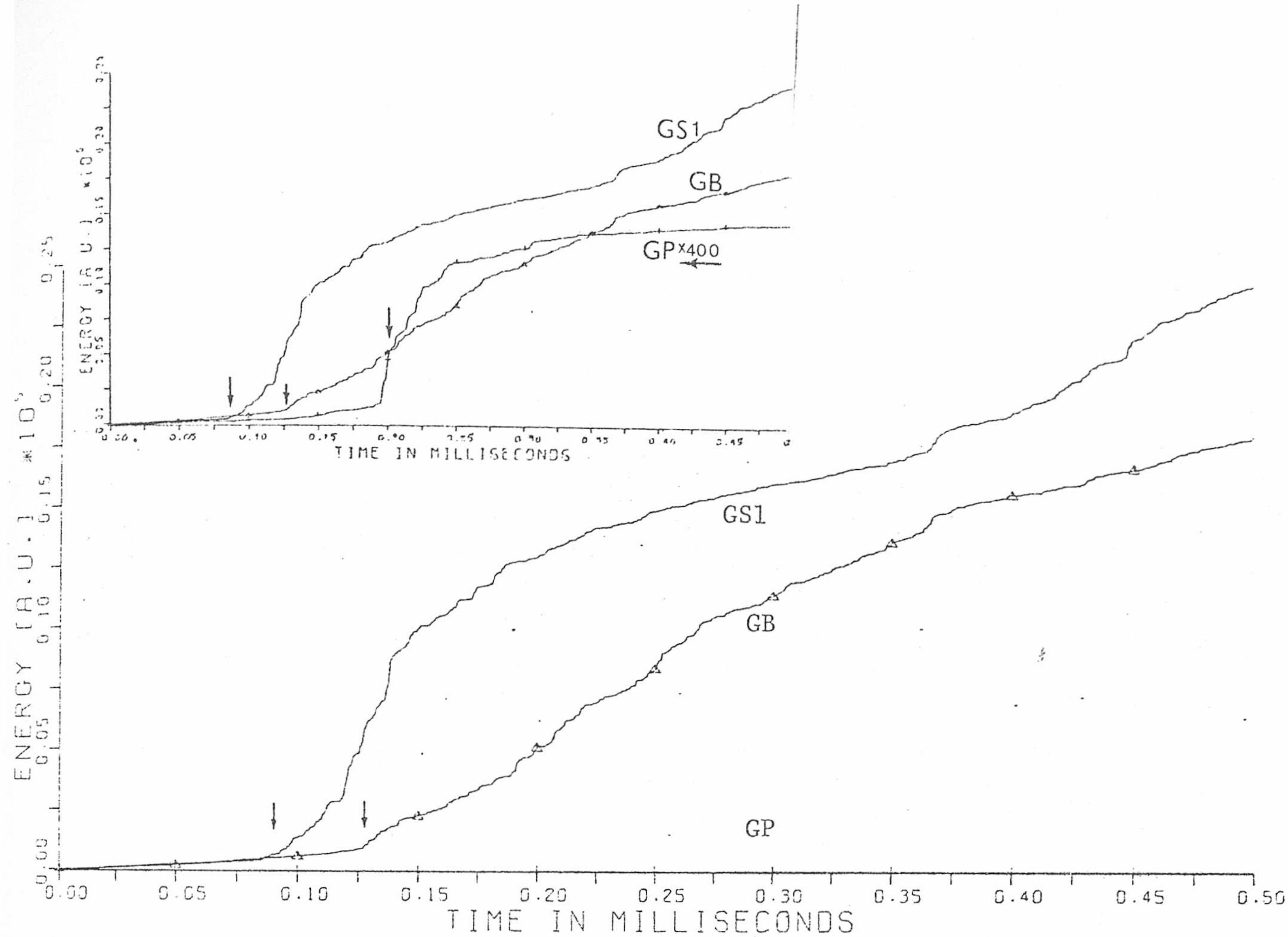

(a) Effects of Specimen Material (Steel- Brass- Perspex).

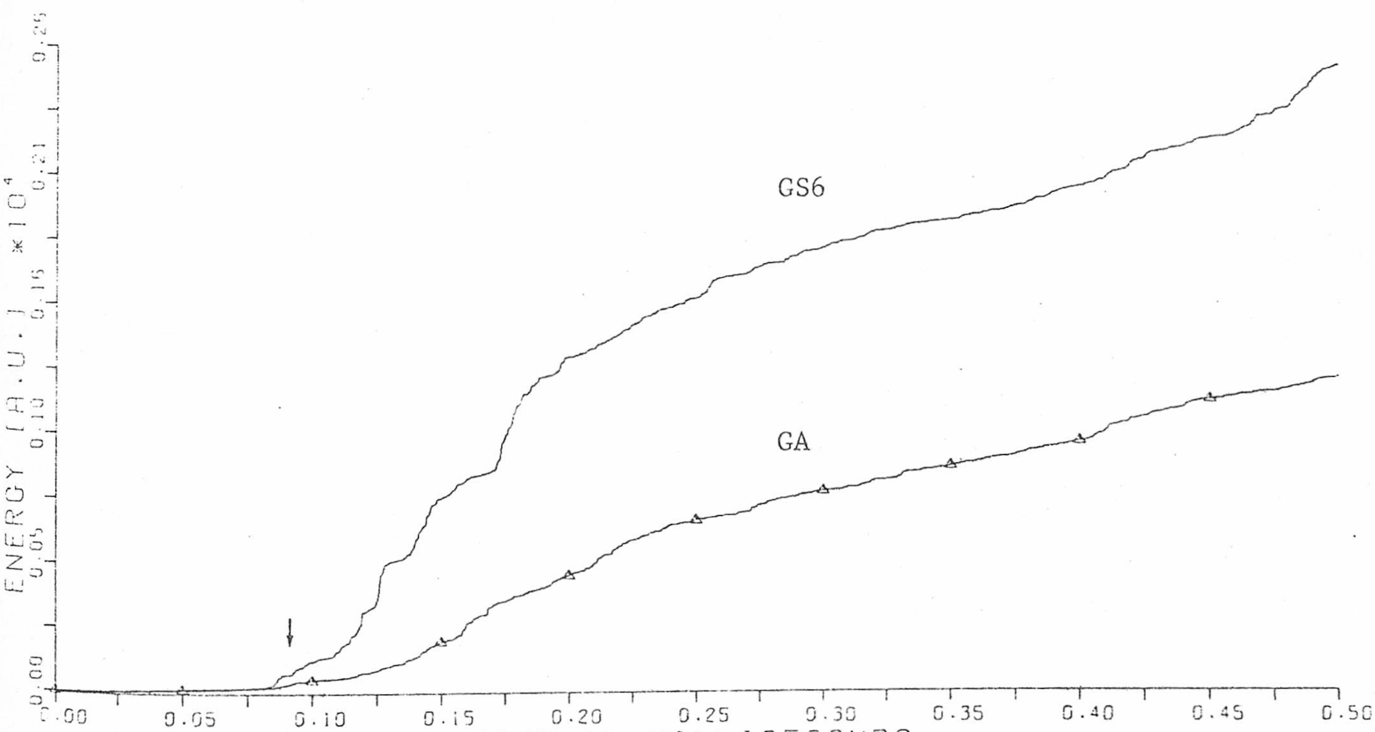

(b) Effects of Specimen Material (Steel- Aluminium).

FIGURE 6.6 : Effects of Specimen Geometry on the Energy Increment.

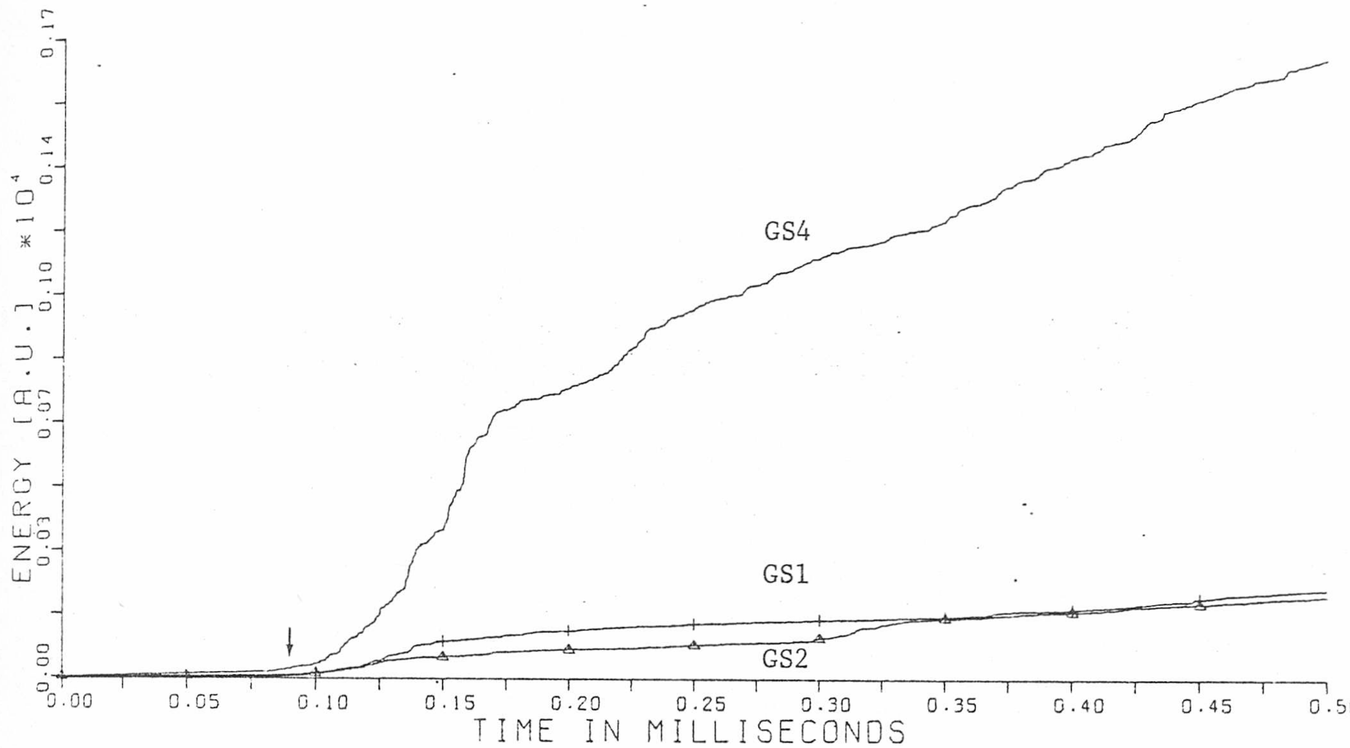

(c) Effects of Specimen Length.

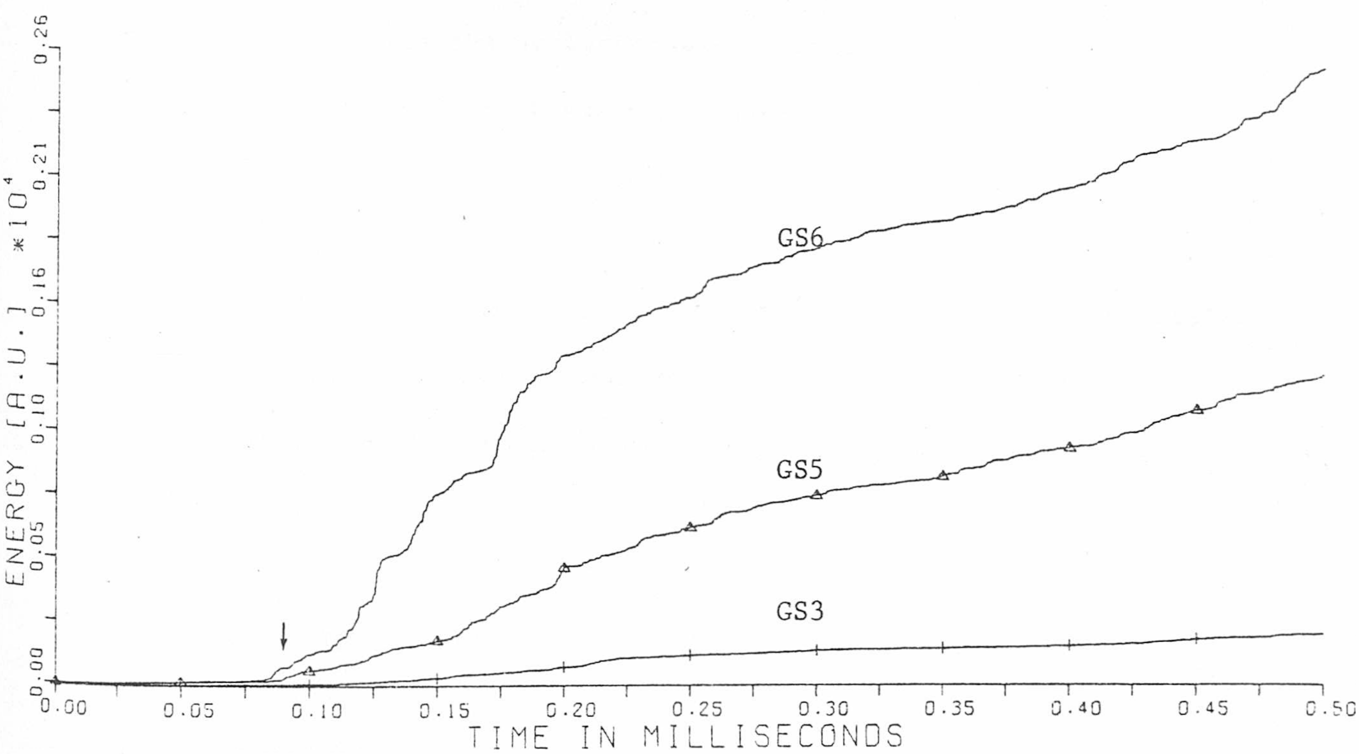

(d) Effects of Specimen Width and Thickness.

FIGURE 6.6 : Cont.

The effect of the specimen width on the energy increment can be observed by comparing the plots for specimens GS3 and GS6 in Fig. 6.6(d). It is clear that an increase of the specimen width has a significant effect in decreasing the received energy. The total energy decreases from 2.608×10^{-5} to 0.216×10^{-5} volts.^{2} sec as the specimen width increases from 25 to 50 mm (other dimensions are identical). Because both the source and detecting transducer are placed on the same surface and in view of the surface wave attenuation mechanisms (167), this observation is not surprising.

Comparison between results from specimens GS3 and GS4 indicates that an increase in specimen thickness decreases the burst energy considerably. This is also expected as increasing the specimen thickness increases the reflected waves paths between the specimen boundaries. Therefore, these bulk waves modes will be subject to more attenuation before they reach the transducer face.

Clearly more analysis is needed before one can draw a realistic relation between the burst total energy and the specimen volume. An attempt to use the acoustic diffuse theory will be discussed in Section 6.5.

ENERGY METHOD FOR SURFACE SOURCE LOCATION

To the right on the energy increment plots, sudden changes in the rate can be easily noted (time indicated by arrows). It is found that at these points the energy increment calculation can yield a superior technique to locate the acoustic emission surface sources.

To demonstrate this, Table 6.III presents detailed analysis of the changes of the energy increment rate at times before, within, and just after the time of the sudden change itself. An important point to note is the significant increase of the energy increment rate at the arrival time of the surface wave. It can be seen that the series of the calculated velocities correspond rather well with the published surface wave velocities. The deviation is shown to be less than ±9% for all specimens.

That is, the time of arrival of the surface wave could be located very well when the average increment rate is suddenly changed.

TABLE 6.III LOCATION OF THE ARRIVAL TIME OF THE SURFACE WAVE MODE BY COMPARING THE SUDDEN CHANGE OF THE ENERGY INCREMENT RATE

Specimen Code	Energy Increment Rate, V^2			Time of Sudden Change (sec.) (10^{-4})	Surface Wave Velocity m s^{-1}		
	Before (Av.) (10^{-2})	Within (10^{-2})	After (10^{-2})		Calculated	Published*	Deviation %
GS1	0.40	0.44	0.45	0.87	2900	3000	-3
GS2	0.12	0.25	1.00	0.92	2720	3000	-9
GS3	0.03	0.10	0.08	0.82	3050	3000	+2
GS4	0.20	1.00	1.00	0.87	2900	3000	-3
GS5	0.20	1.00	4.00	0.87	2900	3000	-3
GS6	1.00	9.00	5.00	0.87	2900	3000	-3
GA	0.20	2.20	2.80	0.87	2900	2900	0
GB	0.16	1.00	0.80	1.30	1980	1950	+1
GP	0.12×10^{-2}	0.12×10^{-2}	0.78×10^{-2}	1.97	1270	1170	+8

*Compiled from Refs. (167-169).

6.3.4 TRIGGER-LEVEL CROSSING COUNTS

The specimens under test are again grouped in the same order as that for the energy analysis. The number of counts versus trigger-level (threshold-level) are displayed in Figs. 6.7(a) through 6.7(d). The values shown on the graph are the maximum peak-to-peak amplitude, the number of positive zero-crossings, n_0^+, and the number of counts at 0.2 volts level, i.e. $n_{0.2}^+$, which are calculated through the program COUNT .

Apart from the zero-level, it can be seen that the variation in the number of counts at various trigger levels, p-p amplitude and the total burst energy (Table 6.II) are very well connected. Such variation may be clearly observed by comparing the change in area under each level-counting distribution with the corresponding variation in energy increment, Fig. 6.6.

The maximum effect of the system noise can be approximately estimated by comparing each distribution with that for the perspex specimen, GP.

The difference in the maximum number of counts, n_o^+ (zero-crossings) between steel (GS1) and brass (GB) specimens can be seen in Fig. 6.7(a). The illustration also shows the variation in the number of counts at different trigger-levels. For example, at 0.2 volts level the number of counts is found to be 10 counts/burst for the steel specimen and only 3 counts/burst for brass. The effect of the system noise is shown to be neglibible at this level (±0.012 volts).

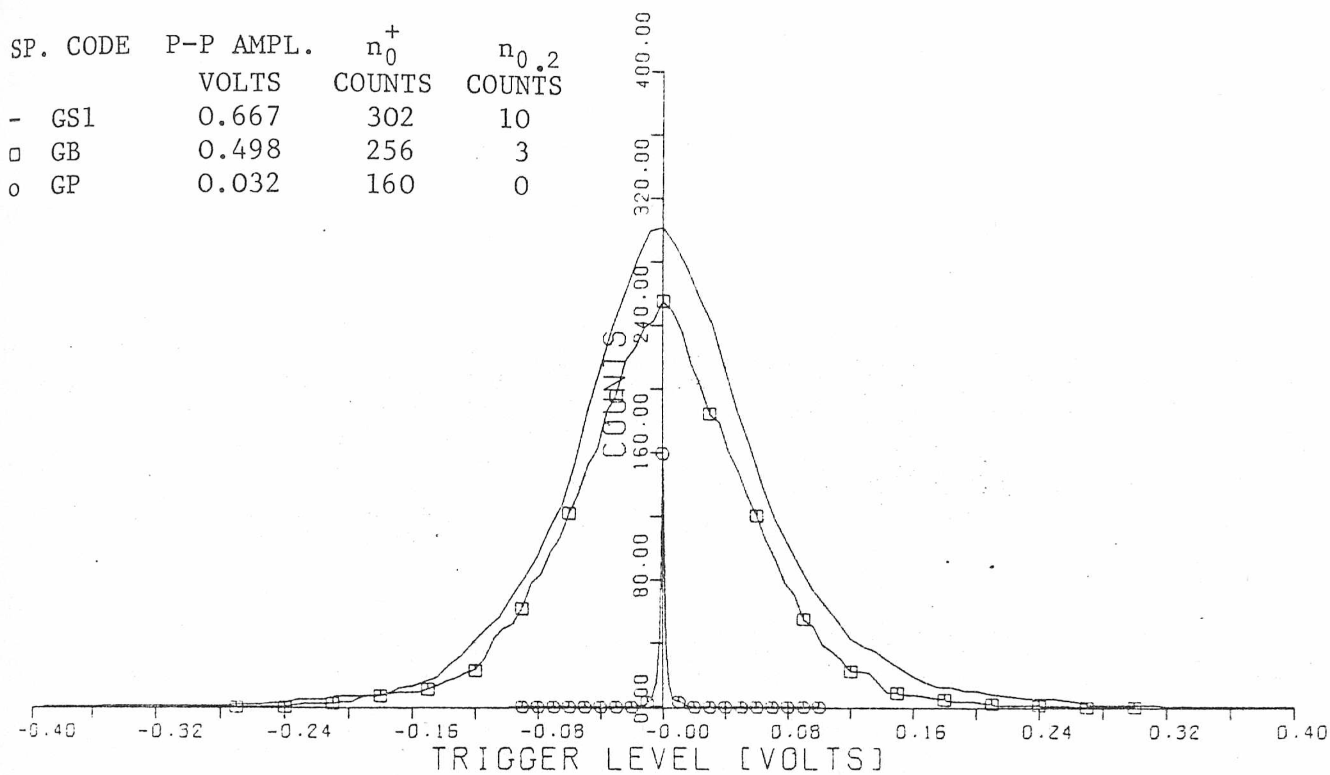

(a) Effects of Specimen Material

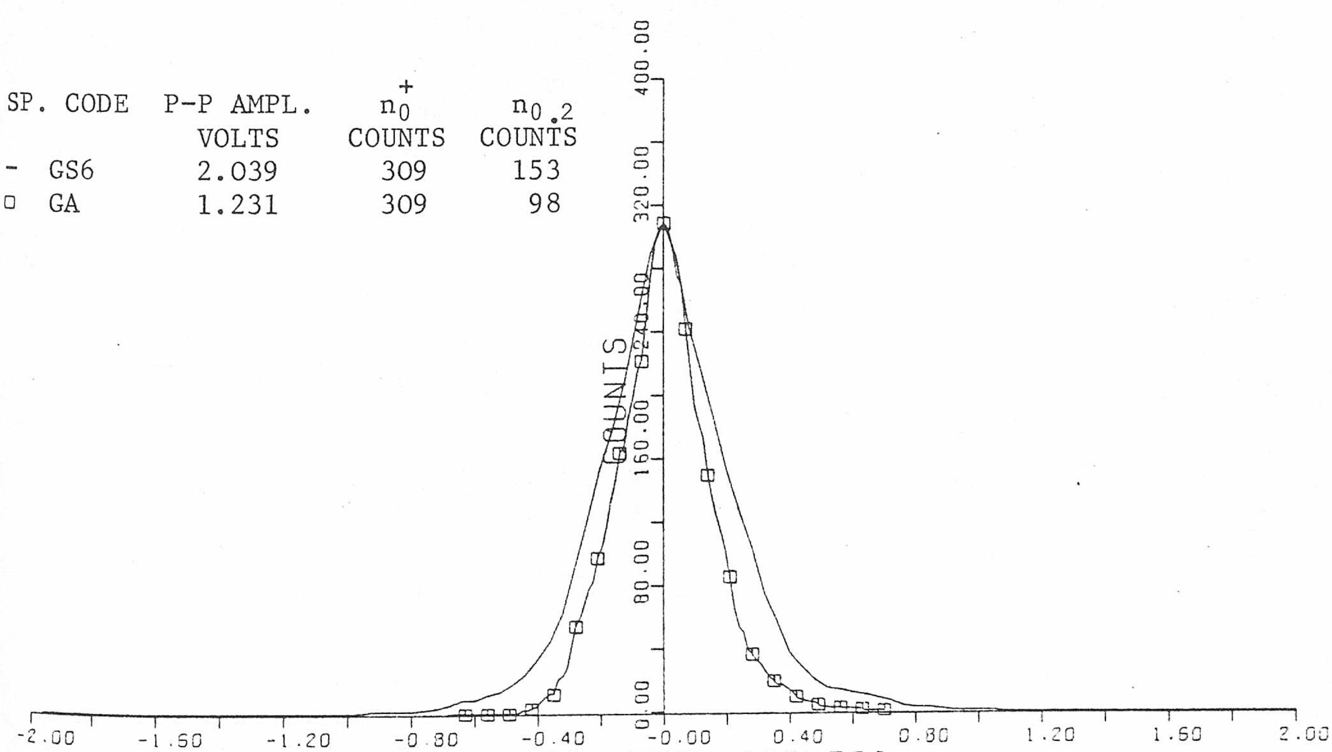

(b) Effects of Specimen Material.

FIGURE 6.7 : Effects of Specimen Geometry on the Trigger-Level Crossing Counts.

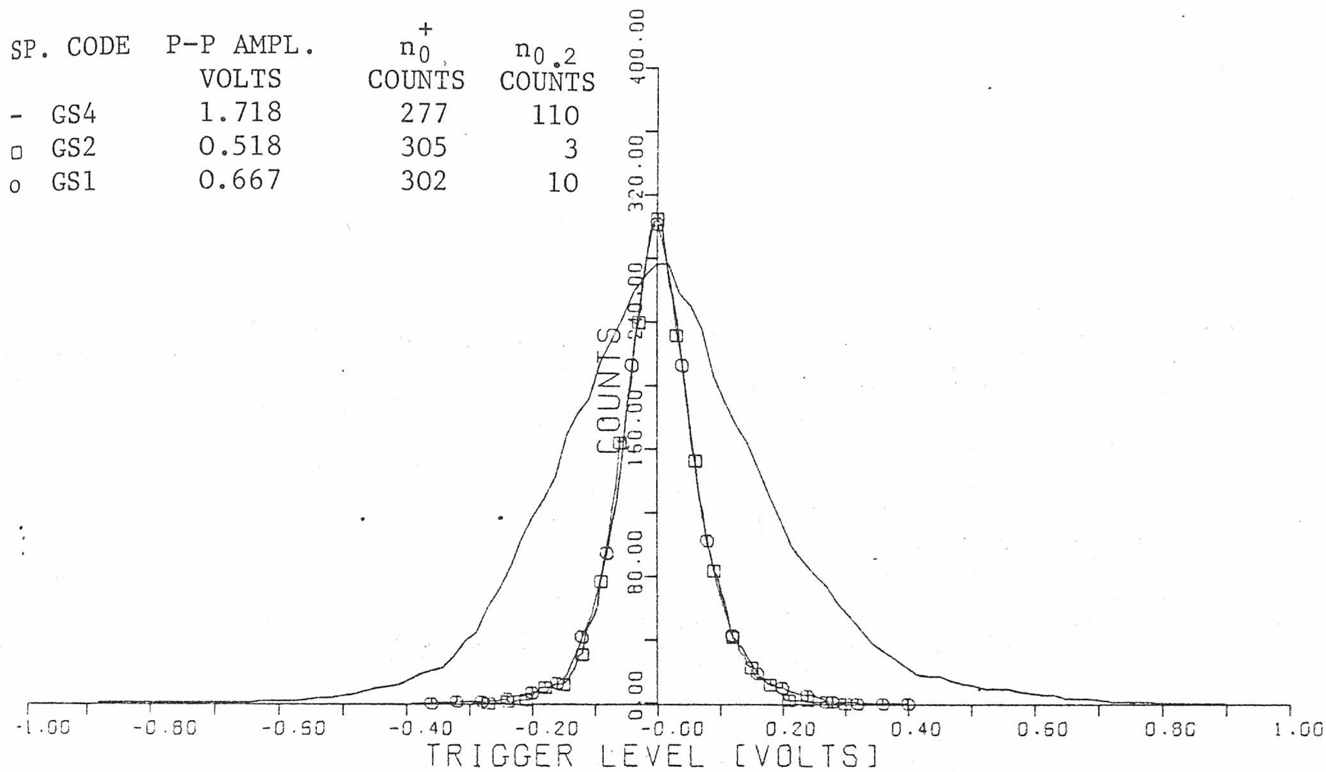

(c) Effects of Specimen Length.

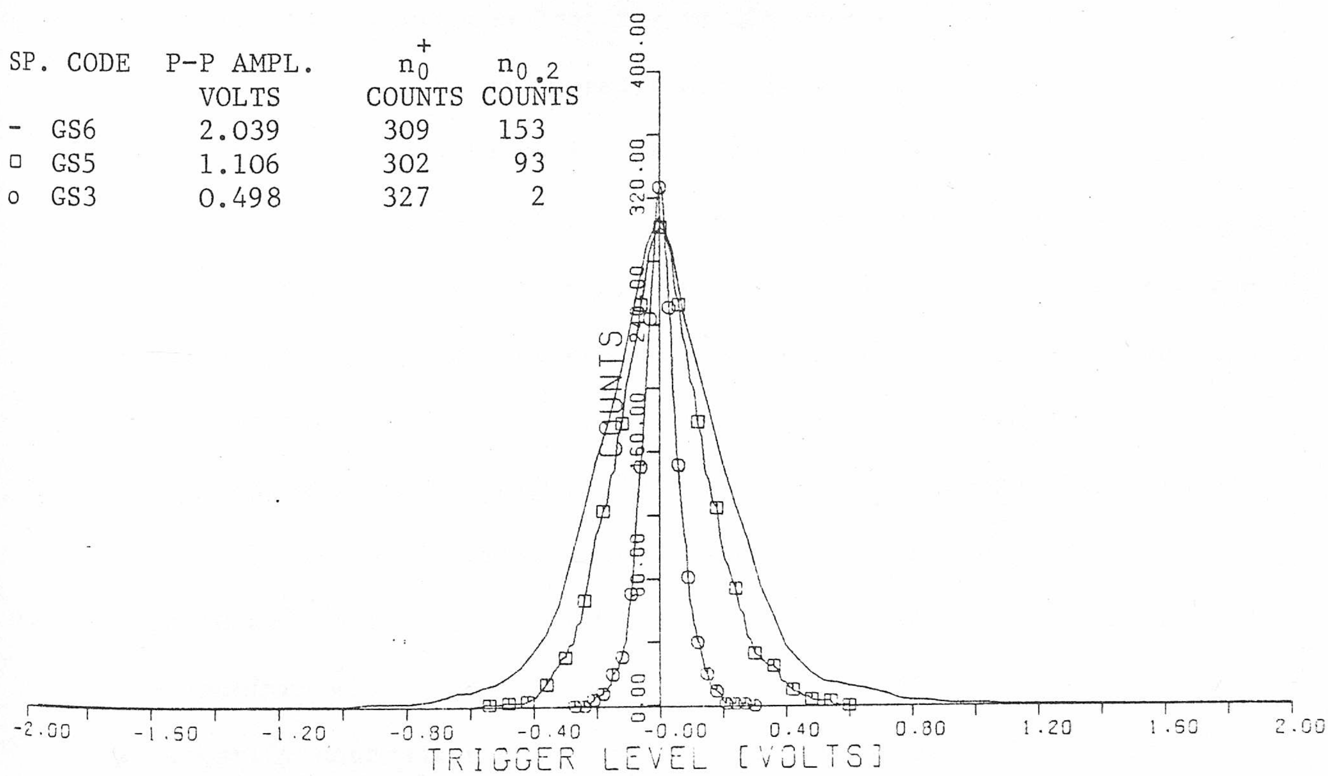

(d) Effects of Specimen Width.

FIGURE 6.7 : Cont.

Figure 6.7(b) shows the variation in level-counts for aluminium (GA) and steel (GS6) specimens of identical dimensions. At 0.2 volts level, the number of counts per burst drops from 153 for steel to 98 for aluminium while no change in the number of zero-crossings occurs. Then as the voltage level decreases to about 0.1 volts the difference in counts decreases.

A comparison between GS3 and GS4 curves in Fig. 6.7(c) shows the effect of the change in specimen length on the level counts. The differences in counts at zero and 0.2 volts levels should be noted. Increasing the specimen length by about one order shows a remarkable reduction in the number of counts at different trigger levels ($n^{+}_{0.2}$ goes down from 110 to 3 counts) while the number of zero-crossings increases from 277 to 305 counts. The plot of GS1 shows how this variation is reduced by increasing the specimen thickness. The observation is seen to be in agreement with early work of Fisher and Lally (170). The authors carried out measurements on magnesium crystals varying in length from 2.54 to 12.70 cm and the results indicated that the acoustic emission pulse rate was proportional to the sample length when the applied strain rates were equal. But, on the opposite side, they found that the pulse rate was insensitive to the change in the cross sectional area over the range of areas from 10 mm^2 to 77.8 mm^2. However our observation on the effect of the specimen width and thickness on emission activities does not necessarily contradict the previous results of ref.(170). Since the minimum cross sectional area in this study was 300 mm^2 for the specimens GS2 and GS3 which is much greater.

The effect of the change in the specimen width on the level-counts is shown in Fig. 6.7(d). Although only a little variation in the number of zero-crossings is found, $n^+_{0.2}$ is increased from 2 to 153 counts/burst as the width decreases from 50 to 25 mm.

The individual effect of the specimen thickness can be demonstrated by comparing the results for the specimens GS4 (Fig. 6.7(c)) and GS3 (Fig. 6.7(d)). Clearly, increasing the specimen thickness increases the number of zero-crossings and decreases both the level-counts and the burst maximum amplitude. Again, it has been reported by Dunegan and Green (12) that thick-notched tensile specimens used in fracture toughness tests tend to give higher emission rates and amplitudes than thin ones. This may not be due purely to the variation in specimen thickness. It may be that the stress-conditions at the crack-tip vary with specimen thickness or, probably, that a large volume of material is presented to the advancing crack front (18).

6.3.5 FREQUENCY SPECTRUM ANALYSIS

The time domain data record $\{X_i(t)\}$ of each burst was converted to the frequency domain by means of digital Fourier transform using the computer program SPECT (Section 2.4). All spectra are plotted in the range of 0-1 MHz with resolution of 2 KHz (the emission signal was filtered first through a bandpass filter of 100-1000 KHz).

Figures 6.8(a) through 6.8(i) show the series of frequency spectra which are calculated for each time domain burst shown in Figures 6.3 (a-i). The Fourier magnitude was first computed and plotted. The power spectral density was next computed as the square modulus of the Fourier magnitude and plotted versus frequency in linear scale, second, and in decibel scale, third. The power spectral density in dB provides detailed information about the non-peaks (valleys) frequencies. No normalization process was applied to either the Fourier magnitude or the linear power spectral density plots, so that the amplitude at different frequencies on all graphs can be compared with each others. However, detailed comparison between different spectra is quite impossible because of the large range of variation in the spectrum amplitudes and frequencies encountered. Nevertheless, a rough comparison of the energy content in different spectra can be made using the values of the zeroth, second and fourth moment, i.e.: σ_x^2, $\sigma_{\dot{x}}^2$ and $\sigma_{\ddot{x}}^2$ (Section 2.5) which are numerically calculated and given on each graph. These parameters are listed later in Table 6.IV and will be used in Section 6.4.2.

The visual analysis of these spectra shows that, generally, the differences between one spectrum and another are in their fine structure and the relative amplitudes of the spectral peaks. Some peaks present on one spectrum are absent in another. All spectra, with the exception of Figure 6.8(i) for the perspex specimen, show that a collection of peaks are usually concentrated around 700 KHz frequency, the strongest peak being at about 725 KHz. This peak or, more precisely, a group of peaks, has a relatively large power spectral density over the 700 to 750 KHz. Although the transducer calibration chart, Fig. 4.3(d); supplied by the manufacturer; shows resonance occurring at 550 KHz, the existence of these prominent strong peaks on all graphs gives a good reason to attribute them to the transducer characteristics.

Now, careful observation of Figs. 6.8(d) and 6.8(h) for specimens GS4 and GB shows that other relatively high peaks amplitude are scattered over the whole frequency range. This may now answer the question of the observed small α (0.87) in section 6.32. The flat response of the perspex specimen GP (above 200 KHz in Fig.6.8(i)) shows also the reason for smaller α (0.67). This indicates that the frequency characteristics may be approximated by studying the emission burst in the time domain.

The occurrence and distribution of other peaks is a much more complicated problem. Transient excitation of a rectangular plate generates a series of different normal mode frequencies (Eq.(5.10)). The normal mode density versus frequency is not equal and depends on the plate dimension (151). In addition to the longitudinal and shear normal modes, symmetric and antisymmetric plate modes can be also excited over the frequency range of interest (123, 171).

Some of the presented spectra were analysed in detail and the spectra peaks are compared with the calculated resonance modes. For example, Figs. 6.9(a) and (b) represent replots of the aluminium specimen spectra and some of the predicted modes are indicated.

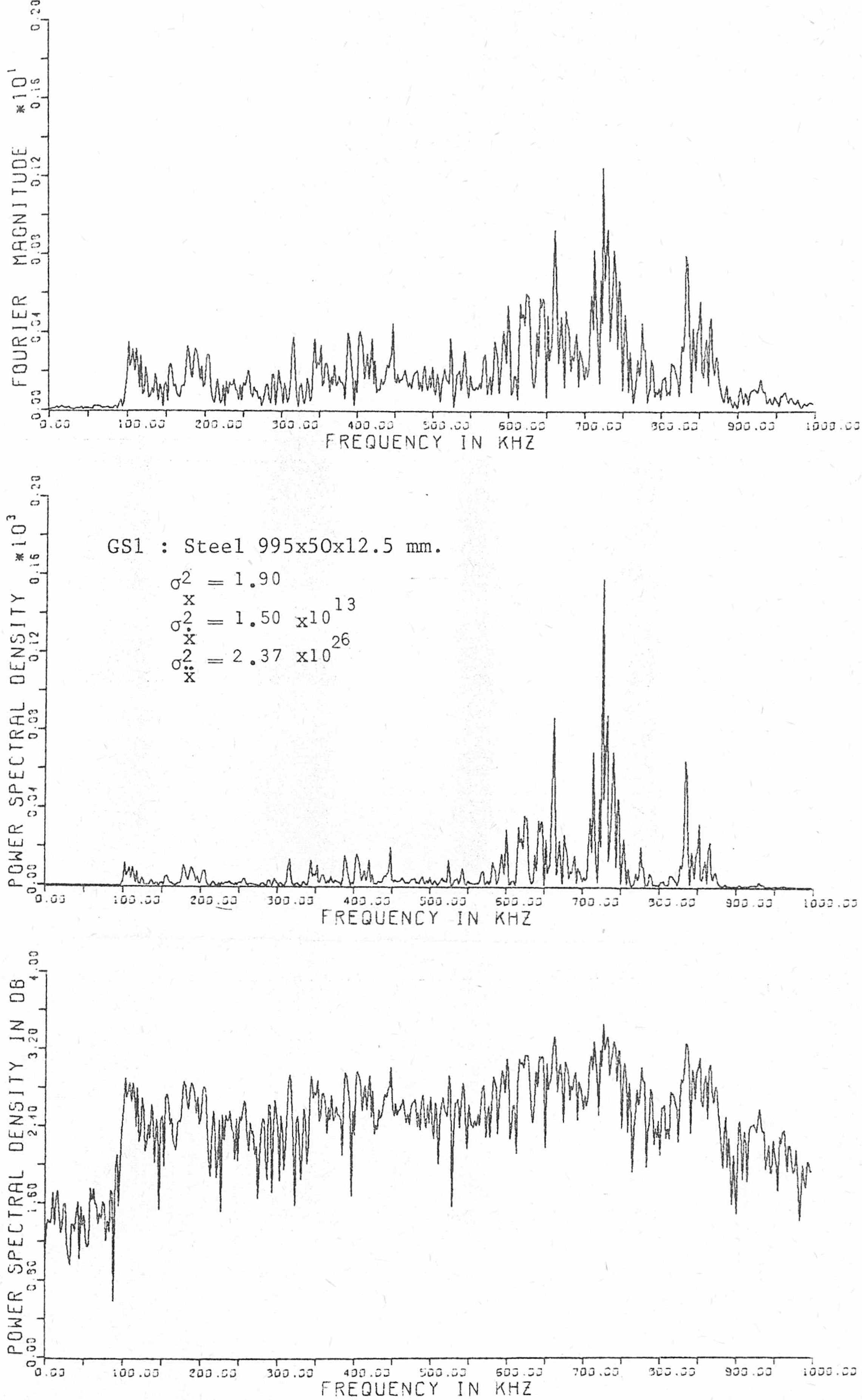

(a) Frequency Response of GS1

FIGURE 6.8 : Fourier Magnitude, Linear and Logarithmic Power Spectral Density of the Received Simulated Emission in Plates of Various Geometries and Materials. (σ_x^2 in Volts.Hz.s., $\sigma_{\dot{x}}^2$ in Volts.Hz^3.s.& $\sigma_{\ddot{x}}^2$ in Volts.Hz^5.s)

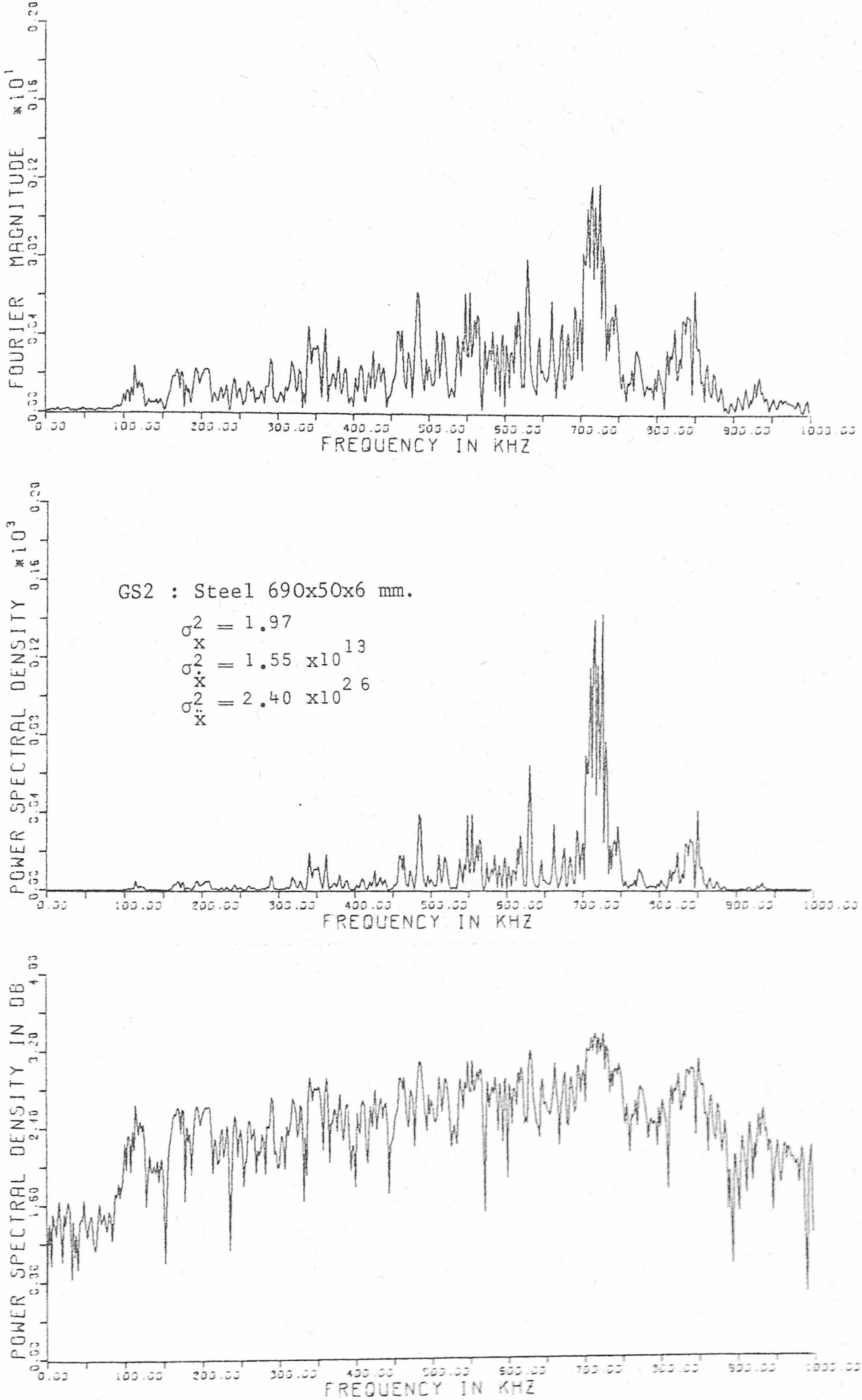

(b) Frequency Response Of GS2

FIGURE 6.8 : Cont.

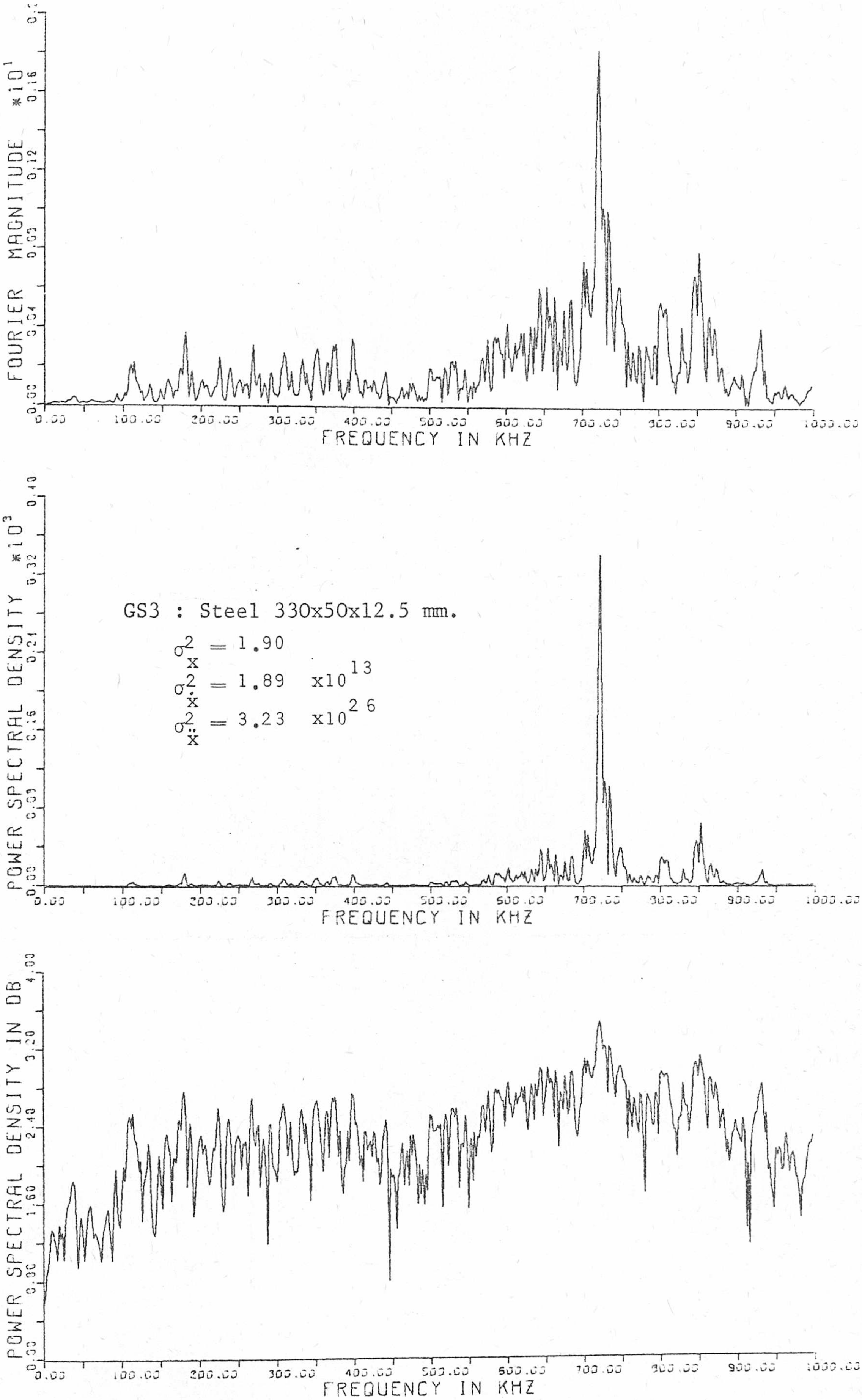

(c) Frequency Response of GS3

FIGURE 6.8 : Cont.

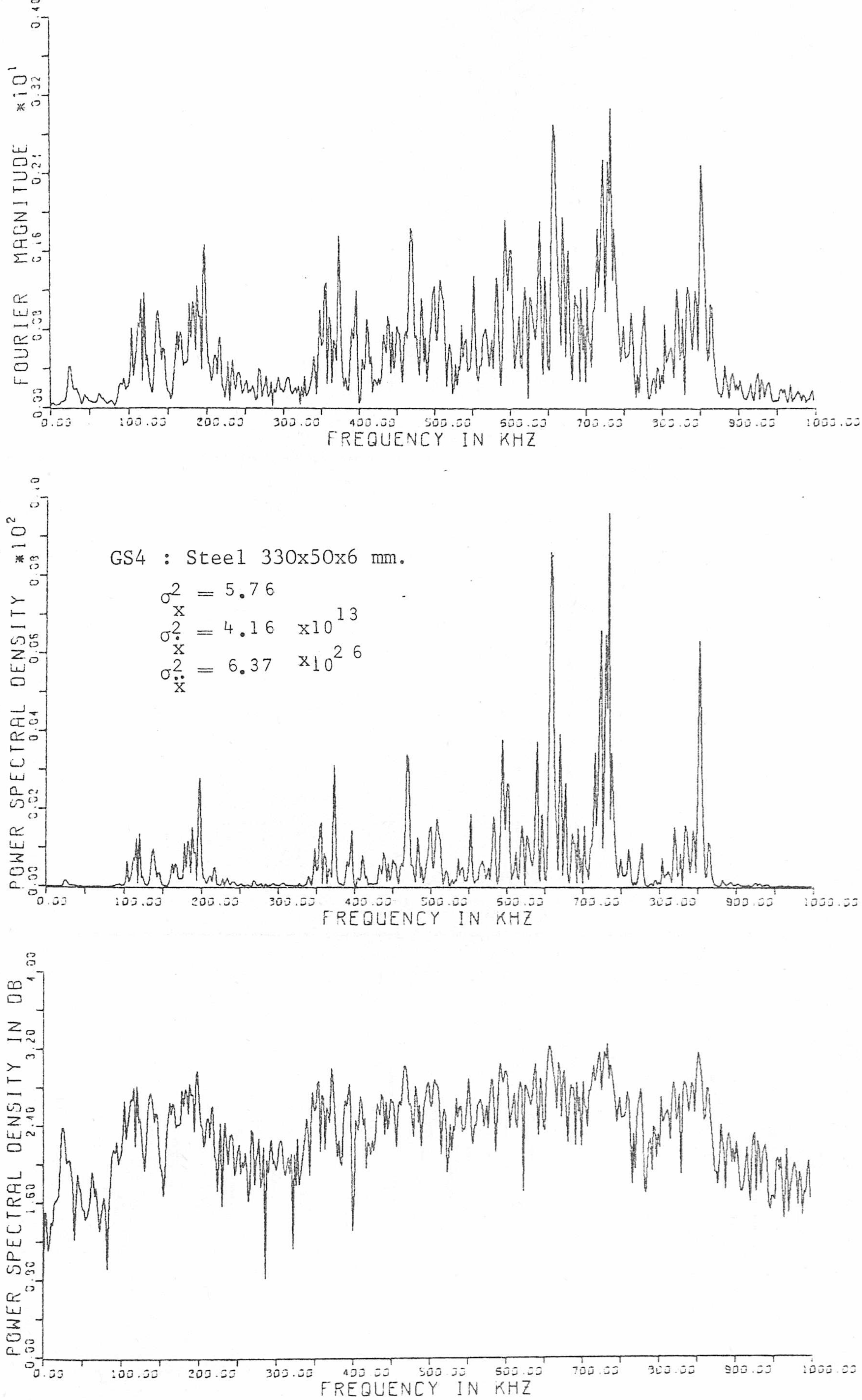

(d) Frequency Response of GS4

FIGURE 6.8 : Cont.

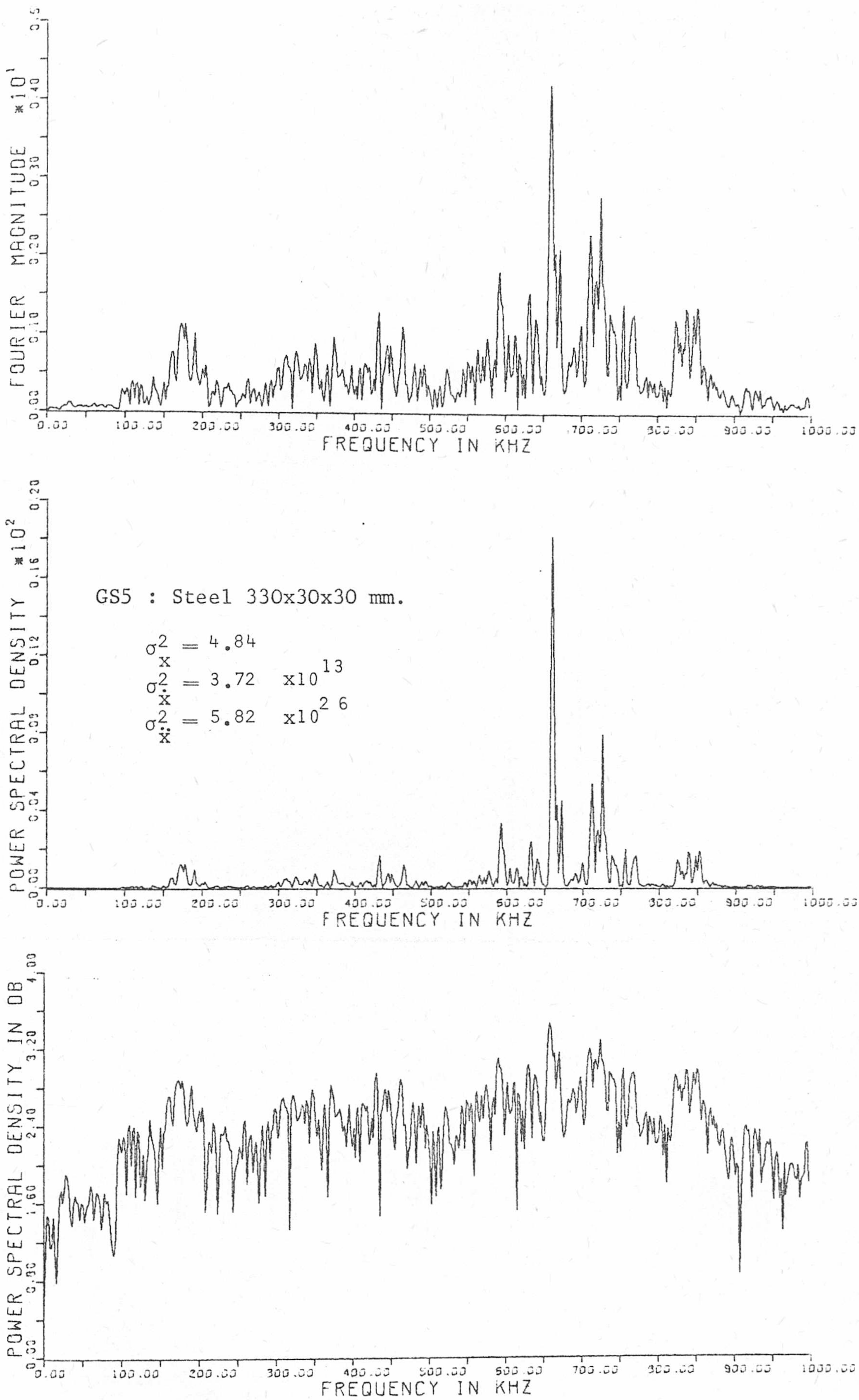

(e) Frequency Response of GS5

FIGURE 6.8 : Cont.

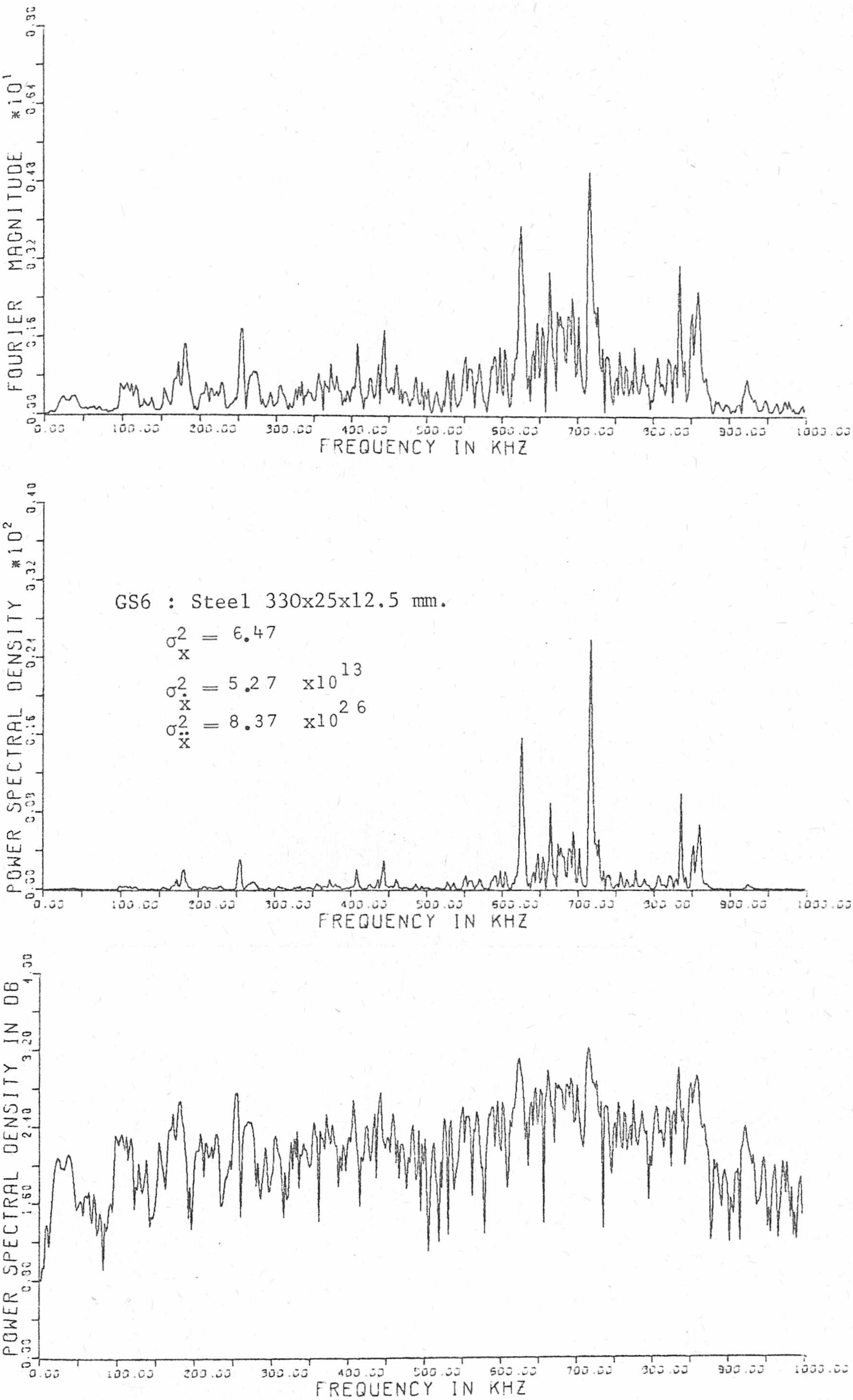

(f) Frequency Response of GS6

FIGURE 6.8 : Cont.

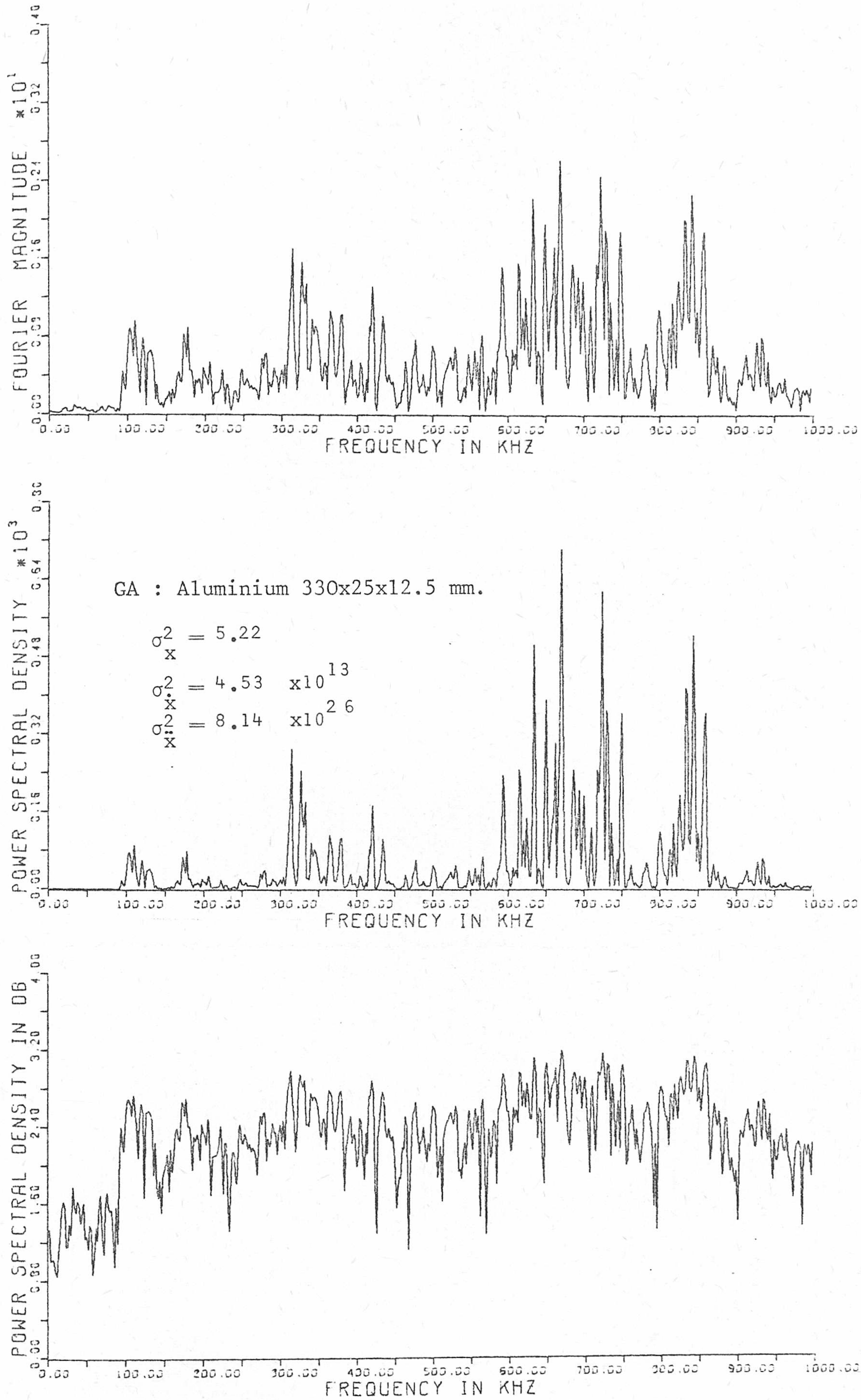

(g) Frequency Response of GA

FIGURE 6.8 : Cont.

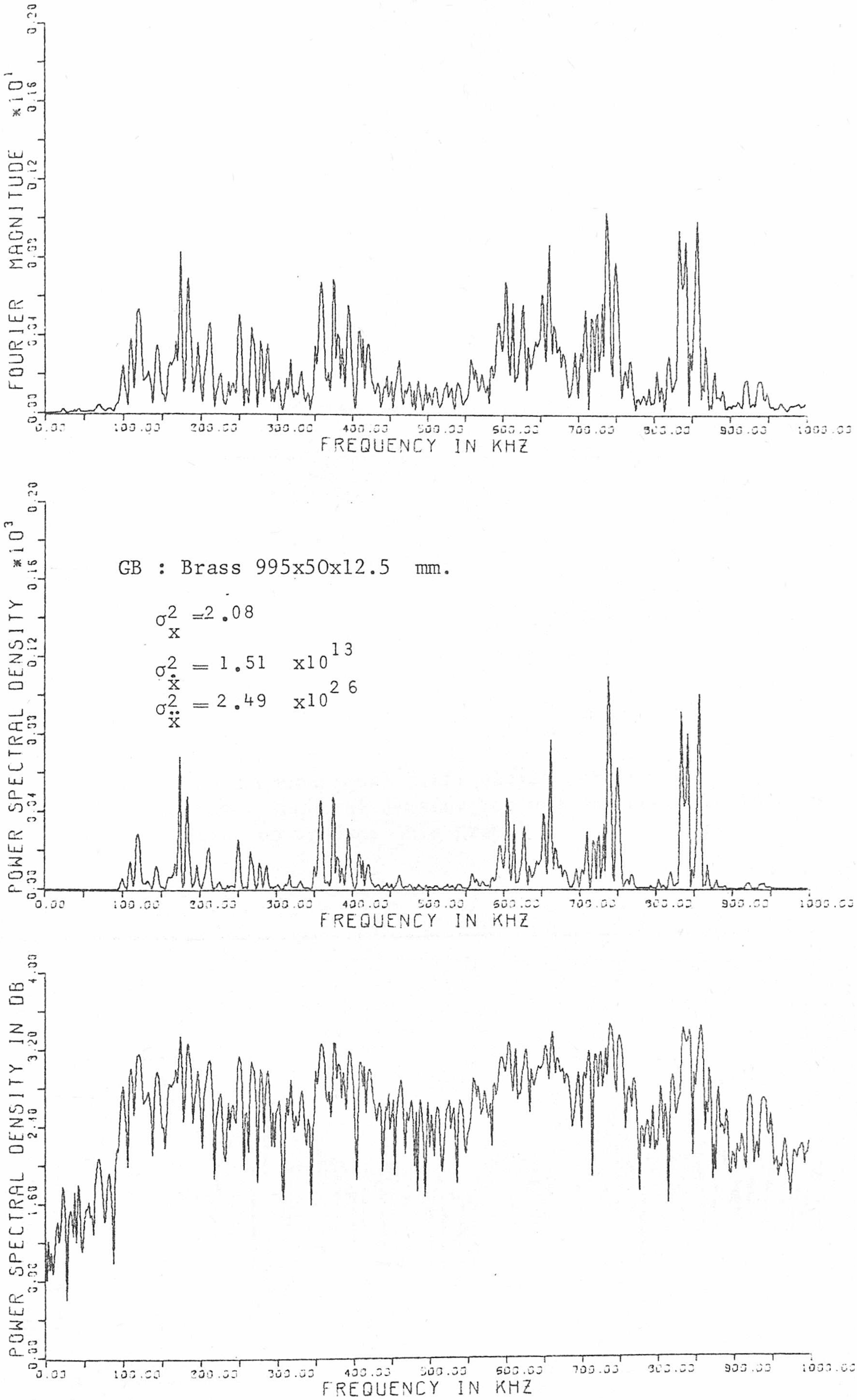

(h) Frequency Response of GB

FIGURE 6.8 : Cont.

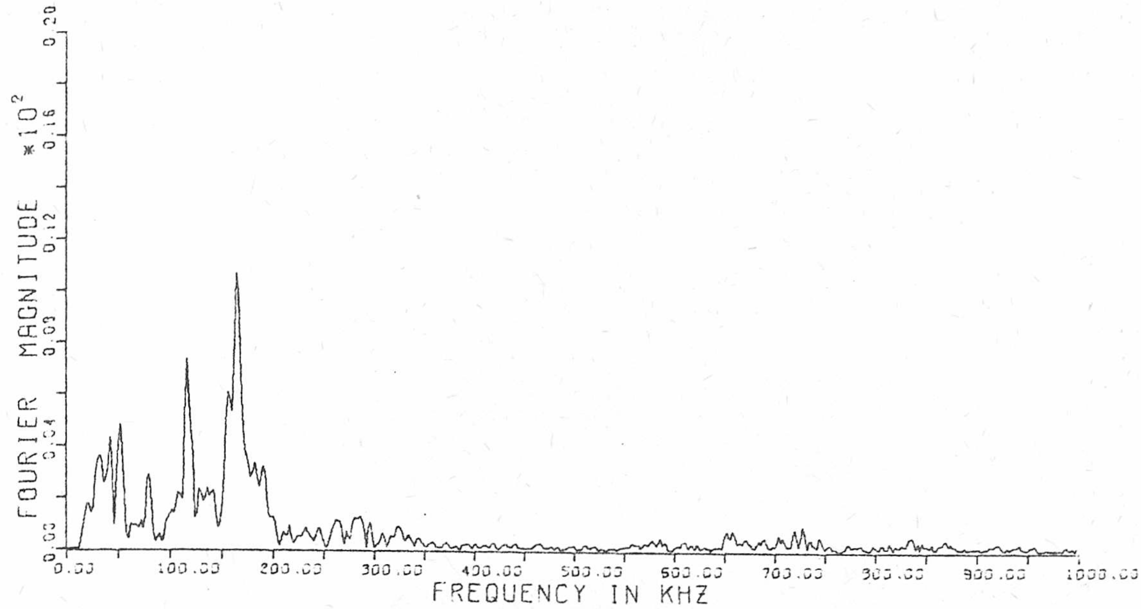

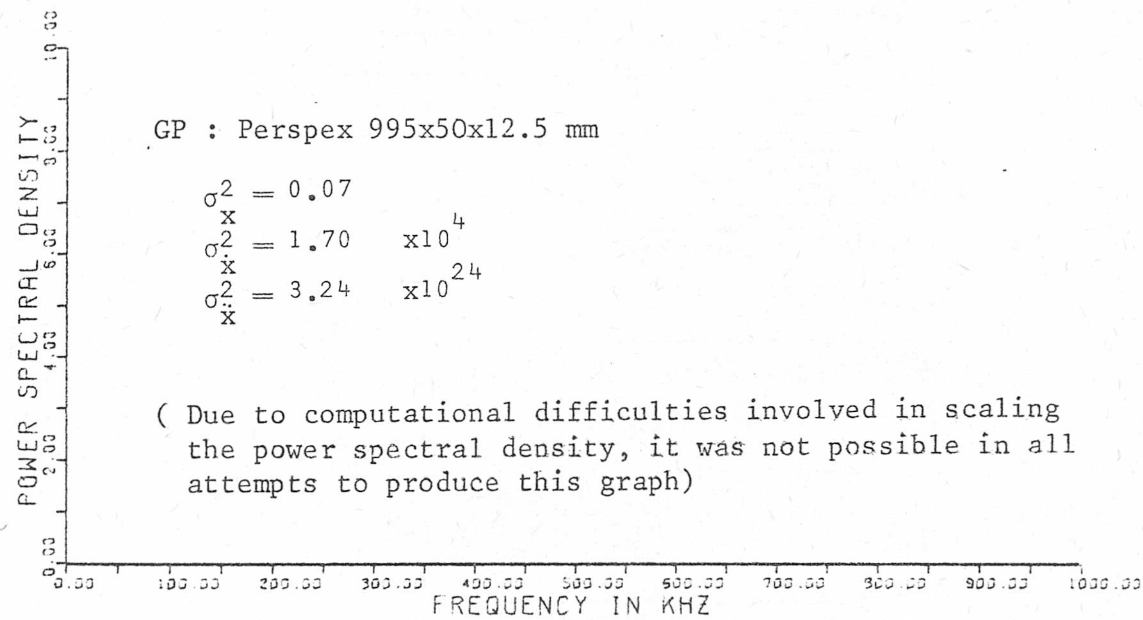

GP : Perspex 995x50x12.5 mm

$\sigma_x^2 = 0.07$

$\sigma_{\dot{x}}^2 = 1.70 \quad x10^4$

$\sigma_{\ddot{x}}^2 = 3.24 \quad x10^{24}$

(Due to computational difficulties involved in scaling the power spectral density, it was not possible in all attempts to produce this graph)

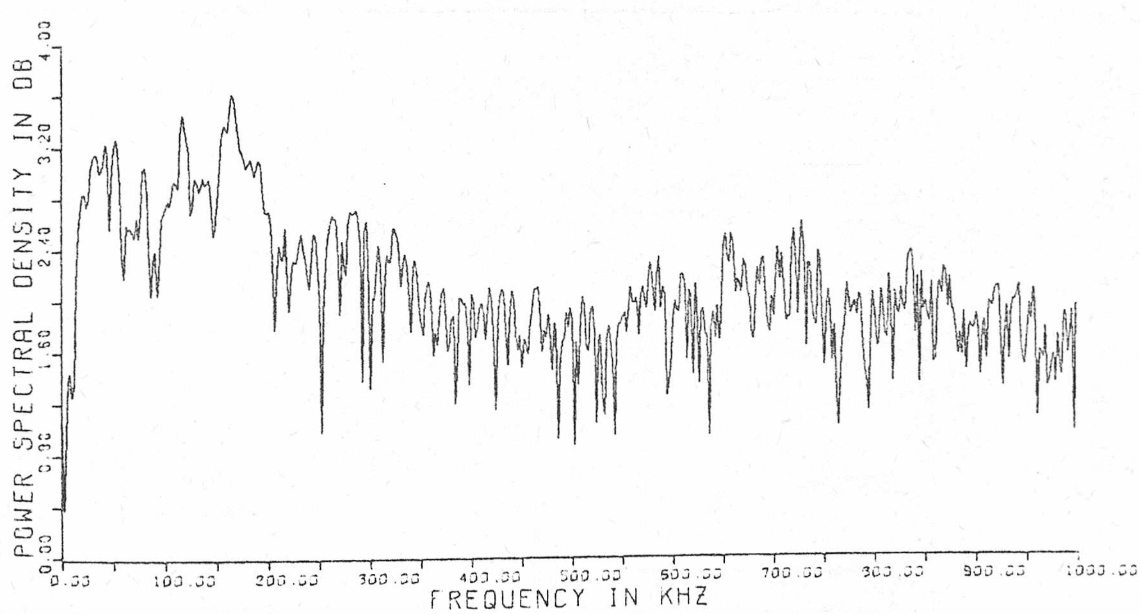

(i) Frequency Response of GP.

FIGURE 6.8 : Cont.

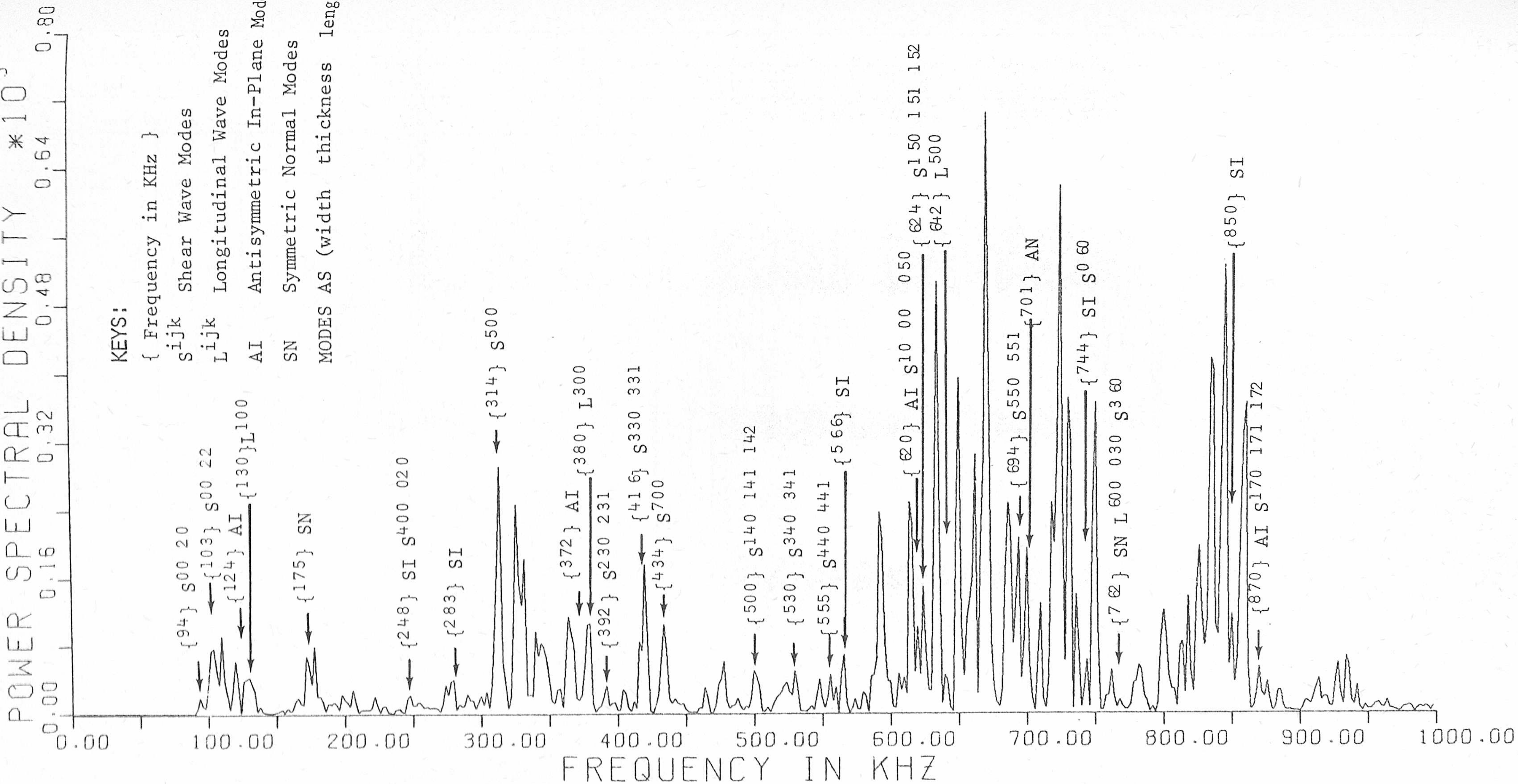

FIGURE 6.9 (a): Locations of the Calculated Resonance Modes on the Power Spectral Density of the Aluminium Specimen.

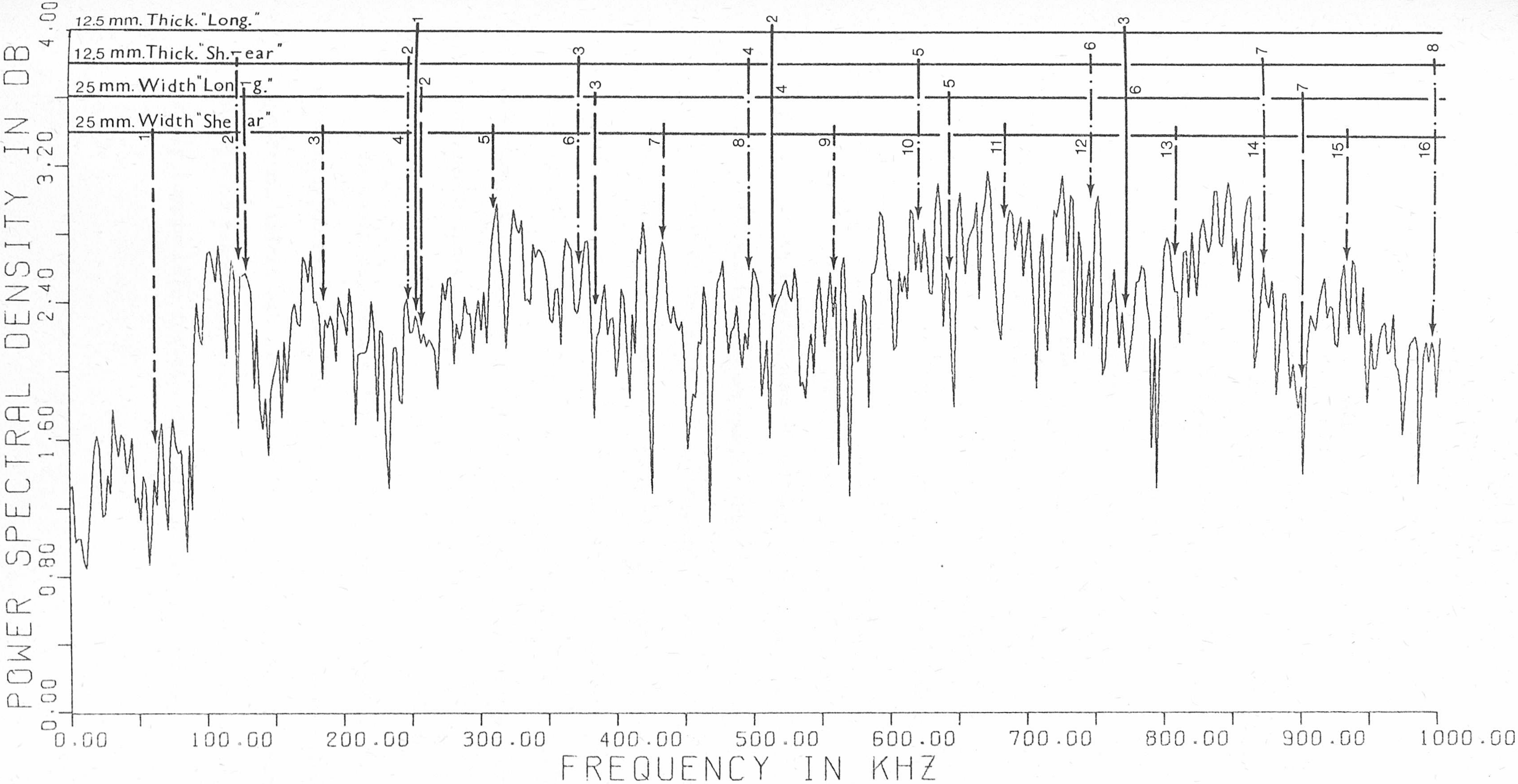

FIGURE 6.9 (b): Locations of the Calculated Principal Modes of the Aluminium Specimen on the Logarithmic Power Spectral Density.

It is found, in general, that when the spectrum frequency is nearly equal to the frequency of a normal mode (longitudinal, shear or Lamb) the magnitude of the power spectrum rises or falls sharply, i.e.: both the peak and valley structures identify the normal modes. The spectrum valleys (non-peaks) are best observed in the logarithmic scale of the decibel plot, Fig. 6.9(b). The principal valleys occur mainly around the longitudinal thickness modes. Notice that the power spectral shown in Fig. 6.9(b) is approximately divided into four regions. There appear to be principal valleys at the specimen longitudinal thickness modes. There is also good evidence of the presence of harmonics, sharp valleys up to the eighth for the specimen thickness shear modes. However, in the same spectra (as well as in others) some peaks were also found to depart somewhat from the calculated resonances. The reasons for this are not certain, especially with the good resolution used. But possibly the effects of the specimen-couplant (PVC)-Shoe-PZT element resonances and the interference with the sided peaks around the strongest resonances account for it. It might also be the effect of frequency dependent attenuation during the propagation of different modes within the specimen volume.

In addition, it was difficult to assign all the calculated resonance modes (Equations (1.14) and (5.10)) to the specimen spectrum, and it was also hard to establish which of the many calculated resonances occurring at the same frequency was the one really responsible for the existence of peak or valley.

To date, the properties of the complex peaks distribution in the frequency spectrum have not been studied in any depth. The results illustrated in this section indicate that the properties of these complex peaks are complicated and suggest that a study of their properties may be attempted in future by using statistical and probability approaches.

6.4 PARAMETERS RELATIONSHIPS AND INTERPRETATION

The conditions under which the statistical model can be applied, which have been considered in Chapter Two, allow the derivation of some mathematical expressions for the relation between the emission burst parameters both in the time and the frequency domains. Consideration of the current experimental results, although limited in specimens used, demonstrates that the burst data set can be of normal distribution. In such case, the derived parameters relationships may now be confidently tested with the experimental data.

6.4.1 LEVEL-COUNTINGS VERSUS ENERGY AND BURST DURATION

It was derived in Section 2.5 that:

$$\Sigma N_\ell = f_o \; e^{-V_\ell^2/2\bar{E}}$$

which relates the burst total number of counts at various trigger level V_ℓ, the burst central frequency f_o and the burst total energy $\bar{E}$ (per unit time). If one first takes the natural logarithm of each side of this expression and substitutes n_o^+ (the number of zero-crossings) for f_o, the above equation becomes:-

$$\ln \Sigma n_\ell = \ln n_o^+ - \frac{TV_\ell^2}{2E_T} \qquad (6.1)$$

where E_T is now the total energy of emission burst with duration T. Expression (6.1) suggests straight line fit between $\ln \Sigma n_\ell$ and V_ℓ^2 for the same burst.

The experimental data of the trigger-level counts Σn_ℓ (in log scale) are plotted against V_ℓ^2 in Fig. 6.10 for different specimens. Notice that, for the GP specimen in Fig. 6.7(a) there is no discernable change in the trigger-level range used in Fig. 6.10. In view of a separate scale being required to represent this particular specimen it was decided not to include the results from this specimen in the rest of this chapter.

As it may be seen in Fig. 6.10, a very good straight line fit is achieved for each specimen. Also shown in the figure the slope and the standard deviation of the least squares fit. The intersection of each straight line with Σn-axis would determine the number of zero-crossings n_o^+. However, the results concerning this parameter will be discussed in the next section. According to Eq. (6.1) each line slope should define the corresponding burst total energy. To demonstrate this, if one takes the first derivative of Eq.(6.1) with respect to V_ℓ^2, i.e.:

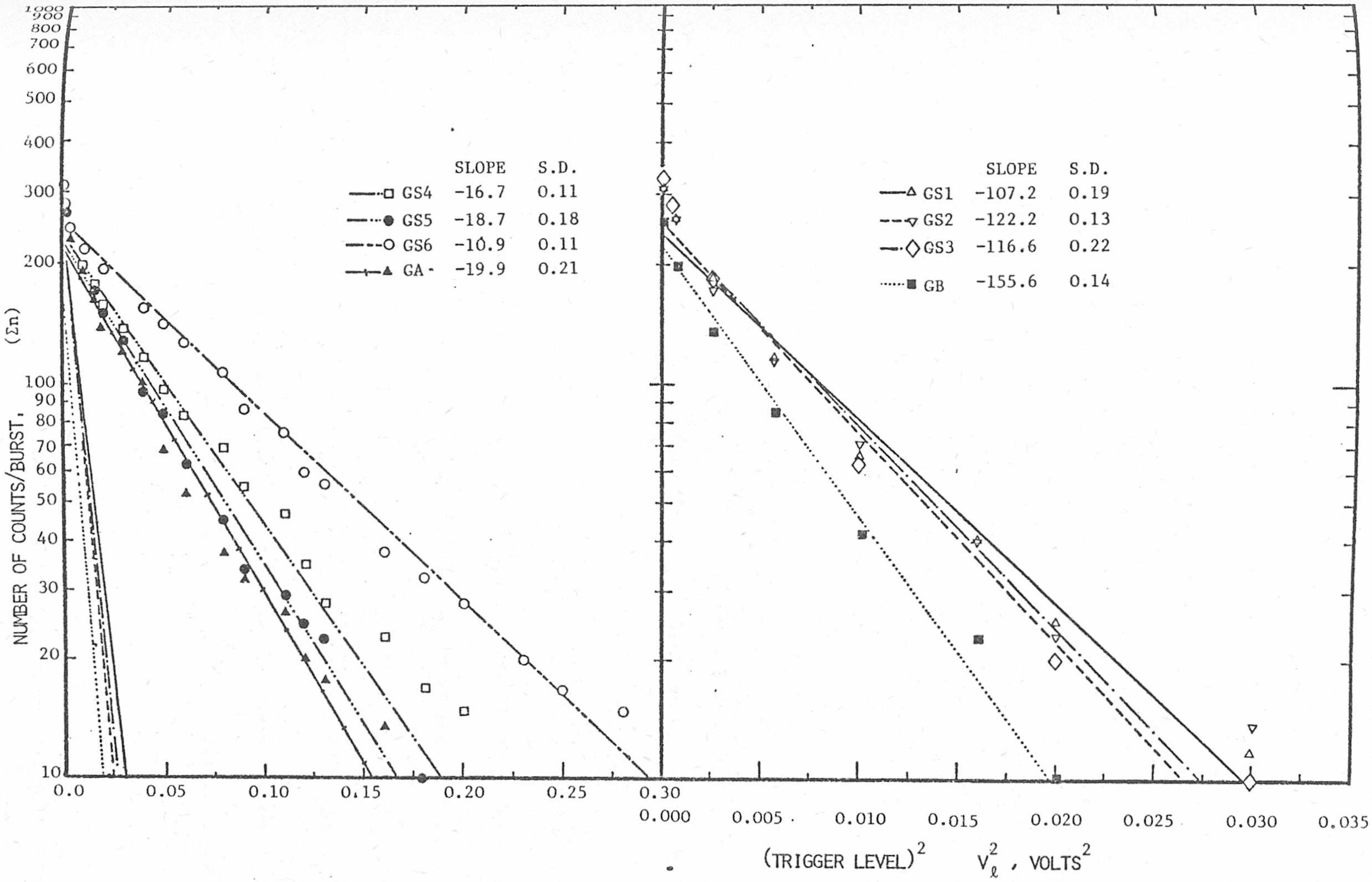

FIGURE 6.10 : Total Number of Counts/Burst (Σn) versus Trigger-Level Square V_ℓ^2 for Simulated Acoustic Emission Source in Plates. (the Least Squares Fit Method was used; S.D is the Standard Deviation).

$$d(\ln \Sigma n_\ell)/dV_\ell^2 = -\frac{T}{2E_T} \qquad (6.2)$$

The adequacy of the functional relationship between $d(\ln \Sigma n_\ell)/d V_\ell^2$ and $\frac{1}{E_T}$ expressed in Equation (6.2) can be judged from Fig. 6.11. The calculated total energy in Table 6.II is plotted versus the corresponding slope from Fig. 6.10. Despite the variation in specimen geometries and materials, an excellent straightline fit is achieved. The slope of the straight line should define the burst duration time T (the analysed portion) or vice versa, i.e.:

$$\text{The slope} = -\frac{T}{2} = -\frac{0.0005}{2} = -2.5 \times 10^{-4} \text{ sec.}$$

which compares favourably to the least squares value (-2.77×10^{-4} sec.).

Now, clearly one can see that the burst total energy, burst duration time and the trigger-level counts are very well connected parameters. Once it is possible to measure two of these parameters, the third one can be calculated. Furthermore, if the burst energy and its duration time are given, the value $d(\ln \Sigma n)/dV_\ell^2$ can be calculated. Then, by knowing only a single trigger-level number of counts, a complete level-counts distribution, similar to those in Figs. 6.7(a-d) can be drawn.

To date, in acoustic emission technology, the measurements made by different researchers in various laboratories are hard to compare quantitatively. This is due to the use of different measurement

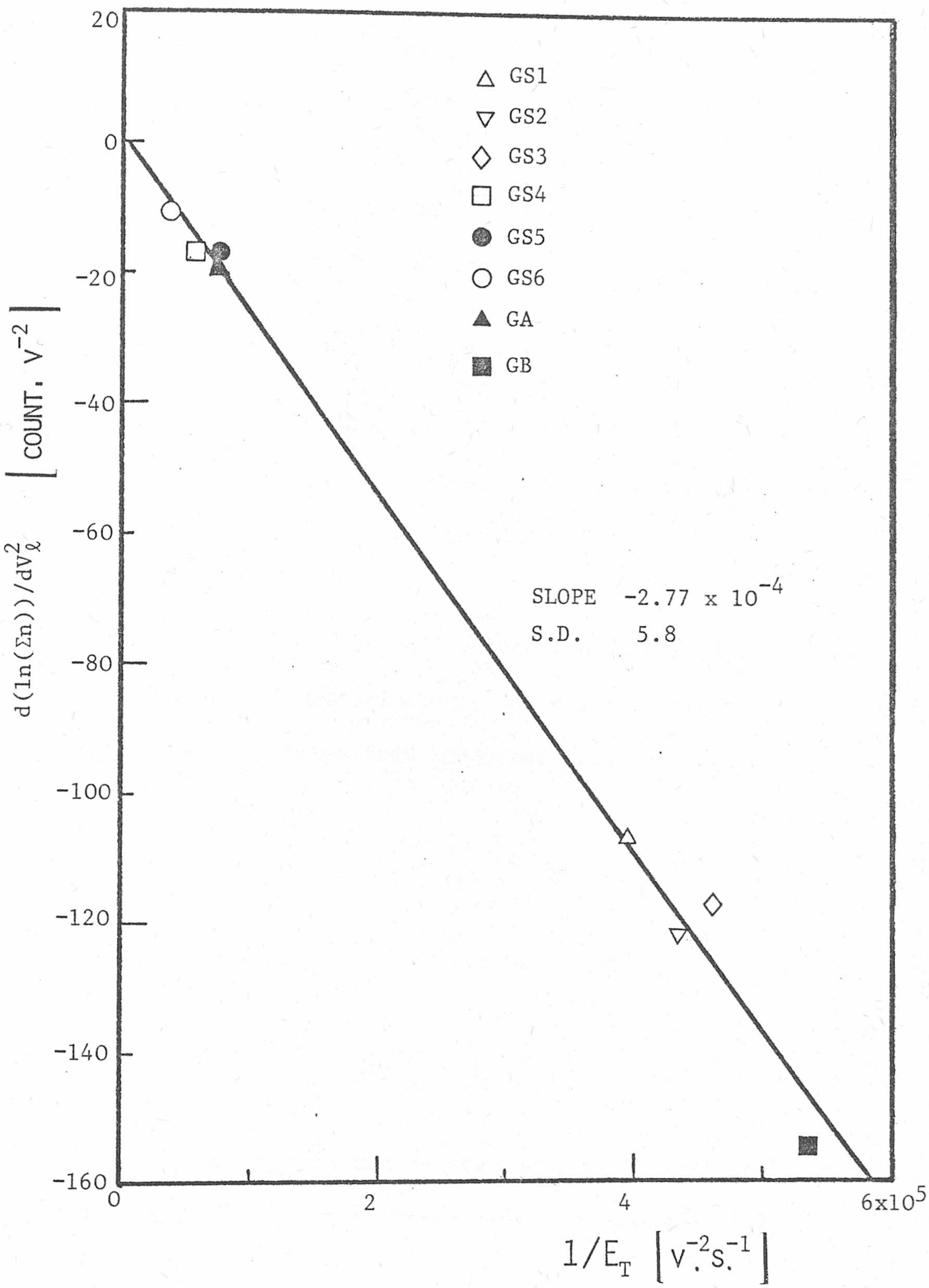

FIGURE 6.11 : The Variation between $d(\ln(\Sigma n))/dV_{\ell}^{2}$ and $1/E_T$.

parameters, equipment and even different settings to measure a similar quantity (e.g. different threshold levels to measure the emission count rate). With the aid of the above mentioned extracting technique it is hoped that one can make an easy interpolation to correlate different published results for useful comparison.

6.4.2 EXTRACTING THE BURST NUMBER OF MAXIMA AND THE NUMBER OF ZERO-CROSSINGS FROM THE BURST FREQUENCY DOMAIN

It was shown in Section 2.5 that the number of positive zero-crossings per unit time, n_o^+, for a narrow frequency band brust can be calculated from the burst frequency domain as:

$$n_o^+ = \frac{1}{2\pi} \frac{\sigma_{\dot{x}}}{\sigma_x}$$

and the burst number of maxima per unit time as:

$$n_{max} = \frac{1}{2\pi} \frac{\sigma_{\ddot{x}}}{\sigma_{\dot{x}}}$$

where σ_x, $\sigma_{\dot{x}}$ and $\sigma_{\ddot{x}}$ are the square roots of the zeroth, second and fourth moments of the burst frequency (Equations (2.33)-(2.35)).

The three frequency moments are calculated from each specimen spectrum and tabulated in Table 6.IV. The table also compares the number of zero-crossings calculated from different time domain

Table 6.IV: Summary of the Frequency Moments and a Comparison between the Number of Maximum Peaks and the Number of Zero-crossings Calculated from the Burst Frequency and Time Domains.

Specimen Code	Frequency Moments			Number of Zero-Crossings Calculated or Measured from: (COUNTS/BURST)							Number of Maxima (COUNTS/BURST)		
	Zeroth σ_x^2 Volts.Hz.S	Second $\sigma_{\dot{x}}^2$ Volts.Hz^3.S (10^{13})	Fourth $\sigma_{\ddot{x}}^2$ Volts.Hz^5.S (10^{26})	Time Domain (COUNT)	Frequency Domain $\frac{1}{2\pi}\frac{\sigma_{\dot{x}}}{\sigma_x}$	% Deviation	Frequency Domain $\frac{2}{3\pi}\frac{\sigma_{\dot{x}}}{\sigma_x}$	% Deviation	Eq.(6.1) & Fig.(6.10)	% Deviation	Time Domain (PEAK)	frequency domain $\frac{1}{2\pi}\frac{\sigma_{\ddot{x}}}{\sigma_{\dot{x}}}$	% Deviation
GS1	1.90	1.50	2.37	302	224	-26	294	-3	240	-21	320	316	-1
GS2	1.97	1.55	2.40	305	223	-27	297	-3	258	-15	311	318	-2
GS3	1.90	1.89	3.23	327	256	-22	334	+2	255	-22	333	328	-1
GS4	5.76	4.16	6.37	277	214	-23	285	-6	234	-16	318	311	-2
GS5	4.84	3.72	5.82	302	221	-27	294	-4	235	-22	315	315	0
GS6	6.47	5.27	8.37	309	227	-27	303	-2	251	-19	326	317	-3
GA	5.22	4.53	8.14	309	234	-24	312	+1	225	-27	322	337	+5
GB	2.08	1.51	2.49	256	214	-16	285	+11	221	-14	296	323	+9
GP	0.07	1.70 $\times10^{-2}$	3.24 $\times10^{-2}$	160	121	-24	165	+3	n.a.	n.a.	240	347	+44

representations and the burst number of maxima with those calculated from the burst frequency domain using the above relationships.

It is of interest to observe the good correlation between the number of maxima calculated from the frequency moments and those measured from Fig. 6.5 (using PEAK). The deviation is less than ±5% with the exception of the specimen GB(+9%) and GP (+44%). Again, these large deviations for the brass and perspex specimen can be explained by observing the corresponding frequency spectra in Figs. 6.8(h) and (i) and by comparing their narrow-band measure α in Figs. 6.5 (h) and (i).

On the other hand, the number of zero-crossings which have been calculated from the frequency moments show lower values than the corresponding time domain (about -25% deviation). Similar deviations are also shown for the values obtained from Eq. (6.1) and Fig. 6.10) in the previous section. These discrepancies can be attributed to the effect of the electronic noise near to the zero-trigger-level in the time domain measurements. The computer program COUNT does not in fact account for this problem. The sudden increase in the number of counts near to the zero voltage in both Figs. 6.7 and 6.10 may explain this point. Also, the small deviation between n_o^+ from the frequency domain and Fig. 6.10 (about ±5% deviation) confirms this explanation.

However, the exact number of zero-crossings, similar to the time domain measurements, including the effect of the system noise are found to follow the empirical relation:

$$n_o^+ = \frac{2}{3\pi} \frac{\sigma_{\dot{x}}}{\sigma_x} \tag{6.3}$$

Results from Expression (6.3) are also presented in Table 6.IV for comparison (±6% deviation). No analytical support can be made for this approximation.

Keeping in mind the narrow-band burst approximation made in developing the theoretical relationships, one should not be surprised to find discrepancies between theory and experiment in this relationship alone.

6.4.3 EMISSION ENERGY AND MAXIMUM PEAK-TO-PEAK AMPLITUDE

In this section, variations between the burst time energy E_T, the energy calculated from the burst spectrum E_f and the burst maximum peak-to-peak amplitude are investigated. At this moment, a dimensional point deserves some mention. First, in calculating the quantity E_T, the expression

$$E_T = \Delta t \sum_{i=1}^{N} x_i^2 (t) \quad \text{Volts}^2 \text{ sec.}$$

was used as shown in Chapter Two. The dimensional unit of this quantity is not actually an energy unit. This approximation, or more precisely individual normalization, has been made in order to avoid the use of dimensionless parameters which would mask the analysis. Second, in calculating the quantity E_f from the frequency spectrum zeroth moment the following expression will be used:

$$E_f = T\,\sigma_x^{\,2} = T \int X\,(f)\;df \qquad \text{volts. sec.}$$

where T is the burst duration time and X (f) is the Fourier magnitude of x(t). The dimension of E_f is different from E_T and is also not an energy unit. Therefore, one should add the term 'measure' to follow 'energy' whenever the parameter energy appears throughout this study.

Figure 6.12(a) represents a plot of E_T versus E_f in linear scale. The major feature of this plot is a distinct well fit quadratic relationship between E_f and E_T given by:

$$E_T = 0.09 \times 10^{-5} - 0.0019\;E_f + 2.795\;E_f^2$$

with standard deviation of 0.139×10^{-5}.

For this reason the burst maximum peak-to-peak amplitude is plotted versus $\sqrt{E_T}$ and directly versus E_f in Figs. 6.12(b) and (c) respectively. Both of the plots verify the general belief that the acoustic emission amplitude is proportional to the burst total energy.

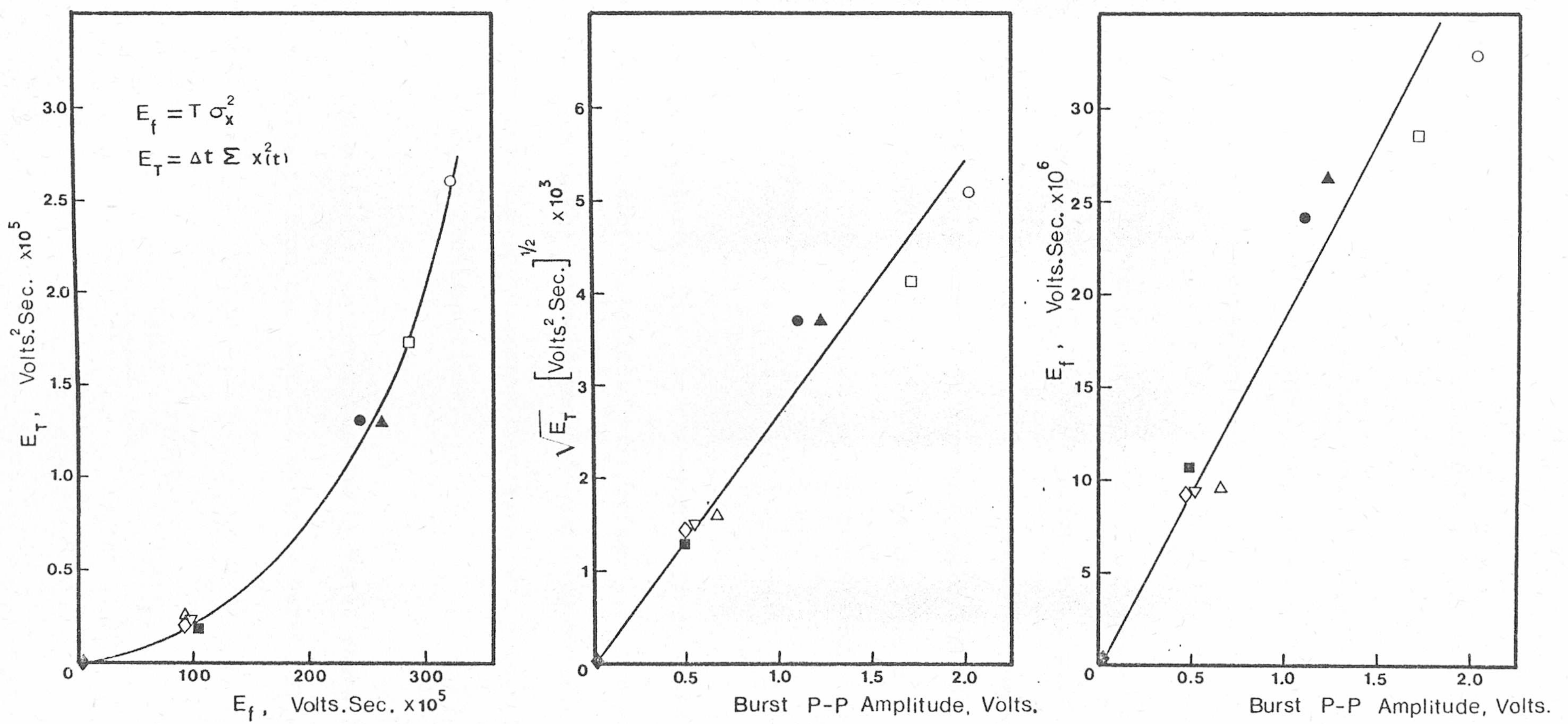

(a) Burst Total Energy E_T, versus Spectrum Total Energy E_f

(b) Burst Total Energy E_T, versus P-P Maximum Amplitude.

(c) Spectrum Total Energy E_f, versus P-P Maximum Amplitude.

FIGURE 6.12 : Variations between Emission Energies and Peak-to-Peak Maximum Amplitude for Different Specimen Geometries.
GS1: △ , GS2: ▽ ,GS3: ◇ ,GS4: □ ,GS5: ● ,GS6: ○ ,GA: ▲ ,
GB: ■ and GP: ◆ .

6.5 THE DEPENDENCE OF THE BURST ENERGY ON THE SPECIMEN VOLUME

Unfortunately, the theoretical investigation carried out in Chapter Two does not provide a direct relationship between the burst total energy and the specimen volume.

An early study by James and Carpenter (172) was carried out on tensile tests of a 7075-T651 aluminium alloy with a wide range of sample size. Although there was a large amount of scatter in the results, the authors claimed that the integrated RMS voltage is directly proportional to the square root of the sample volume. An attempt to apply this assumption to our results has led to remarkable disagreement.

Egle (173) reported that the theory of diffuse sound can be used to predict the effects of specimen size and energy absorption rate in the detected acoustic emission burst. The author shows that the approximated theory was valid only for particular specimen configurations.

The diffuse theory, as interpretated by Egle, shows that the energy released from the acoustic emission burst, E_T, can be estimated as:

$$E_T = \frac{CKS_TS_o}{4V} e^{-bT/V} \qquad (6.4)$$

where: C = the wave velocity,

V = the specimen volume,

T = the burst duration time,

S_o = the source energy released in a very short time,

S_T = the transducer face area,

K = a transducer constant,

b = the energy decay rate, independent of specimen volume.

In the present case K, S_T and S_o are constant since the same source and detector transducers were used in all the specimens. By taking the natural logarithm of Eq. (6.4) one gets:

$$\ln (E_T V) = \ln CA - \frac{bT}{V} \qquad (6.5)$$

For the same emission source, 'A' is constant depending on the receiving transducer characterstics.

Equation (6.5) implies that a straight line will fit between $\ln(E_T V)$ and $\frac{1}{V}$ for a particular group of specimens. The bursts of these specimens should exhibit similar decay rate 'b', close wave velocity 'C' and identical burst duration time 'T'.

Figure 6.14 represents a possible fitting group. Specimens GS1, GS2, GS3 and GB are fitted to the straight line X as they have a similar energy decay rate b. Referring to Table 6.II, the energy analysis results indicate that this group of specimens has approximately equal average energy increment rate with the average

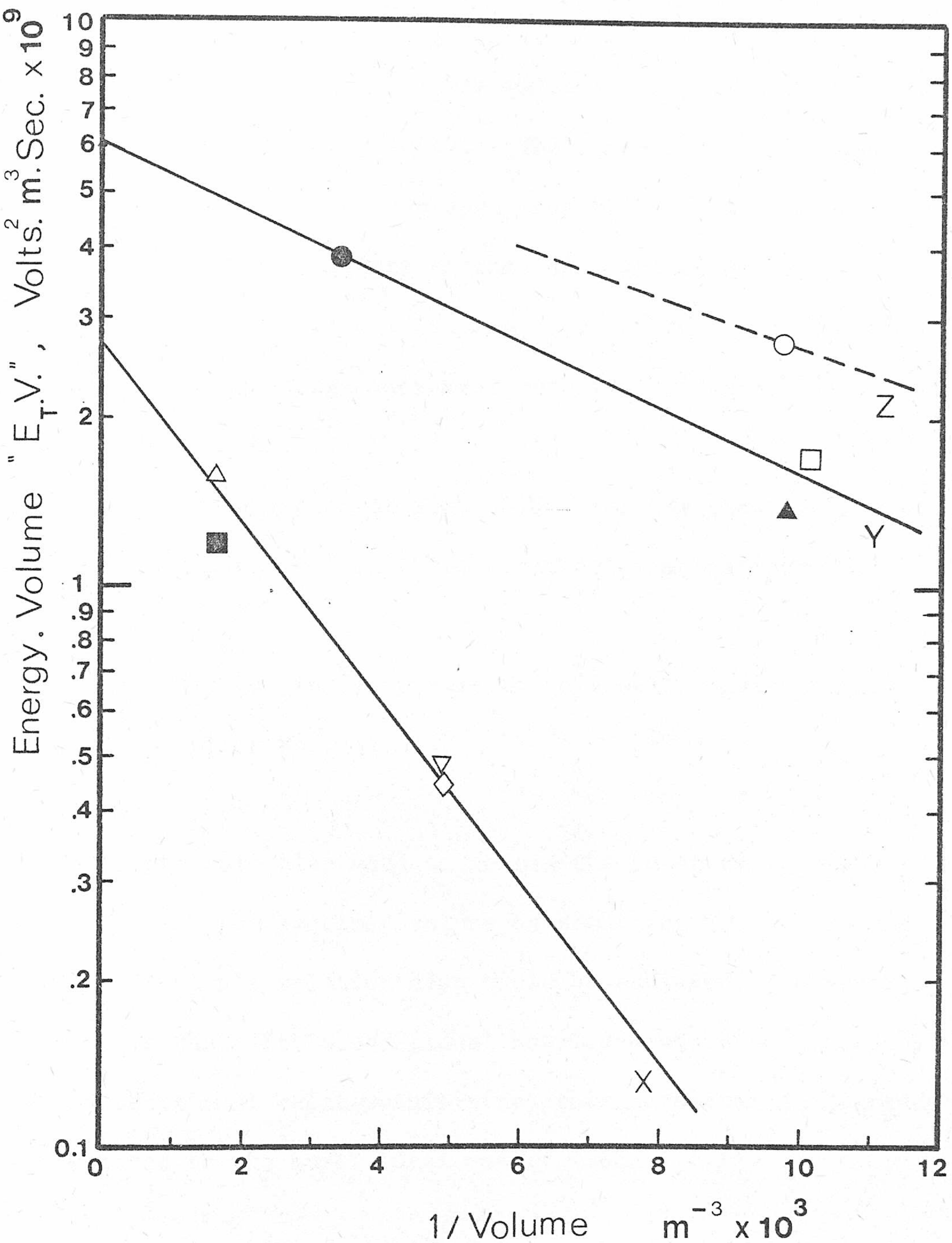

FIGURE 6.13 : The Dependence of Emission Burst Energy E_T on Specimen Volume and the Burst Energy Decay Rate According to the Diffuse Sound Theory.
GS1: △ , GS2: ▽ , GS3: ◇ , GS4: □ , GS5: ● , GS6: ○ ,
GA: ▲ , GB: ■ .

value of 0.49×10^{-5} volts^2 (this value is proportional to the actual burst energy decay rate). The corresponding average energy increment rate for the specimens GS4, GS5 and GA (average 0.33×10^{-4} volts^2) suggests another straight line fit, Y. Similarly a separate line Z is predicted for the specimen GS6 for which the average energy increment rate is 0.564×10^{-4} volts^2.

Careful observation of Fig. 6.10 shows how these groups of specimens are separated in three identical combinations.

In summary Eq. (6.5) appears to hold well considering the assumptions made in Ref. (173).

Attempts were also made to relate the burst trigger-level counts Σn_ℓ and the specimen volume by combining Eqs. (6.5) and (6.1). No simple relationships could be achieved. However, it was felt that little additional knowledge would be gained by such an additional relationship since this parameter has already been related to the burst total energy (Sec. 6.4.1).

6.6 CONCLUSIONS

The study presented in this chapter has attempted to provide additional insight into the characteristics of the acoustic emission burst. The analysis was limited to the plate specimens and ultrasonic simulated acoustic emission source. The results examined were limited to the first 0.5 ms portion of each burst. A final limitation is the small number of specimens used.

On the positive side, all burst parameters that were presented were obtained using a general statistical analysis based on an arbitrary burst function. The bursts upon which these estimated and related parameters were based, were statistically tested for normality and stationarity to ensure their statistical validity. Consequently, the results obtained were more confidently interpreted as being representative of the statistical analysis being sought (Chapter Two).

Of broader interest, this chapter also serves to demonstrate the potential of the data processing technique and the theoretical bases for examining the underlying parameters and their relationships.

As far as specific results are concerned the following conclusions can be made:

1. Emission burst statistical parameters, maximum peak-to-peak amplitude, trigger-level counts, maxima and minima distributions, energy parameters and frequency spectra were obtained and presented for different specimen geometries.

2. The results of the distribution tests indicated that the burst waveforms were of normal distribution. This finding is most consequential to someone concerned with acoustic emission signal analysis and processing.

3. Almost all the bursts failed the reverse arrangement test for stationarity, while visual inspection of the burst waveform shows no serious change on periodic fluctuation in the burst mean level. Because most theoretical burst analysis and models assume that the burst is stationary which makes the mathematics easy, another test program is under investigation.

4. Differences in the burst waveform and frequency parameters are observed for different specimen geometries. Both the size and material of the tested specimen influence the burst pattern considerably.

5. It was found that for a surface emission source, the transducer output waveform is characterized by a sudden rise in the amplitude at the arrival time of the surface wave. This observation could be useful in source location techniques.

6. It was found from the peaks density analysis that the acoustic emission burst is a relatively narrow-band random signal such that the probability density distribution of peaks resembles a Rayleigh distribution.

7. Both the emission total energy and the behaviour of the average energy increment rate are sensitive to both the material and dimension of the specimen. The change in the burst energy increment rate can provide a sensitive means to locate surface emission sources.

8. For the same transducer characteristics and emission source, one obtains emission bursts having significantly different frequency characteristics for different specimen geometries. The resonance peaks on the frequency spectra failed to satisfy all the specimens different resonance modes. The requirement, then, is for further studies to determine the conditions giving rise to particular mode peaks as well as to determine the conditions of modes producing valleys.

9. Experimentally determined parameters relationships from the ultrasonic simulated acoustic emission source show good agreement with the derived relations. It proved possible to relate accurately between the burst trigger-level counts, the number of positive zero-crossings, the burst duration time, peak-to-peak amplitude and the bursts total energy in time and frequency domains.

10. Applying the diffuse sound theory shows that there is no systematic variation of the burst total energy with the specimen volume. This is due to the dependence of the derived relation on the burst energy decay rate of each specimen.

However, it would have been informative to test the statistical model and the derived relationships with other simulated and real acoustic emission sources. This has been left to a later study which should also be extended to complex and compact tension specimens.

The presentation of the burst energy increment demonstrates that it will be possible to fit the acoustic emission bursts to analytical function. Such function will depend on the specimen dimension, material, emission source and transducer characteristics.

PART FIVE

APPENDICES AND REFERENCES

APPENDIX : 2.A

Computer Program Listing

Main Program: STATM.FOR

```
C: A TESTING PROGRAMME FOR NONSTATIONARY TREND BY DIVIDING A SAMPLE
C: RECORD INTO TEN SLICES OF LENGTHS T1,...,T10 ESTIMATING
C: MEAN SQUARE VALUES FOR EACH SLICE AND COUNTING THE NUMBER OF
C: "REVERSE ARRANGEMENTS" OF THESE VALUES.
      DIMENSION A(1025),V(15),ST(150)
      INTEGER POINTS,FREK,OPCORE
      COMMON INDAT
      DATA (ST(I),I=1,5)/.0,.0,.0,.0,.0/
      DATA (ST(I),I=6,45)/.001,.002,.005,.008,.014,.023,.036,
-     1  .054,.078,.108,.146,.190,.242,.300,.364,.431,.5,.569,
-     2  .636,.700,.758,.810,.854,.892,.922,.946,.964,.977,
-     3  .986,.992,.995,.998,.999,.999,.999,.999,.999,.999,
-     4  .999,1.000/
      POINTS=512
      INDAT=20
      TYPE 11
 11   FORMAT(  ' ENTER OUTPUT DEVICE :'$)
      READ(5,12)IPRINT
      IF(IPRINT.EQ.3)CALL CODE
 12   FORMAT(I)

 13   CALL SCALE(POINTS,OPCORE,FREK,NPTS,TEE,V,DELTA,0)
      CALL REABA(A,V,NPTS,255.0,0)
      CALL LEVA(A,NPTS,0,0)

      M=1
      IS=0
      L1=1
      L2=100
      STOT=0.0
 14   SMEN=0.0
      DO 15 I=L1,L2
 15   SMEN=SMEN+A(I)*A(I)
      SMEN=SMEN/100.0
      V(M)=SMEN
      STOT=STOT+SMEN
      WRITE(IPRINT,16)L1,L2,SMEN
 16   FORMAT(  ' FROM',1X,I3,1X,'TO',1X,I4,2X,E20.10)
```

```
      M=M+1
      IF(L2.GT.950)  GO TO 17
      L1=L1+100
      L2=L2+100
      GO TO 14
17    STOT=STOT/10.0
      L1=1
      L2=1000
      WRITE(IPRINT,18)L1,L2,STOT
18    FORMAT(  ' FROM',1X,I3,1X,'TO',1X,I4,2X,E20.10)

      M=1
20    IF(V(M).GE.V(2)) IS=IS+1
30    IF(V(M).GE.V(3)) IS=IS+1
40    IF(V(M).GE.V(4)) IS=IS+1
50    IF(V(M).GE.V(5)) IS=IS+1
60    IF(V(M).GE.V(6)) IS=IS+1
70    IF(V(M).GE.V(7)) IS=IS+1
80    IF(V(M).GE.V(8)) IS=IS+1
90    IF(V(M).GE.V(9)) IS=IS+1
100   IF(V(M).GE.V(10)) IS=IS+1
      M=M+1
      GO TO (110,30,40,50,60,70,80,90,100,110),M

110   WRITE(IPRINT,120)IS
120   FORMAT(  ' THE MAXIMUM POSSIBLE NUMBER OF REVERSE
     1 ARRANGEMENT IS:',I2)
      DEGREE=ST(IS)*100.0
      WRITE(IPRINT,130)DEGREE
130   FORMAT(  ' THE SIGNAL IS (',F6.2,'%) STATIONARY')
      TYPE 140
140   FORMAT( ' ANOTHER RUN ? :'$)
      READ(5,12)ICON
      IF(ICON.EQ.0) STOP
      INDAT=INDAT+1
      GO TO 13
      STOP
      END
$
```

APPENDIX : 2.B

Computer Program Listing

1. Main Program : TIMPLT.FOR

```
C: TIMPLT IS A PROGRAM TO PLOT AN ACOUSTIC EMMISION SIGNAL IN
C: THE TIME DOMIAN.
C::
C::           WRITTEN BY:
C::                              SAMIR EL-DARDIRY
C::                              SCHOOL OF PHYSICS
C::                                   R.G.I.T.
C::                                     1977

      DIMENSION T(1024),A(1024)
      INTEGER FREK,POINTS,OPCORE
      COMMON INDAT

      POINTS=512
      INDAT=20
      CALL PLTS 41
      CALL STARTP(IPRINT,ITEK,FACT)
      CALL SCALE(POINTS,OPCORE,FREK,NPTS,TEE,V,DELTA,0)

      TYPE 1
1     FORMAT( ' ENTER NO. OF POINTS TO BE PLOTTED:'$)
      READ(5,2)FREK
2     FORMAT(G)
      IF(FREK.EQ.0)FREK=1000

      CALL READA(A,V,NPTS,255.0,0)
      CALL TIME(T,DELTA,NPTS)
      CALL LEVA(A,NPTS,0,0)
      CALL GRAPH(A,T,V,FREK)
      CALL WAIT 41
      CALL PLTF 41

      IF(IPRINT.EQ.0)STOP
      LINE=FREK/4
      WRITE(IPRINT,6)
      DO 5 I =1 ,LINE
      LINE2=LINE+I
      LINE3=2*LINE+I
      LINE4=3*LINE+I
```

```
        WRITE(IPRINT,4)I,T(I),A(I),
-       1                     LINE2,T(LINE2),A(LINE2),
-       2                     LINE3,T(LINE3),A(LINE3),
-       3                     LINE4,T(LINE4),A(LINE4)
   4    FORMAT(1H ,4(I6,2X,E10.4,2X,F8.3,3X))

   5    CONTINUE
   6    FORMAT(1H1,9X,'TIME(SEC)',2X,'AMP.(VOLTS)',9X,
-       1'TIME(SEC)',2X,'AMP.(VOLTS)',9X,
-       2'TIME(SEC)',2X,'AMP.(VOLTS)',9X,
-       3'TIME(SEC)',2X,'AMP.(VOLTS)')
        STOP
        END
$
```

2. Subroutine : TIME

```
C: SUBROUTINE TIME GENERATES A VECTOR T WHICH CONTAINS
C:  NM POINTS.

C: THE FIRST DATA POINT IS ZERO .
C: THE INCREMENT USED IS DELTA.

        SUBROUTINE TIME(T,DELTA,NM)
        DIMENSION T(NM)
        T(1)=0.0
        DO 1 N=2,NM
        T(N)=T(N-1)+DELTA
  1     CONTINUE

        RETURN
        END
$
```

3. Subroutine : GRAPH

```
      SUBROUTINE GRAPH(A,T,V,NPT)
      DIMENSION A(NPT),T(NPT),I(10)
      CALL PLOT41(0.0,4.0,-3)

C:: SCALE X & Y AXIS.
C::::::::::::::::::::::
      AX=20.0
      AY=10.0
      DO 1 N=1,NPT
  1   T(N)=T(N)*1000.0
      TMX=0.0
      DT=T(NPT)/AX
      DA=V/AY
      XO=0.0
      AMX=-5.0*DA
      YO=-AMX/ABS(DA)
C::::::::::::::::::::::
      I(1)=4HTIME
      I(2)=4H IN
      I(3)=4HMILL
      I(4)=4HISEC
      I(5)=4HONDS
      CALL AXIS 41(0.0,0.0,I,-20,AX,0.0,TMX,DT)

      I(1)=4HPULS
      I(2)=4HE AM
      I(3)=4HPLIT
      I(4)=4HUDE
      I(5)=4HIN V
      I(6)=4HOLTS
      CALL AXIS 41(XO,0.0,I,24,AY,90.0,AMX,DA)

      CALL LINE 41(T,TMX,DT,A,AMX,DA,NPT,1,0,0)
      CALL PLOT 41(XO,YO,3)
      CALL PLOT 41(AX,YO,2)

      RETURN
      END
 $
```

Computer Program Listing

1. Main Program : COUNT.FOR

```
      DIMENSION A(1024),TRIG(110),COUNT(110)
      INTEGER POINTS,FREK,OPCORE
      COMMON INDAT

      POINTS=512
      INDAT=6
      CALL PLTS41
      CALL STARTP(IPRINT,ITEK,FACT)
      TYPE 1
1     FORMAT(   ' TYPE THE NUMBER OF EXP. TO BE CONSIDERED:'$)
      READ(5,3)NEX
      INTEQ=0

      TYPE 2
 2    FORMAT( ' CHANGE SCALE THROUGHOUT THE RUN <VOLT ; TIME>:'$)
      READ (5,3) SCAL
3     FORMAT(G)
      L=1
4     CONTINUE
      INDAT=INDAT+1

      IF(L.GT.NEX)GO TO 9
      IF(L.EQ.1)GO TO 5
      IF(SCAL.NE.1)GO TO 6

5     CALL SCALE(POINTS,OPCORE,FREK,NPTS,TEE,V,DELTA,0)
6     CALL READA(A,V,NPTS,255.0,0)
      CALL LEVA(A,NPTS,0,0)
      CALL CNT(A,DELTA,TRIG,COUNT,IPRINT,LIMIT)
      IF(L.GT.1)GO TO 7
      CALL CNTP(TRIG,COUNT,XII,DXX,YII,DYY)
      L=L+1
      GO TO 4

7     CONTINUE
8     CALL LINE 41(TRIG,XII,DXX,COUNT,YII,DYY,LIMIT,1,5,INTEQ)
      INTEQ=INTEQ+1
      L=L+1
      GOTO 4

9     CONTINUE
      CALL WAIT41
      CALL PLTF 41
      STOP
      END
$
```

2. Subroutine : CNT

```
      SUBROUTINE CNT(A,DELTA,TRIG,COUNT,IPRINT,LIMIT)
      DIMENSION A(1024),TRIG(110),COUNT(110)
      AMIN=0.0
      AMAX=0.0
      DO 1 I=1,1024
      IF(A(I).LT.AMIN)AMIN=A(I)
      IF(A(I).GT.AMAX)AMAX=A(I)
  1   CONTINUE

      AMPLT=AMAX-AMIN
      IF(IPRINT.NE.0)WRITE(IPRINT,2)AMPLT
  2   FORMAT(1H1,6X,'MAXIMUM PULSE AMPLITUDE =',F8.6,6X,'VOLTS
 -    1'//1H ,6X,'NUMBER OF COUNTS',24X,'TRIGGER LEVEL',6X,'LEVEL
 -    1 NUMBER')

      K=1
      X=AMPLT/2.0
      IF(X.GT.1.0)GO  TO  3
      X=X*10.0
      NOT=IFIX(X)+1
      X=FLOAT(NOT)/10.0
      GO  TO   4

 3    X=X+1.00
      NOT=IFIX(X)
      X=FLOAT(NOT)
 4    CONTINUE

      CENT=X/50.
      TRIG(K)=X
 5    COUNT(K)=0.0
      DO  6  I=2,1023
      IF(A(I-1).LT.TRIG(K).AND.A(I).GE.TRIG(K)) COUNT(K)
 -    1   =COUNT(K)+1.0
  6   CONTINUE

      IF(IPRINT.NE.0)WRITE(IPRINT,7)COUNT(K),TRIG(K),K
  7   FORMAT(1H ,E20.6,16X,F20.5,10X,I3)
      K=K+1
      TRIG(K)=TRIG(K-1)-CENT
      IF (TRIG(K).LT.0.0)  GO  TO  8
      GO  TO 5
```

```
  8     CONTINUE
  9     COUNT(K)=0.0
        DO 10  I=2,1023
        IF(A(I-1).GT.TRIG(K).AND.A(I).LE.TRIG(K))COUNT(K)=COUNT(
-       1                                        K)+1.0
 10     CONTINUE

        IF(IPRINT.NE.0)WRITE(IPRINT,7)COUNT(K),TRIG(K),K
        K=K+1
        TRIG(K)=TRIG(K-1)-CENT
        IF(K.GT.100) GO TO 11
        GO TO 9

 11     LIMIT=K-1
        RETURN
        END
$
```

3. Subroutine : CNTP

```
        SUBROUTINE CNTP(TRIG,COUNT,XII,DXX,YII,DYY)
        DIMENSION TRIG(110), COUNT(110), I(10)
        J=100
        CALL PLOT 41(0.0,4.0,-1)
        AX=20.0
        AY=10.0

        CALL SCAL 41(TRIG,AX,J,1,XII,DXX)
        CALL SCAL 41(COUNT,AY,J,1,YII,DYY)
        YII=0.0

        XO= -XII/ABS(DXX)

        I(1)= 4HTRIG
        I(2)= 4HGER
        I(3)= 4HLEVE
        I(4)= 4HL CV
        I(5)= 4HOLTS
        I(6)= 1H]
        CALL AXIS 41(0.0,YO,I,-21,AX,0.0,XII,DXX)

        I(1)= 4HCOUN
        I(2)= 2HTS
        CALL AXIS 41(XO,0.0,I,6,AY,90.0,YII,DYY)

        CALL LINE 41(TRIG,XII,DXX,COUNT,YII,DYY,J,1,0,0)

        RETURN
        END
$
```

Computer Program Listing

1. Main Program : PEAK.FOR

```
      DIMENSION T(1024),A(1024),AMX(400),AMN(400),TMX(400),TMN(400)
      DIMENSION  DEN (800)
      DIMENSION  LVL(900),DISTN(900)
      INTEGER FREK,POINTS,OPCORE
      REAL LVL, LVLM,LVLP
      COMMON INDAT,DISTP(500),LVLP(500)
      COMMON AY,AIM,DA,AX,YO

      INDAT =6
      POINTS=512

      CALL PLTS 41
      CALL STARTP(IPRINT,ITEK,FACT)
      CALL SCALE(POINTS,OPCORE,FREK,NPTS,TEE,V,DELTA,0)
      CALL READA(A,V,NPTS,255.0,0)
      CALL TIME(T,DELTA,NPTS)
      CALL LEVA(A,NPTS,0,0)
      CALL FACT 41(0.8)

      TYPE 17
      READ(5,18)FREK
      IF(FREK.EQ.0)FREK=1000

      N=0
      L=2
1     IF((A(L)-A(L-1)).GT.0.0.AND.(A(L)-A(L+1)).GT.0.0)GOTO2
      L=L+1

      IF(L.GT.FREK)  GO TO 3
      GOTO 1
2     N=N+1

      AMX(N)=A(L)
      TMX(N)=T(L)
      L=L+1
      IF(L.GT.FREK) GO TO 3
      GO TO 1

3     M=0
      L=2
4     IF((A(L)-A(L-1)).LT.0.0.AND.(A(L)-A(L+1)).LT.0.0)GOTO5
      L=L+1
      IF(L.GT.FREK) GO TO 6
      GO TO 4
5     M=M+1
      AMN(M)=A(L)
      TMN(M)=T(L)
```

```
      L=L+1
      IF(L.GT.FREK)   GO TO 6
      GO TO 4

 6    CONTINUE
      TEP=(FREK-1)*DELTA
      IF(IPRINT.EQ.0)GO TO 20
      WRITE(IPRINT,7)
 7    FORMAT(1H1,' CALCULATION OF MAXIMA'//1H ,6X,'AMPLITUDE(V
     -10LTS)',5X,'TIME(SECONDS)')
      WRITE(IPRINT,8)
 8    FORMAT(1H+,60X,' CALCULATION OF MINIMA'//1H ,66X,'AMPLITUDE(V
     -10LTS)',5X,'TIME(SECONDS)')
      IF(N-M)11,13,9

 9    IM=M
      DO 10 I=N,M
      AMX(I)=0.0
      TMX(I)=0.0
 10   CONTINUE
      GO TO 14

 11   IM=N
      DO 12 I=M,N
      AMN(I)=0.0
      TMN(I)=0.0
 12   CONTINUE
      GO TO 14

 13   IM=N
 14   DO 15 I=1,IM
      WRITE(IPRINT,16)I,AMX(I),TMX(I)
      WRITE(IPRINT,19)I,AMN(I),TMN(I)
 15   CONTINUE
 16   FORMAT(1H ,I3,E16.5,4X,E16.4)
 17   FORMAT( ' ENTER NO. OF POINTS TO BE CONSIDERED:'$)
 18   FORMAT(G)
 19   FORMAT(1H+,60X,I3,E16.5,4X,E16.4)

 20   CALL PEAKP(AMX,AMN,N,M,TMX,TMN,TEP,V)

      NT=M+N
      DO 21  I =1,N
 21   DEN(I)=AMX(I)
      DO 22  J=1,M
 22   DEN(N+J)=AMN(J)

      CALL DIST(DEN,LVL,DISTN,V,IPRINT,LIMIT,NT)
      CALL PLTF 41

      STOP
      END
```

2. SUBROUTINE : DIST

```
      SUBROUTINE DIST(DEN,LVL,DISTN,V,IPRINT,LIMIT,NT)
      DIMENSION LVL(900),DISTN(900),DEN(900)
      DIMENSION INCR(10)
      COMMON DISTP(500),LVLP(500)
      COMMON AY,AIM,DA,AX,YO
      REAL LVL,LVLM,LVLP

      AMIN=0.0
      AMAX=0.0
      NTM=NT-1
      DO 1 I=1,NT
      IF(DEN(I).LT.AMIN)AMIN=DEN(I)
      IF(DEN(I).GT.AMAX)AMAX=DEN(I)
1     CONTINUE
      AMPLT=AMAX-AMIN
      IF(IPRINT.NE.0)WRITE(IPRINT,2)AMPLT
2     FORMAT(1H1,4X,'MAXIMUM PULSE AMPLITUDE =',F8.4,2X,'VOLTS'//1H )
      K=1
      X=V/2.0

      TYPE 3
3     FORMAT( ' ENTER NUMBER OF DENSITY LEVELS :'$)
      READ(5,4)NUML
4     FORMAT(G)
      CENT=V/FLOAT(NUML)
      LP=1
      LVL(K)=X
      LVLM=LVL(K)-CENT
5     DISTN(K)=0.0
      DO  6  I=1,NT
      IF(DEN(I).LT.LVL(K).AND.DEN(I).GE.LVLM)DISTN(K)=DISTN(K)+1.0
6     CONTINUE
      IF(DISTN(K).EQ.0.0)GO TO 8

      IF(IPRINT.NE.0)WRITE(IPRINT,7)DISTN(K),LVL(K),LVLM,K
      DISTP(LP)=DISTN(K)
      LVLP(LP)=(LVL(K)+LVLM)/2.0
      LP=LP+1
7     FORMAT(1H ,E20.6,16X,2F20.5,10X,I3)
8     K=K+1
      LVL(K)=LVL(K-1)-CENT
      LVLM=LVL(K)-CENT
      IF(LVL(K).LE.0.0) GO  TO  9
      GOTO 5

9     CONTINUE
10    DISTN(K)=0.0
      DO 11  I=1,NT
      IF(DEN(I).LT.LVL(K).AND.DEN(I).GE.LVLM)DISTN(K)=DISTN(
     1                          K)+1.0
11    CONTINUE
```

```
      IF(DISTN(K).EQ.0.0) GO TO 12
      IF(IPRINT.NE.0)WRITE(IPRINT,7)DISTN(K),LVL(K),LVLM,K
      DISTP(LP)=DISTN(K)
      LVLP(LP)=(LVL(K)+LVLM)/2.0
      LP=LP+1

12    K=K+1
      LVL(K)=LVL(K-1)-CENT
      LVLM=LVL(K)-CENT
      END=-X
      IF(LVLM.LT.END)GO TO 13
      IF(K.GT.1000) GO TO 13
      GO TO 10

13    LIMIT=K-1
      LP=LP-1
      SCAL=0.0
      DO 14 I=1,LP
14    IF (DISTP(I).GT.SCAL) SCAL=DISTP(I)
      DO 15 I=1,LP
15    DISTP(I)=DISTP(I)/SCAL
      IF(IPRINT.NE.0)WRITE(IPRINT,16),(DISTP(I),LVLP(I),I,I=1,LP)
16    FORMAT(3G)
      IF(IPRINT.NE.0)WRITE(IPRINT,17) SCAL
17    FORMAT(  ' SCALE (FOR PEAKS DENSITY)=',G)
      CALL PLOT 41(20.0,1.0,-3)
C     CALL AXIS 41(0.0,0.0,INCR,0,AY,90.0,AIM,DA)

      INCR(1)=4HPEAK
      INCR(2)=4HS DE
      INCR(3)=4HNSIT
      INCR(4)=1HY
      DX=10.00
      DIX=1.0/10.00
      CALL AXIS 41(0.0,0.0,INCR,-13,DX,0.0,0.0,DIX)

      CALL PLOT 41(0.0,8.0,2)
      CALL PLOT 41(0.0,4.0,-3)
      CALL PLOT 41(10.0,0.0,2)
      CALL PLOT 41(0.0,-5.0,-3)

      DA=V/10.0
      AIM=-5.0*DA
      YO=-AIM/ABS(DA)
      CALL LINE 41(DISTP,0.0,DIX,LVLP,AIM,DA,LP,1,1,3)
      RETURN
      END
$
```

3. Subroutine : PEAKP

```
SUBROUTINE PEAKP(AMX,AMN,N,M,TMX,TMN,TEE,V)          1
DIMENSION AMX(N),AMN(M),TMX(N),TMN(M),I(10)
COMMON AY,AIM,DA,AX,YO                               2
CALL PLOT41 (0.0,4.0,-3)
AX=20.0                                              3
AY=10.0
TIM=0.0
DT=TEE*1000.0/AX                                     4
DA=V/AY
XO=0.0
AIM=-5.0*DA
YO=-AIM/ABS(DA)

I(1)=4HTIME
I(2)=4H IN                                           5
I(3)=4HMILL
I(4)=4HISEC
I(5)=4HONDS                                          6
CALL AXIS41 (0.0,0.0,I,-20,AX,0.0,TIM,DT)

I(1)=4HPULS                                          7
I(2)=4HE AM
I(3)=4HPLIT
I(4)=4HUDE
I(5)=4HIN V
I(6)=4HOLTS
CALL AXIS41 (XO,0.0,I,24,AY,90.0,AIM,DA)             8
                                                     9
DT=DT/1000.0
CALL LINE41 (TMX,TIM,DT,AMX,AIM,DA,N,1,0,0)
CALL LINE41 (TMN,TIM,DT,AMN,AIM,DA,M,1,0,0)
CALL PLOT41 (XO,YO,3)
CALL PLOT41 (AX,YO,2)
RETURN
END
```

10

1. Main Program : ENERGYINC.FOR

```
DIMENSION T(1024),A(1024)
INTEGER POINTS,FREK,OPCORE,SCAL
COMMON INDAT
POINTS=512
INDAT=20

TYPE 1
FORMAT(  ' TYPE THE NUMBER OF EXPTS. TO BE CONSIDERED :'$)
READ(5,2) NEX
FORMAT(G)
TYPE 3
FORMAT( ' FITTING LINE PLOT :'$)
READ(5,2) LINE
TYPE 4
FORMAT( ' CHANGE SCALE THROUGHOUT THE RUN <VOLT ; TIME>:'$)
READ (5,2) SCAL
L=1

CALL PLTS 41
CALL STARTP(IPRINT,ITEK,FACT)
IF(L.EQ.1)GO TO 6
CONTINUE
IF (SCAL.NE.1) GO TO 9

CALL SCALE(POINTS,OPCORE,FREK,NPTS,TEE,V,DELTA,0)

TYPE 7
FORMAT( ' ENTER NO. OF POINTS TO BE PLOTTED:'$)
READ(5,1)FREK
IF(FREK.EQ.0)FREK=1000

CALL   TIME(T,DELTA,NPTS)
DO 8 I=1,NPTS
T(I)=T(I)*1000.0
CONTINUE

CALL READA(A,V,NPTS,255.0,0)
CALL LEVA(A,NPTS,0,0)
CALL ENEGR (A,T,DELTA,TEE,T11,DT,EY,DE,L,IPRINT,NPTS,LINE,FREK)

INDAT=INDAT+1
L=L+1
IF(L.GT.NEX) GO TO 10
GO TO 5
CONTINUE
CALL PLTF 41
STOP  ' PLOT FILE ::  PLOT.PLT'
END
```

2. Subroutine : ENEGR

```
      SUBROUTINE ENEGR(A,T,DELTA,TEE,T11,DT,EY,DE,L,IPRINT,NP,LINE,FRE
        DIMENSION A(NP),T(NP)
        INTEGER FREK
        NPLT=FREK/10
        DO 1 N=1,NP
        A(N)=A(N)*A(N)
    1   CONTINUE
        H=DELTA/2.0
        LNP=NP-1
        A(1)=A(1)*H
        DO 2 I=2,LNP
        A(I)=A(I-1)+(A(I)*DELTA)
C       ED=ED+A(I)
   2    CONTINUE
        A(NP)=A(LNP)+A(NP)*H
        ENERGY=A(NP)
        IF(IPRINT.NE.0)WRITE(IPRINT,3) ENERGY
    3   FORMAT(1H ///'SIGNAL ENERGY=',E30.10,'VOLT**3.SEC.'///)
        IF(IPRINT.NE.0)WRITE(IPRINT,4)
    4   FORMAT(1H1,'ENERGYCALCULATION'///1H ,2X,'I',8X,'TIME IN
   -    1 M.SECONDS',11X,'ENERGY')
        IF(IPRINT.NE.0)WRITE(IPRINT,5)(I,T(I),A(I),I=10,1020,10)
    5   FORMAT(1H ,I4,2X,2E20.10)
        IF(L.EQ.1)CALL ENEG1 (A,T,ENERGY,TEE,T11,DT,EY,DE,FREK)
        CALL  FIT(T,A,FREK,YINT ,SLOPE,IPRINT)
        IF(L.GT.1)CALL LINE 41(T,T11,DT,A,EY,DE,FREK,1,NPLT,L)
        IF(LINE.EQ.0) GO TO 6
        XINT=-(YINT/SLOPE)
        XINT=XINT/DT
        YINT=YINT/DE
        CALL PLOT 41(0.0,YINT,3)
        CALL PLOT 41(XINT,0.0,2)
    6   CONTINUE
        RETURN
        END
$
```

3. Subroutine : ENEG1

```
      SUBROUTINE ENEG1(A,T,ENERGY,TEE,T11,DT,EY,DE,NPT)
      DIMENSION  A(NPT),T(NPT),I(10)
      CALL PLOT 41(0.0,4.0,-3)
        AX=20.0
        AY=10.0
C                CALL SCAL 41(T,AX,NPT,1,T11,DT)
C     CALL SCAL 41(A,AY,NPT,1,EY,DE)
      T11=0.0
      EY=0.0

        YOO=0.0
        XOO=0.0
        DT=T(NPT)/AX
      DE=ENERGY/AY
C      XOO=-T11/ABS(DT)
C      YOO=-EY/ABS(DE)
      I(1)=4HTIME
      I(2)=4H IN
        I(3)=4HMILL
        I(4)=4HISEC
        I(5)=4HONDS
      CALL AXIS 41(0.0,YOO,I,-20,AX,0.0,T11,DT)
      I(1)=4HENER
      I(2)=4HGY [
      I(3)=4HA.U.
      I(4)=1H]
C      I(5)=4H2XSE
C      I(6)=2HC.
      CALL AXIS 41(XOO,0.0,I,13,AY,90.0,EY,DE)
      CALL LINE 41(T,T11,DT,A,EY,DE,NPT,1,0,0)
      RETURN
      END
$
```

APPENDIX : 2.F

Computer Program Listing

1. Main Program : ENERGYDEC.FOR

```
      DIMENSION T(1024),A(1024)
      INTEGER POINTS,FREK,OPCORE
      COMMON INDAT
      POINTS=512
      TYPE 1
1     FORMAT(  ' TYPE THE NUMBER OF EXPTS. TO BE CONSIDERED :'$)
      INDAT=20
      READ(5,3) NEX
      TYPE 2
2     FORMAT( ' FITTING LINE PLOT :'$)
      READ(5,3) LINE
      L=1
      CALL PLTS 41
      CALL STARTP(IPRINT,ITEK,FACT)
3     FORMAT(I)
4     CONTINUE
      IF(L.GT.NEX) GO TO 6
      CALL SCALE(POINTS,OPCORE,FREK,NPTS,TEE,V,DELTA,0)
      CALL READA(A,V,NPTS,255.0,0)
      CALL   TIME(T,DELTA,NPTS)
      DO 5 I=1,NPTS
5     T(I)=T(I)*1000.0
      CALL LEVA(A,NPTS,0,0)
      CALL ENERGY (A,T,DELTA,TEE,T11,DT,EY,DE,L,IPRINT,NPTS,LINE)
      INDAT=INDAT+1
      L=L+1
      GO TO 4
6     CONTINUE
      CALL PLTF 41
      STOP  ' PLOT FILE ::  PLOT.PLT'
      END
$
```

2. Subroutine : ENERGY

```
      SUBROUTINE ENERGY (A,T,DELTA,TEE,T11,DT,EY,DE,L,IPRINT,NP,LINE)
      DIMENSION A(NP),T(NP)
      E=0.0
      NPLT=NP/10
      Q=A(1)
      DO 1 N=1,NP
      A(N)=A(N)*A(N)
  1   CONTINUE
      H=DELTA/2.0
      LNP=NP-1
      DO 2 N=1,LNP
      E=E+(A(N)+A(N+1))*H
  2   CONTINUE
      ENERGY=E
      IF(IPRINT.NE.0)WRITE(IPRINT,3) ENERGY
  3   FORMAT(1H ///'SIGNAL ENERGY=',E20.10,'VOLT**2.SEC.'///)
      IF(IPRINT.NE.0)WRITE(IPRINT,4)
  4   FORMAT(1H1,'ENERGY DECREMENT CALCULATION'///1H ,2X,'I',8X,'TIME
IN
-     1 M.SECONDS',11X,'ENERGY')
      A(1)=ENERGY
      EQ=A(2)
      A(2)=A(1)-H*(A(2)+Q)
      DO  5 I=3,NP .
      EM=EQ+A(I)
      A(I)=A(I-1)-H*(A(I)+EQ)
      EQ=EM-EQ
  5   CONTINUE.
      IF(IPRINT.NE.0)WRITE(IPRINT,6)(I,T(I),A(I),I=10,1020,10)
  6   FORMAT(1H ,I4,2X,2E20.10)
      IF(L.EQ.1)CALL ENEG1 (A,T,ENERGY,TEE,T11,DT,EY,DE,NP)
      CALL  FIT(T,A,NP,YINT ,SLOPE,IPRINT)
      IF(L.GT.1)CALL LINE 41(T,T11,DT,A,EY,DE,NP,1,NPLT,L)
      IF(LINE.EQ.0) GO TO 7
      XINT=-(YINT/SLOPE)
      XINT=XINT/DT
      YINT=YINT/DE
      CALL PLOT 41(0.0,YINT,3)
      CALL PLOT 41(XINT,0.0,2)
  7   CONTINUE
      RETURN
      END
$
```

3. Subroutine : FIT

```
      SUBROUTINE FIT (T,A,N,YINT,SLOPE,IPRINT)
      DIMENSION A(N),T(N)
C *A PROGRAMME TO CALCULATE LEAST SQUARS FIT FOR A STRAIGHT LINE  THROUG
C*
C * A SERIES OF POINTS AND TO CALCULATE THE SLOPE  INTERCEPT AND STANDAR
D *
C *DEVIATION.
C **
C *****SET INITIAL VALUES TO ZERO                                       *
***
      SLOPE=0.0
      YINT=0.0
      CORR=0.0
      SDEV=0.0
      SUMX=0.0
      SUMY=0.0
      SUMX2=0.0
      SUMY2=0.0
      SUMXY=0.0
C *****CALCULATE SUMS                                                   *
**
      DO 1 I=1,N
      SUMX=SUMX+T(I)
      SUMY=SUMY+A(I)
      SUMX2=SUMX2+T(I)**2
      SUMY2=SUMY2+A(I)**2
      SUMXY=SUMXY+A(I)*T(I)
    1 CONTINUE
      DEN=SUMX**2-N*SUMX2
      IF(DEN.NE.0.0) GO TO 3
      IF(IPRINT.NE.0)WRITE(IPRINT,2)
    2 FORMAT(1H ,'THE X COORDINATES ARE ALL THE SAME-EFFECTIVE SLOPE =IN
     1FINSTY')
      STOP
C *****CALCULATE SLOPE , INTERCEPT AND CORRELATION COEFFICIENT          *
**
    3 SLOPE=(SUMX*SUMY-N*SUMXY)/DEN
      YINT=(SUMX2*SUMY-SUMX*SUMXY)/(-DEN)
      DENOM=N*SUMY2-SUMY**2
      IF(DENOM.NE.0.0) GO TO 4
      CORR=1.0
      GO TO 5
    4 CORR=(N*SUMXY-SUMX*SUMY)/SQRT(ABS(-DEN*DENOM))
C *****CALCULATE SUM OF ERRORS AND STANDARD DEVIATION                   *
```

```
**
    5 SUMERR=0.0
      DO 6 I=1,N
      ERR=A(I)-YINT-SLOPE*T(I)
      SUMERR=SUMERR+ERR**2
    6 CONTINUE
      SDEV=SQRT(SUMERR/(N-1))
      IF(IPRINT.NE.0)WRITE(IPRINT,8)SLOPE
    8 FORMAT(1H ,'SLOPE=',E20.10)
      IF(IPRINT.NE.0)WRITE(IPRINT,9)YINT
    9 FORMAT(1H ,'INTERCEPT ON Y AXIS=',E20.10)
      IF(IPRINT.NE.0)WRITE(IPRINT,10) CORR
      IF(IPRINT.NE.0)WRITE(IPRINT,11) SDEV
   10 FORMAT(1H ,'CORRELATION= ',F10.6)
   11 FORMAT(1H ,'STANDARD DEVIATION= ',F10.6)
      RETURN
      END
$
```

APPENDIX : 2.G

Computer Program Listing

1. Main Program : SPECT.FOR

```
      DIMENSION A(513) , B(513)
      DIMENSION C(513) , F(513)
      COMMON INDAT
      EQUIVALENCE (A(1),C(1)),(B(1),F(1))
      INTEGER POINTS,FREK,OPCORE
      INDAT=20
      POINTS=512

      CALL PLTS 41
      CALL STARTP(IPRINT,ITEK,FACT)
      CALL SCALE(POINTS,OPCORE,FREK,NPTS,TEE,V,DELTA,IPRINT)

      TYPE 1
1     FORMAT( ' ENTER NO. OF POINTS TO BE PLOTTED:'$)
      READ(5,8)FREK
      IF(FREK.EQ.0)FREK=500

      CALL READAB(A,B,V,POINTS,255.0,0)
      CALL LEVAB(A,B,POINTS,IPRINT,0)

      CALL HANNG(A,B,POINTS,DELTA,TEE)
      CALL FFT(A,B,POINTS,POINTS,POINTS,1)
      CALL REALTR(A,B,POINTS,1)

      IF(IPRINT.NE.0)WRITE(IPRINT,2   )
2     FORMAT(1H ,20X,'A(N)',26X,'B(N)',18X,'C(N)',17X,'N',15X,'F

      DO 3 N=1,OPCORE
      CVAL=SQRT(A(N)*A(N)+B(N)*B(N))
      A(N)=A(N)/(2.0*FLOAT(POINTS))
      B(N)=B(N)/(2.0*FLOAT(POINTS))
      IF(IPRINT.NE.0)WRITE(IPRINT,4)A(N),B(N),N
      C(N)=CVAL/(2.0*FLOAT(POINTS))
      F(N)=(FLOAT(N-1))/TEE
      IF(IPRINT.NE.0)WRITE(IPRINT,5)C(N),F(N)
3     CONTINUE
4     FORMAT(1H ,10X,F20.16,10X,F20.16,10X,I5)
5     FORMAT(1H+,80X,F16.14,5X,F16.4)
```

```
      DELF=F(2)
      CALL MOMENT(C,F,DELF,FREK,IPRINT,1)

      DO 6 I=1,OPCORE
 6    F(I)=F(I)/1000.0
      DELF=DELF/1000.0

      CALL DRAWD1(C,F,DELF,FREK)

      DO 7 N=1,OPCORE
 7    C(N)=C(N)*C(N)
      CALL WAIT 41

      IF(ITEK.EQ.1)CALL PLOT41(-14.0,0.0,-3)
 8    FORMAT(I)

      CALL DRWD2(C,F,DELF,FREK,ITEK)

      TYPE 9
 9    FORMAT(   ' LOG SCALE ?')
      READ (5,8)LOG
      IF(LOG.EQ.0)GO TO 12

      DO 10 N=1,POINTS
      C(N)=SQRT(C(N))
10    CONTINUE
      DO 11 N=1,POINTS
      C(N)=10.0*ALOG10(C(N))
11    CONTINUE

      CALL WAIT 41
      IF(ITEK.EQ.1) CALL PLOT 41(-14.0,0.0,-3)
      CALL DRAWLG(C,F,DELF,FREK,ITEK)
12    CONTINUE
      IF (ITEK.EQ.1)CALL PLOT 41(2.,0.0,3)

      CALL PLTF 41
      STOP
      END
$
```

2. Subroutine : HANNG

```
      SUBROUTINE HANNG(A,B,IPOINT,DELT,TEE)
      DIMENSION A(IPOINT) , B(IPOINT)
      INTEGER IPOINT
      T=-DELT
      DO 50 N=1,IPOINT
      T=T+DELT
      A(N)=A(N)*ABS(0.5-(0.5*COS(2.0*3.141593*T/TEE)))
      T=T+DELT
      B(N)=B(N)*ABS(0.5-(0.5*COS(2.0*3.141593*T/TEE)))
   50 CONTINUE
      RETURN
      END
$
```

3. Subroutine : MOMENT

```
      SUBROUTINE MOMENT(C,F,DELF,FREK,IPRINT,LS)
      DIMENSION C(1000),F(1000)
      INTEGER FREK
      SM0=0.0
      SM1=0.0
      SM2=0.0
      TOTF2=0.0
      TOTF4=0.0

      DO 1  I=1,FREK
      SOMG=2.0*3.1416*F(I)/1000.0
      SOMG2=SOMG*SOMG
      TERM0=C(I)*DELF/1000.0
      FF=F(I)*F(I)/1000000.0
      TERM1=TERM0*SOMG2*FF
      TERM2=TERM1*SOMG2*FF

      SM0=SM0+TERM0
      SM1=SM1+TERM1
      SM2=SM2+TERM2
    1 CONTINUE

      IF(IPRINT.NE.0) WRITE(IPRINT,2)SM0,SM1,SM2
      IF(LS.NE.0)TYPE 2,SM0,SM1,SM2
    2 FORMAT(1H1,' THE ZEROTH MOMENT=',2X,E18.9/1H ,
 -    1' THE FIRST MOMENT=',2X,E18.9/1H ,
 -    2' THE SECOD MOMENT=',2X,E18.9)
      RETURN
      END
$
```

4. Subroutine : DRAWD1

```
      SUBROUTINE DRAWD1(C,F,DELF,IFREK)

      DIMENSION C(IFREK) , F(IFREK)
      DIMENSION ICHA(5)
C  FOURIER MAGNITUDE PLOT
C ==============================*

         CALL PLOT 41(0.0,4.0,-3)
         AX=20.0
         AY=10.0
C        CALL SCAL 41(F,AX,IFREK,1,FXMIN,DTFX)
         CALL SCAL 41(C,AY,IFREK,1,CYMIN,DTCY)
         FXMIN=0.0
         VAR=DELF*FLOAT(IFREK)
         DTFX=VAR/AX
         CYMIN=0.0
C       XO= -FXMIN/ ABS(DTFX)
C       YO= -CYMIN/ ABS(DTCY)
C        DTCY=C(1)/AY
         XO=0.0
         YO=0.0

         ICHA(1)=4HFREQ
         ICHA(2)=4HUENC
         ICHA(3)=4HY IN
         ICHA(4)=4H KHZ
         CALL AXIS 41 (0.0,YO,ICHA,-16,AX,0.0,FXMIN,DTFX)

         ICHA(1)=4HFOUR
         ICHA(2)=4HIER
         ICHA(3)=4H MAG
         ICHA(4)=4HNITU
         ICHA(5)=2HDE
         CALL AXIS 41 (XO,0.0,ICHA,18,AY,90.0,CYMIN,DTCY)

         CALL LINE 41(F,FXMIN,DTFX,C,CYMIN,DTCY,IFREK,1,0,0)
         RETURN
         END
```

5. Subroutine : DRWD2

```
      SUBROUTINE DRWD2(C,F,DELF,IFREK,ITEK)
      DIMENSION C(IFREK) , F(IFREK)
      DIMENSION ICHA(10)
C POWER SPECTRAL DENSITY PLOT
C ========================================*

      IF(ITEK.EQ.1)GO TO 10
      CALL PLOT 41(30.0,0.0,-3)
      GO TO 20
   10    CALL PLOT 41(14.0,0.0,-3)
   20 AX=20.0
      AY=10.0
C    CALL SCAL 41(F,AX,IFREK,1,FXMIN,DTFX)
      CALL SCAL 41(C,AY,IFREK,1,CYMIN,DTCY)
      FXMIN=0.0
      VAR=DELF*FLOAT(IFREK)
      DTFX=VAR/AX
      CYMIN=0.0
C     X0= -FXMIN/ ABS(DTFX)
C     Y0= -CYMIN/ ABS(DTCY)
      X0=0.0
      Y0=0.0
C     DTCY=C(1)/AY

      ICHA(1)=4HFREQ
      ICHA(2)=4HUENC
      ICHA(3)=4HY IN
      ICHA(4)=4H KHZ
      CALL AXIS 41 (0.0,Y0,ICHA,-16,AX,0.0,FXMIN,DTFX)

      ICHA(1)=4HPOWE
      ICHA(2)=4HR SP
      ICHA(3)=4HECTR
      ICHA(4)=4HAL D
      ICHA(5)=4HENSI
      ICHA(6)=2HTY
      CALL AXIS 41 (X0,0.0,ICHA,22,AY,90.0,CYMIN,DTCY)

      CALL LINE 41(F,FXMIN,DTFX,C,CYMIN,DTCY,IFREK,1,0,0)
      RETURN
      END
$
```

6. Subroutine : DRAWLG

```
      SUBROUTINE DRAWLG(C,F,DELF,IFREK,ITEK)
      DIMENSION C(IFREK) , F(IFREK)
      DIMENSION ICHA(10)
C  LOG. OF  FOURIER MAGNITUDE PLOT
C  =====================================*

      IF (ITEK.EQ.1) GO TO10
      CALL PLOT 41(30.0,0.0,-3)
      GO TO 20
 10   CALL PLOT 41(14.0,0.0,-3)
 20   AX=20.0
      AY=10.0
C    CALL SCAL 41(F,AX,IFREK,1,FXMIN,DTFX)
      CALL SCAL 41(C,AY,IFREK,1,CYMIN,DTCY)
      FXMIN=0.0
      VAR=DELF*FLOAT(IFREK)
      DTFX=VAR/AX
C     XO= -FXMIN/ ABS(DTFX)
C     YO= -CYMIN/ ABS(DTCY)
      XO=0.0
      YO=0.0
C     DTCY=C(1)/10.0

      ICHA(1)=4HFREQ
      ICHA(2)=4HUENC
      ICHA(3)=4HY IN
      ICHA(4)=4H KHZ
      CALL AXIS 41 (0.0,YO,ICHA,-16,AX,0.0,FXMIN,DTFX)

      ICHA(1)=4HPOWE
      ICHA(2)=4HR SP
      ICHA(3)=4HECTR
      ICHA(4)=4HAL D
      ICHA(5)=4HENSI
      ICHA(6)=4HTY I
      ICHA(7)=4HN DB
      CALL AXIS 41 (XO,0.0,ICHA,28,AY,90.0,CYMN,DTCY)

      CALL LINE 41(F,FXMIN,DTFX,C,CYMIN,DTCY,IFREK,1,0,0)
      RETURN
      END
```

7. Subroutine : FFT

(Ref.(138))

```
      SUBROUTINE FFT(A,B,NTOT,N,NSPAN,ISN)
      DIMENSION A(1500),B(1500)
      DIMENSION NFAC(11),NP(209)
      DIMENSION AT(10),CK(10),BT(10),SK(10)
      EQUIVALENCE (I,II)
C  THE FOLLOWING TWO CONSTANTS SHOULD AGREE WITH THE ARRAY DIMENSIONS
      MAXF=23
      MAXP=209
      IF(N.LT.2) RETURN
      INC=ISN
      RAD=8.0*ATAN(1.0)
      S72=RAD/5.0
      C72=COS(S72)
      S72=SIN(S72)
      S120=SQRT(0.75)
      IF(ISN.GE.0) GO TO 10
      S72=-S72
      S120=-S120
      RAD=-RAD
      INC=-INC
   10 NT=INC*NTOT
      KS=INC*NSPAN
      KSPAN=KS
      NN=NT-INC
      JC=KS/N
      RADF=RAD*FLOAT(JC)*0.5
      I=0
      JF=0
C DETERMINE THE FACTORS OF N
      M=0
      K=N
      GO TO 20
   15 M=M+1
      NFAC(M)=4
      K=K/16
   20 IF(K-(K/16)*16.EQ.0) GO TO 15
      J=3
      JJ=9
      GO TO 30
   25 M=M+1
      NFAC(M)=J
      K=K/JJ
   30 IF(MOD(K,JJ).EQ.0) GO TO 25
      J=J+2
```

```
      JJ=J**2
      IF(JJ.LE.K) GO TO 30
      IF(K.GT.4) GO TO 40
      KT=M
      NFAC(M+1)=K
      IF(K.NE.1)M=M+1
      GO TO 80
   40 IF(K-(K/4)*4.NE.0) GO TO 50
      M=M+1
      NFAC(M)=2
      K=K/4
   50 KT=M
      J=2
   60 IF(MOD(K,J).NE.0) GO TO 70
      M=M+1
      NFAC(M)=J
      K=K/J
   70 J=((J+1)/2)*2+1
      IF(J.LE.K) GO TO 60
   80 IF(KT.EQ.0) GO TO 100
      J=KT
   90 M=M+1
      NFAC(M)=NFAC(J)
      J=J-1
      IF(J.NE.0) GO TO 90
C   COMPUTE FOURIER TRANSFORM
  100 SD=RADF/FLOAT(KSPAN)
      CD=2.0*SIN(SD)**2
      SD=SIN(SD+SD)
      KK=1
      I=I+1
      IF(NFAC(I).NE.2) GO TO 400
C   TRANSFORM FOR FACTOR OF 2 (INCLUDING ROTATION FACTOR)
      KSPAN=KSPAN/2
      K1=KSPAN+2
  210 K2=KK+KSPAN
      AK=A(K2)
      BK=B(K2)
      A(K2)=A(KK)-AK
      B(K2)=B(KK)-BK
      A(KK)=A(KK)+AK
      B(KK)=B(KK)+BK
      KK=K2+KSPAN
      IF(KK.LE.NN) GO TO 210
      KK=KK-NN
      IF(KK.LE.JC) GO TO 210
      IF(KK.GT.KSPAN) GO TO 800
```

```
  220 C1=1.0-CD
      S1=SD
  230 K2=KK+KSPAN
      AK=A(KK)-A(K2)
      BK=B(KK)-B(K2)
      A(KK)=A(KK)+A(K2)
      B(KK)=B(KK)+B(K2)
      A(K2)=C1*AK-S1*BK
      B(K2)=S1*AK+C1*BK
      KK=K2+KSPAN
      IF(KK.LT.NT) GO TO 230
      K2=KK-NT
      C1=-C1
      KK=K1-K2
      IF(KK.GT.K2) GO TO 230
      AK=C1-(CD*C1+SD*S1)
      S1=(SD*C1-CD*S1)+S1
C THE FOLLOWING THREE STATEMENTS COMPENSATE FOR TRUNCATION ERROR. IF
C ROUNDED ARITHMETIC IS USED SUBSTITUTE
C     C1=AK
      C1=0.5/(AK**2+S1**2)+0.5
      S1=C1*S1
      C1=C1*AK
      KK=KK+JC
      IF(KK.LT.K2) GO TO 230
      K1=K1+INC+INC
      KK=(K1-KSPAN)/2+JC
      IF(KK.LE.JC+JC) GO TO 220
      GO TO 100
C TRANSFORM FOR FACTOR 3 (OPTIONAL CODE)
  320 K1=KK+KSPAN
      K2=K1+KSPAN
      AK=A(KK)
      BK=B(KK)
      AJ=A(K1)+A(K2)
      BJ=B(K1)+B(K2)
      A(KK)=AK+AJ
      B(KK)=BK+BJ
      AK=-0.5*AJ+AK
      BK=-0.5*BJ+BK
      AJ=(A(K1)-A(K2))*S120
      BJ=(B(K1)-B(K2))*S120
      A(K1)=AK-BJ
      B(K1)=BK+AJ
      A(K2)=AK+BJ
      B(K2)=BK-AJ
      KK=K2+KSPAN
      IF(KK.LT.NN) GO TO 320
      KK=KK-NN
      IF(KK.LE.KSPAN) GO TO 320
      GO TO 700
C TRANSFORM FOR FACTOR OF 4
  400 IF(NFAC(I).NE.4)GO TO 600
      KSPNN=KSPAN
      KSPAN=KSPAN/4
  410 C1=1.0
      S1=0
  420 K1=KK+KSPAN
      K2=K1+KSPAN
      K3=K2+KSPAN
      AKP=A(KK)+A(K2)
      AKM=A(KK)-A(K2)
      AJP=A(K1)+A(K3)
      AJM=A(K1)-A(K3)
      A(KK)=AKP+AJP
      AJP=AKP-AJP
      BKP=B(KK)+B(K2)
      BKM=B(KK)-B(K2)
      BJP=B(K1)+B(K3)
      BJM=B(K1)-B(K3)
      B(KK)=BKP+BJP
      BJP=BKP-BJP
      IF(ISN.LT.0) GO TO 450
      AKP=AKM-BJM
      AKM=AKM+BJM
      BKP=BKM+AJM
      BKM=BKM-AJM
      IF(S1.EQ.0.0)GO TO 460
  430 A(K1)=AKP*C1-BKP*S1
      B(K1)=AKP*S1+BKP*C1
      A(K2)=AJP*C2-BJP*S2
      B(K2)=AJP*S2+BJP*C2
      A(K3)=AKM*C3-BKM*S3
      B(K3)=AKM*S3+BKM*C3
      KK=K3+KSPAN
      IF(KK.LE.NT)GO TO 420
  440 C2=C1-(CD*C1+SD*S1)
      S1=(SD*C1-CD*S1)+S1
C   THE FOLLOWING THREE STATEMENTS COMPENSATE FOR TRUNCATION ERROR
C   IF ROUNDED ARITHMETIC IS USED,SUBSTITUTE C1=C2
      C1=0.5/(C2**2+S1**2)+0.5
```

```
      S1=C1*S1
      C1=C1*C2
      C2=C1**2-S1**2
      S2=2.0*C1*S1
      C3=C2*C1-S2*S1
      S3=C2*S1+S2*C1
      KK=KK-NT+JC
      IF(KK.LE.KSPAN) GO TO 420
      KK=KK-KSPAN+INC
      IF(KK.LE.JC) GO TO 410
      IF(KSPAN.EQ.JC) GO TO 800
      GO TO 100
  450 AKP=AKM+BJM
      AKM=AKM-BJM
      BKP=BKM-AJM
      BKM=BKM+AJM
      IF(S1.NE.0.0) GO TO 430
  460 A(K1)=AKP
      B(K1)=BKP
      A(K2)=AJP
      B(K2)=BJP
      A(K3)=AKM
      B(K3)=BKM
      KK=K3+KSPAN
      IF(KK.LE.NT) GO TO 420
      GO TO 440
C  TRANSFORM FOR FACTOR OF 5(OPTIONAL CODE)
  510 C2=C72**2-S72**2
      S2=2.0*C72*S72
  520 K1=KK+KSPAN
      K2=K1+KSPAN
      K3=K2+KSPAN
      K4=K3+KSPAN
      AKP=A(K1)+A(K4)
      AKM=A(K1)-A(K4)
      BKP=B(K1)+B(K4)
      BKM=B(K1)-B(K4)
      AJP=A(K2)+A(K3)
      AJM=A(K2)-A(K3)
      BJP=B(K2)+B(K3)
      BJM=B(K2)-B(K3)
      AA=A(KK)
      BB=B(KK)
      A(KK)=AA+AKP+AJP
      B(KK)=BB+BKP+BJP
      AK=AKP*C72+AJP*C2+AA
      BK=BKP*C72+BJP*C2+BB
      AJ=AKM*S72+AJM*S2
      BJ=BKM*S72+BJM*S2
      A(K1)=AK-BJ
      A(K4)=AK+BJ
      B(K1)=BK+AJ
      B(K4)=BK-AJ
      AK=AKP*C2+AJP*C72+AA
      BK=BKP*C2+BJP*C72+BB
      AJ=AKM*S2-AJM*S72
      BJ=BKM*S2-BJM*S72
      A(K2)=AK-BJ
      A(K3)=AK+BJ
      B(K2)=BK+AJ
      B(K3)=BK-AJ
      KK=K4+KSPAN
      IF(KK.LT.NN) GO TO 520
      KK=KK-NN
      IF(KK.LE.KSPAN) GO TO 520
      GO TO 700
C  TRANSFORM FOR ODD FACTORS
  600 K=NFAC(I)
      KSPNN=KSPAN
      KSPAN=KSPAN/K
      IF(K.EQ.3)GO TO 320
      IF(K.EQ.5)GO TO 510
      IF(K.EQ.JF)GO TO 640
      JF=K
      S1=RAD/FLOAT(K)
      C1=COS(S1)
      S1=SIN(S1)
      IF(JF.GT.MAXF) GO TO 998
      CK(JF)=1.0
      SK(JF)=0.0
  630 CK(J)=CK(K)*C1+SK(K)*S1
      SK(J)=CK(K)*S1-SK(K)*C1
      K=K-1
      CK(K)=CK(J)
      SK(K)=-SK(J)
      J=J+1
      IF(J.LT.K) GO TO 630
  640 K1=KK
      K2=KK+KSPNN
      AA=A(KK)
      BB=B(KK)
      AK=AA
      BK=BB
      J=1
      K1=K1+KSPAN
  650 K2=K2-KSPAN
      J=J+1
      AT(J)=A(K1)+A(K2)
      AK=AT(J)+AK
      BT(J)=B(K1)+B(K2)
      BK=BT(J)+BK
      J=J+1
```

```
      AT(J)=A(K1)-A(K2)
      BT(J)=B(K1)-B(K2)
      K1=K1+KSPAN
      IF(K1.LT.K2) GO TO 650
      A(KK)=AK
      B(KK)=BK
      K1=KK
      K2=KK+KSPNN
      J=1
  660 K1=K1+KSPAN
      K2=K2-KSPAN
      JJ=J
      AK=AA
      BK=BB
      AJ=0.0
      BJ=0.0
      K=1
  670 K=K+1
      AK=AT(K)*CK(JJ)+AK
      BK=BT(K)*CK(JJ)+BK
      K=K+1
      AJ=AT(K)*SK(JJ)+AJ
      BJ=BT(K)*SK(JJ)+BJ
      JJ=JJ+J
      IF(JJ.GT.JF)JJ=JJ-JF
      IF(K.LT.JF)GO TO 670
      K=JF-J
      A(K1)=AK-BJ
      B(K1)=BK+AJ
      A(K2)=AK+BJ
      B(K2)=BK-AJ
      J=J+1
      IF(J.LT.K) GO TO 660
      KK=KK+KSPNN
      IF(KK.LE.NN)GO TO 640
      KK=KK-NN
      IF(KK.LE.KSPAN) GO TO 640
C  MULTIPLY BY ROTATION FACTOR (EXCEPT FOR FACTORS 2 AND 4)
  700 IF(I.EQ.M) GO TO 800
      KK=JC+1
  710 C2=1.0-CD
      S1=SD
  720 C1=C2
      S2=S1
      KK=KK+KSPAN
  730 AK=A(KK)
      A(KK)=C2*AK-S2*B(KK)
      B(KK)=S2*AK+C2*B(KK)
      KK=KK+KSPNN
      IF(KK.LE.NT) GO TO 730
      AK=S1*S2
```

```
      S2=S1*C2+C1*S2
      C2=C1*C2-AK
      KK=KK-NT+KSPAN
      IF(KK.LE.KSPNN) GO TO 730
      C2=C1-(CD*C1+SD*S1)
      S1=S1+(SD*C1-CD*S1)
C  THE FOLLOWING THREE STATEMENTS COMPENSATE FOR TRUNCATION ERROR.IF
C  ROUNDED ARITHMETIC IS USED,THEY MAY BE DELETED
      C1=0.5/(C2**2+S1**2)+0.5
      S1=C1*S1
      C2=C1*C2
      KK=KK-KSPNN+JC
      IF(KK.LE.KSPAN) GO TO 720
      KK=KK-KSPAN+JC+INC
      IF(KK.LE.JC+JC) GO TO 710
      GO TO 100
C  PERMUTE THE RESULTS TO NORMAL ORDER---DONE IN TWO STAGES
C  PERMUTATION FOR SQUARE FACTORS OF N
  800 NP(1)=KS
      IF(KT.EQ.0) GO TO 890
      K=KT+KT+1
      IF(M.LT.K) K=K-1
      J=1
      NP(K+1)=JC
  810 NP(J+1)=NP(J)/NFAC(J)
      NP(K)=NP(K+1)*NFAC(J)
      J=J+1
      K=K-1
      IF(J.LT.K) GO TO 810
      K3=NP(K+1)
      KSPAN=NP(2)
      KK=JC+1
      K2=KSPAN+1
      J=1
      IF(N.NE.NTOT) GO TO 850
C  PERMUTATION FOR SINGLE VARIATE TRANSFORM(OPTIONAL CODE)
  820 AK=A(KK)
      A(KK)=A(K2)
      A(K2)=AK
      BK=B(KK)
      B(KK)=B(K2)
      B(K2)=BK
      KK=KK+INC
      K2=KSPAN+K2
      IF(K2.LT.KS) GO TO 820
  830 K2=K2-NP(J)
      J=J+1
      K2=NP(J+1)+K2
      IF(K2.GT.NP(J)) GO TO 830
      J=1
  840 IF(KK.LT.K2) GO TO 820
```

```
      KK=KK+INC
      K2=KSPAN+K2
      IF(K2.LT.KS) GO TO 840
      IF(KK.LT.KS) GO TO 830
      JC=K3
      GO TO 890
C  PERMUTATION FOR MULTIVARIATE TRANSFORM
  850 K=KK+JC
  860 AK=A(KK)
      A(KK)=A(K2)
      A(K2)=AK
      BK=B(KK)
      B(KK)=B(K2)
      B(K2)=BK
      KK=KK+INC
      K2=K2+INC
      IF(KK.LT.K) GO TO 860
      KK=KK+KS-JC
      K2=K2+KS-JC
      IF(KK.LT.NT) GO TO 850
      K2=K2-NT+KSPAN
      KK=KK-NT+JC
      IF(K2.LT.KS)GO TO 850
  870 K2=K2-NP(J)
      J=J+1
      K2=NP(J+1)+K2
      IF(K2.GT.NP(J)) GO TO 870
      J=1
  880 IF(KK.LT.K2) GO TO 850
      KK=KK+JC
      K2=KSPAN+K2
      IF(K2.LT.KS) GO TO 880
      IF(KK.LT.KS) GO TO 870
      JC=K3
  890 IF(2*KT+1.GE.M) RETURN
      KSPNN=NP(KT+1)
C  PERMUTATION FOR SQUARE-FREE FACTORS OF N
      J=M-KT
      NFAC(J+1)=1
  900 NFAC(J)=NFAC(J)*NFAC(J+1)
      J=J-1
      IF(J.NE.KT) GO TO 900
      KT=KT+1
      NN=NFAC(KT)-1
      IF(NN.GT.MAXP) GO TO 998
      JJ=0
      J=0
      GO TO 906
  902 JJ=JJ-K2
      K2=KK
      K=K+1
```

```
      KK=NFAC(K)
  904 JJ=KK+JJ
      IF(JJ.GE.K2) GO TO 902
      NP(J)=JJ
  906 K2=NFAC(KT)
      K=KT+1
      KK=NFAC(K)
      J=J+1
      IF(J.LE.NN) GO TO 904
C  DETERMINE THE PERMUTATION CYCLES OF LENGTH GREATER THAN 1
      J=0
      GO TO 914
  910 K=KK
      KK=NP(K)
      NP(K)=-KK
      IF(KK.NE.J) GO TO 910
      K3=KK
  914 J=J+1
      KK=NP(J)
      IF(KK.LT.0) GO TO 914
      IF(KK.NE.J) GO TO 910
      NP(J)=-J
      IF(J.NE.NN) GO TO 914
      MAXF=INC*MAXF
C  REORDER A AND B,FOLLOWING THE PERMUTATION CYCLES
      GO TO 950
  924 J=J-1
      IF(NP(J).LT.0) GO TO 924
      JJ=JC
  926 KSPAN=JJ
      IF(JJ.GT.MAXF) KSPAN=MAXF
      JJ=JJ-KSPAN
      K=NP(J)
      KK=JC*K+II+JJ
      K1=KK+KSPAN
      K2=0
  928 K2=K2+1
      AT(K2)=A(K1)
      BT(K2)=B(K1)
      K1=K1-INC
      IF(K1.NE.KK) GO TO 928
  932 K1=KK+KSPAN
      K2=K1-JC*(K+NP(K))
      K=-NP(K)
  936 A(K1)=A(K2)
      B(K1)=B(K2)
      K1=K1-INC
      K2=K2-INC
      IF(K1.NE.KK) GO TO 936
      KK=K2
      IF(K.NE.J) GO TO 932
```

```
      K1=KK+KSPAN
      K2=0
  940 K2=K2+1
      A(K1)=AT(K2)
      B(K1)=BT(K2)
      K1=K1-INC
      IF(K1.NE.KK) GO TO 940
        IF(JJ.NE.0) GO TO 926
        IF(J.NE.1) GO TO 924
  950 J=K3+1
      NT=NT-KSPNN
      II=NT-INC+1
      IF(NT.GE.0) GO TO 924
      RETURN
C  ERROR FINISH,INSUFFICIENT ARRAY STORAGE
  998 ISN=0
C     PRINT 999
      STOP
  999 FORMAT(44H0ARRAY BOUNDS EXCEEDED WITHIN SUBROUTINE FFT)
      END
```

8. Subroutine : REALTR

```
      SUBROUTINE REALTR(A,B,N,ISN)
      DIMENSION A(1500),B(1500)
      REAL IM
      INC=IABS(ISN)
      NK=N*INC+2
      NH=NK/2
      SD=2.0*ATAN(1.0)/FLOAT(N)
      CD=2.0*SIN(SD)**2
      SD=SIN(SD+SD)
      SN=0.0
      IF(ISN.LT.0) GO TO 30
      CN=1.0
      A(NK-1)=A(1)
      B(NK-1)=B(1)
   10 DO 20 J=1,NH,INC
      K=NK-J
      AA=A(J)+A(K)
      AB=A(J)-A(K)
      BA=B(J)+B(K)
      BB=B(J)-B(K)
      RE=CN*BA+SN*AB
      IM=SN*BA-CN*AB
      B(K)=IM-BB
      B(J)=IM+BB
      A(K)=AA-RE
      A(J)=AA+RE
      AA=CN-(CD*CN+SD*SN)
      SN=(SD*CN-CD*SN)+SN
C  THE FOLLOWING THREE STATEMENTS COMPENSATE FOR TRUNCATION
C  ERROR.IF ROUNDED ARITHMETIC IS USED,SUBSTITUTE
C  20 CN=AA
      CN=0.5/(AA**2+SN**2)+0.5
      SN=CN*SN
   20 CN=CN*AA
      RETURN
   30 CN=-1.0
      SD=-SD
      GO TO 10
      END
$
$
```

Computer Program Listing

1. Main Program : SPECTM.FOR

```
      DIMENSION A(513) , B(513)
      DIMENSION C(513) , F(513)
      EQUIVALENCE (A(1),C(1)),(B(1),F(1))
      INTEGER POINTS,FREK,OPCORE,SCAL
      COMMON INDAT
      POINTS=512
      INDAT=6

      CALL PLTS 41
      CALL STARTP(IPRINT,ITEK,FACT)

      TYPE 1
1     FORMAT(   ' TYPE THE NUMBER OF EXPTS. TO BE CONSIDERED:'$)
      L=1
      READ(5,13)NEX
      TYPE 2
2     FORMAT( ' CHANGE SCALE THROUGHOUT THE RUN <VOLT ; TIME>:'$)
      READ (5,13) SCAL
3     CONTINUE
      IF(L.GT.NEX)GO TO 14
      IF(L.EQ.1)GO TO 5
4     CONTINUE
      IF (SCAL.NE.1) GO TO 7

5     CALL SCALE(POINTS,OPCORE,FREK,NPTS,TEE,V,DELTA,0)

      TYPE 6
6     FORMAT( ' ENTER NO. OF POINTS TO BE PLOTTED:'$)
      READ(5,13)FREK
      IF(FREK.EQ.0)FREK=500

7     CALL READAB(A,B,V,POINTS,255.0,IPRINT)
      CALL LEVAB(A,B,POINTS,IPRINT,0)

      CALL HANNG(A,B,POINTS,DELTA,TEE)
      CALL FFT(A,B,POINTS,POINTS,POINTS,1)
      CALL REALTR(A,B,POINTS,1)

      IF(IPRINT.NE.0)WRITE(IPRINT,8)
```

```
8       FORMAT(1H ,20X,'A(N)',26X,'B(N)',18X,'C(N)',17X,'N',15X,'F')
        DO 10 N=1,OPCORE
        CVAL=SQRT(A(N)*A(N)+B(N)*B(N))
        A(N)=A(N)/(2.0*FLOAT(POINTS))
        B(N)=B(N)/(2.0*FLOAT(POINTS))
        IF(IPRINT.NE.0)WRITE(IPRINT,9)A(N),B(N),N
9       FORMAT(1H ,10X,F20.16,10X,F20.16,10X,I5)
        C(N)=CVAL/(2.0*FLOAT(POINTS))
        F(N)=(FLOAT(N-1))/(TEE*1000.0)
        IF(IPRINT.NE.0)WRITE(IPRINT,11)C(N),F(N)
10      CONTINUE
11      FORMAT(1H+,80X,F16.14,5X,F16.4)
        IF(L.EQ.1)CALL DRAWD3(C,F,TEE,FREK,F1,DF1,C1,DC1)
        IF(L.EQ.1)GO TO 12

        CALL PLOT 41(2.0,2.0,-3)
        CALL LINE 41(F,F1,DF1,C,C1,DC1,FREK,1,0,0)
        CALL PLOT 41(0.0,0.0,3)
        CALL PLOT 41(10.0,0.0,2)
        CALL PLOT 41(0.0,0.0,3)
        CALL PLOT 41(0.0,5.0,2)

12      L=L+1
        GO TO 3
13      FORMAT(G)
14      CONTINUE
        CALL PLTF 41
        STOP
        END
$
```

2. Subroutine : DRAWD3

```
      SUBROUTINE DRAWD3(C,F,TEE,IFREK,F1,DF1,C1,DC1)
      DIMENSION C(IFREK) , F(IFREK)
      DIMENSION ICHA(5)
      INTEGER IFREK
C   FOURIER MAGNITUDE PLOT ,R.HS,MASTER
         AX=10.0
         AY=5.0

      CALL PLOT 41 (0.0,3.0,-3)
      CALL SCAL 41(C,AY,IFREK,1,CYMIN,DTCY)
      FXMIN=0.0
         ISC=IFREK+1
         DTFX=F(ISC)/AX
      CYMIN=0.0
      F1=FXMIN
      DF1=DTFX
      C1=CYMIN
      DC1=DTCY
C        XO= -FXMIN/ ABS(DTFX)
C        YO= -CYMIN/ ABS(DTCY)
         YO=0.0
         XO=0.0
      ICHA(1)=4HFREQ
      ICHA(2)=4HUENC
         ICHA(3)=4HY [K
         ICHA(4)=4HHZ].
      CALL AXIS 41 (0.0,YO,ICHA,-16,AX,0.0,FXMIN,DTFX)
      ICHA(1)=4HFOUR
      ICHA(2)=4HIER
      ICHA(3)=4H MAG
      ICHA(4)=4HNITU
      ICHA(5)=2HDE
      CALL AXIS 41 (XO,0.0,ICHA,18,AY,90.0,CYMIN,DTCY)
      CALL LINE 41(F,FXMIN,DTFX,C,CYMIN,DTCY,IFREK,1,0,0)
      RETURN
      END
$
```

GENERAL NOTES ON THE COMPUTER PROGRAMS

1. All subscribts in the text are advanced by one when they appear in the programs listing, if they start with zero.

2. Subroutines ' name' 41 (var1,var2,.......)
   where 'name '- PLTS
   - PLTF
   - PLOT
   - SCAL
   - AXIS
   - LINE
   - FACT
   - WAIT

   are standard subroutine supplied with the CALCOMP package. For details see \$ CSU/GPF20/1 : Graph Plotting in FORTRAN By F.C. Drain, Computer Services Unit RGIT \$.

APPENDIX : 2.I

Computer Program Listing

1. Main Program: MSES.FOR

```
      DIMENSION A(1024),FREQ(20)
      INTEGER POINTS ,FREK,OPCORE,FREQ,SCALE
      COMMON INDAT
      INDAT=6
      POINTS=512
      ICOT=1
      CALL  PLTS 41
      CALL  STARTP(IPRINT,ITEK,FACT)
      TYPE 1
 1    FORMAT(  ' ENTER NUMBER OF EXPT. :'$)
      READ(5,2)NEX
 2    FORMAT(G)
 3    CALL SCALE(POINTS,OPCORE,FREK,NPTS,TEE,V,DELTA,0)
      CALL READA(A,V,NPTS,255.0,0)
      CALL LEVA(A,NPTS,0,0)
      CALL  HISTGM(FREQ,A,1024,20,30,1,IPRINT)
      CALL STATFQ(V,A,NPTS,IPRINT,20.0)
      ICOT=ICOT+1
      IF(ICOT.LT.NEX+1)GO TO 3
      CALL PLTF 41
      STOP
      END
$
```

2. Subroutine : HISTGM

```
      SUBROUTINE HISTGM(FREQ,A,N,M,LENG,IND,IWRITE)
      DIMENSION IOUT(28),OUT(28),A(1024),FREQ(20)
      INTEGER FREQ, SCALE
      DATA IBLANK,ISTAR,IDASH/1H ,1H*,1H-/
      DATA ETA/1.0E-38/,IWIDTH/70/
 1    FORMAT(6H EACH ,A1,8H EQUALS ,I4,7H POINTS,/)
 2    FORMAT(1H ,I8,3X,28(4X,A1))
 3    FORMAT(12H INTERVAL  ),14(F8.3,2X))
 4    FORMAT(12H MID-POINTS),5X,14(F8.3,2X))
 5    FORMAT(46H0THE PRINTED VALUES MUST BE MULTIPLIED BY
     1 10**,I3)
 6    FORMAT(12H0FREQUENCY  ,28I5)
 7    FORMAT(1H ,120A1)
      K=(IWIDTH-15)/5
      IF(M.GT.K)   M=K
```

```
      LINE=M*5+15
      LENGTH=LENG-10
      IF(LENGTH.LT.0) LENGTH=50
      FM=FLOAT(M)
      IF(IND.EQ.0)GOTO 120
      ETAM=ETA*M
      DO 20 I=1,M
   20 FREQ(I)=0
      XMIN=A(1)
      XMAX=XMIN
      DO 30 I=2,N
      DT =A(I)
      IF(DT.LT.XMIN) XMIN=DT
      IF(DT.GT.XMAX) XMAX=DT
   30 CONTINUE
      IF(XMAX-XMIN.LT.ETAM) GOTO 240
      KEY=1
      KOUNT=0
   40 R=XMAX-XMIN
      B=XMIN
   50 IF(R.GT.1.0)     GOTO 60
      KOUNT=KOUNT+1
      R=R*10.0
      GO TO 50
   60 IF(R.LT.10.0)  GOTO 70
      KOUNT=KOUNT-1
      R=R/10.0
      GOTO 60
   70 IF(KEY.GT.2)  GOTO 80
      B=B*10.**KOUNT
      IF(B.LT.0.0.AND.B.NE.AINT(B))  B=B-1.0
      B=AINT(B)/(10.**KOUNT)
      R=(XMAX-B)/FM
      KOUNT=0
      KEY=KEY+2
      GOTO 50.
   80 STEP=AINT(R)
      IF(STEP.NE.R)  STEP=STEP+1.
      IF(R.LT.1.5)  STEP=STEP-0.5
      STEP=STEP/(10.**KOUNT)
      IF(KEY.EQ.4)  GOTO 90
      RATIO=(XMAX-XMIN)/(FM*STEP)
      IF(RATIO.GT.0.8) GOTO 90
      KOUNT=1
      KEY=2
      GOTO 40
   90 XMIN=B
      C=STEP*AINT(B/STEP)
      IF(C.LT.0.0.AND.C.NE.B)C=C-STEP
      IF((C+FM*STEP).GE.XMAX)  XMIN=C
```

```
100   DO 110 I=1,N
      J=((A(I)-XMIN)/STEP)+1.0
110   FREQ(J)=FREQ(J)+1
120   WRITE(IWRITE,6)(FREQ(I),I=1,M)
      WRITE(IWRITE,7)(IDASH,I=1,LINE)
      MAX=0
      DO 130 I=1,M
      IF(FREQ(I).GT.MAX)MAX=FREQ(I)
130   CONTINUE
      SCALE=1
      DIV=1.0
      IF(MAX.LT.LENGTH)  GOTO 140
      SCALE=(MAX+LENGTH-1)/LENGTH
      WRITE(IWRITE,1) ISTAR,SCALE
      DIV=1./FLOAT(SCALE)
140   DO 150 I=1,M
150   IOUT(I)=IBLANK
      MAX=FLOAT(MAX)*DIV+0.5
      DO 170 I=1,MAX
      K=MAX+1-I
      DO 160 J=1,M
      INDEX=FLOAT(FREQ(J))*DIV+0.5
      IF(INDEX.EQ.K) IOUT(J)=ISTAR
160   L=K*SCALE
170   WRITE(IWRITE,2)L,(IOUT(J),J=1,M)
      WRITE(IWRITE,7)(IDASH,I=1,LINE)
      IF(IND.EQ.0)  GOTO 230
      K=0
      XMIN=XMIN+STEP*.5
      XMAX=XMIN+STEP*FLOAT(M-1)
      XM=AMIN1(ABS(XMIN),ABS(XMAX))
      IF(XM.LT.ETA)XM=XM+STEP
180   IF(XM.GE.0.1) GOTO 190
      K=K+1
      XM=XM*10.0
      GOTO 180
190   XM=AMAX1(XMAX,-XMIN)
200   IF(XM.LT.1000.0) GOTO 210
      K=K-1
      XM=XM/10.
      GOTO 200
210   STEP=STEP*10.**K
      OUT(1)=XMIN*10.**K
      DO 220   I=2,M
220   OUT(I)=OUT(I-1)+STEP
      WRITE(IWRITE,3)(OUT(J),J=1,M,2)
      WRITE(IWRITE,4)(OUT(J),J=2,M,2)
      K=-K
      IF(K.NE.0) WRITE(IWRITE,5) K
```

```
      GOTO 230
240   IND=2
230   CONTINUE
      RETURN
      END
$
```

3. Subroutine : STATFQ

```
      SUBROUTINE STATFQ(V,A,NPTS,IWRITE,TINC)
      DIMENSION IFREQ(100),CONST(101),A(1024)
!! GENERATE THE FREQ. INTERVAL 'CONST'.
      CONST(1)=-V/2.0
      IFREQ(1)=0.0
      ARELF=0.0
      FRESUM=0.0
      FRESQ=0.0
      ASUM=0.0
      ASQ=0.0
      X=V/TINC
      INC= INT(TINC)+1
      DO 11 I=2,INC,1
      CONST(I)=X+CONST(I-1)
      IFREQ(I)=0.0
 11   CONTINUE
      ST=1.0/X
      FN=V+1.0
      DO 100 I=1,NPTS
      ASUM=ASUM+A(I)
      ASQ=ASQ+A(I)*A(I)
      J=ST*A(I)+FN
      IFREQ(J)=IFREQ(J)+1
100   CONTINUE
      WRITE(IWRITE,10)
      DO 200 K=1,INC
      FREQ=IFREQ(K)
      RELFRE=FREQ/NPTS
      ARELF=ARELF+RELFRE
      TEMP=CONST(K)+.5*(CONST(K+1)-CONST(K))
      FRESUM=FRESUM+TEMP*FREQ
      FRESQ=FRESQ+TEMP*TEMP*FREQ
      WRITE(IWRITE,20) CONST(K),CONST(K+1),IFREQ(K),RELFRE,
-     1ARELF
200   CONTINUE
```

```
      WRITE(IWRITE,30) ASUM,ASQ
 10   FORMAT(1H1,9X,'INTERVAL' ,3X,'FREQUENCY' 3X,'RELATIVE
 -    1 FREQUENCY' ,3X,'ACCUM. RELA. FREQ.')
 20   FORMAT(1H ,3X,F7.2,1H:,F7.2,3X,I4,11X,F6.3,15X,F6.3)
 30   FORMAT(1H0,10X,'THE SUM OF THE NUMBERS IS',F10.5,2X,
 -    1'AND',4X,F10.5,2X,'IS THE SUM OF THE SQUARES')
      WRITE(IWRITE,40) FRESUM,FRESQ
 40    FORMAT(1H0,10X,'THE GROUPED SUM OF THE NUMBERS IS'
 -    1,F12.5,2X,'AND' 2X,F12.5,2X,'IS THE SUM OF THE GROUPED
 -    2 SQUARES')
      STPN=FLOAT(NPTS)
      TMEAN=ASUM/STPN
      STD=SQRT((STPN*ASQ)-(ASUM*ASUM))/STPN
      VARC=STD*STD
      WRITE(IWRITE,50)TMEAN,VARC,STD
 50   FORMAT(1H0,' THE MEAN VALUE OF THE DISTRIBUTION IS ='
 -    1,F15.10,1H //' THE SAMPLE VARIANCE IS =',F15.10,1H //
 -    2' THE STANDARD DEVIATION IS =',F15.10)

      RETURN
      END
$
```

APPENDIX 4.A

SUMMARY OF THE ELECTRONIC EQUIPMENT

1. The Bandpass Filter: (Model 3202(R)), Manufactured by The KROHNHITE Corporation of Massachusetts, U.S.A.

   Specifications:

   (i) The cutoff frequencies are continuously adjustable over the frequency range of 20 Hz to 2 MHz.

   (ii) The passband gain is unity (0 dB) with an attenuation rate of 24 dB per octave outside the passband. The maximum attenuation is greater than 80 dB.

   (iii) The maximum input signal is 3 volts (RMS) and the output noise is less than 100 μvolts (RMS) for a bandwidth of 2 MHz rising to 150 μ.volts for a detector bandwidth of 10 MHz.

2. The Transient Recorder:- (Model DL905 Datalab), Manufactured by Data Laboratories Limited, Surrey, England.
   Specifications: (See Chapter Four).

3. The Paper Tape Punch: (Model 1133 Data Dynamics), Manufactured by Data Dynamics Limited, Middlesex, England.
   The recording speed (paper tape): up to 46 characters per second.

4. The High Frequency Rectifier: (Model TM9707 Video Detector full wave rectifier) manufactured by Marconi Insts. Limited.

   Specifications:

   (i) Frequency range: 25 KHz - 30 MHz.

   (ii) Output: positive full wave.

   (iii) Flatness: within ±0.1 dB.

5. The Sweep Wave Generator: (Model 164 (30 MHz) WAVETEK), manufactured by Wavetek, San Diego, California U.S.A.

   Specifications:

   (i) Amplitude Change with frequency: less than

   0.1 dB to 300 KHz
   0.2 dB to 3 MHz
   2.5 dB to 30 MHz

(ii) Amplitude and frequency stability; ±0.25% for 24 hours.

(iii) Amplitude Symmetry: sine wave is symmetrical about ground within ±1% of amplitude range up to 3 MHz.

(iv) Purity: sine wave distortion:

10 Hz - 100 KHz less than 0.5%

0.0003 Hz - 3 MHz less than 1.0%

(v) Output: Maximum output is 20 Volts p-p into open circuit and 10 volts into 50 ohms load. Maximum overal attenuation is -80 dB.

6. The Panametric Pulser: (Model 5052 RR Ultrasonic Pulser -Receiver) manufactured by Panametric, Inc., Massachusetts, U.S.A.

Specifications:(Pulser)

(i) Pulse Amplitude: 250 volts into 50 ohms.
350 volts into 250 ohms.

(ii) Repetition Rate: Internal 200-5000 Hz.

(iii) Damping Range: 5 to 250 ohms.

(iv) Rise time: 5 ns (50 ohms damping at (1) energy setting).

(v) Pulse Width: 20-1000 ns (1/2 amplitude points) adjustable in 4 steps.

Experimental setting: Pulse width of 30 ns.
Pulse Amplitude 200 volts (max.)
rise time ≈5 ns.

7. The Pulse Generator GO 1005: (Model GO 1005 Salatron) Manufactured by Salatron Electronic Group Ltd., England.

Specifications:

(i) Pulse Amplitude: 0.7-100 volts (±3%) continuously variable.

(ii) Repetition Rate: 10 Hz;1MHz cont. variable.

(iii) Pulse Duration: 250 ns-100 ns (±5%) cont. variable.

(iv) Rise time and amplitude:

Amplitude Range (volts)	Rise Time (ns)
3	20
10	30
30	60
100	200

8. Oscilloscopes: (Model D83 Telequipment Solid State) Manufactured by Tektronix, U.K.

   Accuracy: ±1% for voltage
   20% for frequency.

9. The X-Y Chart Recoder: (Model Moseley 7035 B) manufactured by Hewlett Packard.

10. Frequency Counter: (Model 8847 Mulden) Manufactured by Mulden Electronic Limited, England.

    frequency range 0-80 MHz.
    Accuracy: ± 1 Count ±crystal stability.

Subroutine : SCALE

```
      SUBROUTINE SCALE(POINTS,OPCORE,FREK,NPTS,TEE,V,DELTA,IPRINT)
      INTEGER POINTS,FREK,OPCORE
      OPCORE=POINTS+1
      FREK=500
      NPTS=2*POINTS

      TYPE 1
1     FORMAT(  '   TYPE T.R. SWEEP TIME IN SEC. : '$)
      READ(5,3)TEE

      TYPE 2
2     FORMAT( ' TYPE T.R. INPUT VOLTAGE :'$)
      READ(5,3)V
3     FORMAT(G)

      DELTA=TEE/1000.0

      IF(IPRINT.NE.0)WRITE(IPRINT,4)POINTS
4     FORMAT(1H1,5X,'NUMBER OF SAMPLE POINTS=',I4,'*2')
      IF(IPRINT.NE.0)WRITE(IPRINT,5)DELTA,TEE
5     FORMAT(1H ,5X,'SAMPLE PERIOD=',F15.10,4X,'SEC.'/1H ,
     1 5X,         'SAMPLE LENGTH=',F15.10,4X,'SEC.'    )
      RETURN
      END
$
```

Computer Program Listing

1. Subroutine : READA

```
C:   THE SUBROUTINE IS TO BE LOADED WITH ENERGY, TIMEPLOT
C:   AND COUNTING PROGRAMMES, IE;PROGRAMMES NEED THE WHOLE
C:    DATA ONLY AS ONE VECTOR.

      SUBROUTINE READA(A,V,ND,RESOLN,IPRINT)
C:    ===========================================*
C:   SUBROUTINE READ IS TO READ DATA FROM PAPER TAPE OR DSK:
C:   FILES AND SCALES IT ACCORDING TO SCALE FACTOR 'V' (TRANSIENT
C:   RECORDER INPUT VOLTAGE),AND ANALOGUE/DIGITAL CONVERTER AMPLITUDE
C:   RESOLUTION 'RESOLN'
C:
C:   IPRINT: IS THE UNIT NUMBER  OF OUTPUT DEVICE.
C:    USING DEC-20 SYSTEM:-

C:                           0:  NO LIST IS REQUIRED
C:                           3:  IF LIST OF DATA TO BE PRINTED
C:                               BY LPT:
C:                           5:  IF LIST OF DATA TO BE PRINTED
C:                               BY TTY:
C:
C:   USING DL905 TRANSIENT RECORDER THE SUBROUTINE SHOULD
C:   BE CALLED BY 'RESOLN  = 255.0'

C:
C:   DATA RETURN TO THE MAIN PROGRAMME AS A VECTOR A(N).
C:
C

        DIMENSION A(ND)
        DOUBLE PRECISION NAME
        COMMON INDAT

        CALL OPEN (NAME,INDAT)
        READ(INDAT,1)(A(I),I=1,ND)
        CALL    CLOS(NAME,INDAT)
  1     FORMAT(16(F3.1,1X))

C:   CLOSE STATEMENT IS TO ALLOW CALLING THE SAME SUBROUTINE
C:   MORE THAN ONE TIME FOR DIFFERENT FILES FROM IN THE
C:   SAME MAIN PROGRAMME.

        DO 2 N=1,ND
        A(N)=(A(N)*10.0)*V/RESOLN
  2     CONTINUE

        IF(IPRINT.EQ.0)GO TO 4
        WRITE(IPRINT,3)(A(N),N=1,ND)
  3     FORMAT(8(F8.3))
```

```
4       CONTINUE
        RETURN
        END
$
```

2. Subroutine : READAB

```
C:   THIS SUBROUTINE IS TO BE LOADED WITH ANY MAIN PROGRAMME
C:   NEEDS DATA IN TWO ARRAYS SUCH AS FFT.

       SUBROUTINE READAB(A,B,V,NDH,RESOLN,IPRINT)
C:   ===========================================
C:   SUBROUTINE READAB IS TO READ DATA FROM PAPER TAPE OR DSK:
C:   FILES AND SCALES IT ACCORDING TO SCALE FACTOR 'V' (TRANSIENT
C:   RECORDER INPUT VOLTAGE),AND ANALOGUE/DIGITAL CONVERTER AMPLITUDE
C:   RESOLUTION 'RESOLN'
C:
C:   IPRINT: IS THE UNIT NUMBER  OF OUTPUT DEVICE.
C:    USING DEC-20 SYSTEM:-

C:                              0: NO LIST IS REQUIRED
C:                              1: IF THE DATA TO BE STOREDIN FILE
C:                              3: IF LIST OF DATA TO BE PRINTED
C:                                  BY LPT:
C:                              5: IF LIST OF DATA TO BE PRINTED
C:                                  BY TTY:
C:
C:   USING DL905 TRANSIENT RECORDER THE SUBROUTINE SHOULD
C:   BE CALLED BY 'RESOLN  = 255.0'

C:
C:   DATA RETURN TO THE MAIN PROGRAMME  IN TWO ARRAYS A(NDH),B(NDH)
C:
C

        DIMENSION A(NDH),B(NDH)
        DOUBLE PRECISION NAME
        COMMON INDAT

        CALL OPEN (NAME,INDAT)
        DO 2 J=1,64
        K1=(J-1)*8+1
```

```
      K2=K1+7
      READ(INDAT,1)(A(N),B(N),N=K1,K2)
1     FORMAT(16(F3.1,1X))
2     CONTINUE

C:  CLOSE STATEMENT IS TO ALLOW CALLING THE SUBROUTINE MORE
C:  THAN ONE TIME FROM THE SAME PROGRAMME AND FOR
C:  DIFFERENT DATA FILES.

      CALL    CLOS(NAME,INDAT)

      DO 3 N=1,NDH
      A(N)=(A(N)*10.0)*V/RESOLN
      B(N)=(B(N)*10.0)*V/RESOLN
3     CONTINUE

      IF (IPRINT.EQ.0)  GO TO 5
      IF(IPRINT.EQ.1)OPEN(UNIT=1,DEVICE='DSK',FILE='FOR99.DAT')
      WRITE(IPRINT,4)(A(N),B(N),N=1,NDH)
4     FORMAT(1H ,16(F7.3))
      IF(IPRINT.EQ.1)CLOSE(UNIT=1,DEVICE='DSK',FILE='FOR99.DAT')
5     CONTINUE
      RETURN
      END
$
```

3. Subroutine : OPEN

```
      SUBROUTINE OPEN(NAME,INPUT)
      DOUBLE PRECISION NAME
      TYPE 1
1     FORMAT( ' ENTER INPUT DATA FILE NAME :'$)
      READ(5,2) NAME
2     FORMAT(A6)
      OPEN(UNIT=INPUT,ACCESS='SEQIN',DEVICE='DSK',FILE=NAME,
      1           DISPOSE='SAVE')
      RETURN
      END
$
```

4. Subroutine : CLOS

```
      SUBROUTINE CLOS(NAME,INPUT)
      DOUBLE PRECISION NAME
      CLOSE(UNIT=INPUT,DEVICE='DSK',FILE=NAME,DISPOSE='SAVE')
      RETURN
      END
$
```

APPENDIX : 4.D

Computer Program Listing

1. Subroutine : LEVA

```
      SUBROUTINE LEVA(A,ND,IPRINT,IFILE)
      DIMENSION A(ND)

      X=0.0
      DO 7 N=1,ND
      X=X+A(N)
 7    CONTINUE
      Y=X/ND
      DO 6 N=1,ND
      A(N)=A(N)-Y
 6    CONTINUE

      IF(IPRINT.EQ.0) GO TO 4
      WRITE(IPRINT,5)(A(N),N=1,ND)
 5    FORMAT(8(F8.3))
 4    CONTINUE
      IF(IFILE.EQ.0)GO TO 1
      TYPE 3
 3    FORMAT( ' TYPE THE FILE NO. IN WHICH THE DATA TO BE
     1 STORED AS:-'/1H ,'<XXX IN FORXXX.DAT>')
      READ(5,2)  NFILE
 2    FORMAT(I)
      OPEN(UNIT=NFILE,DEVICE='DSK',DISPOSE='SAVE')
      WRITE(NFILE,5)(A(N),N=1,ND)
      CLOSE(UNIT=NFILE,DEVICE='DSK',DISPOSE='SAVE')

 1    CONTINUE
      RETURN
      END
$
```

2. Subroutine : LEVAB

```
      SUBROUTINE LEVAB(A,B,NDH,IPRINT,IFILE)
      DIMENSION A(NDH),B(NDH)

      X=0.0
      DO 1 N=1,NDH
      X=X+A(N)+B(N)
1     CONTINUE

      Y=X/(NDH*2)

      DO 2 N=1,NDH
      A(N)=A(N)-Y
      B(N)=B(N)-Y
2     CONTINUE

      IF(IPRINT.NE.0) WRITE(IPRINT,3)(A(N),B(N),N=1,NDH)
3     FORMAT(8(F8.3))
      IF (IFILE.EQ.0) GO  TO 6
      TYPE 4
4     FORMAT(   ' TYPE THE NUMBER OF FILE WHERE THE DATA TO
     1 BE STORED AS:-'/1H ,'(XXX IN FORXXX.DAT)')
      READ (5,5)NFILE
5     FORMAT(I)
      OPEN(UNIT=NFILE,DEVICE='DSK',DISPOSE='SAVE')
      WRITE(NFILE,3)(A(N),B(N),N=1,NDH)
      CLOSE(UNIT=NFILE,DEVICE='DSK',DISPOSE='SAVE')
6     CONTINUE
      RETURN
      END
$
```

Computer Program Listing

1. Subroutine : STARTP

```
      SUBROUTINE STARTP(IPRINT,ITEK,FACT)
      CALL  DFACT(FACT)
      CALL  FACT 41(FACT)
      TYPE 1
1     FORMAT(  ' PRINT DEVICE :    '$)
      READ(5,3) IPRINT
      IF(IPRINT.EQ.3) CALL CODE
      TYPE 2
2     FORMAT(  ' TEKPLT ? :'$)
      READ(5,3) ITEK
3     FORMAT(G)
      IF(ITEK.EQ.0) RETURN
      CALL  FACT 41(1.6)
      CALL  PLOT 41(1.0,2.0,3)
      RETURN
      END
$
```

2. Subroutine : DFACT

```
      SUBROUTINE DFACT(FACT)
      TYPE 1
      READ(5,2)FACT
1     FORMAT( ' PLOTTING FACTOR :'$)
2     FORMAT(G)
      IF(FACT.EQ.0.0)FACT=1.25
      RETURN
      END
$
```

3. Subroutine : CODE

```
      SUBROUTINE CODE
      DIMENSION CONT(100)
      TYPE 1
1     FORMAT(  '  TYPE EXPT. CODE  :'$)
      READ(5,2) (CONT(I),I=1,10)
      WRITE(3,3)(CONT(I),I=1,10)

2     FORMAT(10A4)
3     FORMAT(1H1,22X,'THE EXPT. CODE  IS::**'
     -1,10A4,1X,'**::')
      RETURN
      END
$
```

APPENDIX 5.A

Physical Constants for Range of Material
Used in the Theoretical Analysis (167-169)

Material	Longitudinal Wave Vel. $m\ s^{-1}$	Shear Wave Velocity $m\ s^{-1}$	Surface Wave Vel. $m\ s^{-1}$	Acoustic Impedance $Kg\ m^{-2}\ s^{-1}(10^6)$
Aluminium (Rolled)	6420	3100	2900	17.3
Brass (70%Cu,30%Zn)	4500	2120	1950	40.6
Copper (Rolled)	5010	2260	1930	44.6
Stainless Steel (347)	5790	3120	2900	45.7
Mild Steel	6000	3230	3000	47.0
Polystyrene	2350	1120	na	2.48
Plastic	2300	1110	na	1.8
Perspex	2700	1300	1170	3.2
Air	344	-	-	0.003

For other material see Chapter Four.

*at a pressure of $1.013 \times 10^5\ N\ m^{-3}$ and 20^oC.

Computer Program Listing

1. Main Program : CPNG3.FOR

```
      DIMENSION F(500),ALPHA(500),FD(500)
      L=1
      CALL SCALCP(VL,Z1,Z2,Z3,XMAXFQ,CENT,NPOINT,L)
      Z13=Z1+Z3
      Z132=Z13*Z13
      Z231=Z2+((Z3*Z1)/Z2)
      Z2312=Z231*Z231
      PYE=2.0*3.1416/VL
      CALL PLTS 41
      CALL STARTP(IPRINT,ITEK,FACT)
      DO 1 I =1,NPOINT
      F(I)= FLOAT(I)*CENT
      FD(I)=F(I)/1000.0
    1 CONTINUE
      CALL CPDB(DB,XMAXFQ,FMX,DT,DA)
    2 CALL THICK(X,L)
      IF(X.EQ.1.0)GO TO 6
      DO 3 I=1,NPOINT
      Q=PYE*F(I)*X
      C=COS(Q)
      S=SIN(Q)
      C2=C*C
      S2=S*S
      ALPHA(I)=2.0*Z3/SQRT((Z132*C2)+(Z2312*S2))
      ALPHA(I)=20.0*ALOG10(ALPHA(I))
    3 CONTINUE
    5 CALL LINE 41(FD,FMX,DT,ALPHA,DB,DA,NPOINT,1,50,L)
      CALL WAIT 41
      L=L+1
      GO TO 2
    6 CONTINUE
      CALL PLTF 41
      STOP
      END
$
```

2. Subroutine : SCALCP

```
      SUBROUTINE SCALCP(VL,Z1,Z2,Z3,XMAXFQ,CENT,NPOINT,L)
C  Z1,Z2,AND Z3 ARE THE ACOUSTIC IMPEDANCES OF
C  1-SPECIMEN MATERIAL
C  2-COUPLANT
C  3-TRANSDUCER (CRYSTAL MATERIAL)
C  VL=LONGITUDINAL ULTRASONIC VELOCITY IN THE COUPLANT LAYER
      TYPE 1
1     FORMAT(1H ,'TYPE VL2   Z1   Z2   Z3 IN ISU')
      READ(5,3) VL
      READ(5,3) Z1
      READ(5,3) Z2
      READ(5,3) Z3
      IF(L.GT.1)RETURN
      TYPE 2
2     FORMAT( ' ENTER NO. OF POINTS TO BE USED IN EACH CURVE : '$)
      READ(5,3) NPOINT

3     FORMAT(G)
      TYPE 4
4     FORMAT(  ' ENTER MAX. FREQ. IN MHZ  :'$)
      READ(5,3) XMAXFQ
      XMAXFQ=XMAXFQ*1000000.0
      CENT=XMAXFQ/FLOAT(NPOINT)
      RETURN
      END
$
```

3. Subroutine : THICK

```
      SUBROUTINE THICK(X,L)
      IF(L.EQ.1)  TYPE 1
1     FORMAT( ' TYPE LAYER THICKNESS IN MM'/1H ,' TO TERMINATE
-     1 THE PROGRAMME TYPE <1000>')
      READ(5,2) X
      X=X/1000.0
2     FORMAT(G)
      RETURN
      END
```

4. Subroutine : CPDB

```
      SUBROUTINE CPDB(DB,XMAXFQ,FMX,DT,DA)
      DIMENSION IA(10)
      CALL PLOT 41(0.0,5.0,-3)
      AA=20.0
      BB=10.0
      TYPE 1
1     FORMAT( ' TYPE MIN , MAX. DB : '$)
      READ(5,2)SM,SX
2     FORMAT(2G)
      DA=(SX-SM)/BB
      DB=SM
      FMX=0.0
      DT=XMAXFQ/(AA*1000.0)
      IA(1)=4HFREQ
      IA(2)=4HUENC
      IA(3)=4HY IN
      IA(4)=4H KHZ
      CALL AXIS 41(0.0,0.0,IA,-16,AA,0.0,FMX,DT)
      IA(1)=4HPRES
      IA(2)=4HSURE
      IA(3)=4H TRA
      IA(4)=4HNS.
      IA(5)=4HCOEF
      IA(6)=4HFICI
      IA(7)=4HENT
      IA(8)=4H[DB]
      CALL AXIS 41(0.0,0.0,IA,32,BB,90.0,DB,DA)
      RETURN
      END
$
```

APPENDIX : 5.C

Computer Program Listing

1. Main Program : DTHREE.FOR

```
A PROGRAMME TO CALCULATE THE OPTIMUM THICKNESSES OF:
  THE ACOUSTIC EMISSION TRANSDUCER WINDOWS USING :
  THREE LAYERS TRANSMISSION SYSTEM.
        REAL I
        TYPE 1
1       FORMAT( ' ENTER Z1 , Z2 , Z3 :'$)
        READ(5,2)Z1,Z2,Z3
2       FORMAT(3G)
        TYPE 3
3       FORMAT( ' ENTER VL2 :'$)
        READ(5,4)VL
4       FORMAT(G)
        SMIN=10E10

        Z13=Z1+Z3
        Z132=Z13*Z13
        Z231=Z2+((Z3*Z1)/Z2)
        Z2312=Z231*Z231
        PYE=2.0*3.1416/VL
        TYPE 5
5       FORMAT( ' ENTER THE CENTRAL FREQ. IN KHZ :'$)
        READ(5,4)FREQ
        FREQ=FREQ*1000.0
6       TYPE 7
7       FORMAT( ' ENTER THE THICKNESS RANGE IN MM :'$)
        READ(5,9)X1,X2
        TYPE 8
8       FORMAT( ' OPT. THICK      TRANS. VALUE(DB)')
        X1=X1/1000.0
        X2=X2/1000.0
9       FORMAT(2G)
        L=1
10      Q=PYE*FREQ*X1
        C=COS(Q)
        S=SIN(Q)
        C2=C*C
```

```
      S2=S*S
      ALPHA=2.0*Z3/SQRT((Z132*C2)+(Z2312*S2))
      ALPHA=20.0*ALOG10(ALPHA)
      IF(L.EQ.1) PRET=ALPHA
      X1=X1+.00001
      L=L+1
      IF(L.EQ.2) GO TO 10
      TERM=ALPHA
      DO 13 I=X1,X2,0.00001
      Q=PYE*FREQ*I
      C=COS(Q)
      S=SIN(Q)
      C2=C*C
      S2=S*S
      ALPHA=2.0*Z3/SQRT((Z132*C2)+(Z2312*S2))
      ALPHA=20.0*ALOG10(ALPHA)
      AFT=ALPHA
      IF(ALPHA.LT.SMIN) SMIN=ALPHA
      IF(TERM.GT.PRET.AND.TERM.GT.AFT) GO TO 11
      GO TO 12
 11   THICK=I*1000.0
      WRITE(5,9)THICK,TERM
 12   PRET=TERM
      TERM=AFT
 13   CONTINUE
      TYPE 14
 14   FORMAT( ' ANOTHER THICKNESS RANGE ? :'$)
      READ(5,4)YES
      IF(YES.EQ.1.0) GO TO 6
      TYPE 15,SMIN
 15   FORMAT( ' THE MINIMUM TRANSMISSION VALUE=',G,'DB.')
      STOP
      END
$
```

2. Main Program : CPDC3.FOR

```
      DIMENSION F(500),ALPHA(500),FD(500)
      CALL PLTS 41
      CALL STARTP(IPRINT,ITEK,FACT)
      DA=0.0
      AMY=0.0
      DT=0.0
      FMX=0.0
      NP=500
      L=1
1     CALL SCALCP(VL,Z1,Z2,Z3,XMAXFQ,CENT,NP,L)
      IF(L.GT.1) GO TO 2
      DO 2 I =1,NP
      F(I)= FLOAT(I)*CENT
  2   CONTINUE
      Z13=Z1+Z3
      Z132=Z13*Z13
      Z231=Z2+((Z3*Z1)/Z2)
      Z2312=Z231*Z231
      PYE=2.0*3.1416/VL
      IF(L.GT.1)  TYPE 9
      CALL THICK(X,L)
      IF(X.EQ.1.0)GO TO 8
      DO 3 I=1,NP
      Q=PYE*F(I)*X
      C=COS(Q)
      S=SIN(Q)
      C2=C*C
      S2=S*S
      ALPHA(I)=2.0*Z3/SQRT((Z132*C2)+(Z2312*S2))
      ALPHA(I)=20.0*ALOG10(ALPHA(I))
  3   CONTINUE
      IF(L.GT.1) GO TO 5
      DO 4 I=1,NP
 4    FD(I)=F(I)/1000.0
      CALL CPDB(DB,XMAXFQ,FMX,DT,DA)
5     CALL LINE 41(FD,FMX,DT,ALPHA,DB,DA,NP,1,50,L)
      CALL WAIT 41
      L=L+1
      TYPE 6
 6    FORMAT( ' ANOTHER CASE ? :'$)
      READ(5,7) YES
      IF(YES.EQ.1) GO TO 1
 7    FORMAT(G)
 8    CALL PLTF 41
 9    FORMAT( ' LAYER THICKNESS :'$)
      STOP
      END
$
```

Computer Program Listing

1. Main Program : CPNG4.FOR

```
      DIMENSION F(500),ALFHA(500),IA(10),FD(500)
      CALL CODE
      TYPE 1
1     FORMAT(1H ,'TYPE VL2  VL3  Z1   Z2   Z3   Z4  IN ISU')
      READ(5,2) VL2
      READ(5,2) VL3
      READ(5,2) Z1
      READ(5,2) Z2
      READ(5,2) Z3
      READ(5,2) Z4
2     FORMAT(G)
      TYPE 3
3     FORMAT( ' ENTER THE NUMBER OF DATA POINTS :')
      READ(5,2) NC
      TYPE 4
4     FORMAT(  ' ENTER THE TRANS. FACE THICK. IN MM.: '$)
      READ(5,2)XTF
      XTF=XTF/1000.0
      TYPE 5
5     FORMAT(  ' ENTER MAX. FREQ. IN MHZ: '$)
      READ(5,2) XMAXFQ
      XMAXFQ=XMAXFQ*1000000.0
      CENT=XMAXFQ/FLOAT(NC)
      TYPE 6
6     FORMAT( ' MIN. VALUE IN DB :'$)
      READ(5,2)DB
      ZO=4.0*Z1*Z4
      ZA=Z1+Z4 .
      ZB=(Z1*Z3/Z2)+(Z2*Z4/Z3)
      ZC=(Z1*Z4+Z2*Z2)/Z2
      ZD=(Z1*Z4+Z3*Z3)/Z3
      PYE2=2.0*3.1416/VL2
      PYE3=2.0*3.1416/VL3
      CALL PLTS 41
      CALL STARTP(IPRINT,ITEK,FACT)
      DO 7 I =1,NC
      F(I)= FLOAT(I)*CENT
7     CONTINUE
      L=1
8     CALL THICK(X,L)
      IF(X.EQ.1.0)GO TO 12
```

```
      DO 9 I=1,NC
      Q2=PYE2*F(I)*X
      C2=COS(Q2)
      S2=SIN(Q2)
      Q3=PYE3*F(I)*XTF
      C3=COS(Q3)
      S3=SIN(Q3)
      AC1=(ZA*C2*C3-ZB*S2*S3)**2
      AC2=(ZC*S2*C3+ZD*C2*S3)**2
      ALPHA(I)=ZO/(AC1+AC2)
      ALPHA(I)=20.0*ALOG10(ALPHA(I))
    9 CONTINUE
      IF(L.GT.1) GO TO 11
      CALL PLOT 41(0.0,5.0,-3)
      AA=20.0
      BB=10.0
C     CALL SCAL 41(ALPHA,BB,NC,1,FFY,DA)
      DA=-DB/BB
      FMX=0.0
      DT=XMAXFQ/(AA*1000.0)
      DO 10 I=1,NC
   10 FD(I)=F(I)/1000.0
      IA(1)=4HFREQ
      IA(2)=4HUENC
      IA(3)=4HY IN
      IA(4)=4H KHZ
      CALL AXIS 41(0.0,0.0,IA,-16,AA,0.0,FMX,DT)
      IA(1)=4HPRES
      IA(2)=4HSURE
      IA(3)=4H TRA
      IA(4)=4HNS.
      IA(5)=4HCOEF
      IA(6)=4HFICI
      IA(7)=4HENT
      IA(8)=4H[DB]
      CALL AXIS 41(0.0,0.0,IA,32,BB,90.0,DB,DA)
   11 CALL LINE 41(FD,FMX,DT,ALPHA,DB,DA,NC,1,50,L)
      L=L+1
      GO TO 8
   12 CONTINUE
      CALL WAIT 41
      CALL PLTF 41
      STOP
      END
$
```

Computer Program Listing

Main Program : CPNG5.FOR

```
      DIMENSION F(500),ALPHA(500),IA(10),FD(500)
      TYPE 1
1     FORMAT(1H ,'TYPE VL2  VL3  VL4   Z1   Z2   Z3   Z4  Z5  IN ISU')
      READ(5,2) VL2
      READ(5,2) VL3
      READ(5,2)VL4
      READ(5,2) Z1
      READ(5,2) Z2
      READ(5,2) Z3
      READ(5,2) Z4
      READ(5,2) Z5
2     FORMAT(G)
      TYPE 3
3     FORMAT( ' ENTER THE NUMBER OF DATA POINTS :')
      READ(5,2) NC
      TYPE 4
4     FORMAT(  ' ENTER THE TRANS. FACE THICK. IN MM.:'$)
      READ(5,2)XTF
      XTF=XTF/1000.0
      TYPE 5
5     FORMAT( ' ENTER THE PZT THICK. IN MM.:'$)
      READ(5,2) XT2
      XT2=XT2/1000.0
      TYPE 6
6     FORMAT(  ' ENTER MAX. FREQ. IN MHZ :'$)
      READ(5,2) XMAXFQ
      XMAXFQ=XMAXFQ*1000000.0
      CENT=XMAXFQ/FLOAT(NC)
      TYPE 7
7     FORMAT( ' MIN. VALUE IN DB :'$)
      READ(5,2)DB
      Z0=4.0*Z1*Z5
      R1=Z1+Z5
      R2=((Z1*Z3)/Z2)+(Z2*Z5/Z3)
      R3=((Z1*Z4)/Z3)+(Z3*Z5/Z4)
      R4=((Z1*Z4)/Z2)+(Z2*Z5/Z4)
      R5=Z3+((Z1*Z5)/Z3)
      R6=Z4+((Z1*Z5)/Z4)
      R7=(Z1*Z5/Z2)+Z2
      R8=(Z1*Z3*Z5)/(Z2*Z4)+(Z2*Z4)/Z3
      PYE2=2.0*3.1416/VL2
      PYE3=2.0*3.1416/VL3
      PYE4=2.0*3.1416/VL4
      CALL PLTS 41
      CALL STARTP(IPRINT,ITEK,FACT)
      DO 8 I =1,NC
      F(I)= FLOAT(I)*CENT
8     CONTINUE
      L=1
```

```
 9      CALL THICK(X,L)
        IF(X.EQ.1.0)GO TO 13
        DO 10 I=1,NC
        Q2=PYE2*F(I)*X
        C2=COS(Q2)
        S2=SIN(Q2)
        Q3=PYE3*F(I)*XTF
        C3=COS(Q3)
        S3=SIN(Q3)
        Q4=PYE4*F(I)*XT2
        C4=COS(Q4)
        S4=SIN(Q4)
        AC1=(R1*C2*C3*C4-R2*S2*S3*C4-R3*C2*S3*S4-R4*S2*S4*C3)**2
        AC2=(R5*C2*C4*S3+R6*C2*C3*S4+R7*S2*C3*C4-R8*S2*S3*S4)**2
        ALPHA(I)=Z0/(AC1+AC2)
        ALPHA(I)=20.0*ALOG10(ALPHA(I))
 10     CONTINUE
        IF(L.GT.1) GO TO 12
        CALL PLOT 41(0.0,5.0,-3)
        AA=20.0
        BB=10.0
C       CALL SCAL 41(ALPHA,BB,NC,1,FFY,DA)
        DA=-DB/BB
        FMX=0.0
        DT=XMAXFQ/(AA*1000.0)
        DO 11 I=1,NC
 11     FD(I)=F(I)/1000.0
        IA(1)=4HFREQ
        IA(2)=4HUENC
        IA(3)=4HY IN
        IA(4)=4H KHZ
        CALL AXIS 41(0.0,0.0,IA,-16,AA,0.0,FMX,DT)
        IA(1)=4HPRES
        IA(2)=4HSURE
        IA(3)=4H TRA
        IA(4)=4HNS.
        IA(5)=4HCOEF
        IA(6)=4HFICI
        IA(7)=4HENT
        IA(8)=4H[DB]
        CALL AXIS 41(0.0,0.0,IA,32,BB,90.0,DB,DA)
 12     CALL LINE 41(FD,FMX,DT,ALPHA,DB,DA,NC,1,50,L)
        CALL WAIT 41
        L=L+1
        GO TO 9
 13     CONTINUE
        CALL WAIT 41
        CALL PLTF 41
        STOP
        END
$
```

Computer Program Listing

Main Program : CPNG6.FOR

```
      DIMENSION F(500),ALPHA(500)
      DIMENSION IA(10),FD(500)
      REAL IM,IM2,MAG
      CALL PLTS 41
      CALL STARTP(IPRINT,ITEK,FACT)
      TYPE 1
1     FORMAT(1H ,'TYPE VL2 VL3 VL4,VL5 Z1,Z2,Z3,Z4,Z5,Z6 IN ISU')
      READ(5,2) VL2
      READ(5,2) VL3
      READ(5,2)VL4
      READ(5,2)VL5
      READ(5,2) Z1
      READ(5,2) Z2
      READ(5,2) Z3
      READ(5,2) Z4
      READ(5,2)Z5
      READ(5,2)Z6
2     FORMAT(G)
      NPTS=500
      TYPE 3
3     FORMAT( ' ENTER THE NUMBER OF DATA CENT  : '$)
      READ(5,2) NC
      TYPE 4
4     FORMAT( ' ENTER THE PZT THICKNESS.')
      READ (5,2)TRAN
      TYPE 5
5     FORMAT(  ' ENTER THE TRANS. FACE THICK.')
      READ(5,2)XTF
      TYPE 6
6     FORMAT( ' ENTER SP. THICK.')
      READ(5,2) XT2
      XTF=3.125E-3
      XT2=3E-3
      TRAN=6.35E-3
      TYPE 7
7     FORMAT(  ' ENTER MAX. FREQ. IN MHZ : '$)
      READ(5,2) XMAXFQ
      TYPE 8
8     FORMAT( ' MIN. VALUE IN DB : '$)
      READ(5,2)DB
      XMAXFQ=XMAXFQ*1000000.0
      CENT=XMAXFQ/FLOAT(NC)
      NNN=NC
      ZE=4.0*Z1/Z6
      Z13=Z1*Z3
      Z14=Z1*Z4
```

```
      Z15=Z1*Z5
      Z26=Z2*Z6
      Z36=Z3*Z6
      Z46=Z4*Z6
      Z25=Z2*Z5
      Z35=Z3*Z5
      Z24=Z2*Z4
      R1=1+(Z1/Z6)
      R2=(Z24/Z35)+((Z13*Z5)/(Z24*Z6))
      R3=(Z2/Z3)+(Z13/Z26)
      R4=(Z3/Z4)+(Z14/Z36)
      R5=(Z2/Z4)+(Z14/Z24)
      R6=(Z4/Z5)+(Z15/Z46)
      R7=(Z2/Z5)+(Z15/Z26)
      R8=(Z3/Z5)+(Z15/Z36)
      G1=(Z1/Z5)+(Z5/Z6)
      G2=(Z1/Z4)+(Z4/Z6)
      G3=(Z1/Z3)+(Z3/Z6)
      G4=(Z1/Z2)+(Z2/Z6)
      G5=(Z13/Z25)+(Z25/Z36)
      G6=(Z14/Z35)+(Z35/Z46)
      G7=(Z14/Z25)+(Z25/Z46)
      G8=(Z13/Z24)+(Z24/Z36)
      PYE2=2.0*3.1416/VL2
      PYE3=2.0*3.1416/VL3
      PYE4=2.0*3.1416/VL4
      PYE5=2.0*3.1416/VL5
      DO 9 I =1,NC
      F(I)= FLOAT(I)*CENT
    9 CONTINUE
      L=1
   10 CALL THICK(X,L)
      IF(X.EQ.1.0)GO TO 15

      DO 12 I=1,NC
C  SOLID SPECIMEN
      Q2=PYE2*F(I)*XT2
      C2=COS(Q2)
      S2=SIN(Q2)
C  COUPLANT LAYER
      Q3=PYE3*F(I)*X
      C3=COS(Q3)
      S3=SIN(Q3)
C  PLASTIC SHOE
      Q4=PYE4*F(I)*XTF
      C4=COS(Q4)
      S4=SIN(Q4)
```

```
       Q5=PYES*F(I)*TRAN
       C5=COS(Q5)
       S5=SIN(Q)
C  REAL PART
       RE   =R1*C2*C3*C4*C5 +  R2*S2*S3*S4*S5
-      1    -R3*S2*S3*C4*C5 -  R4*C2*S3*S4*C5
-      2    -R5*S2*C3*S4*C5 -  R6*C2*C3*S4*S5
-      3    -R7*S2*C3*C4*S5 -  R8*C2*S3*C4*S5
       IM   =G1*C2*C3*C4*S5 +  G2*C2*C3*S4*C5
-      1    +G3*C2*C3*C4*S5 +  G4*S2*C3*C4*C5
-      2    -G5*S2*S3*C4*S5 +  G6*C2*S3*S4*S5
-      3    -G7*S2*C3*S4*S5 +  G8*S2*S3*S4*C5
       RE2=RE*RE
       IM2=IM*IM
       TOT=RE2+IM2
       MAG=SQRT(TOT)
       ALPHA(I)=2.00/MAG
       ALPHA(I)=20.*ALOG10(ALPHA(I))
  12   CONTINUE
       IF(L.GT.1) GO TO 14
       CALL PLOT 41(0.0,5.0,-3)
       AA=20.0
       BB=10.0
C      CALL SCAL 41(ALPHA,BB,NNN,1,FFY,DA)
       DA=-DB/BB
       FMX=0.0
       DT=XMAXFQ/(AA*1000.0)
       DO 13 I=1,NNN
  13   FD(I)=F(I)/1000.0
       IA(1)=4HFREQ
       IA(2)=4HUENC
       IA(3)=4HY IN
       IA(4)=4H KHZ
       CALL AXIS 41(0.0,0.0,IA,-16,AA,0.0,FMX,DT)
       IA(1)=4HPRES
       IA(2)=4HSURE
       IA(3)=4H TRA
       IA(4)=4HNS.
       IA(5)=4HCOEF
       IA(6)=4HFICI
       IA(7)=4HENT
       IA(8)=4H[DB]
       CALL AXIS 41(0.0,0.0,IA,32,BB,90.0,DB,DA)
  14   CALL LINE 41(FD,FMX,DT,ALPHA,DB,DA,NNN,1,50,L)
       CALL WAIT 41
       L=L+1
       GO TO 10
  15   CONTINUE
       CALL WAIT 41
       CALL PLTF 41
       STOP
       END
$
```

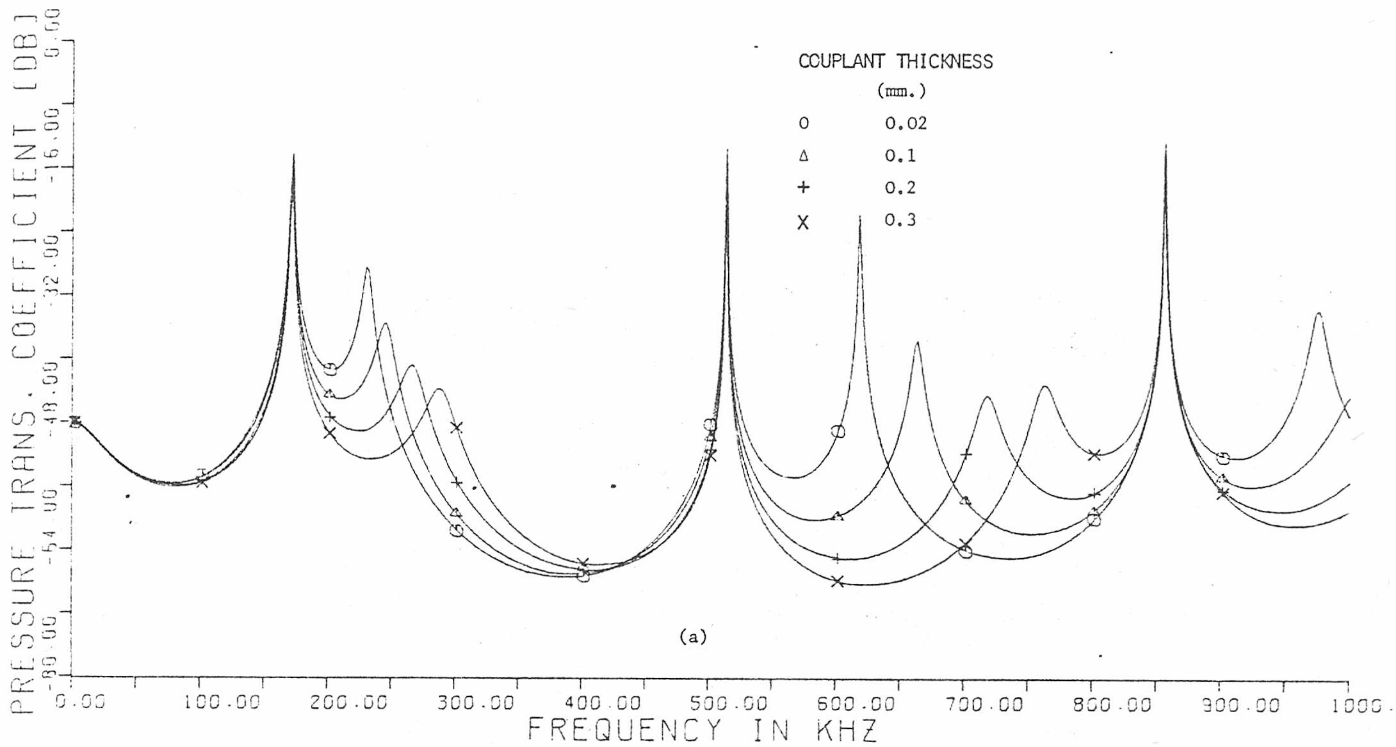

APPENDIX 5.G : Calculated Pressure Transmission Coefficient for Six-layer Transmission System Using Water Couplant and S140 D/E Transducer.

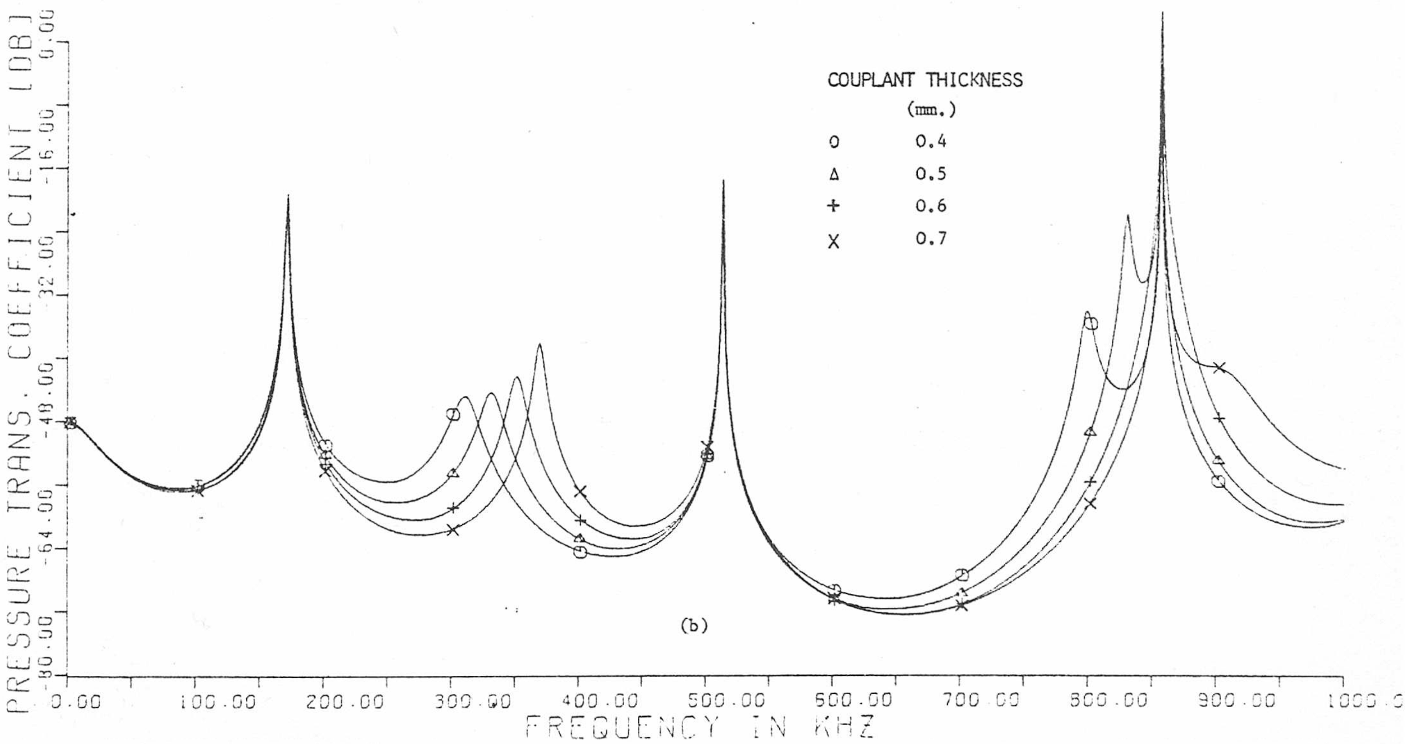

APPENDIX 5.G : Continued.

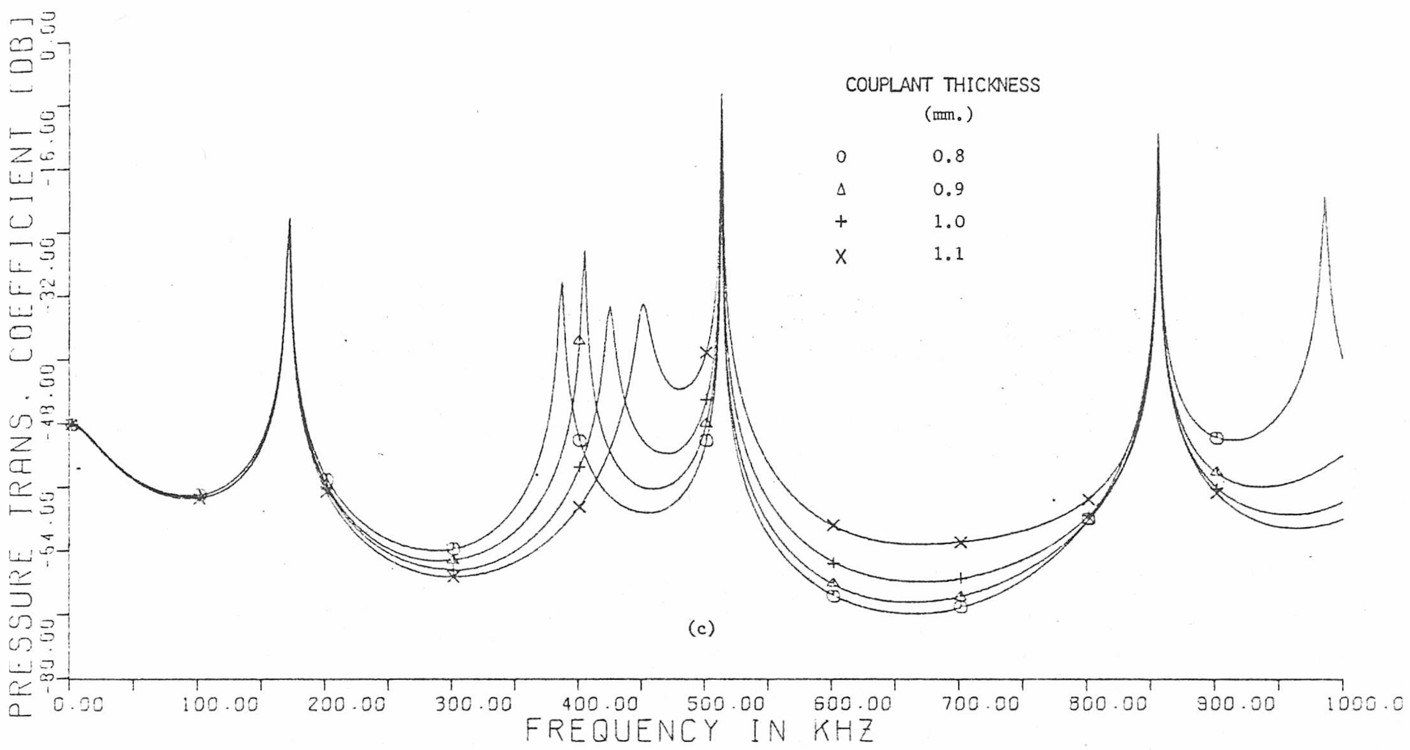

APPENDIX 5.G : Continued.

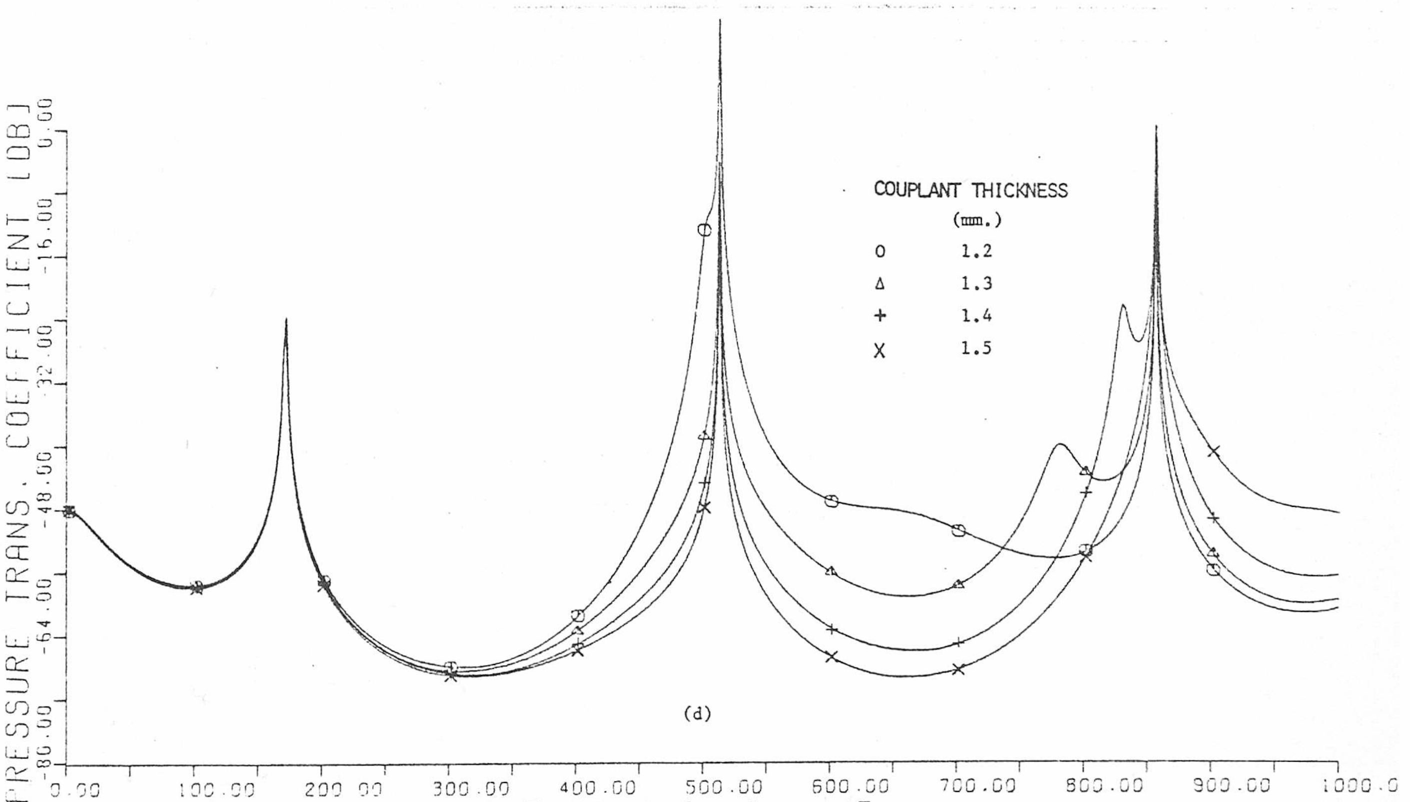

APPENDIX 5.G: Continued.

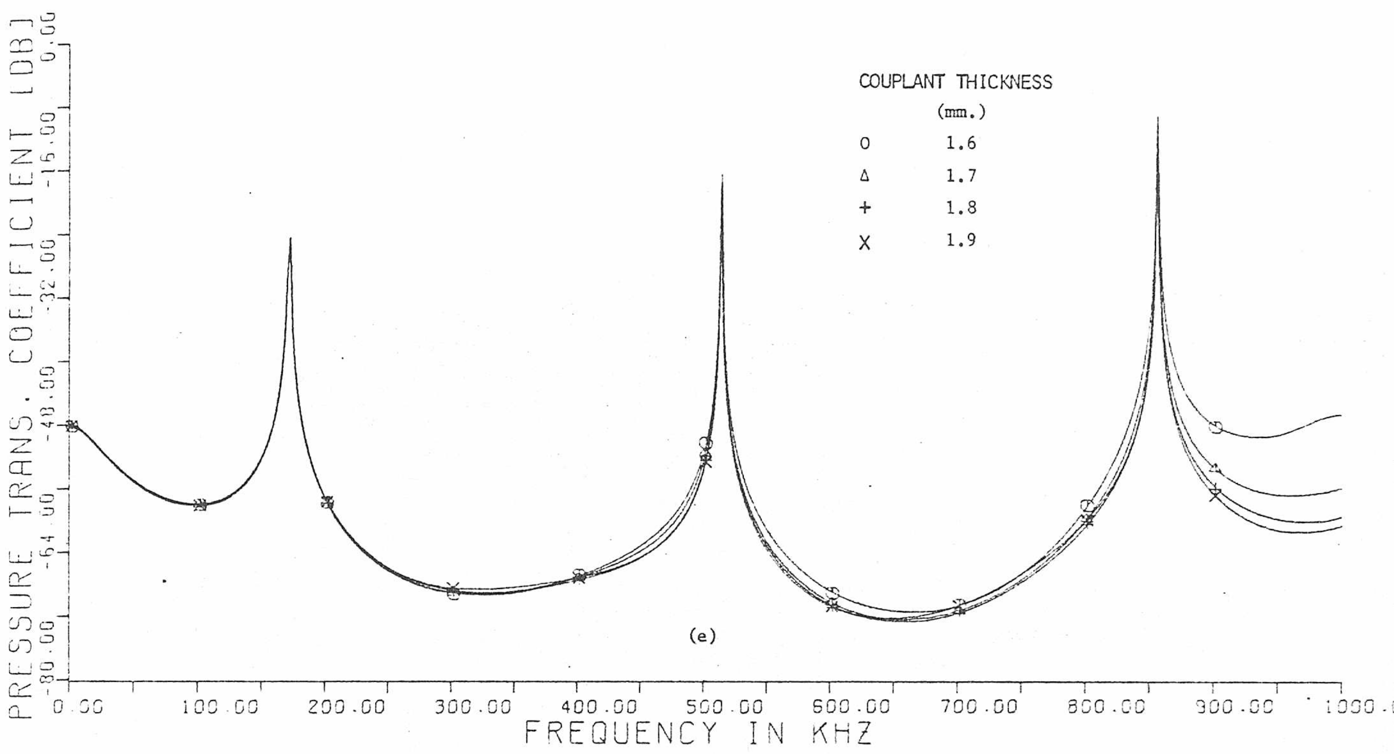

APPENDIX 5.G : Continued.

Computer Program Listing

Main Program : CP6.FOR

```
      DIMENSION F(500),ALPHA(500),VAL(120),FF(100),II(100)
      REAL IM,IM2,MAG
      TYPE 1
 1    FORMAT(1H ,'TYPE VL2 VL3 VL4 VL5 Z1 Z2 Z3 Z4 Z5 Z6 IN ISU')
      READ(5,3) VL2
      READ(5,3) VL3
      READ(5,3)VL4
      READ(5,3)VL5
      READ(5,3) Z1
      READ(5,3) Z2
      READ(5,3) Z3
      READ(5,3) Z4
      READ(5,3) Z5
      READ(5,3)Z6
      NPTS=500
      TYPE 2
2     FORMAT( ' ENTER MIN. VALUE IN DB  : '$)
      READ(5,3)DBM
      EXS=-DBM
3     FORMAT(G)
      TYPE 4
4     FORMAT(  ' ENTER THE TRANS. FACE THICK.  : '$)
      READ(5,3)XTF
      TYPE 5
5     FORMAT( ' ENTER THE SP.THICK.  : '$)
      READ(5,3) XT2
      TYPE 6
 6    FORMAT( ' ENTER THE PZT THICKNESS.: '$)
      READ(5,3) TRAN
      TYPE 7
7     FORMAT(  ' ENTER MAX. COUPLANT THICK. IN MM : '$)
      READ(5,3) XMAXFQ
      XMAXFQ=2.0
      XMAXFQ=XMAXFQ/1000.00
      CENT=XMAXFQ/FLOAT(NPTS)
      ZE=4.0*Z1/Z6
      Z13=Z1*Z3
      Z14=Z1*Z4
      Z15=Z1*Z5
      Z26=Z2*Z6
      Z36=Z3*Z6
      Z46=Z4*Z6
      Z25=Z2*Z5
      Z35=Z3*Z5
      Z24=Z2*Z4
```

```
      R1=1+(Z1/Z6)
      R2=(Z24/Z35)+((Z13*Z5)/(Z24*Z6))
      R3=(Z2/Z3)+(Z13/Z26)
      R4=(Z3/Z4)+(Z14/Z36)
      R5=(Z2/Z4)+(Z14/Z24)
      R6=(Z4/Z5)+(Z15/Z46)
      R7=(Z2/Z5)+(Z15/Z26)
      R8=(Z3/Z5)+(Z15/Z36)
      G1=(Z1/Z5)+(Z5/Z6)
      G2=(Z1/Z4)+(Z4/Z6)
      G3=(Z1/Z3)+(Z3/Z6)
      G4=(Z1/Z2)+(Z2/Z6)
      G5=(Z13/Z25)+(Z25/Z36)
      G6=(Z14/Z35)+(Z35/Z46)
      G7=(Z14/Z25)+(Z25/Z46)
      G8=(Z13/Z24)+(Z24/Z36)
      PYE2=2.0*3.1416/VL2
      PYE3=2.0*3.1416/VL3
      PYE4=2.0*3.1416/VL4
      PYE5=2.0*3.1416/VL5
      CALL PLTS 41
      CALL STARTP(IPRINT,ITEK,FACT)
      DO 8 I =1,NPTS
      F(I)= FLOAT(I)*CENT
  8   CONTINUE
      L=1
  9   IF(L.EQ.1)TYPE10
 10   FORMAT( ' TYPE THE PROPAGATION FREQ. IN KHZ  : '$)
      READ(5,3) X
      X=X*1000.0
      Q2=PYE2*X*XT2
      C2=COS(Q2)
      S2=SIN(Q2)
      Q4=PYE4*X*XTF
      C4=COS(Q4)
      S4=SIN(Q4)
C  TRANSDUCER PZT
      Q5=PYE5*X*TRAN
      C5=COS(Q5)
      S5=SIN(Q)
 11   DO 12 I=1,NPTS
      Q3=PYE3*F(I)*X
      C3=COS(Q3)
      S3=SIN(Q3)
```

```
C   REAL PART
         RE   =R1*C2*C3*C4*C5 +  R2*S2*S3*S4*S5
-        1    -R3*S2*S3*C4*C5 -  R4*C2*S3*S4*C5
-        2    -R5*S2*C3*S4*C5 -  R6*C2*C3*S4*S5
-        3    -R7*S2*C3*C4*S5 -  R8*C2*S3*C4*S5
         IM   =G1*C2*C3*C4*S5 +  G2*C2*C3*S4*C5
-        1    +G3*C2*C3*C4*S5 +  G4*S2*C3*C4*C5
-        2    -G5*S2*S3*C4*S5 +  G6*C2*S3*S4*S5
-        3    -G7*S2*C3*S4*S5 +  G8*S2*S3*S4*C5
         RE2=RE*RE
         IM2=IM*IM
         TOT=RE2+IM2
         MAG=SQRT(TOT)
         ALPHA(I)=2.0/MAG
  12     CONTINUE
         SCA=0.0
          DO 13 I=1,NPTS
         IF(ALPHA(I).GT.SCA)SCA=ALPHA(I)
         F(I)=F(I)*1000.0
  13     CONTINUE
C$$$$$$$$$##########
C22222222222222222222
C33333333333333333333
         DO 15 I=1,NPTS
         ALPHA(I)=ALPHA(I)/SCA
         ALPHA(I)=20.0*ALOG10(ALPHA(I))
  15     CONTINUE

C        CALL PLOT 41(0.0,8.0,-3)
         CALL PLOT 41(0.0,3.0,-3)
         AA=20.0
         BB=10.0
         FMX=0.0
         AMY=EXS
         DT=XMAXFQ*1000.0/BB
         DA=DBM/AA
         II(1)=4HLAYE
         II(2)=4HR TH
         II(3)=4HICKN
         II(4)=4HESS
         II(5)=4HIN M
         II(6)=2HM.
         CALL AXIS 41(0.0,0.0,II,-22,BB,0.0,FMX,DT)
         II(1)=4HRELA
         II(2)=4HTIVE
         II(3)=4H PRE
         II(4)=4HSSUR
         II(5)=4HE IN
         II(6)=4H DB
         CALL AXIS 41(0.0,0.0,II,24,AA,90.0,AMY,DA)
```

```
      THS=AMY
      THI=DA
17    CALL LINE 41(F,FMX,DT,ALPHA,THS,THI,NPTS,1,0,0)
18    TYPE 19
19    FORMAT( ' ENTER EXPT. NO. OF POINTS  : '$)
      READ(5,3) NP
      READ(24,20)(FF(I),VAL(I),I=1,NP)
20    FORMAT( 2G)
      VV=0.0
      DO 21 I=1,NP
      IF(VAL(I).GT.VV)VV=VAL(I)
21    CONTINUE
      DO 22 I=1,NP
      VAL(I)=VAL(I)/VV
      VAL(I)=20.0*ALOG10(VAL(I))
      CLOSE(UNIT=24,DEVICE='DSK',DISPOSE='SAVE')
22    CONTINUE
      CALL LINE 41(FF,FMX,DT,VAL,AMY,DA,NP,1,-1,L)
      L=L+1
      TYPE 23
23    FORMAT( ' MORE DATA  : '$)
      READ(5,3)YES
      IF(YES.EQ.0.0) GO TO 24
      GO TO 18
 24   CONTINUE
      CALL PLTF 41
      STOP
      END
$
```

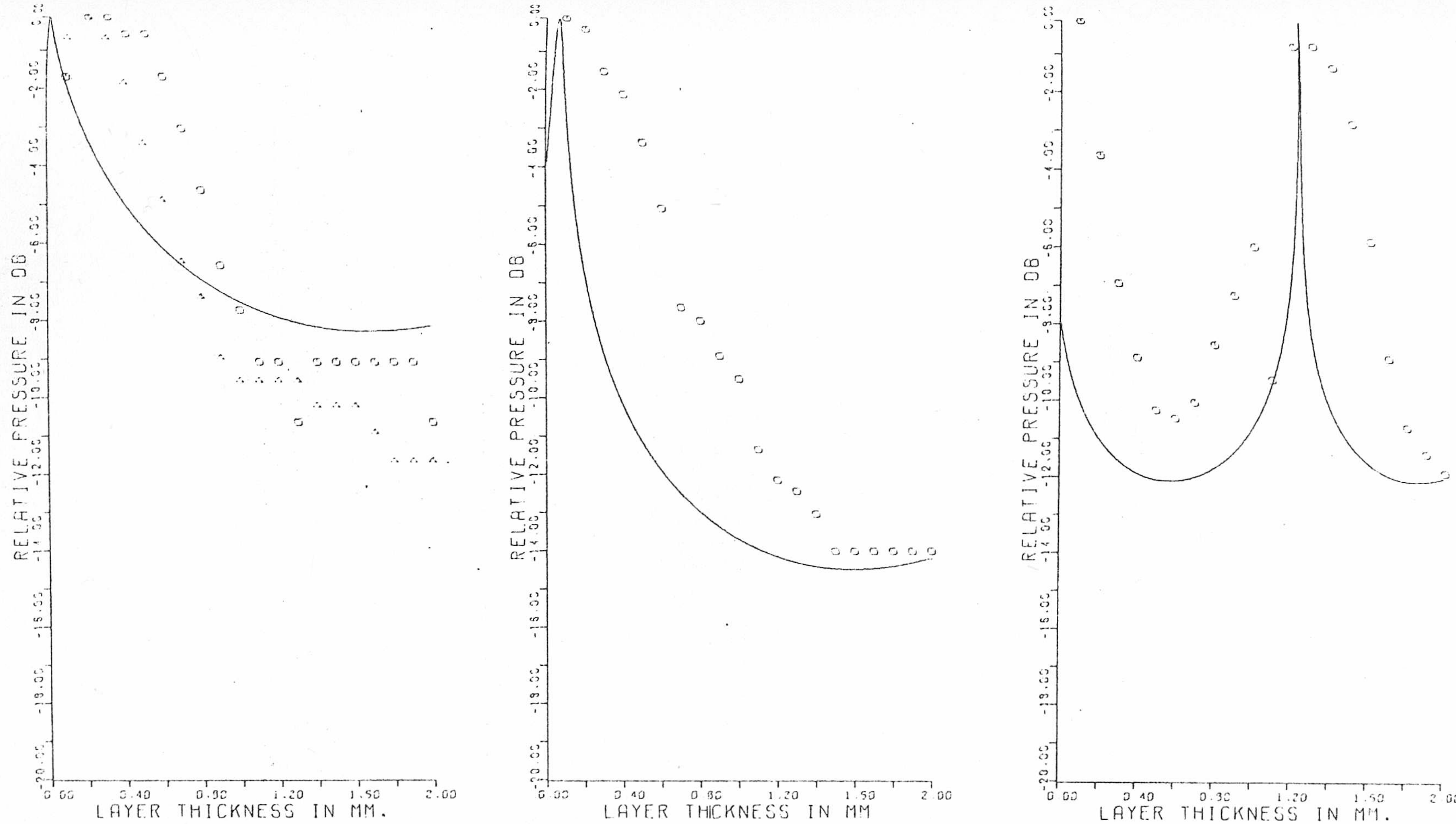

(a) 200 KHz
(Results from Two Experiments)

(b) 240 KHz

(c) 580 KHz

APPENDIX 5.I : Comparison Between Experimental and Theoretical Relative Pressure Transmission as Function of Water Couplant Thickness Using S 140 Transducer.

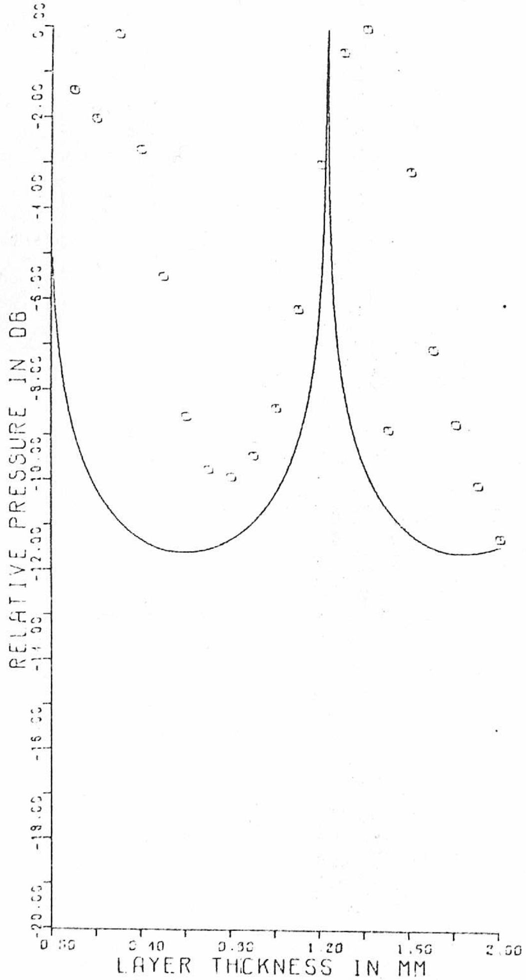

(d) 600 KHz

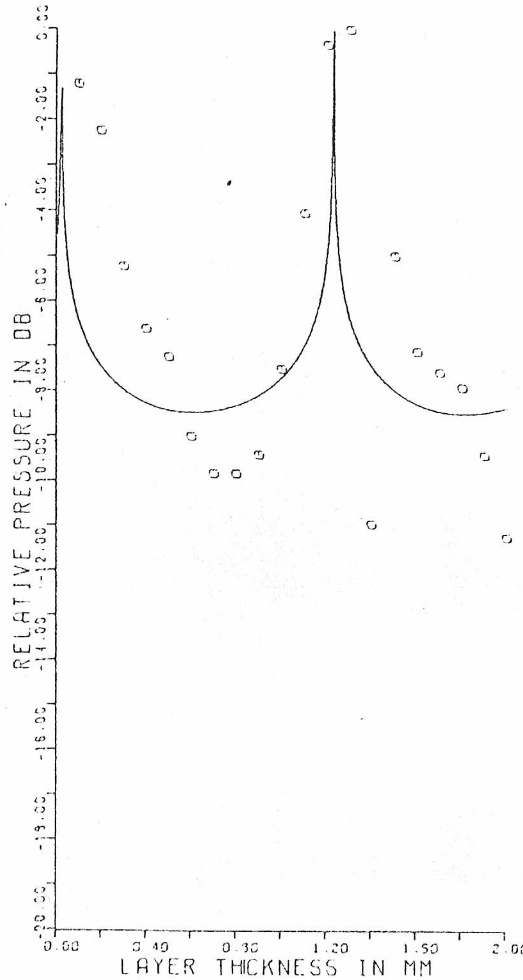

(e) 620 KHz

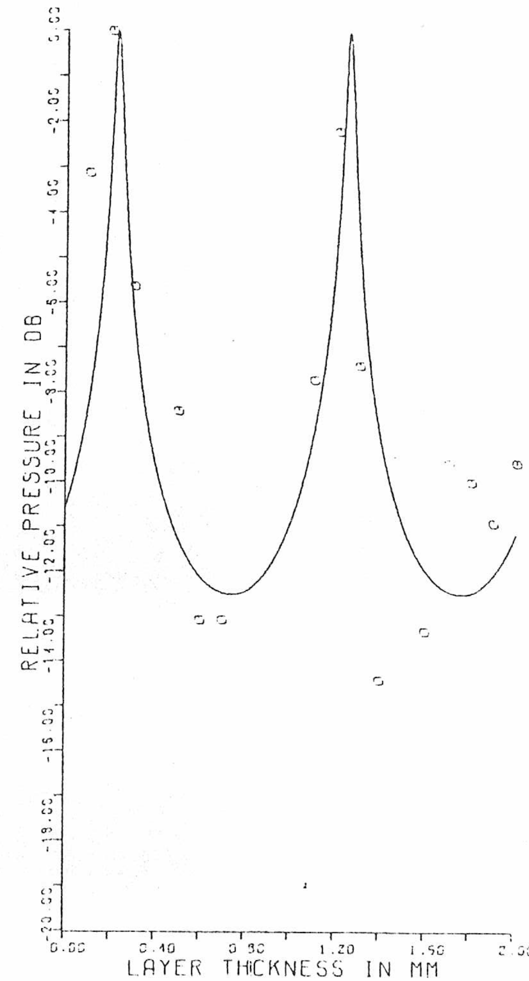

(f) 730 KHz

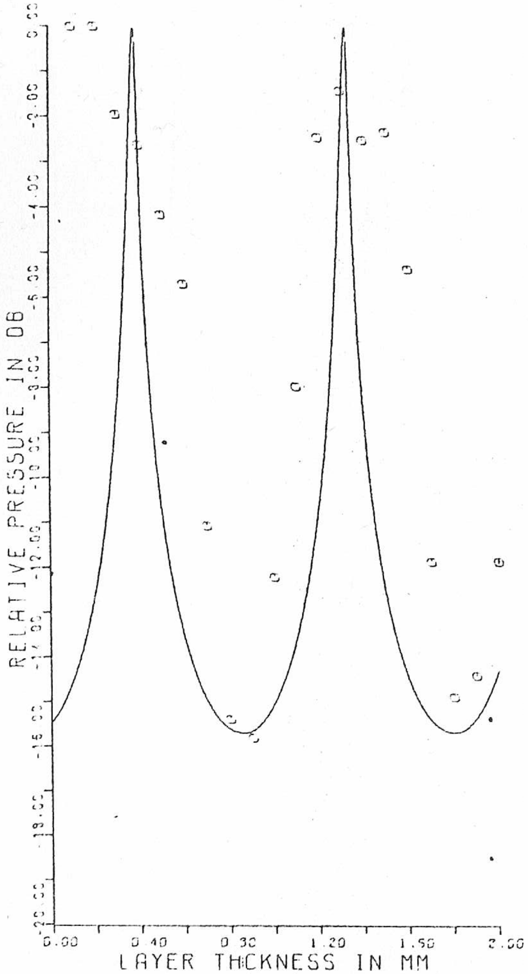

(g) 790 KHz

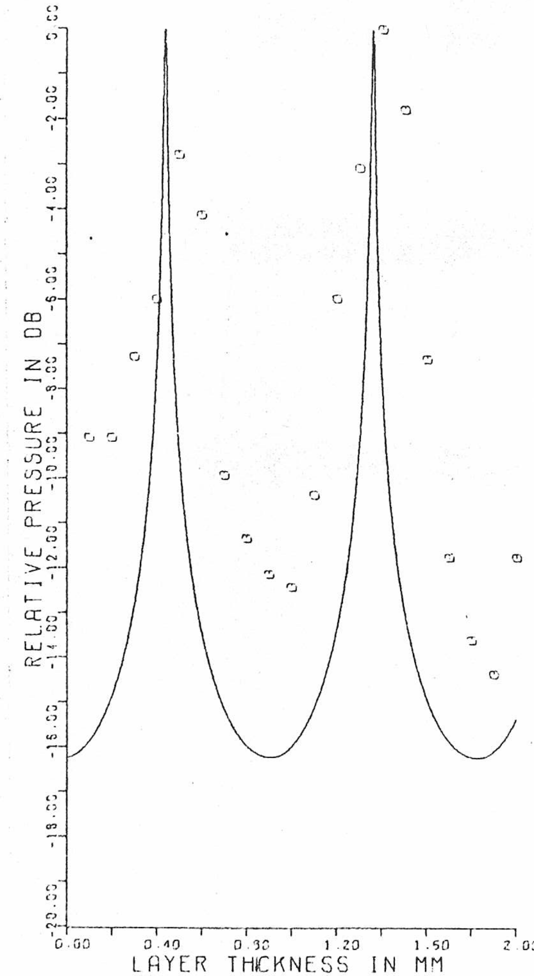

(h) 810 KHz

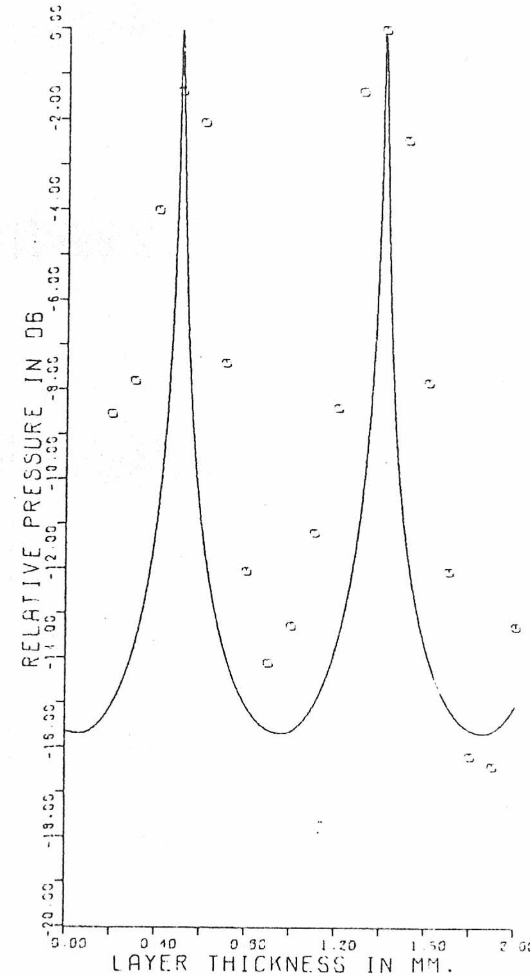

(i) 830 KHz

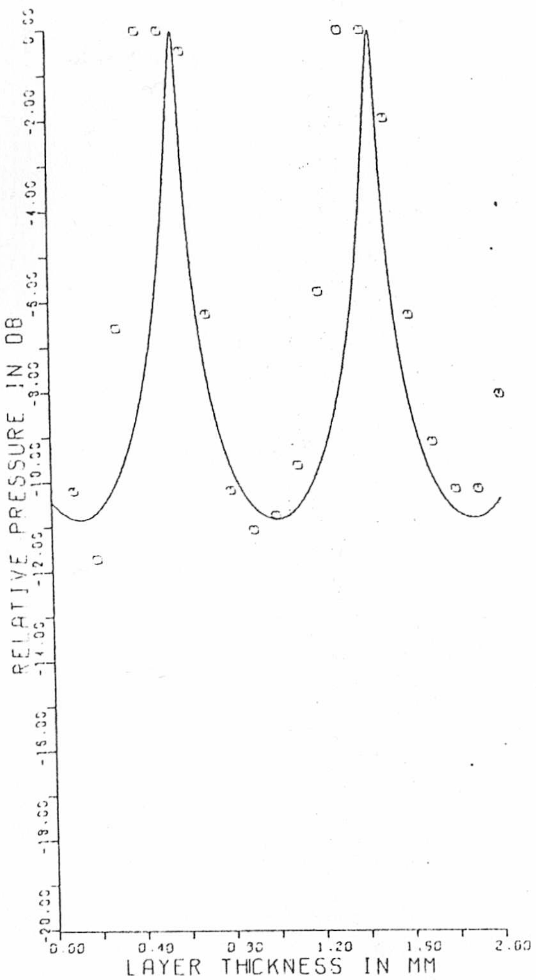

(j) 850 KHz

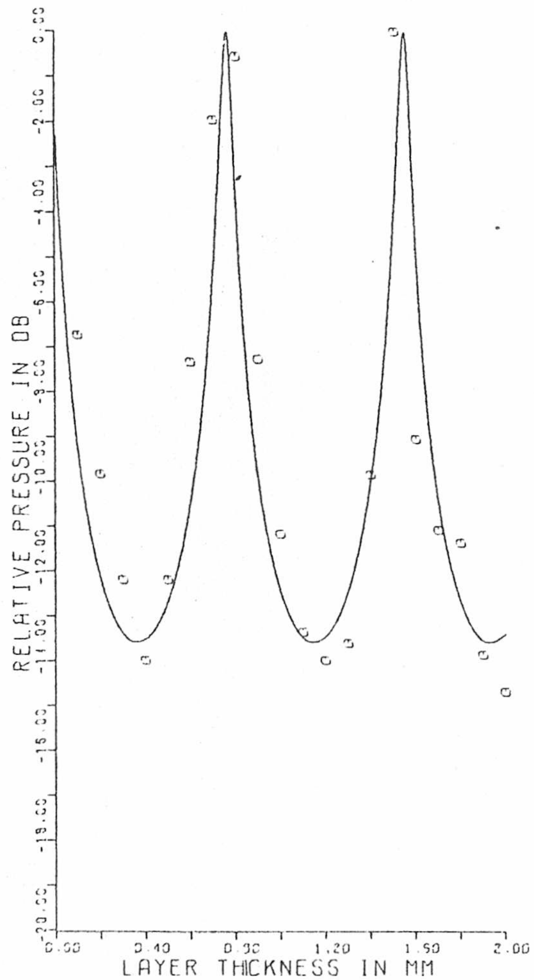

(k) 950 KHz

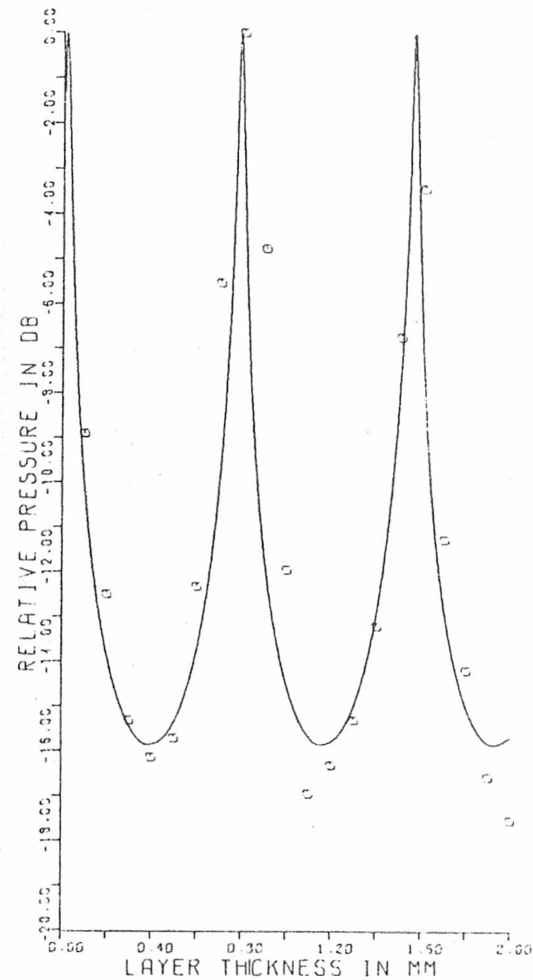

(ℓ) 970 KHz

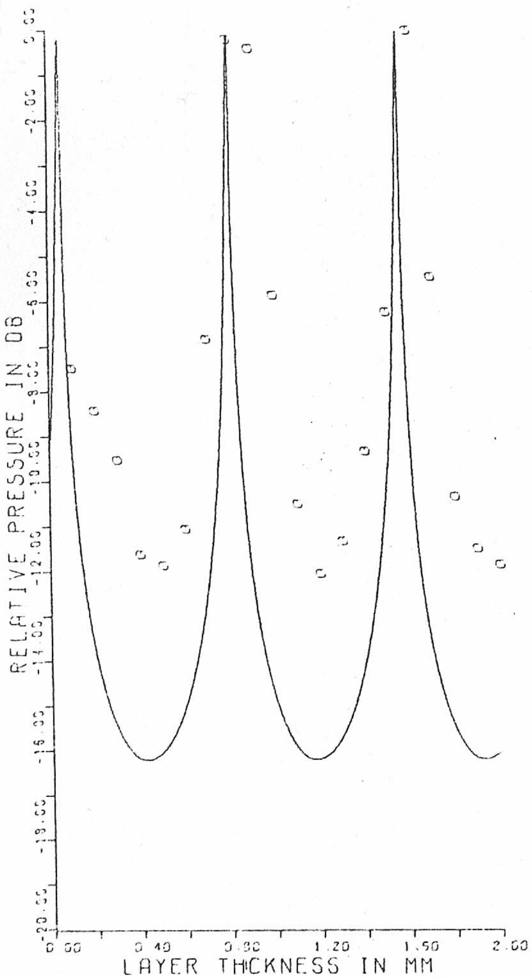

(m) 990 KHz

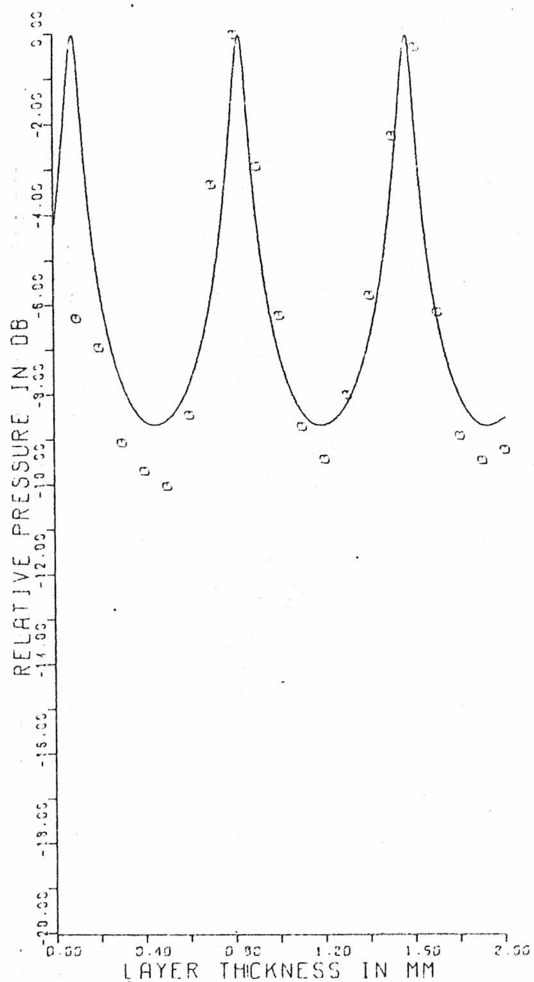

(n) 1010 KHz

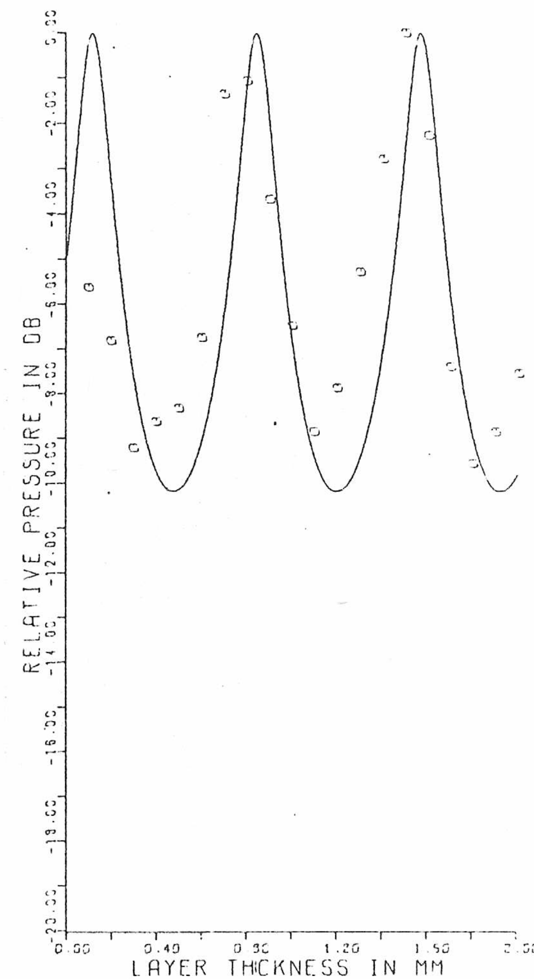

(o) 1030 KHz

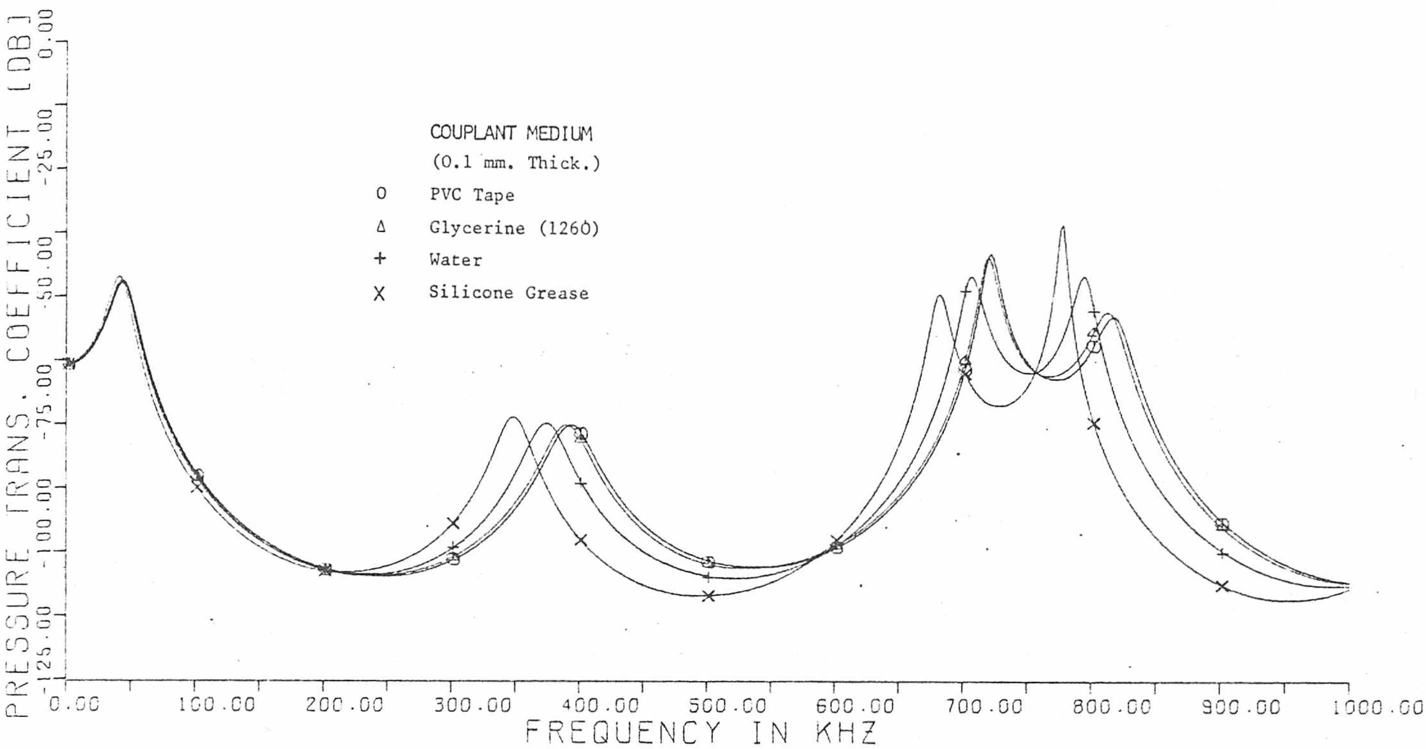

APPENDIX 5.J : Theoretically Calculated PTC Curves for Different Couplant Materials with 0.1 mm. Thickness and S750 Transducer Using The Five-layer Model. (Aluminium -Couplant - Epoxy (Shoe) - PZT- Air)

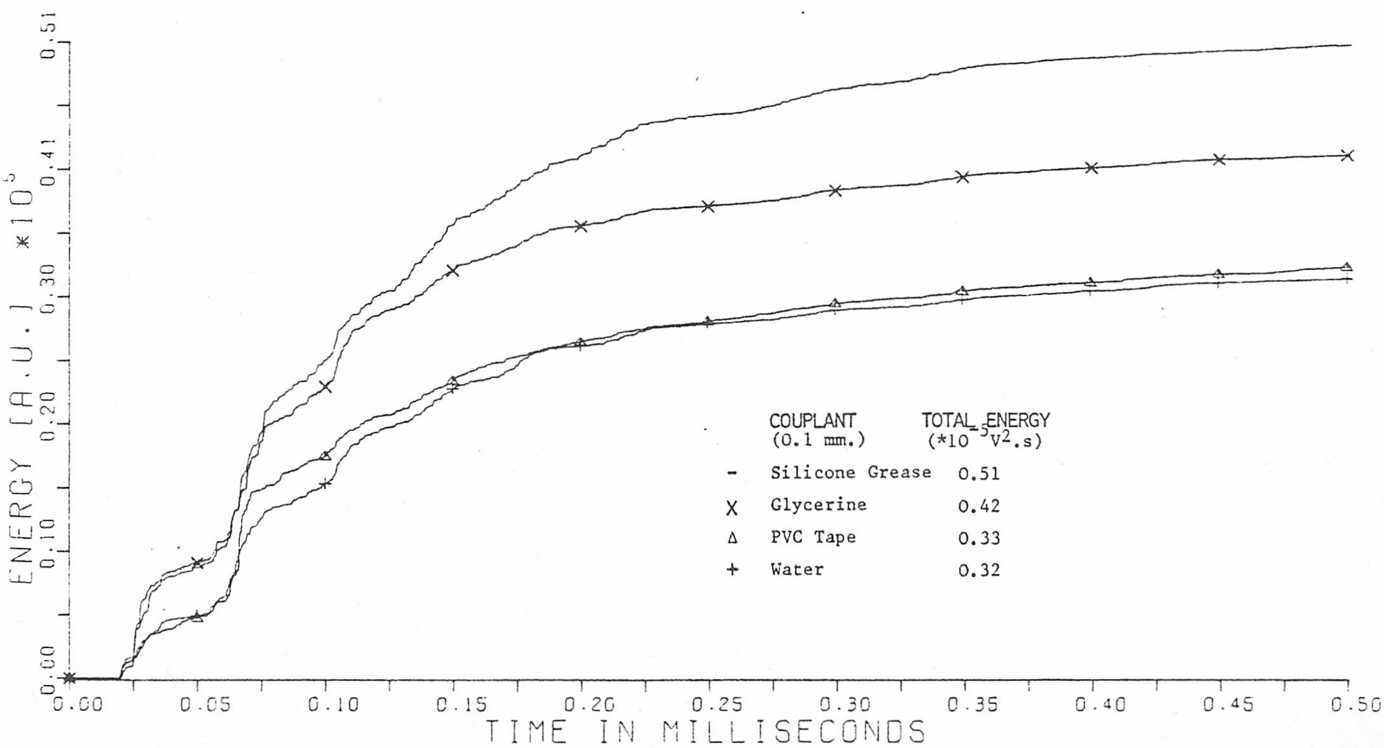

APPENDIX 5.J : Continued.

A Comparison Between The Pulse Energy for Different Couplant Materials Using the Same Source Signal.

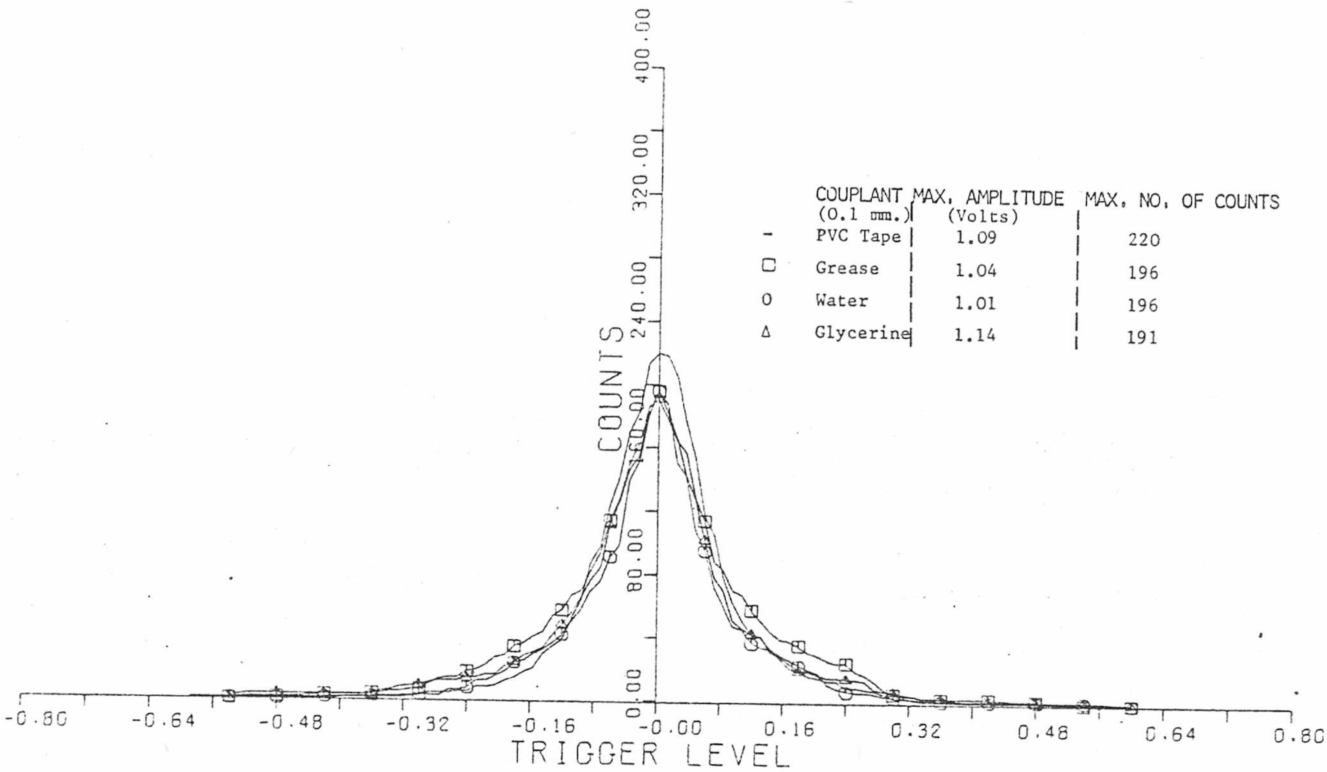

APPENDIX 5.J : Continued.

A comparison Between the Number of Counts versus Trigger Level and Burst Maximum Amplitude for Different Couplant Materials Using the Same Source Signal.

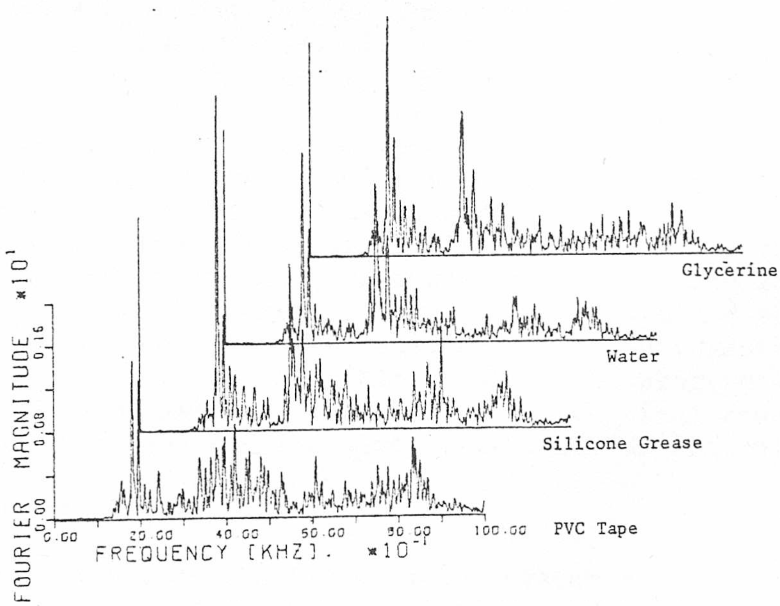

APPENDIX 5.J : Continued.

The Frequency Spectra from Similar A.E. Source (Eléctric Pulse : 30 ns Width, 200 Volts Amplitude and 5 ns Rise Time) for Different Couplant Materials of 0.1 mm. Thickness. Using S750 Transducer and the Air Couplant Block.

APPENDIX 5.K

SUGGESTED OPTIMIZATION METHOD FOR ACOUSTIC EMISSION TRANSDUCER DESIGN

A transmitting multilayer-system computer program, which is based on the number of the transducer components, is essential if any transducer design work is to be undertaken. The programming is not a difficult task, especially if one confines oneself to the case of normal incidence which has been described in Chapter Three. In addition to the standard requirements of calculating the PTC as a function of frequency, it is sometimes important that the program be capable of printing and plotting the phase on transmission for purpose of phase jumps inspection.

A brief general description of a typical simple program flow-chart is shown in the Figure.

The program inputs: transmission-system data, start and finish frequencies, the transducer resonance (central) frequency, and an integer number representing the number of frequency steps in between. From these data, the thickness of the PZT-element can be calculated. The program reads the transducer shoe thickness range to be tried and the appropriate thickness increment at this stage. The PTC and the transmission phase properties are then computed for all the frequencies in the frequency range and repeated for each shoe thickness in the thickness range. In addition to the PTC and phase the program will search for maximum and minimum PTC values and the corresponding frequencies. Then it integrates the area between the PTC curve and the minimum PTC value as a datum line.

As the whole thickness range is complete, the program prints the computed results and a summary will also be displayed on the computer terminal. According to the displayed results, the designer may look more closely at particular shoe thickness results, using smaller increments, or may change the transducer shoe thickness range and/or the frequency range. However, the second and subsequent shoe thickness and frequency ranges could be run without restarting the program. If no further ranges are required the program will open data-file (disk or magnetic tape) to store the final results of the last shoe thickness and frequency ranges for digital plotting.

Data Format and Variables:

i- Physical properties of the transmission system:-
Z1 the propagation medium characteristic impedance
Z2, VL2, L2 the couplant: characteristic impedance, longitudinal wave velocity and thickness
Z3, VL3, L3 the transducer shoe: characteristic impedance, longitudinal wave velocity and thickness
Z4, VL4, L4 the piezoelectric element (PZT): characteristic impedance, long. wave velocity and thickness
Z5 the backing material characteristic Impedance

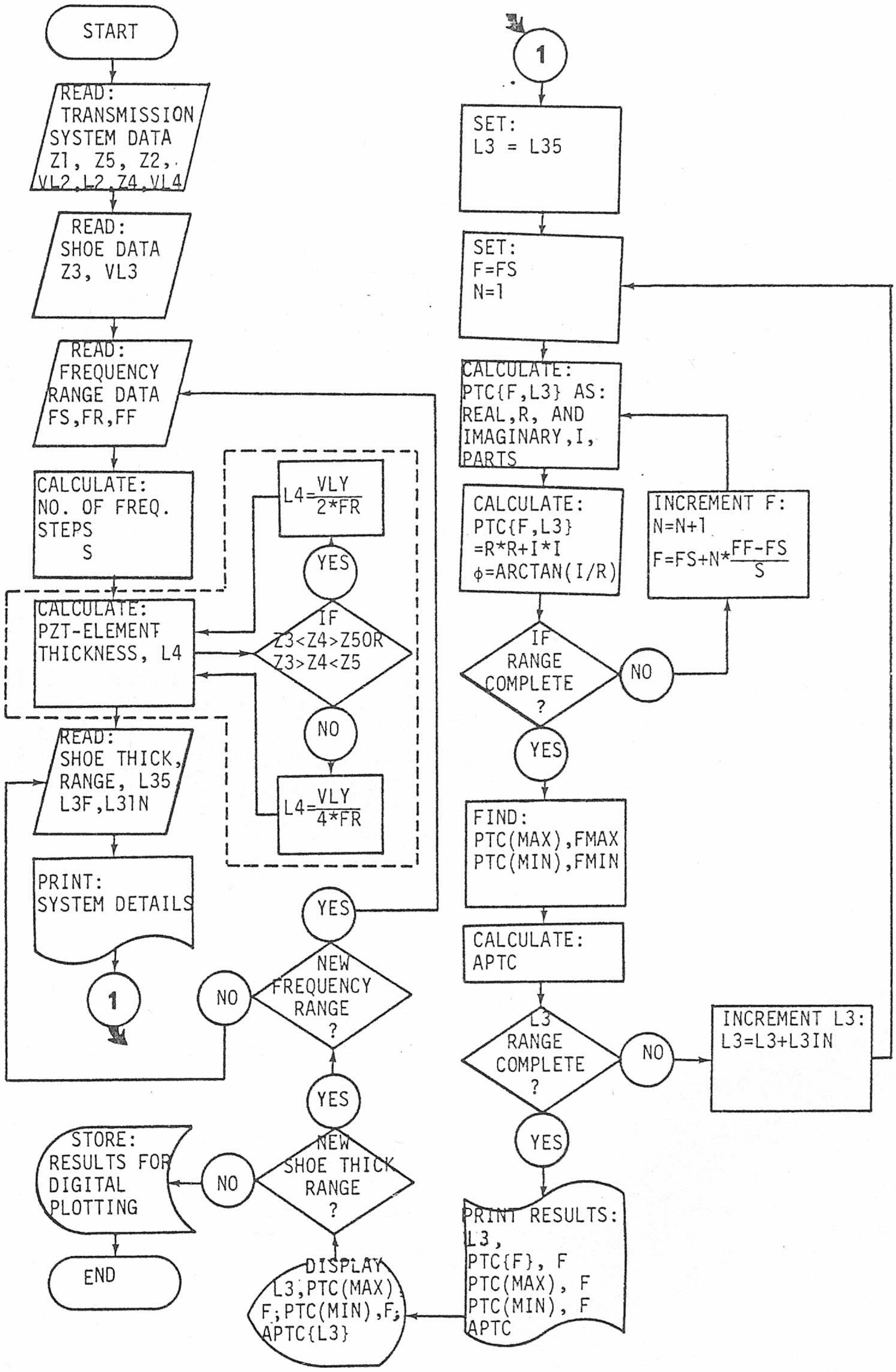

Flowchart for the suggested Transducer Optimization Program

ii- Frequency range:
FS start frequency
FR resonance frequency (or central) for the PZT-element
FF finish frequency
S is an integer such that the PTC values are evaluated for frequencies F(I):

$$F(1) = FS; \; F(2) = FS + \frac{FF-FS}{S}; \; F(3) = FS + 2\,\frac{FF-FS}{S}$$

.........; F(S + 1) = FF. That is S + 1 frequency points in all.

iii- Shoe thickness range:
L3S start transducer shoe thickness
L3F finish transducer shoe thickness
L3IN transducer shoe thickness increment.

X{Y} indicates X is a function of Y

APTC the total area between the PTC curve and a datum line defined as PTC (MIN)

ϕ the transmission phase.

The output will consist of tables of the system details; each one is followed by a table of F, PTC, ϕ for each of L3 value.

REFERENCES

(1) Spanner J.C. :'Acoustic Emission, Techniques and Applications', Intex Publishing Comp., 1974.

(2) Drouillard T.F. :'Acoustic Emission- A Bibliography for 1970-1972', Monitoring Structural Integrity by Acoustic Emission, ASTM STP 571, 1975, pp.241-84.

(3) Drouillard T.F. :'Acoustic Emission- A Bibliography with Abstracts', Plenum Publishing Comp., 1979.

(4) Lord A.E.Jr. :'Acoustic Emission', in Physical Acoustics, Mason, W.P. and Thurston, R.N., Eds., Academic Press, vol. 11, 1975, pp.289-353.

(5) Curtis G.J. :'Acoustic Emission-4: Spectral Analysis of Acoustic Emission', NDT Int., 7 (1974) 82-91.

(6) Ono K., Stern R. and Long M. Jr.:'Application of Correlation Analysis to Acoustic Emission', Acoustic Emission, ASTM STP 505, 1972, pp.152-63.

(7) Brown A.E. and Liptai R.G.:'Round Robin Testing of Acoustic Emission Source', Acoustic Emission, ASTM STP 505, 1972, pp.318-31.

(8) Speich G.R. and Schwoeble A.J.:'Acoustic Emission during Phase Transformation in Steel', Monitoring Structural Integrity by Acoustic Emission, ASTM STP 571, 1975, pp.40-58.

(9) Speich G.R. and Fisher R.M.:'Acoustic Emission during Martensite Formation', Acoustic Emission, ASTM STP 505, 1972, pp.140-51.

(10) Liptai R.G., Dunegan H.L. and Tatro C.A.: 'Acoustic Emissions Generated during Phase Transformations in Metals and Alloys', NDT Int., 1 (1969) 213-21.

(11) Mirabile M. :'Acoustic Emission Energy and Mechanisms of Plastic Deformation and Fracture', NDT Int., 8 (1975) 77-85.

(12) Dunegan H.L. and Green A.T.:'Factors Affecting Acoustic Emission Response from Materials', Acoustic Emission, ASTM STP 505, 1972, pp.100-13.

(13) Frederick J.R. and Felbeck D.K.:'Dislocation Motion as a Source of Acoustic Emission', Acoustic Emission, ASTM STP 505, 1972, pp.129-39.

(14) Gillis P.P. :'Dislocation Mechanisms as Possible Sources of Acoustic Emission', Mat. Res. Stand., 11 (March 1971) 11-3.

(15) Tandon K.N. and Tangri K.:'Acoustic Emissions during Deformation of Polycrystalline Silicon-Iron', Mater. Sci. Eng., 20 (1975) 47-54.

(16) Tandon K.N. and Tangri K.:'An Acoustic Emission Study on Deformation Behaviour of Strain-aged Polycrystalline Samples of Fe-3% Si', Mater. Sci. Eng., 29 (1977) 37-40.

(17) Agarwal A.B.L., Frederick J.R. and Felbeck D.K.:'Detection of Plastic Microstrain in Aluminium by Acoustic Emission', Met. Trans., 1 (1970) 1069-71.

(18) Knott J.F. :'Fundamentals of Fracture Mechanics', Butterworths, London, 1973.

(19) Brindley B.J., Holt J. and Palmer I.G.:'Acoustic Emission-3: The Use of Ring-down Counting', NDT Int., 6 (1973) 299-306.

(20) Swindlehurst W. :'Acoustic Emission-1: Introduction', NDT Int., 6 (1973) 152-8.

(21) Green A.T. :'Detection of Incipient Failures in Pressure Vessels by Stress-Wave Emission', Nuclear Safety, 10 (February 1969) 4-18.

(22) Hutton P.H. :'Acoustic Emission in Metals as an NDT Tool', Mat. Eval., 26 (July, 1968) 125-9.

(23) Mason W.P., McSkimin H.J. and Shockley W.:'Ultrasonic Observations of Twinning in Tin', Phys. Rev., 73 (1948) 1213-14.

(24) Engle R.B. and Dunegan H.L.:'Acoustic Emission: Stress Wave Detection as a Tool for NDT and Material Evaluation', NDT Int., 1(1969) 109-25.

(25) Radon J.C. and Pollock A.A.:'Acoustic Emissions and Energy Transfer during Crack Propagation', Eng. Fract. Mech., 4 (1972) 295-310.

(26) Hill R. and Stephens R.W.B.:'Simple Theory of Acoustic Emission: A Consideration of Measurement Parameters', Acustica, 31 (1974) 224-30.

(27) Tetelman A.S. :'Acoustic Emission Testing and Microfracture Processes', Mat. Res. Stand., 11 (March, 1971) 13-6.

(28) Pollock A.A. :'Stress-Wave Emission in NDT', NDT Int., 2 (1969) 178-82.

(29) Scruby C.B. and Wadley H.N.G.:'A Calibrated Capacitance Transducer for the Detection of Acoustic Emission', J. Phys. D.: Appl. Phys., 11 (1978) 1487-94.

(30) Curtis G.J. :'A Broadband Polymeric Foil Transducer', Ultrasonics, 12 (1974) 148-54.

(31) Speake J.H. :'An Absolute Method of Calibrating Ultrasonic Transducers Using Laser Interferometry', Conf. on The Evaluation and Calibration of Ultrasonic Transducers, London, May 11-12, 1977, 1PC Press, pp.106-14.

(32) Scruby C.B., Collingwood J.C. and Wadley H.N.G.:'A New Technique for the Measurement of Acoustic Emission Transients and their Relationship to Crack Propagation', J. Phys. D.: Appl. Phys., 11 (1978) 2359-70.

(33) Palmer C.H. and Green R.E. Jr.:'Materials Evaluation by Optical Detection of Acoustic Emission Signals', Mat. Eval., 35 (Oct. 1977) 107-12.

(34) Palmer C.H. and Green R.E. Jr.:'Optical Detection of Acoustic Emission Waves', Appl. Opt., 16 (1977) 2333-4.

(35) Hill R. and Stephens R.W.B.:'Acoustic Emission-Evaluation of Transducers and Measuring Systems', Ultrasonics Int., 1973 Conf. Proc., pp.177-82.

(36) Goliamina I.P. :'On the Problem of Axial Oscillations of Polarized Barium Titanate Plates', Sov. Phys. - Acoustics J., 1 (1955) 42-9.

(37) Hueter T.F. and Dozois E.:'The Frequency Response of Barium Titanate Transducers', J.Acoust. Soc. Am., 24 (1952) 85-6.

(38) Shaw E.A.G. :'On the Resonant Vibrations of Thick Barium Titanate Disks', J. Acoust. Soc. Am., 28 (1956) 38-50.

(39) Shaw E.A.G. and Sujir R.J.:'Vibration Patterns of Loaded Barium Titanate and Quartz Disks', J. Acoust. Soc. Am., 32 (1960) 1463-7.

(40) Mason W.P. :'Electromechanical Transducers and Wave Filters', Van Nostrand, Princeton, 1948.

(41) Kossoff G. :'The Effects of Backing and Matching on the Performance of Piezoelectric Transducers', IEEE-SU13 (1966) 20-30.

(42) Bell R.L. :'Acoustic Emission Transducer Calibration: Transient Pulse Method', Tech. Report DE-73-3, Dunegan/Endevco, Livermore, Calif., Feb. 1973.

(43) McBride S.L. and Hutchison T.S.:'Helium Gas Jet Spectral Calibration of Acoustic Emission Transducers and Systems', Can. J. Phys., 54 (1976) 1824-30.

(44) Leschek W.C. :'Acoustic Emission Transducer Calibrator', Mat. Eval., 33 (Feb. 1975) 41-8.

(45) Hatano H. and Mori E.:'Acoustic-Emission Transducer and its Absolute Calibration', J. Acoust. Soc. Am., 59 (1976) 344-9.

(46) Gericke O.R. :'Experimental Determination of Ultrasonic Transducer Frequency Response', Mat. Eval., 24 (Aug., 1966) 409-11.

(47) Hill R. and Adams N.L.:'Reinterpretation of the Reciprocity Theorem for the Calibration of Acoustic Emission Transducers Operating on a Solid', Acustica, 43 (1979)305-12.

(48) Hill R. and Adams N.L. :'A Review of Techniques for the Calibration of Acoustic Emission Transducers', Proc. of the Inst. of Acoustics, 1977.

(49) Breckenridge F.R., Tschiegg C.E. and Greenspan M.:'Acoustic Emission:Some Applications of Lamb's Problem', J. Acoust. Soc. Am., 57 (1975) 626-31.

(50) Hsu N.N., Simmons J.A. and Hardy S.C.: 'An Approach to Acoustic Emission Signal Analysis - Theory and Experiments', Mat. Eval., 35 (Oct., 1977) 100-6.

(51) Harris D.O., Tetelman A.S. and Darwish F.A.:'Detection of Fiber Cracking by Acoustic Emission', Acoustic Emission, ASTM STP 505, 1972, pp.238-49.

(52) Tetelman A.S. and Chow R.:'Acoustic Emission Testing and Microcracking Processes', Acoustic Emission, ASTM STP 505, 1972, pp.30-40.

(53) Pollock A.A. :'Ringdown Versus Energy', Proc. of the 3rd Meeting EWGAE-ISPRA, Sept. 25-26, 1974, pp.144-6.

(54) Gillis P.P. and Hamstad M.A.:'Some Fundamental Aspects of the Theory of Acoustic Emission', Mater. Sci. Eng., 14 (1974) 103-8.

(55) Hill R. and El-Dardiry S.M.A.:'The Effect of Geometry on Acoustic Emission', Proc. of the Inst. of Acoustics, 1976.

(56) Dumousseau P.F. :'Statistical Study of Ring-down Counting Techniques for Characterization of Materials. Influence of Peak Amplitude Function', Proc. of the 3rd. Meeting EWGAE-ISPRA, Sept. 25-26, 1974, pp.141-3.

(57) Palmer I.G. and Heald P.T.:'The Application of Acoustic Emission Measurements to Fracture Mechanics', Mater. Sci. Eng., 11 (1973) 181-4.

(58) Ying S.P. and Grigory S.C.:'Acoustic Emission from Flowed Heavy Section Steel Plates', Mat. Eval., 33 (Feb., 1975) 30-6.

(59) Green A.T. and Dunegan H.L.:'Acoustic Emission Analysis of Crack Propagation and Fracture in Pressure Vessels and Pressure Vessel Materials', Technical Report DE 72-1, Dunegan Corporation, Calif., 1972.

(60) Dunegan H.L., Harris D.O. and Tatro C.A.:'Fracture Analysis by Use of Acoustic Emission', Eng. Fract. Mech., 1 (1968) 105-22.

(61) Dunegan H.L. and Harris D.O.:'Acoustic Emission - a New Nondestructive Testing Tool', Ultrasonics, 7 (1969) 160-6.

(62) Nakamura Y., Veach C.L. and McCauley B.O.:'Amplitude Distribution of Acoustic Emission Signals', Acoustic Emission, ASTM STP 505, 1972, pp.164-86.

(63) Ono K. :'Amplitude Distribution Analysis of Acoustic Emission Signals', Mat. Eval., 34 (Aug., 1976) 177-81, 184.

(64) Ono K. :'Acoustic Emission and Microscopic Deformation, and Fracture Processes', The 2nd. Acoustic Emission Symposium, Tokyo, Sept. 2-4, 1974.

(65) Arii M., Kashiwaya H. and Yanuki T.:'Slow Crack Growth and Acoustic Emission Characteristics in COD Test', Eng. Fract. Mech., 7 (1975) 551-6.

(66) Sinclair A.C.E., Formby C.L. and Connors D.C.:'Fatigue Crack Assessment from Proof Testing and Continuous Monitoring', Acoustic Emission, Proc. of the Int. Inst. of Welding Colloquium, Tel Aviv, 1975, pp.51-64.

(67) Bolin L. :'A Model for Estimating the Signal from an Acoustic Emission Source', Ultrasonics, 17 (1979) 67-70.

(68) Desai J.D. and Gerberich W.W.:'Analysis of Incremental Cracking by Stress-Wave Emission Technique', Eng. Fract. Mech., 7 (1975) 153-65.

(69) Sinclair A.C.E., Connors D.C. and Formby C.L.:'Acoustic Emission Analysis during Fatigue Crack Growth in Steel', Mater. Sci. Eng., 28 (1977) 263-73.

(70) Clarck G.C. and Knott J.F.:'Acoustic Emission and Ductile Crack Growth in Pressure-Vessel Steels', Met. Sci., 11 (1977) 531-6.

(71) Pollock A.A. :'Acoustic Emission-2: Acoustic Emission Amplitudes', NDT Int., 6 (1973) 264-9.

(72) Palmer I.G., Holt J. and Goddard D.J.:'Acoustic Emission Measurements on Type 316 Stainless Steel', Proc. of the 3rd. Meeting EWGAE-ISPRA, Sept. 25-26, 1974, pp.11-26.

(73) Gerberich W.W., Atteridge D.G. and Lessar J.F.:'An Acoustic Emission Investigation of Microscopic Ductile Fracture', Met. Trans. A, 6A (1975) 797-801.

(74) Ishikawa K. and Kim H.C.:'Stress Wave Emission and Plastic Work of Notched Specimens', J. Mat. Sci., 9 (1974) 737-43.

(75) Curtis G.J. :'Acoustic Emission in Stressed Epoxy Bonded Structures', Final Report AERE-R 7684, March, 1974.

(76) Beattie A.G. and Jaramillo R.A.:'The Measurement of Energy in Acoustic Emission', Rev. Sci. Instr., 45 (1974) 352-7.

(77) Harris D.O. and Bell R.L.:'The Measurement and Significance of Energy in Acoustic Emission Testing', Report DE-74-3A, Dunegan/Endevco, Calif., 1974.

(78) Hamstad M.A. and Mukherjee A.K.:'The Dependence of Acoustic, Emission on Strain Rate in 7075-T6 Aluminium', Exp. Mech., 14 (Jan., 1974) 33-41.

(79) Hamstad M.A. and Mukherjee A.K.:'Acoustic Emission vs. Strain and Strain Rate: Measurement and Dislocation Theory Model for Dispersion-Strengthened Aluminium Alloy', Report UCRL-76077, Oct. 5, 1974.

(80) Stephens R.W.B. and Pollock A.A.:'Waveforms and Frequency Spectra of Acoustic Emissions', J. Acoust. Soc. Am., 50 (1971) 904-10.

(81) Woodward B. and Harris R.W.:'The Use of Signal Analysis to Identify Sources of Acoustic Emission', Acustica, 37 (1977) 190-7.

(82) Ono K. and Ucisik J.:'Acoustic Emission Behaviour of Aluminium Alloys', Mat. Eval., 34 (Feb., 1976) 32-44.

(83) Graham L.J. and Alers G.A.:'Acoustic Emission in the Frequency Domain', Monitoring Structure Integrity by Acoustic Emission, ASTM STP 571, 1975, pp.11-39.

(84) Graham L.J. and Alers G.A.:'Spectrum Analysis of Acoustic Emission in A533-B Steel', Mat. Eval., 32 (Feb., 1974) 31-7.

(85) Fleischmann P., Rouby D., Lakestani F. and Baboux J.C.:'A Spectrum Analysis of Acoustic Emission', NDT Int., 8 (1975) 241-4.

(86) Egle D.M. and Tatro C.A.:'Analysis of Acoustic Emission Strain Waves', J. Acoust. Soc. Am., 41 (1967) 321-7.

(87) Bassim M.N., Hay D.R. and Lanteigne J.:'Waveform Analysis of Acoustic Emission Signals from a Mild Steel', Mat. Eval., 34 (May, 1976) 109-13.

(88) Asty M. :'Acoustic Emission Source Location on a Spherical or Plane Surface', NDT Int., 11 (1978) 223-6.

(89) Tobias A. :'Acoustic-Emission Source Location in Two Dimensions by an Array of Three Sensors', NDT Int., 9 (1976) 9-12.

(90) Brihmadesam J.S. and McCormick N.J.:'Acoustic Emission Analysis of Stress Corrosion Cracking in Type 304 Stainless Steels' Nucl. Tech., 29 (1976) 127-35.

(91) Smith S. and Morton T.M.:'Acoustic Emission Detection Techniques for High Cycle-fatigue Testing', Exp. Mech., 13 (1973) 193-8.

(92) Egle D.M. :'Detecting High Cycle Fatigue Crack Growth Using Acoustic Emission', Fracture and Flaws 13th. Annual Symposium, ASME, Albuquerque, March 1-2, 1973.

(93) Guz I.S. and Zotov A.O.:'Emission of Elastic Waves During Crack Growth in Steel that has Passed through Different Heat Treatments', Strength of Materials, 6 (1974) 461-3.

(94) Bell R.L. :'A Progress Report on the Use of Acoustic Emission to Detect Incipient Failure in Nuclear Pressure Vessels', Tech. Report DE-74-1 Dunegan/Endevco, Calif., January 1974.

(95) Bunsell A.R. :'Acoustic Emission for Proof Testing of Carbon Fiber-Reinforced Plastics', NDT Int., 10 (1977) 21-5.

(96) Rotem A. and Baruch J.:'Determining the Load Time History of Fibre Composite Materials by Acoustic Emission', J. Mat. Sci., 9 (1974) 1789-96.

(97) Kelly M.P., Harris D.O. and Pollock A.A.:'Detection and Location of Flaw Growth in Metallic and Composite Structure', Monitoring Structure Integrity by Acoustic Emission, ASTM STP 571, 1975, pp.221-40.

(98) Dean D.S. and Kerridge L.A.:'An Immersion-Technique for the Detection of Acoustic Emission in Carbon-Fibre Reinforced Plastics Pressure Vessels', NDT Int., 9 (1976) 233-8.

(99) Pollock A.A. :'AE Monitoring of Natural and Artificial Defects in the KEMA Vessel', Report DE/74-7, Dunegan/Endevco, Calif., Sept. 1974.

(100) Birchon D., Dukes R. and Taylor J.:'Acoustic Emission Monitoring of a Pressure Vessel', in Periodic Inspection of Pressurized Components, The Inst. of Mech. Eng., 1975, pp.88-94.

(101) Obata Y. and Bentley P.G.:'Acoustic Emission Test on A 1 Meter Diameter Pressure Vessel with a 60% Artificial Defect', the 7th. Meeting of EWGAE-RISLEY, Oct. 18-20, 1978.

(102) Watanabe T., Hashirizaki S. and Arita H.:'Acoustic-Emission Inspection during Water-pressure Testing of Pressure Vessels', NDT Int., 9 (1976) 227-32.

(103) Gopal R. :'Acoustic Monitoring Systems to Assure Integrity of Nuclear Plants', Monitoring Structural Integrity by Acoustic Emission, ASTM STP 571, 1975, pp.200-20.

(104) Hay D.R., Bassim M.N. and Dunbar D.:'In-Service Acoustic Emission Monitoring of a Steam-Methane Reformer Furnace', Mat. Eval., 34 (Jan., 1976) 20-4.

(105) Jolly W.D. :'Acoustic Emission Exposes Cracks During Welding', Weld. J., 48 (Jan., 1969) 21-7.

(106) Hartbower C.E., Reuter W.G., Morais C.F. and Crimmins P.P.: 'Use of Acoustic Emission for the Detection of Weld and Stress Corrosion Cracking', Acoustic Emission, ASTM STP 505, 1972, pp.187-221.

(107) Prine D.W. :'Inspection of Nuclear Power Component Welds by In-process Acoustic Emission Monitoring', NDT Int., 9 (1976) 281-4.

(108) Romrell D.M. :'Acoustic Emission Monitoring of the FFTF Reactor Fuel Pin End Closure Welds', Mat. Eval., 30 (Dec., 1972) 254-8.

(109) Romrell D.M. :'Acoustic Emission Weld Monitoring of Nuclear Components', Weld. J., 52 (Feb., 1973) 81-7.

(110) Compton M.R. :'A Real-Time Software Operating System for a Computer-Controlled Acoustic Emission Flaw Monitor', Mat. Eval., 31 (July, 1973) 121-7.

(111) McElroy J.W. :'Development of Acoustic Emission Testing for the Inspection of Gas Distribution Pipelines', Monitoring Structural Integrity by Acoustic Emission, ASTM STP 571, 1975, pp.59-79.

(112) Stahlkopf K.E. and Dau G.J.:'Acoustic Emission: A Critical Assessment', Nuclear Safety, 17 (Jan.-Feb., 1976) 33-42.

(113) Hill R. and El-Dardiry S.M.A.:'The Influence of Transducer Couplant thickness on Acoustic Emission Parameters', Proc. of the Inst. of Acoustics, 1977.

(114) Hill R. and El-Dardiry S.M.A.:'Variables in the Use and Design of Acoustic Emission Transducers', Proc. of the Int. Conf. on Acoustic Emission, Anaheim, Calif., Sept. 10-13, 1979.

(115) Kroll R.J. :'Stress Waves in Test Specimens due to Simulated Acoustic Emission', Ph.D. Dissertation, Michigan State Univ., 1962.

(116) Fowler K.A. and Papadakis E.P.:'Observation and Analysis of Simulated Ultrasonic Acoustic Emission Waves in Plates and Complex Structures', Acoustic Emission, ASTM STP 505, 1972, pp.222-37.

(117) Fitch, C.E. Jr.:'Acoustic Emission Signal Analysis in Flat Plates', Report BNWL-1008-UC-37 Instruments, April 1969.

(118) Meeker T.R. and Meitzier A.H.:'Guided Wave Propagation in Elongated Cylinders and Plates', in Physical Acoustics, Mason W.P., Ed., Academic Press, vol. 1-A, 1964, pp.111-67.

(119) Mayer W.G. :'Energy Partition of Ultrasonic Waves at Flat Boundaries', Ultrasonics, 3 (1965) 62-8.

(120) Krautkrämer J. and Krautkrämer H.:'Ultrasonic Testing of Materials', Springer-Verlag, 1969.

(121) Birchon D. :'The Potential of Acoustic Emission in NDT', Brit. J. NDT, 18 (1976) 66-70.

(122) Granato A. and Lücke K.:'Theory of Mechanical Damping due to Dislocations', J. Appl. Phys., 27 (1956) 583-93.

(123) Egle D.M. and Brown A.E.:'Considerations for the Detection of Acoustic Emission Waves in Thin Plates', J. Acoust. Soc. Am., 57 (1975) 591-7.

(124) Viktorov I.K. :'Rayleigh and Lamb Waves', Plenum Press, 1967.

(125) Press F. and Healy I.:'Absorption and Rayleigh Waves in Low-loss Media', J. Appl. Phys., 28 (1957) 1323-5.

(126) Tsoi E. and Egle D.M.:'The Influence of Surface Condition on the Acoustic Emission from Aluminium under Cyclic Loading', The 38th National ASNT Fall Conf., Denver, Oct. 2-5, 1978.

(127) Ying S.P. :'Effect of Crack Size on Acoustic Emission Related to Moving Dislocations', J. Appl. Phys., 46 (1975) 2882-8.

(128) Woodward B. :'Identification of Acoustic Emission Source Mechanisms by Energy Spectrum Analysis', Ultrasonics, 14 (1976) 249-55.

(129) Papoulis A. :'Signal Analysis', McGraw-Hill Co., 1977.

(130) Papoulis A. :'Probability, Random Variables, and Stochastic Processes', McGraw-Hill Co., 1965.

(131) Otnes R.K. and Enochson L.:'Digital Time Series Analysis', A Wiley-Interscience, 1972.

(132) Meyer S.L. :'Data Analysis for Scientists and Engineers', John Wiley & Sons Inc., N.Y., 1975.

(133) Newland D.E. :'An Introduction to Random Vibrations and Spectral Analysis', Longman Group Ltd., London, 1975.

(134) Bendat J.S. and Piersol A.G.:'Random Data: Analysis and Measurement Procedures', John Wiley & Sons Inc., N.Y., 1971.

(135) Rice S.O. :'Mathematical Analysis of Random Noise', Bell. Syst. Tech. J., 33 (1944) 282-332, and, 24 (1945) 46-156.

(136) Hamstad M.A. :'On Energy Measurement of Continuous Acoustic Emission', Report UCRL-76286, Dec. 26, 1974.

(137) Hutton P.H. :'Acoustic Emission Applied Outside of the Laboratory', Acoustic Emission, ASTM STP 505, 1972, pp.114-28.

(138) Singleton R.C. :'An Algorithm for Computing the Mixed Radix Fast Fourier Transform', IEEE Trans., AU-17 (1969) 93-103.

(139) Cooley J.W. and Tukey J.W.:'An Algorithm for the Machine Calculation of Complex Fourier Series', Mathematics of Computation, 19 (1965) 297-301.

(140) Beattie A.G. :'Energy Analysis in Acoustic Emission', Mat. Eval., 34 (April 1976) 73-8.

(141) Ono K., Landy R. and Ouchi C.:'On Amplitude Distribution of Burst Emission due to MnS Inclusions in HSLA Steels', Technical Report UCLA 78-03, July 1978.

(142) Onoe M. :'Japanes Experience in Laboratory and Practical Applications of Acoustic Emission to Welded Structures', Acoustic Emission, Proc. of the Int. Inst. of Welding Colloquium, Tel Aviv, 1975, pp.75-101.

(143) Lindsay R.B., Lewis C.R. and Albright R.D.:'Acoustic Filtration in Non-Homogeneous Media', J. Acoust. Soc. Am., 5 (1934) 202-5.

(144) Lindsay R.B. :'Filtration of Oblique Elastic Waves in Stratified Media', J. Acoust. Soc. Am., 11 (1939) 178-83.

(145) Thomson W.T. :'Transmission of Elastic Waves through a Stratified Solid Medium', J. Appl. Phys., 21 (1950) 89-93.

(146) Haskell N.A. :'The Dispersion of Surface Waves on Multilayered Media', Bull. Seism. Soc. Am., 43 (1953) 17-34.

(147) Barnard G.R., Bardin J.L. and Whiteley J.W. :'Acoustic Reflection and Transmission Characteristics for thin Plates', J. Acoust. Soc. Am., 57 (1975) 577-84.

(148) Brekhovskikh L.M. :'Waves in Layered Media', Academic Press, 1960.

(149) Cook R.L. and Lovejoy R.E. :'Acoustic Properties of Epoxy-Fiberglas and Epoxy-Fiberglas-Pb Plates in the Frequency Range 100-700 KHz', J. Acoust. Soc. Am., 57 (1975) 1554-8.

(150) Folds D.L. and Loggins C.D.:'Transmission and Reflection of Ultrasonic Waves in Layered Media', J. Acoust. Soc. Am., 62 (1977) 1102-9.

(151) Kinsler L.E. and Frey A.R.:'Fundamentals of Acoustics', Chapter 6, John Wiley & Sons, Inc., 1962.

(152) Redwood M. :'A Study of Waveforms in the Generation and Detection of Short Ultrasonic Pulses', Appl. Mat. Res., (April, 1963) 76-84.

(153) Lakestani F., Baboux J.C. and Fleischmann P.:'Broadening the Bandwidth of Piezoelectric Transducers by Means of Transmission Lines', Ultrasonics, 13 (1975) 176-80.

(154) Redwood M. :'Transient Performance of a Piezoelectric Transducer', J. Acoust. Soc. Am., 33 (1961) 527-36.

(155) Klerk J. de. :'Thin-Film Piezoelectric Transducers used as Generators and Detectors of Microwave Phonons, with Some Attenuation Measurements in SiO_2', J. Appl. Phys., 37 (1966) 4522-8.

(156) Canella G. :'Resonances and Effects of Couplant Layers in Ultrasonic Contact Testing', Mat. Eval., 31 (April, 1973) 61-6.

(157) Altman H.E. and Beyer R.T.:'Effect of the Parallel Reflecting Surfaces of a Transducer on the Resulting Pulse Shape', J. Acoust. Soc. Am., 59 (1976) 545-50.

(158) Pollock A.A. :The Director of Research and Application of Dunegan/Endevco, Calif., Private Communications, 1977, 1978.

(159) Hamstad M. :At Lawrence Livermore Lab., Calif., Private Communication, 1977.

(160) Peled A. and Liu B. :'Digital Signal Processing', John Wiley & Sons, Inc., 1976.

(161) :'Technical Report on Recommended Practices for Burst Measurements in the Frequency Domain', IEEE Trans., AU15 (1967) 4-14.

(162) Foster F.S. and Hunt J.W.:'The Design and Characterization of Short Pulse Ultrasound Transducers', Ultrasonics, 16 (1978) 116-22.

(163) Speake J. H. :At the NDT Centre, AERE, Harwell, (now with Pantatron Systems Limited, Motherwell HQ), Private Communication, 1978.

(164) Hartman W.F. :'Towards Standards for Acoustic Emission Technology', Nondestructive Testing Standards - A Review, ASTM STP 624, Harold Berger, Ed., 1977, pp.138-45.

(165) Tolstoy I. and Eusdin E.:'Wave Propagation in Elastic Plates: Low and High Modes Dispersion', J.Acoust. Soc. Am., 29 (1957) 37-42.

(166) Pao Y.H. Gajewski R.R. and Ceranoglu A.N.:'Acoustic Emission and Transient Waves in an Elastic Plate', J. Acoust. Soc. Am., 65 (1979) 96-105.

(167) El-Dardiry S.M.A. :'Rayleigh Wave Investigation of Surface Properties of Machined Rolled Bright Steel', M.Phil. Thesis, Brunel Univ., England, 1976.

(168) McGonnagle W.J. :'Nondestructive Testing', Gordon and Breach Sci. Pub., NY, 1971.

(169) Cook E.G. and Van-Valkenburg H.E.:'Surface Waves at Ultrasonic Frequency', ASTM-Bull., 84 (May, 1954) 81-4.

(170) Fisher R.M. and Lally J.S.:'Microplasticity Detected by an Acoustic Technique', Can. J. Phys. , 45 (1967) 1147-59.

(171) Lyon R.H. :'Response of an Elastic Plate to Localized Driving Forces', J.Acoust. Soc.Am., 27 (1955) 259-65.

(172) James D.R. and Carpenter S.H.:'The Effect of Sample Size on the Acoustic Emission Generated During Tensile Deformation of 7075 Aluminium Alloy', Scripta Metallurgica, 10 (1976) 779-81.

(173) Egle D.M. :'On Estimating the Power of Acoustic Emission Events', Soc. Expt. Stress Analysis, SESA Spring Meeting, Chicago, May 11-16, 1975.